PERSPECTIVES IN NEUTRINOS ATOMIC PHYSICS AND GRAVITATION

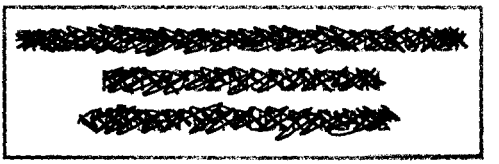

XIIIth Moriond Workshop
Villars sur Ollon, Switzerland - January 30 - February 6, 1993

Perspectives in Neutrinos
Atomic Physics and Gravitation
Series : Moriond Workshops

ISBN 2-86332-136-6

EDITIONS FRONTIERES
B. P. 33
91192 Gif-sur-Yvette Cedex - France

Printed in Singapore by General Printing Services Pte. Ltd.

Proceedings of the XXVIIIth RENCONTRE DE MORIOND
Series : Moriond Workshops
Villars sur Ollon, Switzerland January 30 - February 6, 1993

PERSPECTIVES IN NEUTRINOS ATOMIC PHYSICS AND GRAVITATION

edited by
J. Trân Thanh Vân
T. Damour, E. Hinds
and J. Wilkerson

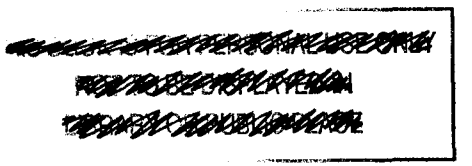

EDITIONS
FRONTIERES

XIIIth Moriond Workshop on :
Perspectives in Neutrinos, Atomic Physics and Gravitation

was organized by

Trân Thanh Vân J. *(Orsay)*

with the active collaboration of :

Boehm F.	*(Caltech)*
Chardin G.	(Saclay)
Cohen-Tannoudji G.	*(Paris)*
Damour T.	*(IHES, Bures sur Yvette)*
Fackler O.	*(Livermore)*
Faller J.	*(Boulder)*
Fischbach E.	*(Purdue)*
Fontaine G.	*(Paris)*
Gerbier E.	*(Saclay)*
Giacobino E.	*(Paris)*
Greene G.	*(NBS)*
Hinds E.	*(Yale)*
Kayser B.	*(Washington)*
Pain R.	*(Paris)*
Petcov S.	*(Sofia/Trieste)*
Spiro M.	*(Saclay)*
Wilkerson J.	*(LANL)*

Sponsored by :

. Centre National de la Recherche Scientifique (IN2P3, MPB)
. Commissariat à l'Energie Atomique(DPhPE)
. National Recherche Foundation

This book is dedicated to Alexander Pomansky
a true scientist and friend

Valentina and Alexander Pomansky

FOREWORD

The XXVIIIth Rencontre de Moriond were held in 1993 in Villars-sur-Ollon (Switzerland) and in Les Arcs, Savoie, (France).

The first meeting took place at Moriond in the French Alps in 1966. There, experimental as well as theoretical physicists, not only shared their scientific preoccupations but also the household chores. The participants in the first meeting were mainly French physicists interested in electromagnetic interactions. In subsequent years, a session on high energy strong interactions was also added.

The main purpose of these meetings is to discuss recent developments in contemporary physics and also to promote effective collaboration between experimentalists and theorists in the field of elementary particle physics. By bringing together a relatively small number of participants, the meeting helps to develop better human relations as well as a more thorough and detailed discussion of the contributions.

This concern of research and experimentation of new channels of communication and dialogue which from the start animated the Moriond meetings, inspired us to organize a simultaneous meeting of biologists on Cell Differenciation and to create the Moriond Astrophysics meeting. Common meetings between biologists, astrophysicists and high energy physicists are organized to study the implications of the advances in one field into the others. I hope that these conferences and lively discussions may give birth to new analytical methods or new mathematical languages.

At the XXVIIIth Rencontres de Moriond in 1993, three physics sessions, one astrophysics session and one biology session were organised :

* January 30-February 6 :	"Perspectives in Neutrinos, Atomic Physics and Gravitation"
* March 13-20	"Electroweak Interactions and Unified Theories"
	"The Cold Universe"
* March 20-27	"QCD and High Energy Hadronic Interactions"
	" Rencontre de Biologie - Méribel "

I thank the organizers of the XXVIIIth Rencontres de Moriond :

- F. Boehm, G. Chardin, C. Cohen-Tannoudji, T. Damour, O. Fackler, J. Faller, E. Fischbach, G. Fontaine, G. Gerbier, E. Giacobino, G. Greene, E. Hinds, B. Kayser, R. Pain, S. Petcov, M. Spiro and J. Wilkerson for the session on Perspectives in Neutrinos, Atomic Physics and Gravitation,

- P. Binetruy, A. Blondel, R. Cahn, G. Coignet, L. Fayard, P. Fayet, J.-M. Frère, L. Krauss, L. Moscoso, C. Savoy and C. Verzegnassi for the Leptonic session,

- Ph. André, C. Césarsky, J.-P. Chièze, F. Genova, C.J. Lada, P.-O. Lagage, E. Mirabel, T. Montmerle, A. Omont, D. Rouan and S. Volonté for the Astrophysics session,

- P. Aurenche, E. Berger, A. Capella, D. Denegri, L. Montanet, B. Pietrzyck, D. Schiff, and C. Voltolini for the Hadonic session,

- M. Caboche, R. Christen, M. Fellous, J.-C. Kader, K. Trân Thanh Vân and A. Ullman for the Biology meeting,

and the conference secretaries : D. Arnoux, L. Besson, D. Davier, V. Demailly, F. Eschenbrenner, D. Josephson, A. Mason, Y. Minssieux, W. Müller, L. Norry, F. and N. Osswald, H. Pham, S. Portut, J. Raguideau, M. Strobel, G. Thiéry, D. Vernet and A. Vernholes.

I am also grateful to Mrs S. Müller, Ms B. Gautron, Mr and Mrs Milan, Ms R. Chenal, Mrs D. Touraille, and Mrs F. Disperati who contributed through their hospitality and cooperation to the well-being of the participants enabling them to work in a relaxed atmosphere.

This Rencontre was sponsored by the Commission of the European Communities (Euroconferences), by the Centre National de la Recherche Scientifique (IN2P3 and FP), and by the Commissariat à l'Energie Atomique (DAPNIA). The workshop on Perspectives in Neutrinos, Atomic Physics and Gravitation was also sponsored by the National Science Foundation. I would like to express my thanks to their encouraging support.

I sincerely wish that a fruitful exchange and an efficient collaboration between the physicists, the astrophysicists and the biologists will arise from this Rencontre as from the previous ones.

J. Trân Thanh Vân

Contents

III. Dark Matter

IV. Atmospheric Neutrinos

V. Neutrino Oscillations

VI. Neutrino Cross Sections

VII. Double β Decay

VIII. 17 KeV Neutrinos

B. ATOMIC/OPTICAL PHYSICS

C. GRAVITATION

I. Equivalence Principle : Experiments

II. Equivalence Principle: Theory

III. Gravitational Waves and Other Gravitational Topics

D. CONFERENCE SUMMARIES

ERRATUM

NEUTRINO PHYSICS

Neutrino Mass

IMPROVED LIMIT ON THE ELECTRON ANTI NEUTRINO REST MASS FROM TRITIUM β-DECAY

Ch.Weinheimer, M.Przyrembel, H.Backe, H.Barth, J.Bonn B.Degen, Th.Edling, H.Fischer, L.Fleischmann, J.U.Grooß, R.Haid, A.Hermanni, G.Kube, P.Leiderer[1], Th.Loeken, A.Molz, R.B.Moore[2], A.Osipowicz, E.W.Otten, A.Picard, M.Schrader, M.Steininger
Institut für Physik, Universität Mainz, Germany

Presented by J.Bonn

ABSTRACT

The endpoint region of the β-spectrum of tritium was remeasured by an electrostatic spectrometer with magnetic guiding field. It enabled the search for a rest mass of the electron anti neutrino with improved precision. The result is $m_\nu^2 = (-39 \pm 34_{stat} \pm 15_{syst})(eV/c^2)^2$, from which an upper limit of $m_\nu < 7.2eV/c^2$ may be derived. The experiment yields the atomic mass difference $m(T) - m(^3He) = (18591 \pm 3)eV/c^2$.

Present addresses:

[1] Fakultät für Physik, Universität Konstanz, Germany
[2] Mc Gill University, Montreal, Canada

In former Moriond conferences we presented progress reports in design and test of a solenoid retarding spectrometer [1, 2] dedicated to study the endpoint of the T_2 β-decay spectrum. First preliminary results were presented in 1991 and 1992. This report gives the first full data analysis yielding a new upper limit on the electron anti neutrino rest mass [3]. The principle of the spectrometer is briefly explained in Fig.1. Due to the adiabatic transforma-

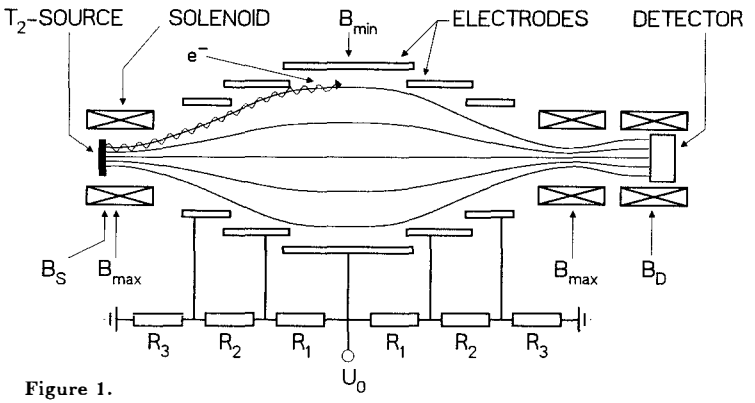

Figure 1.

Principle of the solenoid retarding spectrometer. Electrons emitted from the T_2 source are magnetically guided to the detector. The gradient force $F_\nabla = (\vec{\mu} \times \vec{\nabla}) \times \vec{B}$, acting on the orbital magnetic moment $\vec{\mu}$ of the electrons transforms energy $E_\perp$ in the cyclotron motion around the magnetic field lines into longitudinal motion parallel to the magnetic field. $E_\parallel$ is electrostatically analyzed in the symmetry plane of the spectrometer.

tion of energy in the cyclotron motion $E_\perp$ around the magnetic field lines into $E_\parallel$ parallel to the magnetic field the full foreward solid angle can be accepted. The filter width under these conditions is given by $\Delta E = B_1/B_0 \cdot E$, where B_0 is the maximum and B_1 is the minimum magnetic field.

The experiment described here was performed under the following conditions. The source is placed at a field $B_S = 0.96\ B_0$, slightly in front of the field maximum of the source solenoid which is set to $B_0 = 2.4$ T, limiting the accepted polar angles to $\vartheta < 78°$. The magnetic field reaches its minimum $B_1 = 8 \cdot 10^{-4} T$ in the symmetry plane of the spectrometer, where U_0 maximizes. Retardation of the electrons and reacceleration after the filter is provided by two sets of electrodes arranged symmetrically around the central one. Under these conditions the rise of the transmission from 0 to 1 within the interval $E(1 - B_1/B_0) \leq e \cdot U_d \leq E$ is given by [14]:

$$T(E,U_d) = \frac{1 - \sqrt{1 - \dfrac{E - e \cdot U_d}{E} \cdot \dfrac{B_S}{B_1}}}{\left(1 - \sqrt{1 - \dfrac{B_S}{B_0}}\right)} \qquad (1)$$

where $U_d = U_S - U_0$ is the difference between the potentials of the source and the central electrode. $T(E,U_d)$ was checked with high accuracy by conversion electrons from ^{83m}Kr [14]. As important as the sharpness of the filter is the absence of any tails of $T(E,U_d)$ extending

beyond E. During reacceleration, the electrons are also refocussed by the field of a second solenoid, also set to 2.4 T, and finally reach a silicon detector placed in the central field B_D = 0.8 T of a third solenoid. The active area of the detector has a diameter of 25 mm and is segmented into five rings of equal area. The counts were pulse height analyzed and stored event by event. Cooled down to $-80°C$, the detector has a resolution of 2.0 keV FWHM for 20 keV electrons. The resolution was somewhat degraded with respect to the values reported in ref. [15] due to 15 $\mu g/cm^2$ aluminium evaporated onto the $30\mu g/cm^2$ Kapton foil separating the high vacuum at the detector from the UHV in the spectrometer.

Regarding the source, we decided on molecular T_2 frozen onto an aluminium substrate cooled down to 2.8 K. Compared to any other T-compound, this choice offers the highest specific activity. Because of the lowest possible Z, the spectrum of energy losses by inelastic scattering within the source, as well as by prompt shake up/off processes, is, in comparison, also soft and simple. According to extensive molecular orbit calculations [16], the final state spectrum of the latter is slightly more complicated than that of gaseous T_2 [17]. The present source was constructed following the experience of a feasibility study [18]. The substrate is mounted on the front of a 1.2 m long, horizontal LHe cryostat. The solid angle of T_2- evaporation into the spectrometer is limited to $\Delta\Omega/4\pi = 2.5 \cdot 10^{-3}$ by a LHe-cooled, 10 cm long and 2 cm wide Cu tube in front of the source which itself covers a circular area of 1 cm^2. The tube also reduces condensation of residual gas onto the source. The source is connected to the spectrometer by a bellows allowing it to be moved from the loading to the measuring position through a valve. T_2 is evaporated onto the substrate by covering the respective area with a teflon cup into which T_2 is led through a capillary. Glass windows allow the evaporation process to be controlled by ellipsometry. Films of 40 monolayers, corresponding to a total source strength of 10^8 Bq were prepared. Through on line mass spectrometry we detected tritium contaminations of about 30 % of hydrogen which had probably taken place in the stainless steel container.The source region meets the UHV conditions of the spectrometer [1]. During measurements the source "decayed" almost exponentially with a half-life time of a week. Data were taken for about ten days per source.

Without a source the background spectrum peaked at about 23 keV, well above the tritium spectrum [1]. Therefore, most of it could be suppressed by limiting the window of accepted events between 12 and 19.5 keV. The residual background rate then dropped to 5 mHz for the central segment and to 23 mHz for the outermost one. With the tritium source the background rate rose by a factor of up to 2 for a fresh source. This additional background peaked at the energy $-e \cdot U_0$. A rough estimation showed that it could be attributed to T_2 molecules which evaporate from the source and decay in vacuo within the magnetic flux tube projected onto the detector. After removing the source the background rate returned immediately to the original value showing no obvious sign of contamination of the spectrometer.

Tritium spectra were recorded in the energy interval $18095eV \leq e \cdot U_d \leq 18800eV$ by scanning up and down a negative potential U_S on the source[3] at constant analyzing potential U_0 = -18779 V. The most critical region around the endpoint was scanned in steps of 4 V with an integration time of $2 \cdot 30s$ per point and scan. Elsewhere larger steps and shorter integration times were chosen. The data were screened for false events. By checking the distribution of time differences between events we detected sudden increases in the count rate, possibly triggered by microsparks in the spectrometer. About 14 % of the whole set of about 500 scans have been rejected due to this failure. The scatter of the remaining data obeys a statistical distribution. Fig.2 shows the recorded β-spectrum. The data comprise counts of the two innermost segments

[3] Negative source potential is essential for retaining ions from T_2 decay which are otherwise accelerated into the spectrometer causing a few Hz background rate by ionization of residual gas.

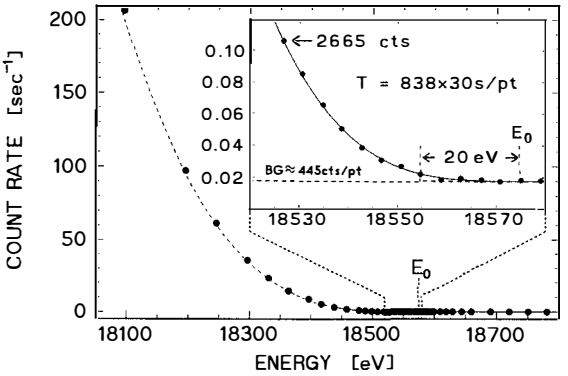

Figure 2.

β-spectrum of tritium recorded during a four week run in 1991. The statistical error bars are too small to be plotted. For energies $E_e \geq 18460eV$ the integral measuring time is 25140s per point. The background level is 450 cts per point ≙18mHz. The full line is the best fit to the data in the interval from 18438 eV to 18800 eV, the broken one is the extrapolation of the fit to lower energies.

of the detector. The other ones are covered only partly by the image of the source and suffer from higher background. An expanded view of the endpoint region is given in the insert. Already 20 eV below the endpoint, the spectrum emerges clearly from the background noise.

Another instructive view to the data is obtained from a linearized plot of the spectrum given in fig.3. Since our spectrometer is integrating the β-spectrum, the linearization is achieved to a first approximation by the cube root of the count rate after substracting the background. The data deviate from the linear slope as soon as transitions to exited states of $(^3HeT)^+$ become significant. The straight line representing transitions to the ground state of $(^3HeT)^+$ intersects the baseline about 4 eV below the endpoint. This is mainly due to the average residual energy in the motion of the electrons around their guiding field lines which is not analyzed by the SRS. The fit, described below, on the other hand slightly overshoots the endpoint, as the best fit value for m_ν^2 is negative. Furthermore, we have plotted into fig.3 fits to the data with m_ν fixed to 0, 10 and 20 eV/c^2 respectively. A value of the order of 20 eV/c^2 is excluded apparently. As to our knowledge, it is the first time that such fine details have ever been resolved in a β-spectrum. In the final evaluation the data were fitted to the sum of a background function

$$b(U_d) = b_0 + b_1 \cdot (E_0 - e \cdot U_d) \tag{2}$$

and a convolution

$$I(U_d) = \int\int T(E', U_d) \cdot D(E', U_d) \cdot L(E, E') \cdot S(E)\, dE \cdot dE' \tag{3}$$

of the transmission function of the spectrometer $T(E', U_d)$ (eq.1), the detector efficiency function $D(E', U_d) = 1 + \alpha_D(E' - eU_d)$ with $\alpha_D = 0.10 \pm 0.01\ keV^{-1}$, the energy loss function L(E,E') and the spectral function of the β-decay S(E).

The background is entirely determined by the data measured beyond E_0 yielding $b_0 = 17.7\ (2)\ mHz$, $b_1 = 5\ (3)\ \mu Hz/V$.

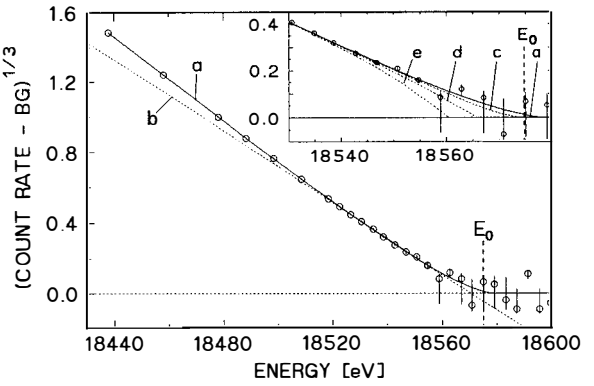

Figure 3.

Linearized β-spectrum close to the endpoint. a: best fit with $m_\nu^2 c^4 = -39 \pm 34 (eV)^2$ and experimental β-endpoint $E_0 = 18574.8 \pm 0.6 eV$, b: linear fit of last 50 eV, c-e: fits with $m_\nu c^2$ fixed to 0, 10, 20 eV in the interval 18438 eV to 18600 eV.

The energy loss function of the sources L(E,E') has been calculated from an inelastic cross section which is approximated by

$$\frac{d\sigma(E,E')}{dE'} = \frac{a_{exc} \cdot \Gamma_{exc}^2}{\Gamma_{exc}^2 + (\Delta E - E_{exc})^2} \cdot \Theta(\Delta E - E_{min}) \cdot \Theta(E_B - \Delta E) + \frac{a_{ion} \cdot \Gamma_{ion}^2}{\Gamma_{ion}^2 + (\Delta E - E_{ion})^2} \cdot \Theta(\Delta E - E_B) \quad (4)$$

with $\Delta E = E - E'$, $E_{min} = 8.8\ eV$, $E_B = 15.4\ eV$,
$a_{exc} = 7.5 \cdot 10^{-19}\ cm^2/(eV \cdot molecule)$, $\Gamma_{exc} = 0.8\ eV$, $E_{exc} = 12.6\ eV$,
$a_{ion} = 1.5 \cdot 10^{-19}\ cm^2/(eV \cdot molecule)$, $\Gamma_{ion} = 7.1\ eV$, $E_{ion} = 17.2\ eV$.
The first Lorentzian approximates the excitation of T_2 [19], the second the ionisation [20]. The parameters a_{exc} and a_{ion} are chosen to match the total stopping power and the total inelastic cross section [21, 22]. The zero loss fraction of electrons is 91% $\pm$ 4% in the average calculated from eq. 4. The error is dominated by uncertainties in the tritium film thickness and homogeneity.

The spectrum is described by

$$S(E) = A \cdot F \cdot p \cdot (E + m_e \cdot c^2) \cdot \sum_i W_i \cdot \varepsilon_i \cdot \sqrt{\varepsilon_i^2 - m_\nu^2 \cdot c^4} \cdot (1 + \alpha_{BS}/3 \cdot \varepsilon_i) \quad (5)$$

with A = amplitude, F = Fermi function[23], p = electron momentum, $\varepsilon_i = (E_0 - V_i - E)$, W_i=relative transition probability to the i'th molecular final state of excitation energy V_i. The backscatter contribution is convoluted with the spectrum in linear approximation by the last factor in eq. 5 with $\alpha_{BS} = 0.20 \pm 0.05\ keV^{-1}$, which was derived from preliminary test measurements. To enable fitting around $m_\nu^2 = 0$ we use a continuation of the term $\varepsilon_i \cdot \sqrt{\varepsilon_i^2 - m_\nu^2 \cdot c^4}$ into the region $m_\nu^2 < 0$ replacing it by $(\varepsilon_i + \mu \cdot exp(-\varepsilon_i/\mu - 1) \cdot \sqrt{\varepsilon_i^2 - m_\nu^2 \cdot c^4}$ with $\mu = 0.76 \cdot \sqrt{-m_\nu^2 \cdot c^4}$. This continuation is smooth and provides a parabolic χ^2-distribution

around $m_\nu^2 = 0$. To save computing time we have replaced the sum over the final states which comprises the product of the final state spectrum of the daughter molecule $(^3HeT)^+$ [17] and the simultaneously excited closest neighbours [16] by 10 discrete states with appropriated Gaussian widths. This procedure has been checked to be sufficiently precise.

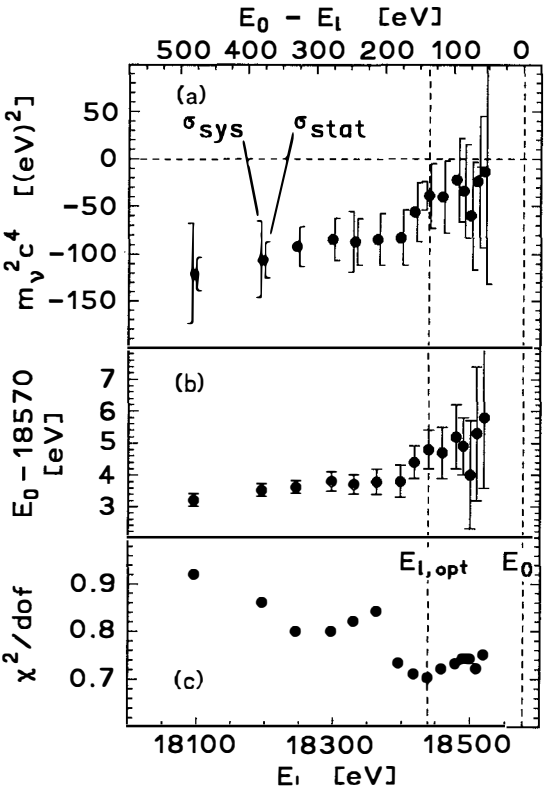

Figure 4.

(a) square of neutrino rest mass m_ν^2, (b) endpoint E_0 and (c) χ^2/dof as function of the lower limit E_l of the fit interval.

The free fit parameters are A, E_0, m_ν^2, b_0 and b_1. Fig.4 shows the best fit results for m_ν^2 , E_0 and χ^2/dof as a function of the lower limit E_l of the fit interval. The significant dependence on this boundary points to residual, systematic errors correlating to m_ν^2 and E_0 further below the endpoint. Although being small they may drag m_ν^2 and E_0 away from the true values because the statistical weight of data points increases rapidly with decreasing energy. As shown by the conservative systematic errors deduced for some of the m_ν-values shown in

fig.4, we believe it unlikely that uncertainties in energy loss, backscatter, spectrometer function etc. could be responsible for this unphysical trend. For $E_l = E_0$ - 137 eV this systematic error is broken down into its components in tab.1. The systematic uncertainties about the final states distribution were checked by using an alternative calculation [29, 30]. The results were essentially unchanged. The trend to negative m_ν^2 arises from an excess count rate far from the endpoint. A simple way to account for this would be to increase the shake off probability. To test this, we changed the shake off probability from 15% as given in ref. [17] over a wide range[4]. At 21% all fit parameters, as well as χ^2/dof, remain stable against variation of the fit interval with m_ν^2 compatible to zero within 1σ statistical error[5].

Table 1. *Influence of variation of critical parameters on m_ν^2 at $E_{l,opt} = E_0 - 137eV$. The coefficients α_D for detector efficiency and α_{BS} for backscatter were changed simultanously since they have the same influence on $I(U_d)$, despite of their different functional dependence. The constant backscatter spectrum was changed by allowing a strong additional linear term keeping the total backscattering probability constant over the interval where the backscatter distribution was investigated. The fraction of energy loss by excitation was changed by 50% while keeping the total inelastic cross section constant. This accounts for different stopping power values given in literature.*

Parameter	Change [%]	$\Delta m_\nu^2 c^4$ $[(eV)^2]$
Inelastic scattering		
total probability	50	14.2
a_{exc} (σ_{tot} =const)	50	3.3
Backscatter & detector eff.		
α_{BS},α_D	25	1.8
different shape	-	3.2
Width of $T(E', U_d)$	10	1.4
Alternative final state		
distribution [29, 30]	-	0.3
Total		15.1

The high resolution and statistics together with the low background of our experiment allow for the first time to reduce the problems associated with including a wider range of the β-spectrum into the data evaluation. We therefore chose $E_{l,opt} = E_0 - 137eV$, where the fraction of ground state transitions is 76 %[6]. The data were fitted for the two sources separately and

[4] Some evidence also seems to exist that shake off probabilities measured in conversion electron spectra [24] exceed calculated ones [25].

[5] An admixture of a second neutrino in the range $m_\nu^2 \leq 100(eV/c)^2$ could remove neither the unphysical value of negative m_ν^2 nor the trends in m_ν^2 and E_0 with increasing data set. In contrast to additional shake off components the inclusion of a second neutrino does not lead to the observed spectral shape due to its essentially different functional dependence.

[6] Extrapolated towards lower energies this fit yields progressively less count rate than measured. When we plot the cube root of this excess count rate (like in Fig.2), a nice, straight Kurie line shows up which intersects with the abscissa 75 eV below the endpoint. Thus it has the signature of a missing spectral component with that endpoint and an amplitude of 4%. We note that the centre of gravity of the shake off electrons is 69 eV.

combined (see tab.2). As a final result we obtain from this interval:

$$m_\nu^2 \cdot c^4 \;=\; (-39 \;\pm\; 34_{stat} \;\pm\; 15_{syst})\;(eV)^2$$

and $E_0 = (18574.8 \pm 0.6) eV$. From E_0 we calculate the mass difference

$$m(T) \;-\; m(^3He) \;=\; (18591 \;\pm 3)\; eV/c^2$$

where the following corrections have been taken into account: recoil energy (1.7 eV), difference in chemical binding energies (16.5 eV), polarization shift (-0.9 eV) [16], difference in work functions between substrate and analyzing electrode (-0.1 eV) [14], potential drop in the analyzing plane (-1.2 eV) [1] . The error is dominated by the uncertainty in the high voltage measurement [14]. Our measurement of the mass difference matches well with recent results [9, 10, 26].

Table 2. *Results for $m_\nu^2/[(eV)^2/c^4]$, $E_0/[eV]$ and χ^2/dof for the two sources S1, S2 and the combined fit Σ.*

	$m_\nu^2 \pm \Delta m_\nu^2$	$E_0 \pm \Delta E$	χ^2/dof
S1	-46 ± 56	18574.2 ± 0.7	0.93
S2	-29 ± 43	18575.3 ± 0.8	0.93
Σ	-39 ± 34	18574.8 ± 0.6	0.70

Following the recipe of the Particle Data Group [27] we calculate from our m_ν^2-result the following upper limit for the electron anti neutrino rest mass with 95 % confidence level:

$$m_\nu \;<\; 7.2\; eV/c^2.$$

In tab.3 we have listed recent measurements of m_ν^2.

Table 3. *Recent results of $m_\nu^2/[(eV)^2/c^4]$ from tritium β-decay. Values of σ_{stat} and σ_{sys} are 1 σ errors. Upper limits on $m_\nu/[eV/c^2]$ according to [27] correspond to 95% c.l.*

Ref.	$m_\nu^2 \pm \sigma_{stat} \pm \sigma_{sys}$	m_ν
LANL [9]	$-147 \pm 68 \pm 41$	< 9.3
Zürich [10]	$-24 \pm 48 \pm 61$	< 11
INS [28]	$-65 \pm 85 \pm 65$	< 13
LLNL [31]	$-60 \pm 36 \pm 30$	< 8
This paper	$-39 \pm 34 \pm 15$	< 7.2

Among the known sources of the systematic error of the present result, uncertainties in the energy loss fraction and the backscatter from the substrate dominate. These values will be checked in detail by measurements with electron conversion lines from ^{83m}Kr covered with D_2 layers of known thickness in the near future. The remaining problem of not fully understanding the measured β-spectrum may be circumvented by restricting the analysis to a region very close to the endpoint which may be even smaller than the one used here. The unique capability of

working very close to the endpoint has not been fully exploited in the past. To this end we will considerably improve the statistical accuracy and make an effort to further reduce background.

The spectrometer was financed by the state of Rheinland-Pfalz and the Bundesminster für Bildung und Wissenschaft providing funds for the new Physics building of the University and its equipment. The Deutsche Forschungsgemeinschaft has contributed to the running and personnel costs of the experiment under the contract number OT33-11. We thank V.M.Lobashev for critical discussions while writing this paper. One of us (R.B.Moore) acknowledges a NATO collaborative grant for support of this work.

References

[1] A.Picard, H.Backe, H.Barth, J.Bonn, B.Degen, Th.Edling, R.Haid, A.Hermanni, P.Leiderer, Th.Loeken, A.Molz, R.B.Moore, A.Osipowicz, E.W.Otten, M.Przyrembel, M.Schrader, M.Steininger, Ch.Weinheimer *Nucl. Instrum. Methods* **B63**(1992)345

[2] H.Backe et al., Proceedings of the 16th Moriond Workshops, 137

[3] Ch.Weinheimer et al. *Phys. Lett.* **B 300**(1993)210

[4] V.A.Lubimov, E.G.Novikov, V.Z.Nozik, E.F.Tretyakov, V.S.Kosik *Phys. Lett.* **94B**(1980)266

[5] S.Boris, A.Golutvin, L.Laptin, V.Lubimov, V.Nagovizin, V.Nozik, E.Novikov, V.Soloshenko, I.Tihomirov, E.Tretyakov, N.Myasoedov *Phys. Rev. Lett.* **58**(1987)2019

[6] E.F.Tretyakov *Bull. USSR Acad.Sci.Phys.*Ser.39,No.3(1975)102

[7] M.Fritschi, E.Holzschuh, W.Kuendig, J.W.Petersen, R.E.Pixley, H.Stuessi *Phys. Lett.* **B173**(1986)485

[8] J.F.Wilkerson, T.J.Bowles, J.C.Browne, M.P.Maley, R.G.H.Robertson, J.S.Cohen, R.L.Martin, D.A.Knapp, J.A.Helffrich *Phys. Rev. Lett.* **58**(1987)2023

[9] R.G.H.Robertson, T.J.Bowles, G.J.Stephenson, D.L.Wark, J.F.Wilkerson, D.A.Knapp *Phys. Rev. Lett.* **67**(1991)957

[10] E.Holzschuh, M.Fritschi, W.Kündig *Phys. Lett.* **B287**(1992)381

[11] V.M.Lobashev, A.I.Fedoseyev, D.V.Serdyuk, A.P.Solodukhin *Nucl. Instrum. Methods* **A240**(1985)305

[12] H.Backe, J.Bonn, Th.Edling, H.Fischer, A.Hermanni, P.Leiderer, Th.Loeken, R.B.Moore, A.Osipowicz, E.W.Otten, A.Picard *Phys. Scr.* **T22**(1988)98

[13] S.Balashov, A.Belesev, A.Bleule et al. *Proc. of the II int. symposium on Weak and Electromagnetic Interactions in Nuclei (W.E.I.N.-89) Montreal*(1989)295,Edition Frontiers, France

[14] A.Picard, H.Backe, J.Bonn, B.Degen, R.Haid, A.Hermanni, P.Leiderer, A.Osipowicz, E.W.Otten, M.Przyrembel, M.Schrader,M.Steininger, Ch.Weinheimer *Z. Phys.* **A342**(1992)71

[15] Ch.Weinheimer, M.Schrader, J.Bonn, Th.Loeken, H.Backe *Nucl. Instrum. Methods* **A311**(1992)273

[16] W.Kolos, B.Jeziorski, J.Rychlewski, K.Szalewicz, H.J.Monkhorst, O.Fackler *Phys. Rev.* **A37**(1988)2297

[17] O.Fackler, B.Jeziorski, W.Kolos, H.J.Monkhorst, K.Szalewicz *Phys. Rev. Lett.* **55**(1985)1388

[18] M.Przyrembel, H.Fischer, A.Hermanni, E.W.Otten, P.Leiderer *Phys. Lett.* **A147**(1990)517

[19] J.Geiger *Z. Phys.* **181**(1964)413

[20] A.E.S.Green, T.Sawada *J.Atm.Terr.Phys.* **34**(1972)1719

[21] L.Pages, E.Bertel, H.Joffre, L.Skalventis *Atomic Data* **4**(1972)1

[22] J.W.Liu *Phys. Rev.* **A7**(1973)103

[23] J.J.Simpson *Phys. Rev.* **D23**(1981)649

[24] D.L.Wark, R.Bartlett, T.J.Bowles, A.G.H.Robertson, D.S.Sivia, W.Trela, J.F.Wilkerson, G.S.Brown, B.Crasemann, S.L.Sorensen, S.J.Schaphorst, D.A.Knapp, J.Henderson, J.Tulkki, T.Åberg *Phys. Rev. Lett.* **67**(1991)2291

[25] Th.A.Carlson, C.W.Nestor *Phys. Rev.* **A8**(1973)2887

[26] R.S.Van Dyck, D.L.Farnham, J.Bare, P.B.Schwinberg *Proc. of the* 6^{th} *Int. Conf. on Nuclei far from Stability and* 9^{th} *Int. Conf. on Atomic Masses and Fundamental Constants Bernkastel-Kues*(1992), ed. by K.L.Kratz et al., in print in the IOP conf. series

[27] Particle Data Group *Phys. Lett.* **204B**(1988)69

[28] H.Kawakami, S.Kato, T.Ohshima, S.Shibata, K.Ukai, N.Morikawa, N.Nogawa, K.Haga, T.Nagafuchi, M.Shigeta, Y.Fukushima, T.Taniguchi *Phys. Lett.* **B256**(1991)105

[29] L.Martin et al. *Phys. Lett.* **110A**(1985)95

[30] D.A.Knapp *doctoral thesis, LANL*(1986)

[31] W.Stoefft *contribution to this workshop*

THE TRITIUM BETA SPECTRUM AND THE NEUTRINO MASS

Wolfgang Stoeffl and Daniel J. Decman

Lawrence Livermore National Laboratory
Livermore, CA 94550

(Presented by Wolfgang Stoeffl)

ABSTRACT

We have set an upper limit of 8 eV for the mass of the electron antineutrino by studying the beta decay of gaseous molecular tritium. Our system uses five super conducting magnets to guide the beta decay electrons from a five meter long source tube into a large toroidal field spectrometer. The spectrometer, which has a resolution of 4 to 18 eV at 23 keV, focuses the electrons onto a liquid-nitrogen-cooled multi-segmented Si(Li) detector. We calibrate our system using conversion electrons from the decay of ^{83m}Kr. Our best fit value for the neutrino mass squared is —60 +/- 36(statistical) +/- 30(systematic) eV^2. We obtain a value of 18586.6(25) eV for the ^{3}H-^{3}He mass difference in good agreement with recent mass spectrometry results.

16

Introduction

Neutrinos play an important role in today's physics research. Massive neutrinos are a prime candidate for the missing mass in the universe. Large underground detectors measure the neutrino flux from the sun and search for supernova neutrinos. Yet despite all efforts there exists no direct measurement of the neutrino mass. The neutrino mass can be measured directly by studying the beta decay of tritium as a massive electron antineutrino will alter the shape of this low-energy beta decay spectrum. This is the only unambiguous way to find a neutrino mass or set an upper limit independent of the structure of the neutrino. In 1980 Lubimov[1] and coworkers reported evidence for a 30 eV neutrino mass in their studies of the beta decay of tritium implanted in valine. Subsequent attempts by groups in Tokyo[2] and Zurich[3], who implanted tritium in thin films, found no evidence for this mass. These groups were able to set upper limits of 13 and 15.4 eV, respectively, for the mass of the electron antineutrino. The group at Los Alamos National Laboratory[4] studied the beta decay of gaseous molecular tritium and found no evidence for a 30 eV mass, but set an upper limit of 9.3 eV. The experiment in Mainz[5] uses frozen tritium and a retarding field spectrometer to set an upper limit of 7.2 eV. However all of the recent results obtained negative values for the best fit value of m_ν^2. This suggests the possibility of an additional systematic error in these measurements or some physics that is not described by the current beta decay theory.

We use a gaseous tritium source combined with a high resolution magnetic spectrometer and a low background counting system to reduce the systematic errors. The gaseous molecular tritium yields the highest specific activity and a system where the final states can be reasonably well calculated. By having a gaseous source we can minimize and measure the scattering of the electrons in the source material. The gaseous source avoids solid state effects, even the effect of tritium bonded to a cooled solid surface. Our experiment has very low background, ~5 counts per day per detector ring in the energy region of interest. We can analyze 23 keV electrons with a resolution between 3 and 20 eV depending on the transmission of the spectrometer. In addition we have a system where we can determine the resolution function and energy loss in the source very precisely. Our data disagree with Lubimov's claim for a 30 eV neutrino mass and we can set an upper limit of 8 eV for the mass of the electron antineutrino at the 95% c.l.

Experimental apparatus

Our gaseous tritium source consists of a 5 meter long tube with a diameter of 3 cm. The source tube is located inside a liquid nitrogen-cooled shield in a high vacuum tube. We can cool the source tube to 50 K. The source vacuum tube and its cryogenic shields fit inside the warm bore of the superconducting magnet assemblies. The gas is differentially pumped at the ends of the source tube by eight turbomolecular pumps, cleaned and is then re-injected into the middle of the tube. The radioactive gas is prevented from entering the spectrometer tank by a 1.5-m-long pumping restriction that is lined with charcoal and cooled to 10 K. In addition to the charcoal we have another section containing a tritium getter pump. Electrons from decays in the gaseous source are

guided into a large toroidal magnetic field spectrometer by five solenoidal super conducting magnets.

We analyze the electrons from the source using a large toroidal field magnetic spectrometer of the Tret'yakov type. The toroidal field is formed by 72 current loops. The inside part of each loop consists of a 25 mm wide, 1 mm thick copper band with a length of 7 meters. The outer conductors are 13 mm diameter aluminum rods. The conductors are supported by a space frame composed of large and small rings held together by aluminum beams. At the first focus of the spectrometer there is a slit system that can be moved by two stepping motors. The slits are two hyperbolic plates and both the position and the gap between them can be changed. In this way we can select different trajectories of the focused electrons. We have a system of 16 deflector plate pairs both before the first focus and in front of the detector. A diagnostic cup with a slit can be positioned over the detector to choose a narrow range of trajectories through the machine. We can then tune the associated deflector plates for those trajectories giving us 16 tunable spectrometers.

The magnetic spectrometer focuses the electrons onto a 12-segment, liquid-nitrogen-cooled Si(Li) detector. The position of the electron impact on this detector determines the energy. Because the detector has good energy resolution, we can distinguish between good events and background from radioactive decays and secondary cosmic-ray interactions. The magnetic spectrometer operates at a constant field and current setting to avoid thermal stresses and misalignment in the spectrometer hardware. We measure electron spectra by changing the electric potential of the source. This accelerating potential is approximately 5 kilovolts for the tritium endpoint. In this way the electrons from the tritium decays in the source tube have an energy of 23 keV throughout the spectrometer and are therefore easily distinguished from the background electrons from tritium contamination in the spectrometer where the maximum energy is 18.6 keV.

A residual gas analyzer, located in the last stage of the differential pumping of the source tube, measures the tritium partial pressure. Our computer then uses the pressure data and a motorized needle valve to regulate the gas pressure. The regulation can keep the tritium source pressure stable to 0.5%. An essential part of the gas regulation is our ability to control the temperature of the experimental hall. By using our computer control system we keep the room temperature constant to with 0.1 K.

We accumulate data by stepping the high voltage to accelerate the source electrons of the energy range of interest to match the analyzing energy of the spectrometer. For each value of the voltage we accumulate 12 spectra on the ring detector. Each of these spectra are written to a disk file along with the pertinent information such as the actual counting time (determined by a precision pulser and scaler), the measured acceleration voltage, dead time parameters, and source gas pressure and temperature corrections. This produces 12 separate spectra for a voltage sweep. In our data analysis fit, we correct the *expected* countrate for the tritium pressure, different timing for each data point etc., and *not* the data itself. This preserves the poisson statistics of the original data.

A source of mono-energetic electrons is a very useful diagnostic tool in measuring and optimizing the performance of the spectrometer system. We have constructed an electron gun to serve this purpose. The gun consists of a quartz window positioned at the end of the source tube farthest from the spectrometer. The vacuum side of the window has a thin, optically half transparent gold coating. This "back wall" of the source is electrically isolated from the rest of the source tube and the support table and we can apply an accelerating voltage to this section of < 25 kV. We illuminate the quartz window with a mercury UV lamp from outside the source tube. The energy of the UV photons is about 100 mV above the work function of the electrons on the gold surface. Therefore the UV light produces very low energy electrons that are then accelerated by the applied high voltage. This gives us a very mono-energetic flood-type beam that is tunable from 0 to 25 keV. One has to take precaution to avoid positively charged energetic tritium or krypton ions from hitting the gold surface. At higher gas densities, the gun-electrons can produce these ions themselves. The ion impact releases electrons with about 5 eV initial energy, causing a high energy tail in the gun emission. Without a positive electric barrier in front of the gun, the ion induced electron emission can falsify the peakposition or energy loss measurements.

Measurements of the system response function

An important aspect of tritium beta decay experiments is the intrinsic resolution function of the spectrometer and source. The finite resolution of the spectrometer will smear out the beta decay spectrum such that the deviation in the distribution expected for a non-zero neutrino mass would appear as a curve. Since we must unfold this system resolution function from the experimentally observed spectrum the accuracy of our knowledge of this function is crucial in determining a neutrino mass limit. We have performed a series of measurements to determine different aspects of our system response function. The measurements include the energy loss contribution and the effects of long tails in the spectrometer response.

Krypton tests

We measure our resolution by using the radioactive calibration source ^{83m}Kr, which is produced by the electron capture decay of ^{83}Rb, approximately 90% of these decays result in the production of a metastable state at 41.5 keV. This isomeric state, which has a half life of 1.8 hours, decays by a cascade of two electromagnetic transitions of 32 and 9 keV. The K-conversion electrons of the 32 keV transition have an energy of 17.8 keV, conveniently close to the end point of tritium. The radioactive krypton gas circulates in the source tube in the same way as molecular tritium and therefore allows us measure our system resolution.

We have made extensive use of the electrons from the ^{83m}Kr decay to study the performance of our source and spectrometer. Although the decay scheme of this isomer consists only of two electromagnetic transitions it gives rise to over 200 structures in its electron spectrum. The lines cover the energy range from 0 to 32 keV and have components that are both nuclear and atomic in origin. The most important feature of the spectrum is the K-conversion line of the 32 keV transition which is shown in figure 1. (The results of the measurements on the 9 keV transition are

presented in reference 6.) The low energy structures are due to the atomic physics processes of shake-up and shake-off. In these processes the electron shells rearrange in response to the K-conversion process, i.e., the electrons suddenly find themselves in a very different nuclear potential. There is not a perfect overlap between the initial neutral krypton orbitals and those with the K vacancy and therefore there is a finite probability that some of the atoms will be left with electrons excited to the 5p, 6p, 7p, levels. This is the shake-up process. The electrons can also be excited into the continuum, this is shake-off. The peak structures show the excitations of the 4p, 3d and 3p atomic shells in a similar manner. Our resolution is sufficiently high that we can resolve the main Lorentzian peak from the first shakeup-shakeoff satellites which allows us to directly determine our resolution without interference from atomic physics. For the Kr 32-keV K line we achieved a resolution as good as 4 eV. In fitting the Lorentzian width for this peak we obtain a value of 2.85 eV, in good agreement with the accepted value for the lifetime of a krypton K vacancy[7].

We use the ^{83}Kr to calibrate the energy scale of our spectrometer using only atomic physics data. The two parameters in our measurement are the calibration constants for the voltage divider, through which we measure the high voltage on the source table, and the shunt for the spectrometer current, which fixes the analyzing energy. We determine the HV-divider constant by measuring the voltage difference of the 32 keV K line and the M-N lines. The M and N binding energies for krypton are known to within .1 eV. The binding energy of the K-shell[8] is 14327.2 eV, known to an accuracy of 0.8 eV. The L-binding energies given in the literature[9,10] are clearly too high by 4 eV. We did not use the L lines to calibrate our spectrometer.

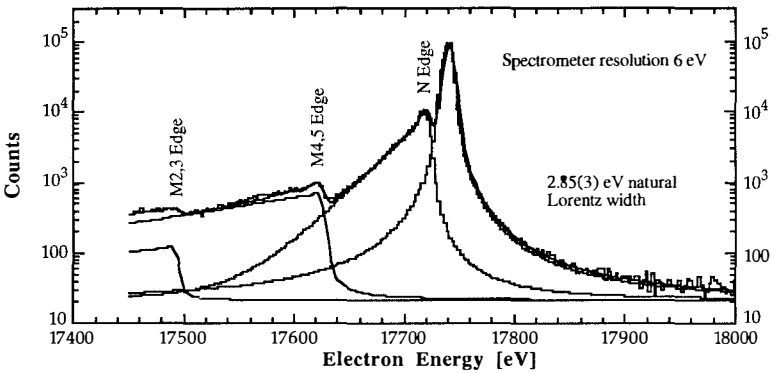

Figure 1. The spectrum of the 32-keV K-conversion line. The shake-up and shake-off satellites are labeled with their atomic shells on the low-energy side of the main peak. The main peak is free from atomic effects and shows the pure Lorentz shape.

To fix the energy scale of our calibration we measure the position of the strong LMM Auger lines at 1460 and 1512 eV[11]. This gives us the zero offset of our calibration, and together with the gain we

have a highly accurate absolute and reproducible energy calibration. To verify the linearity of our HV divider, we have performed this procedure for analyzing energies of 10, 15, 21 and 23 keV and always obtain the same results for the various lines in the ^{83}Kr electron spectrum to within 0.1 eV. Using this system we can then deduce the energies of the gamma rays in the ^{83}Kr cascade. We obtain a value of 17.8213(15) keV for the 32.1485(20) keV K-conversion line, in good agreement with the value deduced from gamma-ray spectroscopy[12]. The energy of the second transition in the cascade is 9.208(3) keV.

Electron gun measurements of the spectrometer resolution.

The scattering of electrons in the spectrometer can produce tails on both sides of the resolution function. Electrons with more energy than the analyzing energy scatter on the slits and conductors of the spectrometer and by losing energy make it through to the detector. This process produces a flat tail on the low energy side of a monochromatic line source with an intensity of 10^{-4} of the total. The low energy tails, i.e. electrons whose initial energy was lower than the analyzing energy, are of more importance to the tritium beta decay measurement since the intensity of electrons increases so rapidly as one moves to lower energies away from the end point. Because of this even a 10^{-4} effect can be significant in the analysis. We have used the high intensity of our electron gun to measure these small effects in our spectrometer resolution function. The data from these measurements is shown in figure 2. We find that the low energy tail extends 200 eV below the peak with 10^{-5} of the total intensity.

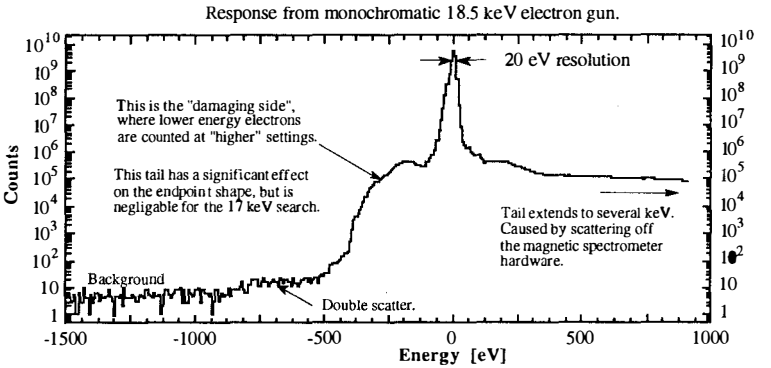

Figure 2: The response function of our spectrometer as measured by the electron gun. Note the 10 orders of magnitude on the intensity scale.

Energy loss measurements

The electron energy loss from scattering with the tritium gas molecules in our source must also be included in our system response function. Ideally we would directly measure this by mixing tritium gas in the source tube with ^{83m}Kr and determine the energy loss from the change in line shape of the 32 keV K-conversion line. However the low energy side of the krypton conversion

lines have large shake-off components in the first 100 eV below the peak. These atomic physics effects mask the bulk of the energy loss spectrum, allowing only a rather crude measure of the energy loss tail. The centroid shift of the total 32 keV K line is a better measure of the energy loss. We determined the relationship of this centroid shift to the total scattering by measuring the shape of the energy loss spectrum with a monochromatic electron beam from our electron gun. The theoretical understanding of the shape and amplitude of the energy loss spectrum for 20 keV electrons is surprisingly poor. We studied the energy loss of 18.5 keV electrons (and other energies) in various pressures of H_2 gas with a spectrometer resolution of 3.9 eV FWHM. The energy loss spectrum of 18.5 keV electrons in H_2 is shown in figure 3. We determine the effect of energy loss by combining the knowledge of the shape of this spectrum with the data from the krypton -- hydrogen mixture. The error in the energy loss determination contributes less than 15 eV^2 in our uncertainty in m_ν^2. To have a more consistent understanding of the energy loss mechanism, we also measured the loss spectra for helium and argon.

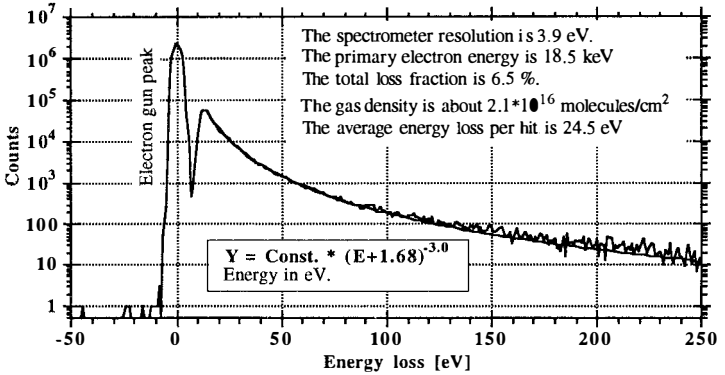

Figure 3 The energy loss spectrum of 18.5 keV electrons in molecular hydrogen.

Tritium end point data and results

We determine the mass of the electron anti-neutrino by measuring the tritium spectrum in the energy range 17.55 to 18.80 keV in steps of 2.25 eV. In order to give the same statistical accuracy to each point we measure longer times for energies close to the endpoint. Also for each run we randomized the order in which these data points were taken. This makes us insensitive to any repeating trend in the source density.

For these data we set the spectrometer to analyze an electron energy of 23 keV with a resolution of about 18 eV FWHM. The density of the source gas at the injection point was about 2 mtorr, at this pressure about 80% of all electrons leave the source without any scattering. In 4 (still preliminary) runs we collected about 15000 counts in the last 100 eV of the spectrum on a background of about 4 counts/eV.

We fit the data to the function produced by folding our system resolution including energy loss with the expression given by

$$P(E) = A[1+\alpha_1(E_{mag}-E)]F(E,Z)pE\sum_i w_i(E_0-E)\sqrt{(E_{01}-E)^2-m_\nu^2}+B \qquad (1)$$

where α_1 describes the linear dependence of the efficiency as a function of the acceleration voltage (E_{mag} is the analyzing energy of the spectrometer), B is a constant background and A is a normalization constant. The summation runs over each of the final states with endpoint energies E_{0i} and population w_i as calculated in reference 13. The term F(E,Z) is the Fermi function which accounts for the effects of the nuclear coulomb field on the beta decay electron. A detailed analysis of this correction has recently been presented by Wilkinson[14] he shows that for the end point region of tritium the Fermi function is given by

$$F(E,Z) = 2\pi y(1 - e^{-2\pi y})^{-1}(1.002037 - 0.001427\beta) \qquad (2)$$

where $y = \alpha Z/\beta$, α is the fine structure constant, Z the atomic number of the daughter nucleus, and β is the electron velocity in units of the speed of light. In fitting the data we vary the values of A, B, m_ν^2 and the end point energy E_0. We determine α_1 and a possible α_2 by measuring a high statistic long range tritium spectrum from 6 to 18.6 keV. This wide range spectrum is taken at a much reduced tritium pressure to avoid a very high counting deadtime at lower energies. The energy loss fraction is different and therefore these spectra can not be combined with the actual endpoint spectra in an easy way.

The results of the least squares fit of these data are shown in table 1. Our end point energy of 18568.5(20) eV can be related to the mass difference of the neutral ^{3}H-^{3}He. We add 16.5 eV for the molecular and atomic binding energy corrections and 1.6 eV for the recoil. The rotation and vibrational excitation of about 2 eV is part of our final state correction. We obtain 18586.6 (25) for the ^{3}H-^{3}He mass difference in good agreement with the latest mass spectrometry measurements[15] of 18590.1(37).

Table 1. The results for the end point spectrum of molecular tritium.

m_ν^2	-60(36+30) eV^2
Endpoint E_0	18568.5(20) eV
Background	4.0(2) eV^{-1} (typical)
Eff. slope α_1	$1.10(1)\cdot10^{-5}$ eV^{-1}

Our data for the end point region of the tritium decay is shown in figure 4 in the form of a Kurie plot where the solid curve represents the best fit to the data. Our data show no evidence for a 30 eV mass for the electron antineutrino, rather it is ruled out by 15 standard deviations. Our best value for m_ν^2 is negative like the other recent results. However at the level of our statistics the result is still consistent with zero within the 2σ confidence range.

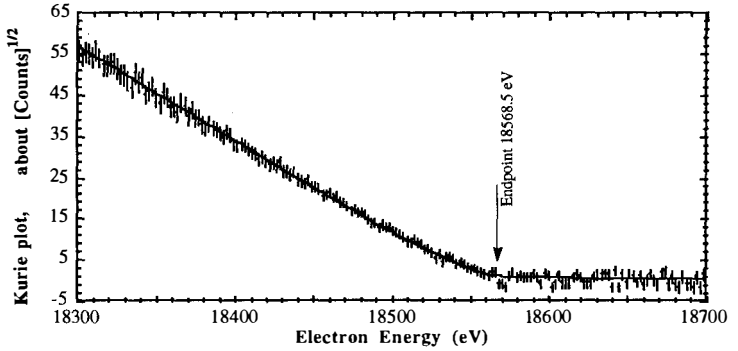

Figure 4. The end point spectrum of molecular tritium for one of the 4 runs. The solid curve is the best fit to the data.

We extract an upper limit for the electron antineutrino mass by fitting our data for fixed values of the mass but allowing the other parameters to vary. We then study the behavior of χ^2 as a function of m_ν^2 and determine how well our data confine the neutrino mass. We study our systematic errors by making small changes in the resolution function, energy loss, and final states to test how sensitive our system is to small changes in these parameters. We also try different error estimation such as maximum likelihood or a modified χ^2 as used by the Los Alamos group. The small difference between the various fit methods is reflected by a 20 eV^2 systematic error. Our present result is an upper limit of 8.0 eV for the mass of the electron antineutrino at the 95% confidence level. The contributions of the various systematic errors are listed in table 2.

Table 2. The contribution to the uncertainty in the mass limit for various parameters of our experiment.

Parameter	Error $(eV)^2$
Statistics	36
Resolution	5
Energy loss shape	4
Energy Loss Amplitude	12
Efficiency (α_1)	6
Recoil Correction	8
Radiative Corrections	10
Final States	10
Fit Method	20

Discussion

A negative value for m_ν^2 has no physical meaning, it is only an indication from the fit analysis that there are too many counts near the end point. This might arise from a systematic error in the measurement such as the presence of an unknown background or a large mistake in the final state corrections. We can point out that a large mistake in the final state calculations is unlikely. If one modifies the final states enough to bring the best fit of m_ν^2 to zero, the end point would shift by 6 eV. The negative value for m_ν^2 might also indicate that there is some additional physics that we must incorporate in our understanding of beta decay. Our negative result is within 2σ of zero so it does not, in itself, warrant the introduction of new physics for beta decay. But it is puzzling to have the same effect in all neutrino mass experiments performed in the last 10 years. It is interesting to note that these tritium beta decay experiments are the first studies of neutrinos at extremely low energies. The physics of these very low energy neutrinos is inaccessible to the techniques of high energy physics and has been largely overlooked by theoretical studies. For the moment, we are aggressively searching for and eliminating any possible flaw in our experimental setup and the data analysis.

Acknowledgments:

This work was performed by LLNL under the auspices of the U. S. Department of Energy under contract No. W-7405-Eng-48.

References

1. S. Boris, A. Golutvin, L. Laptin, V. Lubimov, V. Nagovizin, V. Nozik, E. Novikov, V. Soloshenko, I. Tihomirov, E. Tretjakov and N. Myasoedov, *Phys Rev. Lett.* **58** (1987) 2019.
2. H. Kawakami, S. Kato, T. Ohshima, S. Shibata, K. Ukai, N. Morikawa, N. Bogawa, K. Haga, T. Nagafuchi, M. Shigeta, Y. Fukushima and T. Taniguchi *Phys. Lett.* **256B** (1991) 105.
3. M. Fritschi, E. Holzschuh, and W. Kuendig, *Phys. Lett*. **287B** (1992) 381.
4. R. G. H. Robertson, T. J. Bowles, G. J. Stephenson, D. L. Wark, J.F. Wilkerson, and D. A. Knapp, *Phys. Rev. Lett.* **67** (1991) 957.
5. Ch. Weinheimer, M. Przyrembel, H. Backe, H. Barth, J. Bonn, B. Degen, Th. Edling, H. Fischer, L.Fleischmann, J.U.Grooß, R. Haid, A. Hermanni, G. Kube, P. Leiderer, Th. Loecken, A. Molz, R.B.Moore, A. Osipowicz, E.W. Otten, A. Picard, M. Schrader and M. Steininger, *Phys. Lett.* **300B** (1993) 210.
6. D. J. Decman and W. Stoeffl, *Phys. Rev. Lett.* **64** (1990) 2767.
7. M. H. Chen, B. Crasemann and H. Mark, *Phys. Rev.* **A21** (1980) 436.
8. M. Breinig, *Phys. Rev.* **A22** (1980) 520
9. M.O. Krause, *Phys. Rev* **A140** (1965) 1845
10. J.A.Bearden, A.F.Burr, *Rev. Mod. Phys.* **44** (1972) 716
11. J. C. Levin, S. L. Sorensen, B. Crasemann, M. H. Chen, G. S. Brown, *Phys. Rev.* **A33** (1986) 968.
12. S. T. Staggs, R. G. H. Robertson, D. L. Wark, P.P. Nguyen, J. F. Wilkerson and T. J. Bowles, *Phys. Rev.* **C39** (1989) 1503.
13. O. Fackler, B. Jeziorski, W. Kolos, H. J. Monkhorst, and K. Szalewicz, *Phys. Rev. Lett.* **55** (1985) 13.
14. D. H. Wilkinson, *Nucl. Phys.* **A526** (1991) 131.
15. R. S. VanDyck, D. L. Farnham and P. B. Schwinberg, *Journal of Modern Optics*, **39** (1992) 243.

RECENT DEVELOPMENTS IN METASTABLE SUPERCONDUCTING DETECTORS & POSSIBILITIES FOR NEUTRINO MASS SEARCHES

TA Girard
Centro de Fisica Nuclear / Instituto de Fisica e Matematica
Universidade de Lisboa, 1699 Lisboa Portugal

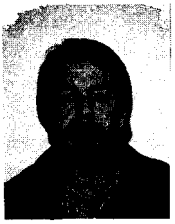

ABSTRACT

We report a preliminary measurement of the beta decay of ^{35}S using a metastable superconducting granular detector. Analyses suggests that, contrary to conventional wisdoms, such measurements may be performed with relatively large grain sizes and size distributions. The consequences for the possibility of several new experiments to search for light neutrino mass in single and double beta decay are considered. These are predicated on observation of structure in the energy loss spectrum of the device, rather than the particle spectra themselves, and depend critically on good knowledge of the detector response.

Detectors based on the radiation-induced phase transitions of superheated Type I superconducting microgranules have been proposed for a variety of new researches[1]. The response of such detectors to β irradiation has been investigated by several groups[2], but have focused on only their sensitivity. Until recently, no precise connection between the results and their origin has existed, and conventional wisdoms of smallest grain size and most uniform size distribution have generated a diminished interest in their pursuit.

The essential principles of their operation have been described previously[3]. For a single grain in a superheated state of temperature and applied magnetic field (T_a,H_a), transitions to the normal state can be induced by increase in either local field or temperature sufficient to move it across the superconductor-normal phase boundary. Thermal transitions can also be induced by the interaction of radiation with the grain, if the energy deposited (ΔE) in the grain is such that

$$\Delta E \geq C_p \Delta T(T_a,H_a), \qquad (1)$$

where ΔT is the temperature distance to the phase boundary, and C_p is the volume heat capacity of the grain. The signal is provided by the accompanying magnetic flux change occuring during the transition as a result of loss of the Meissner effect.

An ensemble of grains requires dilute suspension in a dielectric in order to maintain metastability. Although the simple picture above becomes more complicated owing to the distribution of the local fields resulting from the intrinsic variation in the grains themselves, the basic physics remains unchanged. In this case however, incident radiation interacts with the non-signal producing dielectric as well as the superconducting material.

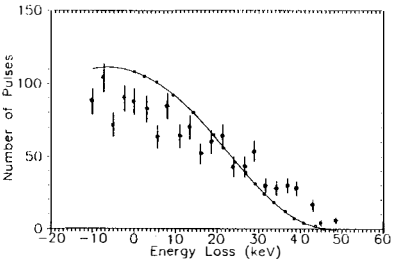

Fig. 1: Comparison of typical results obtained following the "wait" period of real-time tests at 2.3 K (•) and computer simulation (-).

In Fig. 1 we present a recent irradiation result, performed at 2.3 K over a period of 3.4 s. The detector consisted of 10^4 grains, suspended in paraffin to a volume filling factor of 20%, and spaced along a U-shaped copper wire loop, of 225 micron width. The suspension was covered with 1.1 μCi ^{35}S, evaporated onto tissue paper. The grains varied in diameter from 10-25 micron, and were part of a sample made by sonic dispersion of the metal in an oil bath, size filtration and uniform folding[4] into the dielectric.

Fig. 1 also includes a simple, single 17 micron Sn grain diameter simulation of the energy loss spectrum of ^{35}S beta decay as would be measured in accordance with our protocol, based on a recently-developed "hot border" model[5] shown schematically in

Fig. 2. At fixed temperature, the distribution of the maximum of local fields at the equator of each of the grains is represented by the horizontal line xy; at a given H_a, some fraction of the ensemble is normal; each of the remainder sees a different maximum local field (H_l), resulting in a distribution of ΔT required for transitions.

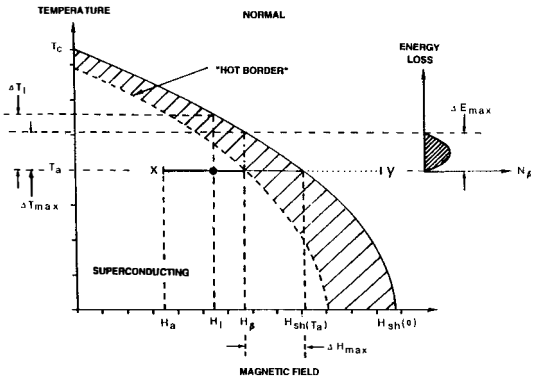

Fig. 2: Effective phase diagram of a grains suspension.

The generic energy loss spectrum in Fig. 2 is fixed at the superheating boundary. Its lowest energy part is only able to induce transitions of those grains for which $H_l \approx H_{sh}(T_a)$; in contrast, the highest loss (ΔE_{max}) is able to transition all grains within the region $\Delta H_{max} = H_{sh}(T_a) - H\beta$, possessing a $\Delta T \leq \Delta T_{max} = C_s^{-1} \Delta E_{max}$. For sufficiently long irradiation times or intense radiation fields, all of the grains in this zone will become normal, thus creating an effective phase boundary, or "hot border", at $H\beta$ which is determined by the maximum energy loss of the beta distribution.

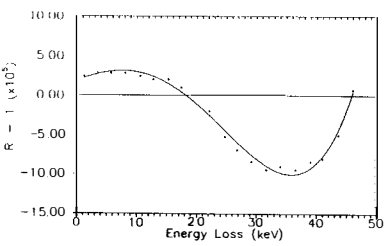

Fig. 3: Ratio of simulated energy loss spectra of ^{35}S decay, with and without a 1% admixture of a 17 keV neutrino, as would be measured in our protocol. R ≡ N(no 17 keV)/N(yes 17 keV).

Increase of H_a by $\delta H << \Delta H_{max}$ similarly increases the local fields of all grains still superconducting, in effect shifting xy to the right across the hot border by δH so that grains in the region $H\beta - \delta H$ enter the active zone. These can however transition to the normal state only as a result of temperature changes induced by the corresponding higher portion of the energy loss distribution, at a rate dependent upon the radiation flux and interaction crossection. Stepping δH across ΔH_{max} is thus equivalent to

piece-wise integration over the loss distribution itself. The results in Fig. 1 obtain from a continuous field ramping of the magnetic field following a 3 s wait period in the irradiation at a midfield value of the superheating curve. The "negative energy" values result from a fixing of the first measurement to the maximum energy loss of the simulation; they are artificial in the sense that the simulation does not include electron straggling in the grain which would lead to greater energy loss.

In Fig. 3 we show the ratio of two simulations of the energy loss spectrum, with and without a 1% mixing of a 17 keV neutrino, as would be observed in our operation of the detector. A 7-fold increase in the detector size and optimization of its operating parameters would require 15 days to statistically achieve the 5×10^{-5} level of sensitivity indicated.

With the 17 keV neutrino demise[6], the question arises as to whether this same detection technique is applicable to the more conventional near-endpoint light mass neutrino searches in beta decay. As shown in Fig. 4, for incident energies below about 0.2 MeV, the electrons are absorbed in the grain, the diameter of which defines the width of the energy loss distribution. For energies above 0.5 MeV, the energy loss decreases to an essentially constant value near 19 keV, increasing by only 1 keV as E_0 rises to 3 MeV. Thus, for decays of $E_0 \geq 1$ MeV, near-endpoint artifacts will occur in the high statistics part of the energy loss spectrum.

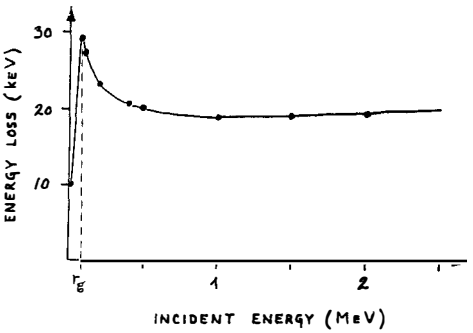

Fig. 4: Energy loss of incident electron energies in a 25 micron Sn grain, via Bethe-Bloch with linear trajectories only.

For electron energies between E_0 and E_0-10 eV, the difference in energy loss $\leq$ 1 eV. Sub-eV resolutions are not however unlikely with such detectors. For the results of Fig. 1, the 0.29 G step size corresponds to 2.3 keV; all else unchanged, this would equal 23 eV at T_a = 0.8 K owing simply to the decrease in the specific heat. In principle, another 1-2 orders of magnitude reduction is achievable by use of a magnetic controller accurate to 10^{-3} G. In this event, the decay of ^{187}Re may be of considerable

interest owing to its 2.5 keV endpoint and superconductivity below 1.6 K.

This resolution requirement is equally true in searching for neutrinoless double beta decay. In this case, a number of theoretical investigations have previously been performed[7]. The basic premise in these was however that the grains should be as small and as uniform as possible, which our current interpretation appears to contradict; this study is now being re-examined for large grain sizes[8].

In either case, counting systematics are reducible via pulse analyses, and the potential spatial resolution of such devices may provide an additional method of background discrimination. The difficulty of either experiment is that it is fundamentally a rare event search. Detector masses of 1 ton or larger are indicated, requiring new developments in cryogenic engineering and instrumentation. Attention to the radioactive backgrounds associated with the detector construction material is required.

In summary, irradiation of a suspension of superheated superconducting grains yields results in contradiction to conventional wisdoms and suggest the possibility of achieving sub-eV resolution in the associated energy loss spectra. These results, cursorily applied to precision searches for light mass neutrino artifacts in single and double beta decay, provide renewed motivation for their further investigation. Such searches are predicated on observation of structure in the energy loss spectrum of the device, rather than the particle spectra themselves, and depend critically on good knowledge of the detector response. The questions of experimental feasibility, such as detector mass requirements, sensitivites and time required to reach them, and systematics associated with both the source and detector operation, are under renewed investigation.

I thank the members of my collaboration - G. Waysand, JI Collar, RP Henriques, D. Limagne, M. Godinho, G. Bonfait, V. Jeudy, O. Heres and V. Pagesy - for the efforts which made this report possible.

References

1. L. Gonzales-Mestres and D. Perret-Gallix, in Low Temperature Detectors for Neutrinos and Dark Matter, ed. K. Pretzl, N. Schmitz and L. Stodolsky (Springer-Verlag, Berlin, 1987), p. 9. and references therein.
2. H. Bernas et al, Phys. Lett. A24 (1967) 721; J Blot et al, J. Appl. Phys. 45 (1974) 1429; A. de Bellefon et al, in Low Temperature Detectors for Neutrinos and Dark Matter-II, ed. L Gonzales-Mestres and D Perret-Gallix (Ed. Frontieres, Gif-sur-Yvette, 1988) p. 425.
3. see for example, BG Turrell et al, Nucl. Instr. & Meth. A289 (1990) 512 and references therein.
4. V. Jeudy, D. Limagne and G. Waysand, Nucl. Phys. B (Proc. Suppl) 28A (1992) 482.
5. TA Girard et al, submitted to Europhys. Lett.
6. H. Kawakami et al, Phys. Lett. B287 (1992) 45; JL Mortara et al, Phys. Rev. Lett. 70 (1993) 394.
7. A Pacheco, Mod. Phys. Lett 1 (1986) 167; A. Larrea and A. Morales, Il Nuov. Cim. 105A (1992) 535.
8. A. Morales, private communication.

THE EFFECT OF A SCALAR BOSON COUPLED TO NEUTRINOS ON THE BEHAVIOR OF THE TRITIUM BETA DECAY SPECTRUM NEAR THE END POINT

G. J. Stephenson, Jr.
Physics Division, Los Alamos National Laboratory
Los Alamos, New Mexico 87545 USA

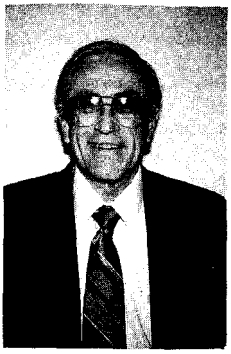

ABSTRACT

Some consequences of a very light scalar boson coupled only to neutrinos are discussed. In particular, I argue that it is possible to sketch scenarios for the evolution of the Universe in which neutrinos cluster to a local density $\approx 10^{16}/cc$, that such clusters would be attracted to matter gravitationally, and that the existence of such a neutrino density in the solar system provides an alternative to $m_{\bar{\nu}_e}^2 < 0$ in fitting tritium beta decay.

The question of neutrino masses, whether they are non-zero and, if so, what their values are, is a major open question in Electro-weak physics. In this conference we are hearing about experiments which study the end point of the beta ray spectrum of ^3H to extract information about $m_{\bar{\nu}_e}$. The actual quantity extracted in the usual analysis is m^2 and modern experiments,[1-5] while differing in experimental techniques, all report a best value of $m_\nu^2 < 0$, roughly by one to two standard deviations. Assuming that the result is not due to some shared systematic, like an error in the molecular final states, and setting aside the possibility that the free neutrino does have a space-like propagator,[6] what could this result mean?

The major assumption in the fitting is that the only difference from the standard, $m_\nu = 0$, description is in the evaluation of the neutrino momentum, $P_\nu = \sqrt{(E_o - E_\beta)^2 - m_\nu^2}$, where E_o is the energy available to the leptons and E_β is the electron energy. This corresponds to multiplying the usual spectrum (dn/dE_β) by $\left[1 - m_\nu^2/(E_o - E_\beta)^2\right]^{1/2}$. This is shown in Figure 1 with the spectrum displayed on 1a and the Kurie plot on 1b with the simplification of only one final state. Solid lines represent $m_\nu = 0$, dashed lines show the effect of a non-zero mass. The vertical bars show the effect of some mechanism that gives added counts near, but below, the end point. Should that be the case, forcing a fit with the standard formula will result in a best value of $m_\nu^2 < 0$. In presenting the Los Alamos result[5], we remarked on this effect and noted that we could obtain a statistically equivalent fit by setting $m_\nu^2 = 0$ and adding a spike of counts at the endpoint. The best fit correspondents to a branching ratio of 10^{-9} or a partial life-time of 10^{10} years.

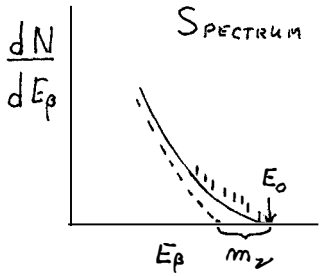

Fig. 1a Spectrum

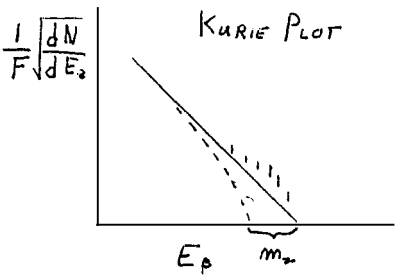

Fig. 1b Kurie Plot

A spike of some height is expected in standard model cosmology through the absorption of relic neutrinos, expected at a density of $\approx 50/cc$ for every flavor, through the mechanism of the usual Weak Interaction, in analogy with K-capture. This rate can be calculated[7] and, for $50/cc$, gives a partial life time of 10^{24} years. Therefore the data would require an increase in the density of relic neutrinos in the vicinity of the earth by some 14 orders of magnitude, which may not be as outrageous as it sounds.

Terry Goldman and I have been investigating the consequences of a light scalar boson which couples to neutrinos but no other light fermion.[8] While scalars coupled to neutrinos may arise in particular gauge theories, we have chosen to view this question phenomenologically, unhindered by other couplings such theories may require. We have concentrated on a scalar rather than a vector for several reasons. First, to avoid anomalies, in particular the coupling to one Z^0 and two new bosons, which cannot be cancelled in the neutrino sector alone. Second, to provide an attractive force between all neutrino species with no shielding. Third, to avoid serious conflict with primordial nucleosynthesis and supernova dynamics. Kolb, Turner, & Walker[9] have shown that this case is equivalent to 1/2 extra family of neutrino for nucleosynthesis, which is tolerable. For the previous statement to hold, there must be two states per light neutrino, i.e. the neutrino must be Majorana, and, hence, the chirality flip induced by the scalar does not produce sterile neutrinos within a supernova. In spite of the fact that, for Majorana neutrinos, there is no sense to the distinction neutrino and anti-neutrino, I shall use the former to denote the left handed state and the latter for the right handed state to facilitate comparisons with other work.

We write $\mathcal{L}_I = ig^{\frac{1}{2}}\overline{\psi}_\nu\psi_\nu\phi = ig(\overline{\psi}_L\psi_R + \overline{\psi}_R\psi_L)\phi$, where R and L refer to chiral projections and ϕ is a scalar field with mass m_ϕ. The region of parameter space of interest (for reasons given below) has m_{ν_e} of several eV and $m_\phi << m_{\nu_e}$. Then for $s - 4m_\nu^2 << m_\nu^2$, the total scattering cross section $\sigma^T \sim \tilde{\alpha}^2/m_\phi^2$, where $\tilde{\alpha} = g^2/4\pi$. For s large compared to m_ν^2, $\sigma^T \sim \tilde{\alpha}^2/s$, hence it is possible to arrange $\tilde{\alpha}$ and m_ϕ so that high energy neutrinos are not affected and low energy neutrinos undergo significant scattering. If $m_\phi << m_\nu$, two Majorana neutrinos will annihilate into two $\phi's$ with a rate given by $\omega = \frac{\pi}{16}\frac{\alpha^2}{m_\nu^2}\rho c$. To sustain a

density of $10^{16}\ v/cc$ now requires that the associated rate be less than $10^{-18}/s$, or $\tilde{\alpha}^2 < 4x10^{-35}\left(m_\nu(eV)\right)^2$. More detailed arguments are presented in ref (8).

Two other processes which can place limits on $\tilde{\alpha}$ directly are the Bremsstrahlung of $\phi's$ during a normal weak transition and the emission of a scalar in place of two neutrinos in nuclear double beta decay. Both processes have been studied. Barger, Keung and Pakvasa[11] use $K \to \ell 2$ decays and Bernatowicz et al[12] compare the deduced $\beta\beta$-decay rates for $^{128,130}Te$. The limits, $\tilde{\alpha}<10^{-6}$, are well satisfied by the parameter set under discussion.

The general many-body problem of relativistic fermions interacting through a attractive scalar exchange and a repulsive vector exchange (provided here by Z^o exchange, although the contribution to this problem is not significant) has been studied as a model of nuclear physics known as OHD[10]. While the parameters for that study are vastly different from the present case, all the necessary formulas are worked out to treat this problem of a self-bound gas of neutrinos. In particular, the effective mass is proportional to $\tilde{\alpha}/m_\phi^2$, so the potential can be scaled independently of the scattering cross-section. However, the scalar potential is scaled by m^*/e^*,[13] where the * refers to effective quantities in the medium, which leads to a transcendental equation for m* (see eq. 3.55, ref. 10),

$$m^* = m - \frac{g^2}{m_\phi^2(2\pi)^3} \int_o^{k_F} d^3k \, \frac{m^*}{\left(k^2 + m^{*2}\right)^{1/2}}.$$

Examination of this equation shows that there is a minimum value of $m^* > 0$, which indicates that the average binding can't exceed m. For ρ of $10^{16}/cc$, $k_F = 16.8\ eV/c$, so the picture would appear to be in trouble for $m_{\nu_e} \sim$ several eV.

There are, however, at least two distinct neutrinos and, most probably, three. Arguments using limits on the amount of dark matter would say that the sum of the three masses must be less than about 100 eV. The inclusion of the other two species, with at least one mass well in excess of 20 eV, circumvents the problem and makes it possible to sustain such a gas.

The evolutionary scenario is then something like this: between e^+e^- annihilation at about 1 MeV and recombination at about 20 eV, the neutrinos, as usual, expand with

$T_\nu = (4/11)^{1/3} T_\gamma$, internally thermalized by ϕ exchange and maintaining contact with the baryons only through gravity. As the Universe approaches the recombination epoch, some neutrinos begin to get cold (i.e., m>kT). On the one hand, given the relatively (to gravity) strong, finite range attraction, those neutrinos will tend to cluster, but, on the other hand, they are still coupled to hot, lighter neutrinos. Shortly after recombination, all the neutrinos are cold, the baryons are decoupled from the photons, so are very cold, and everything is coupled by gravity.

While this system may be rich enough to produce several scales, the most collective mode will be one in which all species condense together, hence, in general, the neutrinos will follow the matter (or vice versa). For a large fraction of the structures in the Universe, neutrinos should cluster where matter clusters. Whether this argument holds on solar system scales is an open question, but the existence of neutrinos clustered about the sun is a possibility. While the density increase from 50 to 10^{16} is nowhere near as large as that for baryons, space is still mainly devoid of neutrinos, allowing the propagation of neutrino signals from extra-Galactic sources. Note that $10^{16}/cc$ corresponds to the primordial density at a temperature of about 10eV; so as long as ϕ-exchange can sustain such a density, or a higher density, the uniform expansion of the early Universe will drive the density down to a value near this.

While these arguments do not prove the existence of neutrinos at a density about $10^{16}/cc$ around the earth, they do provide enough plausibility to examine further the effect on the endpoint of the ^3H beta spectrum. (Should they extend out to the earth's orbit? If neutrinos track the baryons exactly, so $m_\nu = 10^9 m_B$, the neutrino sphere would have a radius of about 0.033 ℓt. yr.) The existence of a Fermi momentum $k_F = 16.8\ eV/c$, and a corresponding $E_F > 16.8\ eV$ means that the previous analysis, done by putting a spike at the endpoint, is inadequate. Robertson, Wilkerson, Knapp and I have revisited that analysis to include the effects of the Fermi distribution,[14] and I shall report here on results using a subset of the data reported in ref. 5, one which gives a very similar $\langle m_\nu^2 \rangle$ to the full set.

Previous discussions[15] of the effect of a filled Fermi sea of neutrinos and anti-neutrinos have been based on the usual assumptions of cosmology and of the Weak Interaction,

a consequence of which is that the neutrinos and anti-neutrinos form completely non-interacting gases and that the particles obey the free dispersion relation. In contrast, the current picture has the neutrinos and anti-neutrinos occupying relatively isolated wells, with the Fermi distribution coming just to the top of the well. None of the other players in the process, the ^3He, ^3H and electron, feel this well, so all of their variables are set by the conditions in a region of space where there is no neutrino background. A cartoon of this description is shown in Figure 2.

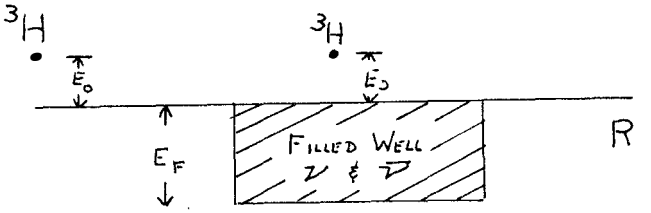

Fig. 2 Cartoon Showing Beta Decay With Neutrino Clusters

The effect of the usual argument is shown, again for only one final state and $m_\nu = 0$ in a Kurie plot on Figure 3a. The filled anti-neutrino sea blocks the emission of $\overline{\nu}'s$ with energy less than $E_F = \sqrt{k_F^2 + m_\nu^2}$, so the beta spectrum is cut off abruptly at $E_0 - E_F$. Neutrinos can be absorbed from the sea giving energies between 0 and E_F to the beta which gains the full E_o from the hadronic system, so there is a non-zero counting rate for $E_o \le E_\beta \le E_0 + E_F$. A non-zero m_ν would not change the spectrum below E_o, but the additional counts would come for $E_o + m_\nu \le E_\beta \le E_o + E_F$.

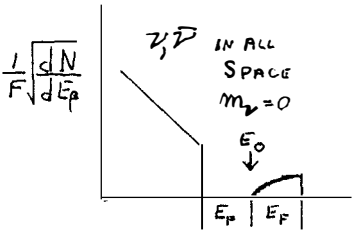

Fig. 3a Kurie Plot, No Clustering

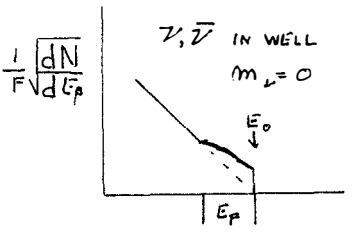

Fig. 3b Kurie Plot With Clustering

However, as I have shown above, that is not a consistent picture if $\rho > 50$, particularly 14 orders of magnitude greater. If the ^3T decays in a region of space where there is no neutrino background, the standard analysis will apply. If, however, the neutrino background is present, the analysis changes, but not as described in the previous paragraph. This is shown in Fig. 3b.

The anti-neutrino emission is not affected. The state into which the anti-neutrino is created has positive energy, is above the top of the well and is orthogonal to all the filled states, hence there is no Pauli suppression. Since, for the case at hand, the emission is s-wave, the change in k multiplied by the nuclear radius does not change j_o, therefore does not change the matrix element. In short, there is no modification.

The neutrinos will be absorbed and will provide extra counts, but, in the main, below E_o. Consider first $m_\nu = 0$ and a neutrino from the bottom of the well. To make that absorption go, E_F must go into the neutrino, so the contribution is at $E_o - E_F$. Since a neutrino at the top of the sea requires no additional energy, it will contribute at $E_\beta = E_0$. Therefore, the neutrino sea will contribute an essentially constant amount to the region $E_0 - E_F \le E_\beta \le E_o$. For fixed E_F, the existence of a neutrino mass, m_ν, will simply shift the interval upwards by m_ν, i. e. extra counts in $E_o - E_F + m_\nu < E_\beta < E_o + m_\nu$.

TABLE 1

$m_\nu^2(eV^2)$	N bins	E(ev)	ρ(#/cc)	Ξ^2
0	"spike"	0	$6x10^{15}$	547.1
0	4	9	$7.2x10^{15}$	547.6
0	6	15	$8.0x10^{15}$	547.2*
0	8	21	$8.6x10^{15}$	547.2
0	12	33	$9.2x10^{15}$	547.5
0	91	60	$14.2x10^{15}$	547.6
5	6	15	$8.2x10^{15}$	546.3
25	6	15	$9.0x10^{15}$	546.3
100	6	15	$11.8x10^{15}$	546.4
0	no relic absorption			549.4
-138.8	no relic absorption			547.2

To implement a fitting procedure, we wish to remain compatible with our earlier work[5], where the data are summed into fixed energy width bins. Therefore we fit to a amplitude distributed over a fixed number of bins, which corresponds to varying the density and the Fermi energy separately. This is done holding m^2 fixed at some value. The results are shown in Table 1. N is the number of bins affected and E is the total width of the added segment. This should correspond to the E_F appropriate to the density of relic neutrinos.

The * indicates the case where that energy and the fit density most nearly match, since $\rho = 8x10^{15}/cc$ implies $k_F = 15.4\ eV/c$. Ξ^2 is the measure of the fit, similar to χ^2, for a discussion, see ref. 16. The first line is the original spike. For comparison, the last two lines show cases where there is no relic neutrino absorption. $m_\nu^2 = 0$ is a forced fit, $m_\nu^2 = -138.8(eV)^2$ is the best fit with the simple function described at the beginning of the paper. For the forced fit there are 553 degrees of freedom, for all other cases there are 552 degrees of freedom.

These results, while preliminary, show certain features which we expect to persist. First, smearing the counts over a Fermi distribution does not destroy the general agreement with the data. Second, one can move the mass, energy width and density around in compensating ways, so there is not a clear preference from Ξ^2. However, ρ uniquely specifies $k_F = \sqrt{E_F^2 - m_\nu^2}$, and not all solutions satisfy this condition, so the result is more robust than is at first apparent.

I have presented a possible scenario for obtaining a high density of neutrinos and shown that such a picture can provide a fit to a subset of the Los Alamos tritium beta decay data. There does not appear to be any show stopper. There are many details to be filled in and the fit needs to be made to the full data set, but this appears to be a viable explanation of the data.

In addition to my colleagues named above, I want to thank the School of Physics, University of Melbourne, for its hospitality while this was being written, Bruce McKellar, Mark Thompson, Bill Spence and John Costella for illuminating conversations, and Prof.'s V. Lobashev and J. Bonn for long discussions during the workshop. This work was supported by the U. S. Department of Energy.

REFERENCES

1) Ch. Weinheimer, M. Przyrembel, H. Backe, H. Barth, J. Bonn, B. Degen, Th. Edling, H. Fischer, L. Fleischmann, J. U. Grooss, R. Haid, A. Hermanni, G. Kube, P. Leiderer, Th. Loeken, A. Molz, R. B. Moore, A. Osipowicz, E. W. Otten, A. Ricard, M. Schrader, and M. Steininger, Phys. Lett B300, 210 (1993).
2) E. Holzschuh, M. Fritschi, and W. Kundig, Phys Lett B287, 381 (1992).
3) H. Kawami, S. Kato, T. Ohshima, S. Shibata, K. Ukai, N. Morikawa, N. Nogowa, K. Haga, T. Nagafuchi, M. Shigeta, Y. Fukushima and T. Taniguchi, Phys Lett B256, 105 (1991).
4) W. Stoeffl, Bull. Am. Phys. Soc. Ser II 37, 1286 (1992).
5) R. G. H. Robertson, T. J. Bowles, G. J. Stephenson, Jr., D. L. Wark, J. F. Wilkerson and D. A. Knapp, Phys Rev Lett 67, 957 (1991).
6) Alan Chodos, V. Alan Kostelecky, Robertus Potting and Evalyn Gater, Mod Phys Lett A7, 467 (1992).
7) Ralph A. Alpher, James W. Follin, Jr. and Robert C. Herman, Phys. Rev 92, 1347 (1953).
8) G. J. Stephenson, Jr. and T. Goldman, in preparation; G. J. Stephenson, Jr., LA-UR-92 (Abstract).
9) Edward W. Kolb, Michael S. Turner and Terrence P. Walker, Phys Rev D34, 2197 (1986).
10) Brian D. Serot and John Dirk Walecka in Advances in Nuclear Physics (J. W. Negele and Erich Vogt, eds.), Vol 16, page 1 (Plenuim Press, New York, 1986).
11) V. Barger, W. Y. Keung and S. Pakvasa, Phys Rev D25, 907 (1982).
12) T. Bernatowicz, J. Brannon, R. Brazzle, R. Cowsik, C. Hohenberg and F. Podsek, Phys Rev Lett 69, 2341 (1992).
13) K. I. Macrae and R. J. Riegert, Nucl Phys B244, 513 (1984); this effect is discussed and incuded in ref. 10.
14) R. G. H. Robertson, G. J. Stephenson, Jr., J. F. Wilkerson and D. A. Knapp, in prep.
15) Karl-Erik Bergkvist, Nucl Phys B39, 317 (1972).
16) David A. Knapp (thesis), LA-10877T (Los Alamos, NM 1986).

COSMOLOGY AND NEUTRINO MASSES

Lawrence KRAUSS
Center for Theoretical Physics and Dept. of Astronomy
Sloane Physics Lab., 217 Prospect St.
Yale University
New Haven, CT 06511 U.S.A.

ABSTRACT

I provide a brief overview of recent developments related to massive neutrinos, from GeV to eV scales which are relevant to cosmology, concentrating on probes for cosmologically interesting neutrino masses, and the reasons for supposing such masses might exist including a discussion of recent COBE data.

1. Introduction

The organizers of this meeting did me the courtesy of announcing my talk without providing me a title to restrict my range. In response to this courtesy I have decided to discuss a menagerie of topics, all losely related to the cosmological implications of neutrino masses.[1] The confirmation that any neutrino has a non-zero mass would be the most important result for particle physics in several decades, because it would provide the first evidence of physics beyond the standard model. For this reason, substantial effort has been devoted in the last few years to terrestrial experimental explorations of this possibility. However, because the implications of a non-zero neutrino mass would be most dramatic for astrophysics and cosmology, it is not surprising that the most sensitive probes of such a possibility derive from research in these areas. New results have been obtained in the last few years which are relevant to neutrinos with masses ranging from TeV scales to sub-eV scales. The bottom line is that neutrinos with masses in most of this range are ruled out. At the same time, there is indirect "evidence", on several fronts, which supports the possibility of a tau neutrino mass in the eV range. This would result in a cosmologically significant mass density of tau neutrinos today.

2. Cosmological constraints and Astrophysical Evidence:

(a) GeV neutrinos:

With the recognition that the number density of GeV-scale neutrinos will automatically evolve in the early universe so that they could have a closure density today, neutrinos became the prototypical Weakly Interacting Massive Particle (WIMP) candidates for dark matter. The arguments which lead to this conclusion are straightforward. The number density of massless or light neutrinos is about 1/10 of that of photons in the microwave background today. This photon background, with a mean energy per particle of about 10^{-4} eV, contributes about 10^{-4} of closure density density. Thus, for neutrinos to close the universe today, one must have:

$$\frac{n_\nu}{n_\gamma}\frac{m_\nu}{10^{-4}\,eV} \approx 10^4 \qquad (1)$$

It is this result which suggests that light neutrinos with mass around 10-100 eV might close the universe. The relic number density of heavy neutrinos can be smaller than that due to light neutrinos because if their interactions are in thermal equilibrium when the temperature of the universe falls below their mass, annihilations of neutrinos and antineutrinos will lower their number density compared to that of photons by a Boltzmann suppression factor. This process will continue until the neutrino interactions fall out of equilibrium. Thus, one finds:

$$\exp\left(-\frac{m_\nu}{T_{freeze\text{-}out}}\right)\frac{m_\nu}{10^{-4}\,eV} \approx 10^4 \qquad (2)$$

For heavy weakly interacting particles such as neutrinos one finds that $m_\nu/T_{freezeout} \approx 20$, so that GeV scale neutrinos will have a remnant energy density today which can close the universe.

I have only brought up this possibility because it can be ruled out, and it has been. While GeV

[1]Some of these discussions also appear in conference proceedings including Neutrino Astrophysics, Takayama, 1992, La Thuile, 1993, and Workshop on Neutrino Telescopes, Venice, 1993, by this author.

mass neutrinos may be heavy by neutrino standards, they are light compared to the Z mass, and thus the Z can decay into such particles with rates almost identical to the decay rate into massless neutrinos[1]. Since both the tau and muon neutrinos are constrained to have masses much less than a GeV, such a massive neutrino would have to exist in addition to the three known neutrino types. In this case, the limit on the Z width, and thus on the number of light neutrinos constains any new massive neutrino to be heavier than O(45) GeV. At the same time, direct search experiments for WIMP dark matter, which are sensitive to massive neutrinos, rule out masses in excess of about 10 GeV[2]. When these limits are combined with the LEP bound, massive neutrino dark matter is ruled out (at weak scales at least).

(b) MeV neutrinos:

As far as I can tell, there is no real motivation to have MeV-scale neutrino masses, but nevertheless, one can rule them out using astrophysical and cosmological arguments. MeV neutrinos will, if they have not yet decayed, begin to dominate the mass density of the universe when the temperature is of the order of an MeV, around the time of big-bang nucleosynthesis (BBN). For this reason, their existence can alter the predicted light-element abundances and thus spoil the apparent agreement between theory and observation. There are three mechanisms by which this can occur:

(i) matter dominated expansion: If indeed a massive neutrino dominates the energy density at the time of BBN, the expansion rate will be faster than it would be in a standard radiation dominated expansion. This causes the neutron-proton ratio to freeze out at a higher value, resulting in greater eventual ^{4}He production. The primordial mass fraction of this element is limited to be less than about 24%, giving stringent limits on the expansion of the universe at the time of BBN (for a recent discussion of the claims and uncertainties see [3]) It has recently been claimed that this increased production is unacceptable unless the neutrino mass is greater than O(25) MeV[4].

(ii) spin flip production: Cline and Fuller[5] recently argued that if neutrinos have Dirac masses, then spin flips, which occur with a probability of order (m_ν^2/E^2), will accompany weak interactions and can result in a thermal abundance ance of right handed neutrino states. This will effectively result in more states in the radiation gas at the time of BBN, resulting in a faster expansion rate, with the same effect as described above. It is claimed that for neutrino Dirac masses in the range of greater than O(200) keV this is a problem for BBN,

(iii) Finally, there exists an older limit on MeV-scale neutrinos from BBN [i.e. 6]. As long as these neutrinos are heavier than about 1 MeV, if they mix with lighter neutrinos, as they almost certainly must if they are to decay sufficiently fast to avoid a cosmological over-abundance today, then their dominant decay mechanism would be likely to be the standard weak decay: $\nu_h \to \nu_e e^+e^-$. In this case, the subsequent interactions of the decay electrons and positrons would produce energetic photons which could photofission deuterium unless the neutrino lifetime were shorter than about 1000 seconds (during which the energetic photons would instead pair produce off of the radiation background). This puts a lower limit on the neutrino mixing angles. At the same time direct kinematic searches for heavy neutrino admixtures in various particle decays put upper limits on such mixing angles. One finds in this way that almost all of the region up to the currently allowed upper limit of 35 MeV for the tau neutrino is excluded. Of course, both this limit, and the one given in (i) can be obviated if the neutrino decays quickly due to some new channel not

accessible in the standard model. However, very exotic new physics is required for this to be viable.

(c) KeV neutrinos:

There are many astrophysical bounds on such particles which have been discussed recently, due to the claimed 17 keV neutrino state (i.e. see [10]). However, the best evidence against such admixtures is now the experiments themselves, described at this meeting by Andrew Hyme, which rule out such a possibility conclusively for a wide range of mixing angles and masses.

(d) eV neutrinos:

These discussions bring us finally to the one case for which there is (circumstantial) astrophysical or cosmological evidence in favor of a neutrino mass rather than against it. This evidence comes most recently from two sources:

(i) Solar Neutrino Numerology: After all the dust has settled, the existing four different solar neutrino detection experiments (Homestake, Kamiokande, SAGE and GALLEX) favor a neutrino based solution, with $m_\nu \neq 0$, iff the Homestake Cl experiment is correct. In this case, a comparison of Homestake with Kamiokande suggests that Be neutrinos are being suppressed more than B neutrinos. (i.e. see [7,8]. Astrophysical solutions to the solar neutrino problem tend to do the opposite.

If the neutrino-based solution is the MSW solution, the favored mass range for the mass eigenstate which is mixed with the electron neutrino is $\approx 10^{-2}$-10^{-3} eV. If one assumes that this mass eigenstate is predominantly the muon neutrino, then one can speculate about the mass of the tau neutrino. Assuming the neutrino mass eigenstates follow the behavior of the quark and charged lepton masses, the tau neutrino should be heavier than the muon neutrino. A reasonable a priori guess for its mass comes from the famous "see-saw" mechanism, which assumes the light neutrino masses arise from mass matrix involving a majorana neutrino mass contribution at some scale M_X, and Dirac mass contributions proportional to the Dirac masses of the known particles. In this case the neutrino mass eigenstates are given roughly by:

$$m_{\nu_i} \approx \frac{m^2_{q_i,l_i}}{M_X} \tag{3}$$

Assuming that the masses in the denominator are the quark, rather than the lepton masses, and setting $m_{\nu(\mu)} \approx 10^{-2}$ -10^{-3} eV, then one obtains an estimate $m_{\nu(\tau)} \approx$ 10-100 eV, in precisely the range of cosmological interest for contributing significantly to the mass density of the universe today.

Of course, as can be seen, this line of reason involves many assumptions, any of which could be wrong. First, the solar neutrino data might change. Next, the MSW solution may not be the correct one. Vacuum oscillations, for example, could solve the solar neutrino problem for a muon neutrino mass in the range of 10^{-5} eV, for example [9,10]. Finally, the see-saw estimate, while plausible, need not be correct.

(ii) COBE-phoria: The observation by the COsmic Background Explorer (COBE) satellite of

fluctuations in the Cosmic Microwave Background (CMB) has caused a great deal of excitement in the cosmology community. Not only do the observed fluctuations presumably represent primordial anisotropies in the distribution of mass and radiation which resulted from microphysical processes in the very early universe, but the scales probed by COBE are so large that they may be combined with observations of large-scale structure to provide a large lever-arm which constrains both the primordial power spectrum of fluctuations and the nature of dark matter. This comes about by comparing numerical simulations for the distribution of matter on large scales resulting from the collapse of primordial density fluctuations with a given power spectrum to observations.

COBE seems to confirm in this regard a claimed problem for the standard Cold Dark Matter (CDM) model of structure formation (involving a flat universe and a flat spectrum of adiabatic primordial density perturbations. CDM apparently results in too little power on large scales and too much power on small scales if it is normalized to fit the galaxy-galaxy two-point function on intermediate scales.

One possible resolution of this problem, which has received some attention after COBE, involves what has become known as "mixed" dark matter. In this case, the dark matter is made of ≈30% "Hot" dark matter such as would result from the existence of a O(10) eV neutrino, and 70% Cold dark matter. This results in more power on large-scales and damps the power on small scales somewhat.

As interesting as this is for neutrino cosmologists, it is important to stress that this motivation for a 10 eV neutrino is very soft. First, "mixed" dark matter agrees better with direct extrapolations of the existing data precisely because it allows another free parameter. It is not clear therefore, that this model is "statistically" any better. Next, it is not clear that the claimed disagreement with CDM cosmology is real. First, the comparison of numerical predictions of the distribution of structure on small scales with observations involves numerical simulations which are still quite crude, in the sense that the calculations involve only dark matter particles, and one must associate visible galaxies with the resulting distribution in some arbitrary way. Next, it is not clear that the primordial power spectrum predicted by inflation is "flat". Inflationary models which produce gravitational wave perturbations which could contribute to the COBE result, for example [11], can involve significant deviations from a flat spectrum [12]. Finally, the predictions of inflationary models involve an *ensemble* of universes. Since we make measurements in a *single* universe, there is an intrinsic uncertainty when comparing predictions to observations.

Because of the importance of these factors for interpreting the COBE data in terms of "mixed" dark matter, I want to spend some time reviewing what it is that COBE measures to determine what information one can glean from the new results. The DMR experiment aboard COBE provides a *differential* measurement of the CMBR temperature, and not an absolute one. In searching for CMBR anisotropies, several larger effects must be first removed. There is a well-known, and well measured, dipole anisotropy in the CMBR signal, at the level of a few parts in a thousand. This is presumably primarily due to the local motion of the satellite with respect to the frame defined by the surface of last scattering of the CMBR. Subtracting the measured dipole from the signal, any analysis of the COBE signal must next concern itself with the chief source of background: our galaxy. A great deal of effort has gone into both modelling the galactic signal, and verifying that it does not contaminate the observed residuals. While the galactic signal is least significant in the 90 GHz band, measurements of the rms temperature deviations at 10^0 separations in all three bands do not go to zero as one moves away from the plane of our galaxy, but instead

approach a constant value of approximately 30 μK by a galactic latitude of about 25^0. It is this residual signal which is claimed to represent true primordial fluctuations in the CMBR.

Averaging over the sky at latitudes greater than 30^0 from the galactic plane, COBE reports an rms temperature deviation:

$$\Delta T_{rms} (\theta > 30^0) \approx 30\ \mu K. \tag{4}$$

Now of course, there is much more information in the CMBR anisotropy than is obtainable from the rms deviation alone. Using a formalism with which particle physicists should be comfortable, it is conventional to define a temperature correlation function, $C(\alpha) \approx \langle T_1 T_2 \rangle$, defined crudely as the average over the sky of the product of temperatures in regions separated by an angle θ. The full temperature correlation function contains all the information gleaned by the experiment. For the purposes of comparing to theoretical predictions, however, it is convenient to expand the measured temperature fluctuations across the sky in a multipole expansion:

$$\delta T (\theta,\varphi) = \sum_{l,m} a_{lm} Y_{lm}(\theta,\varphi) \tag{5}$$

If we define the rotationally invariant quantity:

$$a_l^2 = \sum_m |a_{lm}|^2 \tag{6}$$

Then one can define the various multipole moments of the temperature anisotropy. COBE has measured both the full correlation function of the temperature fluctuations, containing information on all multipoles, and has also reported a value for the quadrupole anisotropy $Q = (a_2^2/4\pi)^{1/2}$:

$$Q = 13 \pm 4\ \mu K. \tag{7}$$

The observed CMBR originated at the epoch when the background matter distribution first became neutral, and decoupled from radiation, at a time of $\approx 3 \times 10^5$ years into the Big Bang explosion. As we look out to high redshifts, and hence to early times, this time defines a "surface", known as the surface of last scattering, beyond which matter was opaque to radiation. After that time, the neutral matter has been transparent, and so the radiation observed by COBE has presumably been travelling unimpeded to the DMR antenna since that time. Thus, the CMBR provides a redshifted picture of the distribution of radiation at that time, on a surface located roughly 10 billion light years away from us in all directions. The horizon size at that time would correspond today to an angle across the sky of about 1^0.

Photons travelling from the last scattering surface to a receiver aboard COBE redshift by a factor of 1000 on average. However, if there are regions of density excess in the dominant energy density at that time, photons leaving such regions at the surface of last scattering will have to "climb up" out of these potential wells, inducing an extra gravitational redshift. Thus, "cool" spots in the CMBR can represent density excesses which, if gravity governs the formation of structure, will eventually collapse to form galaxies, or clusters of galaxies. "Hot" spots can represent regions of under-density, which will eventually form "voids".

Now, the COBE observations, because of their smoothing scale, are only sensitive to fluctuations in temperature on scales of greater than about 10^0. However, *this is much larger than the scale corresponding the the horizon at the last scattering surface. No causal process since the*

beginning of the presently observable Big Bang expansion could have moved energy density around on such scales in order to create potential wells! Thus, if the CMBR has not been further reprocessed since a redshift of z≈1000, the anisotropies observed by COBE are *primordial*, that is, they must represent initial conditions associated with the Big Bang. As a result the COBE observations provide a handle on understanding whatever physics processes at very high energy – i.e. appropriate to particle physics – generated primordial density fluctuations in the early universe.

In addition, a comparison of the COBE signal with distribution of luminous matter in the universe, most of which formed much more recently, provides a long lever arm to help explore how structure has evolved since recombination. After the question of what the geometry of the observable universe is, perhaps the central issue in modern cosmology concerns the origin of the observed structures in the universe: galaxies, clusters, and superclusters. The simplest possibility is that such structures formed out of the gravitational collapse of initially small density excesses in the universe. The previous upper limits on the anisotropy of the CMBR had already provided one of the strong arguments in favor of non-baryonic dark matter.

Since gravity is universally attractive, if initially one starts with small fluctuations $\delta\rho/\rho << 1$, gravity will cause these to increase. Once they exceed unity, they will separate out from the background expansion and collapse to form bound systems. Before the decoupling of matter and radiation at z=1000, baryonic matter density perturbations on scales inside the horizon at that time could not collapse and grow, due to the pressure of the radiation gas to which they were coupled. After decoupling, such fluctuations could grow with time. In order for fluctuations on the scale of present day galaxies to have grown sufficiently to become O(1) by today, they would have had to have been at least $O(10^{-3})$ at the time of last scattering, and would produce comparable temperature anisotropies on the sky.

Since the first scale of fluctuations which can grow after coming inside the horizon in a baryon dominated universe is that associated with the horizon scale at decoupling – about 1^0 on the sky today – one would expect primordial fluctuations on this scale to have been at least this large, if they were to lead to subsequent galaxy formation on smaller scales. This argument suggests that if baryons dominated the matter density at the time of decoupling, that their fluctuations should induce an anisotropy at the level of $O(10^{-3})$ on scales of about 1^0 in the CMBR. Similarly, this suggests that if the spectrum of primordial fluctuations does not vary much as a function of wavelength, that fluctuations in the CMBR on larger scales, those probed at COBE, should not be much smaller.

The fact that the observed fluctuations in the CMBR are not anywhere near this large is one of the many pieces of indirect evidence that we have that baryonic matter does not dominate the energy density of the universe, at least if galaxy formation is to occur by gravitational collapse. However, before the COBE observation the big question was whether fluctuations existed at any level which might be compatible with galaxy formation via gravitational collapse. The present observation now allows us a hope of testing explicit mechanisms, both for the generation of fluctuations, and for their subsequent growth. At present, the only known physical mechanism in the early universe which produces a spectrum of primordial density fluctuations which is calculable completely from first principles is inflation. This is one of the reasons inflationary scenarios are so exciting. They can be tested unambiguously, at least in principle.

Several features of inflationary predictions have recently been stressed which affect the

conclusion that Cold Dark Matter models may have to be supplemented by Hot Dark matter.

(a) The Power Spectrum of Primordial Fluctuations Need not be Exactly Flat.: It used to be said in fact that a flat spectrum was a prediction of inflation. In fact, on the strength of this, most simulations for structure formation have been based on a flat primordial spectrum. Remnant energy density fluctuations today have their origin, in inflationary models, in quantum fluctuations in the scalar field responsible for inflation. The scalar field fluctuations get translated into energy density fluctuations because they cause different regions of the universe to exit the inflationary phase at different times. The stored energy density in the scalar field configuration in those regions that depart from the de Sitter expansion earliest gets redshifted compared to those regions in which the scalar field value has not departed from its false vacuum value. The difference in energy density in regions with different scalar field fluctuations is therefore related to the magnitude of the fluctuations, divided by the time it takes the background scalar field to change by an amount comparible to the size of the fluctuations. Now, if, during the time over which fluctuations on scales relevant to the scales being probed by COBE or studies of galaxy distributions today are pushed outside the horizon, the *slope* of the potential for the scalar field changes, then the magnitude of energy density fluctuations will change and the resultant spectrum of fluctuations will not be flat. This is clearly model dependent, depending on the details of the potential for the scalar field driving inflation.

(b) Inflation Generates Gravitation Wave Modes: These may contribute to the COBE result but may not be directly related to large scale structure formation, and can thus cloud any inferences based on COBE. All massless quantum fields have fluctuations during inflation, but the energy density stored directly in the these fluctuations is usually negligible compared to those which result from the mechanism I have described above. There is one exception, however. Fluctuations in the graviton field end up as direct coherent fluctuations in the metric after inflation, otherwise known as gravitational waves. These produce direct fluctuations in the amount by which radiation travelling to us from the surface of last scattering redshifts, and thus produce temperature fluctuations in the CMBR. Since, miraculously, it turns out that each helicity component of the graviton field acts like a minimally coupled scalar field, at least as far as its equations of motion are concerned in the background expansion, the magnitude of the gravitational wave fluctuations is simply determined by the scalar two point function, which depends purely on the overall *scale* of the potential driving inflation.

(c) The Predicted Anisotropies are Stochastic Variables With Known (but Unobservable) Distributions: Because the classical fluctuations in the fields responsible for observed CMBR anisotropies in inflation result from quantum mechanical fluctuations in the underlying quantum fields, the fluctuations in each mode of the field, while they have a well determined mean value, are themselves Gaussian random variables. But what is the ensemble in which their distribution is Gaussian? It is an ensemble of Universes undergoing inflation! Namely, each time inflation occurs, it produces a set of magnitudes for each independent mode of the relevant fields drawn from a Gaussian distribution.

This has a very important consequence which has taken on new importance now that COBE has measured a non-zero CMBR anisotropy. There is an irremovable uncertainty, a "cosmic" variance in comparing observation with theory. I stress that this uncertainty is completely independent of possible measurement uncertainties. Even if the CMBR anisotropy were measured exactly, there would remain some residual uncertainty in comparing certain theoretical predictions

to observations! This is because we are making measurements in a single Universe! Until someone finds a way to bypass this difficulty, cosmic variance will remain.

These three features of inflationary predictions all play a central role when COBE, and other CMBR observations, are used to constrain our models of the early universe, and of subsequent structure formation, as I alluded to at the beginning of this section. They can dramatically affect the comparison of COBE-scale fluctuations and those observed in the distribution of visible matter in the universe, and must temper one's enthusiasm for a "mixed" dark matter solution of the "COBE problem". Nevertheless, in spite of these caveats a tau neutrino mass in the range of 10-100 eV is certainly more plausible as a result of the existing solar neutrino and COBE data than it would be without it. It thus remains to determine how one might detect such a mass in the laboratory.

3. Detecting a tau neutrino mass with the next Galactic Supernova:

In spite of the obvious interest in exploring such a mass range, terrestrial experiments are quite limited. Experiments are planned at LEP and Fermilab which could detect ν_μ- ν_τ oscillations for tau neutrinos in the eV range. However, the only hope for a direct kinematic measurement would be the observation of tau-neutrinos from stellar collapse. As a result, it is useful to explore techniques which might aid in such a detection in advance of the next supernova, and several groups have been persuing such a course[13,14]. The travel time from a supernova at ≈10 kpc is such that neutrino masses greater than ≈10 eV will result in dispersive time delays on the order of seconds. Unfortunately, tau-neutrinos do not make up the dominant supernova neutrino signal. In a water detector of the size of Super-Kamiokande, for example, the signal will probably involve ≤50 events, out of $\approx 10^4$ total events.

Nevertheless, because of the importance and uniqueness of such a possible measurement, it is worthwhile examining in advance of a galactic supernova how experimenters might optimize their sensitivity. In order to examine in detail this issue, as well as the more general question of what might be learned from the neutrino signal from a galactic supernova, we[13] have developed and tested a comprehensive Monte Carlo program to simulate a supernova neutrino signal, including backgrounds, in underground water detectors. We have suggested several ideas for isolating and analyzing the tau (and muon) neutrino signals in a way which is independent of the details of supernova models, and relies only on relatively ubiquitous assumptions about the late-time thermal signal. A more detailed description of the results, and also of the program appear elsewhere [13,15]

i) The Neutrino Signal: Neutrino events which are detected in a water detector consist of a measured time, energy and angle for each observed e^+ or e^-. Our Monte Carlo program consists of three stages: (1) a neutrino flux is generated at the supernova and propagated to the detector; (2)this flux is convolved with interaction cross sections to determine the scattered events in the detector, involving physical energies and directions; (3) the scattered events are combined with information about the detector (and neutrino masses), including the background event rate and spectrum, to generate detected events with their detected time, energy and direction. Each of the latter stages is generated from the preceding stage by use of a probability distribution. Finally, the time stored with the detection is the time that the neutrino is released from the supernova. We

allowed an additional time-of-flight delay for each massive neutrino event if neutrinos have a mass. The advantage of this procedure is that we can generate a set of events, and then afterwards operate on this set to explore the effect of a mass without having to re-run our Monte Carlo. Thus we obtain, for each supernova explosion, a set of detected events, with each consisting of a time, energy and direction. Sample signals for several different explosions, showing the time signal, and energy spectrum are shown below.

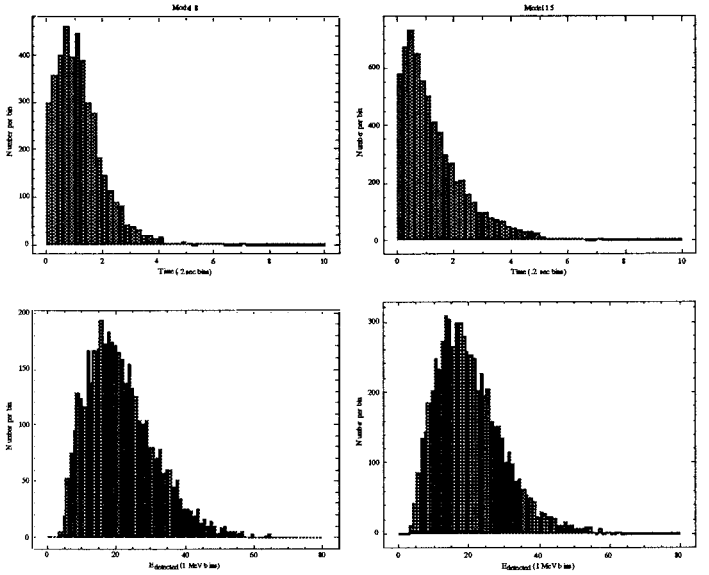

Figure 1: Some sample time signals and energy spectra for two supernova bursts

ii) Analysis Strategy:

Using our Monte Carlo we can examine in detail many features of a supernova neutrino signal. Here, we are most concerned with probing the time delays due to a non-zero tau neutrino mass. Since the characteristic energy for nt is 18-24 MeV, if the tau neutrino mass of is greater than around 500 eV these neutrinos will be delayed beyond the limit of our consideration. For masses between 50 eV and 400 eV, the effect of the mass will be to push events from the first second or so of the signal to 5-50 seconds. The challenge is to see if these effects can be statistically distinguished.

On first thought, such a possibility may seem remote, especially for masses in the 10-50 eV range. Approximately 5000-15000 events are expected, versus 30-100 nt events. Moreover, part of the purpose of the supernova observation will be to pin down the parameters of the supernova explosion. Without pre-ordained knowledge of these parameters, how can we hope to distinguish neutrino mass effects when fitting model predictions to the explosion? We believe one can surmount these difficulties, and extract the tau neutrino signal by exploiting two kinematic

characteristics of the neutrino signals, one of which goes against previous intuition:
(a) First, an angular cut on the data removes most of the electron antineutrino signal. Neutrino-electron scattering at MeV energies is peaked strongly in the forward direction. For example if a scattered electron is produced with only 10 MeV from a neutrino with incident energy E= 20 MeV the scattering angle will be cos $\theta \approx 0.95$. By contrast, the positrons produced by scattering on protons are nearly isotropic, with in fact some mild peaking in the rearward direction. Thus, we should search in the forward cone for the tau neutrino signal. In principle, while one can gain in "signal to noise" by reducing the size of this forward cone (until one runs out of events), in practice the smallest reasonable choice in opening angle corresponds to the angular resolution of the detector itself. For incident ν_τ's with mean energy $\approx$25 MeV, the mean scattered electron energy is $\approx$12 MeV. The angular resolution for electrons of this energy is[16] $\approx 18^0$. Thus, we define the forward cone as corresponding to $\cos\theta > \cos(18^0) \approx 0.95$.
(b) Conventional wisdom suggests that the ν_τ and ν_μ events will have higher mean energy than electron antineutrino events because the former are emitted from the supernova with higher mean temperature. However, exactly the opposite is true. Because the energy distribution in neutrino-electron scattering is flat, the average energy of the scattered electrons will be half that of the incident neutrinos, whereas in antineutrino-proton scattering the outgoing positron takes up almost all the energy of the neutrino. In addition the antineutrino -proton cross section goes as E^2, while the ν - e cross section goes as E. This serves to further enhance the high energy tail of the positron spectrum. As a result of these two factors, we can hope to further suppress the background by making an energy cut. Without this cut, we shall see that it is impossible to demonstrate statistically the existence or absence of the entire ν_τ signal.

While the ability to isolate the overwhelming electron antineutrino signal is very important for extracting the tau neutrino signal, it also provides the essential ingredient which allows a supernova model-independent limit on the tau neutrino mass. By breaking up the signal in to "forward" and "rearward" signals (i.e. $\cos\theta <> 0.95$), we can analyze the internal consistency of the signal itself. In particular, we may use the 5000-15000 events in the rearward cone to provide a fit to the parameters of any sufficiently complex model at the 1% level! We can then compare this fit with a fit to the data in the forward cone. For several key parameters, in particular those governing the late time behavior, which we assume is flavor independent (based on thermal emission), the fits should be identical in the absence of a neutrino mass. The extent to which they disagree then allows us to probe for such a mass. The beauty of this procedure is that it is largely independent of what the actual supernova model is. As long as the model which fits the rearward data is sufficiently complex (incorporating the basic supernova physics) to provide a sufficiently good fit to the rearward data, it should provide a good fit to at least the late time behavior of the forward data in the absence of neutrino masses. One must, of course, take into account that the smaller forward data set limits the statistical accuracy of any fit. Nevertheless, since all late time events will essentially fall in this forward cone, containing far fewer events than the total, even 5-6 such events can be statistically quite significant. In any actual experiment, the experimenters would fit several different models to the rearward data. What we show here is that even a simple fitting algorithm allows one to determine statistically a non-zero tau neutrino mass. The only assumption in this procedure is that the late time supernova signal is independent of neutrino type. Since this is based on thermal cooling, such an assumption seems to be one of the safest one can make.

iii) Analysis and Results:

Using the strategy outlined above, we fit the detector events generated by our Monte Carlo program for the 36 supernova models to a simple 5 parameter model using a maximum likelihood technique (see [13] for details). Shown in figure (a) is the fit to the forward cone for a model explosion, and also the prediction based on the fit to the rearward cone. As can be seen, both predictions are in good agreement, and the both agree with the data. In fig. (b) the same procedure is applied, but now the tau neutrino is given a mass of 100 eV. It can be seen that the rearward fit matches neither the forward data, nor the fit to the forward data. It merely remains to quantify this, in order to determine what kind of neutrino masses can be distinguished.

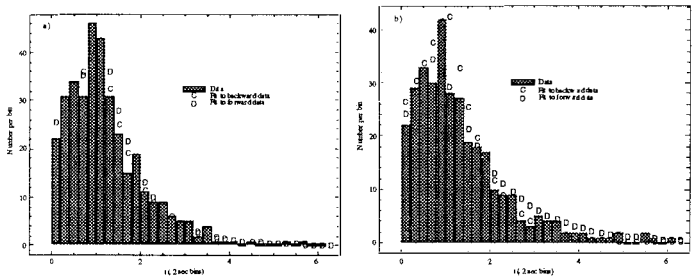

Figure 2: Comparison of fit to forward vs backward cone (a) (0 eV), (b) 100 eV tau neutrino mass

(a) Likelihood matching: This technique is a simple extension of the comparison of forward and rearward fits describe above, which allows a quantitative analytic comparison of fits (see ref. [13] for details)..The results were mixed. For masses ≈40-400 eV we could find strong disagreement between the forward and backward results for some mass values, but instead of the monotonic rise, and then fall we expected, there were valleys where the disagreement is much smaller. This is due to two effects. First of all, if there are late time tau neutrino events which occur in the rearward cone, the rearward fit can be shifted in the direction of the forward fit. Second, if there are enough late-time events in the forward direction, all fits will be bad. This will flatten the likelihood region, allowing a broader range of "acceptable" values. We reduced the first effect by reducing the size of the "rearward" cone, so that it is not contaminated by forward tau neutrino events. The removal of the forward tau neutrino "contamination" more than outweighs the effect of reducing the statistics in the rearward cone.

The second effect, that of all zero mass models providing a poor fit to the forward direction could be reduced by using goodness of fit technique. Better still, we could add a mass parameter to the fitting function, and either perform a best fit for this parameter, or compare the improvement of fits with this extra parameter using an F-test, which quantifies the affect of adding another variable. All of these improvements are currently under investigation. Nevertheless, this technique already demonstrates a sensitivity for masses in the range ≈40-400 eV.

(b) Late time events: The best fit to the rearward data was used to generate a predicted number of events in the forward direction. We then used Poisson statistics to compare the expected number

with the actual number after some time tcut and before 50 seconds. This approach is very model-independent, because it depends only upon the large statistics fit to the late time behavior of the rearward signal.

These results were encouraging, although they are more luminosity dependent. For a medium luminosity burst (at 10 kpc) with short accretion time (0.1 sec), a non-zero mass is indicated at the 99% confidence level for masses between 50-350 eV, and even for masses down to ≈25 eV and up to ≈425 eV, the signal is noticeable at the 90% confidence. If the luminosity of the burst is reduced to the lowest expected, however, sensitivity at the 99% confidence level is restricted to the range 75-150 eV. Similarly, if the constant luminosity phase is longer (1.0 sec), the accessible range is somewhat reduced, to ≈60-325 eV.

These results were obtained without any energy cuts, and without any correlation of energy of events with time, nor do they take into account the spectral differences between the background events and supernova events. When these statistical analyses are combined, we expect the robustness and range of the lower and upper limits will increase. As we include more modelling of the rearward signal in the late time analysis we can make the lower cutoff earlier, thus improving sensitivity to still smaller masses. We made preliminary steps to examine this, by incorporating the same energy and rearward cuts here as were used earlier, and lowering the cutoff time. We can see in this way a sensitivity to masses as low as 25 eV. Incorporating a time interval past 50 seconds could in principle increase the upper end of the sensitive range. It is possible that using the spectral difference between supernova and background events might allow some distinction between signal and noise to be made. Finally, because the time delay is proportional to mass squared, even if the cooling decay constant were twice as large as those chosen here, the lower bounds on mass sensitivity would only be expected to increase by a factor of ≈1.4.

(c) The Early time Signal: Our work also sheds light on an issue which has received some attention in the recently. It has been suggested that because the dispersion due to neutrinos of ≥O(eV) is O(sec), that the early time signal--namely that of the supernova "turn-on"--either the early neutronization burst last O(10 msc) or the O(.05) sec turn on for the thermal burst, followed by possible exotic time structure, as Adam Burrows discussed at this meeting–might allow the strongest sensitivities to small neutrino masses[i.e. see 14]. We display below the early time forward cone events for a represented, average luminosity model. *Note that inherent in the signal is a neutronization burst followed by a smoothly varying thermal cooling signal.*

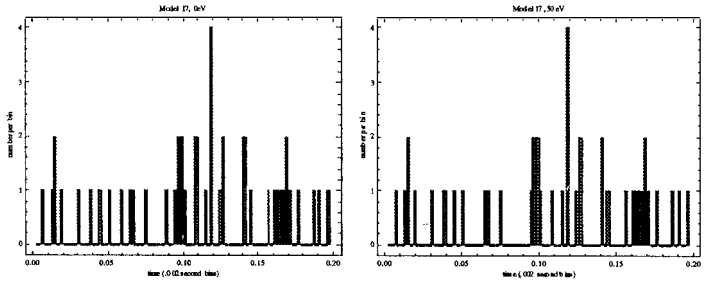

Figure 3: Early time signal in the forward cone: (a) 0 eV, (b) 50 eV tau neutrino mass.

In spite of the potential sensitivity of the neutronization burst to small electron neutrino masses, we find that there is no signal for the neutronization burst. This somewhat surprising result is clear, upon reflection. The total number of expected events from the neutronization burst, even for a detector of the size of Super-Kamiokande, is O(1)!. Thus this signal cannot stand out, even against the thermal turn-on signal. More generally, the neutronization burst has a luminosity of O(5 x1053 ergs/sec), only slightly greater than that in the thermal burst. However, since the ne-e cross section is at least 10 times smaller than the -p cross section, even if there were more than 1 event for the neutronization burst, it would be difficult to extract this from the thermal turn on in a light water detector.

Moreover, in spite of the fact that the thermal cooling signal is smooth, with no instrinsic time structure, it is clear that the Poisson noise makes it impossible to distinguish this from the presence of a modulated signal. It might be possible to look for time modulation in the much larger electron antineutrino signal, given the large number of events in that signal, but any hope of seeing such behavior in the tau neutrino signal seems remote.

Thus, there is no discernible effect of a tau neutrino mass on the early time signal. As our analysis demonstrates, the place to look for a tau neutrino mass in a light water detector is not at early times, but at late times, where delayed events may stand out by their presence or absence.

iv) Extensions:

We have demonstrated that an underground light water detector patterned after Kamiokande could, in principle be sensitive of a neutrino mass as small as $\approx$ 25 eV. We have checked that improvements in the detector, including improved energy resolution, backgrounds, etc. are not likely to increase the sensitivity to neutrino mass significantly.

In order to futher explore this issue, we are now examining the utility of theSudbury Neutrino Observatory (SNO) heavy water detector[17] for this purpose. While this detector is much smaller than Kamiokande it may allow neutral current fission of deuterium to be observed. In this case, non-electron neutrinos would have cross sections which are approximately as large as the antineutrino -proton cross section. Thus, they would contribute a far larger fraction of the signal, and this might improve sensitivity to the tau neutrino.

As far as the analysis we have thus far performed, its strength lies largely in the existence of the signal from the $\approx$10,000 -p events in the large detector. In SNO, one would expect a total of perhaps 500-1000 events from a galactic supernova. Thus, by itself, it is not clear that the SNO detector could take advantage of the strategy we propose to provide limits on the tau neutrino mass. However, in co-ordination with the fitting analysis which could be performed at a Super-Kamiokande detector, the possible neutral current signal at SNO appears at first glance to provide a very useful potential extra handle. Nevertheless, it is not clear, without a detailed analysis of the type we have performed for Kamiokande, and which is now underway for SNO, whether the SNO signal could improve the systematics and statistics. Several comments are in order:

(a) NaCl as a neutron detector for neutral current events will be useless for a supernova signal. The neutron signature is Cerenkov light, which is indistinguishable from the electron signal on an event by event basis, and must be subtracted from a similar signal when NaCl is not in the detector in order to extract neutral current information. However, the supernova neutral signal happens only once in the detector. Thus, in order to get neutral current information on a supernova signal, ^{3}He

detectors must be used.
(b) While the neutral current events, which produce a single neutron are in principle distinguishable from charge current events on deuterium which produce two neutrons, when taken one at a time using ^{3}He detectors, the average time for neutron capture in the detector is estimated to be ≈5-10 msec. Thus, if events are being recorded at a rate exceeding ≈100/sec, it is not clear that the neutron capture signal can be unambiguously associated with a specific electron (positron) signal. Moreover, the efficiency of detecting both neutrons will affect how well one can disentangle these signals. Moreover, the neutral current dissociation signal carries no energy information. These problems may not be severe for the late time analysis. Here the event rate is small enough so that neutral current events can probably be distinguished. However, it would be an important limitation on possible uses of the neutral current fraction at early times to probe the tau neutrino signal, as Burrows et al have suggested[14].

Thus, the next galactic supernova may provide a signal in large underground light and heavy water Cerenkov detectors, which could allow detection of a cosmologically significant tau neutrino mass. More importantly, perhaps, in this area, it is the details which count! Without a detailed analysis of the actual signatures, important features of the signal can go unnoticed, or features of the signal which are unobservable may not be recognized as so. Because of the renewed astrophysical and cosmological interest in light neutrinos which I have alluded to here, it is important to examine these questions seriously before the next supernova.

References:

1. L.M. Krauss, Phys. Rev. Lett. **64**, 999 (1990).
2. i.e. D. Caldwell et al, Phys. Rev. Lett. **61**, 510 (1988); S. Ahlen et al, Phys. Lett. **B195**, 603 (1987); B. Sadoulet et al, Astrophys. J. **324**, L75 (1988).
3. L.M. Krauss, to appear in Proceedings XXVI ICHEP Conference, Dallas, Texas August 1992 (to be published by AIP).
4. E.W. Kolb, et al., Phys. Rev. Lett. **67**, 533 (1991).
5. G.M. Fuller and R.W. Malany, Phys. Rev. D (1991).
6. L.M. Krauss, Phys. Rev. Lett. **53**, 1976(1984).
7. J.N. Bahcall and H.A. Bethe, Phys. Rev. Lett. **65**, 2233 (1990).
8. M. White, L.M. Krauss and E. Gates, Phys. Rev. Lett. **70**, 375 (1993).
9. i.e. P.I. Krastov and S.T. Petcov, Phys. Lett. **B285**, 85 (1992).
10. L.M. Krauss, E. Gates, and M. White, Phys. Lett. B, in press.
11. e.g. L.M. Krauss and M. White, Phys. Rev. Lett. **69**, 869 (1992).
12. e.g. R.L. Davis, et al., Phys. Rev. Lett. **69**, 1856 (1992).
13. L.M. Krauss, et al., Nucl. Phys. **B380**, 507 (1992).
14. A. Burrows, et al., Phys. Rev. **D45**, 3361 (1992).
15. L.M. Krauss, et al., YCTP-P34-92.
16. M. Nakahata, U. Tokyo Ph.D. Thesis, UT-ICEPP-88-01; also A. Suzuki, private communication.
17. G.T. Ewan, et al., Sudbury Neutrino Observatory Proposal, SNO-87-12 (1987).

Solar Neutrinos

IS THERE A SOLAR NEUTRINO PROBLEM? REVIEW OF THEORY AND EXPERIMENTS

Douglas R. O. Morrison
CERN, Geneva, Switzerland

ABSTRACT

The development of the Solar Evolutionary Model since 1957 is described. It is shown that it is a simple model with effectively only two parameters thus limiting its range of application. Although it is robust and remarkable agreement can be obtained with helioseismology, it needs continual and significant updating as the input values and theories change. The ^{7}Li abundance is a factor of a hundred lower than predicted - this can be understood by considering the pattern of the abundances of all stars and a conclusion is that meridional circulation and turbulent diffusion need to be introduced. Together with other uncertainties such as screening effects, it is clear that the errors on the theoretical values cannot be small. A Reference Solar Model is selected and the neutrino flux values from the four experiments, are compared with it. A Fifth Experimental Result is that while pioneering neutrino experiments are admirable, it is found that their numerical results frequently require significant modification. It is concluded that at this time, evidence of a Solar Neutrino Problem is not compelling.

1. INTRODUCTION

In 1957 Schwarzchild [1] proposed the basic scheme for a calculation of the evolution of the Sun from its birth to the present day. In 1961 Bahcall [2] used this model to calculate the flux of neutrinos expected. Davis [3] from 1964 onwards worked towards measuring this neutrino flux using a suggestion by Pontecorvo [4] that solar neutrinos could convert Chlorine37 to Argon37 whose decay electrons could be measured. These pioneering efforts of Bahcall and Davis, well described in Ref. 5, finally led to the Homestake mine experiment where it was found that the flux of neutrinos measured was significantly less, by a factor of more than three, than the theoretical calculations. This has become known as the Solar Neutrino Problem. In recent years the models of solar and stellar evolution have greatly developed with several groups doing independent calculations giving results sometimes significantly different from those of Bahcall. Several major experiments have started to give results which are closer to the model estimates. The situation now is that while some state [6] that there is a significant Solar Neutrino Problem, it is also possible to say that the evidence is "not compelling" [7]. Here recent developments in theory and experiment are reviewed.

2. THEORY

2.1 Basic Problems and Advantages of Evolutionary Models

The basic idea of Schwarzchild [1] was to start from the moment that a star had formed out of the clouds of gases, some 4.5 billion years ago, and follow its evolution to the present when the luminosity, mass and radius could be made to match with the presently measured values, L_0, M_0 and R_0 resp. This was done by taking a large number of shells of different radii and a finite number of time intervals and for each (radius, time) cell, apply the four equations giving balance and continuity across the boundaries (see Ref. 8 for most up-to-date review).

The Sun was considered as consisting of three regions as shown in Fig. 1a; a Core where the nuclear reactions providing the energy, mainly took place; in the middle a Radiation or Intermediate zone where the heat is transferred mainly by radiation; and a Convection zone where the heat is mainly transferred by convection; the boundaries are found to be at about 0.3 and 0.7 R_0. In 1958 Boehm-Vitense [9] introduced the Mixing Length Theory, MLT, in which the whole complex convection and turbulence is described a single parameter, alpha, which was assumed to be the distance, for all radii in the Convective Zone, over which a convective element can be recognized.

Thus the input data to the model calculation has only five elements, the present age, luminosity, mass and radius of the Sun plus its initial composition which is assumed to be known 4.5 Gyr ago. The composition is taken to have three parts, hydrogen, helium and "metals" whose initial fractions are called, X, Y, and Z resp. By "metals" is meant all elements heavier than H and He. The two parameters which are derived from this fit are alpha and the initial helium fraction, Y (it is not possible to obtain reasonable measurements of the primordial helium abundance, except very approximately, by other measurements).

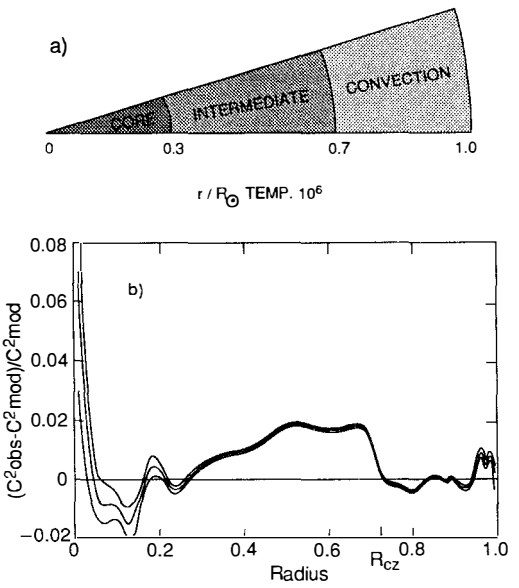

Figures 1: a) Slice of the Sun showing three zones as a function of the fractional radius, $R/R_{\odot}$. b) From heilioseismology [53], difference in sound velocity squared, C^2 between observed (i.e. by inversion calculation) and a Saclay model [18].

At first sight it would seem very optimistic to obtain neutrino fluxes with small errors from such a simple input to a complex system, which to determine the opacity, requires a very detailed knowledge of all the elements and their isotopes 4.5 Gyr ago in a dense cloud collapsing to form a star. However it is better than one expects. The primordial abundances are first obtain by measuring the elements today on or near the Sun's surface and assuming they are the same as 4.5 Gyr ago. This is checked by comparing with certain meteorites which could have the this age and Anders and Grevasse [10] have obtained remarkable agreement (see Fig.3 of Ref. 7b) except in a few cases. These exceptions are principally ^{7}Li which is a factor of 200 too low, ^{9}Be which is a factor of two too low, and iron which has a high value from spectroscopic measurements and a low value from meteorites.

One of the advantages of the model is its remarkable stability because of strong feedback mechanisms. Thus the central temperature cannot easily be varied as this would change the luminosity which is very precisely determined. This applies to the main channels which depend on the initial reaction, pp giving deuterium. It does not apply to very minor branch reactions such as the production of ^{8}B, which is however important here, as it gives almost all the higher energy neutrinos.

Although this evolutionary model is robust, it has many problems of two main kinds. Firstly there are the simplifying assumptions - a) spherical symmetry (though it is known that the rotation rates at the Sun's equator and near the poles are different), b) no magnetic field (though fields of about a million gauss are indicated near the base of the convection zone),

c) one parameter, alpha, is enough to describe all the motion and heat transfer mechanisms in the convection zone, d) there is no movement in the core and intermediate zones. Secondly, there is an enormous amount of diversified input data - the abundances, reaction rates (some measured, many extrapolated while the basic pp reaction giving deuterium has to be calculated as the rate is so low), rate of transfer of radiation (opacity) depends on a very detailed knowledge of ionization and energy levels of all the isotopes, etc. - values of these inputs vary with time as more information is learnt and better theories are developed. There are other problems such as the effects of screening and the choice of the equation of state as a function of the radius. Many of these problems come from the fact that the interior of the Sun is a plasma at such high temperature and pressure that control measurements cannot be made on earth though recent laser work at LLNL [11] has reached just beyond 1% of the Sun's central temperature of 15 million degrees - encouraging agreement has been found [12] with recent opacity calculations by Rogers and Iglesias [13].

It is clear that errors on theoretical calculations cannot be small, but since the aim of studying a solar neutrino problem, is to compare calculated values with experimental ones, the estimate of errors is primordial. These will now be discussed.

2.2 Fluctuating Input Data

In 1988 there were two major calculations of solar models, one by Bahcall and Ulrich [14] and the other by the Saclay group of Turck-Chieze et al. [15] who gave quite different rates for the Chlorine experiment of Davis et al. being 7.9 SNU and 5.8 SNU. resp., also with very different errors of 11% and 22% resp. That this difference is important can be seen by comparing with the Kamiokande II result [16] which was expressed as

$$(\text{Data})/(\text{Theory}) = 0.45 \pm 0.08 \tag{1}$$

where the Theory was taken as Bahcall and Ulrich's value and where the theory error has assumed to be zero. Including the theory error gives;

$$\begin{aligned} \text{Data - Theory} &= (1.00 \pm 0.11) - (0.46 \pm 0.08) \\ &= 0.54 \pm 0.15 \end{aligned} \tag{2}$$

Taking the Saclay calculations gives

$$\begin{aligned} \text{Data - Theory} &= (1.00 \pm 0.22) - (0.71 \pm 0.11) \\ &= 0.29 \pm 0.24 \end{aligned} \tag{3}$$

Thus a significant three and a half standard deviation effect has been converted into one of less than one and a half standard deviations which is not significant. It was mainly the surprisingly small error of 11% of Bahcall et al. [14] which was responsible for making the result seem significant. Thus we have to consider errors of the order of 10% to be very important in deciding whether or not the Kamiokande result is significantly different from evolutionary model calculations.

In 1991/92, there were four major calculations of solar evolutionary models. - the Nice group of Morel et al. [17], the Saclay group of Turck-Chieze and Lopez [18], the Princeton-Yale collaboration, Bahcall and Pinsonneault [19] and the Yale group of Guenther et al. [20] who mainly concentrated on helioseismological comparison. The values given for the Chlorine experiment for the first three are 6.5 ± 20% (model ST3), 6.4 ± 22% and 8.0 ± 12% resp. It

may be seen that there is still significant variations in rates and in errors which come mainly from the choice of input and the choice of errors to be included.

Between 1988 and 1992, there were five major changes to the input data.

It was first pointed out by Courtaud et al. [21] that the abundance of iron as determined from the Sun's surface was significantly higher than the value from meteorites. The surface measurement was based only on HI (i.e. neutral hydrogen) which is only 5% of the total hydrogen. Iron is important as it is the only abundant heavy element which is not completely ionized near the centre of the Sun and since the bound-bound and bound-free rates are dominant in radiation transfer processes, this would change the temperature and hence the neutrino flux significantly. Recent measurements of HII (ionized hydrogen) favour the low value and now other groups follow Turck-Chieze et al. [15] in using the low meteorite value which lowers the neutrino flux by about 10 to 20%.

The flux of high energy ^{8}B neutrinos is directly proportional to the cross section of the $^{7}Be(p,\gamma)^{8}B$ reaction. This reaction has only been measured at high energies above 400 keV and it is necessary to extrapolate down to the Sun's temperature, mainly well below 20 keV. The cross sections are expressed in terms of the astrophysical S-factor which essentially removes the important barrier penetration factor to give an almost flat function. There are two problems - the method of extrapolating and the choice of experiments. In 1988, Turck-Chieze et al. [15] pointed out that previously the extrapolation was done only assuming an s-state but this did not fit the higher energy data. They fitted using s- plus d-states which fitted data better, and found a neutrino flux for chlorine some 12% lower (see Fig., 2a). All groups now use a s- plus d-state extrapolation. Secondly there is the choice of experiments. Most were done at very early times and only two were performed in the critical region below the resonance - these are Kavanagh et al. [22] and Filippone et al. [23] which give extrapolations to zero energy, S(0), values which are significantly different of 27.4 and 20.2 keV-b resp. as shown in Fig. 2b. Long experience of compiling data [24] has shown that newer experiments build on the experience of earlier ones and use better equipment so that it is better to discard the earlier result in case of disagreement - now the Kavanagh experiment dates from 1969 while the Filippone one was 14 years later. Also the Filippone experiment has been well described in a refereed paper while the Kavanagh is only described in 12 lines in an APS abstract - again experience [24] has shown that such results should be rejected as do the Particle Data group. The result is that only the 20.2 keV-b value should be taken whereas the 1992 authors favour the Johnson et al. [25] value of 22.5 keV-b - this change will lower the ^{8}B neutrino flux rate of Ref. 18 and 19 by about 10%.

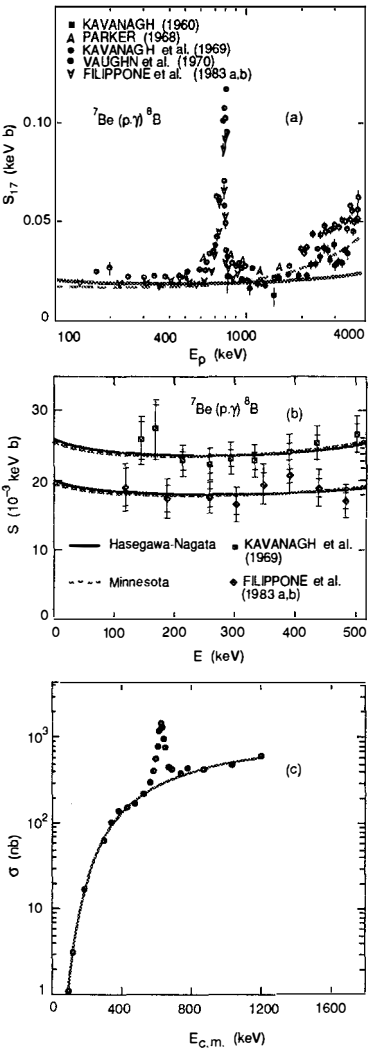

Figure 2: For the reaction ^{7}Be(p,γ)^{8}B: a) astrophysical S-factor (which is essentially the cross section with the barrier penetration factor removed), S_{17}, with experimental values. The solid line is the s-wave fit and the dashed line is with s- and d- waves fitted: b) S_{17} measurements below 450 keV; the Kavanagh et al. [22] and Filippone et al. [23] data are fitted separately by Johnson et al. [25] using s- and d- waves with two slightly different assumptions: c) cross section for the reaction.

The S(0) value has varied appreciably with time as shown in Table 2 of ref. 7a, varying from +34% to -16% of the preferred value. This shows that the error of 12% claimed by Bahcall et al. for the sum of ALL errors, is a gross under-estimate.

New experiments to measure the reaction $^{7}Be(p,\gamma)^{8}B$ are crucial. It is a difficult experiment since as shown in Fig. 2c, the cross section (not the S-value) decreases steeply with energy. Such experiments are being prepared, for example by T. Motobayashi and M. Gai et al. [26], who plan to study it at Riken - they will use a ^{7}Be beam instead of a proton beam to avoid the Coulonb explosion. Other experiments are in preliminary stages at MSU and GSI.

The neutrino flux is proportional to the age assumed for the Sun. Most recent calculations (see Ref. 8) have lowered the age to 4.5 Gyr from values of 4.6 to 4.7 years, correspondingly reducing the ^{8}B flux.

Disagreement with between observations and theory for pulsating stars caused a suggestion [27] in 1982, that the opacity used was incorrect. In 1992 Inglesias and Roberts [13] finally obtained improved values which resulted in an increase of the theoretical neutrino ^{8}B flux of about 10%.

A fifth major change since 1988 is that the effects of diffusion. are beginning to be considered. Diffusion of elements of different masses by gravitational settling was first discussed by Eddington [28] in 1926 and shown to be important for white dwarfs by Schatzman [29] in 1948. Earlier calculations [30] from 1977 on, were re-examined by Proffitt and Michaud [31] who considered helium, CNO and heavier elements. The helium alone reduces the central temperature of the Sun by 0.4% which, following the T^{18} dependence of Bahcall [6], would correspond to an increase in the ^{8}B neutrino flux of about 5%. The heavier elements would have a smaller effect. The diffusion velocities are a few times 10^{-10} cm/s. Bahcall and Pinsonneault [19] estimated that for helium alone, the ^{8}B neutrino flux would increase by about 11%.

Thus these are five effects that have each changed the ^{8}B neutrino flux estimate by 10% or more since 1988. It is clear that a minimum reasonable error is more than 20%. Taking into account the many other errors, probably 30% is a fair estimate. Although these four effects are essentially independent, as it happened, they worked in different directions so that the final ^{8}B flux estimates are not very different from the 1988 ones.

2.3 Lithium, Meridional Circulation and Turbulent Diffusion

The fact that the SSM estimate of Lithium7 abundance is 100 times greater than observed, is clearly an important indication that the model is limited. At first it was thought that it could be easily explained. Lithium is destroyed by proton capture at 2.5 million degrees and the Convective Zone boundary, R_{cz}, has a temperature of just over 2 million degrees, so it was hypothesize that this boundary was unstable and overshooting or vortices, would carry some convection material down to a higher temperature thus destroying most of the ^{7}Li. However many other stars have had their ^{7}Li abundances measured and this theory cannot explain the results for these other stars. The ^{7}Li abundance is shown in Fig. 3a as a function of the effective surface temperature of the star for the Hyades of 0.5 Gyr age. It may be seen that there is a spectacular dip called the Boesgaard dip [32], of a factor of at least a hundred. Lithium abundances for other groups of stars from different globular clusters of various ages, are indicated in Fig. 3b It may be seen that for the young stars of Pleiades of 0.1 Gyr age, the

distribution is smooth, but as the stars get older, the Boesgaard dip appears and the ^{7}Li abundance decreases for the lower temperatures (NGC 752 has an age of 1.7 Gyr and M67 of 5 Gyr which is close to the age of the Sun).

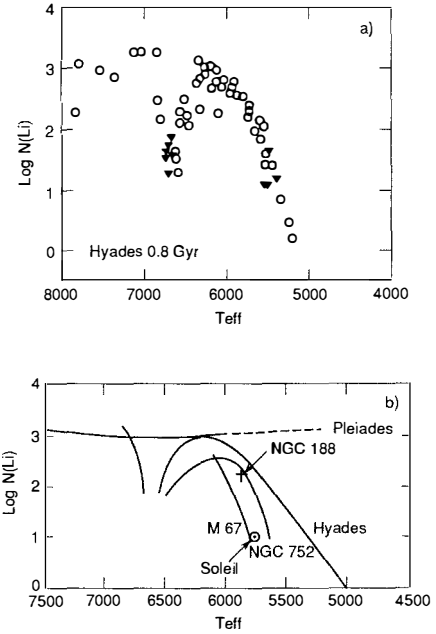

Figure 3: Lithium7 abundances in stars as a function of the effective surface temperature [37]; a) for stars in the Hyades of 0.8 Gigayears age: b) stars in globular clusters of different ages plus the Sun.

The ^{7}Li results cannot be explained simply by overshooting. Several explanations have been proposed - the one that best fits the observations for main sequence stars and for giants and subgiants, is that of Charbonnel and Vauclair [33] which assumes two-loop meridional circulation. Earlier Charbonneau and Michaud [34] had used the classical Eddington-Sweet single-cell meriditional circulation and could reproduce the Boesgaard dip. Vauclair [35] and Charbonnel et al. [36] extended this to two-loops as shown in Fig. 4. Here the outer loop would correspond to the Convection zone. At the surface of the Sun, the rotational velocity at the equator is different from that near the poles, and the outer loop would explain this (but the SSM would not). The full explanation of ^{7}Li depletion is convincing but complicated and is given in the above references or more fully, in Charbonnel [37]. The loops will carry matter and hence cause mixing which will lower the central temperature. The meriditional circulation will also cause turbulence - this turbulence will significantly reduce the matter transport, but will in its turn cause some mixing. These effects need to be include in a new model of stellar evolution which would tend to give lower neutrino fluxes.

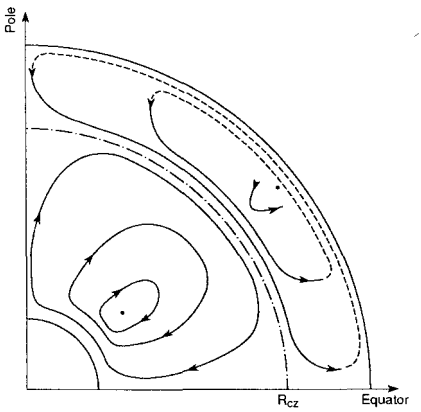

Figure 4: Map of meridional circulation patterns in the Sun [37].

It is natural to identify the boundary between the loops as that of the Convective Zone at R_{cz}. If one looks at the what happens when two rivers with differently coloured water, merge, it may be seen that there is surprisingly little mixing - i.e. the boundary forms an almost impenetrable layer. Also it may be noticed that the inner boundary of the inner loop could be the boundary of a possible core, R_c. These two subjects will be discussed below with helioseismology.

2.4 Helioseismology

The Sun's surface has been observed to vibrate with periods of about 5 minutes. These oscillations are explained as p-waves for pressure (or acoustic) waves which occur in the resonant cavity formed between the Sun's surface and an inner radius Several million such waves are expected to exist and several thousand have been observed with exceptional accuracy. In addition g-waves (g for gravity) are expected to exist but have not been observed though new projects using satellites, such as GOLF, are expected to give first results.

The observations of p-waves have been analyzed and compared with models in two ways. Firstly by comparing the frequencies where generally good agreement has been obtained by Guenther et al. [20] and by Turck-Chieze et al. [8]. Secondly inversion calculations have been done to deduce the velocity of sound, c, as a function of the radius, R. Results from Turck-Chieze and Lopez [18] are shown in Fig. 1b where it can be noticed that there is a discontinuity at $R = 0.713 \pm 0.003\ R_O$ which is interpreted as the boundary of the Convective Zone, R_{cz}. A sharp rise is seen at very small radii, marked as R_c - it will be discussed later as to whether this could be evidence for a core. With certain assumptions, the temperature can be deduce as a function of the radius and generally good agreement is obtained.

Thus helioseismology can be considered as a very important confirmation of the Solar Evolutionary Model but in future it will provide input data to new generations of models. The central region of the Sun is only investigated by oscillations with low l (the waves are classified as harmonics with three numbers, l, m, and n) and therefore results in the central region must

still be treated with caution, but if gravity waves can be studied, then the central region will be fully investigated.

2.5 Does the Sun have a Core?

When the Sun was first formed from a gaseous cloud, it was spinning very quickly and lost angular momentum by its solar wind - it was a T Tauri star. The model calculations found it had a core which gradually decreased with time and it was generally considered to have vanished after a short time, about 100 million years. The solar wind is now very small, 10^{-14} M_O per year. showing that angular momentum loss is now unimportant. Looking at the meridional circulation pattern deduced for the necessity to fit the ^{7}Li depletion results from all star, shown in Fig. 4, it is possible to consider that there is a small residual core. The helioseismological results shown in Fig. 1b indicate a marked variation of the sound speed at small radii, less than 0.1 R_O. This result could be interpreted as a convective core or as unexpected mixing effects. However other helioseismological results, in particular, the frequencies, are inconsistent with calculations [38] assuming that there is a core. So it probably best to neglect the possibility of a core until more experimental results, especially from gravity waves, are available.

2.6 Choice of Reference Model

When comparing experimental results with theory, it is necessary to look at the various model calculations and choose one as a reference. In the past it has been a convention to chose the latest Bahcall et al. calculation for a variety of reasons and this was perhaps valid especially in view of his pioneering work and regular updates. However with a selection of 1992 models, one can choose more critically. The outstanding difference between Bahcall et al. [19] and the other models is the exceedingly small errors of the former. It can be seen from table 10 of Ref. 17, that the errors taken come almost entirely from experimental values so that the serious question of theoretical errors from many factors such as screening, choice of weak or intermediate coupling, choice of equation of state, etc, are neglected or underestimated. The work of the Nice group [17] is excellent but they offer such a choice of models that it could be confusing. The calculation of Turck-Chieze and Lopez [18] has still some problems - diffusion is not included but neither is meridional circulation with turbulent diffusion - these act in opposite directions and in first approximation balance [35]; also the value chosen for the ^{7}Be(p,γ)^{8}B rate is about 10% too high, but it has the most complete comparison with helioseismology. In conclusion would recommend that the model of Turck-Chieze et al. be taken as the reference model but with the ^{8}B neutrino flux lowered by 10%.

The 1992 values that they give [18] are (122.5 ± 7) SNU for gallium, (6.4 ± 1.4) SNU for Chlorine and (4.4 ± 1.1) 10^6 cm^{-2}s^{-1} for the water detector.

If one were to give the values preferred above i.e. to lower the latter two values by 10% and give 30% errors, then this gives for Chlorine, (5.8 ± 1.7) SNU and for the water detector, (4.0 ± 1.2) 10^6 cm^{-2}s^{-1}.

2.7 Errors

Whether there is a solar neutrino problem or not depends crucially on the estimates of the errors on the theory and on the experiments.

The question of the interpretation of the errors given on the theory values is controversial. Turck-Chieze and Lopez [18] write "We consider any theoretical error as a minimal error (absence of error on the assumptions of the calculation) and only indicative of the present status and of the occurring improvements. A statistical distribution is not justified for all sources of error, so it seems to us dangerous to use the "so-called" 1 or 3 sigma error." ..... "As all errors are not statistical errors, we believe that it is unjustified to multiply by 3 the error we suggest, in order to get a "3 sigma" error. as it has sometimes been done." On the other hand Bahcall wrote [39] "You can of course divide the errors I quote by three if you prefer dealing with effective 1 sigma errors". The basic problem of the errors on theoretical values is that some errors are well defined and some not. The models have hundreds of pieces of experimental input data which have fairly well-defined errors, but have have also theoretical uncertainties depending on the choice of the equation of state, of screening effects, etc. which are very difficult to quantify. It would be helpful if the theoretical errors were given in two parts, one from experimental input and the other some guesstimate of the pure theoretical uncertainties. At present the best recommendation is to take the errors of Turck-Chieze and Lopez [18] and remember that they say that these are minimal errors. As a consequence this means that if the value of

{ theory value- expt. value }

is say, N standard deviations then this should be interpreted as meaning less than or equal to N standard deviations.

3. FOUR SOLAR NEUTRINO EXPERIMENTS

3.1 Introduction

There are four experiments that are measuring solar neutrino fluxes. One, Kamiokande measures neutrino elastic scattering while the other three use a "radiochemical" technique where the neutrinos convert atoms of the target into a short-lived isotope which is extracted from the target mass and its decay measured. This is not easy as the target contains some 10^{30} atoms and the number of radio-active atoms extracted is only a few. These few decays are observed against a background which is estimated by continuing the counting for several months. As the problem of background is so severe, the four experiments are performed deep underground to reduce cosmic ray effects and in very clean conditions to reduce radioactivity from natural sources such as radon and from uranium, thorium etc in the materials.

3.2 Kamiokande

The elastic scattering of solar neutrinos on electrons in water is measured by detecting the Cherenkov light from the electron. The peak of events pointing in the direction of the Sun allows a clean distinction of the signal from the large background. Overall the Kamiokande experiment is large, well-funded and well-organized and the raw results are considered trustworthy.

For the Kamiokande II experiment [16] (1040 days of data taking), they find $(2.67 \pm 0.28).10^6$ $cm^{-2}s^{-1}$. Comparing with the Reference .Solar Model value [18] of $(4.4 \pm 1.1).\ 10^6$ $cm^{-2}s^{-1}$, this gives;

$$\text{Theory - Expt.} = (100 \pm 25)\% - (61 \pm 6)\% = (39 \pm 26)\%$$

that is a one and half standard deviation effect, which is not significant. If the preferred value had been taken the effect would have been less, (33 ± 31)%. It may be noted this is rather different from the result given in table 8 of Ref. 18 where the ratio Exp/Theory is taken and it is not too clear what the percentage is so that it is unclear as to the statistical significance. It is strongly recommended that the ratio Expt/Theory be not used but the result be expressed as

Theory - Expt

where 100% is defined as the theory value, so that the errors used are clearly presented.

The Kamiokande III experiment (395 days) gives a higher value; combining it with Kamiokande II gives [40] for 1435 days above a threshold of 7.5 MeV,

$$\text{Data/SSM} = 0.49 \pm 0.04 \pm 0.06$$

where SSM was taken as the Bahcall and Ulrich 1988 value of 7.9 SNU. To estimate the statistical significance of this, it should be noted that the error of the SSM value was not included. If one uses the above recommended Reference Solar Model of Ref. 18, this gives

$$\text{Theory - Expt.} = (100 \pm 25)\% - (64 \pm 6)\% = (36 \pm 26)\%$$

which is slightly less than a one and a half standard deviation effect.

The Kamiokande group plan to carry out some further calibration runs at the KEK accelerator.

3.3 The GALLEX Experiment

The GALLEX experiment is strong and well-organized. It started later than the SAGE experiment but was able to measure cleanly electrons down to about 1 keV so that unlike SAGE, they could also study the 10.3% of electrons of 1.2 keV from L-shell capture and also the 46% of electrons of about 1 keV from the K-shell which decay together with X-rays of about 9 keV. The result is that although they have less gallium, about 30 tons, than Sage, they have a higher counting rate. They generously acknowledge that they have benefited from the help given by the SAGE Collaboration.

From 15 runs each of about a month, they find [41] a neutrino rate of

$$83 \pm 19 \pm 8 \text{ SNU}$$

which is some 1.8 standard deviations less than the reference Solar model value.

3.4 The SAGE Experiment

The Soviet-American Gallium Experiment, SAGE pioneered the use of gallium as a target where ^{71}Ga decays to ^{71}Ge which has a half-life of 11.4 days and were the first to discover all the problems such as the ^{68}Ga being converted to ^{68}Ge by cosmic rays when the gallium was on the earth's surface - this created a major background problem and took considerable work underground for SAGE (and later for Gallex), to eliminate this dominating background. This was a difficult pioneering experiment. Finally in 1990, SAGE considered five of their runs to be satisfactory and presented their results at the Singapore conference [42] in 1990 and in a paper [43] in 1990. The results caused great excitement as it seemed that there were almost no

solar neutrinos - they gave a best fit value of 20 SNU and 90% confidence upper limit of 79 SNU which indicated major disagreement with all the Solar Models which predicted values in the range of 115 to 132 SNU. Normally the graph of the integrated count rate is published, however if one looks at the detailed differential spectrum (shown in Fig. 1 of Ref. 7a and Fig. 8 of Ref. 7b), it can be seen that the statistics are best described as ultra-low and of the five runs, three appear to give a negative neutrino flux. Now there is a controversy, as is frequent with ultra-low statistical analysis, as the SAGE group consider that negative numbers are non-physical and should be put to zero. Hence for them the five runs give two positive rates and three runs with rates of 0.0 SNU. Another interpretation would say that for some reason no counts were recorded and it is only by putting the three negative values to zero, that an overall positive value of 20 SNU is obtained - this can be seen by studying the differential plot of the counts.

In 1991, more runs were performed [44] and a value for these of (85 +22/-32 ± 20) SNU given. SAGE considered that these 1991 runs were not inconsistent with the 1990 runs so that it was justified to combine the two sets to give [45] a rate of (58 +17/-24 ± 14) SNU.

There was a difference in the analysis criteria in this new work. In 1970 the Chlorine experiment appreciated that a decay in their counter occurred at a point so that all the ions took about the same time to reach the wire so that the pulse had a sharp rise-time whereas if a cosmic ray passed through their counter, the ions produced were spread out along the trajectory and hence arrive at the wire at different times giving a slow rise-time for the pulse. Hence in 1970 the Chlorine experiment introduced a fast rise-time selection and considered it so important that they rejected their first three years of data for 1967 - 1970. Initially the SAGE experiment used the same criteria, but have now decided that they can include data without the rise-time selection.. Hence their 1990 data now includes a sixth run, May 1990, with 27 SNU and their 1991 data has five runs with fast rise-time selection and a sixth run, June 1991, with no selection. It is explained [46] that the June 1991 had low background and the May 1990 run quite high background. The effect of including these two runs is not statistically significant, increasing the 1990 data by about 1 SNU and lowering the 1991 value from 89 SNU [47] to 85 SNU.

There are two approaches to the interpretation of the SAGE data. It could be said that all 12 runs are consistent and the best fit is (58 +17/-24 ± 14) SNU. It could also be assumed that the 1990 run was a pioneering one and that the 1991 was a second generation one, hence one should take the best SAGE result as (85 +22/-32 ± 20) SNU or 89 SNU(no error calculated). It should be remarked that since the total number of counts above background is 25 for 12 runs, it is not surprising that all subsets are statistically consistent. Future running where they hope to measure also electrons down to one keV, will help.

3.5 Chlorine Experiment

After earlier trials, the Chlorine experiment was started by Ray Davis and co-workers in 1967. The ^{37}Cl is converted by neutrinos to ^{37}Ar. They have observed both the 11.4 day half-life of ^{37}Ar and the electrons of 2.8 keV as expected - this was the first evidence of neutrinos from the Sun and was a major confirmation of Solar Evolutionary Models - both major results.

The actual rate of solar neutrinos has been a subject of great interest as it has consistently been much lower than the theoretical estimates and it was this that gave rise to "the Solar neutrino problem". An early estimate in 1982 [48] gave less than one SNU, but the result has

increased with time being 2.05 ± 0.3 SNU [6] for 1970-84 and 2.53 ± 0.32 [49] for 1986-92. The latest value is 40% of the reference Solar model. The significance of this result is;

$$\text{Theory - Expt.} = (100 \pm 22)\% - (40 \pm 13)\% = (60 \pm 26)$$

which is a 2.3 standard deviation effect.

It has often been concluded that the Chlorine experiment is definitive significant evidence for a Solar Neutrino problem. However it can be seen that with a more careful choice of reference Solar Model which has reasonable though minimal, errors, the discrepancy is not as much as three standard deviations. Also it should be appreciated that there are a number of difficulties [see Ref. 7] with this pioneering experiment of which two are serious.

Firstly it was claimed for some years that there was an oscillation with a period of about 10 years which was in anti-coincidence with the solar sunspot number, and this was described [50] as a five-standard deviation effect. As the sunspots are a near-surface phenomenon and the neutrinos are produced deep inside the Sun and any signal would take some million years to propagate to the surface, this claim caused great surprise. However the Kamiokande experiment has shown [16, 40] strong evidence that there is no such effect and more recently the Chlorine experiment has reduced their estimate of the effect to two standard deviations. It is now generally considered that there is no sunspot correlation.

Secondly, the Chlorine value is in contradiction with the Kamiokande rate. While the Chlorine threshold at 0.83 MeV is much lower than the Kamiokande threshold of 7.5 Mev, in fact the neutrinos involved in both, are mainly those from ^{8}B with similar energies. This is because the $^{37}Cl(\nu,e)^{37}Ar$ reaction proceeds through excited states of ^{37}Ar and the main one, 62%, is at 5 MeV (see Ref. 51 for complete level diagram). Now it has been shown that it is possible to make the two results consistent but this requires some extraordinary assumptions and it is wiser to wait until more data are available.

Thus it is perhaps premature to conclude that the Chlorine experiment is definitely in contradiction with Solar Models in view of these problems.

3.6 The Fifth Experimental Result

It is well known by practioners that experiments with neutrinos are difficult since they have zero charge, zero or almost zero mass, and have very small reaction cross sections. A surprisingly high number of neutrino experiments have turned out to be qualitatively wrong and even more have seen their numbers corrected by more than three of their standard deviations. In particular, pioneering neutrino experiments have a very high problem rate. This statement that pioneering neutrino experiments, while admirable, have a high problem rate, should be considered as an experimental result established with adequate statistics.

4. EXPERIMENTAL CONCLUSIONS

It has been shown above that none of the four experiments reported so far, are definitively in significant disagreement with the reference Solar Evolutionary Model. It may also be noted that first generation experiments are further from model values than second generation experiments (Kamiokande, GALLEX, SAGE 1991). If one takes into consideration the Fifth Experimental Result that pioneering neutrino experiments have been found to have

frequent need for re-considering their numerical values, then the evidence for any disagreement is weakened.

Both the SAGE and GALLEX experiments have decided to calibrate their rates by using a neutrino source of about a million curies. It is hoped to perform these two experiments in late 1994 and major conclusions may have to await these important calibrations.

On the other hand it is noteworthy that all four experiments find values which are less than the model values. This could be an indication that the first generation Solar Evolutionary Model are too simple and need modification to include new features. Also it may indicate that the temperature near the centre of the SUN is too low - such a hypothesis is weakly supported by the helioseismological result shown in Fig. 1b where the inferred sound velocity is different from expectations at radii less than 0.1 R_0.

5. CONCLUSIONS

It is concluded that relatively simple stellar evolutionary models have been remarkably successful in explaining many features of the Sun and other stars. However over the last 40 years considerable progress has been made and second generation models with more parameters are required to explain more complicated features that are now being measured such as light element abundances in stars, magnetic fields etc. Another progress is the realization that errors on the solar neutrino fluxes are larger than previously thought - this has greatly reduced the significance of any discrepancy between theory and experimental rates. At present no single experiment is seriously in discrepancy with model predictions, though the fact that they are lower than the model values may suggest that the central temperature is too high as is mildly indicated by helioseismological analysis. Several of the present experiments are increasing their data significantly and there are many new major experiments being prepared such as SuperKamiokande, SNU, Icarus and Borex, which will greatly increase the data-taking rate. Further it may be possible to measure the neutrino energy so accurately that different Solar reactions can be individually measured as proposed by Ypsilantis et al. [52].

Thus while there is no clear evidence for a Solar Neutrino Problem today, the Sun is our nearest star and it is essential that we study it as well as possible because of the information that it yields can be used generally in Astrophysics.

ACKNOWLEDGEMENTS

It is a pleasure to acknowledge many helpful dicussions, in particular with Drs. J.N. Bahcall, T. Bowles, C. Charbonnel, J. Christensen-Darmsgaard, G.N. Garvin, A. Mader, M.H. Pinsonneault, M. Spiro, A. Suzuki, Y. Totsuki, S. Turck-Chieze, D. Vignaud, and J.F. Wilkerson, though the responsibility for the content is the author's.

REFERENCES

[1] M Schwarzchild et al. Astrophys. J., **125** (1957) 233.

[2] J.N. Bahcall, Phys. Rev. **124** (1961) 495.

[3] R. Davis, Phys. Rev. Lett. **12** (1964) 303.

[4] B. Pontecorvo, Chalk River report, P-D205, 1946.

[5] J.N. Bahcall and R. Davis, Appendix to Ref. 6.

[6] J.N. Bahcall, "Neutrino Astronomy', CUP, 1989.

[7] a) D.R.O. Morrison, Intl. J. of Mod. Phys. **D1** (1992) 281;
b) Particle World, **3** (1992) 30.

[8] S. Turck-Chieze et al., to be publd. Physics Reports, Saclay Report, SAp 1993/4, 1993.

[9] E. Boehm-Vitense, Z. Astrophys. J. **46** (1958) 108.

[10] E. Anders and N. Grevesse, Geochim. Cosmochim. Acta **53** (1989) 197.

[11] L.B. Da Silva et al., Phys.Rev. Lett. **69** (1992).

[12] D.B. Guenther, Nature, **359** (1993) 585.

[13] F.J. Rogers and C.A. Inglesias, Astrophys. J. Suppl. **79** (1992) 507.

[14] J.N. Bahcall and R.K. Ulrich, Rev. Mod. Phys. **60** (1989) 297.

[15] S. Turck-Chieze et al. Astrophys. J. **335** (1988) 415.

[16] K.S. Hirata et al. Phys. Rev. Lett. **63** (1989) 16; **65** (1990) 1297; **65** (1990) 1301; Phys. Rev. **D44** (1991) 2241.

[17] P Morel et al., "inside the Stars", Vienn, 1992 and to appear, 1992.

[18] S. Turck-Chieze and I Lopez, "Inside the Stars", Vienna, 1992, Saclay report, SAp 1992/64, to appear in Astrophys. J. (1993).

[19] J.N. Bahcall and M.H. Pinsonneault, to be publd. Rev. Mod. Phys. 1993.

[20] D.B. Guenther et al. Astrophys. J. **387** (1991) 377.

[21] D Courtaud et al. Solar Phys. **128** (1990) 49.

[22] R.W. Kavanagh et al. Bull. Am. Phys. Soc.

[23] B.W. Filiponne et al., Phys. Rev. Lett. **50** (1983) 412; Phys. Rev. **C28** (1983) 2222.

[24] A. Baldini et al., Landold-Bornstein New Series, vol. 12a and 12/b (1988); V.V. Ezhala et al., Vol. 14 (1992), Springer-Verlag, Berlin,

[25] C.W. Johnson et al., Astrophys. J. **392** (1992) 320.

[26] M. Gai, priv. comm.

[27] N. Stone, Astrophys. J. **260** (1982) L87.

[28] A.S. Eddington, "The Internal Constitution of the Stars", CUP, (1926).

[29] E. Schatzman, J. Phys. et Rad. **9** (1948) 46; "White Dwarfs", North Holland Publ. (1958).

[30] P.D. Noerdlinger, Astron. Astrophys., **57** (1977) 407; J. Wambganss, Astron. Astrophys, **205** (1988) 125; A.N. Cox et al., Astrophys. J. **342** (1989) 1187.

[31] C.R. Proffitt and G. Michaud, Astrophys. J. **380** (1991) 238.

[32] A.M. Boesgaard and M.J. Tripicco, Ap. J. **303** (1986) 724.

[33] C. Charbonnel and S. Vauclair, sub. to Astron. Astrophys. (1992).

[34] P. Charbonneau and G. Michaud, Astrophys. J. **334** (1988) 746.

[35] S. Vauclair, Astrophys. J. **335** (1988) 971.

[36] C. Charbonnel et al. Astron. Astrophys. **255** (1992) 191.

[37] C. Charbonnel, Thesis, Universite de Toulouse III (1992).

[38] F. Betrix, Diplome, EPFL, Lausanne, 1993

[39] J.N. Bahcall, Ref. 6, page 38.

[40] Y. Totsuka, Texas/PASCOS conference, Berkeley, Dec. 1992.

[41] GALLEX, P. Anselbaum et al., Phys.Lett. **B285** (1992) 376 and 390.

[42] V.N. Gavrin, High Energy Physics Conf., Singapore 1990

[43] V.N. Gavrin, Phys. Rev. Lett. **67** (1990) 3332.

[44] V.N. Gavrin, High Energy Phys. Conf., Dallas 1992.

[45] T. Bowles, Moriond Conference, Jan./Feb. 1993, Villars.

[46] J.F. Wilkerson, priv. comm.

[47] T. Bowles, priv. comm.

[48] See Ref. 6, p319.

[49] See Ref. 18, table 8.

[50] See Ref. 6 p. 329 and R. Davis, Proc. Informal Conf. on Status and Future of Solar neutrino Research, BNL report no. 50879, Vol.1 p1, 1987.

[51] A. Garcia et al., Phys. Rev. Lett. **67** (1991) 3654.

[52] T. Ypsilantis, priv. comm.

[53] J. Christensen-Dalsgaard et al, "Seismology of the Sun and Sun-like Stars", ed. E. Rolfe ESA SP-286 p 499, 1988.

GALLEX : RESULTS, STATUS AND FUTURE

Th. STOLARCZYK

DAPNIA, Service de Physique des Particules
C.E. Saclay, 91191 Gif-sur-Yvette, France

for the GALLEX collaboration[1)]

Abstract : The GALLEX collaboration has now taken solar neutrino data for 22 months. The first set of data, GALLEX I, corresponding to the detection of solar neutrinos from May 1991 to April 1992, has been fully analyzed and lead to a production rate of 82 ± 17 (stat.) ± 8 (syst.) SNU which represents about 65% of the value predicted by standard solar models (around 124-132 SNU). Data taking is going on, while the collaboration is now preparing the crucial probe of the experiment with a 2 MCi ^{51}Cr neutrino source.

1. Purpose of the experiment

GALLEX detects solar neutrino using the ß-inverse reaction $\nu_e + {}^{71}Ga \rightarrow {}^{71}Ge + e^-$, where the neutrino interaction is signed by the decay of the ^{71}Ge atoms ($\tau = 16.49$ d) in a small proportional counter. The very low threshold of the reaction (233 keV) is such that GALLEX has the opportunity to study two main aspects of the solar physics. First the hypothesis of hydrogen fusion: if this hypothesis is correct the fusion of hydrogen into helium in the deep solar interior should begin by the $p + p \rightarrow {}^2H + e^+ + \nu_e$ reaction, a very slow reaction governing the hydrogen burning, constraining most of the solar luminosity and leading to the so-called ν_{pp} neutrinos, the lowest energy and most abundant neutrinos produced in the sun (91% of the total neutrino flux). The energy endpoint of the ν_{pp} neutrinos is 420 keV thus explaining the necessity of a very low threshold reaction for the detection.

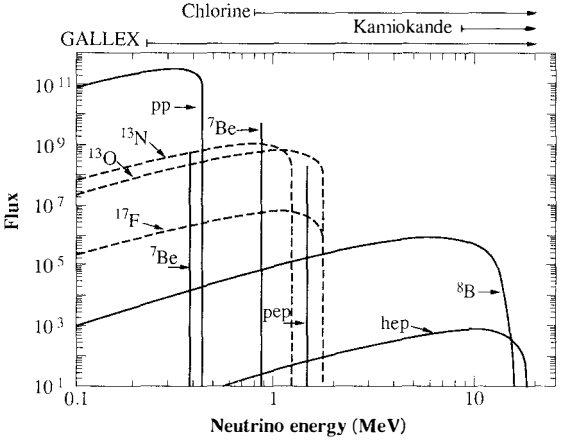

Fig.1 : The solar neutrino spectrum. The fluxes are expressed in $cm^{-2}.s^{-1}.MeV^{-1}$ except for the monoenergetic lines ($cm^{-2}.s^{-1}$).The detection thresholds of GALLEX, the chlorine experiment and Kamiokande are shown at the top of the plot. One can see the importance of the ν_{pp} flux compared to the other sources (from [2])

But GALLEX is also sensitive to more energetic neutrinos produced in secondary solar reactions: Standard Solar Models [3,4,5] (SSM) predict that the GALLEX signal comes for 54% from ν_{pp}, for 26% from $\nu_{^7Be}$ (produced in $^7Be + e^- \rightarrow {}^7Li + \nu_{^7Be}$ reactions, leading to 2 lines at 383 keV and 861 keV), for 11% from $\nu_{^8B}$ (produced in

the $^8B \rightarrow {}^8Be + e^+ + \nu_B$ reactions, energy up to 14 MeV), the remaining 9% consisting in fluxes produced in minor processes, dropped for our discussion. The solar neutrino spectrum is shown on figure 1.

The second topic of importance for GALLEX is the confrontation of its results with the chlorine and Kamiokande results, which have lead to the so-called "solar neutrino problem". The chlorine experiment has now claimed a depletion of the ν_B and ν_{Be} neutrinos for 25 years. The measured flux lies between 28% and 35% of the predictions of the solar models [6]. This fact has been confirmed by Kamiokande since 1987 (despite the fact that Kamiokande is sensitive only to ν_B): only $\approx 50\%$ of the predicted flux is detected [7].

2. Description of the experiment

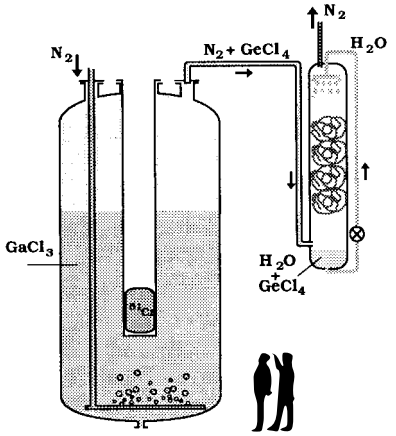

Fig.2 : Simplified scheme of the GALLEX tank ($70\,m^3$) and extraction facility (view of the main tank with the thimble which will receive the chromium source).

The target is in the form of a $54\,m^3$ gallium-chloride solution containing 30.3 tons of natural gallium (see figure 2). According to SSM, solar neutrinos should produce roughly 1.2 ^{71}Ge atom per day among the 10^{29} ^{71}Ga atoms of the solution (natural gallium is composed of 39.9% of ^{71}Ga and 60.1% of ^{69}Ga). The production rate is so low that all the experimental process has to be maintained in conditions of extremely low background.

An exposure to the Sun lasts 3 or 4 weeks after which around 15 or 20 atoms are present in the solution. To measure the ^{71}Ge extraction efficiency, ≈ 1 mg of pure non-radioactive germanium isotope is added at the beginning of each exposure.

The germanium inside the solution is in the form of $GeCl_4$ which has the particularity to be very volatile in an acidified medium. $2000\,m^3$ of pure nitrogen are circulated inside the tank to carry out the germanium. Then we proceed to a gas-water exchange in a scrubber, the $GeCl_4$ being very soluble in a neutral medium. At the end of the extraction the few solar neutrino produced atoms plus the carrier are concentrated in

some ten liters of water. This solution is concentrated again as a 1 liter solution which is brought on a synthesis line where the $GeCl_4$ is converted into a gas, the germane (GeH_4), using tritium-free chemicals. After a chromatographic process removing all impurities like natural air components or radon, the GeH_4 is pushed inside a small proportionnal counter. The final counting gas is obtained by adding old xenon, which lead to a 30%GeH_4-70%Xe gas mixture at 1 atm.

The counters are all similar (6.4mm diameter, 32mm length, 1 cm^3 total volume) and are made of hyperpure Suprasil quartz [8]. They have an iron or a silicon cathode (in that last case, made from single silicon-crystals) and a 13 µm diameter tungsten anode. The proportion of gas inside the actual counting volume is roughly 87%. Once the proportional counter has been filled, it is imbedded in its lead box, fitted into the preamplifier box and transported into a large shield tank in a Faraday cage. There ^{71}Ge decays will be observed: they consist in two peaks at 1.17 keV and 10.37 keV corresponding respectively to the L- and K-electronic capture of ^{71}Ge toward ^{71}Ga. The shield tank is fitted with 8.6 tons of lead. Two sliding-end doors, also filled with lead, are attached to a flexible air lock design with glove boxes to enable counter change without venting the low-radon atmosphere inside. We can simultaneously operate eight "active" counter lines positioned in the well of a NaI-pair spectrometer at the front end of the shield tank (for gamma anti-coincidences) and sixteen "passive" lines positioned in a low radioactivity copper block at the opposite end.

A Tektronix (R7912) fast transient digitizer serves for complete pulse shape analysis for background reduction. The data are handled by CAMAC oriented electronics, electrically decoupled from a MicroVax and its periphery via optical fibre link. Inserting the newly filled counter into the counting shield requires run-stop for all lines. The foil-sealed door is opened and the counter box is inserted through an air lock without venting. After connection to the respective line cables, it is calibrated with a Gd-Ce X-ray source (see below) on a little bench inside the tank shield and then inserted into its counting position. The operating voltage is roughly 1600 V.

During routine periods, tank interventions occur approximately every 3 weeks, the normal run sequence, and each time many counters are at work since we normally count for up to 6 or even 8 months. We have then made it a routine to calibrate half of the counters at each enforced interruption, thus normally every six weeks a counter is recalibrated.

For energy calibration, we use X-ray fluorescence induced on xenon in the counting gas by quartz-penetrating 35 keV Ce-X-rays which are excited from cerium by europium X-rays from the EC-capture decay of a ^{153}Gd source (half life 242 d) [9]. This has the great advantage that the whole active volume is illuminated and that three lines are available at the very relevant energies of 1.03, 5.09 and 9.75 keV, to be compared with the Ge-decay lines at 1.17 keV (L peak) and 10.37 keV (K peak).

3. Signal analysis

Experiments made with counters filled with $^{71}GeH_4$ have permitted to derive the spectrum characteristics of any counters used for the detection of ^{71}Ge produced by solar neutrinos. The average counting efficiencies of the counters, defined as the part of events being at ± FWHM around the peaks (what we called the "energy windows"), are respectively 30.6% and 35.2% for L and K peak. Hence the overall counting efficiency is 65.8%. Test runs in Gran Sasso have shown that on the passive side the counter background is only 0.04 count per day in the L window and 0.02 count per day in the K window (these values are slightly larger on the active side).Once energy selection has been made, the fast transient digitizer signal which records the pulse shape in the counter allows to discriminate background events from good candidates. Indeed background events, like electrons from Compton scattering or alpha particles, lead to an extended track inside the counting gas and therefore to a slow signal. On the contrary ^{71}Ge decays leads to Auger electrons which have a very small path (<1 mm at 10 keV) corresponding to a fast signal. Good candidates are defined using the value of the rise-time between 10% and 70% of the signal amplitude, and are located in windows defined by comparison with calibrations and the $^{71}GeH_4$ filled counter experiments. These cut efficiencies for ^{71}Ge decays are respectively 97.7% and 95% for L and K windows. This set of good candidates has then to be cleaned from events in coincidence with a signal in the NaI crystal (for active side) and from events which may be due to the radon decay chain (see details in [10]). On figure 3 are plotted the energy spectra of selected events for various time cuts (first, second and between

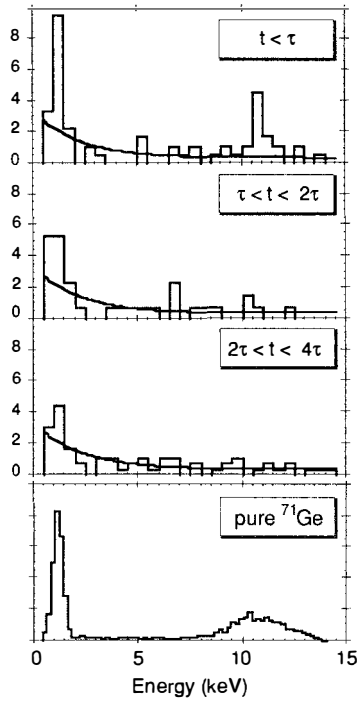

Fig.3 : Behaviour of the energy spectrum of selected events with time (Number of events per 5 days of counting per exposure x 10^2 for the first 3 plots, arbitrary unit for the last plot).

second and fourth ^{71}Ge life-time). One sees very clearly an accumulation of counts in K and L regions which vanishes with time.

Finally the number of ^{71}Ge produced in the solution is obtained from a maximum likelihood method. The likelihood function is composed of:

1) two time-constant backgrounds (one for K and one for L),

2) an exponentially decreasing term $\propto a_{71} e^{-t/\tau_{71}}$ corresponding to the ^{71}Ge decay,

3) an exponentially decreasing term $\propto K_{68} e^{-t/\tau_{68}}$ corresponding to the decay of the few residual ^{68}Ge atoms ($\tau_{68} = 415$ d) extracted from the solution, which were produced at the ground level at the early stages of the experiment[10]. The amplitude of this contribution has been measured to be $K_{68} = 3.6$ ^{68}Ge atoms released per day from the solution at the time of the first exposure used for the analysis and is decreased with the time at which exposures are performed.

Figure 4 shows the time distribution of selected events on which is superimposed the τ_{71} life-time fitted by the maximum likelihood analysis.

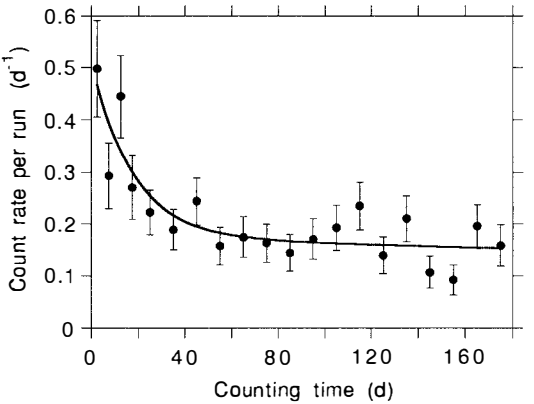

Fig. 4 : Time distribution of selected events (dots) and fitted distribution from the maximum likelihood analysis ($\chi^2 = 20.1$ for 18 degrees of freedom, namely 30% of confidence level).

4. Results and implications

The result of the maximum likelihood analysis has to be corrected for background cut inefficiencies and side reaction contributions. Separated measurements with counters filled with radon show that the radon time cuts used for event selection cover 90% of the cases. Independent analysis show that this inefficiency lead to a correction of

2 ± 1 SNU*. ^{69}Ge isotopes can be produced in the solution by side reactions (see below). The contribution coming from ^{69}Ge which could have been considered as good ^{71}Ge decays is 1 ± 1 SNU. Then, one has to remove the ^{71}Ge production rate due to side reactions. In that case ^{71}Ge atoms are mainly produced via ^{71}Ga(p,n)^{71}Ge reaction (threshold: 1.02 MeV). Protons are either produced in the hadronic showers due to high energy cosmic muon nuclear interactions (muon flux ≈ 1 m^{-2}.h^{-1}) in the solution, or by fast neutron scattering on the atoms of the solution. The first contribution has been evaluated after measurement of the ^{71}Ge production rate in a CERN muon beam and is equal to 3.7 ± 1.1 SNU [11]. The contribution of fast neutrons inside the tunnel, whose flux is continuously monitored by a calcium nitrate detector, has been calculated to be only 0.15 ± 0.10 SNU [11].

Finally one has to substract from the signal the contribution of U, Th, Ra in the solution which is also very low, less than 0.2SNU.

Therefore the maximum likelihood result has to be reduced by 7SNU.

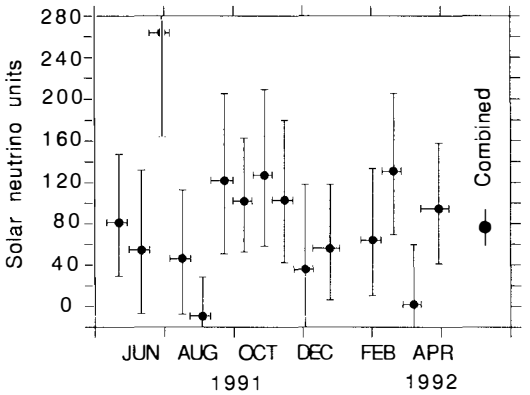

Fig. 4 : Results for the 15 individual runs and the combined analysis (7 SNU correction taken into account) for data taken between May 14th, 1991 and April 29th, 1992.

After 15 solar neutrino exposures (324 days) between May 14th, 1991 and April 29th, 1992 and the equivalent of 7 years of quasi-uninterrupted counting ($\approx$ 15x7 months, counting stopped on November 2nd, 1992) the measured solar neutrino production rate is 0.8 ^{71}Ge atom produced per day inside the solution, namely 82 ± 17(stat.) ± 8 (syst.) SNU (68% C.L.), which corresponds to ≈ 75 ^{71}Ge atoms

* 1 SNU corresponds to 10^{-36} neutrino capture per second per target atom

detected. Systematical errors take into account 5.5 SNU for the ^{68}Ge correction uncertainty, 1.8 SNU for the side reactions and 4.3 SNU for various efficiencies. On figure 4 are shown the results for the individual runs.
The predicted production rates are 132 SNU, 125 SNU and 128 SNU for respectively Bahcall et al.[3], Turck-Chièze et al.[4] and Berthomieu et al.[5]. Namely GALLEX detects only 65% of the predicted signal (2σ). The *first order conclusion* is that GALLEX has for the first time detected the full ν_{pp} flux, thus confirming the hypothesis of the hydrogen fusion in the sun core, and a depletion of roughly one third of the high energy part of the solar neutrino spectrum ($\nu_B + \nu_{Be}$) as claimed by the two previous experiments (chlorine and Kamiokande).

The SAGE result for its last period (1991) is in good agreement with GALLEX ($85^{+22}_{-32} \pm 20$ SNU) and its combined result ($58^{+17}_{-24} \pm 14$ SNU), taking into account the first period of counting in 1990 [12] ($20^{+15}_{-20} \pm 32$ SNU), is compatible within 1σ. The statistical significance of the data spreading and the comparison with Sage result is discussed elsewhere in these proceedings [13].
The three experimental results could be matched either by a $\approx 5\%$ solar center temperature reduction or by assuming matter enhanced neutrino oscillations (MSW effect). The first assumption seems difficult to be tuned with respect to the solar model present status. The second assumption would lead, in the case of pure $\nu_e \rightarrow \nu_\mu$ oscillations, to two possible regions for neutrino mass difference and mixing angle : $\Delta m^2 \approx 10^{-5}$ eV^2 and $\sin^2 2\theta \approx 4.10^{-3}$ or $\sin^2 2\theta \approx 0.8$ [14].

5. Status of the experiment

The exact GALLEX result has important implications on our understanding of the fusion processes in the Sun and on neutrino properties. Therefore it is essential to reduce the statistical uncertainty.
The neutrino exposure period GALLEX II started on August 19th, 1992, after transfer of the target solution from the emergency tank to the main tank. This tank has an improved sparging capability and is equipped with a thimble which will permit the chromium source experiment. Since this date, 8 solar neutrino runs have been performed and are now counting. As the first preliminary data come in, they support our results from GALLEX I and most importantly indicate no surprises following the transfer of the solution to a completely different and improved tank arrangement. In particular, after the transfer, 8 technical runs were performed to test our understanding of a tailing ^{68}Ge release discussed in [10]. In these runs the target solution was heated and then cooled in order to measure the release rates of any ^{68}Ge.

The release rates basically conform to our model predictions and thus support our approach to the correction utilized in GALLEX I.

6. Future : the source experiment

The source experiment will be a crucial probe of the validity of the extraction efficiency and more generally of the whole GALLEX process. It will be done using a 1.9 MCi ^{51}Cr artificial neutrino source (τ=40.4 d, $^{51}Cr + e^- \rightarrow {}^{51}V + \nu_e$) producing neutrinos similar to ν_{Be} produced in the Sun ($E_\nu(90\%) = 746$ keV and $E_\nu(10\%) = 426$keV). This source will be installed in the thimble of the main tank. It will be obtained after neutron irradiation in the Grenoble Siloe reactor [15] of 40kg of ultra-pure chromium, enriched at 38% in ^{50}Cr ($n + {}^{50}Cr \rightarrow {}^{51}Cr + \gamma$).
11 kg of chromium have already been received. The first irradiation will be done around May 1994 : after two months of exposure, 190 ^{71}Ge atoms will have been produced, to be compared to the $\approx$75 ^{71}Ge atoms detected so far. A second irradiation is planned for middle of 1995. End of 1995, after 3 full years of counting, GALLEX will have detected about 300 ^{71}Ge decays which will lead to a statistical uncertainty of less than 10% on the solar neutrino flux.

References :

1) The GALLEX collaboration : P.Anselmann, W.Hampel, G.Heusser, J.Kiko, T.Kirsten, E.Pernicka, S.Pezzoni, R.Plaga, U.Rönn, M.Sann, C.Schlosser, H.Völk, R.Wink, M.Wójcik, *Max-Planck-Institut für Kernphysik (MPIK), Postfach 103980, D-6900 Heidelberg, Germany* - R.v.Ammon, K.Ebert, T.Fritsch, K.Hellriegel, E.Henrich, L.Stieglitz, F.Weyrich, *Institut für Heiße Chemie, Kernforschungszentrum Karlsruhe (KFK), Postfach 3640, D-7500 Karlsruhe, Germany* - M.Balata, E.Bellotti, N.Ferrari, H.Lalla , *Laboratori Nazionali del Gran Sasso (LNGS), S.S. 17/bis Km 18+910, I-67010 L'Aquila, Italy* - C.Cattadori, O.Cremonesi, E.Fiorini, L.Zanotti, *Dipartimento di Fisica, Università di Milano e INFN, Via Celoria 16, I-20133 Milano, Italy* - F.v.Feilitzsch, R.Mößbauer, U.Schanda, *Physik Department E15, Technische Universität München, James-Franck Straße, D-8046 Garching b.München, Germany* - G.Berthomieu, E.Schatzman, *Université de Nice-Observatoire, B.P.139, F-06003 Nice Cedex, France* - I.Carmi, I.Dostrovsky, *Department of Isotope Research, The Weizmann Institute of Science, P.O.Box 26, 76100 Rehovot, Israel* - C.Bacci, P.Belli, R.Bernabei, S.D'Angelo, L.Paoluzi, *Dipartimento di Fisica dell'Università Tor Vergata e INFN, Via*

Carnevale, I-00173 Roma, Italy - S.Charbit, M.Cribier, G.Dupont, L.Gosset, J.Rich, M.Spiro, Th.Stolarczyk, C.Tao, D.Vignaud, *DAPNIA/SPP, CE Saclay, F-91191 Gif-sur-Yvette Cedex, France* - R.L.Hahn, F.X.Hartmann, J.K.Rowley, R.W.Stoenner, J.Weneser, *Department of Chemistry, Brookhaven National Laboratory, Upton, NY 11973, USA.*

2) Neutrino Astrophysics, J.N.Bahcall, Cambridge University Press, 1989

3) J.N.Bahcall and M.H.Pinsonneault, Rev. of Mod.Phys. 64(1992)885
J.N.Bahcall and R.K.Ulrich, Rev. of Mod.Phys. 60(1988)297

4) S.Turck-Chièze et al., Astrophys.J. 335(1988)415
S.Turck-Chièze and I.Lopes, Astrophys.J., May 1993

5) G.Berthomieu et al., Astron.Astrophys. 268(1993)775

6) R.Davis et al., Proc. 21th ICRC, Vol.12, p.143, Protheroe ed., Univ. of Adelaide Press, Adelaide, Australia, 1990

7) K.Hirata et al., Phys.Rev.Lett. 65(1990)1297 and Phys.Rev. D44(1991)2241

8) R.Wink et al., to be published in Nucl.Instr. and Meth. A

9) Th.Stolarczyk, GALLEX Internal Note GX4, January 1992
A.Urban, Thesis, TU München, 1989

10) P.Anselmann et al., Phys.Lett. B285(1992)376

11) Th.Stolarczyk, PhD Thesis, Université de Paris-Sud, October 1990

12) A.I.Abazov et al., Phys.Rev.Lett. 67(1991)3332
T.J.Bowles, these proceedings

13) M.Spiro, these proceedings.

14) P.Anselmann et al., Phys.Lett. B285(1992)390

15) M.Cribier et al., Nucl.Instr. and Meth. A265(1988)574

PRESENT STATUS OF SAGE

Thomas J. Bowles
(for the SAGE Collaboration*)
Physics Division, MS D449
Los Alamos National Laboratory
Los Alamos, New Mexico 87545

ABSTRACT

A radiochemical ^{71}Ga-^{71}Ge experiment to determine the primary flux of neutrinos from the Sun began measurements of the solar neutrino flux at the Baksan Neutrino Observatory in 1990. The number of ^{71}Ge atoms extracted from 30 tons of gallium in 1990 and from 57 tons of gallium in 1991 was measured in twelve runs during the period of January 1990 to December 1991. The combined 1990 and 1991 data sets give a value of 58 +17/-24 (stat) ± 14 (syst) SNU. This is to be compared with 132 SNU predicted by the Standard Solar Model.

INTRODUCTION

A fundamental problem during the last two decades has been the large deficit of the solar neutrino flux observed in the radiochemical chlorine experiment[1] compared with the Standard Solar Model (SSM) theoretical predictions[2],[3]. Recent results of the Kamiokande II water Cherenkov experiment[4] have confirmed this deficit. These results may be explained by deficiencies in the solar model in predicting the ^{8}B neutrino flux or may indicate the possible existence of new properties of the neutrino.[5] The role new neutrino properties may play in the suppression of the solar neutrino flux[5] can be determined by a radiochemical gallium experiment. An experiment using ^{71}Ga provides the only feasible means at present to measure low energy solar neutrinos produced in the proton-proton (p-p) reaction[6]. Exotic hypotheses aside, the rate of the p-p reaction is directly related to the solar luminosity and is insensitive to alterations in the solar models. An observation in a gallium experiment of a strong suppression of the low energy solar neutrino flux requires the invocation of new neutrino properties.

THE BAKSAN GALLIUM EXPERIMENT

Extraction Procedure

The experimental layout as well as the chemical and counting procedures have been described previously and are only briefly outlined here.[7]

Each measurement of the solar neutrino flux begins by adding approximately 700 μg of natural Ge carrier equally divided among the reactors holding the gallium. After a typical exposure interval of 1 month, the Ge carrier and any ^{71}Ge atoms that have been produced by neutrino capture are chemically extracted from the Ga using the following procedure. A weak HCl solution is mixed with the Ga metal in the presence of H_2O_2 which results in the extraction of Ge into the aqueous phase. The extracted solutions from the reactors are combined and reduced in volume by vacuum evaporation. Additional HCl is then added and an Ar purge is initiated which sweeps the Ge as $GeCl_4$ from the acid solution into 1.2 liters of H_2O. The Ge is then extracted into CCl_4 and back extracted into 0.1 liters of low-tritium H_2O. The counting gas GeH_4 (germane) is then synthesized and purified by gas chromatography. The extraction efficiency is measured at two stages of the extraction procedure by atomic absorption analysis. The final determination of the quantity of

germanium is made by measuring the volume of synthesized GeH_4. The overall extraction efficiency is typically 80 ± 6%.

Counting Procedure

The GeH_4 is then mixed with a measured amount of Xe and inserted into a low-background proportional counter. The proportional counter (with a volume of about 0.75 cm^3) is placed in the well of a NaI detector inside a large passive shield and counted for 2-4 months. ^{71}Ge decays by electron capture to the ground state of ^{71}Ga with an 11.4 day half life. The low-energy K- and L-shell Auger electrons and X-rays produced during electron shell relaxation in the ^{71}Ga daughter atom are detected by the proportional counter. Pulse shape discrimination based on rise time measurements is used to separate the ^{71}Ge decays from background. The energy, amplitude of the differentiated pulse, and any associated NaI signal are recorded for each event in the counter.

The counter is typically calibrated at one month intervals using an external ^{55}Fe source. The K-peak acceptance window is then determined by extrapolation from the ^{55}Fe peak. The extrapolation procedure was verified by filling a counter with $^{71}GeH_4$ together with the standard counter gas.

EXTRACTION HISTORY

The experiment began operation in May, 1988 when purification of 30 tons of Ga commenced. The large quantities of long-lived ^{68}Ge (half life = 271 days) produced by cosmic rays while the Ga was on the surface were removed. New extraction procedures were implemented beginning with the January 1990 extraction which resulted in the elimination of radon contamination in the extractions.

Monthly extractions were carried out from January through July of 1990 with sufficiently low backgrounds to begin measurements of the solar neutrino flux. The May run had no rise time information which was lost due to electronic problems. Although the resulting high background gave essentially no sensitivity to the solar neutrino flux, the May run is shown here for completeness. The extraction sample for the June run was lost due to a vacuum accident.

Useful solar neutrino data were not obtained after the July 1990 run due to a Cr engineering test run. Following completion of the test run, a total of about 30 tons of new

Ga were purified, the gallium used in the previous solar neutrino runs was removed and the chemical reactors were extensively cleaned, and then the chemical extraction system was carefully cleaned. Separate extractions of the new and old Ga were carried out in June and July 1991. Rise time information was lost for the June run due to unstable electronics, but the background was still sufficiently low that a measurement of the solar neutrino flux could be made. Beginning in August 1991, combined extractions of the old and new Ga were begun. The run from October 1991 was lost due to a counter failure.

MEASUREMENT OF THE SOLAR NEUTRINO FLUX

Statistical Analysis

Results from measurements carried out in 1990 and 1991 are reported here. Earlier data taken during 1989 are not presented here due to the presence of radon and residual ^{68}Ge.

The data analysis selects events that have no NaI activity in coincidence within the ^{71}Ge K-peak acceptance window. The K-peak acceptance window in energy is a 2 FWHM wide energy cut centered on the K-peak and the inverse rise time cuts are 95% acceptance. A maximum likelihood analysis[8] is then carried out on these events by fitting the time distribution to an 11.4-day half-life exponential decay plus a constant rate background. Table 1 shows the results of the maximum likelihood analysis.

Table 1. Statistical analysis of runs.

Extraction Date	Ga Mass (Tons)	Best Fit (SNU)	N_W^2	68% CL (SNU)	Probability
Jan 24, 90	28.7	0	0.367	60	9%
Feb 28, 90	28.6	39	0.310	83	13%
Mar 29, 90	28.5	90	0.035	175	96%
Apr 20, 90	28.4	0	0.060	94	81%
May 22, 90	28.3	79	0.073	204	73%
Jul 24, 90	21.0	0	0.250	149	19%
Jun 28, 91	27.4	8	0.142	100	41%
Jul 23, 91	27.4	27	0.079	131	70%
Aug 25, 91	49.3	300	0.050	421	96%
Sep 23, 91	56.6	48	0.064	91	79%
Nov 22, 91	56.3	75	0.088	131	65%
Dec 20, 91	56.2	93	0.037	147	95%
Combined 1990 and 1991		**58**	**0.094**	**80**	**61%**

The data from each of the twelve extractions are shown in Figure 1, which shows the integral plot of events versus time within the ^{71}Ge K-peak acceptance window. In this figure, the value of the curve is incremented by one count every time an event occurs and thus shows the time distribution of ^{71}Ge-like events. The best fit line to each data set is shown by the dashed line. The Smirnov-Cramer-Von Mises parameter N_W^2 provides a measure of the goodness of fit[9], which is independent of the binning of the data. For this parameter, it is expected that 50% of the fits should have values greater than 0.119, and 50% less than 0.119. (In some sense, one can consider a N_W^2 value of 0.119 as being analogous to a χ^2 value of 1.0.) The probability that a measurement would exceed the value of N_W^2 determined for each of the runs is also given in Table 1.

Systematic Effects

The systematic uncertainties in the chemical extraction and counting efficiencies were typically 6% and 10%, respectively, corresponding to a 7 SNU uncertainty.

The systematic uncertainty in extrapolating the inverse rise-time cuts is estimated using a cut that includes all events not in coincidence with the NaI counter which are within the energy cut of the K-peak acceptance window with no cut made on inverse rise time. This results in an uncertainty of 9 SNU (68% CL) for the combined 1990 and 1991 data.

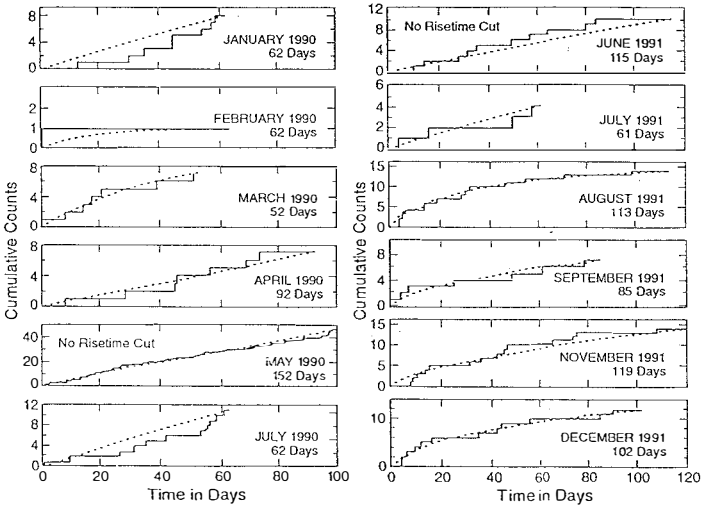

Figure 1. Data from the 1990 runs (final) and 1991 runs (preliminary).

In the 1990 data set in which there was an apparent increase in the background at late counting times (see figure 1) for some runs. The uncertainty in background determination under the ^{71}Ge decay curve due to possible time variations of the counter background was checked in a number of ways[10]. All tests are consistent with the hypothesis that the apparent increase in background at late times is purely a statistical fluctuation. However, such a fluctuation could suppress the signal by causing an overestimation of the background at early times. In order to minimize any assumptions, an uncertainty for any possible time variation of the background for the 1990 data was assigned to be 30 SNU (68% CL). A possible time variation of the background was checked for in the 1991 data and the combined 1990 and 1991 data and none was found. As there is no evidence for any time variation in the 1991 or the combined 1990 and 1991 data, it is assumed that the background is constant in time and no systematic uncertainty is assigned for a possible time variation in the background to the combined 1990 and 1991 data sets.

The final possible systematic effect is due to possible background reactions which could produce ^{71}Ge and the possible presence of radon, which can mimic a ^{71}Ge signal. The total background production rate in 30 tons of liquid gallium metal of all germanium activities has been calculated to be less than 2.5% of the SSM production rate[7], resulting in an uncertainty of 3 SNU (68% CL). The data has been examined to search for a possible presence of radon. Checks included looking at overflow events, looking outside of the K-peak acceptance window, looking for delayed coincidences of events, and fitting the data to allow for both ^{71}Ge and radon. A systematic uncertainty for the presence of radon of 8 SNU (68% CL) was assigned.

RESULTS

The results[10] of the analysis of the five runs with rise time selection in the 1990 data indicated a flux of solar neutrinos of only 20 SNU (statistically one sigma above zero). However, the large systematic uncertainties of a possible time variation of the background led to an upper limit of the ^{71}Ga capture rate of 79 SNU (90% CL). With the additional data from 1991, it appears that the the increased count rates at late times observed in some of the runs were simply statistical fluctuations. Monte Carlo simulations of the data indicate that both the 1990 and 1991 data are statistically distributed as expected with a central value of 58 SNU.

For the combined 1990 and 1991 data, the rate was determined to be:

^{71}Ga Capture Rate = 58 + 17/-24 (stat) ± 14 (syst) SNU.

This assumes that the extraction efficiency for ^{71}Ge atoms produced by solar neutrinos is the same as that measured using natural Ge carrier. This corresponds to 24 counts assigned to ^{71}Ge decay, compared to the SSM prediction of 55 counts.

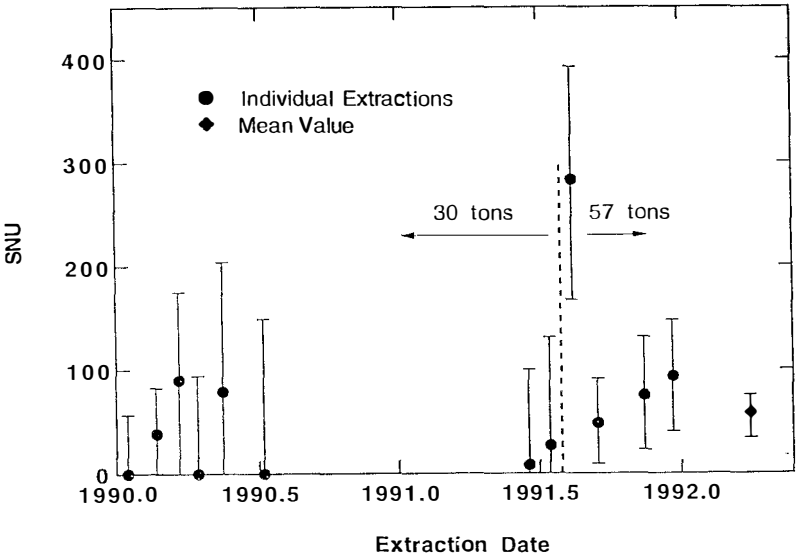

Figure 2. Best fit values and 1-σ uncertainties for each of the runs during 1990 and 1991, together with the best fit value and 1-σ uncertainty for the combined 1990 and 1991 data.

EXTRACTION EFFICIENCIES

While all available information leads one to expect that the extraction efficiency for ^{71}Ge atoms produced by solar neutrinos should be the same as for the carrier, it is important to test this assumption. A test to search for possible losses in the extraction of ^{71}Ge atoms was carried out by doping the Ge carrier with a known number (6555 ± 359) of ^{71}Ge atoms. The doped carrier was added to one of the reactors holding 7 tons of gallium, three successive extractions were carried out, and the number of ^{71}Ge atoms in each extraction was determined by counting. The overall chemical extraction efficiency was

determined to be 101 ± 5%, while that for the ^{71}Ge was 99 + 6/-8%, indicating that the extraction efficiency of the natural Ge carrier and ^{71}Ge track closely.

The measurement with the ^{71}Ge doped carrier does not test for possible losses which might occur during the formation process. In inverse beta decay, the resultant ^{71}Ge atom may be in an excited state and in some fraction, the ^{71}Ge atom is ionized. It is possible, albeit very unlikely, that these excitations may drive some chemical reaction which may result in the ^{71}Ge atom being tied up in a chemical form which we cannot efficiently extract. That atoms which have been produced in excited states can be extracted from metallic gallium has been demonstrated at some level during the cleanup of the gallium, as we efficiently extracted in excess of 99.9% of the cosmogenic ^{68}Ge.

We are currently carrying out a set of measurements in which we look at beta decay of Ga isotopes in the gallium. In the sudden impulse approximation, atomic excitations of an atom during beta decay should be the same as those in inverse beta decay. In this experiment, we have taken a few grams of gallium from the reactors and then chemically removed all of the residual Ge carrier. The gallium was then irradiated to form several μg each of ^{70}Ga and ^{72}Ga by (n,γ) reactions. The ^{70}Ge and ^{72}Ge subsequently decay to stable ^{70}Ge and ^{72}Ge with half-lives of 21.1 minutes and 14.1 hours, respectively. The gallium metal is kept liquid (in order to simulate conditions in the solar neutrino runs) and allowed to sit for a few weeks so that all of the ^{70}Ga and ^{72}Ga has decayed. The stable ^{70}Ge and ^{72}Ge are then extracted from the irradiated gallium using the same procedure as in the full scale solar neutrino runs. Both the absolute amounts of ^{70}Ge and ^{72}Ge and their ratio are determined by mass spectroscopy. Preliminary results show the efficiencies for ^{70}Ge and ^{72}Ge to be 98% and 92%, respectively, with uncertainties of ± 10%. Thus, it appears that ^{70}Ge and ^{72}Ge are formed in the amounts expected.

Finally, an experiment using a neutrino source is planned in order to test the overall extraction efficiency in situ. A suitable neutrino calibration source can be made using ^{51}Cr, which decays with a 27.7 day half-life by electron capture, emitting monoenergetic neutrinos of 751 keV (90.2% BR) and 426 keV (9.8% BR). An engineering test run with a lower-intensity ^{51}Cr source was carried out during the fall of 1990. A full-scale calibration run is scheduled for 1994 using a 1-MCi ^{51}Cr source.

CURRENT STATUS AND FUTURE PLANS

With the combined 1990 and 1991 data sets, SAGE is observing a signal consistent with ^{71}Ge produced by solar neutrinos. The first results from SAGE, and the data from 1991 appear consistent taking into account the systematic uncertainties. The combined data sets show a good overall fit to a value of 58 SNU. However, these results are still based on limited statistics and assume that the extraction efficiency for ^{71}Ge atoms produced by solar neutrinos is the same as that measured using natural Ge carrier. It is clearly necessary to accumulate more data with higher signal to noise and better efficiencies, as well as to test the extraction efficiency with a ^{51}Cr artificial neutrino source.

Intensive work has been carried out to reduce noise pulsing and backgrounds in the L peak. Preliminary data indicates that beginning with the September 1992 run, we are able to count the L peak, which will almost double our counting efficiency.

Preparations are also underway to fully calibrate the system using an artificial ^{51}Cr source. We expect to be able to carry out this experiment in 1994.

Finally, we are continuing to study possible systematic effects from the data, including additional studies of possible background sources and Monte Carlo simulations.

CONCLUSIONS

Different SSMs predict that the total expected capture rate in ^{71}Ga to be in the range[2), 3)] of 125 to 132, with the dominant contribution (71 SNU) coming from the p-p neutrinos. The minimum expected rate in a Ga experiment, assuming only that the Sun is presently generating nuclear energy at the rate at which it is radiating energy, is 79 SNU[5)]. Observation of significantly less than 79 SNU in a gallium experiment is difficult to explain without invoking new neutrino properties.

The first measurements from a gallium solar neutrino experiment have observed fewer ^{71}Ge atoms than predicted by the SSM. From the 1990 and 1991 data, we observe only 44% of the predicted flux. Assuming the extraction efficiency for ^{71}Ge atoms produced by solar neutrinos is the same as for natural Ge carrier, the first measurements indicate that the flux may be less than that expected from p-p neutrinos alone.

ACKNOWLEDGEMENTS

The SAGE collaboration wishes to thank A.E. Chudakov, G.T. Garvey, M.A. Markov, V.A. Matveev, J.M. Moss, S.P. Rosen, V.A. Rubakov, and A.N. Tavkhelidze. We are also grateful to J.N. Bahcall, Yu. Smirnov, and many members of the GALLEX collaboration for useful discussions. We acknowledge the support of the Russian Academy of Sciences,, the Institute for Nuclear Research, the Ministry of Sciences of the Russian Federation, the Division of Nuclear Physics of the US Department of Energy, the National Science Foundation, Los Alamos National Laboratory, and the Univ. of Pennsylvania.

* The SAGE Collaboration: O.L. Anosov, E.L. Faizov, V.N. Gavrin, A.V. Kalikhov, T.V. Knodel, I.I. Knyshenko, V.N. Kornoukhov, I.N. Mirmov, A.V. Ostrinsky, A.M. Pshukov, A.A. Shikin, P.V. Timofeyev, E.P. Veretenkin, G.T. Zatsepin, *Institute for Nuclear Research of the Russian Academy of Sciences*, T.J. Bowles, S.R. Elliott[#], J.S. Nico, H.A. O'Brien, D.L. Wark[##], J.F. Wilkerson, *Los Alamos National Laboratory*, B.T. Cleveland, R. Davis, Jr., K. Lande, *University of Pennsylvania*, M.L. Cherry, *Louisiana State University*, R.T. Kouzes[###], *Princeton University*

[#]Present Address: L-421, Lawrence Livermore National Laboratory, Livermore, CA 94550
[##] Present address: Dept. of Particle and Nuclear Physics, Oxford University, Keble Road, Oxford, OX1 3RH, England
[###]Present address: Batelle Pacific Northwest Laboratories, P.O. Box 999, Richland, WA 99352

REFERENCES

1) R. Davis et al., Proc. 25th Int. Conf. on High Energy Physics, edited by K.K. Phua and Y. Yamaguchi, (World Scientific, Singapore, 1991), p. 667
2) J.N. Bahcall and R. Ulrich, Rev. Mod. Phys. **60**, 297 (1988).
3) S. Turck-Chieze, S. Cahen, M. Casse, and C. Doom, Ap. J. **335**, 415 (1988).
4) K.S. Hirata et al., Phys. Rev. Lett. **65**, 1297 (1990).
5) J.N. Bahcall, Neutrino Astrophysics, Cambridge University Press, 343 (1989).
6) V.A. Kuzmin, Sov. Phys. JETP **22**, 1051 (1966).
7) V.N. Gavrin et al., Proc. of "Inside the Sun", Conference, Versailles, edited by G. Berthomieu and M. Cribier (Kluwer Academic, Dordrecht, 1989), p. 201.
8) B.T. Cleveland, Nucl. Instrum. Methods **214**, 451 (1983).
9) A.W. Marshall, Ann. Math. Stat. **29**, 307 (1958).
10) A.I. Abazov et al., Phys. Rev. Lett. **67**, 3332 (1991).

Radiochemical Solar Neutrino Experiments

JAMES RICH AND MICHEL SPIRO

DAPNIA, Service de Physique des Particules,
CE Saclay
F-91191 Gif-sur-Yvette Cedex

INTRODUCTION

This review will cover the three presently running radiochemical solar neutrino experiments, namely the Chlorine, SAGE and GALLEX experiments. It is mostly focussed on a discussion of statistical consistency checks of the data available to us.

THE CHLORINE EXPERIMENT

Since 1967 Davis [1] and co-workers have performed a pioneering experiment by extracting ^{37}Ar atoms created by the reaction $\nu_e + {}^{37}Cl \rightarrow {}^{37}Ar + e^-$, (threshold 814 keV) from a tank of 615 t of tetrachlorethylene C_2Cl_4. The steps in the experimental procedure (see figure 1) are:

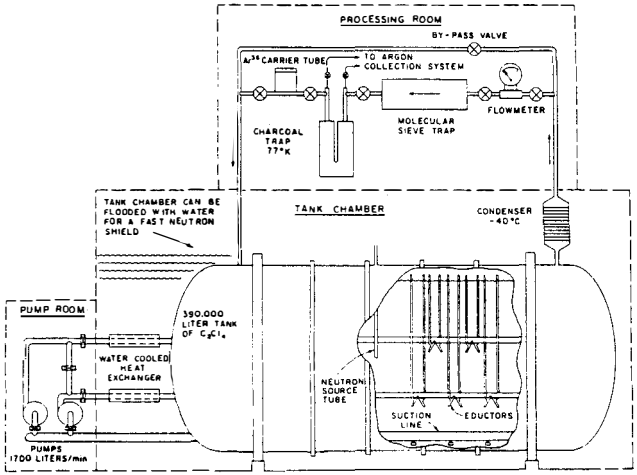

FIGURE 1. Schematic view of the Chlorine experiment [1].

1. At the beginning of a run approximately 0.2 cm^3 of either ^{36}Ar or ^{38}Ar is added to serve as a carrier.

2. The tank is exposed for the desired length of time (about 80 days).

3. After exposure, the argon (carrier and produced ^{37}Ar) is removed by circulating a large quantity of He through the tank. The argon is then separated from the helium in a charcoal trap cooled to the temperature of liquid nitrogen where argon is absorbed.

4. The Argon is transferred from the heated charcoal trap to a line where it is purified and its volume is measured (recovery efficiency measurement). It is then loaded into a small (0.3 - 0.5 cm^3) proportional counter along with tritium-free methane which serves as a counting gas.

5. The sample is counted for approximately 8 months and often longer.

6. The carrier yield is verified by mass spectroscopy of the argon.

The ^{37}Ar decays by electron capture: $^{37}Ar + e^- \rightarrow {}^{37}Cl + \nu_e +$ X rays . The resulting hole in the K shell can give X rays and Auger electrons with a total energy of 2.5 keV. The counter is designed to measure these electrons. They show up in a rise-time versus energy window (fig.2) since we expect these events to be fast (point like ionization) and with a well defined energy. The half life of the decay is 35 days. On the other hand the background due to radioactivity in the counter and shielding has flatter rise-time and energy distributions and occurs randomly in time.

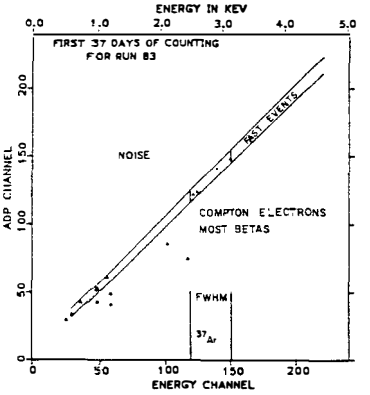

FIGURE 2. Plot of rise-time versus energy for the first counting period of run 83.

For the period 1970-1992 the data were analyzed to give about 600 counts of ^{37}Ar. This gives an uncorrected ^{37}Ar counting rate of about 6 events per run. The evidence for ^{37}Ar is striking. The energy distribution (fig.3a and fig.3b) obtained by combining all the runs (first 70 days of counting) show a clear peak which is absent when selecting the events which occur after 105 days). The time distribution (fig. 3c) of the events occuring in the peak region is clearly compatible with the ^{37}Ar lifetime plus a time independent background.

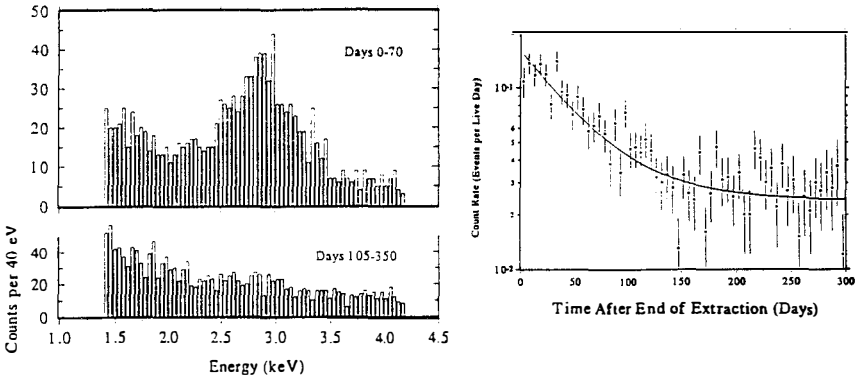

FIGURE 3. Energy spectra and time distribution showing evidence for ^{37}Ar production in the Chlorine experiment.a) Energy spectrum in the first two half lives after the end of extraction.b)Same after three half lives. c) Time distribution for the events in the energy - risetime window

The data are analyzed by a maximum likelihood method assuming a time independent background and a ^{37}Ar decaying component. The results are shown for each run in figure 4 which all together give the combined value: 2.3 ± 0.3 SNU.

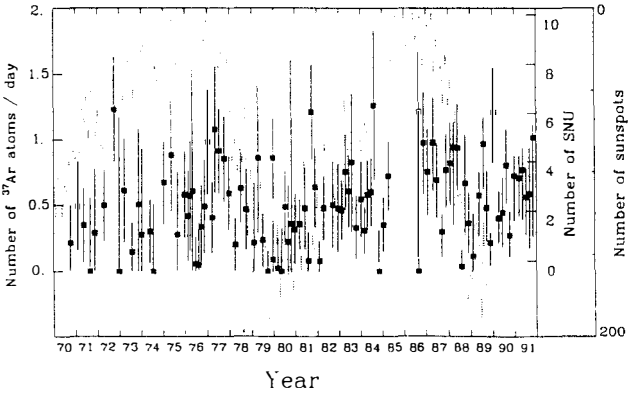

FIGURE 4. Results of the Chlorine experiment for all runs.

We have analyzed through Monte-Carlo simulations whether or not these data depart from statistical behaviour, by assuming a constant production rate of 0.5 ^{37}Ar atom per day. We take the background distribution, the efficiencies and the dead times roughly as they were observed in the actual experiment. In fig. 5 we plot the histogram of the production rate for individual runs as expected from this Monte-Carlo and compare it with the data (97 runs). The peaks at zero are due to negative values which occur due to statistic fluctuations and which are then forced to zero. To quantify the agreement, we compare the width of the two distributions (σ=.28 atoms for Monte-Carlo, σ=.32 for data). By running Monte-Carlo experiments of 97 runs, we estimate a 5% probability of finding a width of the distribution broader than that observed in the actual experiment. Our analysis shows then that at a 2σ level, there is no hint for a non poissonian behaviour of the data. We emphasize that our Monte-Carlo is very simple and ignores variations in experimental procedures or efficiencies that would widen the distribution.

It has often been claimed that the Chlorine data show a time dependence. Any significant time dependence of the production rate would have induced a significant increase of the width of the distribution through the convolution of the spread due to the time dependence and the spread due to to Poisson statistics. Quantitatively, the width of the experimental distribution is less than σ=0.36 ^{37}Ar production rate per day. We can then exclude any time dependence with a spread greater than 0.2 ^{37}Ar production rate per day or equivalently 1 SNU.

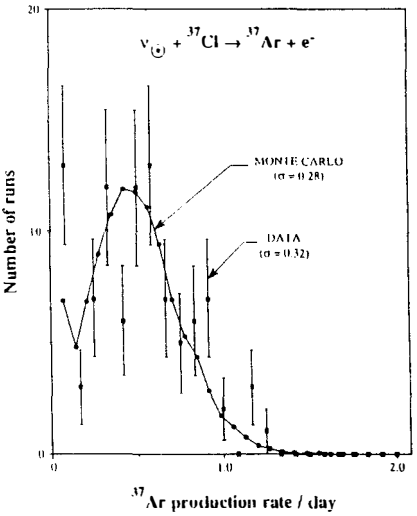

FIGURE 5. Comparison of the SNU distribution expected from Monte-Carlo and the measured one (97 runs of the Chlorine experiment).

It has been suggested in [2] that the time distribution for events in 6 runs where a low production rate was observed is not consistent with that expected for ^{37}Ar decay and a time independent background. The suspect distribution is shown in figure 6 along with that for 9 runs where a high production rate was observed. We have used the Smirnov-Cramer-Von Mises Nw^2 parameter together with the Monte-Carlo simulations to determine whether or not the two distributions are consistent with expectations. We find 6% confidence level for the high runs and 17% for the low runs which indicates again that there is nothing pathological with the time distributions of those runs.

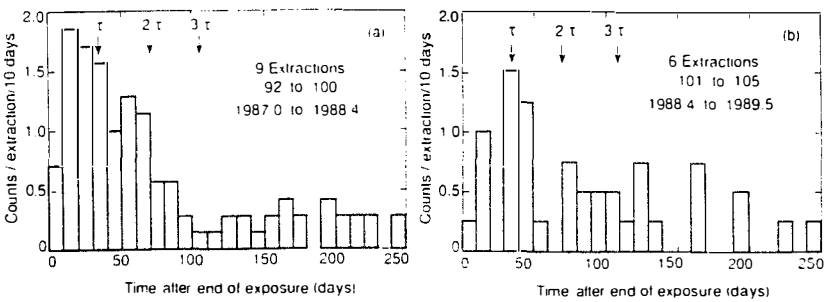

FIGURE 6. Time distribution for (a) the "high runs" and (b) the "low runs".

The result of the Chlorine experiment (2.25 ± 0.3 SNUs) , when compared to the predictions of the Sun Standard Models, which range from 6 to 8 SNUs [6], is the strongest evidence of the solar neutrino problem. It cannot be discarded easily since this experiment is probably the simplest of all solar neutrino experiments performed so far and since the statistical tests applied to this experiment do not show any evidence for something pathological. Moreover, according to our analysis, no individual runs can be discarded in view of statistical arguments, and the results of the chlorine experiment are compatible with a stable behaviour as a function of time at the 2.0 sigma level.

More recently, the Chlorine collaboration presented a new analysis of the data based on an energy weighting procedure. The final result does not change, but the results run per run do change. We cannot discuss here whether the new distribution agrees with Poisson statistics. This would have to be done by the Collaboration itself.

FIRST RESULTS OF THE GALLIUM EXPERIMENTS

Two experiments are now underway, SAGE in USSR which published the first results in December 1991 [3] and GALLEX in Italy, which published their first results in June 1992 [5]. The recipes are similar to that of the Chlorine experiment: introduce 1mg of inactive germanium in the 30t of Gallium, expose the Gallium to solar neutrinos in a low background environment, extract by a chemical method the solar ν-produced ^{71}Ge atoms together with the inactive Germanium, transform into a counting gas (GeH_4), fill a proportional counter and count the decays of ^{71}Ge (11.4 d half life). The main difference is that the SAGE experiment uses metallic liquid Gallium target while the GALLEX experiment uses acidic aqueous Gallium Chloride solution. This induces important differences in the chemistry.

SAGE

The Soviet-American Gallium Experiment is being performed by the Moscow-Los Alamos-Pennsylvania Collaboration. It is located in the Baksan Valley in the Caucasus mountains (Russia) under about 4700 meter water-equivalent of rock. The Gallium (now 60 tons) is in the form of of gallium metal contained in several tanks (7 tons each) equipped with stirrers and heaters that maintain the temperature above the melting point (29.8 C) (fig.7).

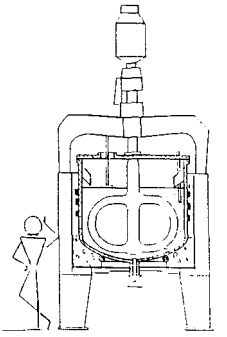

FIGURE 7. Schematic of SAGE

SAGE started to take data in January 1990 and presented results for the first five exposures during year 1990. The data used the first 30 tons of gallium target. The expected rate for 30 t target and 132 SNU is 1.2 ^{71}Ge atom created per day and the exposures last about 4 weeks. Taking into account all the efficiencies, one expect to observe only 3 desintegrations due to ^{71}Ge K electron capture ($^{71}Ge + K\ e^- \rightarrow {}^{71}Ga + \nu$ + X-rays + Auger electrons). Four of the runs had preferred values of 0 SNU. Altogether they published [3] an average result of 20 SNU, an upper limit of 55 SNU (68% C.L.) and 79 SNU (90% C.L.). More recently they announced the results they obtained in later runs when they increased the total mass of gallium from 30 to 60 tons [4]. This is shown on fig.8. A signal seems now to emerge. The preliminary value for a combined analysis of all runs is 58 ± 20 (stat) ± 14 (syst) SNU [4].

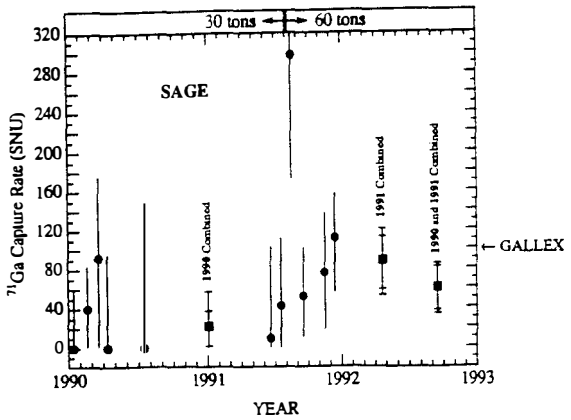

FIGURE 8. Results for all runs of the SAGE experiment.

Again, we have performed Monte Carlo simulations and compared the expected distribution of the number of SNU for individual runs to the measured one (fig. 9).

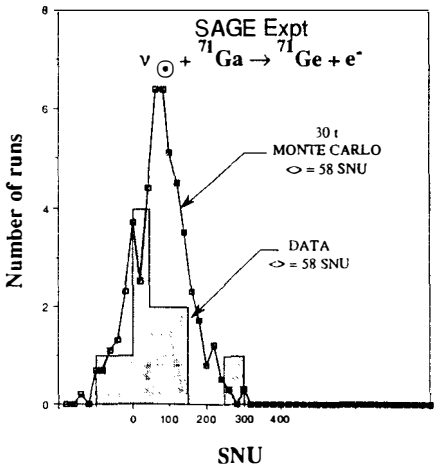

FIGURE 9. Comparison of the SNU distributionexpected from Monte-Carlo and the measured one (11 runs from SAGE).

The agreement is good. We have even performed Monte-Carlo experiments of 5 runs , like in the first publication of SAGE, and found that there is a 10% probability to find an average result lower or equal to 20 SNUs. This is due to the poor statistical

level reached so far by this experiment. This can be seen on fig.10 which shows the combined time distribution for all the runs. The excess at small times is the evidence for the signal which seems to emerge now. The number of excess events is around 25.

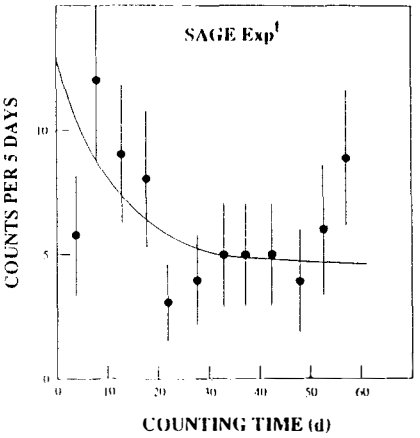

GALLEX

Gallex is located in the Gran Sasso Underground Laboratory in Italy and is being performed by the Heidelberg-Karlsruhe-Munich-Gran Sasso-Milano-Roma-Nice-Saclay-Rehovoth-Brookhaven collaboration. Fig. 11 shows a schematic view of the detector. The 30.3 tons of Gallium are in the form of a solution of $GaCl_3$ acidified in HCl. The Ge atoms form the volatile compound $GeCl_4$. At the end of 3 weeks exposures, these molecules are swept out by bubbling a large flow of gas (N_2) through the solution. A concentration step is then followed by a transformation of the $GeCl_4$ into GeH_4. A small amount of given stable isotope of germanium is added as a carrier in the tank before each run. Its purpose is twofold: to check the extraction efficiency and to be used as the counting gas which fills a small (1 cm^3) proportional counter.

The small proportional counters are made with ultrapure material and have been built specially for this experiment. The experiment is sensitive to both K-shell and L-shell electron captures in the decay of ^{71}Ge atoms. Seven counts (for 132 SNU) are then expected after each run, in the K and L regions. The data used in the analysis consist of 14 runs taken from May 1991 to May 1992. They are now published [5]. There is compelling evidence for a signal: the peaks in energy at 1.2 keV and 10 keV for L and K electron capture are seen, the 11.4 half life of ^{71}Ge is well identified over a flat background (Fig.12) both for the combined energy spectrum and time distribution of all runs. Fig. 13 shows the results for all runs together with the combined result of 83 ± 19 (stat) ± 8 (syst) SNU.

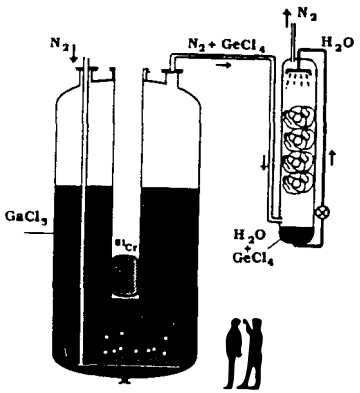

FIGURE 11. Schematic view of the GALLEX detector.

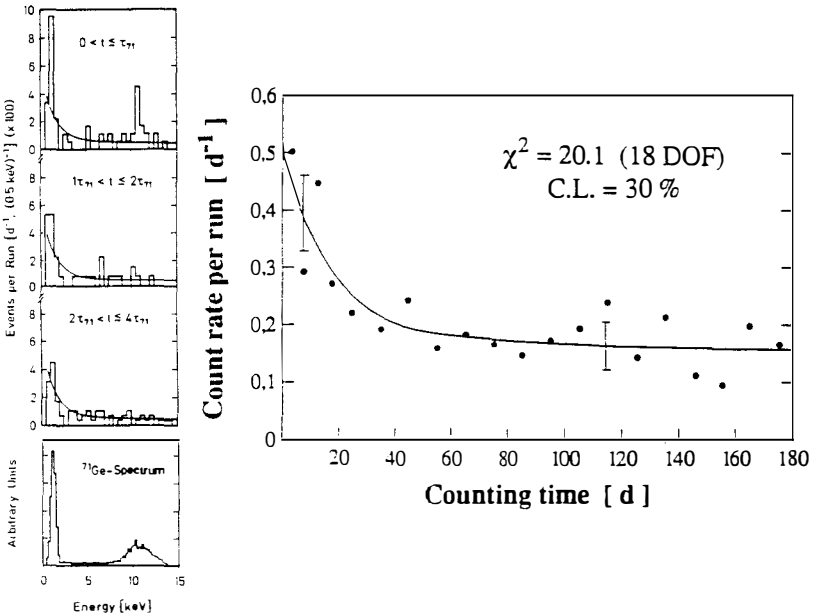

FIGURE 12. Energy spectra and time distribution showing evidence for a L and K peak signal in the GALLEX experiment. a)energy spectrum in the first mean life of ^{71}Ge after the end of extraction. b)energy spectrum for events occuring between one and two mean lifetimes. c)energy spectrum for events occuring after two mean lifetimes. d)measured energy spectrum for a ^{71}Ge calibration sample. e) time distribution of all events in the K and L windows

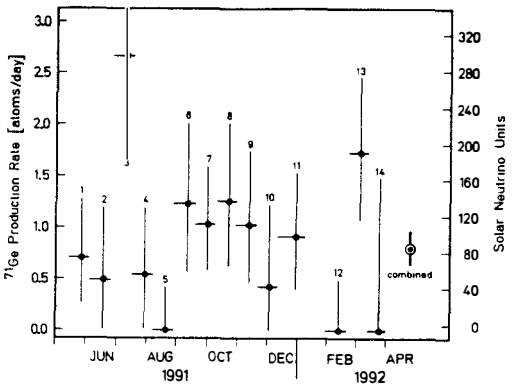

FIGURE 13. Results of the GALLEX experiment for all runs.

Here also, the Monte-Carlo expectations on the distribution of the number of SNU for individual runs and for the data agree (fig. 14).

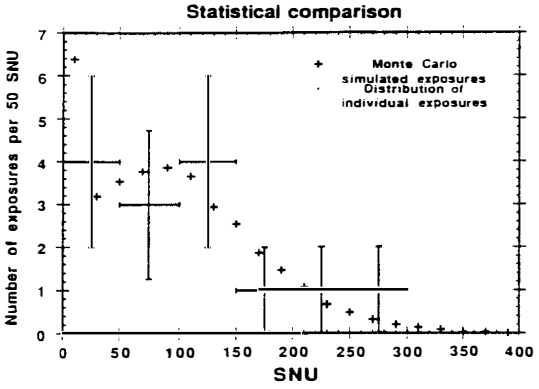

FIGURE 14. Comparison of the SNU distribution expected from Monte-Carlo and the measured one (14 runs) for GALLEX

We have also performed extensive Nw^2 analyses to verify that the time distributions of individual runs are consistent with that expected for ^{71}Ge decay and background. The Nw^2 distribution for all runs is compared with Monte-Carlo distribution (Fig. 15).

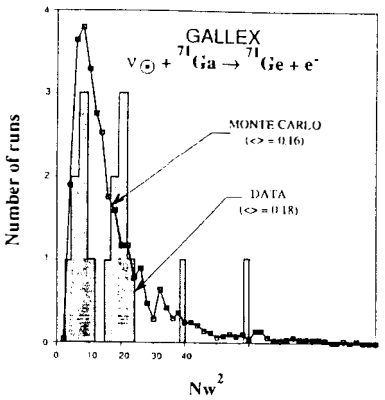

FIGURE 15. Comparison of Monte-Carlo Nw^2 distribution and the measured values.

By performing Monte-Carlo of the full experiment (14 runs, we compare the actual observed average Nw^2 to the expected average distribution. We find a 30% probability to find an average larger than the actual measured value. Finally we have recently completed GALLEX phase I, namely by adding SR15 and completing the counting time of SR1 to SR14. The result is stable: $82 \pm 17 \pm 8$ SNUs.

CONCLUSIONS

The chlorine radiochemical experiment is conceptually simple and shows no strong indication of any statistical anomalies. It still forms the basis of the solar neutrino problem. Each of the two gallium experiments shows internal statistical consistency. SAGE's recent preliminary results are consistent with the published GALLEX results. If this convergence is confirmed by a more definitive analysis, we would suggest that the combined result of the two gallium experiments, SAGE and GALLEX, (74 ± 15 SNU combining statistical and systematic errors) be used for comparisons with theoretical expectations.

AKNOWLEDGEMENTS

We thank B. Cleveland, K. Lande, M. Cribier and D. Vignaud for many helpful discussions and N. Lelièvre for helping to edit the manuscript.

REFERENCES

1. R. Davis et al. Phys. Rev. Let. **20** (1968) 1205
R. Davis et al., 1990 in Proc. Int. Conf. "Neutrino 90", Geneva
R. Davis et al., Proc. of the 21st Int. Cosmic Ray Conf., ed. by R.J. Protheroe, vol.12 p.143, (Univ. Adelaide)
K. Lande, Blois Conf. on Particle Astrophysics, June 1992, to be published in the proceedings.

2. D.R.O. Morrison, Particle World **3** (1992) 30.

3. A. I. Abazov et al., Phys. Rev. Lett. **67** (1991) 3332.

4. V. Gavrin, Blois Conf. on Particle Astrophysics, June 1992, and HEP International Conf., Dallas, August 1992.

5. P. Anselmann et al., Phys. Lett. **B285** (1992) 390.

6. J. N. Bahcall and R.K. Ulrich, Rev. Mod. Phys. 60 (1988) 297
J. N. Bahcall and M.H. Pinsonneault, Rev. Mod. Phys. 64 (1992) 28
S. Turck-Chièze et al., Ap. J. 335 (1988) 415
S. Turck-Chièze and I. Lopes, to appear in Ap. J., April 1993.

THE CURRENT STATUS OF SOLAR NEUTRINO OBSERVATION FROM KAMIOKANDE AND SUPER KAMIOKANDE

The Kamiokande Collaboration

Presented by;
Kenji Kaneyuki
Department of Physics, Tokyo Institute of Technology
O-okayama, Meguro-ku, Tokyo 152, Japan

ABSTRACT

The current status of Kamiokande solar neutrino observation is presented. The preliminary result based on 1040 + 395 live days of Kamiokande-II and Kamiokande-III gives the relative ^8B solar neutrino flux to the prediction of Standard Solar Model; $\frac{data}{SSM} = 0.49 \pm 0.04 \pm 0.06$. And there is no statistically significant time variation of solar neutrino flux observed in Kamiokande on the full solar neutrino observation period. And the current status of Super Kamiokande is also presented.

1 Introduction

The solar neutrino observation was started by Davis using the ^{37}Cl detector in 1969 [1]. And the large deficit in the observed neutrino capture rate to a theoretical one gives so-called "the solar neutrino problem". Now, there are four solar neutrino experiments in operation, Homestake, Kamiokande [2], SAGE [3] and Gallex [4], and the deficit in the observed neutrino flux to a calculated one by the standard solar model (SSM) [5] is reported by each experiment. Therefore the solar neutrino problem has remained unsolved and it has been one of the most interesting problems in elementary particle physics and astrophysics. A lot of solutions have been presented to explain this large discrepancy; modification of solar model, neutrino oscillations, magnetic moment of neutrinos and so on. However, more appreciation of the solar model as well as more experimental data are needed to solve this problem .

In Kamiokande, solar neutrinos are detected through the elastic scattering of a neutrino an the electron, therefore the threshold energy of solar neutrinos is higher than other radio chemical experiments. The energy threshold of the ^{37}Cl experiment is 0.814 MeV and ^{7}Be and ^{8}B neutrinos can be observed, and the Ga experiments can detect pp neutrino with an energy threshold of 0.233 MeV. However, Kamiokande have a big advantage to the solar neutrino observation. In the detector, neutrinos from the sun interact with electrons, and the recoil electrons emitting Čerenkov photons are detected on real time, and the direction and energy of the recoil electrons are determined event by event. The angular distribution of the recoil electrons with respect to the direction to the sun gives a clear peak of the signal against flat background, therefore the signal can be clearly distinguished from the background.

2 Kamiokande experiment

KAMIOKA nucleon decay experiment is a large ring-imaging water Čerenkov detector and started its operation in 1983 in search of nucleon decays. For the solar neutrino observation, the detector was upgraded in 1985 to lower the trigger threshold. A new electronics system was installed to measure timing information. An anti-counter surrounding the inner detector was constructed for vetoing of the external background, and the detector was also air-tighted for the reduction of background coming from ^{222}Rn. Thanks to these improvements, the solar neutrino observation could be started in January 1987 with an analysis threshold of 9.3 MeV.

The analysis threshold was then lowered to 7.5 MeV by the gain doubling of photomultiplier tubes after we accumulated the 450 live days of solar neutrino data. Kamiokande-II shut down for the replacement of dead photomultiplier tubes in April 1990 until when a total of 1040 live-day solar neutrino data was taken. And we restarted our solar neutrino observation with new electronics and a reflective mirror attached to each photomultiplier in December 1990. In this paper, the preliminary result is presented from the 395 live-day data in Kamiokande-III.

The Kamiokande-III detector is a 2140 ton water Čerenkov detector located 2700 m.w.e underground. The 948 20-inch photomultiplier tubes are set on the inner surface of the cylindrical inner detector, and inner tank is surrounded by the 4π solid-angle anti counter with 123 20-inch photomultiplier tubes for vetoing external cosmic rays and gamma rays from the rock. The fiducial volume of the solar neutrino analysis is defined to be 680 tons. The trigger threshold is set $\sim$ 5MeV for an electron with 50% efficiency. The energy of a low energy event is estimated by the number of photomultiplier tubes which detect Čerenkov photons. The energy calibration is made by 9MeV γ-rays from the $Ni(n,\gamma)Ni^*$ reaction. And the error in the absolute scale is estimated within 3%.

The improvements of the detector are replacement of electronics with a better timing resolution, higher light collection area due to a reflective mirror attached to each photomultiplier tubes, and better timing resolution of photomultiplier tubes which replace the dead photomultiplier tubes. The energy resolution in Kamiokande-III is 19% and position resolution is 1m at 10MeV for an electron compared with 20% and $1.1m$ respectively in Kamiokande II. The angular resolution is 28% for a 10 MeV electron because the angular resolution is limited by the Coulomb multiple scatterings in water.

3 Data analysis

Even with the large volume of detector, the event rate of solar neutrinos is as low as 0.8 events/day with 7.5MeV threshold. Therefore, the signal has to be selected from a overwhelming background such as external γ rays, β rays from ^{214}Bi, spallation products generated by energetic cosmic ray muons. The analysis chain of the solar neutrino observation in Kamiokande is as follows. First, low energy events are selected, and reconstructed using the timing and charge information, and the position, direction and energy of the events are determined. Then

the events in the fiducial volume are selected to remove external γ rays. Subsequently, the spallation products are eliminated using the timing and the spatial correlation of the low energy event with the preceding muons which generate the spallation products. Finally, the remaining external γ rays in the fiducial volume are removed using the directional information, because external γ rays come into fiducial volume normal to the detector surface. After these selections, a final sample of 1693 events is obtained during 395 days of detector live time in the Kamiokande-III. The trigger rate in Kamiokande-III is about 1Hz, among which, 0.37Hz comes the cosmic ray muons. The low energy event rate in the all detector volume with an energy threshold of 7.5 MeV is 380 events/day, 23 events/day after the fiducial volume cut, 6.8 events/day after the spallation cut and the event rate in the final sample is 4.3 events/day. Figure 1 shows the event rate at each reduction step as a function of recoil electron energy.

Figure 2 shows the event rate of the latest few month's data in the fiducial volume as a function of recoil electron energy in the Kamiokande-III compared with that of the first half year data in Kamiokande-III. The study of removal of low energy background has lowered the event rate, the event rate at the threshold of 7.5 MeV during the first half year of Kamiokande-III operation is equivalent to that at 7.0 MeV threshold in the latest few month's operation.

4 Result

Figure 3 shows an angular distribution of the final sample with an energy threshold of 7.5 MeV during 395 live days. A clear peak at $cos\theta_{sun} = 1$ and an isotropic background are seen, where θ_{sun} is the angle between the direction of an event and that from the sun. From this angular distribution and energy distribution of the recoil electrons, a relative ^8B solar neutrino flux is obtained as follows;

$$\frac{data}{SSM} = 0.55 \pm 0.07 \pm 0.06$$

where SSM is the central value calculated by Bahcall and Ulrich 1988, i.e., $\phi_\nu(^8B) = 5.8 \times 10^6 cm^{-2} sec^{-1}$, and the quoted errors are statistical and systematic, respectively. The solid line in this figure shows the prediction by Standard Solar Model, and the dashed line shows the best fit. This result is consistent with the Kamiokande-II result of $0.46 \pm 0.05 \pm 0.06$ within the statistical errors. The combined result of the Kamiokande-II 1040 live day data and the

Kamiokande-III 395 live day data gives;

$$\frac{data}{SSM} = 0.49 \pm 0.04 \pm 0.06$$

The ^{37}Cl experiment claimed an anti-correlation of sun spot number with the observed solar neutrino flux [6]. Figure 4 (a) shows the observed neutrino flux relative to SSM as a function of time, where each data point contains approximately 200 live-days data, while Figure 4 (b) shows the sun spot number as a function of time. From these figures, there is no statistically significant time variation of solar neutrino flux observed in Kamiokande during this period which includes both solar minimum and maximum periods.

5 Super Kamiokande

Super Kamiokande is a 50,000 tons water Čerenkov detector with 11200 20-inch photomultiplier tubes. In Super Kamiokande, significantly higher statistics with a better detector performance can be obtained than in the current Kamiokande. Now, the excavation of the detector site and production of 20 inch photomultiplier tubes are going on. The data taking will be started in April 1996.

Table 1 shows the summary of the detector performance of Super Kamiokande compared with Kamiokande-II. The improvement of the photomultiplier tubes and higher photosensitive coverage is essential to the improvement of detector. New 20 inch photomultiplier tubes to be developed for Super Kamiokande have a better timing resolution and a better charge response than the current 20 inch photomultiplier tubes, and the photosensitive coverage in Super Kamiokande is twice larger than in Kamiokande-II. They will lead to better energy and position resolutions, $16\%/\sqrt{E}$ and $50cm$ at 10 MeV for an electron compared with 20% and $110cm$ in Kamiokande-II respectivelly. And these better energy and position resolution are essential to remove the low energy background. In the case of observation of solar neutrinos, 100 times higher statistics, namely, 23 events per day can be obtained at an energy threshold of 5 MeV in Super Kamiokande than in the current Kamiokande. And the energy spectrum of the recoil electrons will provide a decisive test of neutrino oscillations. Figure 5 shows expected energy spectra of the non-adiabatic and the quasi-vacuum cases allowed by Homestake, Kamiokande and Gallex experiments during 3 year's operation of the Super Kamiokande detector. This figure shows a clear difference between the non-adiabatic case and the quasi-vacuum case in

the shape of energy distribution. Of course, a lot of physics will be also anticipated from Super Kamiokande, i.e., nucleon decays, atmospheric neutrinos, super novae neutrino, relic neutrinos and so on.

6 Conclusion

In conclusion, the solar neutrino observation in Kamiokande-III has successfully continued. The preliminary result from 395 live-day data in Kamiokande-III gives a relative neutrino flux: $\frac{data}{SSM} = 0.55 \pm 0.07 \pm 0.06$ and it is consistent with the published Kamiokande-II result. The combined result gives $\frac{data}{SSM} = 0.49 \pm 0.04 \pm 0.06$. And no statistically significant time variation has been observed based on the full solar neutrino observation period. And Super Kamiokande, a next generation experiment now under construction, will start data taking in April 1996.

References

[1] R. Davis *et al., in Proceedings of the 21st International Cosmic Ray Conference, Adelaide, Australia, 1990, edited by R. J. Protherioe (Graphic Services, Northfield, South Australia, 1990)*

[2] K.S. Hirata *et al., Phys. Rev. Lett.* **65** *(1990) 1297.*
K.S. Hirata *et al., Phys. Rev.* **D44** *(1991) 2241.*

[3] A.L. Abazov *et al., Phys. Rev. Lett.* **67** *(1991) 3332.*

[4] P. Anselmann *et al., Phys. Rev.* **B285** *(1992) 376.*
P. Anselmann *et al., Phys. Rev.* **B285** *(1992) 380.*

[5] J.N. Bahcall *et al., Rev. Mod. Phys.* **60** *(1988) 297.*

[6] B. Cleveland *et al., in Proceeding of the 25th International Conference on High energy Physics,* **Vol.1,** *(1990) 667.*

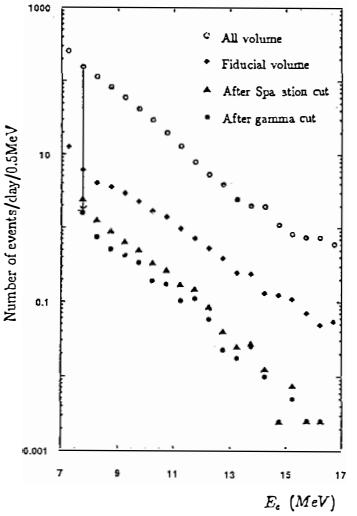

Figure 1: Event rate at each reduction step as a function of recoil electron energy.

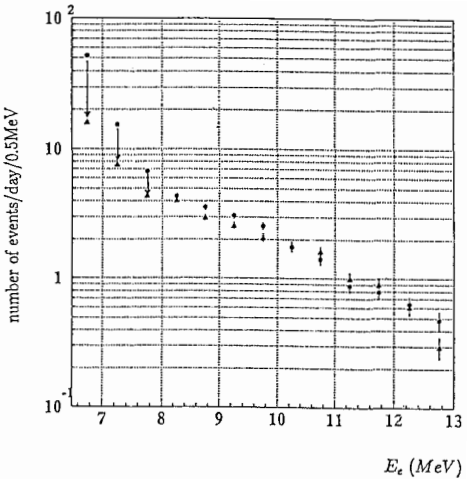

Figure 2: Event rate in the fiducial volume as a function of recoil electron energy during the latest few months in Kamiokande-III (▲) and during the first half year (•).

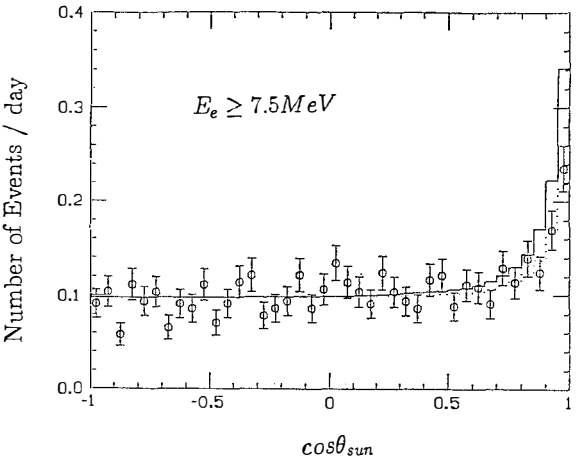

Figure 3: Angular distribution of the recoil electrons with respect to the direction of the Sun in the final sample at an energy threshold of 7.5MeV during 395 live-day in Kamiokande-III.

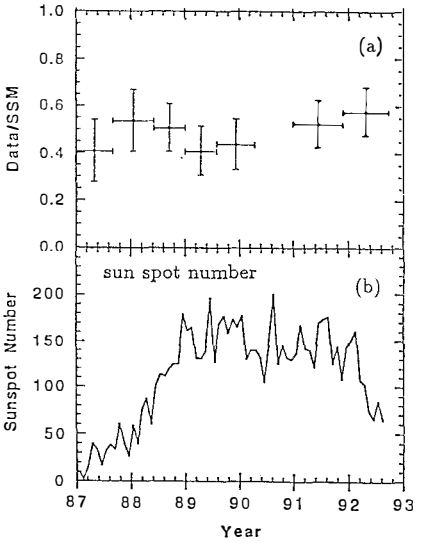

Figure 4: The observed neutrino flux relative to the standard solar model calculation as a function of time (a), together with the sun spot number as a function of time (b).

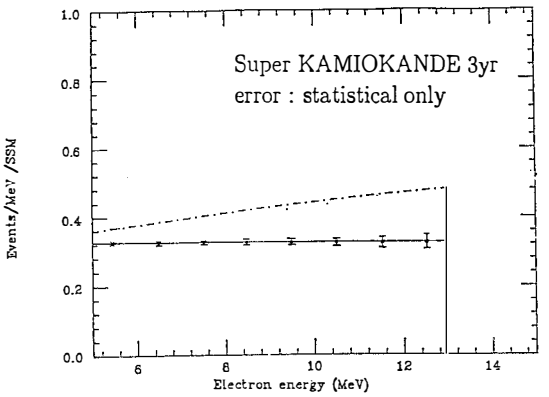

Figure 5: The energy spectra relative to the standard solar model calculation for typical neutrino oscillation parameters in the non-adiabatic ($\Delta m^2 = 10^{-5.22}, sin^2 2\theta = 10^{-2.15}$) and the quasi-vacuum ($\Delta m^2 = 10^{-5.0}, sin^2 2\theta = 10^{-0.22}$) regions allowed by Homestake, Kamiokande and Gallex.

	KAM-II	Super KAM	
detector	$16mh$ $\times 19m\phi$	$41mh$ $\times 39m\phi$	
total mass	3000t	50000t	
fiducial mass	2140t 1040t 680t	32000t 22000t 22000t	super novae p decay solar neutrino
anti counter	1.5m	2m	
number of PMT	948	11200	
photosensitive coverage	20%	40%	
TTS of PMT	4nsec	2.5nsec	1 p.e.
Energy resolution	$3.6\%/\sqrt{E}$ $20\%/\sqrt{E}$	$2.6\%/\sqrt{E}$ $16\%/\sqrt{E}$	e (GeV) e (MeV)
position resolution	110cm 15cm	50cm 10cm	10MeV e $p \rightarrow e^+\pi^0$
trigger threshold	$\sim 5MeV$	$4 \sim 5MeV$	
analysis threshold	7.5MeV	5MeV	solar neutrino
e/μ separation	98%	99%	

Table 1: Summary of the detector performance of Super Kamiokande compared with Kamiokande-II.

SNO, A MULTIFUNCTION SPECTROMETER FOR SOLAR NEUTRINOS

B. C. Robertson
Physics Department, Queen's University
Kingston, Ontario, Canada K7L 3N6

ABSTRACT

The present plans for detector layout and the expected performance characteristics of the Sudbury Neutrino Observatory are described. Details of the controlling factors for the data quality of the μ and τ neutrino signal are discussed, as well as expected sensitivity of the observed ^{8}B spectrum to different neutrino oscillation scenarios.

The Sudbury Neutrino Observatory (SNO) detector is a 1000 tonne D_2O Čerenkov detector, designed to be sensitive to all neutrino types as well as being able to provide detailed spectral information about solar neutrinos. The detector is located 6800' underground in INCO's Creighton mine near Sudbury, Ontario. The great depth of overlying rock assures that there will not be a significant cosmic ray background. The detector itself consists of 1000 tonnes of D_2O contained in a 6 m radius, 5 cm thick transparent acrylic spherical shell suspended in the centre of the detector cavity by 20 low-activity ropes. Surrounding the D_2O at an inner radius of 8.5 m are $\sim$ 9450 20 cm dia. Hamamatsu photomultiplier tubes (PMTs). These are mounted in panels on a stainless steel geodesic support structure which in turn is held in place by cables suspended from the deck. The cavity is filled with low-activity H_2O which serves both as a neutrino target and a shield for the D_2O. The general layout of the detector is illustrated in Figure 1.

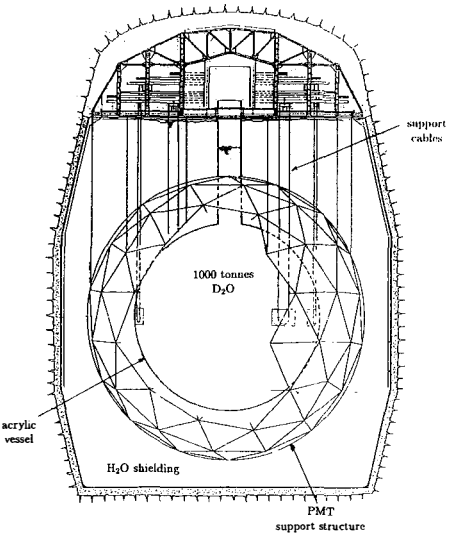

Figure 1: Detector Configuration

The light-collecting area of the PMTs is increased by 87% to 59% of 4π through the use of light-concentrating reflectors placed on the PMT front face. The reflectors also restrict the effective view to a 7 m radius sphere concentric with the D_2O. A recent addition to the detector design is a cosmic ray veto consisting of about 100 outward-looking PMTs without reflectors. The energy threshold for analysis is approximately 5 MeV so that the detector will only be sensitive to ^8B neutrinos from the sun. However, as will be discussed later, ongoing improvements indicate that a somewhat lower threshold should be achieved.

The basic property that gives the SNO detector its unique capabilities is the D_2O target, which allows neutrinos to be detected via three different reactions with quite different characteristics. The first reaction (*C*harged *C*urrent),

$$\nu_e + d \rightarrow p + p + e^+$$

produces energetic electrons approximately 1.4 MeV lower in energy than the incident neutrino. This reaction allows a very good spectral characterization of the incident neutrino flux and so is a sensitive indicator of possible ^{8}B spectral distortions.

The second reaction (*N*eutral *C*urrent),

$$\nu_x + d \rightarrow p + n + \nu_x,$$

is equally sensitive to *all* neutrino types and so provides a good measure of the total solar neutrino flux above the 2.2 MeV threshold for this reaction. The neutrons will be identified by one of two different mechanisms: detection of high-energy γ-rays from neutron capture in the chlorine from 2.5 tonnes of NaCl dissolved in the D_2O, or direct detection of neutrons using 112 ^{3}He neutron counters distributed throughout the D_2O (no salt added). Both techniques will be used, but not simultaneously.

The third reaction (*E*lastic *S*cattering),

$$\nu_x + e \rightarrow \nu_x + e,$$

is mainly sensitive to electron neutrinos but also weakly sensitive to μ and τ neutrinos. This reaction only has about one-tenth the strength of the charged current and neutral current reactions. It has poor energy response but very good direction sensitivity. This fact has been used to good effect in the Kamiokande detector.

A Monte Carlo calculation of the expected detector performance is shown in Figure 2 for a running period of one year with salt. Only events that have been reconstructed to be inside

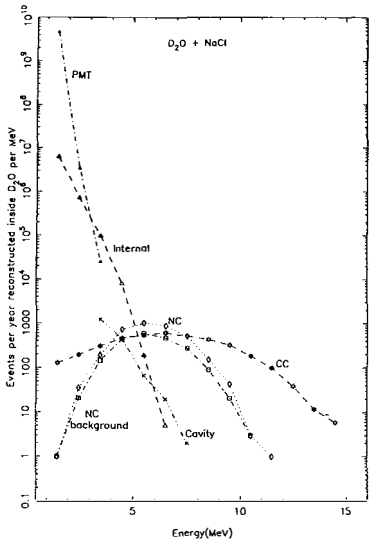

Figure 2: Monte Carlo calculation of signal and background spectra, D_2O plus salt.

the 6 m radius containing the D_2O are included. The curve labelled CC (charged current) gives a good characterization of the ^8B spectrum, and is shown for an assumed intensity of one-third of the "standard solar model" (SSM) value of $5.7 \times 10^6\ \nu \cdot cm^{-2} \cdot s^{-1}$ at the earth's surface. The curve labelled NC is due to neutral current interaction neutrons that generate chlorine neutron capture γ rays. The intensity shown is for a full SSM neutrino flux. For clarity the expected elastic scattering yield is not shown.

In addition to the neutrino signals there are several backgrounds that arise from contaminants in various parts of the detector. The background labelled internal is due to cascades of β and γ radiation emitted at the bottom of both the uranium and thorium decay chains in the heavy water, the acrylic vessel and light water. Thorium in the acrylic vessel is the dominant component of the internal background, which itself is the dominant background from about 3 to 6 MeV. At lower energies the background is due to the same uranium and thorium activities in the photomultiplier components (the background labelled PMT). At energies greater than about 6 MeV the main background (labelled Cavity) is due to high-energy γ rays from activity in the surrounding rock that reach the D_2O.

Underlying the neutral current signal is a neutral current background - neutrons created by photodissociation of deuterons by the same γ-ray flux responsible for the "internal" background. Here again, thorium is the main activity responsible for background neutron generation. The various components responsible for the neutral current background are given in Table 1, together with their assumed thorium contamination level and their contribution to the neutral current background. The background contributions are listed in terms of chlorine captures so that they can be compared directly with the neutral current signal chlorine capture rate, which is 3650 per year for the full standard solar model. The main contributors to the background are the D_2O and the acrylic vessel. The acrylic vessel contribution is lower

Table 1: Neutron Captures, D_2O + NaCl

Component	*Mass* (t)	*Th Level* (g/g)	*Th Mass* (μg)	*Cl Captures* (y^{-1})
D_2O	1000	1.1×10^{-14}	11	950
NaCl	2.5	1×10^{-12}	2.5	210
Acrylic	30	2×10^{-12}	60	1100
Support Ropes	0.12	4×10^{-10}	50	170
H_2O	1670	2×10^{-14}	33	25
PMTs	9.5	8×10^{-8}	760,000	25

than its thorium load would indicate because the associated neutrons have a relatively high probability of escaping into the light water rather than being captured in chlorine. In fact all the thorium sources external to the D_2O generate neutrons only at the edge of the detector which therefore have a relatively high escape probability. Furthermore chlorine captures due to the acrylic and the other external sources can be identified by their distinct radial distribution, so that their effective contribution to the neutral current background can be reduced to a residue from an explicit fit to about 20% of the initial value. This is approximately equivalent to reducing the radial fiducial cut for these backgrounds from 6.0 to 5.5 meters.

The expected signal to background ratio for the neutral current data can be discussed using the above considerations. It can be seen from Figure 2 that the daily neutral current signal for a threshold of 5 MeV would be about 7.0 counts per day. For the same energy threshold the corresponding neutron background would be about 4.0 counts per day. Ac-

counting for the external neutron background using its radial distribution would reduce the background to about 2.6 counts per day. It is also expected that as a result of significant improvements in radiopurity that have been achieved, the acrylic vessel is likely to be about a factor of ten cleaner than the value listed in Table 1. Similarly initial evaluations of the water purification system performance have resulted in the design aim for the light and heavy water being improved by a factor of ten. Incorporating these changes would reduce the neutron background to about 0.7 per day, and allow considerable confidence in the neutral current measurement of the total $e + \mu + \tau$ neutrino flux using the SNO detector.

The spectral sensitivity of the SNO detector provided by the charged current signal can also yield valuable information. The existing results from the chlorine and gallium radiochemical experiments together with those of the Kamiokande water Čerenkov detector have been widely interpreted in terms of the MSW effect. In particular, the analyses [1] indicate that the combined results are consistent with a non-adiabatic MSW solution in the region of $\delta m^2 \sim 6 \times 10^{-6} eV^2$, $\sin^2 2\theta \sim 7 \times 10^{-3}$ and with a large-mixing solution of $\delta m^2 \sim 8 \times 10^{-6} eV^2$, $\sin^2 2\theta \sim 0.6$. A Monte Carlo calcualtion of the charged current spectrum accumulated in one year for these two cases is shown in Figure 3. For easier comparison the data have been binned in 1 MeV intervals, and the 1 σ statistical uncertainties are indicated. No contribution to the error from other yields has been included. The spectrum shows a statistically significant relative suppression of the non-adiabatic yield for energies below about 6 MeV compared to the large mixing case.

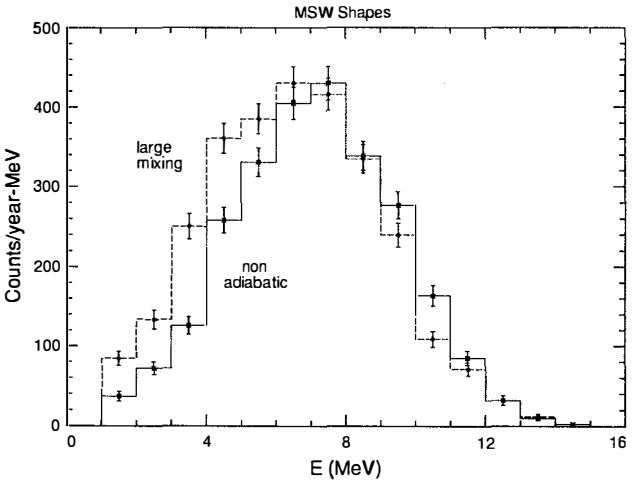

Figure 3: Monte Carlo calculation of the charged current spectrum of MSW solutions.

The strong divergence in shapes below 6 MeV indicates the importance of achieving as low a threshold energy as possible. The nominal threshold value of 5 MeV is the approximate energy where the CC signal level meets the internal background (Figure 2). The improvements in both the acrylic and water purity levels discussed earlier would lower the threshold up to about 200 keV. Also, initial estimates of the effect of the protective coating on the PMT

reflectors indicate that the gain for the acrylic and H_2O component of the internal background should be reduced relative to that for the CC and NC signals. This also would result in an effective reduction of the threshold of up to 200 keV. These changes will clearly improve SNO's ability to constrain possible MSW solutions.

The combined chlorine, gallium and Kamiokande results have also been shown to be consistent with a range of so-called "just so" neutrino oscillations [2] (also described as long wavelength oscillations or LWO). In this case the vacuum oscillation length is comparable to the sun-earth separation, causing strong suppressions in different energy regions. The parameter space consistent with the data spans a segmented band in $\delta m^2 - \sin^2 2\theta$ space ranging approximately from 0.5 to 1 $\times 10^{-10}$ eV^2 in δm^2 and from 0.5 to 1.0 in $\sin^2 2\theta$. In order to indicate the shape sensitivity of the charged current spectral shape to changes within this band of solutions, a Monte Carlo calculation of the spectrum accumulated in one year for paramters near each of the ends of the allowed band is shown in Figure 4. Again the 1 σ statistical uncertainties have been shown. The spectra shown are for $\delta m^2 = 1.1 \times 10^{-10} eV^2, \sin^2 2\theta = 1.0$, at the top of the allowed band (labelled "large δm^2"), and $\delta m^2 = 6.4 \times 10^{-11} eV^2, \sin^2 2\theta = 0.83$, near the bottom of the allowed band (labelled "small δm^2").

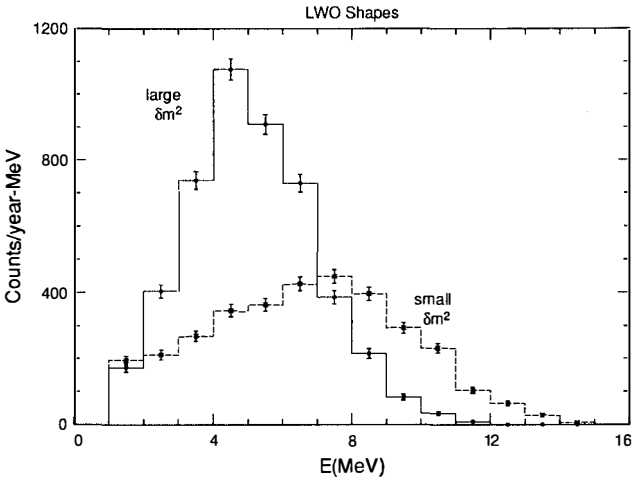

Figure 4: Monte Carlo calculation of charged current spectrum for LWO solutions.

The spectra show a very marked shape change over the allowed parameter range that is clearly distinguishable statistically. In addition a detailed comparison indicates that the long wavelength oscillation shapes shown can be statistically distinguished from the MSW solutions shown in Figure 3.

The analysis of possible ^{8}B spectral distortions discussed above can be used as an independent confirmation of results obtained from the evaluation of neutral current and total charged current yields. Combined, the two analyses should provide a very stringent restriction

on possible solutions to the solar neutrino problem. Clearly the combined ability to measure the total $e + \mu + \tau$ neutrino flux plus the shape sensitivity inherent in the charged current spectrum makes the SNO detector a uniquely powerful instrument.

References

1. P. Anselmann *et al.*, Physics Letters **B285**(1992)390,
X. Shi, D. N. Schramm and J. N. Bahcall, Physical Review Letters **69**(1992)717,
J. M. Gelb, W. Kwong and S. P. Rosen, Physical Review Letters **69**(1992)1864,
S. A. Bludman, N. Hata, D. C. Kennedy and P. G. Langacker, to be published.

2. V. Barger, R. J. N. Phillips and K. Whisnant, Physical Review Letters **69**(1992)3135,
P. Kratsev and S. Petkov, Physics Letters **285B**(1992)85.

NEUTRAL-CURRENT DETECTION IN THE SUDBURY NEUTRINO OBSERVATORY

T.J. BOWLES, P.J. DOE, M.M. FOWLER, A. HIME, R.G.H. ROBERTSON, P.M. THORNEWELL, J.B. WILHELMY, J.F. WILKERSON, and J.M. WOUTERS,
Los Alamos National Laboratory, Los Alamos, NM 87545, U.S.A.

ABSTRACT

The Sudbury Neutrino Observatory (SNO) will have the capability of detecting all active species of neutrinos with energies greater than 2.2 MeV by the neutral-current disintegration of deuterium. The comparison of this rate with the rate of inverse beta decay of the deuteron will yield a nearly model-independent answer to the question of whether electron neutrinos from the sun oscillate into mu or tau neutrinos. The signal of a neutral-current interaction is the liberation of a free neutron in the heavy-water detector, and we discuss a technique employing ^{3}He proportional counters for registering these neutrons, particularly from the standpoint of the ultra-low backgrounds needed.

1 INTRODUCTION

The Sudbury Neutrino Observatory (SNO) is a laboratory to study the properties of neutrinos and to resolve the "solar neutrino problem" [1, 2]. The heart of the detector is 1000 tonnes of 99.92% isotopically pure heavy water (D_2O) in a specially excavated chamber 2100 m below ground in the INCO Creighton nickel mine near Sudbury, Ontario.

Deuterium has unique nuclear properties that make it ideal for the study of neutrino interactions. There are four principal modes by which neutrinos can interact with heavy water:

$$\begin{aligned} d + \nu_e &\rightarrow p + p + e^- - 1.44 \text{ MeV} \quad (\text{CC} : 9750 \text{ yr}^{-1}) \\ d + \nu_x &\rightarrow p + n + \nu_x - 2.22 \text{ MeV} \quad (\text{NC} : 5000 \text{ yr}^{-1}) \\ d + \bar{\nu}_e &\rightarrow n + n + e^+ - 4.03 \text{ MeV} \quad (\text{CA} : 0 \text{ yr}^{-1}) \\ e^- + \nu_x &\rightarrow e^- + \nu_x \quad (\text{ES} : 1100 \text{ yr}^{-1}) \end{aligned}$$

The first of these reactions proceeds by the charged-current (CC) interaction of electron neutrinos specifically. The second is the neutral-current (NC) disintegration of deuterium and can be initiated with equal probability by any of the left-handed neutrinos (ν_e, ν_μ or ν_τ) and their antiparticles. The third is the charged-current interaction of electron antineutrinos (CA). The fourth is the elastic scattering of neutrinos (ES). While all flavors can scatter, the cross section for electron neutrinos is about 6 times that for other flavors as a result of the additional charged-current channel. In the standard models of the sun (SSM; [3]) and of particle physics, only electron neutrinos are produced by the sun. However, if neutrino oscillations occur, then the neutrinos may reach the Earth as other flavors.

SNO therefore has the capability to reveal the presence of neutrino oscillations largely independent of solar properties. If the NC rate exceeds the CC rate (suitably normalized for cross sections), then neutrinos must be oscillating. If the CC energy spectrum differs from the known ^8B spectrum, then neutrinos must be oscillating via the MSW mechanism [4] or the Voloshin-Vysotsky-Okun' mechanism [5]. Unlike the kinematically convolved ES spectrum, the CC electron spectrum measured in SNO directly reflects the incoming ν_e spectrum (with quite good energy resolution) simply shifted down by 1.44 MeV.

SNO is a high-rate experiment. The interaction rates listed with the reactions above are for a ^8B ν_e flux of 6×10^6 cm^{-2} s^{-1} and a detection threshold of 5 MeV electron kinetic energy (the NC threshold is the binding energy of the deuteron).

The Čerenkov light from charged-current and elastic-scattering events is detected in SNO by an array of 9,500 photomultipliers surrounding the acrylic sphere that holds the D_2O.

Neutral-current interactions release a free neutron, and a number of strategies for detecting the neutron can be devised. One is to dissolve in the heavy water a fraction of a percent of chloride ion. When a neutron captures on 75% abundant ^{35}Cl, it emits an 8.6-MeV γ, which showers. The resulting Čerenkov radiation can be detected by the PMT array in the same way CC events are detected.

Another method, the one discussed here, is to detect the neutron in ^{3}He proportional counters dispersed in the heavy water so that the NC and CC events become completely distinct and no longer represent "backgrounds" to each other. Because of the central importance of SNO's neutral-current capability to the potential discovery of new physics, there are strong incentives to develop independent techniques.

2 ^{3}He DETECTORS FOR SNO

The use of ^{3}He proportional counters for neutron detection is a well-established technique that relies on the exothermic reaction,

$$^3\mathrm{He} + \mathrm{n} \rightarrow \mathrm{t} + \mathrm{p} + 0.764\ \mathrm{MeV},$$

for which the thermal-neutron cross section is enormous, 5330 b. As heavy water is an excellent moderator, it is possible to distribute counters sparsely and still realize high capture efficiencies.

The planned arrangement for SNO is approximately 900 m of 5-cm diameter tubular detectors organized end-to-end in strings anchored to the bottom of the acrylic vessel on a square 1-m lattice. On average, 15% of the light from Čerenkov events is obstructed by the detector array, which somewhat degrades the energy resolution and increases the threshold.

2.1 THE SIGNAL

In the usual mode of operation of proportional counters, the total charge collected at the anode wire is converted to a voltage in a charge-sensitive (integrating) preamplifier, and gives a measure of the energy deposited in the gas. More information than just the total charge is actually available, however. The primary ionization from a track drifts in and is multiplied over a period of time that depends on track length, track orientation, and the drift velocity. Thus the ionization density projected onto a plane perpendicular to the wire can be deduced from the current profile of the pulse. This information reveals a great deal about the event that created the track. An example is shown in Fig. 1. The ionization density peaks near the end of an α-particle track (the "Bragg peak"). That part of the track arrives first at the wire, creating a sharp initial maximum in the current followed by a period of decreasing current terminating after 4 μs when the most distant ionization reaches the wire. The signal shown is the digitized output of a current preamplifier. (The total energy can be derived from the integral.) By contrast, the ^{3}He(n,p)T event displays the double peak produced by the back-to-back proton and triton tracks. Each event has a distinctive ionization "fingerprint." In the simplest analysis, the maximum drift duration of a ^{3}He(n,p)T event is 2.9 times that of an alpha of the same energy, and it is possible merely by sorting with respect to current-pulse duration and total charge to obtain a subset of neutron events, more than 50%, that are completely free of α competition.

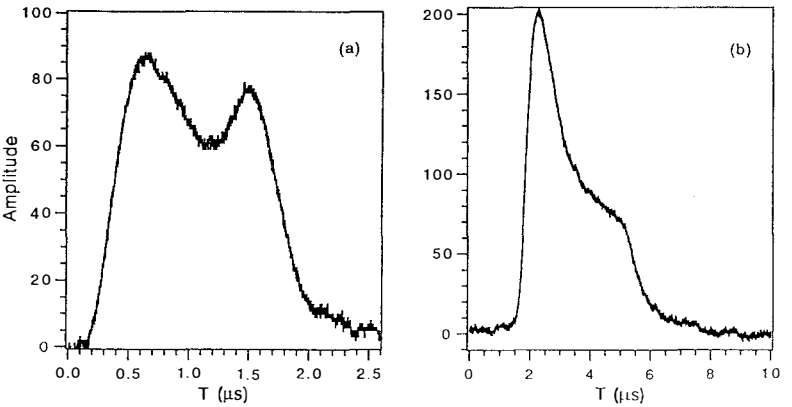

Figure 1: (a): Current pulse from ^{3}He(n,p)T event in a 30-cm proportional counter. (b): Pulse from 5.4-MeV α.

2.2 Efficiency

Monte Carlo neutron-transport calculations indicate that the counter array, filled with 3 atm of ^{3}He and 0.75 atm of CF_4, has a raw capture efficiency of 45% for neutrons generated in the 99.92% enriched heavy water.

2.3 Energy Resolution

Short counters with the ^{3}He – CF_4 gas fill have yielded 2.5% FWHM. However, gas gains must be restricted to values less than about 10 to avoid space-charge effects with alphas, and electronic noise becomes a significant factor. Under actual running conditions (long cables, long counters, capacitor termination), a resolution of 10% is expected.

2.4 Wall Effect

For pure ^{3}He in a semi-infinite detector, in 31% of captures, either the triton or the proton strikes the wall before the end of its range. The wall effect drops with the addition of another gas, because the ratio of neutron-capture range to charged-particle range increases. The choice of CF_4 as an additive is motivated by its high stopping power, low **Z**, and good counting properties. In the 80:20 ratio selected, the wall effect is 18%. Wall-effect events can be used since the spectrum is known, but the signal-to-background ratio is worse in that part of the spectrum.

2.5 Position Coordinate

Position information is required in order to reconstruct the radial distribution of events from NC interactions and from the acrylic-vessel background, as well as to establish connections between Čerenkov events and related neutrons (e.g., in the detection of $\bar{\nu}_e$ interactions).

To reduce the amount of material in the heavy water, to minimize interference with Čerenkov light, and to minimize the number of cables running through the neck of the vessel, a single-ended readout is highly desirable. A group at Nagoya University [6] has developed an ingenious solution which is essentially charge division, but in which the charge delivered to one end (the remote end) is stored in a capacitor to leak back into the line with a long time constant. Position information is derived from the ratio of charges in the fast and slow components, and can be extracted from the digitized pulse profiles.

In tests carried out at LANL on this method a position resolution of 1.6% FWHM was obtained. (The position-resolution requirements are modest, since the mean distance to capture is 113 cm.) Position readout by this technique can be combined with fast measurement of the current-pulse shape by adding a resistance in series with the termination capacitor. This effectively lengthens the detector electrically and allows pulse-shape information to be derived for the entire active length of the device.

3 BACKGROUNDS

At the design levels of radiopurity (4 pg/g maximum each of U and Th), the principal backgrounds are approximately 140 neutrons per year released in the heavy water by photodisintegration, and approximately 1000 α events from the walls of the detectors. To achieve these levels, the counter bodies will be constructed of pure Ni formed by chemical vapor deposition from $Ni(CO)_4$. [One sample of tubing made this way was assayed recently at 7.4(4) pg/g Th and $\leq$ 0.8 pg/g U.] The photodisintegration background will be measured *in situ* from Čerenkov light produced by the 2.6-MeV and 2.44-MeV gammas at the bottom of the Th and U chains, while the alpha backgrounds can be determined directly from the spectra recorded in the counters. An additional source of alphas is ^{210}Pb deposited on the inner surface of the counter from radon, which sets a limit in the range 10-1000 hours for unprotected exposure to room air during construction.

4 STATISTICAL CONSIDERATIONS

The possible presence of MSW distortions (and possible time variations therein) in the CC spectrum make it prudent to avoid assumptions about the shape of that spectrum. In that case, the CC spectrum must be derived by subtraction of all non-CC contributions, and the statistical advantages of separate detection of NC and CC interactions are self-evident.

Assume a detected CC rate of C per year, a detected NC rate of N per year, and a detected neutron background rate of B per year. A likely running scenario would be t_1 years with pure D_2O, followed by t_2 years with salt or ^3He counters for a total of t years. Defining the fractional precision in quantity i as σ_i, for the ^3He method, one has:

$$\sigma_C^2 = \frac{1}{Ct}$$

$$\sigma_N^2 = (1 + \frac{B}{N})^2 \frac{1}{(N+B)t_2} + (\frac{B}{N}\sigma_B)^2,$$

Then the fractional precision in the ratio is:

$$\sigma_R = (\sigma_N^2 + \sigma_C^2)^{1/2}.$$

With the salt technique, statistics for CC alone are accumulated only to the end of interval t_1:

$$\sigma_C^2 = \frac{1}{Ct_1}.$$

Thereafter, statistics accumulate in the sum N + C = T:

$$\sigma_T^2 = (1 + \frac{B}{T})^2 \frac{1}{(T+B)t_2} + (\frac{B}{T}\sigma_B)^2$$

$$\sigma_R = (\sigma_T^2 + \sigma_C^2)^{1/2}$$

The ratio (N+C)/C must be determined approximately twice as accurately to achieve a desired precision in the ratio N/C, as illustrated in Table 1. For these calculations, B = η(1176 + 294[salt] or 140[^{3}He]) and $\sigma_B = 0$ (σ_B represents additional, non-statistical sources of error; η is the neutron detection efficiency).

Table 1: Fractional precisions needed in SNO for a 5-σ demonstration that, when the SSM flux is present, 1/3 is ν_e, and 2/3 ν_μ or ν_τ.

					Data Ratio N/C or T/C		
Method	η	N	C	N/3	No Osc	SSM + Osc	For 5σ
^{3}He	0.4	2000	2200	667	0.303	0.909	σ_R=14.7%
Salt	0.5	2500	2200	833	1.379	2.136	σ_R=7.1%

The foregoing equations are illustrated graphically in Figure 2, with t_1 = 0.5 years. The necessary precision for a 5-σ effect is achieved very rapidly in both cases. After one year total the salt and ^{3}He methods achieve 10- and 19-σ significance, respectively.

The magnitude of any photodisintegration background present must be determined by some auxiliary measurements. For example, if the heavy water contains 11 fg/g each of Th and U, and 2.5 tonnes of added NaCl contains 1 pg/g each of those isotopes [7], then the detected background neutron rate is B = η(1176 + 294) per year above 6 MeV, to be compared to the SSM rate of N = η(5000). If the background can be determined to a precision of only 50%, then the ^{3}He and salt methods become dominated by that uncertainty, and differ little in their ultimate statistical precision (in this rather pessimistic example, still a 5-σ effect after a year).

As described, the ^{3}He counters also in general have a continuous α background underlying part of the neutron-capture spectrum. If the fraction of events free of alpha

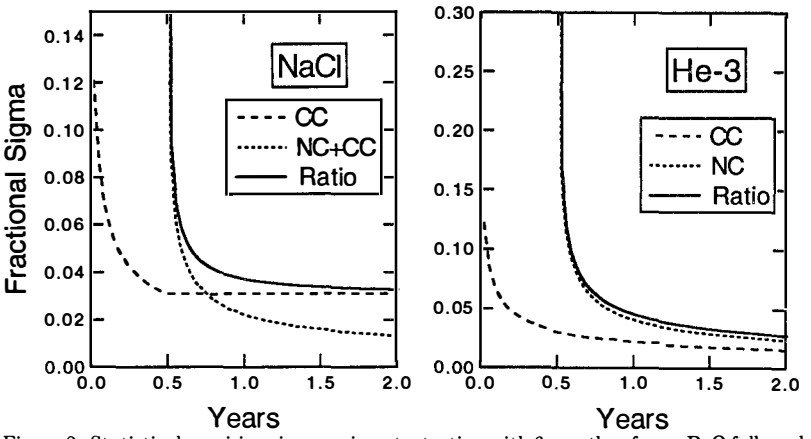

Figure 2: Statistical precisions in experiments starting with 6 months of pure D_2O followed by installation of either salt (left) or ^{3}He counters.

background is f and the ratio of the alpha rate (after energy cuts) to the total neutron rate (including photodisintegration neutrons) is α, then it may be shown that

$$\sigma_N^2 = (1+\frac{B}{N})^2 \left\{ \frac{1}{(N+B)t_2} \left(\frac{1-f+\alpha}{1-f+f\alpha} \right) + \alpha^2 (\Delta f)^2 \left(\frac{1-f+\alpha(2f-1)}{1-f+\alpha} \right)^2 \right\} + (\frac{B}{N}\sigma_B)^2,$$

where Δf is the uncertainty in f. The value of f is of order 0.5. The effects of alpha backgrounds are minor as long as $\alpha \leq 1$.

5 CONCLUSION

The value of a measurement of the neutral-current interaction rate of solar neutrinos in distinguishing astrophysical and particle-physics solutions to the solar neutrino problem cannot be overstated. Analysis and measurements of neutron-detection efficiencies and backgrounds indicate that SNO will be capable of detecting the neutral-current process with good efficiency and low backgrounds. Two quite different approaches, dissolved salt and ^{3}He proportional counters, will be used as a check on systematic effects. The latter approach has the desirable feature that NC interactions will be distinguishable event-by-event from other types of interaction.

References

[1] G. Aardsma et al., Phys. Lett. **B194**, 321, 1987.

[2] B.C. Robertson, these Proceedings.

[3] J.N. Bahcall and M.H. Pinsonneault, Rev. Mod. Phys. **64**, 885 (1992).

[4] S.P. Mikheyev and A. Yu. Smirnov, Yad. Fiz. **42**, 1441 (1985) [Sov. J. Nucl. Phys. **42**, 913 (1985)]; L. Wolfenstein, Phys. Rev. **D17**, 2369 (1978).

[5] M.B. Voloshin, M.I. Vysotskii, and L.B. Okun', Yad. Fiz. **44**, 677 (1986) [Sov. J. Nucl. Phys. **44**, 440 (1986)].

[6] A. Uritani, C. Mori, T. Watanabe, and A. Miyahara, "Novel Position Sensing Method Using Fast and Slow Components in an Output Signal from a Proportional Counter" Proc. 7th Symp. on Radiation Measurements and Applications, Univ. of Michigan, Ann Arbor, MI, May 21-24, 1990.

[7] SNO Collaboration, "Sudbury Neutrino Observatory Proposal", SNO-87-12, 1987.

ICARUS. STATUS AND PROGRESS

P.Cennini, S.Cittolin, J.P.Revol, C.Rubbia
CERN, CH-1211, Geneva 23, Switzerland

L.Fortson, P.Picchi
Lab. Naz. di Frascati dell'INFN, via E.Fermi 40, Frascati (Roma), Italy

F.Cavanna, G.Piano Mortari, M.Verdecchia
Dipartimento di Fisica e INFN, Università dell'Aquila, via Vetoio, Coppito (AQ), Italy

M.Cheng, D.Cline, S.Otwinowski, M.Zhou, H.Wang
Department of Physics, UCLA, Los Angeles, CA 90024, USA

A.Bettini, F.Casagrande, P.Casoli, S.Centro, B.Dainese, C.De Vecchi,
F.Gasparini, G.Muratori, A.Pepato, F.Pietropaolo, P.Rossi, S.Suzuki, S.Ventura
Dipartimento di Fisica e INFN, Università di Padova, via Marzolo 8, Padova, Italy

P.Benetti, E.Calligarich, R.Dolfini, A.Gigli Berzolari, F.Mauri,
L.Mazzone, C.Montanari, A.Piazzoli, A.Rappoldi, G.L.Raselli, D.Scannicchio
Dipartimento di Fisica e INFN, Università di Pavia, via Bassi 6, Pavia, Italy

L.Periale
ICGF del CNR di Torino, corso Fiume 4, Torino, Italy

ABSTRACT

We briefly report on the present status of the ICARUS R&D program. Results from the continuous running of a 3 ton LAr TPC by more than 18 months demonstrate that the ICARUS technique is reliable giving bubble chamber quality images of ionising particles. The analysis of the data taken in this period on atmospheric muons enabled us to determine various detector parameters (electrons lifetime in LAr, electrons diffusion parameter, spatial resolution, charge recombination). During the last months of the past year we successfully tested the possibility to purify the Argon directly in liquid phase. The high purification speed allowed by this method is an important tool to extend the ICARUS technique to very large mass detectors.

1. INTRODUCTION

A liquid argon time projection chamber (LAr-TPC) working as an electronic bubble-chamber, continually sensitive, self-triggering, able to provide 3-D imaging of any ionising event together with a good calorimetric response was first proposed by C. Rubbia in 1977 [1]. In order to verify the feasibility of such a detector, the ICARUS collaboration started in 1985 an intensive R&D program aiming to solve the main technological problems:

1) the liquid argon purity that has to be kept at the level of 0.1 ppb of electronegative molecules to allow the ionisation electrons for long drift distances;
2) the extreme cleanliness of the material employed in the construction of the detector and the complete reliability of the feed-throughs between pure argon and out-side world to avoid contamination due to degassing or leaks;
3) the realisation of wire chambers able to perform a non destructive read-out (in order to get a 3-D image of the event) made of several wire planes with few mm pitch; this requires high precision very reliable mechanics and good knowledge of the electric field in the detector;
4) the development of low noise preamplifiers to get a good signal to noise ratio.

The satisfactory results obtained on small scale tests [2, 3, 4] allowed us to start in 1989 the construction of a 3 ton prototype [5] which is presently working at CERN under stable conditions without interruptions since May 1991.

The step from small to large volumes has been made possible by:

a) the argon purification performed in gas phase with industrial methods with special care for the cleaning of the materials that come in contact with the purified argon [4];
b) the use of a recirculation system that purifies continually the gas due to the heat leakage of the dewar and liquefies it back into the detector. This inhibits the diffusion inside the liquid of electronegative impurities produced by degassing of materials in the high temperature region of the detector;
c) the use of signal feed-throughs made on vetronite support with the technique of the printed circuit board and welding each pin on it.

2. GENERAL FEATURES

The 3 ton detector configuration is well described in our proposal [5]. Here we want to remind the following aspects.

a) The LAr is contained in a stainless steel cryogenic vessel. The detector set is suspended from the top flange together with all the service elements (heat

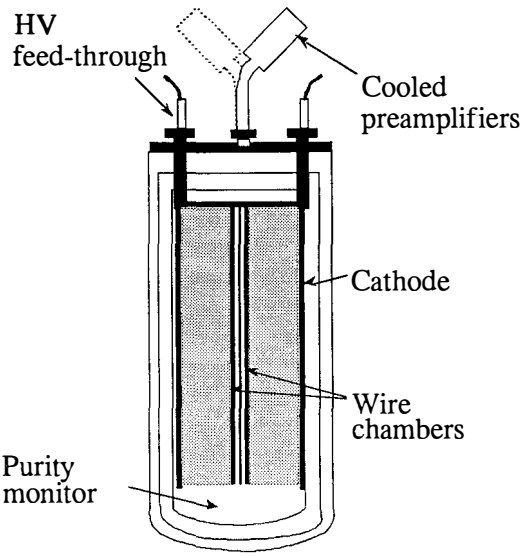

Fig. 1

exchanger, purity monitor, level and pressure indicators). The active volume, defined by the wire chamber and the field shaping electrodes, is split into two independent semi-cylindrical sections (fig. 1).

b) Each section is faced by a wire chamber that covers a surface of $2.4 \cdot 0.9$ m^2 and consists of three parallel grids. Drifting electrons go successively through the following wire planes:
   1. a plane with the function of screen transparent to the electrons;
   2. a sense wire plane where the electrons give an induction signal (again completely transparent);
   3. a plane with the wires perpendicular to the previous ones where the charge is collected.

   The pitch of each sense wire is 2 mm. The separation between planes is also 2 mm. The maximum drift path is 42 cm. The chambers are constituted of 3600 vertical wires (stainless steel, 100 μm diameter) 2.4 m long and 4800 horizontal wires 0.9 m long. The signal cables are kapton flat cables 3.5 m long inside the detector with low capacitance (40 pF/m). The 2100 signal feed-throughs are grouped in 8 flanges located on top of the dewar. Low noise pre-amplifiers are placed inside cooled boxes mounted directly on top of the signal feed-throughs flanges.

c) A purity monitor constituted by a double gridded ionisation chamber with a drift length of 6 cm is located at the bottom of the dewar separated from the active volume by a metal plate (fig. 1). The electron lifetime in LAr inside the detector is continually monitored by measuring the attenuation of an electron cloud produced by a laser UV pulse impinging on the photo-cathode [4].

3. DETECTOR RESPONSE

A large amount of data have been collected with the 3 ton prototype using atmospheric muons. An event that illustrates very well the peculiar characteristics of the detector is shown in fig. 2: a cosmic muon stopping with electron decay. The event is seen by the detector in two orthogonal views: the induction plane (non-destructive read-out) and the collection plane (destructive read-out) with the sense wire direction at 90° in one plane with respect to the other and with the drift time (third orthogonal coordinate) in common to both of them; the last feature together with the charge deposited along the tracks allows a 3-D reconstruction. The electric field in the drift volume is 350 V/cm corresponding to an electron drift velocity of 1.24 mm/μs. The sampling time is 200 ns. The charge deposited over one wire is about 10000 electrons for minimum ionising particles. The signal to noise ratio is ≈6 for the induction wires and ≈10 for the collection ones. This event proves, with the many others we are collecting, that the LAr-TPC works as an electromagnetic calorimeter with high granularity (2•2•2 mm^3 cell) and low electronic noise (equivalent to 25 KeV). In fact the measure of dE/dx along the muon track allows the determination of the total energy deposited, the incoming direction (by the increase of ionisation near the stopping point), the particle identification (by dE/dx vs range near the stopping point), the exact point of the decay

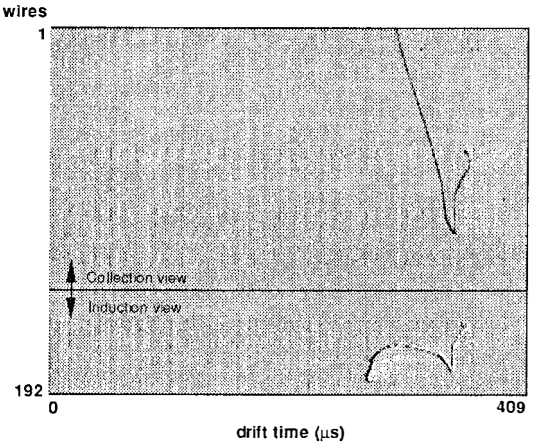

Fig. 2

Furthermore the energy of the electron from muon decay track is also measurable both by energy loss and range: in particular, for the event in fig. 2, the measured electron energy is 18 MeV.

From the analysis of through-going cosmic muons it has been possible to extract several parameters characterising the detector: electron lifetime, electron recombination, electron diffusion,

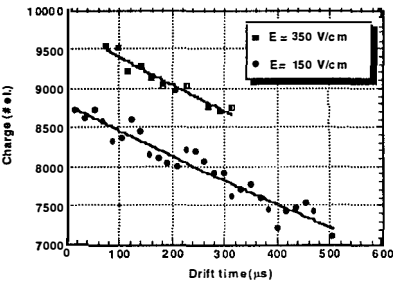

E.F. (V/cm)	Lifetime (μs)	Free charge (# el.)
350	2584	9775
150	2540	8800

Fig. 3

energy resolution, space resolutions.

The electron lifetime value given by the purity monitor has been checked by means of cosmic ray muons crossing vertically the drift volume. The trigger was constituted three scintillators placed two on top and one on the bottom of the dewar in coincidence with the signal on the wires planes. The events have been selected requiring that there was no evidence of large multiple scattering and delta rays ensuring thus that they were minimum ionising particles. The distribution of the charge deposited along the tracks is measured for each drift time slice with a binning of 17 μs, the most probable value is extracted and plotted as a function of the drift time; an exponential fit to this plot gives directly the free electron yield and the electron lifetime (fig. 3). This measure has been repeatedly performed giving a stable value of lifetime of about 2.5 ms, in agreement with the data from the purity monitor.

The dependence of the electron-ion recombination on the ionisation density have been obtained analysing data from muons stopping inside the detector. The charge yield as a function of the dE/dx is well described by the formula (Birk's law) $dQ/dx = A\,dE/dx/(1+K\,dE/dx)$ with A = 35 el/keV and K = 0.13 cm/MeV for a

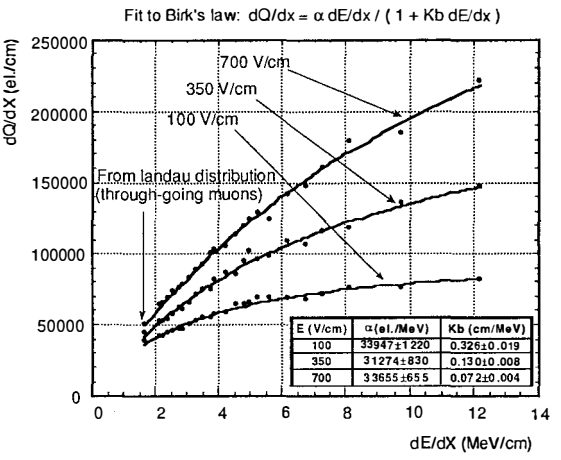

E (V/cm)	α(el./MeV)	Kb (cm/MeV)
100	33947±1220	0.326±0.019
350	31274±830	0.130±0.008
700	33655±655	0.072±0.004

Fig. 4

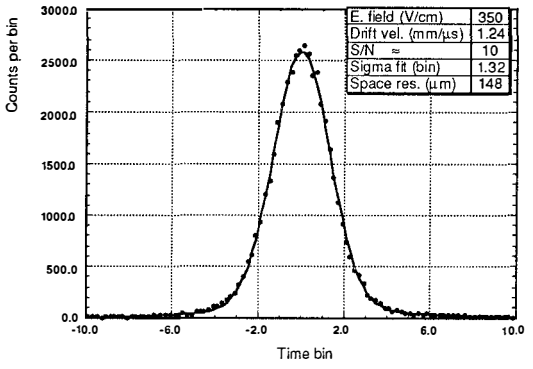

Fig. 5

drifting field of 350 V/cm (fig. 4). The increase in recombination at the end of the range shows that the detector energy response at low fields is non-linear.

A big effort is now in course to fully understand the effects of the recombination on the energy response of the detector. At present we are analysing crossing muons data of in order to extract the recombination dependence on the electric field strength and on the angle between the track and the electric field. As part of our next program we plan to dope the LAr in order to lower the recombination and thus avoid the related problems.

The space resolution along the drift direction has been measured from the distribution of the residuals to a linear fit of the tracks of high energy crossing muons. An r.m.s. resolution of 150 μm has been found roughly independent from the electric field (fig. 5) and the drift distance. In a dedicated test on a small scale with the preamplifiers immersed in LAr and a low input capacitance we got a signal to noise ratio of ≈ 20 and a spatial resolution of 58 μm [6].

The analysis of the signal rise time allows the determination of the longitudinal diffusion as a function of the drift time. The rise time (RT) is proportional to the spread (s) of the signal due to diffusion and $s^2 = 2Dt$ (where D is the longitudinal diffusion coefficient and t is the drift time), hence a linear fit of RT^2 versus drift time gives directly D. The data taken 350 V/cm and at 250 V/cm give a value of D = 4.8 ± 0.2 cm^2/s in agreement with the measurement of other authors [7] and the value expected from brownian motion and electrostatic repulsion between the electrons.

From the results presented above turns out that a certain amount of technical work has to be done in order to improve the S/N ratio. This can be accomplished by connecting the preamplifiers directly to the wires inside the LAr thus reducing the input capacitance due to the cables and the intrinsic thermal noise.

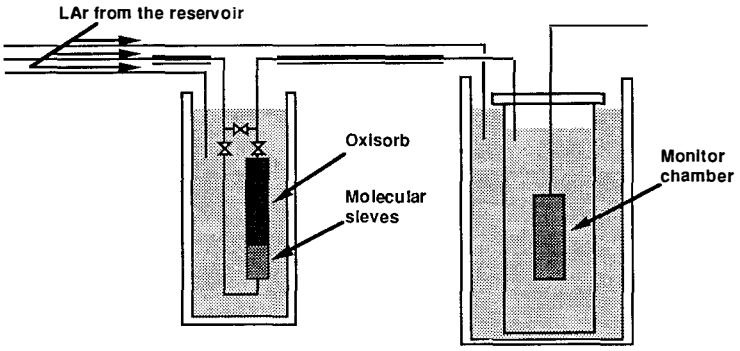

Fig. 6

5. LIQUID PHASE PURIFICATION

During the last months of the past year we made a test in order to verify the possibility to purify the Argon directly in liquid phase. A schematic view of the apparatus we used is shown in fig. 6. Industrial LAr (1ppm O_2 equivalent) from a storage dewar passes, through vacuum lines, into a filter immersed in LAr and then fills a second dewar (130lt volume) where is contained a monitor chamber similar to the one used into the 3 ton prototype. The filter is constituted of 2lt of molecular sieves (5A type) that mainly remove H_2O and 4lt of Oxisorb [9] that remove O_2 and can purify up to 75000lt of industrial LAr.

The flow rate was controlled by setting the appropriate pressure drop into the circuit.

We performed a series of purifications/fillings of the detector dewar at different fluxes up to a maximum rate of 800lt/h and always found an electron lifetime above 3-4ms, that is the limit of our experimental sensitivity. The maximum rate was determined by the impedance of the Oxisorb cartridge and has not to be taken as the limit of this technique; two or more filters in parallel can be used to increase the flux.

4. CONCLUSIONS

We reported on the latest results from the R&D program of the ICARUS project. The continuous running by more than 18 months of the 3 ton prototype demonstrates that the ICARUS technique is reliable. The detector provides electronic bubble-chamber quality images with millimetre size "bubbles". It is continually sensitive and

self-triggering. Spatial resolution is in the range of 150 μm. Ionisation and range measurements provide particle identification.

Extension of this technique to very large volume detectors is now possible thanks to the Argon purification in liquid phase nevertheless for the full completion of our R&D activity we still need to investigate some point:

a) LAr doping, in order to reduce the recombination rate.
b) Development of low noise low temperature pre-amplifiers to increase the signal to noise ratio.
c) Design of very large wire chambers mechanically reliable.

5. REFERENCES

[1] C. Rubbia, CERN-EP Internal Report 77-8 (1977).
[2] E. Buckley et al., Nucl. Instr. and Meth. A275 (1989) 364.
[3] E. Bonetti et al., Nucl. Instr. and Meth. A286 (1990) 135.
[4] A. Bettini et al., Nucl. Instr. and Meth. A305 (1991) 177.
[5] ICARUS collaboration, "ICARUS I: An Optimized Real Time Detector of Solar Neutrinos", LNF - 89/005 (R).
[6] P. Astier et al., "Detecting n_t with electronic techniques", Univ. Paris VI, LPNHEP/8907 (1990) and LPNHEP/9006 (1990).
[7] E. Shibamura et al., Phys. Rev. A20 (1979) 2547.

NEUTRINO PHYSICS SOLUTIONS OF THE SOLAR NEUTRINO PROBLEM

S.T. Petcov[1,2]

[1]Scuola Internazionale Superiore di Studi Avanzati, and Istituto Nazionale di Fisica Nucleare, Sezione di Trieste, I-34014 Trieste, Italy.
[2]Permanent address: Institute of Nuclear Research and Nuclear Energy, Bulgarian Academy of Sciences, 1784 Sofia. Bulgaria.

Abstract

The interpretations of the solar neutrino observations in terms of vacuum oscillations, MSW transitions, and spin-flavour precession of solar neutrinos are reviewed, and the corresponding implications for future solar neutrino experiments are discussed.

1. INTRODUCTION

The publication in 1991 and 1992 of the results of the Ga-Ge solar neutrino experiments [1,2,3] made practically complete the set of data on solar neutrinos which could be obtained with the first generation of solar neutrino detectors. Although the pioneer experiments of Davis et al. [4], Kamiokande [5], SAGE [1,3] and GALLEX [2] will continue to run for at least few more years and the accuracy of the data they provided will improve, no substantial changes of the latter are expected * and no new data will be available before solar neutrino detectors of the second generation (SNO, Super Kamiokande, ICARUS, BOREXINO, HELLAZ) become operational in the second half of the 90'ies.

The implications of the results of the solar neutrino experiments, which concern the intrinsic neutrino properties (mass, mixing, magnetic moment, etc.), are among the most significant and interesting and they have been thoroughly studied [6-12] (for earlier analyses see refs. [13,14]). In the present article we shall discuss the interpretations of the solar neutrino observations in terms of vacuum oscillations [15], MSW transitions [16], and spin-flavour precession [17] of solar neutrinos. Possible tests of the "unconventional" neutrino properties suggested by the indicated interpretations, in the future solar neutrino experiments will also be considered.

2. THE SSM PREDICTIONS VERSUS THE SOLAR NEUTRINO DATA

According to the standard solar model [18,19], the solar ν_e flux consists of several components (pp, ^{7}Be, ^{8}B, pep, ^{13}N, ^{15}O, etc.), three of which will play a major role in our discussion: the least energetic pp-neutrinos ($E_\nu(pp) \leq 0.42$ MeV), the intermediate energy monochromatic ^{7}Be-neutrinos ($E_\nu(^7Be) = 0.862$ MeV (90% of the ^{7}Be-neutrinos), 0.36 MeV (10%)), and the higher energy ^{8}B-neutrinos ($E_\nu(^8B) \leq 14$ MeV). Three different methods of detection of the solar neutrinos have been exploited in the five experiments that have provided data so far: the radiochemical Cl-Ar method, proposed by Pontecorvo in 1946 [20] (in Davis et al. experiment), the neutrino-electron elastic scattering reaction (in Kamiokande experiments), and the Ga-Ge radiochemical method [21] (in SAGE and GALLEX). The Cl-Ar and the Ga-Ge radiochemical methods permit to detect electron neutrinos with energies exceeding 0.816 MeV and 0.233 MeV, respectively. The Kamiokande-II and -III experiments can register any active neutrino (i.e. $(\bar{\nu}_e)$, $(\bar{\nu}_\mu)$, $(\bar{\nu}_\tau)$) having energy greater than 7.5 MeV.

It follows from the presently existing results based on SSM calculations [22, 19] that from 70% to 77% of the event rate in the experiment of Davis et al. should be due to the ^{8}B-neutrinos, while the ^{7}Be- neutrinos should generate only from 14% to 17% of the solar neutrino induced events. The pp-neutrinos do not give contribution to the event rate in the Cl-Ar detectors because they possess energies which are below the threshold energy of the ν_e induced Cl-Ar reaction. With a threshold energy of 7.5 MeV the Kamiokande-II and Kamiokande-III detectors are sensitive only to the ^{8}B component of the solar neutrino flux. Finally, the pp-, the ^{7}Be- and the ^{8}B-neutrinos are predicted to produce, respectively, from 54% to 57%, from 24% to 27% and from 7.4% to 10% of the events in the Ga-Ge experiments SAGE and GALLEX. Thus, the largest fractions of the solar neutrino induced signals in the Davis et al. and Kamiokande detectors, and in the SAGE

* A priori, one cannot totally rule out the possibility of surprises in the next few years. The planned calibrations of the GALLEX and SAGE detectors will be crucial for conclusive determination of the characteristics of the solar neutrino flux inferred from the current data.

and GALLEX detectors are produced, according to the SSM, by very different components of the solar neutrino flux, namely by the ^{8}B– and the pp–neutrinos. Although the ^{7}Be–neutrinos contribute to the event rates in both Cl–Ar and Ga-Ge detectors, their respective contributions, being nonnegligible, do not exceed considerably, as we shall see, the experimental uncertainties in the presently existing data of the corresponding experiments. All these facts are more or less well known.

We shall summarize next briefly some of the solar neutrino data and the relevant SSM results which will be used in the further analysis. The average rate of production of ^{37}Ar by the solar neutrinos, $\bar{R}(Ar)$, observed in the experiment of Davis et al. [4] during approximately a 20 year period of data taking (altogether 750 solar neutrino induced events registered), reads:

$$\bar{R}(Ar) = (2.19 \pm 0.25)\ \text{SNU}. \tag{1}$$

The current SSM prediction for $\bar{R}(Ar)$ vary between the recent result of Bahcall and Pinsonneault [22]

$$\bar{R}(Ar)_{BP} = (8.0 \pm 3.0)\ \text{SNU}, \tag{2}$$

where 3 SNU corresponds to an "effective three standard deviations uncertainty", and the prediction of Turck–Chieze et al. [19]

$$\bar{R}(Ar)_S = (6.4 \pm 1.4)\ \text{SNU}, \tag{3}$$

1.4 SNU representing estimated 1 s.d. uncertainty.

Kamiokande–II and Kamiokande–III collaborations have measured the flux of ^{8}B–neutrinos during a total of 1040 days (in the period 1986–1990) and of 395 days (in 1991-1992), respectively. The combined result of the two experiments for the inferred average flux of ^{8}B neutrinos, $\bar{\Phi}(B)$, has the form [5]

$$\bar{\Phi}(B) = (0.49 \pm 0.05 \pm 0.06)\Phi^0, \tag{4}$$

where $\Phi^0 = 5.8 \times 10^6\ \nu_e/\text{cm}^2/\text{sec}$. It differs very little from the result of the Kamiokande–II collaboration [5]. The values of $\bar{\Phi}(B)$, calculated theoretically in ref. [22] and in ref. [19] are again to a large extent representative for the possible variations in the current SSM predictions. They are given respectively by:

$$\bar{\Phi}(^8B)_{BP} = 0.98(1 \pm 0.43)\Phi^0\ \ (3s.d.), \tag{5}$$

$$\bar{\Phi}(^8B)_S = 0.74(1 \pm 0.25)\Phi^0\ \ (1s.d.). \tag{6}$$

Let us note that apart from differences in the used input data (notably the cross–section of the reaction $p + {}^7Be \rightarrow {}^8B + \gamma$), the calculations performed in refs. [22] and [19] leading to the predictions (2), (5) and (3), (6) differ in the treatment of the diffusion of ^{4}He in the Sun: the latter is taken into account in the analysis of the authors of ref. [22] and is not accounted for in ref. [19].

Finally, let us quote the results of the two Ga–Ge experiments GALLEX and SAGE (based on signals of 75 and 25 events, respectively) [2,3]:

$$\bar{R}_{GALLEX}(Ge) = (83 \pm 19 \pm 8)\ \text{SNU}, \quad \bar{R}_{SAGE}(Ge) = (58^{+17}_{-24} \pm 14)\ \text{SNU}. \tag{7}$$

The SSM predictions for $\bar{R}(Ge)$ vary very little [18,19, 22]:

$$\bar{R}_{th}(Ge) = [(122 \div 132) \pm (5 \div 7)]\ \text{SNU}\ \ (1s.d.). \tag{8}$$

A detailed statistical analysis of the data of the GALLEX and SAGE experiments [23] revealed that the results of the two collaborations, eqs. (7) and (8), are statistically compatible with each other (which to certain extent is not surprising [6] given the small numbers of events the two experiments have).

In what follows we shall assume that the differences between the solar neutrino data and the SSM predictions are not due to unaccounted for astrophysical effects, poorly known nuclear reaction cross-sections, etc. (see, e.g., ref. [24]), but rather are related to a "nonstandard" behaviour of the solar electron neutrinos on their way to the Earth. Taken together, the current solar neutrino observations contain evidences in favour of this possibility. In fact, the strongest indications in favour of the neutrino physics solution of the solar neutrino problem come from the current results (1) of the experiment of Davis et al. and the corresponding current SSM predictions, eqs. (2)–(3), as well as from the difference in the observed levels of suppression of the signals in the Davis et al. and Kamiokande experiments [25]. Here we will be primarily concerned with the possibility that the solar neutrinos take part in oscillations in vacuum while they travel to the Earth, or undergo matter-enhanced transitions or spin-flavour precession (in the solar magnetic field) while they propagate from the central region to the surface of the Sun.

3. VACUUM OSCILLATIONS OF SOLAR NEUTRINOS

Consider first the possibility that solar neutrinos take part in two-neutrino oscillations in vacuum [15,26,6,7,10,11,14]: $\nu_e \leftrightarrow \nu_{\mu(\tau)}$, or $\nu_e \leftrightarrow \nu_s$, where ν_s is a sterile neutrino. The oscillations of interest are characterized, as is well known, by two parameters: $\Delta m^2 = m_2^2 - m_1^2 > 0$ and $\sin^2 2\theta$, $m_{1,2}$ being the masses of two neutrinos with definite mass in vacuum, and θ being the neutrino mixing angle in vacuum *. The regions of values of the parameters Δm^2 and $\sin^2 2\theta$, for which the oscillations $\nu_e \leftrightarrow \nu_{\mu(\tau)}$, or $\nu_e \leftrightarrow \nu_s$ of ν_e in vacuum permit to reconcile the Davis et al., Kamiokande and the GALLEX and SAGE results have recently been determined in refs. [6,7,10,11] (for earlier analyses see [26,14]). The results obtained in ref. [6] are presented graphically in Fig. 1a and Fig. 1b (grey + black + hatched shaded areas). They are based on the SSM predictions of ref. [22] (or of ref. [18], which is practically equivalent). The method of analysis of the data of the Davis et al. and Kamiokande experiments used in ref. [6] (and [7]) is, in particular, especially sensitive to the dependence of the neutrino oscillation probability on the Sun–Earth distance. Only the average rates of Ga production (7) observed by the GALLEX and SAGE collaborations (with uncertainties corresponding to 1 s.d. and 2 s.d.) have been used. The values of Δm^2 and $\sin^2 2\theta$ forming the shaded areas in Fig. 1a and Fig. 1b lie in the intervals [6,7]:

$$0.5 \times 10^{-10}\text{eV}^2 \leq \Delta m^2 \leq 1.1 \times 10^{-10}\text{eV}^2, \quad 0.75 \leq \sin^2 2\theta \leq 1. \tag{9}$$

Let us mention that for $\Delta m^2 \simeq 10^{-10}\text{eV}^2$ the oscillation length in vacuum [15], $L_\nu = 4\pi p/\Delta m^2$, p being the absolute value of the neutrino momentum, is comparable for the solar neutrinos having an energy $p \simeq 10$ MeV with the average distance between the Sun and the Earth, $R_\oplus \simeq 1.49 \times 10^8$ km.

It is interesting to note [7,6] that if the solar electron neutrinos take part in two-neutrino oscillations in vacuum characterized by the values of Δm^2 and $\sin^2 2\theta$ allowed

* For further details concerning the theory of the neutrino oscillations in vacuum see, e.g., refs. [26,27].

by the solar neutrino data, i) the one year averaged rate of ^{71}Ge–production in the Ga–Ge experiments, $\bar{R}_y(Ge)$, should lie in the interval

$$40 \text{ SNU} \leq \bar{R}_y(Ge) < 90 \text{ SNU}, \tag{10}$$

and ii) there can be seasonal variations of $\bar{R}(Ge)$, the absolute difference between the one-month average values of $\bar{R}(Ge)$ for December and June being not larger than approximately 20 SNU and 15 SNU for the cases of $\nu_e \leftrightarrow \nu_{\mu(\tau)}$ and $\nu_e \leftrightarrow \nu_s$ oscillations, respectively. The predicted seasonal changes of $\bar{R}(Ge)$ are associated with the strong dependence (for the values of Δm^2 and $\sin^2 2\theta$ belonging to the regions determined by eq. (9)) of the vacuum oscillation probability for the monochromatic ^{7}Be neutrinos on the Sun–Earth distance which varies due to the eccentricity of the Earth orbit around the Sun.

The values of Δm^2 and $\sin^2 2\theta$ forming the black areas in Figs. 1a and 1b are allowed including the GALLEX and SAGE data at 68% C.L. (1s.d.). Even at this confidence level, the solar neutrino data can be described perfectly well on the basis of the hypothesis of two–neutrino oscillations in vacuum of the solar ν_e. The corresponding region of values of Δm^2 and $\sin^2 2\theta$ is somewhat reduced by the restrictions following from the GALLEX and SAGE results *. At 95% C.L. the GALLEX and SAGE observations (7) do not lead to new constraints on the values of Δm^2 and $\sin^2 2\theta$ allowed by the results of the other two solar neutrino experiments (grey+black+hatched areas on Figs. 1a and 1b).

One can perform an analogous analysis assuming that the solar ν_e take part in three-neutrino oscillations in vacuum [28]. As can be shown [6], the important predictions concerning the maximal value of $\bar{R}_y(Ge)$, $\bar{R}_y(Ge) < 90$ SNU, and the possibility of large seasonal variations of the ^{7}Be–neutrino flux, remain valid also in the three–neutrino oscillation case.

4. THE CASE OF MATTER–ENHANCED TRANSITIONS

Let us turn now to the possibility that the solar neutrinos undergo two–neutrino transitions $\nu_e \to \nu_{\mu(\tau)}$ in the Sun, which are resonantly enhanced by solar matter effects [16]. At present there exists a well developed theory and a complete, simple and very accurate analytic description of the indicated transitions of the solar neutrinos in the Sun (see, e.g., ref. [29]). The transitions of interest depend on the same two parameters Δm^2 and $\sin^2 2\theta$ which enter into the expression for the vacuum oscillation probabilities. For a solar ν_e with momentum $\vec{p}$ they depend also on the value of the electron number density N_e in the point of neutrino production in the Sun, $N_e(t_0)$, on the resonance density [16], $N_e^{res} = (\Delta m^2 \cos 2\theta)/(2p\sqrt{2}G_F)$, as well as on the way (relatively "fast" or "slow") N_e changes along the neutrino path in the Sun. The latter, in particular, determines the type of the solar neutrino transitions in the Sun, which can be adiabatic or nonadiabatic [16] (see also [27]). According to the SSM [18,19,22], N_e decreases approximately exponentially with a scale height $r_0 \cong 0.1R_s$, $R_s \cong 6.96 \times 10^5$ km being the solar radius, in the radial direction from the centre to the surface of the Sun. The probability that a ν_e having momentum $\vec{p}$ and produced at time t_0 in the central part of the Sun will not transform into $\nu_{\mu(\tau)}$ on its way to the surface of the Sun (reached at time t_s), $P(\nu_e \to \nu_e; t_0, t_s)$, is given by [30,31]

$$P(\nu_e \to \nu_e; t_0, t_s) = \frac{1}{2} + \left(\frac{1}{2} - P'\right) \cos 2\theta_m(t_0) \cos 2\theta. \tag{11}$$

* The inclusion of the latest SAGE data, eq. (7), leads to additional restrictions in this case which were not accounted for in refs. [6] and [10] and which are indicated as hatched areas in Fig. 1a.

Here

$$P' = \frac{\exp\left[-\pi r_0 \frac{\Delta m^2}{2p}(1-\cos 2\theta)\right] - \exp\left[-2\pi r_0 \frac{\Delta m^2}{2p}\right]}{1-\exp\left[-2\pi r_0 \frac{\Delta m^2}{2p}\right]} \tag{12}$$

is [30,31] the level crossing probability (i.e., the analog of the Landau–Zener probability) for exponentially varying density N_e, and $\theta_m(t_0)$ is the neutrino mixing angle in matter [16] in the point of ν_e production, $\tan 2\theta_m(t_0) = \tan 2\theta/(1 - N_e(t_0)/N_e^{res})$. For the adiabatic (nonadiabatic) $\nu_e \to \nu_{\mu(\tau)}$ transitions the probability P' is negligible (nonnegligible).

In the calculations performed for the study of the possible MSW solutions of the solar neutrino problem one can utilize a certain procedure [31] which makes the analytic description of the matter–enhanced transitions of the solar neutrinos based on eqs. (11) and (12) remarkably precise * (the precision is typically not worse than 95 % in the domain of values of Δm^2 and $\sin^2 2\theta$ of interest [31]).

The interpretation of the solar neutrino observations in terms of the MSW effect for solar neutrinos was studied in several articles [6,8,9,11,12] after the publication of the GALLEX and the latest SAGE data last year. The results obtained in ref. [6] are presented graphically in Fig. 2a and Fig. 2b, where respectively the 68 % C.L. and the 95 % C.L. iso–SNU and iso–suppression contours, corresponding to the data (1), (7), and (4) of the Davis et al., GALLEX, SAGE and the Kamiokande experiments, are shown. The iso–SNU contours associated with the GALLEX result (7) give the values of Δm^2 and $\sin^2 2\theta$ for which $\bar{R}_y(Ge)$ is within the limits 62 SNU $\leq \bar{R}_y(Ge) \leq$ 104 SNU (Fig. 2a) and 41 SNU $\leq \bar{R}_y(Ge) \leq$ 125 SNU (Fig. 2b). The elements of the iso–SNU contours shown on Fig. 2a (corresponding to 80 SNU and 30 SNU) and on Fig. 2b (102 SNU) indicate the constraints following from the SAGE .. The curves were derived taking the mean values of the SSM predictions (2) and (5); the value of 132 SNU [18,22] has been used as a SSM prediction for the event rate in the Ga–Ge experiments. As it is clear from Figs. 2a and 2b, the current solar neutrino data can be described rather well on the basis of the hypothesis that the solar neutrinos undergo two-neutrino matter-enhanced transitions into active neutrinos of a different flavour (i.e., $\nu_e \to \nu_{\mu(\tau)}$) in the Sun. The values of Δm^2 and $\sin^2 2\theta$, for which the matter-enhanced transitions of the solar ν_e allow to reproduce the results of the Davis et al., Kamiokande, GALLEX and SAGE experiments are shown as black areas on Figs. 2a and 2b *. The restrictions following from the absence of a difference between the event rates observed during the day and during the night by the Kamiokande–II experiment were also taken into account on Figs. 2a and 2b. The 95% C.L. allowed values of the parameters Δm^2 and $\sin^2 2\theta$, forming the three disconnected black areas on Fig. 2b, lie in the intervals:

$$3.2 \times 10^{-6}\text{eV}^2 \lesssim \Delta m^2 \lesssim 1.1 \times 10^{-5}\text{eV}^2, \quad 5 \times 10^{-3} \lesssim \sin^2 2\theta \lesssim 1.6 \times 10^{-2}, \tag{13a}$$

$$\Delta m^2 \sin^2 2\theta \cong (4.3 \pm 1.1) \times 10^{-8}\text{eV}^2, \tag{13b}$$

$$5.4 \times 10^{-6}\text{eV}^2 \lesssim \Delta m^2 \lesssim 1.1 \times 10^{-4}\text{eV}^2, \quad 0.39 \lesssim \sin^2 2\theta \lesssim 0.86, \tag{14}$$

and

$$10^{-7}\text{eV}^2 \lesssim \Delta m^2 \lesssim 1.8 \times 10^{-6}\text{eV}^2, \quad 0.74 \lesssim \sin^2 2\theta \lesssim 0.93. \tag{15}$$

* This procedure was used in refs. [6,11]. For a concise summary see ref. [29].

* The grey areas on Figs. 2a and 2b are allowed by the GALLEX data, but are excluded by the SAGE results.

The results (13)–(15) were obtained [6] on the basis of a somewhat simplified analysis. First, the uncertainties in the theoretical predictions (2), (5), and (8) were not taken into account. Second, in a more refined statistical treatment of the experimental observations one should treat the data from the different experiments simultaneously and thus determine the relevant allowed regions of the values of the parameters Δm^2 and $\sin^2 2\theta$ at a chosen confidence level. However, one could expect that the results one would obtain using the more consistent approach taking care of the indicated inaccuracies will not be very much different from those represented by eqs. (13)–(15) as the effects on the results from the improvements of the analysis along these two points tend to mutually cancel. This is confirmed by the study performed in ref. [9] (see also ref. [11]), where the indicated inaccuracies were taken into account and at 95% C.L. results practically coinciding with those shown in Fig. 2b were obtained *.

For Δm^2 and $\sin^2 2\theta$ belonging to the intervals (13a)–(13b) (the small mixing angle case) the MSW transitions of the ^{8}B–neutrinos are nonadiabatic, while the transitions of the pp– and the ^{7}Be–neutrinos are adiabatic. This solution is usually called "nonadiabatic". In the case of the nonadiabatic solution the probability of ν_e survival in the Sun strongly depends on the energy of the solar ν_e: it is very small ($\sim 10^{-3}$) for the ^{7}Be–neutrinos, close to 1 for the pp–neutrinos, and varies with the energy for the ^{8}B–neutrinos. The large mixing angle solutions corresponding to values of Δm^2 and $\sin^2 2\theta$ from (14) and (15) are associated with adiabatic transitions of the ^{8}B–, ^{7}Be– and the pp–neutrinos ("adiabatic" solutions). For the values of Δm^2 and $\sin^2 2\theta$ from the intervals (15), for instance, the survival probability for the ^{8}B, ^{7}Be and pp electron neutrinos is roughly the same and is approximately equal to $\sin^2\theta$. The same is true for the allowed values of Δm^2 and $\sin^2 2\theta$ from the intervals (14) when $\sin^2 2\theta \gtrsim 0.65$. For $0.39 \lesssim \sin^2 2\theta \lesssim 0.65$ and the corresponding values of Δm^2 from (14) the survival probability for the ^{8}B–, ^{7}Be–, and the pp–neutrinos can differ substantially [6].

The specific energy dependence of the solar neutrino survival probability in the cases of the solutions considered in Sections 3 and 4 is reflected, e.g., in the spectrum of electrons from solar $\nu_e - e^-$ elestic scattering, as is illustrated on Figs. 3a and 3b.

How the solutions we have described above are going to change if the solar neutrinos undergo transitions into sterile neutrinos, $\nu_e \to \nu_s$, in the Sun? The 1 s.d. solutions (see Fig. 2a) can disappear, while the two regions on Fig. 2b associated with eqs. (14) and eqs. (15) will "shrink" somewhat in $\sin^2 2\theta$: the first towards the smaller values of $\sin^2 2\theta$ from the corresponding interval in (14), and the second– towards the larger values of $\sin^2 2\theta$ from the interval in (15) [6]. Actually, one can use cosmological arguments [32] to rule out the "large" mixing angle solutions in this case.

5. A SPIN-FLAVOUR CONVERSION SOLUTION

Finally, let us consider briefly a solution of the solar neutrino problem based on the hypothesis of matter–enhanced spin–flavour conversion [17] $\nu_{eL} \to \bar{\nu}_{\mu R}$ of solar neutrinos in the toroidal magnetic field in the Sun **. As is well known, the possibility of spin–flavour conversion of solar neutrinos is being discussed in connection with the suggested time variation of the signal in experiment of Davis et al. in (anti)correlation with the solar

* The "large" mixing angle solution (15) disappears if utilizing the χ^2– criterium to determine the allowed regions of values of Δm^2 and $\sin^2 2\theta$ at 95% C.L. one does not take into account (or underestimates) the uncertainties in the theoretical predictions [8,12].

** For a detailed discussion of the theory of spin–flavour conversion of neutrinos see, e.g., refs. [33].

activity [34]. Such time variation cannot be produced, e.g., by vacuum oscillations of solar neutrinos.

The interpretation of the solar neutrino observations in terms of the spin–flavour conversion hypothesis has been studied after the publication of the GALLEX and the latest SAGE data in refs. [35-38]. We shall present here a brief summary of the results obtained in ref. [35]. The simplest case of i) conversion involving only two active neutrinos ν_{eL} and $\bar{\nu}_{\mu R}$, ii) negligible lepton mixing (ν_{eL} and $\nu_{\mu L}$ ($\bar{\nu}_{\mu R}$) are supposed to be neutrinos with definite masses m_1 and m_2 in vacuum), iii) existence of ν_{eL}–$\bar{\nu}_{\mu R}$ transition moment of magnetic dipole type, μ, and of iv) nontwisting solar magnetic field *, $B_\perp$, was considered. The rate of Ar production observed in the experiment of Davis et al. in the period of low (high) solar activity was taken to lie in the interval [4] 3.6 SNU $\leq \bar{R}(Ar) \leq$ 4.8 SNU ($0 \leq \bar{R}(Ar) \leq$ 1.9 SNU). The event rate in the Kamiokande experiments, and correspondingly, the value of the ratio $\bar{R}(K) = \bar{\Phi}(B)/\Phi^0$ extracted from the data, is consistent with being constant in time. However, time variations of $\bar{R}(K)$ which do not exceed approximately 30% cannot be ruled out by the data [5]. In ref. [35] the values of $\bar{R}(K)$ at minima (maxima) of solar activity were taken to lie in the interval 0.58–0.68 (0.30–0.40). The numbers 0.68 and 0.30 correspond to the observed maximal and minimal values of $\bar{R}(K)$ (including 1 s.d. uncertainties in the data from the corresponding runs); the width of the allowed $\bar{R}(K)$ regions was taken rather arbitrarily.

The $\nu_{eL} \to \bar{\nu}_{\mu R}$ conversion probability in the case considered depends, in particular, on the parameter Δm^2 and on $\mu B_\perp$. The results quoted below correspond to $\mu = 10^{-11}\mu_B$, where μ_B is the Bohr magneton; results for any other value of μ can be obtained from those derived by corresponding rescaling of $B_\perp$. Unfortunately, very little is known about the structure of the magnetic field inside the Sun so that one is forced to utilize various physically plausible magnetic field configurations. Several different spatially nonuniform (spherically symmetric) profiles of $B_\perp$ have been used in the analysis [35] **. The case of existence of a frozen magnetic field in the central part of the Sun in addition to the field in the convective zone was also investigated. The quality of the fit of the data was found to be very sensitive to the form of the magnetic field profile used in addition to the assumed strenght of the magnetic field. In principle, this may allow to get detailed information about the magnetic field in the solar interior in the future. The best fit (in the simplest case of no inner magnetic field) was achieved with the "triangle" magnetic field configuration

$$B_\perp(x) = B_0 \frac{x - x_0}{x_c - x_0}, \quad x_0 \leq x < x_c, \tag{16a}$$

$$B_\perp(x) = B_0 \left(1 - \frac{x - x_c}{1 - x_c}\right), \quad x_c \leq x \leq 1, \tag{16b}$$

with $x_0 = 0.70$ and $x_c = 0.85$, x being the distance from the centre of the Sun in units of the solar radius R_s, and B_0 being the maximal value of $B_\perp$. It was assumed for simplicity that only B_0 changes with time. The results obtained are presented graphically on Fig. 4. The shaded areas on Fig. 4 correspond to values of the parameters Δm^2 and B_0 for which the values of $\bar{R}(Ar)$ and $\bar{R}(K)$ in the periods of low and high solar activity lie in

* The case of convective zone magnetic field $B_\perp$ which changes its direction in the plane perpendicular to the neutrino momentum, i.e. twists, along the neutrino trajectory in the Sun was analyzed in ref. [36].

** The solar magnetic field $B_\perp$ was assumed to be spatially uniform and present everywhere in the Sun in the study performed in ref. [37]. This assumption is not supported by the current views about the structure of the solar magnetic field.

the intervals specified above *. With the magnetic field configuration (16) used one finds that always $\bar{R}(Ar) \geq 1.5$ SNU, while the rate of Ge production in the Ga-Ge experiments is 62 SNU $\leq \bar{R}_y(Ge) \leq 102$ SNU. Note that the GALLEX and the lates SAGE data were collected during a period of high solar activity. The allowed ranges of the parameters which follow from Fig. 4 correspond to

$$\Delta m^2 \simeq (4 \times 10^{-9} - 2 \times 10^{-8})\ \mathrm{eV}^2,\ (B_0)_{min} \simeq 28\ \mathrm{kG},\quad (B_0)_{max} \simeq 50\ \mathrm{kG}. \qquad (17)$$

Similar results are obtained if one takes $x_0 = 0.75$ instead of 0.70 in the magnetic field profile of eq. (16). All the other magnetic field configurations considered in ref. [35] either resulted in very poor fits of the experimental results or completely failed to reproduce the chlorine, Kamiokande and gallium data simultaneously.

6. IMPLICATIONS FOR FUTURE SOLAR NEUTRINO EXPERIMENTS

The implications of the above results for the future solar neutrino experiments SNO [39], Super Kamiokande [40], BOREXINO [41] and ICARUS [42] have been studied in refs. [6,10,12,37,43,44]. The designed characteristics of the BOREXINO detector [41] and the remarkably narrow width of the ^{7}Be–neutrino 0.86 MeV line make the BOREXINO experiment appear best adapted to test the vacuum oscillation solution of the solar neutrino problem [7,6,10] and to distinguish between it and the matter-enhanced transitions (or MSW) solutions. In the case of the vacuum oscillation solution (see eq. (9)) a rather strong monthly and/or seasonal variations of the flux of the ^{7}Be electron neutrinos at the Earth surface is predicted to take place (in addition to the expected standard $\sim$ 7% seasonal variation), as the probability of the ^{7}Be–neutrino survival, P(^{7}Be), exhibits typically a strong oscillatory dependence on the Sun– Earth distance. For instance, for $\Delta m^2 = 7.9\times10^{-11}$ eV^2; 6.3×10^{-11} eV^2 and $\sin^2 2\theta = 0.8$ ($\sin^2 2\theta = 0.9$), the one month average values of P(^{7}Be) for December and June read, respectively: 0.19 and 0.35; 0.35 and 0.19 (0.10 and 0.26; 0.28 and 0.10). Let us recall that the suppression factor F of the signal in the BOREXINO experiment is approximately equal to the suppression factor F(^{7}Be) of the 0.86 MeV ^{7}Be–neutrino flux, F $\approx$ F(^{7}Be), which in turn is given by F(^{7}Be) $\approx$ P(^{7}Be) + 0.22(1 - P(^{7}Be)) in the case of $\nu_e \leftrightarrow \nu_{\mu(\tau)}$ oscillations ($\nu_e \rightarrow \nu_{\mu(\tau)}$ transitions), and coincides with P(^{7}Be), F(^{7}Be) = P(^{7}Be), if $\nu_e \leftrightarrow \nu_s$ oscillations ($\nu_e \rightarrow \nu_s$ transitions) take place. It should be noted that the seasonal variations of the flux of the ^{8}B electron neutrinos (and therefore of the event rates in the SNO, Super Kamiokande and ICARUS detectors) predicted to take place due to the vacuum oscillations only are not larger than 15% [6]. For some of the allowed values of Δm^2 and $\sin^2 2\theta$ from (9) (e.g., for $\Delta m^2 \sim 10^{-10}$ eV^2) they can compensate the standard 7% seasonal change of the flux of ^{8}B–neutrinos reaching the Earth, associated simply with the change of the Sun–Earth distance.

In contrast to the behavior of P(^{7}Be) in the vacuum oscillation solution case, the averaged probability of ν_e survival in the Sun (and therefore, the corresponding suppression factors) does not exhibit in the case of the MSW solutions monthly and/or seasonal variations, being independent on the Sun–Earth distance for any of the components (^{8}B, ^{7}Be, pp, etc.) of the solar ν_e flux. Thus, a constant value of F(^{7}Be) all through the year will be an evidence in favour of the MSW solutions of the solar neutrino problem. Would it be possible to distinguish between the different MSW solutions on the basis of the BOREXINO data? Values of F(^{7}Be) $\approx$ 0.22 and F(^{7}Be) $\sim 10^{-3}$ are predicted in the case of the

* The shaded area at values of $B_0 \sim 75$ kG corresponds to values of Δm^2 for which there is a direct correlation of neutrino signals with solar activity instead of anticorrelation.

nonadiabatic solution: the first corresponds to $\nu_e \rightarrow \nu_{\mu(\tau)}$ transitions, while the second – to $\nu_e \rightarrow \nu_s$ transitions. If the adiabatic solution is valid and $\sin^2 2\theta = 0.40; 0.50; 0.60; 0.70; 0.80; 0.90$, the suppression factor F(^{7}Be) should take respectively the values F(^{7}Be) = (0.69 to 0.78); (0.58 to 0.72); (0.47 to 0.67); (0.53 to 0.61); (0.36 to 0.55); (0.34 to 0.37), an interval for a given value of $\sin^2 2\theta$ corresponding to the interval of allowed values of Δm^2 for this value of $\sin^2 2\theta$.

The SNO, Super Kamiokande and the ICARUS experiments will provide, in particular, information about the spectrum of the final state electrons in the ν–e^- elastic scattering reaction. The predicted spectra [6] for several typical values of Δm^2 and $\sin^2 2\theta$ from (9), (13), (14) and (15), and ν_e oscillations or transitions in $\nu_{\mu(\tau)}$ are shown in Figs. 3a and 3b. It is clear from Figs. 3a and 3b that the experiments using detectors with lower "thresholds" will have greater capabilities to descriminate between the different solutions. Spectral information can also be of crucial importance for distinguishing between the spin-flavour precession solution and the vacuum oscillation and the MSW ones [44].

To conclude, the vacuum oscillations and the matter-enhanced transitions of the solar neutrinos continue to be viable and aesthetically very appealing solutions of the solar neutrino problem. The solar neutrino observations (including the suggested time variation of the signal in the experiment of Davis et al. in anticorrelation with the solar activity) can also be described on the basis of the spin-flavour conversion hypothesis. In the latter case the quality of the fit of the data depends strongly on the assumed type of the profile of the magnetic field in the convective zone of the Sun. Future real time high statistics solar neutrino experiments (SNO, Super Kamiokande, BOREXINO, ICARUS) will be able to test further and possibly discriminate between these solutions.

ACKNOWLEDGMENTS. The author would like to thank the members of the Organizing Committee of the Moriond Workshop for ensuring pleasant working atmosphere at the Workshop. This work was supported in part by the Bulgarian National Science Foundation via grant PH–16.

References

1. A.I. Abazov et al. (SAGE collaboration), Phys. Rev. Lett. 67 (1991) 332.
2. P. Anselmann et al., (GALLEX collaboration), Phys. Lett. 285B (1992) 376.
3. V. Gavrin, Talk given at the XXVIth Int. Conference on High Energy Physics, August 5 - 13, 1992, Dallas (U.S.A.).
4. R. Davis et al., XXI Int. Cosmic Ray Conf., January 6–19, Adelaide, Australia, Conference papers, vol. 7, p. 155, 1990; K. Lande, Talk given at the Int. Conf. "Neutrino '90", June 10-15, 1990, Geneva.
5. K.S. Hirata et al. (Kamiokande II collaboration), Phys. Rev. Lett. 63 (1989) 16; 65 (1990) 1297 and 1301; Y. Suzuki, ICRR Report 92-15; Y. Totsuka, Talk given at the "Neutrino '92" Int. Conf., Granada, June 7–12, 1992.
6. P.I. Krastev and S.T. Petcov, Phys. Lett. 299B (1992) 99.
7. P.I. Krastev and S.T. Petcov, Phys. Lett. 285B (1992) 85.
8. P. Anselmann et al., (GALLEX collab.), Phys. Lett. 285B (1992) 390.
9. X. Shi, D.N. Schramm, and J.N. Bahcall, Phys. Rev. Lett. 69 (1992) 717.
10. V. Barger, R.J.N. Phillips, and K. Whisnant, preprint MAD-PH-708 (1992).
11. L. Krauss, E. Gates, and M. White, Phys. Lett. 299B (1993) 94.
12. S.A. Bludman et al., preprint UPR-0516T (revised), December 1992.
13. P.I. Krastev, S.P. Mikheyev and A.Yu. Smirnov, INR preprint P-695, Moscow, 1991; J.N. Bahcall and W.C. Haxton, Phys. Rev. D40 (1989) 931; A.J. Baltz and J.

Weneser, Phys. Rev. D37 (1988) 3364; J. Bouchez et al., Z. Phys. C32 (1986) 499; S.P. Rosen and J.M. Gelb, Phys. Rev. D34 (1986) 969.
14. V. Barger, R.J.N. Phillips and K. Whisnant, Phys. Rev. D43 (1991) 1110; A. Acker, S. Pakvasa and J. Pantaleone, Phys.Rev. D43 (1991) 1754.
15. B. Pontecorvo, Zh. Eksp. Teor. Fiz. 33 (1957) 549, 34 (1958) 247, 53 (1967) 1717.
16. S.P. Mikheyev and A.Yu. Smirnov, Yad. Fiz. 42 (1985) 1441; L. Wolfenstein, Phys. Rev. D17 (1978) 2369.
17. C.-S. Lim and W. Marciano, Phys. Rev. D37 (1988) 1368; E.Kh. Akhmedov, Phys. Lett. 213B (1988) 64.
18. J.N. Bahcall and R.K. Ulrich, Rev. Mod. Phys. 60 (1988) 298.
19. S. Turck–Chièze et al., Astrophys. J. 335 (1988) 425; S.Turck–Chièze, Talk given at the "Neutrino '92" Int. Conf., Granada, June 7–12, 1992.
20. B. Pontecorvo, Chalk River Lab. Report PD–205 (1946).
21. V.A. Kuzmin, Sov. Phys. JETP 22 (1966) 1050.
22. J.N. Bahcall and M. Pinsonneault, preprint IASSNS-AST 92/10. This paper contains a review of the results obtained by other authors and references to their work.
23. M. Spiro, these Proceedings.
24. M. Pinsonneault, these Proceedings.
25. J.N. Bahcall and H.A. Bethe, Phys. Rev. D47 (1993) 1298.
26. S.M. Bilenky and B. Pontecorvo, Phys. Rep. 41 (1978) 225.
27. S.M. Bilenky and S.T. Petcov, Rev. Mod. Phys. 59 (1987) 671.
28. A. De Rujula et al., Nucl.Phys. B168 (1980) 54.
29. S.T. Petcov, Nucl. Phys. B (Suppl.) 13 (1990) 527.
30. S.T. Petcov, Phys. Lett. 200B (1988) 373, 214B (1988) 139.
31. P.I. Krastev and S.T. Petcov, Phys. Lett. 207B (1988) 64; (E): ibid. 214B (1988) 661; J. Rich and S.T. Petcov, Phys. Lett. 224B (1989) 426.
32. K. Enqvist et al., Nucl. Phys. B373 (1992) 498.
33. P.B. Pal, Int. J. Mod. Phys. A (1992); J. Pulido, Phys. Rep. 211 (1992) 167.
34. G.A. Bazilevskaia et al., JETP Lett. 35 (1982) 273 and Yad. Fiz. 39 (1984) 856; B. Filippone and P. Vogel, Phys. Lett. 246B (1990) 546; L. Krauss, Nature 348 (1990) 403; J.W. Bieber et al., Nature 348 (1990) 407.
35. E.Kh. Akhmedov, A. Lanza and S.T. Petcov, Phys. Lett. 303B (1993) 85.
36. P.I. Krastev, Phys. Lett. 303B (1993) 75.
37. H. Minakata and H. Nunokawa, these Proceedings.
38. J. Pulido, Inst. Math. Phys. preprint IFM 19/92, Lisboa.
39. G. Ewan et al., Sudbury Neutrino Observatory Proposal, SNO-87-12, 1987.
40. T. Kajita, Physics with the Super Kamiokande Detector, ICRR Report 185-89-2, 1989.
41. C. Arpesella et al., BOREXINO proposal (eds. G. Bellini, R. Raghavan et al., Univ. of Milano, Milano 1992), vols. 1 and 2.
42. J.N. Bahcall, M. Baldo-Ceolin, D. Cline, and C. Rubbia, Phys. Lett. 178B (1986) 324; ICARUS I: An Optimized, Real Time Detector of Solar Neutrinos, by the ICARUS collaboration, LNF–89/005(R), 1989.
43. J.W. Gelb et al., Phys. Rev. Lett. 69 (1992) 1846.
44. P.I. Krastev and S.T. Petcov, in preparation.

Figure Captions

Fig. 1a. Regions of values of the parameters Δm^2 and $\sin^2 2\theta$ allowed by the Homestake and Kamiokande–II individual run data (grey+black+hatched area), and by the 68% C.L. (black area) and 95% C.L. (grey+black+hatched area) GALLEX and SAGE results in the case of solar neutrino oscillations into active neutrinos: $\nu_e \leftrightarrow \nu_{\mu(\tau)}$. Shown are also the iso-SNU contours corresponding to an average rate of ^{71}Ge production in the Ga–Ge experiments of 83 SNU (dash–dotted line), 104 SNU and 63 SNU (solid lines). The grey (hatched) area is excluded at 68% C.L. by the GALLEX (SAGE) result.

Fig. 1b. The same as in fig. 1a, but for solar neutrino oscillations into sterile neutrinos: $\nu_{e'} \leftrightarrow \nu_s$.

Fig. 2a. Regions of values of Δm^2 and $\sin^2 2\theta$ for which the matter-enhanced two–neutrino transitions $\nu_e \rightarrow \nu_{\mu(\tau)}$ provide a solution to the solar neutrino problem (black areas): the iso–SNU and the iso-suppression contours correspond to the 68% C.L. Homestake (solid lines), Kamiokande–II and –III (dashed lines), SAGE 1990 [1] (dotted line), GALLEX (dash-dotted lines), and SAGE 1992 [3] (dash-dotted elements of lines) results. The region allowed by the Homestake data is located between the two solid line contours, etc.

Fig. 2b. The same as in fig. 2a, but for the 95% C.L. Homestake, Kamiokande–II and –III, GALLEX and SAGE 1992 results. The dotted line corresponds to the SAGE 90% C.L. upper limit of 79 SNU, obtained in 1990.

Fig. 3a. The spectrum of the final state electrons from the ν–e^- elastic scattering reaction in the case of vacuum oscillations $\nu_e \leftrightarrow \nu_{\mu(\tau)}$ of solar neutrinos, characterized by values of Δm^2 and $\sin^2 2\theta$ from (9) for which one obtains a description of the solar neutrino data. The spectrum is normalized to the standard one (for ν_e–e^- elastic scattering) in the absence of oscillations. The values of Δm^2 (in eV^2) and $\sin^2 2\theta$, for which the curves have been obtained, are given in brackets at the curves.

Fig. 3b. The same as in fig. 3a, but for the case of matter-enhanced $\nu_e \rightarrow \nu_{\mu(\tau)}$ transitions of solar neutrinos. The dashed curve corresponds to nonadiabatic transitions, while the solid curves correspond to adiabatic transitions.

Fig. 4. The iso-SNU (iso-suppression) contours for ^{37}Cl, Kamiokande and ^{71}Ga experiments in the (B_0, Δm^2) plane. The magnetic field configuration is described by eq. (16). The full lines are chlorine iso-SNU curves (1.5, 1.9, 2.2, 3.6, 4.8, 5.2 and 5.8 SNU), the dotted lines correspond to the ratio $\bar{R}$=0.30, 0.40, 0.58 and 0.68 for the Kamiokande experiment, and the dash-dotted lines represent the gallium iso-SNU curves (62.0, 83.0, 104.0 and 120 SNU). The shaded areas show the allowed ranges of values of the parameters Δm^2 and B_0 (see the text).

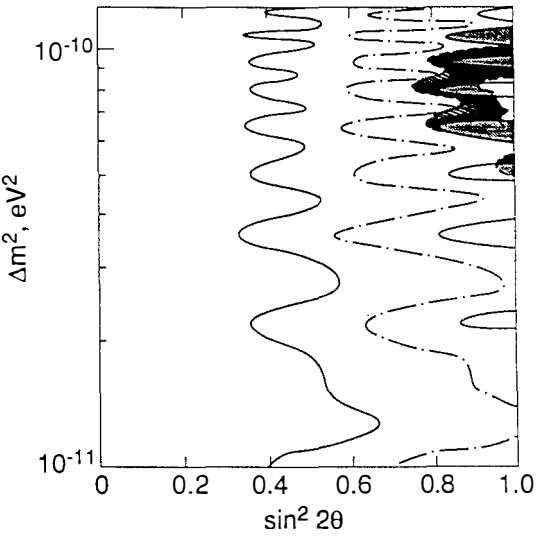

Figure 1a.

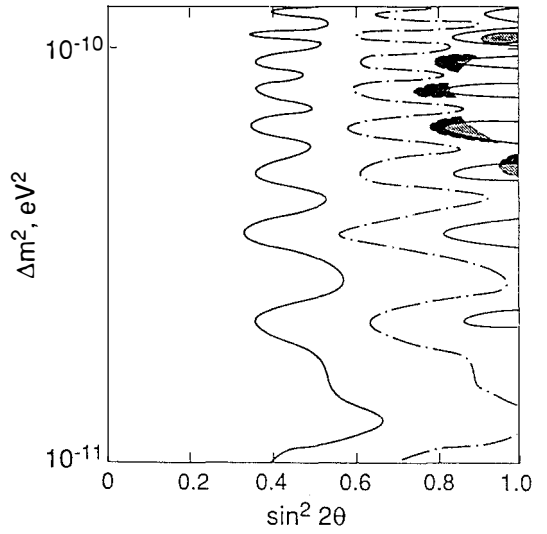

Figure 1b.

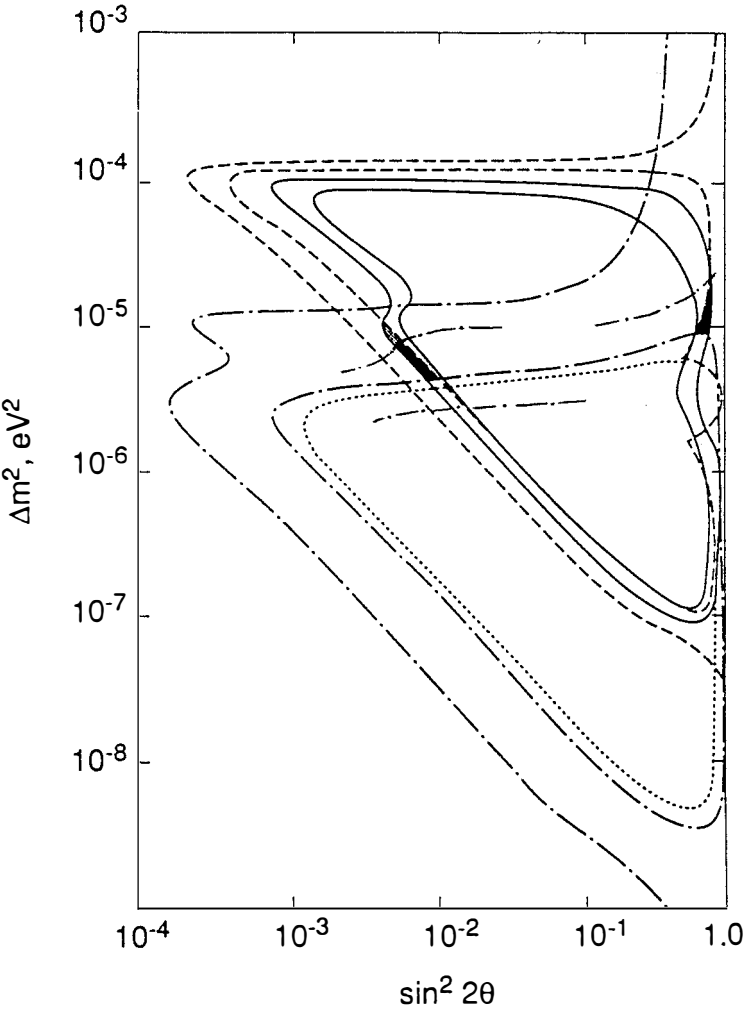

Figure 2a.

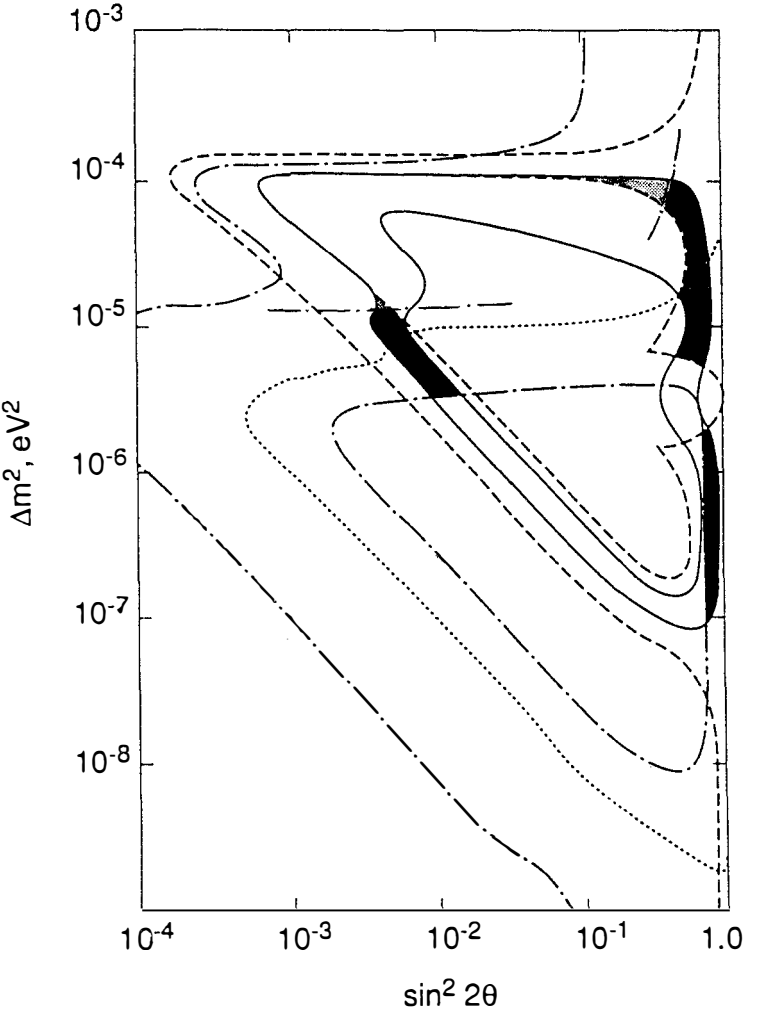

Figure 2b.

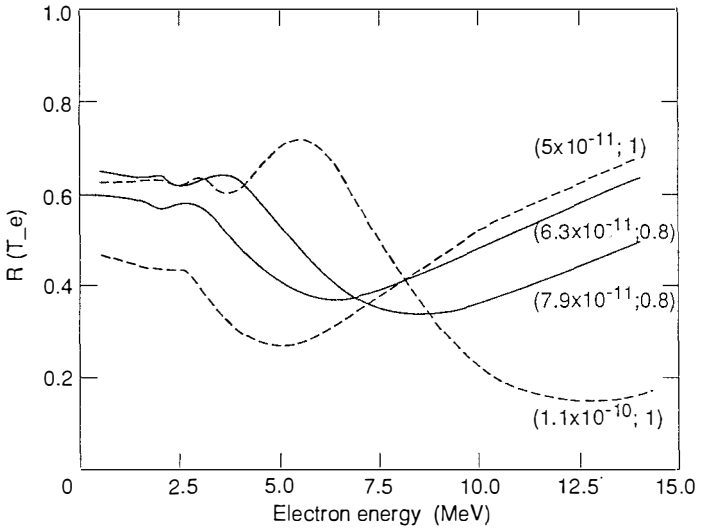
1.0
0.8
0.6
0.4
0.2
0
R (T_e)
2.5
5.0
7.5
10.0
12.5
15.0
Electron energy (MeV)
(5x10-11; 1)
(6.3x10-11;0.8)
(7.9x10-11;0.8)
(1.1x10-10; 1)

Fig. 3a

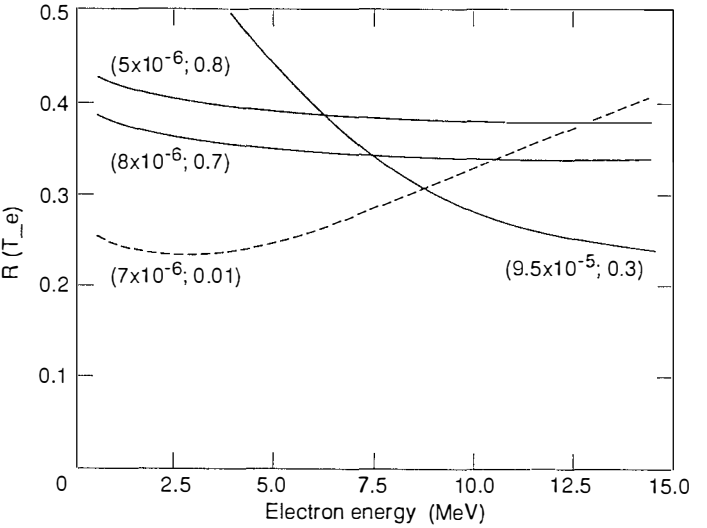
0.5
0.4
0.3
0.2
0.1
0
R (T_e)
2.5
5.0
7.5
10.0
12.5
15.0
Electron energy (MeV)
(5x10-6; 0.8)
(8x10-6; 0.7)
(7x10-6; 0.01)
(9.5x10-5; 0.3)

Fig. 3b

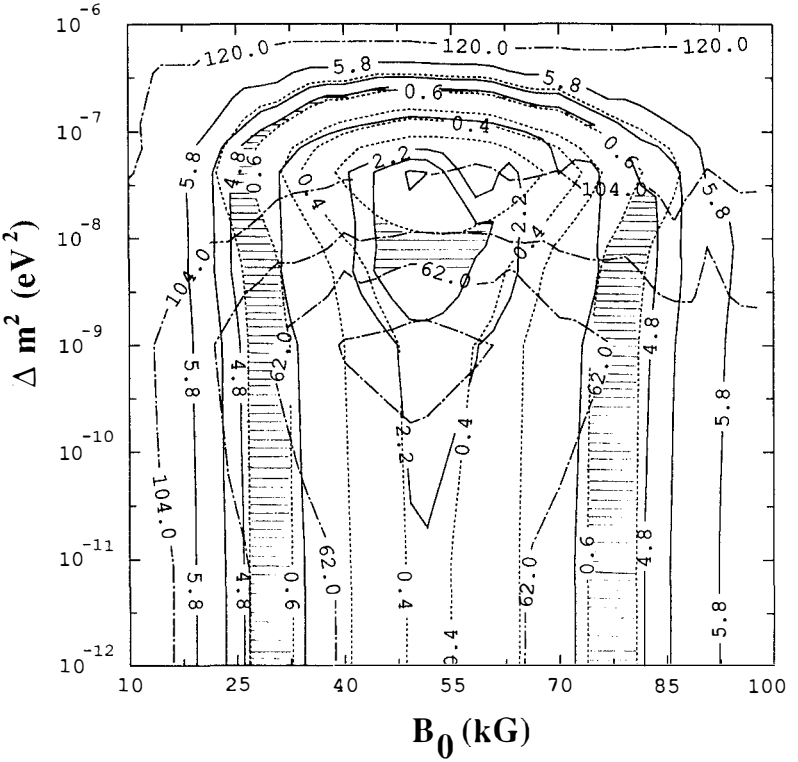
10^{-6}
10^{-7}
10^{-8}
10^{-9}
10^{-10}
10^{-11}
10^{-12}
Δm^2 (eV^2)
10
25
40
55
70
85
100
B_0 (kG)
120.0
5.8
0.6
0.4
2.2
104.0
62.0
4.8

Figure 4.

NEUTRINO SPIN PRECESSION WITH FLAVOR MIXING AND THE SOLAR NEUTRINO PROBLEM

Hiroshi Nunokawa[1,2] and Hisakazu Minakata[1]

[1] *Department of Physics, Faculty of Science*
Tokyo Metropolitan University
1-1 Minami-Osawa Hachioji, Tokyo 192-03 Japan

[2] *Theory Group, National Laboratory for High Energy Physics (KEK)*
1-1 Oho, Tsukuba-shi, Ibaraki-ken, 305 Japan

presented by H. Nunokawa

ABSTRACT

We focus our attention to the combined mechanism of the Mikheyev-Smirnov- Wolfenstein (MSW) and the spin-flavor resonance effects as a solution to the solar neutrino problem. We will report some results of our detailed numerical analysis of the mechanism and will show the parameter regions by which the mechanism can explain the solar neutrino deficit. If the parameters are located in this region, we can explain existing three types of experiments, the ^{37}Cl, the Kamiokande-II and the ^{71}Ga, at the 2σ level. This new solution contains the spin-flavor resonance effect as its key ingredient.

1. Introduction

One of the most promising solution to the solar neutrino problem is the reduction of electron neutrino by the matter enhanced neutrino oscillation, the Mikheyev-Smirnov- Wolfenstein (MSW) mechanism[1]. From the data of the ^{37}Cl, the Kamiokande-II and the Gallex experiments, one can pick out the two restricted parameter regions of $\sin^2 2\theta$ and Δm^2 where the MSW mechanism acts as the solution[2]. The another attractive possibility is that the observed neutrino flux is reduced because of the spin rotation of the left handed neutrino into the right handed one in the solar magnetic field[3]. Of particular interest is the mechanism of resonant enhancement of neutrino spin rotation in matter with the magnetic field which is found by Lim and Marciano[4], and by Akhmedov[5]. The spin rotation is the natural explanation of the anticorrelation between the sunspot number and the solar neutrino flux which is reported in the ^{37}Cl experiment[6] . It has been pointed out [7] that the two resonant mechanism can work simultaneously to reduce the flux of ν_e from the sun for certain values of the parameters $\sin^2 2\theta$, Δm^2 and μB where μ is the neutrino magnetic moment and B is the solar magnetic field. Several authors[8] have studied the spin-flavor resonance in the presence of flavor mixing from the different points of view. Here, we will report some results of our extensive analysis of this combined mechanism of the MSW and the resonant spin rotation and examine whether this mechanism can be a new solution to the solar neutrino problem.

2. Spin-Flavor Resonance with Flavor Mixing

The evolution equation for neutrinos in matter with the magnetic field for two generation of Majorana type neutrinos is given by

$$i\frac{d}{dt}\begin{bmatrix}\nu_e\\ \nu_\mu\\ \bar{\nu}_e\\ \bar{\nu}_\mu\end{bmatrix} = H\begin{bmatrix}\nu_e\\ \nu_\mu\\ \bar{\nu}_e\\ \bar{\nu}_\mu\end{bmatrix} \tag{1}$$

The Hamiltonian matrix for this system [4] is given by

$$H = \begin{bmatrix} a_{\nu_e}(r) - \frac{\Delta m^2}{2E}\cos 2\theta & \frac{\Delta m^2}{4E}\sin 2\theta & 0 & \mu B \\ \frac{\Delta m^2}{4E}\sin 2\theta iso & a_{\nu_\mu}(r) & -\mu B & 0 \\ 0 & -\mu B & -a_{\nu_e}(r) - \frac{\Delta m^2}{2E}\cos 2\theta & 0 \\ \mu B & 0 & \frac{\Delta m^2}{4E}\sin 2\theta & -a_{\nu_\mu}(r) \end{bmatrix} \tag{2}$$

where $a_{\nu_e} \equiv \sqrt{2}G_F(N_e - N_n/2)$, $a_{\nu_\mu} \equiv \sqrt{2}G_F(-N_n/2)$ with N_e, N_n the electron and neutron density in the sun and B is the solar magnetic field. Note that diagonal elements of magnetic moment vanish for Majorana neutrinos. Since we do not know the detailed structure of the magnetic field in the sun, we assume the simplest case, the uniform magnetic field throughout the sun. We have calculated the capture rate or the event rate which are predicted by this combined mechanism for the ^{37}Cl, the Kamiokande-II and the ^{71}Ga experiments. To estimate capture rates in the ^{37}Cl and the ^{71}Ga experiments, we have used the neutrino flux from various sources in the sun which is predicted from the Standard Solar Model (SSM)[9]. We have taken into account neutrinos from pp, ^{7}Be, ^{13}N, ^{8}B and pep

and neglected neutrinos from ^{17}F, ^{13}O and hep because their flux are very small. To estimate the event rate in the Kamiokande-II experiment, we have taken into account the trigger efficiency of the detector.

Fig. 1 shows the contour plot of the region allowed by the combined mechanism of the MSW and the Spin-Flavor resonance for $\mu B = 1, 2, 3$ and 4 in units of $10^{-10}\mu_B \cdot$kG where μ_B is the Bohr magneton. When $\mu B = 1$, the allowed region is almost the same as the pure MSW case ($\mu B = 0$), but for μB greater than 2 the equal yield contour, so called the MSW triangle, changes its shape drastically. For example, when $\mu B = 2$, the oblique line of the MSW triangle extends outward from the triangle. Let us now discuss how to distinguish these solutions. We have picked out three parameter sets of Δm^2 and $\sin^2 2\theta$ from three black areas, respectively in Fig. 1 (b) as the candidate of two pure MSW solutions and one MSW-spin-flavor solution. Fig. 2 represents the survival probabilities of ν_e as a function of neutrino energy for three parameter sets. From Fig. 2, we can expect that three solutions can be distinguished[12] by accurately measuring the solar neutrino energy spectrum in high statistic future experiments such as SNO, Super Kamiokande and BOREXINO.

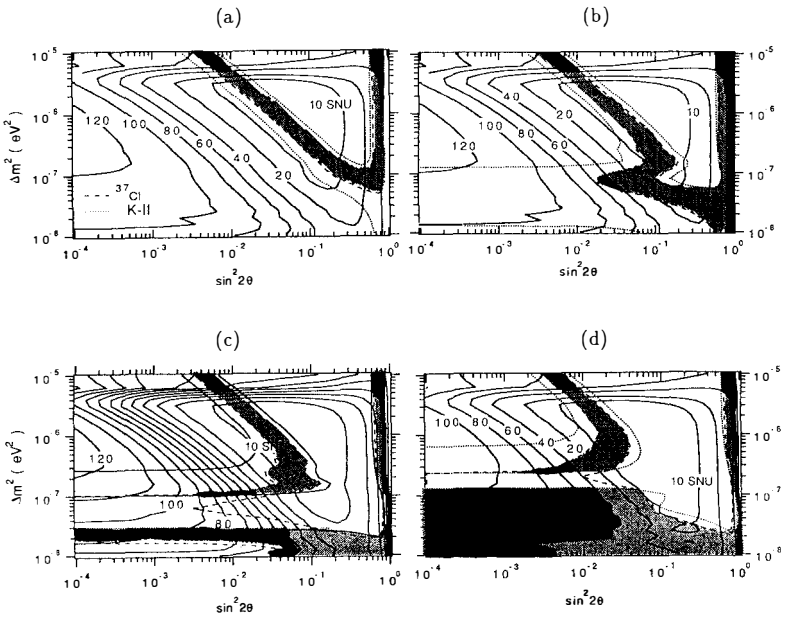

Fig. 1: Contour lines with number is the -SNU plot for the ^{71}Ga experiment. The shaded region shows the 2 σ allowed region for the ^{37}Cl and Kamiokande-II experiments. The black area show the simultaneous 2σ allowed region for the ^{37}Cl (2.2±0.6 SNU)[6], Kamiokande-II (0.46 ±0.16 of SSM) [10] and Gallex (83 ±42 SNU)[11] experiments. Fig. 1 (a), (b), (c) and (d) show the case of $\mu B = 1, 2, 3$ and 5 in units of $10^{-10}\mu_B \cdot$kG, respectively.

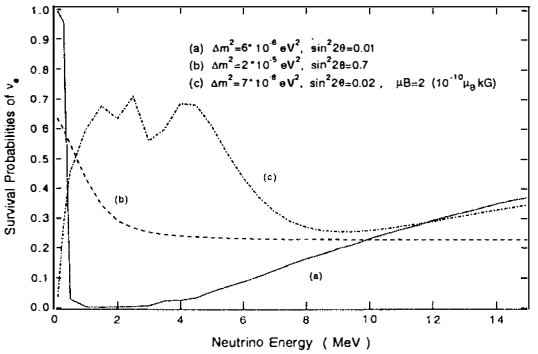

Fig. 2:
This figure presents the survival probabilities of electron neutrinos at the terrestrial detectors as a function of neutrino energy for three parameter sets (a), (b) and (c) defined in the figure.

3. Conclusions

We show that the combined mechanism gives the new parameter region of $\sin^2 2\theta$ ($\lesssim 0.01$) and Δm^2 ($\lesssim 10^{-7}\mathrm{eV}^2$) as a solution to the solar neutrino problem when $\mu B \gtrsim 2$ in units of $10^{-10}\mu_B \cdot$ kG. This new solution is located in a parameter region different from that of the two known MSW solutions and is characteristic to the spin-flavor precession. These solutions are expected to be distinguished by accurately measuring the neutrino energy spectrum in the future solar neutrino experiments. For more detailed discussions on this topic, see ref. 12) and 13).

References

1) S. P. Mikheyev, A. Y. Smirnov, Yad. Fiz. **42** (1985) 1441 [Sov. J. Nucl. Phys. **42**, (1985) 913]; L. Wolfenstein, Phys. Rev. **D17**, (1978) 2369.
2) GALLEX Collaboration, Phys. Lett. **B285** (1992) 390.
3) L. B. Okun, M. B. Voloshin and M. I. Vysotsky, Yad. Fiz.**44** (1986) 677. [Sov. J. Nucl. Phys. **44**, (1986) 440].
4) C. S. Lim and W. Marciano, Phys. Rev. **D37** (1988) 1368.
5) E. Akhmedov, Phys. Lett. **B213** (1988) 64.
6) B. Cleveland et al., *Proceedings of the 25th International Conference on High Energy Physics*, Vol. I, page 667, edited by K. K. Phua and Y. Yamaguchi (World Scientific, Singapore, 1991).
7) H. Minakata and H. Nunokawa, Phys. Rev. Lett. **63** (1989) 121.
8) A. B. Balantekin, P. J. Hatchell and F. Loreti, Phys. Rev. **D41** (1990) 3583; K. S. Babu, Rabindra N. Mohapatra and I. Z. Rothstein, Phys. Rev. **D44** (1991) 2265; E. Gates, L. Krauss and M. White, Phys. Rev. **D46** (1992) 1263.
9) J. Bahcall and R. Ulrich, Rev. Mod. Phys. **60** (1988) 297 ; J.Bahcall, *Neutrino Astrophysics* (Cambridge University Press, Cambridge, England, 1989).
10) K. S. Hirata *et al.* , Phys. Rev. **D44** (1991) 2241.
11) GALLEX Collaboration, Phys. Lett. **B285** (1992) 376.
12) H. Nunokawa and H. Minakata, Fermilab preprint, FERMILAB-PUB-92/193-T.
13) H. Nunokawa, Dr. of Science thesis, 1992.

COMMENT ON SUPERNOVA NEUTRINOS AND THE MSW SOLAR NEUTRINO SOLUTIONS

H. Nunokawa and H. Minakata

At Neutrino '92, Stodolsky made a comment about the relation between ν_e from the supernova SN1987A and the MSW solutions of the solar neutrino problem[14]. His comment is as follows. First event at Kamiokande from SN1987A pointed back to Magellanic Cloud [15] so this suggests that the first event may be due to ν_e from neutronization burst. If we take this one event seriously and if we require that the MSW mechanism of the same two flavor neutrinos is responsible for the solar neutrino deficit and ν_e from the supernova then even one ν_e event is too large to be detected in KamII. However, there is a restricted parameter region of $\sin^2 2\theta$ and Δm^2 in which the MSW resonance is efficient for solar neutrino but is not efficient for supernova neutrino. Interestingly, this region contains the small mixing angle MSW solution. (See dashed line of Fig. 3.)

Now we would like to point out that similar result is obtained even if ν_e is converted to other type of neutrino (ν_μ or ν_τ) in the supernova. In that case, we require the regeneration of supernova neutrino into ν_e in the earth. Interestingly again, the parameter region in which regeneration of ν_μ or ν_τ into ν_e in the earth efficiently occur coincides with the large mixing angle MSW solution. Fig. 3 shows the two MSW solutions (black areas) [2] and the region allowed by the regeneration in the earth for supernova neutrino (hatched region) [16]. We can see that large mixing angle MSW solution overlap with the hatched region.

We would like to thank Prof. K. Nakamura of ICRR for pointing out this possibility to us.

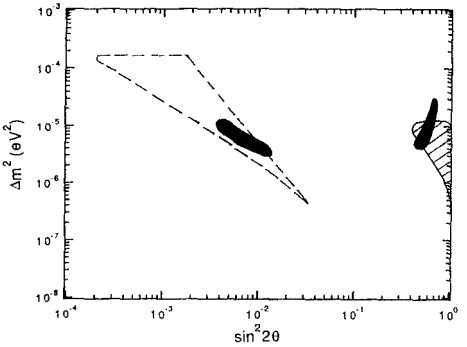

Fig. 3 : Two black areas are the MSW solutions of the solar neutrino problem and the hatched region indicates the region in which the probability of regeneration of supernova neutrino into ν_e in the earth is more than 50 %[16]. The area surrounded by the dashed line is the region mentioned in Stodolsky's talk.

References

14) L. Stodolsky, Talk given at 15th International Conference on Neutrino Physics and Astrophysics (Neutrino '92), Granada, Spain, 7-12 Jun 1992.
15) K. Hirata et al., Phys. Rev. Lett. **58** (1987) 1490.
16) H. Minakata et al. Mod. Phys. Lett. **A2** (1987) 827; J. Arafune et al. Phys. Rev. Lett. **59** (1987) 1864.

PONTECORVO'S ORIGINAL OSCILLATIONS REVISITED

E.Kh. Akhmedov[a], S.T. Petcov[b),c)], A.Yu. Smirnov[d)]

[a)]SISSA, I-34014, Trieste, Italy and Kurchatov Institute, 123182 Moscow, Russia
[b)]SISSA and INFN, Sezione di Trieste, I-34014 Trieste, Italy
[c)]INRNE, Bulgarian Academy of Sciences, BG-1784 Sofia, Bulgaria
[d)]ICTP, I-34100, Trieste, Italy and INR, 117312 Moscow, Russia

ABSTRACT

We show that a left-handed neutrino ν_L can oscillate into its CPT- conjugate state $\bar{\nu}_R$ with maximal amplitude, in direct analogy with $K^0 - \bar{K}^0$ oscillations. Peculiarities of such oscillations under different conditions are studied.

1. 35 years ago Pontecorvo suggested the possibility of neutrino oscillations [1] by analogy with the oscillations of neutral K mesons. The question he raised was "...whether there exist other mixed neutral particles besides the K^0 mesons which differ from their antiparticles and for which the particle $\rightarrow$ antiparticle transitions are not strictly forbidden"[1].

Direct analogy with the $K^0-\bar{K}^0$ case would imply oscillations of a neutrino into its CPT-conjugate state with large amplitude. We shall refer here to such a process as "Pontecorvo's original oscillations".

The essential difference between the K^0 mesons and neutrinos is related to the spin of neutrinos. It was realized after the $V-A$ structure of weak interactions had been established that neutrinos are produced and interact in chiral states. In particular, only left-handed neutrinos ν_L have been observed. The CPT conjugation transforms ν_L into a right-handed antineutrino $\bar{\nu}_R$, and so the realization of the Pontecorvo's original idea would mean the existence of the oscillations $\nu_L \leftrightarrow \bar{\nu}_R$. Strictly speaking, such transitions are not just a process of lepton number oscillations, but also simultaneously neutrino spin precession.

Since the helicity of a free particle is conserved, in vacuum the oscillations $\nu_L \leftrightarrow \bar{\nu}_R$ cannot occur. Particle-antiparticle transitions in vacuum can in principle take place for 4-component neutrinos. In terms of chiral states these oscillations would imply transitions of ν_L into $\bar{\nu}_L$ (or $\bar{\nu}_R$ into ν_R), so that the neutrino helicity is conserved. However, such transitions are not analogous to the $K^0 - \bar{K}^0$ oscillations: $\bar{\nu}_L$ is not the true antiparticle of the left-handed neutrino, the existence of which is required by the CPT invariance, but rather a different neutrino state. In the ultrarelativistic limit ν_L and $\bar{\nu}_L$ can be considered as independent particles with quite different interactions (ν_L is active whereas $\bar{\nu}_L$ is sterile in the standard model).

For the above reasons it was generally supposed that Pontecorvo's original oscillations are just the oscillations of active neutrinos into sterile states, whereas the true neutrino-antineutrino oscillations $\nu_L \leftrightarrow \bar{\nu}_R$ were considered impossible. In this report we show that under certain conditions maximal-amplitude $\nu_L \leftrightarrow \bar{\nu}_R$ oscillations can nevertheless occur.

2. Consider for definiteness the transitions involving electron neutrinos, $\nu_{eL} \leftrightarrow \bar{\nu}_{eR}$. As we already stressed, this imply helicity flip of the neutrino states. Such a flip can be induced, for example, by interactions of neutrinos with external magnetic fields provided the neutrinos have magnetic (or electric) dipole moments. However, the magnetic-moment interaction cannot transform a neutrino into its own antineutrino because of CPT invariance.

Nevertheless, it can convert a neutrino into an antineutrino of another species [2]. From this fact it follows that the $\nu_{eL} \to \bar{\nu}_{eR}$ transition can in principle proceed via an additional neutrino ν_x in the intermediate state (assuming that the usual flavour mixing also exists), and $\nu_{eL} - \bar{\nu}_{eR}$ mixing appears as a second-order effect. However, it can be shown[3] that CPT invariance results in vanishing the amplitudes of such transitions as well. The crucial points are that for any chain of transitions with a ν_{xL} in the intermediate state there is another chain mediated by $\bar{\nu}_{xR}$ with its amplitude having opposite sign and the same absolute value.

Thus, in order to induce the $\nu_{eL} \leftrightarrow \bar{\nu}_{eR}$ transitions, one needs to break CPT. However, this does not necessarily require the existence of CPT-noninvariant interactions: the CPT symmetry can be broken by the external conditions. In particular, this can be the case if the process takes place in matter or in a transverse magnetic field whose direction changes along the neutrino trajectory. Matter breaks C and CPT because it consists of particles and not of antiparticles, and a twisting field breaks parity P (and hence CPT) since it rotates either clockwise or counter clockwise along the neutrino path. In fact, both matter and twisting fields lift the degeneracy of the intermediate neutrino states ν_{xL} and $\bar{\nu}_{xR}$ and so induce $\nu_{eL} \leftrightarrow \bar{\nu}_{eR}$ transitions.

The possibility of $\nu_{eL} \leftrightarrow \bar{\nu}_{eR}$ transitions in matter and transverse magnetic field was first pointed out in[4]. However, for fixed-direction magnetic fields the transition probability was shown to be small even for large neutrino mixing and magnetic moments [5]. As we shall see, the magnetic field rotation can change the situation drastically.

3. Consider a system of four neutrino states ν_{eL}, $\bar{\nu}_{eR}$, $\nu_{\mu L}$, and $\bar{\nu}_{\mu R}$ with vacuum mixing and transition magnetic moment μ relating ν_{eL} with $\bar{\nu}_{\mu R}$. Assuming that the energy levels of ν_{eL} and $\bar{\nu}_{eR}$ are sufficiently well separated from the $\nu_{\mu L}$ and $\bar{\nu}_{\mu R}$ ones, one finds for the $\nu_{eL} - \bar{\nu}_{eR}$ transition probability in a medium with constant matter density, absolute value of the magnetic field $B_\perp$ and angular velocity of the magnetic field rotation $\dot{\phi}$[3]:

$$P(\nu_{eL} \to \bar{\nu}_{eR}; t) = \frac{(2H_{e\bar{e}})^2}{(2H_{e\bar{e}})^2 + (2N + \dot{\phi} - \eta)^2} \sin^2 \left(\frac{1}{2} \sqrt{(2H_{e\bar{e}})^2 + (2N + \dot{\phi} - \eta)^2}\, t \right) \qquad (1)$$

Here $N \equiv \sqrt{2} G_F (n_e - n_n/2)$ where G_F is the Fermi constant, n_e and n_n are the electron and neutron number densities, the angle $\phi(t)$ defines the direction of the magnetic field $\mathbf{B}_\perp(t)$ in the plane orthogonal to the neutrino momentum, $\dot{\phi} \equiv d\phi/dt$. The effective $\nu_{eL} \to \bar{\nu}_{eR}$ mixing term $H_{e\bar{e}}$ is

$$H_{e\bar{e}} \simeq s_2 \delta \mu B_\perp \frac{\dot{\phi} - 2rN}{[(-rN + \dot{\phi}/2)^2 - (2c_2\delta)^2]}, \qquad (2)$$

where $r \equiv n_n/(2n_e - n_n)$, $\delta \equiv \Delta m^2/4E$, $s_2 \equiv \sin 2\theta_0$, $c_2 \equiv \cos 2\theta_0$, E is the neutrino energy, $\Delta m^2 = m_2^2 - m_1^2$, m_1, m_2 and θ_0 being the neutrino masses and mixing angle in vacuum. In eq. (1) η is a small energy-dependent term: $\eta = (\tan\omega - \cot\omega)H_{e\bar{e}}$, where $\tan\omega \equiv s_2\delta/\mu B_\perp$. It follows from (2) that the effective $\nu_{eL} - \bar{\nu}_{eR}$ mixing is caused by an interplay of flavour mixing and the one induced by the interaction of the magnetic moment with magnetic field. In accordance with our general discussion, it arises due to the transitions through the $\nu_{\mu L}(\bar{\nu}_{\mu R})$ states: $\nu_{eL} \to \nu_{\mu L}(\bar{\nu}_{\mu R}) \to \bar{\nu}_{eR}$. In vacuum the contributions of ν_μ and $\bar{\nu}_\mu$ cancel each other. Matter ($n_n \neq 0$) and magnetic field rotation ($\dot{\phi} \neq 0$) lift the degeneracy of the ν_μ and $\bar{\nu}_\mu$ levels and so give rise to the $\nu_{eL} - \bar{\nu}_{eR}$ mixing.

One can readily make sure that in nonrotating magnetic fields the $\nu_{eL} - \bar{\nu}_{eR}$ mixing is always strongly suppressed. On the contrary, in a twisting field the $\nu_{eL} \leftrightarrow \bar{\nu}_{eR}$ oscillations can be *resonantly enhanced*. For

$$\dot{\phi} = -2N + \eta \simeq -2N \tag{3}$$

the $\nu_{eL} - \bar{\nu}_{eR}$ mixing becomes maximal and the oscillations proceed with maximal depth. Eq. (3) is nothing else but the resonance condition for the $\nu_{eL} \leftrightarrow \bar{\nu}_{eR}$ oscillations. It implies that the field rotation compensates for the energy splitting of the ν_{eL} and $\bar{\nu}_{eR}$ levels caused by their interaction with matter. Up to the small term $\eta \sim H_{e\bar{e}}$, it does not depend on the neutrino energy. Due to this fact the energy width of the resonant peak can be fairly large. This means that for a neutrino beam with continuous energy spectrum a large fraction of neutrinos can undergo resonantly enhanced $\nu_{eL} \leftrightarrow \bar{\nu}_{eR}$ oscillations.

Let us assume now that

$$\frac{\dot{\phi}}{2} = -N = -\frac{2c_2\delta}{1+r}, \tag{4}$$

Now the energy levels of three neutrino states, namely, those of ν_{eL}, $\bar{\nu}_{eR}$ and $\nu_{\mu L}$, cross in one point (this means that the resonances of the $\nu_{eL} \leftrightarrow \bar{\nu}_{eR}$, $\nu_{eL} \leftrightarrow \nu_{\mu L}$ and $\nu_{\mu L} \leftrightarrow \bar{\nu}_{eR}$ transitions merge in one point). The influence of the ν_μ state on the $(\nu_{eL}, \bar{\nu}_{eR})$ system becomes maximal. For constant N, r, $B_\perp$ and $\dot{\phi}$ one obtains the following probability of the $\nu_{eL} \leftrightarrow \bar{\nu}_{eR}$ oscillations:

$$P(\nu_{eL} \to \bar{\nu}_{eR}; t) = \sin^2 2\omega \sin^4 \frac{1}{2} ft + \sin^2 2\omega \sin^2 \frac{3}{4}\epsilon' t \cos ft + d \sin \epsilon' t \sin ft, \tag{5}$$

where $f = \sqrt{(\mu B_\perp)^2 + (s_2\delta)^2}$, $\epsilon' = -\epsilon \sin 2\omega (s_2\delta)(\mu B_\perp)/(H_{\bar{\mu}} - H_e)$, $H_{\bar{\mu}}$ and H_e being the energy levels of the corresponding flavour neutrinos and $d = O(\epsilon')$. We see that the

depth of the $\nu_{eL} - \bar{\nu}_{eR}$ oscillations, $\sin^2 2\omega$, does not exhibit any suppression; moreover, in the symmetric case $s_2\delta = \mu B_\perp$, when the vacuum mixing is equal to that induced by the magnetic moment interaction, one has $\sin 2\omega = 1$ and the oscillation depth becomes maximal. For $s_2\delta \neq \mu B_\perp$ the oscillation depth is less than unity and it decreases when the difference between $s_2\delta$ and $\mu B_\perp$ increases.

Let us stress that the maximal-amplitude short-wavelength oscillations described by eq. (5) are only possible in a rotating field, when the merging condition (4) can be fulfilled. The merging condition and $\nu_{eL} - \bar{\nu}_{eR}$ oscillation length depend on the neutrino energy, and so the enhancement of the $\nu_{eL} \leftrightarrow \bar{\nu}_{eR}$ oscillations in this case has a resonant character, too.

4. Our previous discussion was constrained to the case of constant N, r, $B_\perp$ and $\dot{\phi}$. In a medium with matter density, and magnetic field varying along the neutrino path, the maximum-amplitude $\nu_{eL} \leftrightarrow \bar{\nu}_{eR}$ oscillations will take place if the functions $N(t)$ and $\phi(t)$ satisfy the resonance condition (3) over a sufficiently large space interval Δt.

Eq. (3) is in fact just the condition of crossing of the ν_e and $\bar{\nu}_e$ levels. Thus, if the parameters of the medium vary in such a way that at a certain point t_r eq. (3) holds, resonant $\nu_{eL} \to \bar{\nu}_{eR}$ conversion may take place in the resonant region[6,3]. The conversion can be nearly complete if the matter density and $\dot{\phi}$ vary slowly enough (adiabatically) along the neutrino path.

The maximum-amplitude $\nu_{eL} \leftrightarrow \bar{\nu}_{eR}$ oscillations we have discussed, especially those in the merging point, can provide an efficient mechanism of generation of $\bar{\nu}_e$ flux in the sun. They can also have important consequences for neutrinos created in collapsing stars.

It should be emphasized that the merging condition (4) does not require any fine tuning provided the neutrinos have a continuos spectrum and matter density changes monotonously along the neutrino path. N_0.

REFERENCES

1. B. Pontecorvo, Zh. Eksp. Teor. Fiz. 33 (1957) 549; 34 (1958) 247.
2. J. Schechter, J.W.F. Valle, Phys. Rev. D24 (1981) 1883; Phys. Rev. D25 (1982) 283 (E); M.B. Voloshin, M.I. Vysotsky, L.B. Okun, Sov. Phys. JETP 64 (1986) 446.
3. E. Kh. Akhmedov, S.T. Petcov, A.Yu. Smirnov, SISSA 170/92/EP, SISSA 9/93/EP.
4. C.-S. Lim, W.J. Marciano, Phys. Rev. D37 (1988) 1368.
5. E.Kh. Akhmedov, Sov. Phys. JETP 68 (1989) 690.
6. S.P. Mikheyev, A.Yu. Smirnov, Sov. J. Nucl. Phys. 42 (1985) 913; Prog. Part. Nuc. Phys. 23 (1989) 41; L. Wolfenstein, Phys. Rev. D17 (1978) 2369.

NEUTRINO INTERACTIONS IN MATTER

Palash B. Pal
Center for Particle Physics
Physics Department, University of Texas
Austin, TX 78712, USA

– Electronic mail addresses –
BITNET: phbd070@utxvms.bitnet
INTERNET: phbd070@utxvms.cc.utexas.edu
DECNET: 25643::phbd070

If a fermion is travelling through a medium, it can have matter-induced magnetic and electric dipole moments. These contributions conserve chirality, and can be non-vanishing even for a Majorana neutrino. Several implications for neutrino physics are discussed.

1 Neutrino propagation in matter

This subject beacame popular when Wolfenstein calculated neutrino refractive index in matter, and subsequently Mikheyev and Smirnov recognized resonant nature of flavor oscillations triggered by matter effects. Application to the solar neutrino problem is now standard [1].

To set up the stage, we outline a covariant calculation leading to Wolfenstein's result. One evaluates the self-energy function to determine the dispersion relation, which can give the refractive index [2, 3, 4]. Consider a massless neutrino for simplicity. Chirality dictates that its self-energy is of the form

$$\Sigma = RSL\,, \tag{1}$$

where R and L are chirality projection operators. In vacuum, the most general form of S is

$$S = a(k^2)\not{k}\,. \tag{2}$$

Thus, the pole of the propagator is at $k^2 = 0$, i.e., the particle is massless to all orders.

In a medium characterized by the center-of-mass velocity v^μ,

$$S = a\not{k} + b\not{v} \tag{3}$$

in general. Thus, the dispersion relation changes, which is responsible for a refractive index different from unity.

2 Electromagnetic vertex

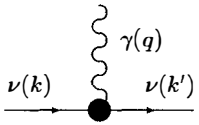

Figure 1: The effective vertex with photon.

In general, the vertex in Fig. 1 can be written as

$$\bar{u}(k')\Gamma_\lambda(k,k',v)u(k)A^\lambda\,, \tag{4}$$

where the vector v^μ has been defined earlier. Conservation of charge implies the condition:

$$q^\lambda\Gamma_\lambda \;=\; 0\,. \tag{5}$$

In the vacuum where v^μ does not exist, the neutrino has no charge, so that

$$\Gamma_\lambda(k,k,0) = 0\,. \tag{6}$$

These imply the following most general form for Γ_λ in the vacuum [5, 6, 7]:

$$\Gamma_\lambda = (q^2\gamma_\lambda - q_\lambda\not{q})(R + r\gamma_5) + i\sigma_{\lambda\rho}q^\rho(D_M + D_E\gamma_5)\,. \tag{7}$$

In matter, additional terms are possible because of the 4-vector v [8, 9]:

$$\Gamma'_\lambda = iD'_E(\gamma_\lambda v_\rho - \gamma_\rho v_\lambda)q^\rho\gamma_5 + iD'_M\epsilon_{\lambda\rho\alpha\beta}\gamma^\rho\gamma_5 q^\alpha v^\beta\,. \tag{8}$$

It is easy to understand these terms in co-ordinate space if all form factors are assumed to be momentum *in*dependent. The vacuum part can then be written as

$$\bar{\psi}\gamma_\lambda\psi\partial_\rho F^{\lambda\rho}(R + r\gamma_5) + \bar{\psi}\sigma_{\lambda\rho}\psi F^{\lambda\rho}(D_M + D_E\gamma_5)\,, \tag{9}$$

whereas the extra terms in a medium are

$$D'_E\bar{\psi}\gamma_\lambda\gamma_5\psi\, v_\rho F^{\lambda\rho} + D'_M\bar{\psi}\gamma_\lambda\gamma_5\psi\, v_\rho\tilde{F}^{\lambda\rho}\,. \tag{10}$$

In the non-relativistic limit, since $\bar{\psi}\gamma_0\gamma_5\psi \to 0$, $\bar{\psi}\vec{\gamma}\gamma_5\psi \to \vec{\sigma}$, in a frame where $v^\rho = (1, \vec{0})$, we can write (10) as

$$D'_E\vec{\sigma}\cdot\vec{E} + D'_M\vec{\sigma}\cdot\vec{B}\,. \tag{11}$$

Hence, these are new contributions to dipole moments [8, 9]. Notice that these terms are chirality conserving, and can be non-zero even for a Majorana neutrino [8]. Both these properties are different from the vacuum dipole moment terms.

3 Calculations at the leading order

To the leading order in the Fermi constant [10, 11],

$$\Gamma_\lambda = \mathcal{T}_{\lambda\rho}\gamma^\rho L\,, \tag{12}$$

$$\mathcal{T}_{\lambda\rho} = \mathcal{T}_T R_{\lambda\rho} + \mathcal{T}_L Q_{\lambda\rho} + \mathcal{T}_P P_{\lambda\rho}\,, \tag{13}$$

where, with $\tilde{g}_{\lambda\rho} = g_{\lambda\rho} - q_\lambda q_\rho/q^2$ and $\tilde{v}_\lambda = \tilde{g}_{\lambda\rho}v^\rho$,

$$R_{\lambda\rho} = \tilde{g}_{\lambda\rho} - Q_{\lambda\rho} \tag{14}$$

$$Q_{\lambda\rho} = \tilde{v}_\lambda\tilde{v}_\rho/\tilde{v}^2 \tag{15}$$

$$P_{\lambda\rho} = i\epsilon_{\lambda\rho\alpha\beta}q^\alpha v^\beta/\sqrt{(q\cdot v)^2 - q^2}\,. \tag{16}$$

The form factors $\mathcal{T}_T$, $\mathcal{T}_L$, $\mathcal{T}_P$ have been calculated in the leading order in G_F, in the general case when the incoming and the outgoing neutrinos in Fig. 1 may or may not be the same. From this, one can obtain various physical effects, as described below.

Radiative decay : In the vacuum, this is suppressed due to leptonic GIM. A medium full of electrons and not muons or taons is not flavor symmetric. Thus, the GIM mechanism is no more operative. The rates are enhanced tremendously [12, 13].

Modification of forward scattering amplitude : This occurs through the electromagnetic vertex, if the electron scatters from the photon. This was originally supposed to be large, as large as the Wolfenstein term [14]. Later, it was pointed out that protons can also scatter from the photon, and this cancels exactly the electron-scattering contribution in the forward scattering amplitude for neutrinos [15, 16].

Induced electric charge : Neutrinos in medium have a small charge induced by matter effects [17], $e^{\nu}_{ind} = -(eG_F/\sqrt{2})(1 + 4\sin^2\theta_W)(e^2 r_D^2)^{-1}$ where the Debye screening length is given by $r_D^2 = T/n_e e^2$ for a non-relativistic plasma at temperature T. This gives $e^{\nu}_{ind} \approx -2 \times 10^{-32}(1\,\mathrm{cm}/r_D)^2$. This is not measurable even for the densest known plasma for which $r_D \simeq 10^{-4}$ cm.

Plasmons : Plasmons can decay into $\nu\bar{\nu}$. The rate has been calculated [10]. Neutrinos can produce plasmons in a medium [11, 18].

4 Outlook

The effects may be large compared to the vacuum effects, but still not hopeful for being observable. However, the subject is interesting, and I am sure that the resonant neutrino oscillation is *not* the only interesting physical effect. Maybe some other process, like the Majoronic decay of neutrinos [19], or other systems like the early universe [20, 21], will yield some non-trivial effects. Or maybe in more non-trivial matter distribution as in a crystal, some of the electromagnetic effects will be enhanced enough to be observable.

I end by thanking my friend José F Nieves, with whom I have done most of the work on this subject. I also thank R Cowsik for some discussions after my talk at the conference.

1. For references and a recent review, see, e.g., P B Pal: IJMP A7 (1992) 5387.
2. D Nötzold, G Raffelt: NP B307 (1988) 924.
3. P B Pal, T N Pham: PR D40 (1989) 259.
4. J F Nieves: PR D40 (1989) 866.
5. J F Nieves: PR D26 (1982) 3152.
6. B Kayser, A Goldhaber: PR D28 (1983) 2341.
7. B Kayser: PR D30 (1984) 1023.
8. J F Nieves, P B Pal: PR D40 (1989) 1693.
9. V B Semikoz, Y A Smorodinskii: JETP 68 (1989) 20.
10. J C D'Olivo, J F Nieves, P B Pal: PR D40 (1989) 3679.
11. V N Oraevskii, A Y Plakhov, V B Semikoz, Y A Smorodinskii, JETP 66 (1987) 890.
12. J C D'Olivo, J F Nieves, P B Pal: PRL 64 (1990) 1088.
13. C Giunti, C W Kim, W P Lam: PR D43 (1991) 164.
14. R Horvat: PL B266 (1991) 431.
15. J F Nieves, P B Pal: PL B283 (1992) 117.
16. V B Semikoz: PL B284 (1992) 337.
17. V N Oraevsky, V B Semikoz: Physica 142A (1987) 135.
18. R F Sawyer: PR D46 (1992) 1180.
19. C Giunti, C W Kim, U W Lee, W P Lam: PR D45 (1992) 1557.
20. R Barbieri, A Dolgov: NP B349 (1991) 743.
21. K Enqvist, K Kainulainen, J Maalampi: NP B349 (1991) 754.

TEST OF COHERENT NEUTRINO DETECTION USING SAPPHIRE CRYSTALS

M. P. McHugh and P. T. Keyser[a]
Air Force Phillips Laboratory/GPEG
Hanscom AFB, MA 01571 USA

ABSTRACT

An experiment to detect solar neutrinos using the method of Weber was undertaken. Two sapphire crystals of about 82 g each, along with compensating lead masses, were placed in a liquid-supported torsion balance (LSTB) in a symmetric configuration. If the sapphire has a sufficiently large coherent scattering cross section (proportional to the *square* of the number of scatterers) then the momentum transfer from solar neutrinos will produce an observable one day period in the angular position of the balance. To the limit of experimental sensitivity, no such effect was observed.

[a]Present address: University of Alberta, Edmonton Alberta T6G2E8 Canada.

INTRODUCTION

Joseph Weber has proposed that neutrino scattering from single crystals can give total cross sections proportional to the square of the number of scattering sites[1-4]. This would produce enhancements of the cross section on the order of Avogadro's number for very modest sized crystals, making a table-top sized neutrino detector possible. The effect differs from ordinary coherent scattering of radiation in that the neutrinos have Compton wavelengths that are short compared to the crystal lattice spacing (for a discussion of long wavelength coherent scattering see ref. 5 page 683). Despite many theoretical arguments against the validity of this claim[6-10], Weber has presented experimental results[3] in apparent agreement with very large scattering cross sections for neutrinos from single crystals of sapphire (Al_2O_3). We decided that an attempt to reproduce his results was merited.

Weber published results for three types of experiments --detection of tritium β-decay neutrinos, nuclear reactor neutrinos, and solar neutrinos; all three utilizing a torsion balance as the detector. We pursued detection of neutrinos from the Sun using essentially the same method as Weber. The technique employs a torsion balance that holds test masses of lead and single-crystal sapphire. If the sapphire has a large scattering cross section and the lead has a negligible cross section then the solar neutrinos will impart momentum to one side of the torsion balance, producing a measurable torque. The torque changes sign as the earth rotates, and the 24 hour periodic motion that results is the solar neutrino signal.

Weber's results were for a torsion balance holding a 26 g sapphire crystal. With 65 days of data averaged together, the amplitude of the 24 h signal implied a force of $\sim 4.6\times10^{-6}$ dynes which he attributed to solar neutrinos. This is an astounding result in that if one assumes that all of the neutrinos that pass through the geometric cross section of this crystal are scattered through a random angle; and that the neutrino flux is that given by the standard solar model (see ref 11), then the maximum force on the crystal would be 5.3×10^{-6} dynes. The curve

designated "predicted signal" in Figure 2 was calculated for our experiment using the same assumptions. The curve is not a sinusoid due to the fact that the geometric cross section of the cylindrically shaped crystals changes throughout the day as the direction of the neutrinos changes. The maximum magnitude of the calculated force is ~2×10^{-5} dynes. Other methods for predicting the size of the effect give even larger forces. By simply scaling the results of Weber by the square of the mass for the two 82 g crystals used in this work, we calculate a force of 9×10^{-5} dynes for our torsion balance.

APPARATUS

The apparatus used for this work is a liquid-supported torsion balance (LSTB) that was developed at the Joint Institute for Laboratory Astrophysics (JILA) by Jim Faller and his students[12-14]. The LSTB shown in Figure 1 consists of an aluminum cylinder that floats in water that is kept at its temperature of maximum density (3.98°C). The water provides the support while the spherical and ovoid electrodes on the top of the LSTB are used to provide the centering force and the restoring torque. An optical lever, using four lenses mounted on the lid of the LSTB, provides for the detection of the angular position of the LSTB.

The test masses are two Pb/Al_2O_3 "sandwiches" and six gold-plated Pb cylinders each weighing about 510 g. The crystals themselves weigh 82 g each and are about 4.5 cm in diameter, 1.3 cm in height. The overall height of all eight masses is the same, with the crystal/lead masses having a larger diameter due to their lower density. The symmetric design is used to minimize the effect of gradients in the gravitational field. A calibration of the LSTB sensitivity to applied torques is done in the following way. First the oscillation period is measured for several different electrode voltages. This along with the moment of inertia about the vertical axis is used to calculate the torsion constant (the torque per unit angular displacement). The sensitivity is checked using the gravitational attraction of lead bricks placed near the apparatus. This produces an "order of

magnitude" response and demonstrates that the LSTB is moving freely. The gravitational torque has large uncertainties and cannot be used independently as a calibration.

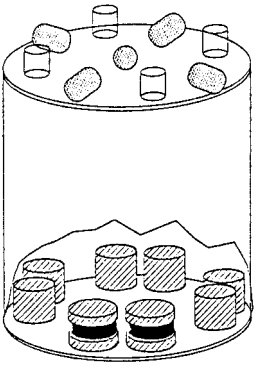

Fig. 1 A cutaway view showing the test masses inside of the LSTB. The sapphire is shown in black. On top are shown the lenses and the electrodes.

DATA

A data run consists of a computer reading multiple channels of an A/D data logger (optical lever output, thermistor resistances, magnetometer output, etc.) at one minute intervals. Ten minute averages are then stored on a disc. The signal is of the form of a 24 h periodic signal of the proper phase on the optical lever output voltage. This is converted into an angle using a calibration (done just prior to the experiment) and then into a torque using the torsion constant discussed above. Finally this is converted into a force using the length of the moment arm of the crystals about the vertical axis. A graph of the data time series is shown in Fig. 2 along with the predicted signal. A least-squares fit to a function of the form of the expected signal is performed. This functional form is just a cosine of the angle between the zenith and the direction to the Sun. This zenith angle is a fairly complicated function of the time of day and, of course, depends on the time of

year as well. An average of the least-squares fits for three such data runs gives the result of $-3.3\pm2.8\times10^{-8}$ dynes of extra force on the sapphire.

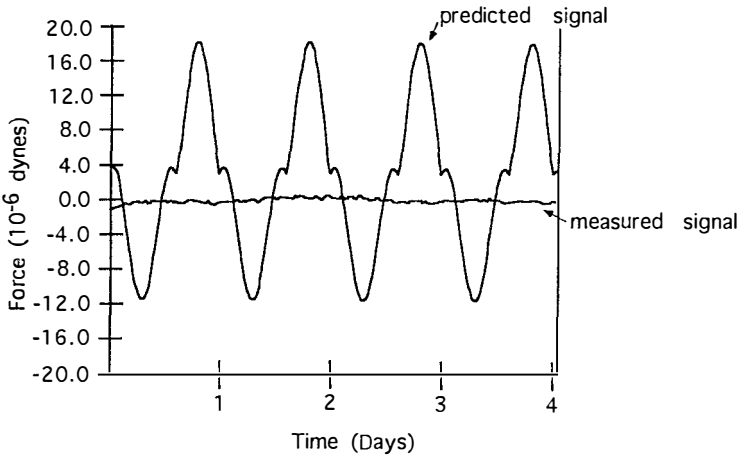

Fig. 2. This graph shows the data from one of the runs (starting at 17:30 EST on 7 Jan. 1993) along with the predicted signal based on the results of Weber. The angular position of the LSTB is converted into a force on the sapphire test masses.

EXPERIMENTAL UNCERTAINTIES

In an experiment of this nature the systematic errors must be dealt with very carefully. The fact that the signal has a period of 24 h presents difficulties in that many effects (e.g. temperature, tilts, motion of people) also occur with this period. The main sources of error considered are, gravity gradients, temperature fluctuations, magnetic field, and tilt. The temperature at various points on the apparatus, the tilt and the magnetic field were all monitored during the data runs in order to look for possible systematic errors.

The gravity multipole couplings are dealt with by first measuring the moments of the float by producing large gradients with nearby lead bricks. Then these moments are used with estimates of the local mass motions to give limits on

the torque produced by varying gravtational gradients. This error is estimated to be less than 0.5×10^{-8} dynes. The magnetic field on top of the LSTB tank was monitored with a three-axis flux-gate magnetometer, which combined with measurements of the torques produced by temporary large magnetic fields gave an estimated uncertainty of 0.2×10^{-8} dynes. The tilt was measured with a 2-axis electronic bubble level and in a similar manner the uncertainty was estimated to be 4.0×10^{-8} dynes. The temperature fluctuations at various points on the apparatus were monitored with thermistors, and combined with large artificial thermal gradients to make a worst-case estimate of the uncertainty as 4.0×10^{-7} dynes. The temperature fluctuation contribution dominates the systematic uncertainties, but this seems an overestimate as it is an order of magnitude larger than the "signal". However, temperature effects are very difficult to model and a less conservative estimate seemed unjustified.

An assumed feature of the coherent scattering is that the quality of the crystals is important for the effect. The more nearly perfect the crystals the better the coherence. We had our crystals tested by double crystal X-ray topography, by the same group at NIST that tested Weber's crystals, and they were found to be good single crystals with no extraordinary defects, comparable to his.

CONCLUSION

This experiment shows no observation of enhanced neutrino scattering cross sections for single crystals of sapphire. The extra force on the sapphire was $-0.3\pm4\times10^{-7}$ dynes, consistent with zero. The fraction of the predicted result is -0.002 ± 0.027 compared to 0.86 ± 0.26 observed by Weber. This uncertainty is obtained from his stated uncertainty in the solar neutrino flux[3]. A slightly different approach has also recently obtained a null result[15].

The authors would like to thank Crystal Systems of Salem Massachusetts for providing the high quality sapphire crystals used in this work. Thanks also to Richard Deslattes and Albert Henins of the National Institute of Standards and

Technology in Gaithersburg Maryland for performing the X-ray diffraction topography. We are indebted to Jim Faller for encouraging us to pursue this work.

REFERENCES

1. J. Weber, Found. Phys. **14**, 1185 (1984).

2. J. Weber, Phys. Rev. C **31**, 1468 (1985).

3. J. Weber, Phys. Rev. D **38**, 32 (1988).

4. J. Weber in *New and Exotic Phenomena '90*, proceedings of the Xth Moriond Workshop, Les Arcs, France, 20-27 January 1990 (Editions Frontières, Gif Sur Yvette, 1990) Edited by O. Fackler and J. Tran Thanh Vân, pp. 323-8.

5. J. D. Jackson, *Classical Electrodynamics*, 2nd ed. (Wiley, New York, 1975) p. 683.

6. G. F. Bertch and Sam M. Austin, Phys Rev. C **34**, 361 (1986).

7. T. H. Ho, Physics Letters **168B**, 295 (1986).

8. Y. Aharonov, F. T. Avignone, III, A. Casher and S. Nussinov, Phys. Rev. Lett. **58**, 1173 (1987).

9. Harry J. Lipkin, Phys. Rev. Lett. **58**, 1176 (1987).

10. M. N. Butler, Phys. Rev. C **35**, 1164 (1987).

11. J. N. Bahcall, *Neutrino Astrophysics* (Cambridge University Press, 1989).

12. G. M. Keiser and J. E. Faller in *Proceedings of the Second Marcel Grossmann Meeting on General Relativity* (North-Holland Publishing Company, 1982) Edited by R. Ruffini, pp. 969-76.

13. P. T. Keyser, Ph.D. thesis, University of Colorado, Boulder, 1986.

14. M. P. McHugh, P.T. Keyser and J. E. Faller in *New and Exotic Phenomena '90*, proceedings of the Xth Moriond Workshop, Les Arcs, France, 20-27 January 1990 (Editions Frontières, Gif Sur Yvette, 1990) Edited by O. Fackler and J. Tran Thanh Vân, pp. 233-6.

15. J. D. Franson and B. C. Jacobs, Phys. Rev. A **46**, 2235 (1992).

Dark Matter

REVIEW OF DARK MATTER

David O. Caldwell*
Physics Department, University of California, Santa Barbara, CA 93106-9530, USA

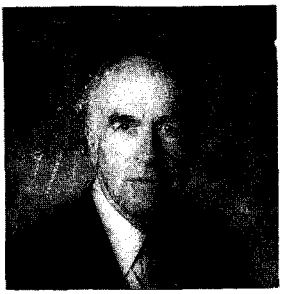

ABSTRACT

There is increasing evidence that baryons constitute < 10% of the mass of the universe. It is likely that the non-luminous matter, which must be particles outside the Standard Model of particle physics, is made up of $\sim$ 70% cold dark matter and $\sim$ 30% hot dark matter. If the solar ν_e and atmospheric ν_μ deficits are manifestations of neutrino mass, then there is a unique pattern of neutrino masses to accommodate the hot dark matter, pointing to needed terrestrial experiments. The cold component can be searched for directly, and already the exclusion of Dirac candidates extends over 12 orders of magnitude in particle mass and 20 orders of magnitude in cross section. This search must now get to cross sections less than one-tenth that of the weak interaction for Dirac masses > 20 GeV and utilize detector nuclei with spin for Majorana masses $\gtrsim$ 10 GeV. A program to achieve these goals is being implemented with a cryogenic detector.

* Supported in part by the U.S. Department of Energy Grant DE-FG03-91ER40618

1. EVIDENCE FOR DARK MATTER

Observational information increasingly points to the density of the universe's being far greater than the mass one can detect by other than gravitational means. Some of that non-luminous mass is in familiar baryonic form, but much more of it must be particles which are not in the Standard Model of particle physics. Thus the search for this dark matter is of great importance to particle physics, astrophysics, and cosmology.

The success of nucleosynthesis theory in predicting the abundance in the universe of ^{4}He, ^{3}H, ^{2}H, and ^{7}Li, as well as three flavors of neutrinos, gives confidence that the ratio of the mass density to the density required to just close the universe is $\Omega = 0.05 \pm .03$.[1] Observed baryons give only $\Omega \approx 0.007$, so there must be some unseen baryonic matter. This is most likely in the form of Jupiters (stars too small to have initiated nuclear burning), very small black holes ($< 10^{-6}$ solar masses) or neutral hydrogen.

The need for non-baryonic mass increases with increasing scale. The tangential velocity, v, of a mass, m, in a galaxy remains constant out to a radius, r, about an order of magnitude beyond the luminous mass, M, whereas from $GmM/r^2 = mv^2/r$, $v \propto r^{-1/2}$ would be expected. Unobserved mass increasing linearly with r must exist, giving $\Omega = 0.05$–0.10, but the fall-off in v is seldom observed. On the scale of galactic clusters, need for $\Omega = 0.1$–0.3 is required both by the motion of galaxies with respect to the center of luminous mass of the cluster and by gravitational lensing by the cluster of a distant light source. Very large scale velocity fields from the flow of galaxies and galactic clusters require $\Omega > 0.3$ at the 4–6 standard deviation level,[2] and these data favor $\Omega = 1$. The flat universe of $\Omega = 1$ is very likely because it is the only time-stable value for a zero cosmological constant. Unless there is severe fine tuning in the early universe, the present density should have been driven far out of the present range, toward 0 or ∞, unless $\Omega = 1$. Inflation theory, which provides an explanation for several otherwise inexplicable puzzles, also requires $\Omega = 1$.

2. APPARENT NEED FOR MIXED DARK MATTER

An explanation is required for the need for larger Ω the bigger the scale. Another dark matter conundrum to be understood is how it affects the formation of structure in the uni-

verse. Both of these issues can be explained in a model[3] which, in addition to the required small amount of baryonic dark matter, has a mixture of hot and cold dark matter. Relativistic hot dark matter tends to wash out density fluctuations, while slowly moving cold dark matter would enhance initial fluctuations to seed the concentration of baryons.

Data on the extent of structure in the universe is now available on a wide range of distance scales. Evidence from the COBE results on the anisotropy of the cosmic microwave background radiation, galaxy-galaxy angular correlations, large-scale velocity fields, and correlations of galactic clusters can all be fit[4] if the universe contains 70% cold dark matter and 30% hot dark matter contributed by $\sim$ 7 eV in neutrino mass. Such a model provides a consistent explanation not only of the shape of the density fluctuation spectrum, but also the observed estimates of the absolute density on small and large scales. While the fits have been made with a single neutrino, dividing the mass among more than one neutrino would work even better.[5]

3. BARYONIC DARK MATTER

It is barely possible that there could be enough baryonic dark matter to account for all the dark matter in our galaxy. In that case we would have to rely on accelerator experiments and theoretical input to determine the nature of non-baryonic dark matter. While solely baryonic dark matter is unlikely in view of the probable need for cold dark matter for galaxy formation, it is certainly important to ascertain the nature of the baryonic dark matter.

The most likely baryonic candidates are objects which can be between 10^{-7} and 10^{-1} solar masses. If lighter than the lower limit, they would have evaporated away in a galactic time scale, and if heavier than the upper limit, they would have become visible by nuclear ignition. These MAssive Compact Halo Objects, or MACHOS, are being looked for by gravitational microlensing, a search for the brightening of one of $\sim 10^7$ stars in the Magellanic Cloud as a MACHO passes across the line of sight to that star. This brightening has a characteristic time dependence and would be achromatic. So far the three groups[6] doing this work have demonstrated feasibility, in that the photographic plates and CCD cameras have discovered many variable stars, but with no MACHO candidates yet, the background problems seem

well in hand. The present results are still well below the level of the few events per year expected if all the galactic dark matter were baryonic.

4. HOT DARK MATTER

The light, but not massless (as it is in the Standard Model) neutrino has long been a candidate for dark matter, since there are $\sim 10^2/\mathrm{cm}^3$ of each family everywhere, and a mass of ~ 25 eV would give $\Omega = 1$. The problem of galaxy formation has to be solved by introducing topological seeds, such as cosmic strings, and there is also the difficulty that dwarf galaxies cannot hold enough such light neutrinos to provide their needed dark matter. A better use for neutrinos, mentioned above, is as a minority component of dark matter.

Since the direct detection of relic neutrinos appears to be impossible, their existence will have to be deduced from neutrino oscillation information. Conventional wisdom has the ν_τ playing this role, but if all current hints of neutrino mass are correct, that scheme is wrong, and there is a more likely scenario.[7] There are at present three indications of neutrino mass: (1) the deficit of solar ν_e's, (2) the depletion of atmospheric ν_μ's relative to ν_e's, and (3) the apparent need for some hot dark matter. If all of these are indeed due to neutrino mass, there are only three logical possibilities for the pattern of neutrino masses and mixings: (A) ν_e, ν_μ, and ν_τ are all about 2.3 eV in mass, (B) ν_e, ν_μ, and ν_τ are all very light, and one or more sterile neutrinos, ν_s, provide the dark matter, or (C) ν_e and ν_s are very light and ν_μ and ν_τ are about 3.5 eV each. Case (A) is probably ruled out by the non-observation of neutrinoless double beta decay. Case (B) is also probably ruled out because the ν_s decoupled so early in the expansion of the universe that their numbers depleted, making their required mass $\gg 7$ eV, which in turn makes them too slow to perform the function of the hot dark matter. That leaves only case (C), which explains the ν_e solar deficit via $\nu_e \rightarrow \nu_s$, with about the same Δm^2 and mixing angle as for $\nu_e \rightarrow \nu_\mu$. There is also no difficulty with too many neutrinos at the time of nucleosynthesis, since a ν_s that light (and with the mixing angles of either the non-adiabatic MSW or vacuum oscillation cases) was not then in equilibrium. Case (C) explains the atmospheric ν_μ depletion via $\nu_\mu \rightarrow \nu_\tau$, with these nearly degenerate heavier neutrinos also providing an even better fit to the structure information than a single

7 eV neutrino.[5)]

The question of ν_e to ν_s or ν_μ should be settled by the neutral current detection at SNO or BOREXINO. A check on the $\nu_\mu \to \nu_\tau$ of the atmospheric ν_μ depletion could be provided by long baseline neutrino oscillation experiments planned at Brookhaven and Fermilab. The essential feature of a $\Delta m^2 \sim 10$ eV^2 mass difference between the ν_e–ν_s and ν_μ–ν_τ sectors can be tested best by a $\nu_\mu \to \nu_e$ oscillation experiment, although the less sensitive and more difficult $\nu_e \to \nu_\tau$ experiment should also be done, because these mixings are model dependent. The LSND experiment at Los Alamos as early as 1994 could achieve a limit on $\sin^2 2\theta_{e\mu} \sim 3 \times 10^{-4}$ at this Δm^2, if current funding problems do not interfere.

5. COLD DARK MATTER

There are a very large number of cold dark matter candidates, of which only a few are motivated by needs other than to be dark matter. One is the axion, which would result from a possible solution to the strong CP problem. Despite requiring a mass $\sim 10^{-5}$ eV to give $\Omega = 1$, axions are a cold dark matter candidate. The lack of evidence for energy transport by axions in stellar cooling and from SN1987A limits axion mass to $\lesssim 10^{-3}$ eV. Two experiments[8)] have been developed to detect axions by looking for the conversion of axions to photons in a magnetic field, but lack a factor of $\sim 10^2$ in sensitivity for doing so. A new experiment[9)] is currently being constructed with a much higher field superconducting magnet which could have the required sensitivity.

There used to be also considerable motivation for a heavy fourth-generation neutrino as dark matter. The SLC/LEP limitation to three generations of weak isodoublet neutrinos of mass $\lesssim 45$ GeV eliminated a fourth Majorana neutrino, since to be dark matter its mass would have to be $\sim$ 5–8 GeV, which is determined by its annihilation rate when such neutrinos could have been in thermal equilibrium in the early universe. Such a Majorana neutrino may have been ruled out previously by indirect dark matter searches performed at the proton decay detectors, Fréjus, Kamioka, and IMB. The Majorana particles could be captured by the sun or earth, annihilate in pairs, and produce energetic neutrinos from the cascade decays of heavy flavor annihilation products. The energetic neutrinos then need to be detected above the

background of atmospheric neutrinos. Space limitations prevent discussing the observations or the controversy about the interpretation of the complex chain of events involved.

In contrast to the Majorana case, a Dirac neutrino could have had a wide mass range, since an initial particle-antiparticle asymmetry would allow the annihilation rate to be adjusted suitably. The SLC/LEP result conclusively ruled out the 4–10 GeV Dirac mass range. Masses larger then 10 GeV had already been eliminated by underground Ge semiconductor detectors sensitive to nuclear recoils struck by such a particle. Three experiments[10,11] have searched for dark matter. Results presented here are from the UCSB/LBL/UCB data, although the others are similar. The exclusion plot of Fig. 1 assumes a conservative dark matter galactic halo density of 0.3 GeV/cm^3 = 5×10^{-25} g/cm^3 and a Maxwellian dark matter velocity distribution of $v_{rms} \approx 300$ km/s. Each particle mass is assumed in turn to be the source of dark matter, and the results are for the case of spin-independent interactions, for which there is nuclear coherence. Particles having the normal weak interaction would lie along the line in Fig. 1 labelled "Dirac ν," and are excluded between 10 GeV and $\sim$ 3 TeV. Since $\sim$ 30 eV–4 GeV would give $\Omega > 1$, all isodoublet Dirac neutrinos $\gtrsim$ 30 eV are eliminated as dark matter, if the upper mass limit is really[12] $\sim$ 1 TeV. Also ruled out as dark matter are the lightest technibaryon and any particle above and to the right of the solid line.

A region shown in Fig. 1 refers to a class of Weakly Interacting Massive Particles (WIMPs) called Cosmions, which could be dark matter and also solve the solar ν problem. The Cosmion could be captured in the sun and fall toward the center, where its motion to larger radii would cool the solar core by the $\sim$ 10% needed to reduce the flux of ^{8}B solar neutrinos.[13] The Cosmions were essentially excluded[14] using Si detectors in the UCSB/LBL/UCB apparatus, since these are more sensitive to lower masses than is Ge.

The exclusion region does not end at the boundaries of Fig. 1, as seen in Fig. 2. Note that the cross section of Fig. 1 is on Ge, while that of Fig. 2 is for protons. Interest in Strongly Interacting Massive Particles (SIMPs) as dark matter prompted Starkman et al.[15] to find regions of mass-cross section space viable for dark matter candidates. The most likely remaining region was the mass range $10^6 - 10^8$ GeV with a cross section on protons of

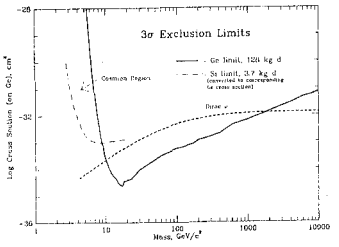

Fig. 1. Exclusion plot for the mass and elastic cross section on Ge for dark matter particles. The weak interaction cross section is indicated by "Dirac ν."

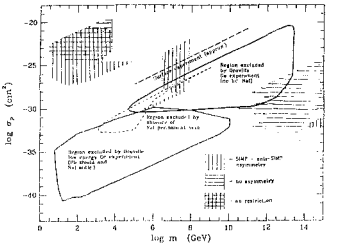

Fig. 2. Exclusion plots for the mass and cross section on protons for dark matter particles, showing also the regions Ref. 15 found were not excluded by other information.

10^{-28}–10^{-22} cm^2 and a narrow "finger" reaching down to 10^5 GeV and 10^{-30} cm^2. To search this region the Pb shielding and NaI veto above the Ge detectors in the UCSB/LBL/UCB apparatus were removed, giving the "no-lid, NaI" exclusion region shown. To extend the upper boundary, some data were taken with a Ge detector at the surface, giving the dashed line. Another exclusion region is dashed in and labeled "absence of a NaI permanent veto", since in this region there would always be a SIMP in the NaI within the electronics dead time. This region extends into the exclusion area of Fig. 1, which is shown completely here.

With so much of the SIMP mass–cross section space eliminated, it is improbable that any particle with stronger than the standard weak interaction can be the main component of dark matter. There is also a limit[12,16] that any stable elementary particle which was once in thermal equilibrium in the early universe has to have a mass less than $\sim 10^3$ TeV.

6. FUTURE DIRECT DETECTION OF DARK MATTER

The need is now to go to cross sections well below weak for Dirac particles and especially to achieve sensitivity to Majorana particles with their spin-dependent interactions, particularly the lightest supersymmetric particle (LSP). The LSP is a well motivated dark matter candidate, since it was invented for a purpose other than to be dark matter, and an $\Omega = 1$ density is achieved quite naturally for a range of LSP parameters. If R-parity ($+1$ for particles, -1 for their supersymmetric partners) is conserved, the LSP is stable, but in any case it

is likely to be long lived. The LSP is generally considered to be a neutralino, some mass state which is a mixture of the interaction states of the superpartners of the hypercharge gauge boson, the neutral SU(2) gauge boson, and the neutral components of Higgs doublets. The nature of that mixture determines how readily the particle can be detected, but already accelerator and nonaccelerator experiments have considerably restricted the parameter space. The large number of free supersymmetric parameters are reduced in the Minimal Supersymmetric Standard Model (MSSM), particularly when grand unification (GU) is assumed, typified by the association with SU(5). Under these conditions LEP and CDF results restrict the neutralino to be more massive than $\sim$ 20 GeV. If one relaxes the assumption of GU,[17] neutralino masses giving $\Omega = 1$ can be $\sim$ 10 GeV, and outside the MSSM there are not well-defined limits on neutralino mass. However, the accelerator results and the requirement of $\Omega = 1$ still restricts the parameters considerably. In general it is likely that if the neutralino is dark matter, its mass is between 20 and 150 GeV.[18]

With the limitations from LEP and those shown in Fig. 1, for Dirac particles also masses > 20 GeV are of interest. Reduction of backgrounds to get to smaller cross sections for both the Dirac and Majorana particles is essential. In the latter case it is also necessary to have a nucleus with spin. Since the semiconductor experiments have involved extensive efforts to reduce backgrounds, significant further reductions require a new technique.

7. A CRYOGENIC EXPERIMENT

As backgrounds are due mainly to electrons (from β decays, Compton scattering, or photoelectrons), which ionize efficiently at low energies, whereas the nuclear recoil signal produces mainly phonons, a simultaneous measurement of phonons and ionization energies would provide an excellent discriminant. A semiconductor detector requires an electric field of $\sim 10^3$ V/cm to remove free charge carriers and fully deplete the crystal, but such a field moving the ionization charge creates phonons which swamp the original phonon component of the particle interaction. However, the phonon signal can be detected using very low temperatures ($\sim 0.03°$ K), since the impurity charges are then frozen out from the bands, and only about 0.5 V/cm is needed to collect ionization electrons and holes. The low temperature

also provides a measurable temperature rise resulting from the particle interaction, as the heat capacity of the detector is proportional to the cube of the absolute temperature.

The Center for Particle Astrophysics group demonstrated[19] this technique using a 60 g. crystal of Ge and neutron-transmutation-doped thermistors. Figure 3 shows the ionization and phonon response to X-rays from ^{241}Am, while Fig. 4 displays a measurement with that X-ray source and a ^{252}Cf neutron source. With the current resolutions (FWHM of 1.7 keV for ionization and 1.9 keV for phonons at 60 keV), an additional background rejection of $> 10^2$ is calculated, and it is likely that those numbers will improve.

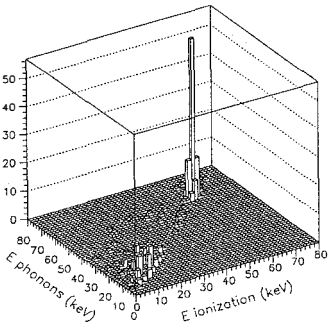

Fig. 3. Signals from 14, 18, and 60-keV X-rays (from ^{241}Am) in a 60 g. Ge crystal operated at 0.03° K, for which both the ionization and heat (phonons) have been measured.

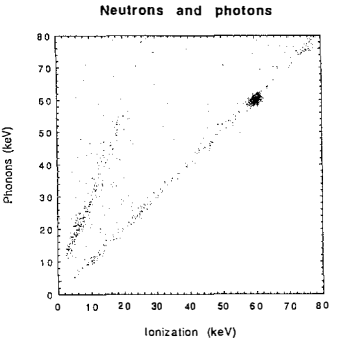

Fig. 4. Response of the 60 g. Ge crystal to a ^{252}Cf neutron source, shielded by 11" of Pb, and X-rays from ^{241}Am. Resolution of the two populations begins at ~ 3 keV of ionization.

This technique will be applied in an experiment presently being implemented at a shallow (20 m.w.e.) site on the Stanford campus by the UCSB/LBL/UCB/Stanford/INR Baksan group. Since the technique is new and dilution refrigerators require attention, a location was chosen on the basis of ready access. The Oroville site[12] at 600 m.w.e. was by far the shallowest heretofore used for a dark matter search. Cosmic ray muons are a problem in that they produce neutrons which can give nuclear recoils. A highly efficient muon veto counter must be constructed and provide a deadtime after the passage of the muon until the neutron is at least of too low an energy to give a measureable recoil. The neutrons, produced mainly in the Pb shield needed to reduce external radioactivity, are moderated by polyethylene.

According to calculations, the main remaining source of neutrons are the Cu fixtures needed to contain the detectors at low temperature. The shielding can be quite complete because the dilution refrigerator has been constructed with an unusual side exit so that cooling can be achieved in a separate cold box.

Current plans are to take data with three 0.5 kg detectors, one of normal Ge, one enriched in ^{73}Ge (spin 9/2), and one enriched in ^{76}Ge (spin 0). This will provide appropriate cross checks and allow the simultaneous search for Dirac and Majorana dark matter. If we can achieve electron background levels comparable to those we now have in the semiconductor experiment at Oroville, this should begin the exploration of the region in which the lightest supersymmetric particle could exist, as shown in Fig. 5.

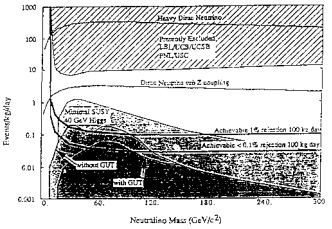

Fig. 5. Exclusion plot of event rate vs. particle mass showing the already excluded region of Fig. 1 and the neutralino region with various theoretical assumptions. The lines show limits to be achieved after 100 kg days using a ^{73}Ge crystal and having 1% and 0.1% additional rejection from simultaneous ionization and phonon measurements.

8. CONCLUSIONS

If dark matter is indeed 70% cold and 30% hot, the nature of the latter will have to be determined by terrestrial experiments, guidance for which comes from present indications for neutrino mass. These suggest a unique pattern for neutrino masses. The cold component is amenable to direct search, and already by this means Dirac candidates covering 12 orders of magnitude in mass and 20 orders of magnitude in cross section have been eliminated. Some Majorana particles have also been ruled out. Further progress can come from new techniques, including the simultaneous measurement of phonons and ionization, now being implemented.

REFERENCES

1. T.P. Walker et al., *Ap. J.* **376**, 51 (1991) and OSU-TA-1/93 (1993).
2. A. Nusser and A. Dekel, *Ap. J.* **405**, 437 (1993).
3. Q. Shafi and F.W. Stecker, *Phys. Rev. Lett.* **53**, 1292 (1984).
4. E.L. Wright et al., *Ap. J.* **396**, L13 (1992); M. Davis, F.J. Summers and D. Schlegel, *Nature* **359**, 393 (1992); A.N. Taylor and M. Rowan-Robinson, *Nature* **359**, 396 (1992); R.K. Schaefer and Q. Shafi, BA-92-28 (1992); J.A. Holtzman and J.R. Primack, *Ap. J.* **405**, 428 (1993).
5. M. Davis and J. Primack, private communications.
6. Center for Particle Astrophysics, Lawrence Livermore, Mt. Stromlo; Princeton, Carnegie Obs., Warsaw Univ.; IAP, Obs. de Paris, Marseille, Saclay, Orsay.
7. D.O. Caldwell and R.N. Mohapatra UCSB-HEP-93-03 (1993, submitted to Phys. Rev. Lett.); references to the original literature can be found therein.
8. W. Wuensch *et al.*, *Phys. Rev. D* **40**, 3153 (1989); C. Hagmann *et al.*, *Phys. Rev. D* **42**, 1297 (1990).
9. LLNL, Florida, INR, UCB, Chicago, SLAC Collaboration.
10. S.P. Ahlen et al., *Phys. Lett.* , B195, 603 (1987); F. Boehm et al., *Phys. Lett.* **B255**, 143 (1991).
11. D.O. Caldwell et al., *Phys. Rev. Lett.* **61**, 510 (1988).
12. K. Griest and M. Kamionkowski, *Phys. Rev. Lett.* **64**, 615 (1990).
13. R.L. Gilliland et al., *Ap. J.* **306**, 703 (1986) and earlier references therein.
14. D.O. Caldwell et al., *Phys. Rev. Lett.* **65**, 1305 (1990).
15. G.D. Starkman et al., *Phys. Rev. D* **41**, 3594 (1990).
16. A.-C. Davis and R.H. Brandenberger, *Phys. Lett.* **B284**, 81 (1992).
17. K. Griest and L. Roszkowski, *Phys. Rev. D* **46**, 3309 (1992).
18. L. Roszkowski, *Phys. Lett.* **B262**, 59 (1991).
19. T. Shutt *et al.*, *Phys. Rev. Lett.* **69**, 3425, 3531 (1992).

Atmospheric Neutrinos

ATMOSPHERIC NEUTRINOS AND NEUTRINO OSCILLATIONS

R.Barloutaud
DAPNIA-CEN SACLAY

ABSTRACT

The results on the composition of atmospheric neutrinos interacting in underground detectors and on the rate of atmospheric muon neutrino interactions in the earth surrounding the detectors are reviewed. Up to now, systematic errors on the neutino flux and on the electrons and muons neutrino interaction identifications are not yet reliable enough to prove that atmospheric neutrinos oscillate before being detected.

The study of neutrinos produced in the high atmosphere offers a possibility to search for neutrino oscillations occuring during their travel through the earth and atmosphere in a range varying between about 10 and 13.000 Kms. As they are mainly produced in the decays of charged pions and muons, they consist on twice more ν_μ or $\bar{\nu}_\mu$ than ν_e or $\bar{\nu}_e$. Therefore, the fluxes, the energy and angular distributions of these particles are sensitive to ν_μ ν_e or ν_μ ν_τ oscillations if the mass squared difference between two neutrino flavors is larger than 10^{-4} ev^2 and, due to systematic uncertainties, if the corresponding mixing angles are such that $\sin^2 2\theta$ is larger than about 0.4.

The interactions of atmospheric neutrinos are observed in large underground detectors where both ν_μ and ν_e interactions can be identified. Moreover high energy charged current ν_μ interactions in the earth surrounding the detectors, producing upward or nearly horizontal going muons may be separated from the high rate of downward going atmospheric muons. During the recent years more than one thousand neutrino interactions occuring inside the underground detectors have been measured, and a similar amount of ν_μ earth interactions were observed. Several reviews have been recently presented[1,2,3] on the results obtained by these experiments.

1. Atmospheric neutrino flux calculations

The atmospheric ν_μ and ν_e fluxes, their energy and angular distributions must be calculated as accurately as possible in order to find experimentally some deviations which could be attributed to neutrino oscillations.

Starting from primary cosmic ray fluxes, their interactions on nitrogen and oxygen nuclei, and the propagation of the decay pions and muons in the atmosphere, many groups[4 to 11] have calculated the fluxes of ν_μ and ν_e reaching the earth, taking into account the geomagnetic effects and the time dependent solar activity. The results may be summarized as follows:

a) Mainly due to uncertainties on cosmic primary flux and composition, the total neutrino flux is known to about 20% at low energy ($\lesssim$ 10 Gev) and to 30% at high energy ($\gtrsim$ 10 Gev).

b) The composition of the atmospheric neutrinos agrees in all the models and the uncertainty on the flux ratio ν_μ / ν_e is probably smaller than 5%[4 to 11].

c) The shapes of the energy and angular distributions of the atmospheric neutrinos are rather well predicted.

d) The interaction rate of the ν_μ in the earth depends also on their cross section; this introduces an additional uncertainty of about 10%[12]. However, the shapes of the energy and angular distributions of the muons produced in the earth are reliably calculated[12].

2 Experimental studies

2.1 Detection of neutrino interactions inside underground detectors

These detectors originally designed to study the nucleon decays are in principle able to measure and to identify the ν_μ and ν_e charged current interactions and in some cases, with a smaller efficiency, the neutral current interactions. The interaction rate is of the order of 100 events/Kt.year. The large Cerenkov detectors experiments (1 to 5 Kt. of fiducial volume for the Kamioka[13,18] and I.M.B.[14] have analysed 4.9 and 7.7 Kt.years of data respectively. The energy thresholds vary between 0,1 to 0,2 Gev for the ν_e and 0,2 to 0,3 Gev for the ν_μ interactions. In order to reach a good identification efficiency of the electrons and muons, the single ring events, fully contained in the detector are selected, limiting the energy to about 1.4 Gev. This allows to detect the decay electron of the muons with a pulse delayed by the muon lifetime. The tracking calorimeter experiments have analysed 0,3 1,6 and 0,5 Kt.year of data in the NUSEX[15] Frejus[16] and SOUDAN2[17] detectors respectively. These experiments are in principle able to separate all ν_μ and ν_e interactions and, according to their atmospheric muon background, to make use of the events produced in the fiducial volume, but not necessarily fully contained in the detector. The threshold energy varies between 0,2 and 0,3 Gev for ν_μ and ν_e interactions.

2.2 Detection of the ν_μ interactions in the earth surrounding the detector

a) Upward going muons (zenith angle $\theta_Z \sim 90°$, energy larger than $\sim$10 Gev)

In order to separate the muons produced by ν_μ interactions in the earth from the huge flux of downward going atmospheric muons an excellent separation in directionnality is required. This is obtained by the water Cerenkov detectors Kamioka[18] and IMB[19], and by time of flight in

scintillator telescopes (BAKSAN and MACRO). Until now, only results from the BAKSAN experiment have been published[20]. The IMB experiment[19] has also recorded the upward going muons stopping in the detector; they correspond to ν_μ energy of the order of 50 Gev[12].

b) The nearly horizontal neutrinos may be separated without directionnality information from the downward going muons in an angular region, which depends on the depth of the detector and the shape of the ground over the laboratory. This corresponds in the Frejus experiment[21] to $75° < \theta_Z < 105°$ in which the muon rate amounts to about 60% of the upward going muons.

3. Results on atmospheric neutrino flavor composition and oscillations

3.1 ν_μ and ν_e fluxes

In each experiment, the data are compared to the expectation obtained by a Monte Carlo simulation, taking into account the response of the detector for each type of interaction, the calculated neutrino fluxes, their energy and angular distributions.

The published results allow to calculate the following ratios where ν_μ and ν_e represent the rate of the interactions.

$$R_T = (\nu_\mu+\nu_e)\text{data} \;/\; (\nu_\mu+\nu_e)\text{simul.}$$

$$R_S = \frac{\text{single ring (prong) data}}{\text{multi rings (prongs)}} \;/\; \frac{\text{single ring (prong) simul.}}{\text{multi rings (prongs)}}$$

$$R = (\nu_\mu/\nu_e)\text{data} \;/\; (\nu_\mu/\nu_e)\text{simul.}$$

$$R_D = (\mu\text{decay/no }\mu\text{ decay})\text{data} \;/\; (\mu\text{decay/no }\mu\text{ decay})\text{simul.(in Cerenkov exp.)}$$

The values of these ratios are represented in fig.1 (a,b,c,d).The calculated fluxes are all normalized to the Bartol flux predictions[6]. The errors shown are purely statistical.

The following comments can be made on these results.

a) As indicated in the fig.1 caption, the event selections applied by the experiments to obtain these results are very different.In particular only 30% of the neutrino interactions are common in the Frejus and the water Cerenkov experiments.

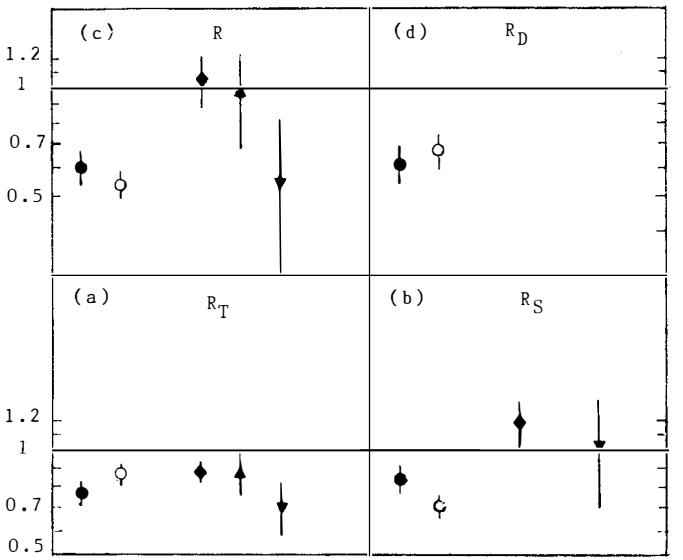

Fig.1 Data over simulation rate ratios for ν interactions produced inside the detector
●Kamioka exp. 310 one ring, 147 multiring fully contained events[18].
○IMB exp. 610 one ring, 325 multiring fully contained events[14].
◆Frejus exp.188 events (except 1 prong uncontained), 70 one prong events[16].
▲NUSEX exp. 50 fully contained events[15].
▼SOUDAN2 exp. 25 one prong, 12 multiprong, fully contained events[17].

b) The ratios R_T (fig.1a) are compatible and lower than unity in all experiments, suggesting that the Bartol flux[6] used in the simulations may be slightly overestimated but compatible with the estimated systematic error.

c) The flux independent ratios R_S (fig.1b) are lower than unity in the water Cerenkov experiments.(especially in the IMB results where it differs by more than 5 s.d. from unity). This shows that the fraction of the single ring events is not well described by the simulation in the IMB experiment. In case of a deficit of ν_μ , for which the energy threshold is higher than for ν_e, it is expected that the ratio R_S should be larger

than unity.

d)The ratios R (fig.lc) are definitely lower than unity in the water Cerenkov but compatible with unity in the tracking calorimeter experiments. This has been interpreted by the Kamioka group as an indication for neutrino oscillations $\nu_\mu \nu_e$ or $\nu_\mu \nu_\tau$ .This deficit of ν_μ interactions is also visible in the ratio R_D (fig ld) which is also lower than unity.

Beside the statistical errors on R plotted in fig.lc, some systematic errors have been evaluated to take into account the possible misidentification of muons and electrons which could be different in the data and in the simulation. These errors R_{sys} are 0.05, 0.12, 0.15 and 0.10 in the Kamioka, IMB, Frejus and SOUDAN2 experiments respectively.(In the Frejus experiment[22] they have been checked by making three completely independent simulations and analyses of the data). An important question is to know how reliable are these errors; a test of the electrons and muons identification efficiency will be performed in a water Cerenkov detector in a near future[3] to clarify this point.

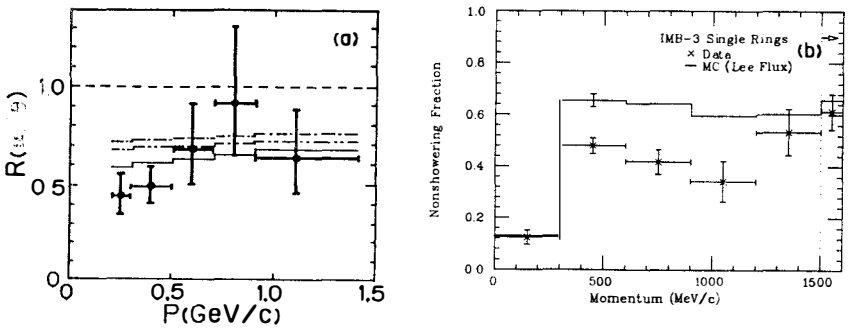

Fig.2 a)Momentum dependence of the ratio R in the Kamioka experiment.The dashed and dashed-dotted lines correspond to no oscillation and some oscillation hypotheses

b) Non showering fraction of events versus momentum in IMB experiment. The full line corresponds to no oscillation.

3.2 Energy and zenith angle distribution

The ν_μ deficit found in the water Cerenkov experiments is clearly visible in the shape of the energy distribution of R (fig2a) in the Kamioka experiment and to a lesser degree in the IMB experiment (fig2b). However the shape of the zenithal angle θ_Z distributions are not showing any evidence for an angular dependence of this deficit[13-19]). The corresponding

Frejus distributions in energy and zenith angle are compatible, within the statistical accuracy to the Monte Carlo simulations[16].

3.3 Neutrino oscillation analyses

Assuming that the differences between the data and the simulations are due to neutrino oscillations, some exclusion plots in the diagrams Δm^2-$\sin^2 2\theta$ have been calculated by the Kamioka[13] and the Frejus[22] experiments. The errors used are the quadratic sum of statistical and systematic errors and the 90% c.l. exclusion regions have been determined for $\nu_\mu \nu_e$ and $\nu_\mu \nu_\tau$ oscillations (fig.3a and 3b). The Kamioka analysis requires an oscillation in the region $\Delta m^2 \gtrsim 4\ 10^{-3}$ ev^2, $\sin^2 2\theta \gtrsim 0.4$ for $\nu_\mu \nu_e$ or $\Delta m^2 \gtrsim 10^{-3}$ ev^2, $\sin^2 2\theta \gtrsim 0.4$ for $\nu_\mu \nu_\tau$, while the Frejus analysis excludes the region $\Delta m^2 \lesssim 3\ 10^{-3}$ ev^2, $\sin^2 2\theta \lesssim 0.5$ for $\nu_\mu \nu_e$ and $\Delta m^2 \lesssim 6\ 10^{-3}$ ev^2, $\sin^2 2\theta \lesssim 0.6$ for $\nu_\mu \nu_\tau$. The presence of oscillations which could explain the ν_μ deficit in the Kamioka experiment does not change appreciably the shapes of the energy (fig.2a) and angular distributions[3].

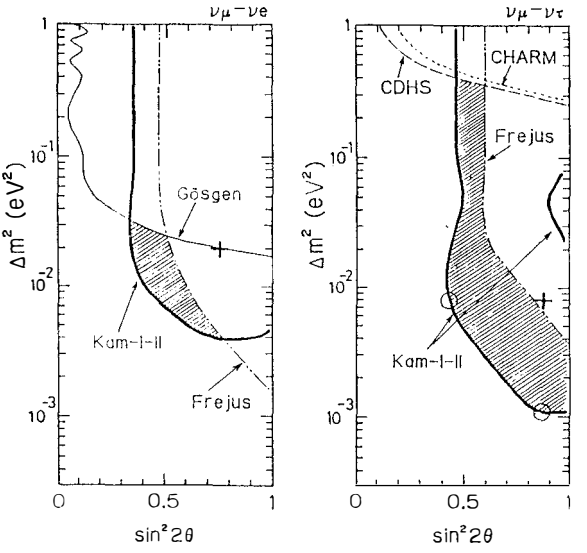

Fig.3 Allowed neutrino oscillation parameters from Kamioka experiment (right of the full line) and from Frejus experiment (left of the dashed line) for $\nu_\mu \nu_e$ and $\nu_\mu \nu_\tau$ oscillations.

4.Results on upward and horizontal going muons and neutrino oscillations.

A detailed review of the results obtained by the Kamioka[18,3], IMB[19] and Baksan[20] experiments has been recently made by the Bartol-Penn. group[12]. A result on the rate of horizontal muons obtained in the Frejus experiment[21] will also be included in the report.

4.1 Upward and horizontal going muons fluxes.

In each experiment, the observed muon rate is compared to the predicted one and their ratio r

r = observed rate / predicted rate

has been measured using the energy and angle dependent ν_μ flux calculated by Volkova[4]. With other models of ν_μ flux and recent neutrino cross sections, the predicted rate may vary by about 30%[12]. The results on r with the statistical errors are presented in fig.4a. All values are compatible with unity , but somewhat lower than 1.3 expected by the larger Bartol flux. The shape of the angular distributions presented by Kamioka and Baksan are found to be compatible with the distributions calculated by the various models[12].

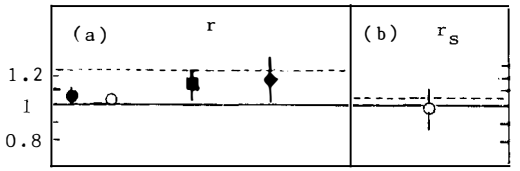

Fig.4 Data over simulation rate ratios over the ν_μ interactions produced in earth
● Kamioka exp. 252 up going muons.
○ IMB exp. 617 up going muons.
85 stopping up going muons.
■ Baksan exp. 421 upgoing muons.
◆ Frejus exp. 55 horizontal muons.
The dashed lines correspond to the maximum predictions.

The IMB experiment has measured[19] the ratio of the muon rates stopping in the detector and crossing it:

f = stopping muon rate/through muon rate = 0.16±0.02

This ratio is almost independent of the ν_μ flux and is calculated to be

0.158±0.05. Therefore the ratio

r_s = f data / f simulation

presented in fig.3b is found in excellent agreement with unity.

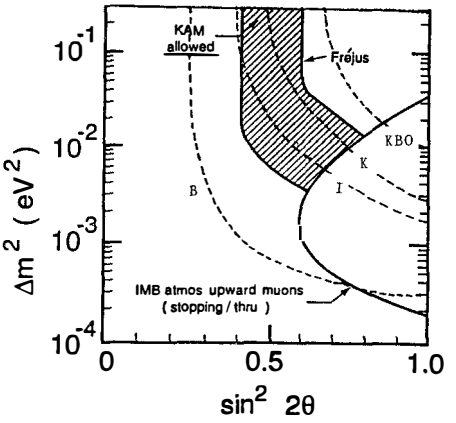

Fig.5 Allowed ν_μ ν_τ oscillation parameter regions for the atmospheric interactions in detector (Kamioka and Frejus experiments) and for interactions in earth.
The dashed lines represent the B, K, and I limits obtained by Baksan, Kamioka, and IMB respectively and calculated with the Volkova flux. The line labelled KBO is calculated with the Kamioka data, the Bartol flux and Owen cross-section. The allowed regions lie to the left of the dashed curves.The full line is obtained by the IMB experiment, with the fraction of stopping up going muons.

4.2 Neutrino oscillation analyses

No evidence for ν_μ deficit is found in the results of upward going muon fluxes. In order to see whether or not these results were in contradiction with the ν_μ deficit found in the composition of the neutrinos interacting in the detector, some exclusion zones in the oscillation parameter plot were calculated by the Kamioka, IMB and Baksan groups assuming various ν_μ flux models. Some of these zones exclude completely the previous allowed region (fig.5). However, the region remains untouched by the Kamioka limit calculated with the Bartol flux and the Owens cross section[12]. The excluded zone for $2\ 10^{-4}\text{ev}^2 \lesssim \Delta m^2 \lesssim 2\ 10^{-2}\text{ev}^2$ and $\sin^2 2\theta \gtrsim 0.7$

is due to the absence of discrepancy between the experimental and the calculated value of the fraction f.

Conclusion.

The evidence for oscillation of the atmospheric neutrinos is still far to be compelling. No effect is found in the results of the ν_μ interaction in the earth. The deficit of ν_μ in the Cerenkov detector interactions might suggest an oscillation $\nu_\mu \nu_e$ or $\nu_\mu \nu_\tau$ in the region $\Delta m^2 \gtrsim 10^{-2}$ to 0.4 ev^2, $\sin^2 2\theta \simeq 0.5$. However, this conclusion must be confirmed by a check of the systematic uncertainties of the Monte Carlo simulations used to demonstrate this deficit.

References

1. J.Schneps, Neutrino 92 Proceedings,Granada 1992
2. E.W.Beier et al, Phys. Lett. B283 (1992) 446
3. Y.Totsuka, Neutrino 92 Proceedings, Granada 1992
4. L.V.Volkova, Yad. Fiz. 31,1510 (1980)
5. T.K.Gaisser et al, Phys. Rev. D38 (1988) 85
6. G.Barr et al, Phys. Rev. D 39 (1989) 3532
7. E.V.Bugaev et al, Phys. Lett. B232 (1989) 391
8. A.V.Butkevich et al. Yad. Fiz. 50, 142, (1989)
9. M.Honda et al Phys. Lett. B248 (1990) 883
10. H.Lee et al, Nuovo Cimento 105 B (1990) 193
11 M.Kawasaki et al, Phys. Rev. D 43 (1991) 2900
12. W.Frati et al Int. Report BA 92-71, UPR 0218 E (1992)
13. K.S.Hirata et al, Phys. Lett. B205 (1998) 416
    B280 (1992) 146
14. R.Becker-Szendy et al Phys. Rev. D46 (1992) 3720
15. H.Aglietta et al, Europhysics letters 8 (1989) 611
16. Ch. Berger et al, Phys. Lett. B227 (1989) 489
17. M.Goodman (Soudan2 Coll.) Internal report (FDK-540) (1992)
18. Y.Oyama (Kamioka Coll.) Moriond Jan. 1992 Proceedings p.59
19. R.Becker- Szendy et al, Phys. Rev. Lett. 69 (1992) 1010
20. M.M.Boliev et al, Venice Workshop Proceedings (1991) 235
21. H.Meyer (Frejus Coll.) Moriond Jan.1992 Proceedings p.169
    Y.Wei, Thesis University of Wuppertal (1993)
22. Ch. Berger et al, Phys. Lett. B245 (1990) 305

THE CURRENT STATUS OF ATMOSPHERIC NEUTRINO FROM KAMIOKANDE

The Kamiokande collaboration

Presented by;
Kenji Kaneyuki
Department of Physics, Tokyo Institute of Technology
O-okayama, Meguro-ku, Tokyo 154, Japan

ABSTRACT

A preliminary result of contained events during the detector exposure of 1.28 kt·yr in Kamiokande-III is presented. The updated result from Kamiokande-III is consistent with the previous result from Kamiokande-I and II, and the combined result during a total of 6.18 kt·yr exposure gives $(\mu/e)_{data}/(\mu/e)_{MC} = 0.60 \pm 0.06 \pm 0.05$.

1 Introduction

Neutrino physics using a large underground detector has an advantage over an experiment using an accelerator or a reactor, in that neutrinos travel longer path length in vacuum and matter. Therefore, the study of atmospheric neutrinos approach from a different side to neutrino physics.

Primarily, atmospheric neutrinos have been studied as background against nucleon decay experiments deep underground. Atmospheric neutrinos come from the interactions of primary cosmic rays with nuclei composing the atmosphere. The generated neutrinos travel a distance ranging from the depth of the atmosphere to the diameter of the earth. Therefore, the sensitivity of an experiment using the atmospheric neutrino beam to neutrino oscillations is $\Delta m^2 \sim 10^{-4} eV^2$, as the average neutrino energy around $1GeV$.

The difficulty in the study of atmospheric neutrinos comes from the ambiguity in theoretical calculations of the neutrino flux. The atmospheric neutrino flux has been calculated by several authors in detail. The difference in absolute value of flux falls within 30% among the calculations by Gaisser [1], Honda [2] and Lee [3]. However, the ambiguity in the ratio of muon neutrino flux to electron neutrino flux cancels out, because they originate from the same decay chains $\pi^{\pm} \rightarrow \mu^{\pm} + \overset{(-)}{\nu}_{\mu}$ or $K^{\pm} \rightarrow \mu^{\pm} + \overset{(-)}{\nu}_{\mu}$ followed by $\mu^{\pm} \rightarrow e^{\pm} + \overset{(-)}{\nu}_{\mu} + \overset{(-)}{\nu}_{e}$. The three calculations agree within 5% at neutrino energies larger than 100 MeV/c.

A relative deficit in ν_{μ} to ν_e has been already reported by Kamiokande [4] [5], and IMB [6] based on contained neutrino events. As for up-going muons as a probe of neutrino oscillations, they should be treated carefully since the models of the neutrino flux and the models of neutrino interactions directly affect the event rate calculations [7]. In this talk, a recent result of contained events during detector exposure of 1.26 kt·yr in Kamiokande-III is presented in addition to the previous result from Kamiokande-I and II during 4.92 kt·yr exposure.

2 Event selection

The analysis sequence of atmospheric neutrinos is as follows; First, an event is required to be contained. The events should be fully contained in the inner detector and should not have any particles exiting into the anti counter, therefore the selection criteria are;

1. total number of photoelectrons lies between 110 p.e. and 4500 p.e.

30MeV/c - 1350MeV/c for electron

205MeV/c - 1500MeV/c for muon

2. maximum number of photoelectrons in an event < 200 p.e.

3. no signal in the anti counter (Kamiokande-II,III)

The number of tracks, position of event vertex and direction of each track are reconstructed using the timing and charge information of each photomultiplier. After that, the fiducial volume is defined to be 2m (1.5m) inside from the photomultiplier plane in Kamiokande-I (Kamiokande-II,III), and the events in the fiducial volume are selected. The fiducial mass is 880 ton in Kamiokande-I and 1040 ton in Kamiokande-II, III respectively.

A Monte Carlo study shows 75% of single ring events come from quasi elastic interactions, and only 4% of the events come from neutral current interactions, therefore single ring events are a good probe of the parent neutrino flavors. Each single ring event is classified as muon-like event or electron-like event using the Čerenkov ring pattern and the opening angle of the Čerenkov ring. The efficiency of particle identification is 98% from a Monte Carlo study, and it is backchecked by real stopping μ and μ-decay electrons. In addition to these cut, each electron like event is required the momentum to be larger than 100MeV/c.

3 Result

Table 1 show a summary of fully contained events in Kamiokande-I, II (4.92 kt·yr) with an additional 1.26 kt·yr data from Kamiokande-III. The total detector exposure is 6.18 kt·yr. The additional data from Kamiokande-III are consistent with the previous data, and the combined result gives a total of 557 events. They include 389 single ring events and 168 multi ring events. Single ring events are then classified as 191 muon-like events and 198 electron-like events. And Monte Carlo predictions based on the callculations, by Gaisser, Honda and Lee are also given in the table 2. To avoid the large ambiguity in the absolute neutrino flux and the cross sections of neutrino interactions, we take a double ratio of muon-like events to electron-like events in comparison with the Monte Carlo prediction based on the Gaisser's calculation. The result gives;

$$\frac{(\mu-\mathrm{like}/\mathrm{e}-\mathrm{like})_{\mathrm{data}}}{(\mu-\mathrm{like}/\mathrm{e}-\mathrm{like})_{\mathrm{M.C.}}} = 0.60 \pm 0.06 \pm 0.05$$

where the quoted errors are statistical and systematic, respectively. The detail of systematic errors is given in Table 3. And it should be stressed here that the double ratio shows a good agreement among the three flux calculations, 0.60 ± 0.06 based on Gaisser's, 0.59 ± 0.06 on Honda's and 0.59 ± 0.06 on Lee's. And this result is also consistent with a result of contained events from the IMB-III, $(\mu/e)_{data}/(\mu/e)_{M.C.} = 0.54 \pm 0.05 \pm 0.12$.

Figure 1 shows the momentum distributions of electron-like events and muon-like events, where solid line shows the Monte Carlo prediction based on the Gaisser's calculation. The distribution of the electron-like events are consistent with the Monte Carlo prediction, while the distribution of the muon-like events shows an apparent deficit compared with the prediction in the all momentum regions. However, the absolute normalization factor of the neutrino flux has a large ambiguity therefore the only thing one can claim is a relative deficit in muon-like events to electron-like events. Figure 2 3 shows the momentum and zenith angle dependence of the double ratio of $(\mu/e)_{data}/(\mu/e)_{M.C.}$, and this figure demonstrates that there is no strong dependence on the momentum and zenith angle within the statistical error.

The ratio of ν_μ to ν_e can checked independently using the μ-decay signal, because charged current ν_μ interactions are accompanied by an electron from μ decay. The following double ratio gives;

$$\frac{(\mu - \text{decay/no } \mu - \text{decay})_{\text{data}}}{(\mu - \text{decay/no } \mu - \text{decay})_{\text{M.C.}}} = 0.63^{+0.07}_{-0.06}$$

where the error is statistical one. This result is in good agreement with the result from the particle identification. The relative deficit in muon-like events to electron-like events is also confirmed by μ decay signal.

4 Future plan

A beam test using a 1000 ton water Čerenkov detector will be done at KEK in Japan for Kamiokande and IMB in 1994. The electron, muon and pion beams will be used in the momentum range from $200 MeV/c$ to $1000 MeV/c$. The aim of this beam test is a check of the current analysis procedure in the water Čerenkov detectors, both Kamiokande and IMB.

And Super Kamiokande has been under construction since 1991, the data taking will start in April 1996. Super Kamiokande will accumulate 22 times more events than the present Kamiokande. Figure 4 shows an expected zenith angle dependence during 5 years operation

of the Super Kamiokande detector assuming some neutrino oscillation parameters allowed by Kamiokande [5], and in some case the difference dependence on oscillation parameters may be clearly seen.

5 Conclusion

In conclusion, Kamiokande observed a relative ν_μ deficit to ν_e in atmospheric neutrinos based on the data during detector exposure of 6.18 kt·yr. The double ratio of muon-like events to electron-like events is $0.60 \pm 0.06 \pm 0.05$, and this result is confirmed by an independent analysis of the fraction of single ring events with μ decay signals. And IMB also gave a consistent result, using contained events.

As future plans, a beam test using charged particle beams will start in 1993 as a check of the current analysis, and Super Kamiokande, under construction now, will be able to test neutrino oscillations using atmospheric neutrinos with the 22 times higher statistics than obtained in Kamiokande.

References

[1] G. Barr *et al., Phys. Rev.* **D39** *(1989) 3532.*

[2] M. Honda *et al., Phys. Lett.* **B248** *(1990) 193.*

[3] H. Lee *et al., Nuobo Cimento* **B105** *(1988) 883.*

[4] K.S. Hirata *et al., Phys. Lett.* **B205** *(1988) 416.*

[5] K.S. Hirata *et al., Phys. Lett.* **B280** *(1992) 146.*

[6] D. Casper *et al., Phys. Rev. Lett.* **66** *(1991) 2561.*

[7] W. Frati *et al., preprint* **UPR-0218E** *(1992).*

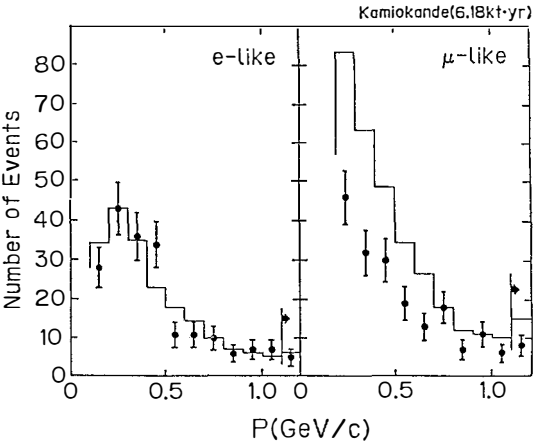

Figure 1: Momentum distribution of electron-like events and muon-like events. Solid line shows a Monte Carlo prediction based on the Gaisser's neutrino flux calculation.

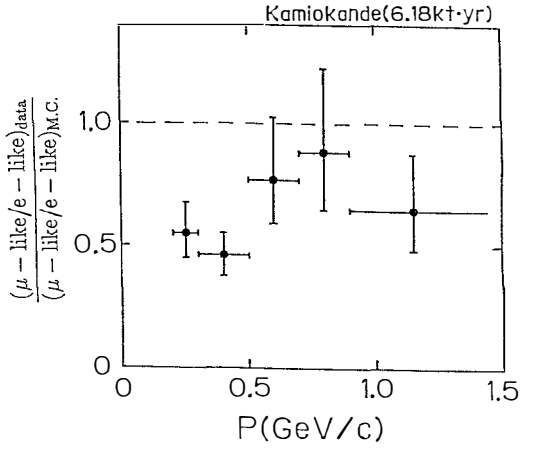

Figure 2: Momentum dependence of the double ratio of $(\mu/e)_{data}/(\mu/e)_{M.C.}$.

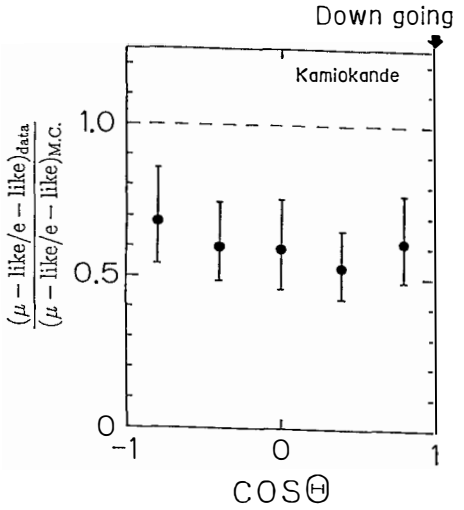

Figure 3: Zenith angle dependence of the double ratio of $(\mu/e)_{data}/(\mu/e)_{M.C.}$.

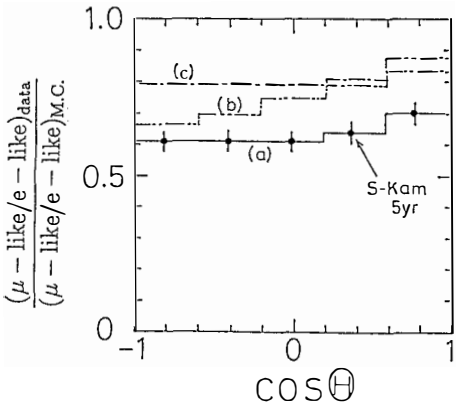

Figure 4: Expected zenith angle dependence assuming neutrino oscillation parameters, $(\Delta m^2, sin^2 2\theta)$ = (a) $(0.8\times10^{-2}eV^2, 0.85)$, (b) $(1.0\times10^{-3}eV^2, 0.85)$ and (c) $(0.8\times10^{-2}eV^2, 0.45)$. The statistical error in this figure is equivalent to 5 years operation of Super Kamiokande.

	Data		ν M.C.	
	total	μ-decay	total	μ-decay
Single-ring events	389	142	528.1	252.4
μ-like	191	126	325.2	230.6
e-like	198	16	202.9	21.8
Multi-ring events	168	64	208.0	86.0
Total	557	206	736.1	338.4

Table 1: Summary of the fully contained events during detector exposure of 6.18 kt·yr of Kamiokande-I,II and III.

	μ-like	e-like	$\frac{(\mu\text{-like/e-like})_{\text{data}}}{(\mu\text{-like/e-like})_{\text{M.C.}}}$
Gaisser	325.2	202.9	0.60 ± 0.06
Honda	292.5	179.4	0.59 ± 0.06
Lee	256.1	157.1	0.59 ± 0.06

Table 2: Summary of Monte Carlo predictions based on the callculations, by Gaisser, Honda and Lee.

Flux		
	$(\nu_\mu+\bar{\nu}_\mu)/(\nu_e+\bar{\nu}_e)$	<5%
	$\bar{\nu}_e/\nu_e$	2%
Analysis		
	Particle ID	4% (2×2%)
	1Ring/2Ring separation	2%
	Vertex pos. determination	1%
	Absolute E. calibration	1%
	External background	< 1%
MC		
	σ(CC, ν_μ)/σ(CC, ν_e)	~3%
	Ambiguity in NC cross section	~2%
	γ-ray from exited nuclei	1%
	Statistical fluctuation of MC	3.6%
	Total(added in quadrature)	9%

Table 3: Summary of the systematic errors on the μ/e ratio.

FLAVOUR COMPOSITION OF ATMOSPHERIC NEUTRINOS MEASURED IN IMB-3 DETECTOR [1]

Danka Kiełczewska [2]
The University of California, Irvine, California 92717, USA
Warsaw University, Warsaw, Poland

for the IMB Collaboration:

R. Becker-Szendy[a], C. B. Bratton[b], D. Casper[c], S. T. Dye[c], W. Gajewski[d], M. Goldhaber[e], T. J. Haines[f], P. G. Halverson[d], D. Kielczewska[d,g], W. R. Kropp[d], J. G. Learned[a], J. M. LoSecco[h], G. McGrath[a], C. McGrew[d], S. Matsuno[a], R. S. Miller[i], L. Price[d], F. Reines[d], J. Schultz[d], H. W. Sobel[d], J. L. Stone[c], L. R. Sulak[c], R. Svoboda[i]

[a] *The University of Hawaii, Honolulu, Hawaii 96822, USA*
[b] *Cleveland State University, Cleveland, Ohio 44115, USA*
[c] *Boston University, Boston, Massachusetts 02215, USA*
[d] *The University of California, Irvine, California 92717, USA*
[e] *Brookhaven National Laboratory, Upton, New York 11973, USA*
[f] *The University of Maryland, College Park, Maryland, USA*
[g] *Warsaw University, Warsaw, Poland*
[h] *The University of Notre Dame, Notre Dame, Indiana 46556, USA*
[i] *The Louisiana State University, Baton Rouge, Louisiana, USA*

Abstract

As a result of a 7.7 kt-year exposure of IMB-3 underground water Čerenkov detector 935 interactions of neutrinos with energies above 50 MeV were recorded. A sample of 610 single-ring events, consisting primarily of quasi-elastic $\nu_l N \rightarrow l^{\pm} N$ interactions, has been selected and the identification of lepton l has been performed using two independent procedures. The relative population of μ-like events is compared with the expected values obtained from a detailed simulation of atmospheric neutrino interactions with water. Three different ν flux calculations and two models of ν interactions are considered. Systematic uncertainties due to approximations involved in the models are discussed.

[1] This research was funded in part by the U.S. Department of Energy
[2] Supported by KBN grant Nr 2 0100 91-01

1 INTRODUCTION

Atmospheric neutrinos are produced in a layer of about 15 km as a result of hadronic cascades originated from interactions of cosmic rays. The neutrino flux decreases rapidly with energy, following approximately E^{-k} function, with $k = -2.7$ around 1 GeV. At energies below 500 MeV the flux changes less quickly with energy and reaches a maximum at 35 MeV. The ratio $\phi(\nu_\mu + \overline{\nu}_\mu)/\phi(\nu_e + \overline{\nu}_e)$ is close to 2 in this energy region, as a result of $K^\pm$ and $\pi^\pm$ meson decays into $\nu_\mu\mu^+$ and $\overline{\nu}_\mu\mu^-$ followed by $\mu^+ \to \overline{\nu}_\mu\nu_e e^+$ and $\mu^- \to \nu_\mu\overline{\nu}_e e^-$ decays.

A number of models have been developed to calculate the fluxes of atmospheric neutrinos [1, 2, 3, 4, 5] at energies below 5 GeV. This energy region requires careful treatment of the muon polarization as well as of the influence of the Earth magnetic field, which strongly depends on the geomagnetic location of a detector. All calculations are required to reproduce the same measurements of the high energy muon flux.

The fluxes below 5 GeV are large enough to allow for a detection of significant samples of neutrino interactions occuring inside of massive underground detectors primarily constructed for proton decay searches. The flavour composition of atmospheric neutrinos was studied in the earlier IMB-1 experiment [6] by measuring the fraction of events containing a muon decay signal. In 3.77 kt-year exposure the measured fraction was smaller than expected from Monte-Carlo studies.

A difference in Čerenkov ring patterns formed by electrons and muons was utilized first by Kamiokande Collaboration. A 39% deficit of μ-like events found first in a 3.4 kt-year exposure [7] attracted wide attention and was interpreted by many authors as a result of neutrino oscillations. A recent analysis of the data from 6.2 kt-year exposure of the Kamiokande detector, reported also at this conference, confirms previous finding [8].

In IMB detector the interactions are observed in the fiducial volume of 3.3 ktons of water as mostly fully contained events [9, 10]. A total of 935 events with visible energy above ~50 MeV were identified in data collected between May 1986 and ending March 1991, corresponding to a total exposure of 7.7 kt-year. The results and their comparison with simulations using flux calculations by Lee and Koh [2] were published in ref. [11]. Here we present the same data compared with results of a simulation using different flux calculations and different neutrino interaction model. Systematic uncertainties involved in the simulations are emphasized.

2 EXPERIMENTAL DATA

The IMB detector, filled with 8 kt of water, records Čerenkov light emitted by relativistic particles with 2048 photomultiplier tubes (PMTs). Particle energies are measured using the number of collected photo-electrons. Approximately one photo-electron corresponds to one MeV of visible energy, which is defined as the energy of an electron which would produce the same number of Čerenkov photons. The visible energy resolution is $3\%/\sqrt{E_{vis}(\mathrm{GeV})}$, plus a constant systematic term of $\pm 7\%$.

The data reported here consists of events with a vertex inside the 3.3 kt fiducial volume firing from 70 to 900 PMTs. A total of 935 events were found during 852 days of the detector livetime, with an efficiency of 93% . As a result of the visual scanning a single ring was identified in a sample of 610 events and multiple rings in the remaining 325 events. By searching for coincidences among delayed PMT hits, muon decay electrons were detected with greater than

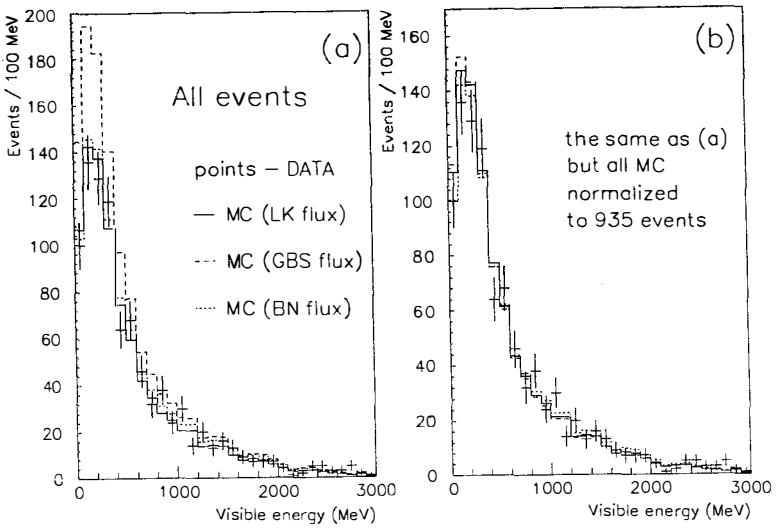

Figure 1: Visible energy distribution of all 935 events compared with MC simulations.

80% efficiency. At least one muon decay signal was found in $34 \pm 2(stat)$% of single-ring events and 43 ± 3% of multiple-ring events. The simulation based on Lee and Koh flux calculations predicts these fractions at $43 \pm 1(stat) \pm 4(syst)$% and $48 \pm 1(stat) \pm 5(syst)$% respectively.

An independent procedure for particle identification is provided by the pattern of Čerenkov rings. Diffuse, showering patterns S are associated with $e^{\pm}$ and γ, while sharper, non-showering patterns NS originate from $\mu^{\pm}$, $\pi^{\pm}$ and p. Only single ring events allow reliable particle identification. Using three independent, automated algorithms, 378 events were identified as showering and 232 as non-showering. Studies with cosmic-ray muons as well as simulated electron and muon tracks indicate that the identification procedure correctly identifies 92% of the events with visible energy above 100 MeV, with a possible systematic bias toward one classification or the other being less than 5% . Simulations of atmospheric neutrino interactions indicate that the correlation between ν_e-induced (ν_μ-induced) events and identified single-ring S (NS) events is 87% (92%).

In order to explore possible uncertainties due to the applied momentum cuts we use here event energies and momenta obtained with a different calibration that the measurements published in ref. [11]. The visible energy distribution is shown in Fig. 1 for all the sample and in Fig. 2 for single-ring events. Fig. 3 displays momenta distributions of S and NS tracks.

3 RESULTS AND DISCUSSION

Two independent models have been developed to simulate neutrino interactions in water (both quasi-elastic and pion production channels), nuclear interactions of produced hadrons and de-

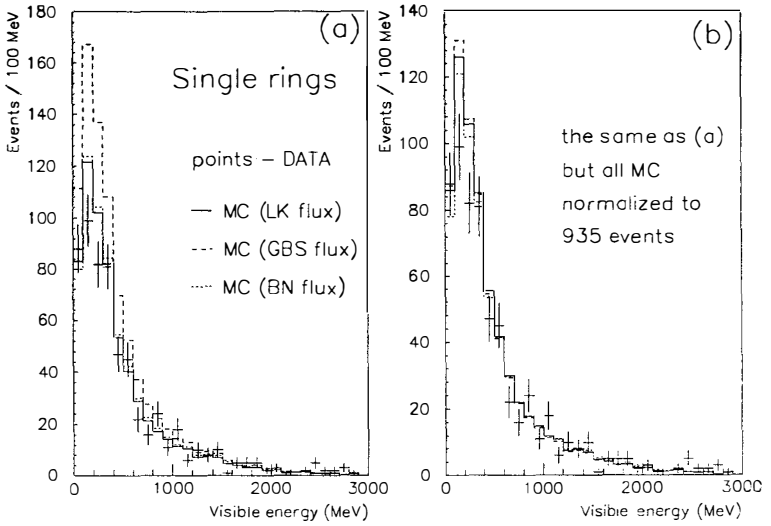

Figure 2: Visible energy distribution of 610 single-ring events compared with MC simulations.

tector response to Čerenkov radiation. A model described in ref. [13] was employed in ref. [11] (called henceforth Model A). In order to further investigate possible uncertainties in simulated predictions we employ here a model described in ref. [14] (Model B).

We use three different atmospheric neutrino flux calculations [1, 2, 3]. The results of ref. [3] were corrected to take into account the effect of muon polarization on the neutrino spectra: the size of the effect was taken from ref. [1].

The simulated events were subjected to the same analysis procedures as the data. however the pattern recognition was approximated by imposing 8% random misidentification for both type of the tracks. The simulated energy and momentum distributions are compared in the figures. As all the absolute flux predictions are subject to a 30% uncertainty, we present also the simulated distributions normalized to the total of 935 events found in the experiment. It is seen that after the normalization the outcome of different neutrino flux models is essentially the same.

In Table 1 the predicted ratios r of NS to S event populations are compared with the data. To assure a good, constant with energy efficiency of identification only events with momentum $>$ 100 MeV/c and $>$ 300 MeV/c are considered for S and NS tracks respectively. Also an upper cut on 1500 MeV/c is used to veto exiting particles.

For illustration purposes we quote also the ratio of calculated fluxes $r_\phi = \phi(\nu_\mu + \overline{\nu}_\mu)/\phi(\nu_e + \overline{\nu}_e)$ for the neutrino energies of interest as well as the ratios of actual numbers of quasi-elastic interactions $r_{QE} = Q.E.(\nu_\mu + \overline{\nu}_\mu)/Q.E.(\nu_e + \overline{\nu}_e)$ occurring in water, no matter whether detected or not. It is seen that the undetected interactions with muons produced below Čerenkov

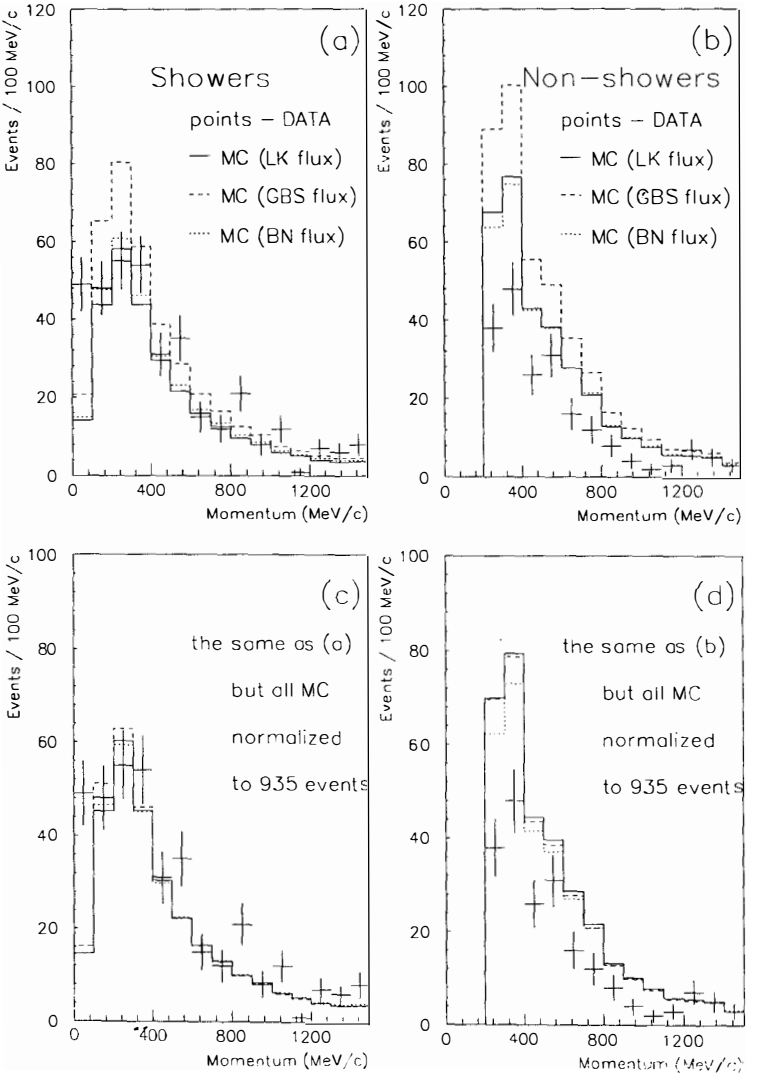

Figure 3: Momentum distributions of showering and non-showering events compared with MC simulations.

Table 1: Ratios r, r_ϕ and r_{QE}.

$r_\phi = \phi(\nu_\mu + \overline{\nu}_\mu)/\phi(\nu_e + \overline{\nu}_e)$:		~ 2
$r_{QE} = Q.E.(\nu_\mu + \overline{\nu}_\mu)/Q.E.(\nu_e + \overline{\nu}_e)$:	Model A - LK flux	1.82
	Model B - LK flux	1.68
$r = NS/S$:	Model A - LK flux	1.04
	Model B - LK flux	1.16
	Model B - BGS flux	1.10
	Model B - BN flux	1.08
	DATA	$0.53 \pm 0.05 \pm 0.05$

threshold or just above it, result in the NS/S ratio being significantly lower than r_{QE}.

The significant reduction of the observed muon neutrino interactions due to subthreshold muons indicates that the ratio r depends not only on flux ratio r_ϕ (which is the same within 5% for different flux calculations) but also on how steep is the neutrino spectrum at very low energies. The employed flux calculations have certain elements in common, e.g. the geomagnetic effect is calculated using the same approximate formula. In order to study how this affects the r ratio, we assumed a spectrum shape E^{-k} extending down to energies as low as 100 MeV, the same for all the neutrino flavours, but with fixed $r_\phi = 2$. The obtained ratios r were 0.87 for $k = -2.6$ and 0.79 for $k = -2.7$. Further steepening of the spectrum leads to momenta distributions clearly softer than the measured ones.

There are also common elements in the employed ν interaction models, e.g. both of them use Fermi Gas Model approximations, which assumes that there is no momentum transfer to the recoiling nucleus and no final state interactions between the final nucleon and the nucleus. The interaction occurs on a nucleon moving with a Fermi momentum, and the resulting nucleon is required to be energetic enough to obey Pauli exclusion principle. The interactions of produced hadrons with the surrounding nuclear matter are taken into account, but the lepton energy is in no way affected by them. From inspecting Figs 2 and 3 it is clear that a 100 MeV/c shift in momentum transfer would diminish the observed disagreement between the data and the expectations.

4 SUMMARY

It is estimated that uncertainties in the ratio r_ϕ, the cross-sections for ν interactions on a nucleon and the Fermi sphere energy lead to a systematic error on the simulated ratio r of 20% (which corresponds to 10% error on the fraction of μ-like events among all single-rings [13]). This estimate is confirmed here by the numbers quoted in Table 1.

We have also discussed effects that are not included in the estimated uncertainties on the expected ratios. They may originate from approximations that are common in the models predicting ν spectra and lepton distributions. It seems that a more detailed calculations are necessary before the observed μ deficit is ascribed to such an exotic phenomena as neutrino oscillations.

Most of the systematic uncertainties would be canceled out in the following ratio of events:

$$\frac{\nu_\mu N \rightarrow \mu N \pi^0}{\nu_x N \rightarrow \nu_x N \pi^0 \; + \; \nu_e N \rightarrow e N \pi^0} \tag{1}$$

where ν stands for both $\overline{\nu}$ and ν. Subthreshold muons would be signaled by decay electrons accompanying π^0's. With a good identification and statistics of the π^0 events expected in Super-Kamiokande detector this ratio would show a 5 s.d. effect after 5 years of data-taking for the oscillation parameters derived as an explanation of the current data.

References

[1] S. Barr, T. K. Gaisser, S. Tilav and P. Lipari, *Phys. Lett.* **B214**, 147 (1988)
G. Barr, T. K. Gaisser and T. Stanev, *Phys. Rev.* **D39**, 3532, (1989)

[2] H. Lee and Y. Koh, *Il Nuovo Cim.* **B105**, 883 (1990)

[3] E. V. Bugaev and V. A. Naumov, *Phys. Lett.* **B232**, 391 (1989)

[4] M. Honda, K. Kasahara, K. Hidaka and S. Midorikawa, *Phys. Lett.* **B248**, 193 (1990)

[5] M. Kawasaki and S. Mizuta, *Phys. Rev.* **D43**, 2900 (1991)

[6] T. J.Haines et al., *Phys. Rev. Lett.* **57**, 1986 (1986)

[7] K. S. Hirata et al., *Phys. Lett.* **B205**, 416 (1988)

[8] K. S. Hirata et al., *Phys. Lett.* **B280**, 146 (1992)
T. Kajita, talk presented at the *International Symposium on Neutrino Astrophysics* in Takayama, Japan, 19 - 22 Oct., 1992
K. Kaneyuki, this conference

[9] R. Claus et al., *Nucl. Instr. Meth.*, **A261**, 540 (1987)

[10] R. Becker-Szendy et al., to be published in *Nucl. Inst. Meth.*

[11] D. Casper et al., Phys. Rev. Lett. **66**, 2561 (1991)
R. Becker-Szendy et al., *Phys. Rev.* **D46** 3720 (1992)

[12] R. Becker-Szendy et al., *Phys. Rev. Lett.* **69**, 1010 (1992)

[13] D. W. Casper, *Ph.D. Thesis*, University of Michigan (1990)

[14] T. Haines, *Ph.D. Thesis*, University of California, Irvine (1986)

Neutrino Oscillations

OVERVIEW OF ACCELERATOR LONG BASELINE NEUTRINO OSCILLATION EXPERIMENTS

STEPHEN PARKE

Fermi National Accelerator Laboratory,
P.O. Box 500, Batavia, IL 60510, U.S.A.

Abstract

There is renewed interest in performing a long baseline neutrino oscillation experiment using accelerator neutrinos because of a discrepancy between the measured and the predicted values of the ratio of electron to muon neutrinos produced in the upper atmosphere by cosmic rays. The approximate range in oscillation parameter space indicated by the Kamiokande atmospheric neutrino results and confirmed by IMB is bounded by $10^{-3}\ eV^2 < \Delta m_0^2 < 10^{-1}\ eV^2$ and $\sin^2 2\theta_0 > 0.4$. To reach such small Δm_0^2 , using an accelerator as the source of neutrinos where the energy is typically 1 GeV or greater, requires baselines in the range of 10 km to 1000 km. In this talk I will give an overview of the most likely possibilities for such a long baseline accelerator neutrino oscillation experiment.

1 Introduction

The recent indications of a deficit in the ν_μ flux of atmospheric neutrinos and the long-standing solar neutrino problem have motivated new searches for neutrino oscillations with small neutrino Δm^2. The results of the Kamiokande collaboration on atmospheric neutrinos suggest oscillation parameters in the range bounded by $10^{-3}\ eV^2 < \Delta m_0^2 < 10^{-1}\ eV^2$ and $\sin^2 2\theta_0 > 0.4$. This result has renewed interest in using accelerator neutrinos to perform a long baseline neutrino oscillation experiment. Many possibilities have been discussed; it is almost like picking an accelerator from column A and a detector from column B and there you have a possible experiment! In this overview I will brief review the range of parameter space a neutrino oscillation experiment can explore and then discuss the most likely possiblities.

The transition probability of producing one flavor of neutrino ν_a, of energy E, at the source, letting the neutrino propagate to the detector, a distance L away, and then detecting the neutrino as a different flavor ν_b, is (for a derivation see, for example, ref [1])

$$\mathcal{P}_{ab} = \sin^2 2\theta_0 \ \sin^2\left(1.27\frac{\Delta m_0^2 L}{E}\right) \tag{1.1}$$

where Δm_0^2, E and L are measured in eV^2, GeV, and km respectively. Δm_0^2 is the difference of the squares of the masses for the two neutrino mass eigenstates and θ_0 is the mixing angle relating these mass eigenstates to the flavor eigenstates. The experiments that measure this probability either measure a finite value for $\mathcal{P}_{ab}$ or assign a limit $\mathcal{P}_{ab} < P_{min}$; the value of P_{min}, the energy spectrum of detected neutrinos and the source-detector distance then define a region in the $(\sin^2 2\theta_0,\ \Delta m_0^2)$ plane for each experiment. This P_{min} is the minimum measurable oscillation probability for the experiment in a given analysis mode. The size of P_{min}, or the limit in our ability to measure $\mathcal{P}_{ab}$, arises from many sources; statistical uncertainties, the contamination of the beam with other neutrino species, the fractional uncertainty in the neutrino flux calculations, the knowledge of the experimental acceptance for the different neutrino species, the backgrounds to the ν_b signal and many other systematic uncertainties.

For large Δm_0^2 ($\gg E/L$) an experiment can explore any

$$\sin^2 2\theta_0 \geq 2\ P_{min}. \tag{1.2}$$

For $\sin^2 2\theta_0 = 1$ the limit on the mass difference squared is

$$\Delta m_0^2 \geq \frac{\sqrt{P_{min}}}{1.27}\frac{E}{L}, \tag{1.3}$$

assuming $P_{min} << 1$. For smaller $\sin^2 2\theta_0$ a good *approximation* to the probability contour is a straight line with slope $-1/2$ in a log-log plot in the $(\sin^2 2\theta_0,\ \Delta m_0^2)$ plane until this line intersects the vertical line from Eq. 1.2.

Therefore, for the range indicated by the atmospheric neutrino data, an interesting experiment for this purpose will need to have a $P_{min} \approx 10\%$ or better and E/L at least one but preferable two orders of magnitude smaller than 0.4 GeV/km.

2 Fermilab - Soudan 2

The new Main Injector at Fermilab will be a 120 GeV proton accelerator that can deliver 2×10^{20} protons on target (POT) in a 10^7sec-year. If a new neutrino beamline is constructed at Fermilab

for both a short baseline experiment, P803 [2], as well as for a long baseline experiment, using this accelerator as a source of protons, then the average energy of muon neutrinos produced would be approximately 10 GeV. The contamination from muon anti-neutrinos and electron neutrinos will be at the percent level. Initially there were three proposals for the long baseline detector: IMB, Soudan 2 and DUMAND. Since that time, IMB has ceased to exist and the engineering and environmental issues of sending a beam 30 degrees below the horizontal to DUMAND, make it prohibitively expensive.

Soudan 2 is 710 km from Fermilab in a direction 3.2 degrees below the horizontal [3]. This detector is a modular fine-grain tracking calorimeter with a mass of 1 kTon (with a possible upgrade to 5 kTon) surrounded on all sides by a two-layer active shield of proportional tubes. The analysis would be based on the ratio of events that appear in the far detector to be of neutral current type to that of charged current type compared to the same ratio in a near "identical" detector. The exclusion plots are shown in Fig.1. The difference in the limits between the two oscillation modes comes from the difference in the ν_τ charged current cross section compared to ν_e or ν_μ.

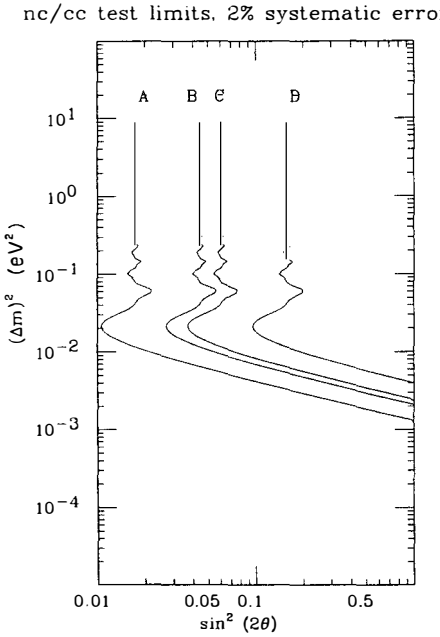

Figure 1: Fermilab/Soudan 2 90% CL limits: A and B are for a 4 year run and a 5 kTon fiducial volume detector (14k events) for $\nu_\mu \leftrightarrow \nu_e$ and $\nu_\mu \leftrightarrow \nu_\tau$ respectively. C and D are for a 9 month run using only the current 0.9 kton (680 events) for $\nu_\mu \leftrightarrow \nu_e$ and $\nu_\mu \leftrightarrow \nu_\tau$ respectively.

3 BNL - New Detector

Mann and Murtagh [4] have proposed a long baseline experiment using the BNL-AGS which can deliver 6×10^{13} POT every 1.7 sec, thus achieving 2×10^{20} POT in 100 days. The average neutrino energy is approximately 1 GeV and the contamination from ν_e is about 1%. A new neutrino beamline will need to be constructed for this experiment.

The detectors consist of three massive imaging Çerenkov counters at 1, 3 and 20 km from the source. These detectors will have masses of 0.8, 0.8 and 6.3 kTons respectively. This experiment will be a ν_μ disappearance experiment using the quasi-elastic events as the signal. The raw event rate in the far detector is 18k per 100 days of running. The analysis will be performed by measuring the event rate in the far, intermediate and near detectors as a function of neutrino energy. Fig. 2 contains the exclusion plots for this experiment.

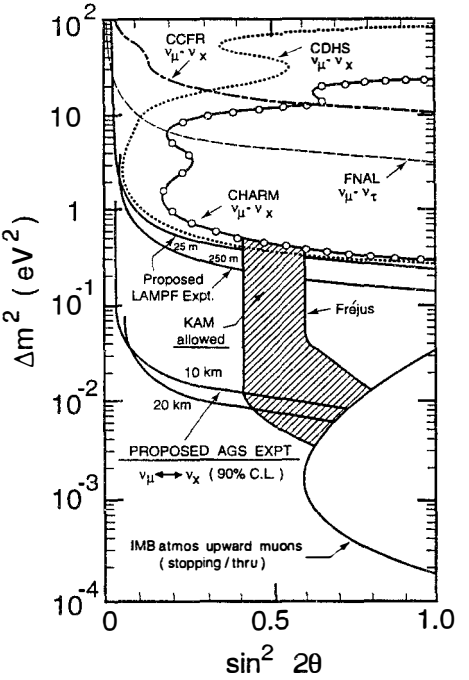

Figure 2: The regions accessible to the BNL-AGS experiment with the far detector at 10 km and 20 km.

4 CERN - Detector in Gran Sasso

The CERN-SPS is an 80 to 450 GeV proton accelerator which can conveniently be used to send a neutrino beam from CERN to the Gran Sasso Laboratory. The SPS-LHC transfer line is the the direction of Gran Sasso Laboratory and the distance of 730 km makes the beam a modest 3.3 degrees below the horizontal. The SPS accelerator is capable of delivering 10^{20} POT per 10^7 sec - year and the contamination of the muon neutrino beam from muon anti-neutrinos or electron neutrinos is at the per cent level. At 80 GeV the average energy of the neutrinos would be approximately 6 GeV.

The ICARUS detector[6] in the Gran Sasso tunnel would be a 5 kTon large liquid Argon TPC and that would have 4k charged current events per 10^{20} POT from the CERN neutrino beam. The $\nu_\mu \leftrightarrow \nu_e$ analysis would be based on ν_e appearance plus a precise understanding of the beam contamination and the backgrounds from ν_μ neutral current interactions with π^0 faking electrons. Whereas the results in the $\nu_\mu \leftrightarrow \nu_\tau$ mode would be based on a combination of analyses; ν_μ disappearance, the neutral current to charged current ratio, and direct appearance of ν_τ. The exclusion plots for the ICARUS/CERN experiment are given in Fig. 3.

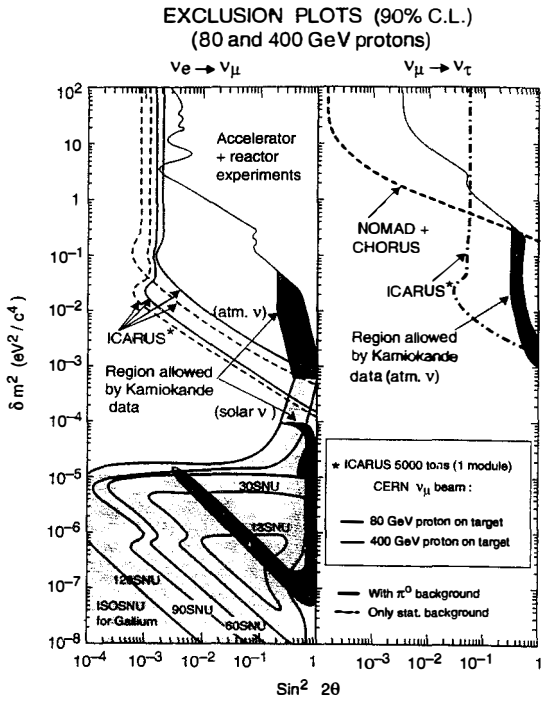

Figure 3: CERN/ICARUS exclusion plots for both $\nu_\mu \leftrightarrow \nu_e$ and $\nu_\mu \leftrightarrow \nu_\tau$.

The GeNIUS (GeV Neutrino-Induced Underground Shower) [7] detector is a 17 kTon (15 kTon fiducial volume) fine-grained sampling calorimeter to be placed, if approved, in the Gran Sasso tunnel. With a neutrino beam similar to the FNAL beam from the Main Injector this detector would have 18k charged current events for 10^{20} POT. The analysis would be performed using the neutral current to charged current ratio for $\nu_\mu \leftrightarrow \nu_\tau$ and the electron-type to muon-type events for $\nu_\mu \leftrightarrow \nu_e$. The exclusion plots for this detector with the CERN-PS producing a neutrino beam with average energy of 5 GeV are given in Fig. 4.

CERN has also discussed the possibility of sending a neutrino beam, produced from 450 GeV protons, to SuperKamiokande, 9000 km away. The beam would have to be aimed 44 degrees below the horizontal. With such large separation between source and detector this experiment will be able to study matter enhanced oscillation effects in the $\nu_\mu \leftrightarrow \nu_e$ mode. An exclusion plot for this possibility can be found in Ref. [6].

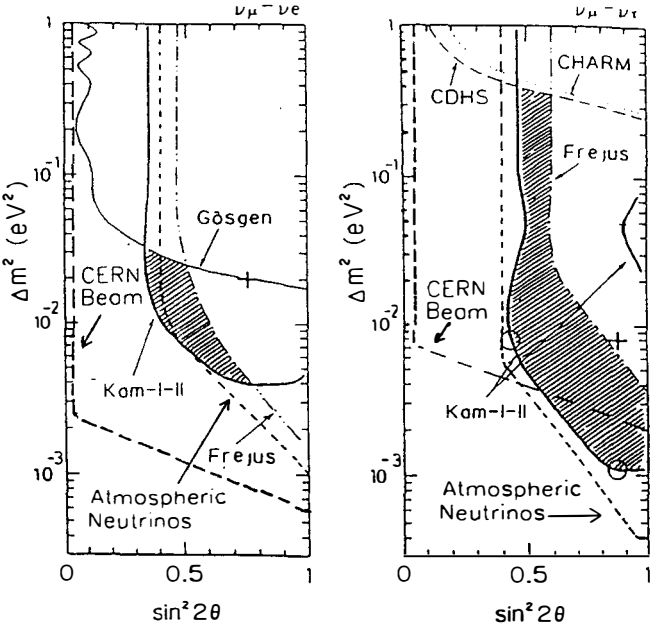

Figure 4: Area of oscillation parameter space ruled out at the 90% confidence level for one year of running for the GeNIUS detector and the CERN neutrino beam.

5 KEK - SuperKamiokande

The possibility of sending a muon neutrino beam the 250 km between SuperKamiokande and KEK has been discuss in detail by Nishikawa[5]. The KEK-PS is a 12 GeV proton accelerator which can currently deliver 4×10^{12} protons on target every 2.5 sec. Therefore a modest upgrade is required to the KEK-PS to deliver 10^{20} POT in a period of a few years. The average energy of the neutrino beam is approximately 1 GeV and the contamination of ν_e is a few percent.

SuperKamiokande is a 50 kTon water Çerenkov detector which is scheduled for completion in April of 1996. The event rate in the 20 kTons of fiducial volume of SuperKamiokande is 400 CC events for 10^{20} POT using a two radiation length target. The analysis for the $\nu_\mu \leftrightarrow \nu_\tau$ mode is based on the neutral current to charged current ratio for SuperKamiokande and a small water Çerenkov detector on the KEK site. This requires distinguishing an EM showering particle (e or γ) from a non-showering particle (μ or π) which can be attained with this detector above a few hundred MeV, whereas the $\nu_\mu \leftrightarrow \nu_e$ mode requires distinguishing between an electron and a π^0 which can be separated for neutrino energies greater than 2 GeV for this detector. The exclusion plots for this combination of accelerator and detector are given in Fig. 5.

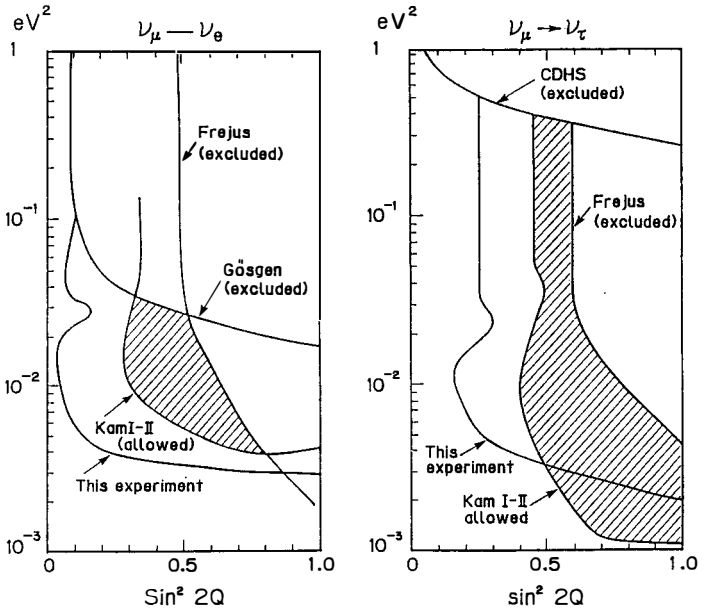

Figure 5: The 90% exclusion plots for the KEK-PS - SuperKamiokande experiment for both $\nu_\mu \leftrightarrow \nu_\tau$ and $\nu_\mu \leftrightarrow \nu_e$.

6 Other and Conclusions

Another possibility is to use the proposed new accelerator at TRIUMF (KAON), aimed at either a new detector approximately 40 km from the source or to SuperKamiokande in Japan. Details of these possibilities are still under discussion. Using the SSC as a source of neutrinos has also been discussed in conjunction with GRANDE as a detector.

Given the results from the atmospheric neutrino data, it is important to explore the oscillation parameter region $10^{-3}\ eV^2 < \Delta m_0^2 < 10^{-1}\ eV^2$ and $\sin^2 2\theta_0 > 0.4$ [8]. Accelerator neutrinos are ideal for this purpose because the intense beams are well understood, with a more sharply peaked energy spectrum and can be manipulated as opposed to atmospheric neutrinos. There are a number of very exciting possibilities for experiments to explore this region of parameter space; let us hope that at least one of these experiments is actually performed. Remember that the fermion mass question is one of particle physics' great mysteries beyond the Standard Model, and any clues from neutrinos may unleash our imagination to further our understanding of nature.

7 Acknowledgements

I would like to thank R. Bernstein, M. Goodman, A.Mann, D. Michael, M. Murtagh, K. Nishikawa, J.-P. Revol and N. Weiss for providing me with many details for this review. Fermilab is operated by the Universities Research Association Inc. under contract with the United States Department of Energy.

References

[1] R. H. Bernstein and S. J. Parke, Phys. Rev. **D44** 1991, (2069).

[2] K. Kodama *et al.*, "Muon Neutrino to Tau Neutrino Oscillations", FNAL Proposal P–803.

[3] W. Allison *et al.*, "A Long Baseline Neutrino Oscillation Experiment Using Soudan 2", FNAL Proposal P-822.

[4] A. Mann and M. Murtagh, "Proposal for a Long Baseline Neutrino Oscillation Experiment at the AGS", January, 1993.

[5] K. Nishikawa, U. of Tokyo Preprint, INS-Rep-924, April 1992.

[6] J.-P. Revol, CERN Preprint, CERN-PPE/93-01, January 1993; C. Rubbia, CERN Preprint, CERN-PPE/93-08, January 1993.

[7] D. G. Michael, "Searching for Oscillations of Atmospheric and Accelerator Neutrinos", Caltech Preprint, August 1992.

[8] This region will be also explored by reactor neutrino oscillation experiments in the $\nu_\mu \leftrightarrow \nu_e$ mode. See other contributions to this workshop.

A LOW ENERGY NEUTRINO-OSCILLATION DETECTOR AT THE SAN ONOFRE NUCLEAR REACTOR

N. C. Mascarenhas, F.H. Boehm, M. Chen, R. Hertenberger, V. Novikov, and P. Vogel
Physics Department, California Institute of Technology
Pasadena, CA 91125, USA

Presented by
Nicholas C. Mascarenhas

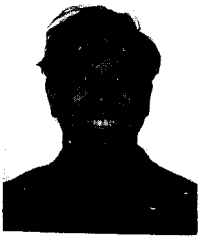

ABSTRACT

The San Onofre experiment consists of a large liquid scintillation detector for studying neutrino oscillations with a projected sensitivity for Δm^2 of $10^{-3}eV^2$ and a mixing angle sensitivity of $sin^2 2\theta = 0.1$. The detector is a segmented 13 ton liquid scintillator. A novel scheme of neutron background rejection based on a positron annihilation coincidence requirement has been developed. Our detector will be installed at a distance of 650 m from the San Onofre reactors in Southern California, 20 mwe below surface. We employ a passive neutron buffer and an active muon veto to reduce the background. The event rate is expected to be 22/d with a signal-to-background of about 2 : 1.

1. Physics Goals

There exist strong indications of a solar neutrino anomaly[1], and of an anomaly in the atmospheric neutrino flux as observed by the Kamiokande[2] and IMB[3] experiments. The exclusion plot of figure 3 indicates the allowed areas and motivates us to search for evidence of neutrino oscillations below the present limit of Δm^2 of $2 \times 10^{-2} eV^2$. Reactor neutrinos have low energies (0 - 10 MeV) and a detector positioned at about 1 km from a reactor will be sensitive to Δm^2 down to $10^{-3} eV^2$ and mixing angles $\sin^2 2\theta$ of 0.1. The detector reaction is, $\bar{\nu_e} + p = e^+ + n$, requiring a proton rich target. No evidence for oscillation has been seen with the best current limits for reactor based $\bar{\nu}_e$ disappearance from the Goesgen[4] experiment. These limits (90% CL) are shown in figure 3.

In the Goesgen and Bugey[5] experiments, detectors were moved to different distances from the reactor (for Goesgen: 38m, 46m, and 65m). the relative neutrino spectra obtained are independent of neutrino flux and detector efficiency. Oscillation parameters are obtained from the ratios of the spectral yields, by virtue of the fact that oscillations are energy dependent, thus modifying the neutrino spectrum (and the positron spectrum) reaching the detector. Given that the detector absolute efficiency is calibrated and the reactor power and status of the fuel elements is well known at all times, the absolute neutrino yield is known for each position. This independently determines the oscillation parameters. Such experiments that search for a decrease in the measured flux of neutrinos are known as disappearence experiments.

The limitations here arise from the uncertainty in the absolute normalization of the reactor neutrino spectrum (3% at 68% CL for the Goesgen experiment), the detector efficiency (4%), the reaction cross section (2%), and the reactor power (2%). Therefore, in these disappearance experiments, the sensitivity for the mixing strength, $\sin^2 2\theta$, will be limited to about 6%. Progress for improved sensitivity for Δm^2, i.e. larger oscillation length can be made by placing a large detector at a greater distance from the reactor.

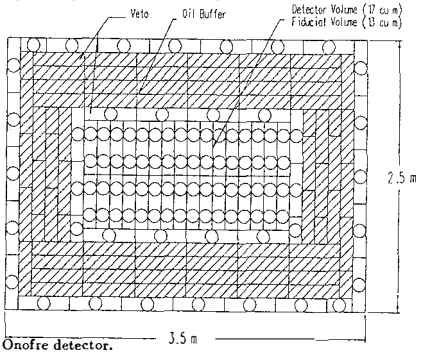

Figure 1. The San Onofre detector.

2. Our Detector

The Caltech group has proposed a long baseline experiment at San Onofre (0.65 km)[6] in Southern California. San Onofre has two large reactors of 3.3 GW each. Other experiments with a 10km baseline have been proposed by Boehm et al.[8] and by Steinberg et al.[9].

The San Onofre experiment[6] employs a 13ton (fiducial volume) segmented liquid scintillator as illustrated in figure 1, to be installed in an underground vault (20mwe below ground) at a distance of 0.65 km from the 6.6GW(th) San Onofre reactors (operated by the Southern California Edison Company). A fast coincidence between a positron (1MeV $\leq E \leq$ 8MeV) in one cell and two 511keV annihilation gammas (50keV $\leq E \leq$ 600keV) in two or more adjacent cells defines a positron annihilation signal (see figure 2). Following the fast triple coincidence, the reaction neutron is detected via the proton capture gamma ray (2.2MeV) in a time window of 500μs. For a shallow detector the muon flux is not attenuated much. Neutrons from muon interactions in matter are a possible source of background. Energetic neutrons can recoil on protons in the scintillator leaving a signal that mimics a positron. Our triple coincidence reduces this background by about 500. We have measured our detector efficiency to be 10 % using a tagged positron source, the signal rate will be 22/d and the background event rate will be about 10/d, as explained below.

The detector is surrounded by an active muon veto and passive boron loaded mineral oil neutron buffer for a total of 80 cm of hydrogen rich buffer. All cells are made of clear acrylic and have dimensions 9m x 0.5m x 0.13m. The outer 0.80m of the center detector cells serves both as a double layer muon veto as well as neutron and gamma ray (^{40}K from PMs) absorber. The detector thus is modular allowing later rearrangement and enlargement. About 1,500 muons/s will hit the central volume of the detector. They will be signaled by the tight, 2 layer active muon veto. The veto time for a stopped muon is 500μs and that for a through muon 10μs resulting in a dead time of 5%.

A small 12 cell detector (170 liters of liquid scintillator) has been installed in the basement (tendon gallery) of unit 2 reactor at 24.5m from the core. The detection scheme is similiar and it will verify efficiency and background. Later as a monitor detector. The event rate of this prototype detector will be 10/d with negligible background. We are currently adding 6 cells to increase the event rate to about 20/d.

The neutron yeild from capture of cosmic ray muons and from muon spallation in the detector and in the surrounding earth and concrete has been studied by experiment and simulations. Both processes, especially the latter, give rise to production of neutrons up to 100MeV or more in energy. About 1800/d fast neutrons enter the fiducial volume after attenuation in the buffer. Fast neutrons may excite ^{12}C nuclei producing a 4.4MeV gamma ray. This, together with a contribution from fast neutron related triple coincidences creates a correlated background of about 4/d. The triple coincidence requirement, thus, rejects

neutron induced events by a factor of 500.

The neutrons produced by incident muons in the fiducial volume are tagged and can be rejected by the muon veto. Scant data exists on the high energy neutron production . Our 12 cell detector in the tendon gallery (at 20 mwe) is currently measuring muon nuclear spallation neutron production. We will also obtain neutron flux vs. neutron energy (for muon capture neutrons) from an experiment we performed in the Stanford tunnel (20mwe).

Th and U concentration in the scintillation liquid are found to be about 0.3×10^{-12}g/g[9] and thus negligible. ^{40}K in the scintillator has been measured and is negligible. ^{40}K gammas from the PMTs can be reduced sufficiently by both the definition of the fiducial volume (80cm dead region) and the use of PMs with low ^{40}K glass windows. The background from the surrounding rock is attenuated by an 0.8m thick sulfurcrete lining and the 80 cm mineral oil buffer. The residual gamma background is about 6/d.

We have constructed and studied the optical and mechanical properties acrylic scintillation cells similar in dimension to those in our experiment and determined the timing (1ns for 1MeV) and position accuracy $\approx$ 15cm and light yield. We are using Philips XP4512 5 inch dia.PMs. We have developed a scintillator using the single component wavelength shifter PMP, with an attenuation length of 10m at 440nm and a light output 60% of anthracene. The PM coverage of the end faces is 38%. The energy resolution in a 2.5m long test cell is 10% at 1 MeV.

References

1. T. Kirsten, in *International Symposium on Neutrino Astrophysics*, Takajama, Japan (October 1992), Universal Academic Press; Y. Suzuki, ibidem
2. T. Kajita, ibidem
3. S. Dye, ibidem
4. G. Zacek et al. *Phys. Rev.* **D34** (1986) 2621.
5. J. Bouchez, in *Neutrino 88*, eds. Schneps et al. (1989), World Scientific, Singapore, p. 28.
6. F. Boehm et al. *The San Onofre Experiment*, Progress Report, Caltech (1992); see also ref. 8.
7. Y. Declais et al. *Search for Neutrino Oscillations at the Chooz Reactor*, Letter-of-Intent, LAPP (1992) and private communication.
8. F. Boehm et al. *Nucl. Instr. Meth.* **A300** (1991) 395.

9. R. Steinberg and C.E. Lane, *The Perry Experiment*, in *Proceedings of the Franklin Symposium* (1992), to be published.

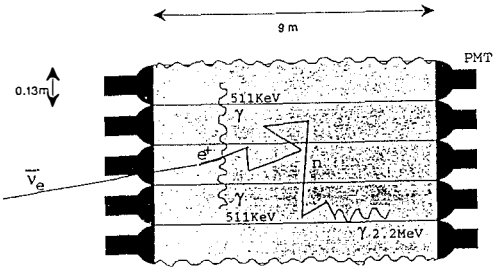

Figure 2. Sketch of the reaction in the segmented detector.

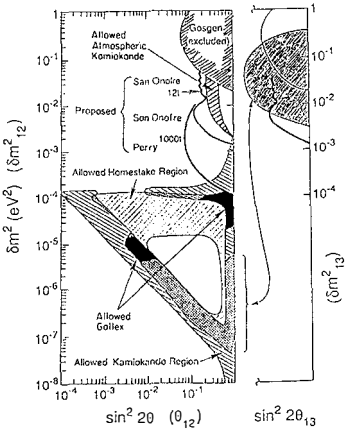

Figure 3. Oscillation parameters for ν_e disappearance experiments. The dark areas show the allowed region from the solar neutrino experiments. The cross-hashed region indicates the allowed region for ν_μ - ν_e oscillations from atmospheric neutrinos. The excluded area from the Goesgen experiment is shown, as are the proposed long baseline reactor experiments at San Onofre, Chooz[7] and Perry. The region for Δm^2_{13} shown on the right is obtained using seesaw scaling.

$\nu_\mu \to \nu_\tau$ OSCILLATIONS IN THE CASE OF HIERARCHY AND SEE-SAW TYPE MIXING

S.M. Bilenky

Joint Institute of Nuclear Research
Dubna, Russia
and
Istituto Nazionale di Fisica Nucleare, Sezione di Torino
Via P. Giuria 1, I-10125 Torino, Italy

ABSTRACT

Neutrino oscillations are discussed under the assumption that there is a hierarchy of neutrino masses and a hierarchy of couplings among lepton families. It is shown that $\nu_\mu \rightleftharpoons \nu_\tau$ oscillations which at present are investigated at CERN and Batavia have the largest amplitude. $\nu_\mu \rightleftharpoons \nu_\tau$ oscillations are considered also in the case of neutrino mixing and see-saw type mixing of light neutrinos with heavy Majorana particles.

The problem of neutrino masses and mixing is one of the most important problems of today's neutrino physics. In many experiments on the search for neutrino oscillations, on the measurement of the hard part of the β-spectrum of ^{3}H, on the search for neutrinoless double β-decay of different nuclei no evidence of non-zero neutrino masses and mixing have been found. On the other hand some indications in favour of neutrino mixing was obtained from the analysis of all existing solar neutrino data under the assumption that the standard solar model is correct [1]. Let us notice that some anomaly in the ratio of fluxes of atmospheric ν_μ and ν_e have been observed in some experiments [2]. It seems, however, that this anomaly requires further investigations.

New experiments on the search for effects of neutrino mixing are under preparation at present. We will discuss here $\nu_\mu \rightleftharpoons \nu_\tau$ oscillations in the beam of accelerator neutrinos [3].

Let us consider first the case of a mixture of three massive neutrinos

$$\nu_{\ell L} = \sum_{i=1}^{3} U_{\ell i} \nu_{iL} , \qquad \ell = e, \mu, \tau . \tag{1}$$

Here ν_i is the field of the neutrino with mass m_i and U is a unitary mixing matrix. For the probability of the transition $\nu_\ell \to \nu_{\ell'}$ we have

$$P(\nu_\ell \to \nu_{\ell'}) = \left| \sum_{i=2,3} U_{\ell' i} U_{\ell i}^* \left[\exp\left(-i \frac{\Delta m_{i1}^2 R}{2p} \right) - 1 \right] + \delta_{\ell' \ell} \right|^2 , \tag{2}$$

where $\Delta m_{ij}^2 \equiv m_i^2 - m_j^2$, $R \simeq t$ is the distance between the source and the detector and p is the neutrino momentum.

Let us assume now [4] that there is a hierarchy of neutrino masses

$$m_1 \ll m_2 \ll m_3 \tag{3}$$

and, as suggested by solar neutrino data, Δm_{21}^2 is so small that in terrestrial neutrino experiments $\Delta m_{21}^2 R/2p \ll 1$. For the $\nu_\ell \to \nu_{\ell'}$ transition probability ($\ell' \neq \ell$) we obtain

$$P(\nu_\ell \to \nu_{\ell'}) = \frac{1}{2} A(\nu_\ell \to \nu_{\ell'}) \left[1 - \cos\left(\frac{\Delta m_{31}^2 R}{2p} \right) \right] , \tag{4}$$

where

$$A(\nu_\ell \to \nu_{\ell'}) = 4 |U_{\ell' 3}|^2 |U_{\ell 3}|^2 \tag{5}$$

is the oscillation amplitude.

Let us assume also that in analogy with quarks there is the following hierarchy of couplings among the lepton families

$$|U_{e3}|^2 \ll |U_{\mu 3}|^2 \ll 1 , \qquad |U_{\tau 3}|^2 \simeq 1 . \tag{6}$$

From Eqs.(5) and (6) we get

$$A(\nu_e \to \nu_\tau) \ll A(\nu_\mu \to \nu_\tau) \ll 1 \,. \tag{7}$$

For the amplitude of the transition $\nu_\mu \to \nu_e$ we have

$$A(\nu_\mu \to \nu_e) = \frac{1}{4} A(\nu_\mu \to \nu_\tau) A(\nu_e \to \nu_\tau) \,. \tag{8}$$

Thus, if a quark-like hierarchy is realized in the lepton sector, the amplitude of the transition $\nu_\mu \to \nu_\tau$ will be the largest one. The transition $\nu_\mu \to \nu_e$ is a "second" order effect with the smallest amplitude. Notice that if the mixing matrix U coincides with the CKM quark mixing matrix [5] we have

$$A(\nu_\mu \to \nu_\tau) = (1.0 \pm 0.2) \times 10^{-2} \,, \qquad A(\nu_e \to \nu_\tau) \simeq 10^{-4} \,, \qquad A(\nu_\mu \to \nu_e) \simeq 3 \times 10^{-7} \,. \tag{9}$$

What about the value of m_3? There are some indications at present that m_3 could lie in the electronvolt region. This indications follows from the analysis of the solar neutrino data with a see-saw formula for the neutrino masses and from a hot and cold dark matter scenario [6] that is suggested by the recent COBE observation of the anisotropy of the background radiation and observations of the large scale structure of the universe. Thus the experiments searching for $\nu_\mu \rightleftharpoons \nu_\tau$ oscillations [3] look very promising at the moment.

Up to now we have considered the case of mixing of three massive neutrinos. In the general case (Dirac-Majorana mass term [7]) the current neutrino fields $\nu_{\ell L}$ are superpositions of the left handed components of the fields of six massive Majorana particles

$$\nu_{\ell L} = \sum_{i=1}^{3} U_{\ell i} \nu_{iL} + \sum_{i=a}^{3} U_{\ell a} N_{aL} \,. \tag{10}$$

Let us assume that N_a are the fields of heavy Majorana particles ($m_a \gg m_Z$). As is well known, the see-saw mechanism for the neutrino mass generation is based on this assumption. In this case the state vectors of flavour neutrinos $|\nu_\ell\rangle = \sum_{i=1}^{3} U^*_{\ell i} |i\rangle$ are non-orthogonal

$$\langle \nu_{\ell'} | \, \nu_\ell \rangle = \delta_{\ell'\ell} - \Omega_{\ell'\ell} \,, \qquad \Omega_{\ell'\ell} = \sum_{a=1}^{3} U_{\ell' a} U^*_{\ell a} \,. \tag{11}$$

Let us consider $\nu_\mu \rightleftharpoons \nu_\tau$ oscillations in the case of neutrino mixing and non-orthogonality of the neutrino states [8]. For the $\overset{(-)}{\nu}_\mu \to \overset{(-)}{\nu}_\tau$ transition probability we have

$$\begin{aligned} P\left(\overset{(-)}{\nu}_\mu \to \overset{(-)}{\nu}_\tau\right) \;=\; & 2\,|U_{\tau 3}|^2\,|U_{\mu 3}|^2 \left[1 - \cos\left(\frac{\Delta m^2_{31} R}{2p}\right)\right] \\ & -2\,|U_{\tau 3}|\,|U_{\mu 3}|\,|\Omega_{\tau\mu}| \left[\cos\left(\frac{\Delta m^2_{31} R}{2p} \mp \chi\right) - \cos\chi\right] \\ & + |\Omega_{\tau\mu}|^2 \,, \end{aligned} \tag{12}$$

where $\chi \equiv Arg\left\{U_{\tau 3}U^*_{\mu 3}\Omega^*_{\tau\mu}\right\}$. As it is seen from Eq.(12), if CP is violated in the lepton sector and $\Omega \neq 0$ then

$$P(\nu_\mu \to \nu_\tau) \neq P(\bar{\nu}_\mu \to \bar{\nu}_\tau)\,. \tag{13}$$

Informations about the value of $|\Omega_{\tau\mu}|$ can be obtained from the analysis of the data on weak decays [9] and from the LEP data on the measurement of the number of neutrino flavours. We have

$$|\Omega_{\tau\mu}| \lesssim 2.8 \times 10^{-2}\,. \tag{14}$$

Taking into account Eq.(14) we can conclude [8] that in the case of hierarchy (the element $|U_{\mu 3}|$ is small) the second term in Eq.(12) can be comparable with the first one. Thus the investigation of $\nu_\mu \rightleftharpoons \nu_\tau$ oscillations can allow to obtain informations not only about neutrino masses and mixing but also about the possibility of mixing of the light neutrinos with heavy Majorana particles.

It is a pleasure for me to thank Carlo Giunti for collaboration and fruitful discussions.

References

[1] GALLEX Collaboration, *Phys. Lett.* B **285** (1992) 390.

[2] K.S. Hirata et al., *Phys. Lett.* B **280** (1992) 146; R. Becker-Szendy et al., *Phys. Rev.* D **46** (1992) 3720.

[3] J. Schneps, Talk presented at the 15^{th} International Conference on Neutrino Physics and Astrophysics (NEUTRINO 92), Granada, Spain, June 1992; CHORUS Collaboration, CERN-SPSC/90-42 (1990); NOMAD Collaboration, CERN-SPSC/91-21 (1991); R. Bernstein et al., Neutrino Physics after the Main Injector Upgrade, FNAL 1991.

[4] S.M. Bilenky, M. Fabbrichesi and S.T. Petcov, *Phys. Lett.* B **276** (1992) 223.

[5] E. Witten, *Phys. Lett.* B **91** (1980) 81.

[6] M. Davis, F.J. Summers and D. Schlegel, *Nature* **359** (1992) 393; A.N. Taylor and M. Rowan-Robinson, *Nature* **359** (1992) 396.

[7] See the review: S.M. Bilenky and B. Pontecorvo, *Phys. Rep.* **41** (1978) 225.

[8] S.M. Bilenky and C. Giunti, Torino University preprint DFTT 66/92.

[9] P. Langacker, Lectures presented at TASI-90, Boulder. June 1990, UPR 0470T; S.M. Bilenky, W. Grimus and H. Neufield, *Phys. Lett.* B **252** (1990) 119.

The NOMAD $\nu_\mu \leftrightarrow \nu_\tau$ oscillations experiment

Jean-Michel Levy
L.P.N.H.E.
IN2P3-CNRS and Universites Paris 6 et 7
4 place Jussieu, T33 RdC
75252 Paris Cedex 05
France

Abstract

The CERN WA96 (NOMAD) experiment now at the building stage is aimed at detecting $\nu_\mu \leftrightarrow \nu_\tau$ oscillations with a sensitivity which should lower by one order of magnitude the present limit on the mixing parameter for high mass differences. Its originality resides in the τ identification method and the use of a light, high resolution, active target. The following article briefly reviews the motivations for the search, the basic ingredients of the method and describes the apparatus and its present stage of developpement.

1 The what's and why's in a nutshell.

1. Neutrino oscillations are reviewed at length in other papers in these proceedings. Here we only wish to remind the reader that one has to admit that neutrinos born in weak processes are mixtures of mass eigenstates. Since these acquire different phases during their propagation, the subsequent interaction of, say, a ν_μ -born neutrino has a certain probability to give rise to a lepton of another flavour (say, τ).
The probability of occurence of this phenomenon in a simplified two-flavour world where ν_μ and ν_τ would be linear combinations of two mass-eigenstates, is given by:

$$P(\nu_\mu \rightarrow \nu_\tau) = sin^2(2\theta) sin^2(\frac{\pi x}{L})$$

where:
1. θ is the mixing angle, that is $cos(\theta)$ is the amplitude of the lighter mass-eigenstate in the state $|\nu_\mu>$.
2. x is the distance from the production point to the interaction point.
3. $L = 4\pi p/\Delta m^2 = 2.48E(GeV)/(|m_2^2 - m_3^2|(eV^2))\ km$ where m_2 and m_3 are the two mass-eigenvalues.
From this one sees that for given θ the upper limit on Δm^2 an experiment can possibly set varies as E/x and that one has to go to large distances to probe small mass differences, whilst the upper limit on $\sin^2(2\theta)$ depends on the accumulated statistics only. However for 'high' Δm^2, the oscillating factor is washed out by the experimental spreads in E and x and averages to 1/2, yielding a constant limit on the mixing.

2. Why $\nu_\mu \leftrightarrow \nu_\tau$ oscillations ?
By analogy with the quark sector, one expects that
1. the τ - associated neutrino is dominated by the amplitude of the heaviest mass state.
2. mixing is stronger with ν_μ (associated to the next lower-mass charged lepton, the so-called 'adjacent generation') than with ν_e .
Most models based on the 'see-saw' mechanism have this kind of association built-in.
On the other hand, it is known that the Universe embodies a large amount of non- shining mass. Recent results (COBE) on the microwave background fluctuations favour a 30-70 % mixing of 'hot' and 'cold' dark matter. Since neutrinos were abundantly produced during the Big Bang, they are a natural candidate for the former, if they have masses in the region of a few $10's\ eV$. However, LEP results show that there are only three light neutrino species, and upon interpreting the solar neutrino deficit as due to an oscillation, one suspects very low masses for ν_e and ν_μ .
All this strengthens the likelihood of a ν_τ dominated by a few $10's\ eV$ mass state, and therefore the possibility of detecting $\nu_\mu \leftrightarrow \nu_\tau$ oscillations in terrestrial experiments with a short ($\sim$ 1 km) baseline. The present limit on the mixing is $sin^2(2\theta) \leq 5.10^{-3}$ [2]. The above quark analogy argument encourages strongly going an order of magnitude lower [1].

2 The problem in a wallnut shell.

Detecting ν_τ 's means 'seeing' the τ 's they generate in Charged Current (C.C.) weak interactions on nuclei. τ 's lifetime is $\sim 3.10^{-13} sec.$, meaning a track length of $100\mu m$ to $1mm$ at S.P.S. energies. This can only be imaged using very high resolution techniques, like nuclear emulsions [3] or holographic bubble chambers. An alternate possibility

choosen by the NOMAD collaboration is to forsake visualisation and identify τ 's by the kinematics of their decay products. The backgrounds to be fought are due to ordinary neutrino (ν_e , ν_μ) interactions, direct ν_τ production being very low ($\sim 10^{-6}$) at S.P.S. energies. Given that ν_e represents but $\sim 1\%$ of the beam, the cleanest decay channel w.r.t. C.C. interaction backgrounds is *a priori* $\tau \rightarrow e^- \nu_\tau \bar{\nu}_e$.

3 The kinematical method

1. Leptonic τ decays. To reject the ν_e C.C. background , we take advantage of the effect of the two escaping ν's from τ decays on the event's kinematics in the plane transverse to the beam. Let p_T^h, p_T^{miss}, p_T^e be the transverse components of, respectively, the total hadronic, $e^{-}s$ and missing momenta; let $\phi_{mh} = \angle(p_T^{miss}, p_T^h)$ and $\phi_{lh} = \angle(p_T^e, p_T^h)$. For well-reconstructed ν_e events one expects a small ϕ_{mh} and $\phi_{lh} \approx \pi$, whilst for ν_τ events ϕ_{mh} can be large since p_T^{miss} essentially stems from the two escaping ν's. The difference shows clearly on a scatter plot where the ν_e sample exhibits a depletion in the high ϕ_{mh} region which does not exist in the ν_τ sample [4, 5]. The cut used in this region reduces the ν_e background by a factor $2 - 3\ 10^{-3}$, while keeping 40% of the τ events. Another requirement is to demand that the transverse mass computed from p_T^{miss} and p_T^e be less than a τ mass.
Other potential sources of $e^{-}s$ are: asymetrical photon conversions or π^0 and η Dalitz decays, Compton electrons, μ^- and K_{e_3} decays in flight. Knock-on $e^{-}s$ and π_{e2} decays proved innocuous because of the low rate for the later and the visible recoil hadron for the former. All the others, with the exception of in-flight μ decays, have their origin in the hadronic shower. Hence, the underlying principle of the cuts against these is to demand the electron to be somehow isolated from the hadrons (angle,relative p_T,mass(e^-, γ) against Dalitz decays).
The μ decay channel has also been considered. It does not suffer of many backgrounds which affect the e^- channel, but requires strengthening of the angle-plot cut and some isolation cuts because of the huge ν_μ background and the sizeable π to μ decay rate.

2. Semi-leptonic τ decays. Three channels have been studied: $\nu_\tau\ \pi^-$, $\nu_\tau\ \rho^-$, $\nu_\tau\ a_1^-$.
The background here is mainly Neutral Current interactions, and the selection of τ 's against them is based on the following facts:
1. In a true τ event, the most energetic hadron originates most of the time from the decay of the τ .
2. The genuine τ decay hadron is separated from the rest of the hadronic shower.
More details can be found in [4, 6, 7].

4 The experimental set-up

The method just outlined requires clear electron identification and measurement. These are fulfilled by the use of Transition Radiation detectors, an electro-magnetic calorimeter and a preshower. The good spatial resolution of the system also allows proper reconstruction of the $p_T^{\prime}s$ of hadrons decaying into $\gamma^{\prime}s$ and helps identify the electron through its bremsstrahlung photons and its preshower signature. High precision on the p_T's from charged hadrons and $e^{-}s$ implies a low Z target material to minimize multiple scattering and keep b'strahlung moderate, together with a number of high-resolution measuring planes. Compromising between often contradictory requirements,

the following design was arrived at : (see fig.)

1. The detector will be housed in the former UA1 horizontal field dipole magnet set at .4 Tesla and moved to the location of the old BEBC. It has an inner volume of about 3 by 3 m in cross-section and 6 m long.

2. The target is made of 44 3-by-3 meter drift chambers built with a self-supporting structure of composite materials (C and H nuclei), making up a fiducial mass of 2.97 tons. Each d.c. represents $\sim$ 2% of a radiation length; it has three planes of sense wires at $-5°, 0°, +5°$ w.r.t. the magnetic field, which should give a precision of $200\mu m$ per wire in the bending plane (y) and $2mm$ per chamber parallel to the beam. The maximum drift distance is 3.6 cm . Tests of a prototype actually yielded $\sigma_y = 160\mu m$.

3. 10 T.R. Detectors follow the target. They are made of a radiator of 400 polypropylene foils 20 μm thick spaced by 250 μm and an X-ray detector consisting of vertical straw tubes of $\varnothing 1.6cm$. These are made of aluminized mylar $25\mu m$ thick and filled with a mixture of 70% Xe and 30% CH_4 at atmospheric pressure. Extrapolation of the results of a prototype test forecasts a 90% efficiency for e^{-}'s and a π/e rejection of 10^{-3}. To increase the lever arm, each couple of T.R. detectors will be followed by a D.C. of the type described above.

4. The preshower is made of 1.5 X_0 of Pb followed by two orthogonal planes of extruded aluminium tubes 1 by 1 cm in cross-section. Tests of a prototype reveal a $5 - 10$ π/e rejection factor, depending on the energy.

5. The calorimeter is made of 1100, 10.6 by 8 cm lead-glass blocs, 20 X_0 in depth, read by tetrodes with their axes at 45° w.r.t. the B field. Zero field tests of a 3 by 3 blocs prototype stack give $\sigma(E)/E = 5\%/\sqrt{E\ (GeV)}$. Taken together, the preshower-calorimeter system gives a π/e rejection of $\sim 10^{-3}$ for 90% efficiency to e^{-}'s. With the T.R. detector rejection one is thus well above what is needed to eliminate the $\sim$ 18500 π^{-}'s predicted to go through the cuts.

6. Muons are identified by large drift chambers separated by a Fe filter downstream of the magnet, which serves itself as a first filter.

5 Expected sensitivity

Monte Carlo simulations of the experiment were performed with the previous characteristics to define different sets of cuts for the decay channels which have been mentionned above. Assuming two years of exposure in the CERN-SPS wide-band neutrino beams, 1.1 10^6 ν_μ C.C. events together with 3.7 10^5 N.C. and 13200 ν_e C.C are expected in the fiducial volume. The following table summarizes the estimated efficiencies, expected backgrounds and sensitivities with these statistics.

τ decay mode	Fraction	Efficiency	Predicted background	Limit on ν_τ / ν_μ
$\tau^- \rightarrow e^- \nu_\tau \bar{\nu}_e$	.178	.12	4.6	$3.5\ 10^{-4}$
$\tau^- \rightarrow \mu^- \nu_\tau \bar{\nu}_\mu$	.178	.039	2.2	$8.4\ 10^{-4}$
$\tau^- \rightarrow \pi^- \nu_\tau$	.108	.014	l.t. 2	$2.2\ 10^{-4}$
$\tau^- \rightarrow \rho^- \nu_\tau$	.227	.023	l.t. 2	$6.6\ 10^{-4}$
$\tau^- \rightarrow 3\pi^{\pm} \nu_\tau$	.138	.087	l.t. 2	$2.9\ 10^{-4}$

Merging these results, a negative search would yield a limit $sin^2 2\theta \leq 3.8\ 10^{-4}$ at the 90% c.l.

We conclude by noting that 83 % of the τ width is probed in 5 different channels, which will allow conclusive consistency checks in case a signal is observed and that backgrounds can be estimated from the data themselves (ν_e and ν_μ C.C. events share the same production dynamics, and N.C. backgrounds are charge-symmetric.)

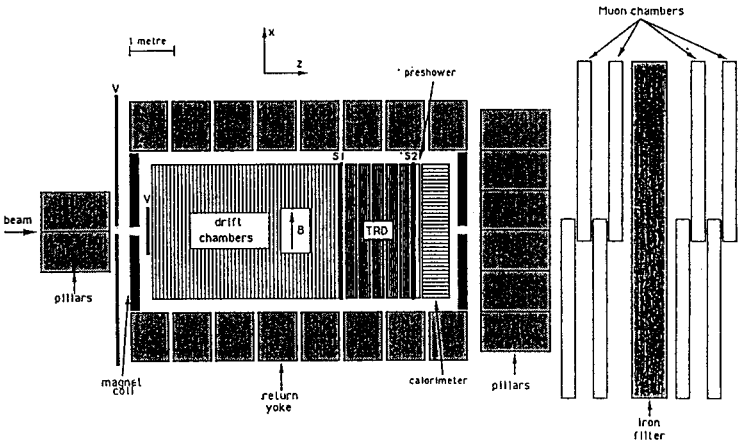

The NOMAD experimental set-up.

References

[1] H.Harari Phys. Lett. **216B** 413 (1989)

[2] N. Ushida *et al.* Phys. Rev. Lett. , **57** (1986) 2898.

[3] FNAL draft proposal P803 (1990). CERN proposal SPSC/90-42 .

[4] CERN proposal SPSC/P261, March 1991 and addenda.

[5] Jacques Dumarchez in Proc. of the XIIth Moriond Workshop (1992)

[6] Search for $\nu_\mu \leftrightarrow \nu_\tau$ oscillations by electronic techniques.
J.M. Lévy, contribution to the XV international conference on neutrino physics and astrophysics, Granada, Spain, june 1992. Preprint LPNHE 92/09

[7] Luigi Dilella in proc. of the XV international conference on neutrino physics and astrophysics, Granada, Spain, june 1992.

Neutrino Cross Sections

The MUNU Experiment

MUNU collaboration

C. Broggini

I.N.F.N. Laboratori Nazionali del Gran Sasso, I-67010 Assergi (AQ), Italy

M. Avenier, G. Bagieu, R. Brissot, J.F. Cavaignac, D.H. Koang, D. Lebrun, and A.Stutz

Institut des Sciences Nucléaires, IN2P3-UJF, 53 Avenue des Martyrs, F-38026 Grenoble CEDEX, France

H.W. Becker

Institut für Kernphysik, Wilhelm Klemmstr. 9, D-4400 Münster, Germany

J. Busto, J. Farine, V. Jörgens, A. Tadsen, M. Treichel, and J.-L. Vuilleumier

Institut de Physique, A.-L. Breguet 1, CH-2000 Neuchâtel, Switzerland

D. Gibin, A. Guglielmi, M. Mezzetto, G. Puglierin, and L. Visentin

Dipartimento di Fisica dell'Università and INFN, Via Marzolo 8, I-35100 Padova, Italy

C. Amsler, S. von Dombrowski, E. Holzschuh, and F. Ould-Saada

Physik-Institut, Schönberggasse 9, CH-8001 Zürich, Switzerland

Abstract

We intend to build a low background detector based on a gas TPC to be installed near a nuclear reactor in Bugey for the experimental study of $\bar{\nu}_e e^-$ scattering. The threshold on the electron recoil energy can be set very low, around 500 keV, giving the experiment a good sensitivity to the magnetic moment of the $\bar{\nu}_e$, extending down to $2\text{-}3 \cdot 10^{-11}$ Bohr magnetons.

Introduction

The neutrino magnetic moment matrix $\mu_{\ell,\ell'}$ $(\ell,\ell' = e,\mu,\tau)$, like the mass matrix $m_{\ell,\ell'}$, is fundamental and its experimental study may provide insight on new physics. In the standard model, neutrinos are massless Dirac particles and have vanishing magnetic moments. But models predicting moments up to 10^{-10} Bohr magnetons have been built (see for instance [1] [2]).

Magnetic moments will give the neutrinos electromagnetic interaction, allowing scattering from the active left handed $\nu_{\ell L}$ states into the sterile $\nu_{\ell' R}$ states. The contribution, compared to that of the usual weak interaction, increases with decreasing neutrino energy [3] and the best way of looking for the magnetic moment of the ν_e seems to be the detailed study of $\overline{\nu}_e e^- \rightarrow \overline{\nu}_e e^-$ scattering at low energy.

The most spectacular consequence of magnetic moments is the precession of neutrinos from left handed $\nu_{\ell L}$ states to right handed $\nu_{\ell' R}$ states in the presence of a transverse magnetic field $\vec{B}_\perp$. In fact, solar neutrino astronomy is at the origin of the recent interest in the magnetic moment of the neutrino. Depending on the choice of parameters, it seems possible to explain with such an hypotesis [4] [5] the fluxes and time dependence of the ^{37}Cl and Kamiokande experiments, as well as the flux of low energy neutrinos, below expectations, reported by the ^{71}Ga experiment.

Nuclear reactors are the best source of $\overline{\nu}_e$ with energies between 0 and 8 MeV and are ideally suited for such an experiment. The energy spectra are known with good precision, better than 3 % for E_ν between 2 and 8 MeV [3].

Only two attempts have been made to measure $\overline{\nu}_e e^-$ scattering [6] [7]. The signal was marginal in comparison with the background and the threshold on the recoiling electron energy was rather high (1.5 MeV). The only way they had to extract the signal was the comparison of the reactor-on and reactor-off rate. It clearly appears important to improve by a large factor on these results.

We propose to measure $\overline{\nu}_e e^- \rightarrow \overline{\nu}_e e^-$ scattering with much better precision, by using a detector which should be ready before the end of 94.

The experiment

We are planning to use a gas time projection chamber (TPC), the drift volume of which serving as electron target. We should thus be able to identify well single electrons originating from inside a predefined fiducial volume. Such a good signature should help

in keeping the background down. For instance, multi-Compton events inside the drift volume can be rejected. Beta activities from the walls will be identified as such.

Since we have tracking, we can measure the scattering angle φ_e of the electron. It is not so small at these energies and multiple scattering is non negligible. So this will only give a modest background suppression. But it will allow a simultaneous measurement of signal plus background events in the forward direction and background events only in the backward direction. Background can thus be measured on-line, while the reactor is on. This is particularly important in the case of a non optimal signal to background ratio, since the reactor off periods are in general too short to reach good statistical precision.

We note that part of the background will be due to natural activities. Much progress has been accomplished these recent years in low background techniques, and cleaner materials are available. The materials to be used must, in addition, also have little cosmogenic activation, since all power reactors are aboveground.

We will use a hydrogen free medium for the detector, so we will completely suppress the background from $\bar{\nu}_e + p \rightarrow e^+ + n$ scattering.

Our TPC will be immersed in a liquid scintillation detector which will work as an anti-Compton.

The detector must be placed near a reactor as powerful as possible to maximize the $\bar{\nu}_e$ flux, and as close as possible, keeping the reactor correlated background at a negligible level. The Bugey reactor (2800 $MWth$) appears ideal. It has for a long time been used to search for neutrino oscillations [8]. It emits about $5 \cdot 10^{20}$ $\bar{\nu}_e$ s^{-1} and is on 11 months out of 12. The spectrum is known with uncertainties of order 3.5 % in the energy region between 2 MeV and 8 MeV.

A lab has been installed underneath the core, with a room large enough for the detector at a distance of 18.6 m from the core. This is the preferred location for the experiment. The gamma activity of this area measured without shielding with a same NaI crystal is slightly lower than that of the ISN laboratory. No neutron flux associated with the reactor has been measured in the BUGEY-I experiment, placed closer to the reactor core.

The central detector

The gas of the TPC should have low Z to minimize multiple scattering, and have a high electron density. The most attractive appears CF_4, which has a very high density (3.68

$g \cdot l^{-1}$ at 1 *bar* and thus a very high electron density, $1.06 \cdot 10^{21}\ cm^{-3}$ at 1 bar). We will work at 5 bar of pressure, and have a total number of target electrons of $N_e = 5.29 \cdot 10^{27}$. Its drifting properties have been studied by various authors [9]. The drift velocity is very high, $\sim 4\ cm \cdot \mu s^{-1}$ for an electric field of 600 $V \cdot cm^{-1}$ at 5 bar. The total drift time for a distance of 1.5 m would thus be 38 μs, making the detector reasonably fast. The lateral drift is small and would amount to 2.5 mm after 1 m at the same field strength. The longitudinal drift, 2.2 mm would be somewhat less.

All these parameters have been obtained from measurements at 1 bar and over a drift distance of a few cm. We have shown however that electrons can be drifted over long distances in 5 bar of pure CF_4 with a mini-TPC prototype. The drift length was 20 cm and the active diameter 10 cm. To achieve good purity, the gas was circulated continuously through an Oxysorb filter to remove oxygen and a cold trap to remove water and possible freon contaminations. A mean drift distance longer than 6 m at 5 bar and at 600 $V \cdot cm^{-1}$ was achieved [10].

The cosmogenic activation of C and F is reasonably low since these nuclei are light. Also CF_4 is not toxic, not flammable, and relatively cheap ($\sim$2 SF per liter).

The CF_4 gas at 5 bar is contained in a cylindrical acrylic vessel of inner diameter 90 cm and 158 cm long. Acrylic is choosen because of its very low radioactivity.

We verified that the outgassing of acrylic does not lead to a degradation of gas purity leading to reduced attenuation length or energy resolution. For this, a prototype TPC with acrylic containement vessel has been constructed in Gran Sasso. The TPC has been successfully operated with CF_4 up to a pressure of 5 bar. With an improved gas purification system we could reach an attenuation length longer than 9 m at 5 bar [11].

The drift volume is delimited by a cathode on one end of the vessel, and a grid on the other one. These, along with field shaping rings at successive potentials on the outside of the vessel cylinder, provide an homogeneous drift field. With this design, the CF_4 volume is active over its entire diameter.

Behind the grid is an anode plane. The anode wires are separated by potential wires. The inner diameter of the frame is 90 cm. All anode wires are connected together to give the energy signal. The following plane contains two sets of isolated perpendicular strips to pick up the induced signals. The pitch, 3.3 mm, is well adapted to the lateral drift in CF_4. This $x - y$ plane provides the spatial information along the x and y axis

in the anode plane. The $x - y$ plane is kept at ground potential, while the anode plane is at a positive high voltage large enough to have good amplification around the anode wires. This way the number of high voltage feed-throughs is minimal, which is important for the low background environment. The third coordinate, along the drift field (z) is determined from the time evolution of the signals. This only allows a determination relative to the point of the track closest to the grid. An absolute determination of z may be possible if we can exploit the cathode or grid signal. We are exploring this point.

To fully exploit the information provided by the TPC, we will use a read-out electronic with fast flash ADC's for the anode and each x or y strip. For an electron drift velocity of 4 cm/μs in 5 *bar* CF_4 gas the FADC system has to be operated at a 25 MHz sampling frequency, corresponding to 40 ns sampling time. In order to cover the maximum drift length (1.58 m) a memory depth of 1024 words is required. We will use the commercially available Struck DL350 FADC system, which fullfills these criteria.

The active veto

The acrylic vessel will be immersed in a stainless steel tank filled with a mineral oil based liquid scintillator (NE235H or equivalent). The scintillator will serve to veto the cosmic muons and as anti-Compton detector. This liquid scintillator is compatible with acrylic and it can be procured with a transmission length of more than 10 m, and a light yield of 50% anthracene. The thickness is 60 cm for the ends, and 50 cm on the cylindrical periphery.

Top and bottom lid of the vessel will be instrumented with photomultipliers. We need a good photomultiplier coverage, about 20 % for a light transmission length of several meters, and triggering at the 10 photoelectron level, which seems doable. This corresponds to a total of 38 photomultipliers of 20 cm diameter. With this it will be possible to reach good anti-Compton efficiency, say of order 99 % as well as a threshold around 100 keV.

The 38 photomultipliers (8" EMI 9351 low activity tubes) will be attached on two frames to form two concentric circles at each of the ends. Surfaces between photocathodes will be painted with titanium oxyde (TiO_2)or covered with a thin teflon sheet for light reflection. The phototubes will be directly immersed into the liquid for optimum light coupling.

The steel vessel, a cylinder 2.80 m long and 2 m in diameter, will be pressurized so as to

Table 1: Event rates

$T(MeV)$	Acceptance	$\bar{\nu}_e e^-$ Events/day	
	(Contained)	$\mu_\nu = 0$	$\mu_\nu = 10^{-10}$
0.5--1	0.85	5.3	8.1
> 1	0.65	4.2	5.3

have a small pressure difference between the inside and the outside of the lucite vessel. The liquid scintillator and the steel vessel will also serve as passive shielding, but will not be sufficient. It will be necessary to add 15 cm of low activity Pb around the steel vessel to reduce the local activities. To reduce the neutron flux created in the lead by the cosmic muons, there will be a layer of 10 cm of borated polyethylene surrounding the steel vessel. Concerning the cosmic rays, the Bugey lab is in a favorable situation. It is below the core, and has a large overburden of steel, concrete and water corresponding to about 20 m water equivalent. This attenuates the muons by a factor 4, and eliminates the nucleons. Nevertheless, materials with low cosmogenic activation must be selected for the construction of the detector.

Signal and background

The expected rates at 18.6 m from the 2800 $MWth$ Bugey reactor have been calculated, for $\mu_\nu = 0$, assuming W and Z exchange only, with $\sin^2\theta_w = 0.2325$, and for $\mu_\nu = 10^{-10}$, and are given in table 1 (the electromagnetic signal goes as $\mu_\nu{}^2$). The acceptance for fully contained electrons was estimated by Monte-Carlo simulation using the GEANT code. These rates have to be compared to background rates, which are estimated in the following.

We define as background a fully contained event which has a minimum energy deposition of 500 keV in the gas, together with a maximum energy deposition of 100 keV in the anti-Compton liquid scintillator.

Two main sources of background have been identified: cosmic muons and natural radioactivity. While cosmic rays crossing the detector will be easily identified and rejected, muon interactions in the surrounding material or in the detector itself can create long-lived radioactive nuclei in the TPC, generating electron-like background events. Interactions within the fiducial volume can produce activity in two ways: stopped muons

Table 2: Simulated background event rates from cosmic rays and $\overline{\nu_e} - p$ reactions

origin	medium	type	events/day	rejection	Total
Cosmics	Gas	^{19}O	0.45		0.45
		^{18}N	0.20	veto	~ 0
		^{12}B	0.37	μ-track	~ 0
	Liquid + Acrylic	(n,γ)	0.90	veto $200\mu s$	0.30
	Lead + Steel	(n,γ)	0.45	veto	0.30
	Gas	^{20}F	0.15		0.15
$\overline{\nu_e} - p$	Liquid	(n,γ)	0.48	veto	0.16
Total			5.8		1.36

leading to capture, and inelastic scattering of through-going muons inducing production of spallation nuclei. These interactions of muons within the large amount of surrounding material (shielding, scintillator) produce neutrons (and gamma rays) which can penetrate the TPC and be absorbed.

The background event rate induced by the cosmic muons and by the $\overline{\nu_e} - p$ reactions is given in table 2. For all the detector components we will choose low radioactivity materials. For instance, mineral oil can be procured with a concentration in Th and U well below 10^{-12} g/g [12]. This level can be maintained in the scintillator, since the additives (pseudo-cumene) are also very clean [13]. Different techniques have been developed by the SNO Collaboration to determine ultra low concentrations of Uranium and Thorium in the acrylic. It was shown that acrylic sheets with a concentration in U and Th of $\sim 10^{-12}$ g/g are commercially available. This more than fullfills our needs.

We found an upper limit on the background rate due to natural activity of 1.76 + 1.35 $event \cdot day^{-1}$. The former contribution is due to the radioactivity of the steel vessel and the latter one is due to the inner part of the TPC (resistors, epoxy frame, solder, feed-throughs and so on). This background has been estimated from the background measured in the Xe TPC in the Gotthard lab, correcting for the differences in gas and

geometry. It should be considered an upper limits. It is hoped that the CF_4 TPC can be made cleaner than the $Xe\ TPC$ with the experience gained. In particular, cleaner resistors, developped in the meantime (factor ten lower in activity) will be used for the resistor chain, and crimps will be used instead of solder for the wires. To conclude, the total rate from the three main components of background - namely cosmics, natural activities from the outer and inner parts of the TPC, should be:

$$N_{bkgd} < 1.36 + 1.76 + 1.35 = 4.47 \cdot day^{-1}.$$

This is to be compared to the expected signal rate of $9.5 \cdot day^{-1}$ (see table 1)

Capability of the experiment

The total background rate which will be measured during two reactor- off periods (~ 2 months) is thus expected to be smaller than the signal rates in the bin $0.5 < T(MeV) < 1$ ($5.1 \cdot day^{-1}$). We remind that the background will be also determined with better precision from the event rate in the backward half sphere and subtracted. The isotropy of the backgroud could be verified by relaxing some of the selection conditions. Considering the signal rates at 18.6 m in table 1, a statistical error less than 3 % should be achievable in the bin $0.5 < T(MeV) < 1$ in one year of measuring time. Combined with a systematic error of 5 %, essentially from the reactor spectrum (3.5 %), reactor power and burn-up (2 %) and detection efficiency (3 %), this leads to a sensitivity of $\mu_\nu \sim 3 \cdot 10^{-11}$ Bohr magnetons, more than a factor 10 better than in previous experiments. This sensitivity is mainly dominated by the systematic uncertainties and changes only slowly as a function of the signal versus background ratio. The limit value on μ_ν would be around $4 \cdot 10^{-11}$ if background is increased by a factor of 4.

The signal rates for the bin $T > 1.MeV$ ($4.2 \cdot day^{-1}$) is equivalent to the lower energy bin, while the contribution from the magnetic moment term is more than a factor of two lower. We will exploit the ratio of this two energy bins to reduce the systematic uncertainties. However, to attain lower limits, significantly longer data taking time would then be necessary. Also we will explore ways to improve the sensitivity by exploiting the angular information.

With some luck the threshold may be lowered more, say down to 300-350 keV, and a sensitivity around $2 \cdot 10^{-11}$ seems then achievable. Depending on the actual background situation it may be possible, after the first data taking period at 5 bar, to lower pressure

and threshold without loosing too much in event rate since the electron recoil spectrum peaks at low energies. That would improve the μ_ν sensitivity even more.

We would also like to add that a change of 5 % in $\sin^2\theta_W$ changes the event rate by 4.3 % in the energy bin 0.5-1 MeV, and by 5.8 % above 1 MeV. A 5 % determination of $\sin^2\theta_W$ appears thus possible in our experiment, assuming a small magnetic moment. This accuracy is rather good, considering that we are dealing with a purely leptonic process. It is comparable to that achieved by the CHARM II collaboration in the study of $\nu_\mu e$ scattering [14].

References

[1] M.B. Voloshin, Sov. J. Nucl. Phys. 48(1988)

[2] R. Barbieri et al., Phys. Lett. B 252(1990)251

[3] P. Vogel and J. Engel, Phys. Rev. D 39(1989)3378

[4] P.I. Krastsev and A.Yu Smirnov, Z. Phys. C 49(91)675; P.I. Krastsev, *Time Variation of Solar Neutrino Signals and the RSFC hypothesis*, CERN TH 6648/92;

[5] E.Kh. Akhmedov, A. Lanza, S.T. Petcov, preprint SISSA-172/92/EP

[6] F. Reines, H.S. Gurr and H.W. Sobel, Phys. Rev. Lett. 37(1976)315

[7] G.S. Vidyakin et al., JETP Lett. 49(1989)740

[8] E. Kajfasz in Proc. of Moriond Workshops April(1992)

[9] A. Peisert and F. Sauli, CERN yellow report 84-08, 1984;

[10] C. Broggini et al., Nucl. Inst. and Meth. A 311(1992)319

[11] C. Broggini, to be published in Nucl. Inst. and Meth. A (1993)

[12] F. Boehm et al., Caltech Report CALT-63-630 (Nuclear Physics)

[13] BOREXINO proposal, August 1991

[14] D. Geiregat et al., Phys. Lett. B 259(1991)499

Measurement of CC and NC ν - ^{12}C Cross Sections at Beam Dump Energies

KARMEN Collaboration represented by

Jonny Kleinfeller
Kernforschungszentrum Karlsruhe, Institut für Kernphysik I,
D-7500 Karlsruhe, Germany

Abstract

The Karlsruhe-Rutherford InterMediate Energy Neutrino Experiment KARMEN at the pulsed spallation neutron facility ISIS makes use of the 'beam dump' neutrinos ν_μ, ν_e and $\bar{\nu}_\mu$ from the $\pi^+ \rightarrow \mu^+ \rightarrow e^+$ decay chain at rest. Neutrinos are detected in a 56 t high resolution liquid scintillation calorimeter. Consisting entirely of hydrocarbons the calorimeter serves as a massive live target of ^{12}C- and ^{1}H- nuclei for the investigation of various ν-induced reactions. The exclusive CC reaction $^{12}C(\nu_e, e^-)^{12}N_{g.s.}$, which is observed with negligible background and spectroscopic quality, allows to measure for the first time the spectral shape of ν_e emitted in μ^+-decay. On the other hand, the observation of the NC reaction $^{12}C(\nu, \nu')^{12}C^*$ $(1^+1; 15.1\ \text{MeV})$ induced by neutrinos with different flavour, allows a first direct laboratory test of the flavour universality of the ν-Z^0 coupling at low energies.

KARMEN Collaboration :

B. Armbruster, G. Drexlin, V. Eberhard, K. Eitel, H. Gemmeke, W. Grandegger, T. Jannakos, M. Kleifges, J. Kleinfeller, R. Maschuw, P. Plischke, J. Rapp, J. Wochele, J. Wolf, S. Wölfle, B. Zeitnitz; *Kernforschungszentrum Karlsruhe and Universität Karlsruhe*

D. Blaser, B. Bodmann, A. Dirschbacher, E. Finckh, T. Hanika, M. Hehle, J. Hößl, W. Kretschmer, F. Schilling, H. Schmidt, O. Stumm; *Universität Erlangen-Nürnberg*

J.A. Edgington, B. Seligmann; *QMWC London*

A.C. Dodd, A.G.D. Payne; *Rutherford Appleton Laboratory*

N.E. Booth; *Oxford University*

1. Introduction

The KARMEN experiment is performed at the neutron spallation facility ISIS of the Rutherford Appleton Laboratory. From the decay of stopped pions produced in the UD_2O 'beam dump' of the pulsed 800 MeV proton beam of ISIS equal numbers of ν_μ, ν_e and $\bar{\nu}_\mu$ are emitted isotropically with energies up to 52.8 MeV according to the decay sequence $\pi^+ \rightarrow \mu^+ + \nu_\mu$; $\mu^+ \rightarrow e^+ + \nu_e + \bar{\nu}_\mu$. Because of the different lifetime of π^+ (26 ns) and μ^+ (2.2 μs) a prompt ν_μ- burst within the first 0.5 μs after proton beam-on-target is followed by a $(\nu_e, \bar{\nu}_\mu)$- pulse in the later time window of 0.5 - 9 μs, where ν_μ are no longer present. The ISIS proton extraction frequency of 50 Hz defines a duty cycle factor of the order of 10^{-4} which allows effective suppression of cosmic background. Neutrinos are detected in a high resolution 56 t liquid scintillation calorimeter located at a mean distance of 17.5 m from the neutrino source and housed in a massive 6 000 t shielding blockhouse.

2. Exclusive CC reaction $^{12}C(\nu_e, e^-)^{12}N_{g.s.}$

Detection of the exclusive charged current reaction $^{12}C(\nu_e, e^-)^{12}N_{g.s.}$ is based on a spatially correlated delayed coincidence between an electron from the inverse β- decay on ^{12}C during the ν_e- time window and a positron from the subsequent ^{12}N - decay, which uniquely identifies ν- induced transitions to the ground state of ^{12}N. The data sample used for the present analysis was taken from April 1990 to June 1992 corresponding to 2641 C of protons on target. Software cuts on the time, energy and spatial correlation of the prompt and delayed signal (for details see [1]) selected 130 coincidence events from the data sample. The proof that these ν- candidates are indeed due to exclusive CC reactions is given by fig. 1 a- d): the measured time- and energy distributions of the prompt and delayed signal are in very good agreement with what one expects from the reaction sequence $^{12}C(\nu_e, e^-)^{12}N_{g.s.} \rightarrow {}^{12}C + e^+ + \nu_e$. In particular the time distribution of the prompt signal (fig. 1 b) clearly demonstrates the origin of these events to be induced by ν_e from μ^+ - decay. From 123.7 ± 11.4 of these CC events left after background subtraction (signal - background ratio ≈ 20) the cross section was deduced to be

$$\langle \sigma_{\text{excl.CC}} \rangle^{\text{exp}} = [\, 8.0 \pm 0.75\,(\text{stat.}) \pm 0.75\,(\text{syst.})\,] \times 10^{-42}\ \text{cm}^2$$

This result is in good agreement with recent theoretical calculations [2, 3, 4] as well as with another experimental result [7].

The spectroscopic quality of the measured electron energy spectrum (fig. 1 a) of the exclusive CC reaction $^{12}C(\nu_e, e^-)^{12}N_{g.s.}$ allows the experiment to measure for the first time the spectral shape of ν_e emitted in μ^+ -decay. Recently it has been shown [9] that a precise determination of the ν_e shape parameter ω_L (the neutrino analogon to the famous Michel parameter ϱ) is sensitive to the Lorentz structure of muon decay. The experiment will therefore be able to set stringent upper limits on non V - A contributions in muon decay (especially to the interference term $|\, g_{RL}^S + 2 g_{RL}^T \,|$ of scalar and tensor interactions with lefthanded ν_e).

3. NC nuclear excitation $^{12}C(\nu, \nu')^{12}C^*$ $(1^+1; 15.1\ \text{MeV})$

Improved trigger conditions since July 1990 allowed to identify for the first time the inelastic ν- scattering off ^{12}C - nuclei, i.e. NC events of the type $\nu + {}^{12}C \rightarrow \nu' + {}^{12}C^*$ $(1^+1; 15.1\text{MeV})$ [5]. The signal for this process is the detection of a localized scintillation event of 15 MeV visible

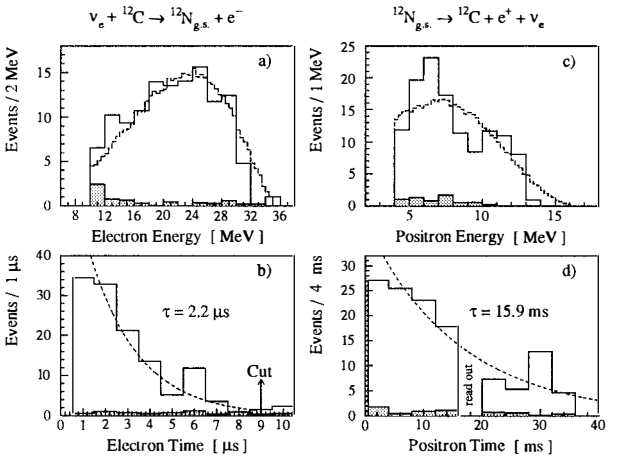

Fig. 1: Energy- and time distributions of the prompt and delayed signals of exclusive ${}^{12}C(\nu_e, e^-){}^{12}N_{g.s.}$ reactions. Energy spectra are compared to MC simulations (broken lines), time distributions are shown with the decay curves of μ^+ ($\tau = 2.2$ µs) and ${}^{12}N$ ($\tau = 15.9$ ms) superimposed. The normalized 'beam off' background is shown as shaded area.

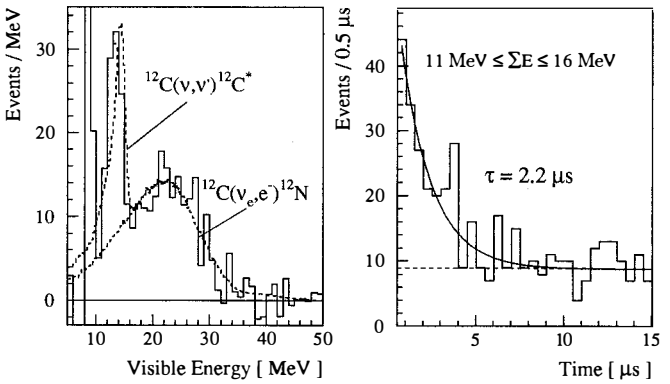

Fig. 2: a) Visible energies of single prong events in the ($\nu_e, \bar{\nu}_\mu$) time window with background subtracted. The dotted line corresponds to MC simulations for inclusive CC reactions and the NC excitation of ${}^{12}C$, respectively; b) event time with respect to beam-on-target in the NC-energy window, cosmic background (broken line) *not* subtracted.

energy from photons emitted as the ($1^+ 1$) analogue state of ^{12}C decays back to the ground state with a 94 % γ - decay branching ratio. In order to optimize the signal to background ratio evaluation was restricted to the (ν_e , $\bar{\nu}_\mu$) - time window of 0.5 - 3.5 μs after beam-on-target. The energy spectrum of events satisfying these criteria with residual background from off beam analysis subtracted is shown in fig. 2 a). Above 17 MeV there is a broad distribution of events corresponding to inclusive charged current reactions. Between 11 and 16 MeV lies a clearly recognizable peak which is ascribed to the $^{12}C(\nu, \nu')^{12}C^*$ ($1^+ 1$; 15.1 MeV) reaction. The time distribution of all events between 11 - 16 MeV shows an exponential time slope of 2.2 μs above a flat background (see fig. 2 b) indicating that indeed these events are induced by ν_e and $\bar{\nu}_\mu$ from μ^+ - decay. The flux averaged cross section for the *sum* of ν_e and $\bar{\nu}_\mu$ induced NC transitions was deduced to be

$$\langle \sigma_{NC} (\nu_e + \bar{\nu}_\mu) \rangle^{exp} = [9.5 \pm 1.8 \, (stat.) \pm 1.35 \, (syst.)] \times 10^{-42} \, cm^2$$

which again is in good agreement with theoretical calculations for this reaction [2, 4, 6] giving values ranging from (9.9 - 10.3) $\times 10^{-42}$ cm^2.

4. Flavour universality of ν - NC coupling

Except for an isospin factor $1/\sqrt{2}$ the matrixelements of the dominant isovector axialvector hadronic weak currents for the NC transition $^{12}C(\nu_e , \nu_e')^{12}C^*(1^+ 1)$ and the CC reaction $^{12}C(\nu_e , e^-)^{12}N_{g.s.}$ are the same [2, 4]. As the NC transition is simultaneously induced by two neutrino flavours of the *same* intensity, i.e. ν_e and $\bar{\nu}_\mu$, the ratio R of $\sigma_{NC} (\nu_e + \bar{\nu}_\mu)$ / $\sigma_{CC} (\nu_e)$ is about 1, provided the ν_e couples in the same way to the Z^0 as $\bar{\nu}_\mu$. Because of the slightly different energy spectra of ν_e and $\bar{\nu}_\mu$ and also accounting for the small ν - $\bar{\nu}$ difference in the NC cross section the theoretical expectation for this ratio is R = 1.08 [2], where from our measurement we get $R = 1.19 \pm 0.26$. This is a flux independent implicit test of the flavour universality in the neutrino neutral current coupling, which is going to be significantly improved with increasing statistics.

5. Conclusions

After three more years of data taking KARMEN will have contributed significantly to the experimental investigation of neutrino - nucleus interactions in an energy regime which is of great astrophysical interest (ν - induced nucleosynthesis during SN explosions, measurement of the bolometric flux of SN and/or solar neutrinos).

References

[1] B. Bodmann et al. (KARMEN Coll.), Phys. Lett. **B 280** (1992) 198.
[2] M. Fukugita, Y. Kohyama and K. Kubodera, Phys. Lett. **B 212** (1988) 139.
[3] T.W. Donnelly , Phys. Lett. **B 43** (1973) 93, and priv. communication (1992).
[4] S.L. Mintz et al., in 'Progress in Nuclear Physics' (Elsevier, 1991) p. 290.
[5] B. Bodmann et al. (KARMEN Coll.), Phys. Lett. **B 267** (1991) 321.
[6] J. Bernabéu and P. Pascual, Nucl. Phys. **A 324** (1979) 365.
[7] D.A. Krakauer et al., Phys. Rev. **C 45** (1992) 2450.
[8] E. Kolbe et al., Nucl. Phys. **A 540** (1992) 599.
[9] W. Fetscher, Phys. Rev. Lett. **69** (1992) 2758, and preprint (1993)

Double β Decay

New Results in the Gotthard ^{136}Xe Double Beta decay experiment

F. Boehm[a], K. Gabathuler[c], H. Henrikson[a],
D. Imel[a], M.Z. Iqbal[a], V.J. Jörgens[b], J. Farine[b],
L.W. Mitchell[b], B.M. O'Callaghan-Hay[a], J. Busto[b],
M. Treichel[b], J.-C. Vuilleumier[b],
J.-L. Vuilleumier[b], H. Wong[a]

a) California Institute for Technology, Pasadena, CA 91125, USA
b) Institut de physique, Université de Neuchâtel, CH-2000 Neuchâtel, Switzerland
c) Paul Scherrer Institute, CH-5232 Villigen PSI, Switzerland

Presented by J. Busto

Abstract

We have built a Xenon TPC to study neutrinoless double beta decay in ^{136}Xe. After a period of 6820 hours, from which we extract limits, a background study of the most evident backgound sources, has been performed. The results of this preliminary studies are presented.

Introduction

The detection of neutrinoless double beta decay provides a sensitive test of the structure of weak interactions. This non-conserving lepton-number process would be the evidence that the neutrino has a non vanishing Majorana mass which could possibly be coupled to right handed currents[1].

The Gotthard Experiment

The ^{136}Xe is a good candidate for $\beta\beta$ decay with a total energy of 2.48 MeV. On the other hand, Xe gas possess adequate properties to be used in a drift chamber. In our experiment, a 180 liters active volume T.P.C. filled with enriched Xe (62.5% ^{136}Xe) and operated at 5 atm. is used (figure 1). The caracteristics of this setup has been presented elsewere[2,3].

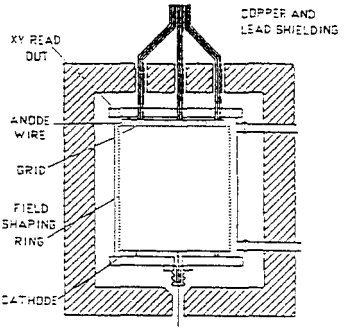

Fig. 1. Shematic view of the experimental setup

The detection of a $\beta\beta$ decay event in the TPC is characterized by a track with two particular "end feactures" coming from the high energy deposition and the large multiple- scattering for slows electron. A typical "two electron event" is depicted in figure 2.

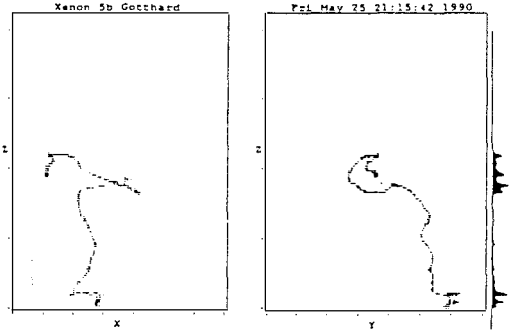

Fig. 2. A typical "two electron" event

Firts results

The energy spectrum of "two electrons" events is presented in figure 3, corresponding to 6820 hours of statistic. Considering some energy windows where the signal/background ration is optimized, for a given mode we, obtain the following half-life limits for differents $\beta\beta$ decays modes.

- Neutrinoless mode (mass mecanism, right handed currents)

$$T^{0\nu}_{\frac{1}{2}}(\langle m_\nu \rangle) > 0.78(0.42) \times 10^{24}\,y \;\Rightarrow\; \langle m_\nu \rangle \begin{cases} 3.0 - 3.8\,eV\,(Caltech^4) \\ 2.5\,eV\,(Heidelberg^5) \end{cases}$$

$$T^{0\nu}_{\frac{1}{2}}(RHC) > 0.50(0.28) \times 10^{24}\,y$$

- Neutrinoless (Majoron mode) ($E \in [2.0 - 2.5\ MeV]$)

$$T^{0\nu}_{\frac{1}{2}}(\chi) > 7.2 \times 10^{21}\,y \;\Rightarrow\; \langle g \rangle \begin{cases} 2.3 \times 10^{-4}\,(Caltech^4) \\ 1.8 \times 10^{-4}\,(Heidelberg^5) \end{cases}$$

- Two neutrino mode ($E \in [1.67 - 2.0\ MeV]$)

$$T^{0\nu}_{\frac{1}{2}}(2\nu) > 2.5 \times 10^{20}\,y$$

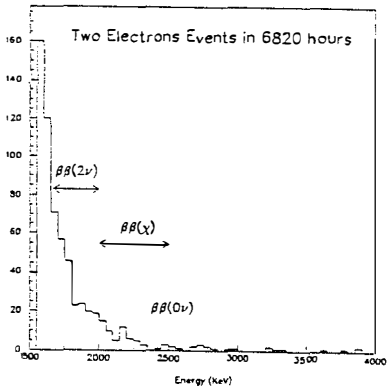

Fig. 3. Two electrons spectrum (6820 hours). The limits are obtained for several energy regions where signal/background is optimized.

Background studies

In order to increase the performances of our setup, a background study concerning the most evident background sources has been performed recently.

Cosmic muons

The μ flux in the Gotthard laboratory is $\sim 15\mu\ m^{-2}\ day^{-1}$. The interaction of these particles with the surrounding matter represents a potential background source. To

prevent this, a $2m^2$ plastic scintillator has been placed on the top of the detector. Actually, after two month of statistics, no " two electron" event has been observed with cosmic flag.

Neutrons background

The interaction of cosmic muons and the spontaneous fission of uranium and thorium present in the rocks, produce a neutron flux in the laboratory ($< 2.5 \times 10^{-5}\ n\ cm^{-2}\ s^{-1}$). These neutrons interacting, for example, with the copper TPC walls, give γ of high energy up to $\sim$ 8 MeV ($\sigma \sim 4$ barns) and appear as a dangerous background in our experiment. To reduce this, and other backgrounds induced by neutrons, a schielding of 5 mm of B_4C surrunding the total detector must be installed in the near future.

Field shaping ring resistors

The homogeneous electric field between anode and cathode is provided by a set of copper rings (70 rings) surrounding the active volume. These rings are separated by 1 cm, and connected by 10 MΩ resistors (figure 1). The high amount of U, Th and K, present in calssical resistors, represents, via the γ emission of these isotopes, the higher background know in the TPC. In ordre to reduce this background component, old resistors are replaced by new ones, showing less radioactive contamination. This contamination is reduced by a factor 6 in U, and Th and by factor 40 in 40K. Figure 3 presents the two germanium spectrum corresponding to the two differents resistors used in the experiment.

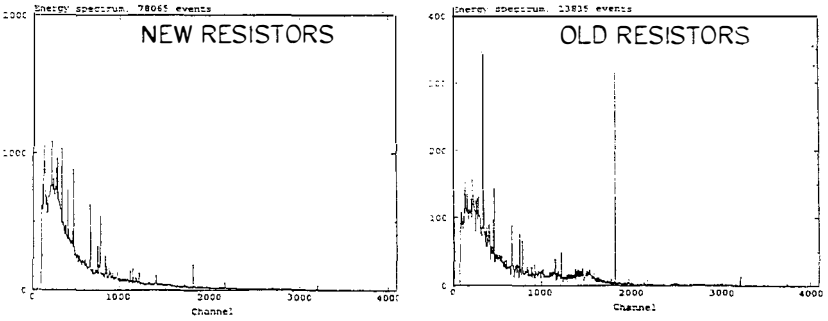

Fig. 3. Germanium spectrum corresponding to "old" (100 pieces/10^5 sec.) and "new" (200 pieces/10^6 sec.) resistors

The reduction of the resistors contamination, must be followed by a reduction in for the counting rate in the TPC. These results are depicted in table 1. We can observe that the number of events recorded are reduced by a factor 7 for all the events betwen 1.6 and 3 MeV. This effect is observed in the same way for single electrons events in a [2-3 MeV] energy window. However it is interesting to note that the counting rate for the two electrons events remains unchanged.

Table 1. Counting rate with "old" and "new" resistors for differents kinds of events

Kind of events	"Old resistors" (6820 h)	"New resistors" (550 h)
All evevts (1.6 - 3.0 MeV)	7.93 c/h	1.16 c/h
All events (2.0 - 3.0 MeV)	4.20 c/h	0.63 c/h
Single e^- (2.0 - 3.0 MeV)	2.97 c/h	0.41 c/h
Two e^- (2.0 - 3.0 MeV)	0.015 c/h	0.020 c/h
Two e^- (1.6 - 3.0 MeV)	0.051 c/h	0.070 c/h

In summary, after the first period corresponding to 6820 hours of statistics, we have initiated a work to reduce the background in our experiment. This work leads today to a global reduction of a factor 7 in the one electron events counting rate. A more important reduction is expected in future from the neutron shielding, and other background considerations like the gas radioactive pollution, etc. Finaly, even if the new statistics is not very high ($\sim$ 550 hours), one interesting aspect of this background studies, contrasting whith the global reduction, is the unchanged counting rate for the two electrons events.

References

1. See, for example, F. Boehm and P. Vogel, *Physics of Massive Neutrinos* Cambridge University Press, Cambridge (1987).
2. H.T. Wong, Ph. D. Thesis, Caltech (1991).
3. H.T. Wong *et al.*, Phy. Rev. Lett. **67** 1218 (1991).
4. J. Engel, P. Vogel and M.R. Zirnbauer, Phys. Rev. **C37**, 731 (1988).
5. A. Staudt *et al.*, Europhys. Lett. **13(1)**, 31 (1990).

Acknowledgements

This work was supported by the Fonds National pour la Recherche Scientifique and by the US Department of Energy.

RESULTS OF A SEARCH FOR DOUBLE POSITRON DECAY AND ELECTRON-POSITRON CONVERSION OF ^{78}Kr

E.Garcia, A.Morales, J.Morales, R.Nunez-Lagos, A.Ortiz de Solorzano, J.Puimedón, C.Sáenz, A.Salinas, M.Sarsa, J.Villar
Instituto de Fisica Nuclear y Altas Energias,
Universidad de Zaragoza, Spain

A.A.Klimenko, V.V.Kuzminov, N.A.Metlinsky, V.M.Novikov, A.A.Pomansky, B.V.Pritychenko
Baksan Neutrino Observatory, Institute for Nuclear Research,
Russian Academy of Sciences, Russia

Presented by A.A.Pomansky

Abstract

The preliminary resulta of a search for the $2\beta^+$ and $K\beta^+$ in a coincidence experiment using a high pressure ionization chamber of enriched ^{78}Kr inside NaI scintillators are presented. After 4434 hours of counting time the half-life limits obtained are $T_{1/2}(K\beta^+)_{0\nu} \geq 5.8 \times 10^{21}$ y and $T_{1/2}(2\beta^+)_{0\nu+2\nu} \geq 2.0 \times 10^{21}$ y at 68% C.L. These are the best world limits for the $2\beta^+$ and $K\beta^+$ decay modes.

On general grounds, it is established that the $2\beta^+$ decay rates 1,2,3) are about six orders of magnitude lower than the $2\beta^-$ decay of emitters of the same region of nuclides (say ^{78}Kr versus ^{82}Se), when assuming similar nuclear matrix elements. That strong reduction stems from the smaller energy available and the Coulomb repulsion factor in the positron emission. The cleaning of the background implied by the annihilation photons (when performing coincidence experiments) might somehow compensate the smallness of the expected rate. A favourable nuclear matrix element also enhance the rate bringing it to more optimistic perspectives. Notice that no detailed theoretical estimates are available. On the other hand the electron-positron conversion is a more probable process than the double positron emission because of the higher available energy and the smaller Coulomb repulsion. The relative rates are roughly a factor 10^3-10^4 for the two neutrino mode with respect to the corresponding $2\beta^+$ emissions.

Suitable candidates because of their experimental capabilities as detectors themselves or because of a favourable theoretical expected rate are the $2\beta^+$ emitters ^{78}Kr, ^{124}Xe and ^{106}Cd, the last one being particularly favourable from the theoretical point of view. There are no theoretical estimates of the ^{78}Kr processes expect in the simple [4] or naive [5] approaches. On the other hand, the phase space integrals appearing in the ^{78}Kr and ^{124}Xe cases have been recently computed by using relativistic wave functions for the lepton[6].

The ^{78}Kr transition to ^{78}Se has a Q-value of 2.881 Mev and the transitions (A,Z) - (A,Z-2) are indicated in the scheme depicted in Figure 1. The three processes, double positron emission, electron captured followed by positron emission and double electron capture are energetically allowed for the transitions to the ground states. Transitions to the excited states of ^{78}Se are also possible, but they are no considered here. We are interested in exploring the processes $2\beta^+$ and $K\beta^+$ searching for the coincidences (with and without neutrino emission) between the positron(s) signal recorded in a source-detector high pressure ionization chamber (IC) of krypton gas (enriched in the isotope 78) and the

511 kev annihilation photons detected in a set of sodium iodine detectors which surround the chamber. The signature of the neutrinoless $^{78}Kr - ^{78}Se$ electron-positron conversion would be an energy deposition of 1859 keV in the IC (positron kinetic energy plus the selenium K-shell binding energy) in coincidence with the two annihilation gammas in the NaIs, whereas the $2\beta^+$ decay would show up as four annihilation gammas in the scintillators coincident with a positron deposition energy of 837 keV in the IC. In the case of no operation of the IC, i.e. when using the chamber only as a source of potential emitters, the recording of gammas will only provide inclusive $(0\nu + 2\nu)$result.

The experimental device consists of a high pressure, high resolution ionization chamber placed within an hexagonal system of large NaI scintillators. The dimensions of the IC are 10.6 cm of diameter and 14.0 cm long, and its internal volume V=1.54 liters. The wall is 2 mm thick, acting as the grounded cathode. The central anode has a diameter of 12 mm. Surrounding the central anode, there is a grid of 40 mm diameter, formed by wires on tungsten (50 μm of diameter) spaced 2 mm. With these parameters, the estimated shield inefficiency of the grid is less than 3.5%. The body flanges and electrodes of the chamber have been made in titanium. Quartz has been used as insulator. The chamber is filled with 35 liters (fiducial volume) of Krypton gas, isotopically enriched up to 94.15% in ^{78}Kr, to be used both as double beta decay source and as detector medium at a pressure of 25 atmospheres. The total number of potentially double beta emitters in the chamber is $N_{2\beta} = 1.024 \times 10^{24}$ atoms of ^{78}Kr. The operating conditions were: grid voltage $V_g = +1000V$, anode voltage $V_a = +2600$ V, cathode is grounded; a pressure is 25 atmospheres. The energy resolution achieved with a mixture of $^{78}Kr + 0.2\%H_2$ is fairly good. In the energy regions relevant for the $2\beta^+$ and $K\beta^+$ neutrinoless searches, one can quote, conservatively, an energy resolution of 3% at 837 keV and 2% at 1859 keV as deduced from the nearby ^{88}Y gamma lines of 1836.2 keV, 898.0 keV and 814.2 keV (1836.2 keV - 2x511 keV).

The scintillator system is composed of a set of six large BICRON NaI detectors of dimensions 15.94 cm of diameter and

23.30 cm long, of hexagonal cross-section. The detectors are made from especially chosen low-background materials and have been underground for more than four years before the starting of this experiment. The dimensions of the crystals are 13.5cm diameter, 20.4cm long and are wrapped in teflon, canned in low background steel, 0.5 mm thick, having quartz windows and standard magnetic shielding. The measured energy resolution of the NaI is 6% at the ^{60}Co line of 1.33 MeV. The six hexagonal detectors have been arranged in a honeycomb-like structure, leaving the central hexagonal hole to host the ionization chamber (see Figure 2). A 20 cm layer of low activity lead bricks shields the detectors from enviromental radioactivity.

The experiment has been carried out in the Canfranc Tunnel Laboratory (Spanish Pyrenees) at a depth of 675 m w.e. The acquisition system for the experiment is a fast-slow coincidence device using NIM and CAMAC electronics. The first scintillators open a 100 ns coincidence window in a CAMAC multiplicity arithmetic logic unit which construct the scintillators configuration mask (scintillators fired during the coincidence time) and generate a look at me signal through the Camac bus weaking an interrupt service routine in the PDP 11/73 computer. For each event, we store in a hard disk the configuration mask, the time of the day with a 20 ms precision, the energies of the scintillators fired, as wellas the corresponding time distributions. The slow coincidence is done by opening a 60 μs window and looking the energy detected by the chamber as well as the time difference distribution between the scintillators (acting as start) and the chamber signal (stop) in a range of about 60 μs. The chamber energy is also stored in the same way as before. In order to minimize the access time to disk we use a software flip-flop between two 2Kw, 16 bits, buffers which fill a big 16 Kw, 16 bits, buffer in memory which is transferred to disk when full.

To compute the efficiency of the photon(s) detection by the NaI array a standard Monte Carlo simulation was used. It was found that after an atom of ^{78}Kr Kβ^+ decays in the active volume of the chamber the probability of detecting two 511keV

gammas generated in the active volume of the chamber in any pair of scintillators is $\varepsilon_{2\gamma}$=0.19. We note that the coincidences between adjacent sodium iodines are negligible, so the two gamma coincidences refer mostly to opposite scintillators and non-opposite but non-adjacent scintillators. On the other hand, the probability of detecting two 511 keV gamma in any pair of NaI detectors in coincidence also with an energy deposit of 1850 keV in the IC has been computed by MC to be 2.8%. In the case of a $2\beta^+$ decay following the annihillation of both positrons inside the krypton volume, the probability of detecting the two pairs of 511 keV gamma rays in any set of four different detectors is 1.7%.

To give a half life limit of the neutrinoless electron followed by positron conversion we have accumulated 4434.5 hours of three-fold coincidence data. Recording the chamber signals in coincidence with the two 511 keV photons allows to distinguish between the positron annihilation inside the krypton gas from those two 511 keV gamma coincidences due to other background sources. The two annihilation gamma ray coincidence background registrated also in coincidence with a IC signal (of unspecified energy) is 0.026 c/h (for opposite NaIs), 0.022 c/h (for non opposite, non adjacent NaIs) and 0.007 c/h (for adjacent ones), i.e. a reduction by factors 20, 40 and 500 with respect to the corresponding annihilation coincidence backgrounds obtained with a vessel of similar dimensions containing about one third less atoms of ^{78}Kr.

To set a lower limit for the neutrinoless $K\beta^+$ process in ^{78}Kr we have looked for the coincidences between 2γ's in their respective energy windows each one of 2.35σ =54 keV width centred around 511 keV and a IC signal of energy 1859 ± 200keV. Even in such a large IC window there were no events at all in the 4434.5 hours of counting time (versus about two hundred and fifty events recorded when the IC was also fired by the coincidence but without selecting any energy deposited in it). To derive half-life limits we have used the standard expression $T_{1/2} \geq \ln 2 N_{2\beta} \varepsilon\, tk/A$ where A is the upper limit of the events searched for and k the probability of the events to fall in the searched energy bin(s). The factor ε stands for

the efficiency which according to the process under consideration was given above. The half-life limit obtained from the absence of events taking into account $N_{2\beta}=1.024\times10^{24}$, t=0.506y, $\varepsilon_{K\beta^+}=0.028$ and $k = (0.76)^2$ is

$$T_{1/2}(K\beta^+)_{0\nu} \geq 5.8\times10^{21}\ y, \quad 68\%C.L.$$

A very conservative 2ν-mode half-life limit for the process $K\beta^+$ can be quoted if we assign the registered counts in the upper part of the coincidence spectrum shown in Fig.3 (N(E > 700 keV)=141 events) to the corresponding area of the theoretical spectrum[6] of the two-neutrino decay mode in the process $K\beta^+$ of ^{78}Kr. This has been a usual procedure employed to get half-life limits, avoiding the higher background of the low energy region which could mask the double beta signal. By using the fact that the theoretical upper part of the 2ν spectrum accounts for 2/3 of the total number of double beta counts (E=700 keV is the energy of the maximum of the theoretical 2ν spectrum), one gets, using the standard half-life formula cited above. However, this estimation may be significantly improved. Matter of fact, visible peaks in the Fig.3 at the energies about 0.45 MeV, 0.73 MeV, 1.2 MeV and may be even 1.6 MeV are consequences of the e^+-e^- pair production inside the IC by gammas of 1.46(^{40}K)MeV, 1.76(^{214}Bi)MeV, 2.204(^{214}Bi)MeV and 2.62(^{208}Tl)MeV. Therefore, a real quantity of counts inside the IC which could be refered to the $K\beta^+_{2\nu}$ decay of ^{78}Kr will be much less and the respective limit be much higher. The present limit without above mentioned consideration is $T_{1/2}(K\beta^+)_{2\nu} \geq 2\times10^{20}$y, 68%C.L.

Finally we have looked also for coincidences of four annihilation gammas in the NaIs together with a signal output from the IC (intended at an energy of 837 keV in a given window). In fact, after 4954.25 hours of counting time no coincidences of four gamma showed up independently of whatever could have happen in the chamber. In fact, due to the chosen trigger (i.e. NaIs first) nothing was obviously registered by the IC which in this case has played the role of a mere source of double positron emitters. The limit one gets is

$$T_{1/2}(2\beta^+)_{0\nu+2\nu} \geq 2.0\times10^{21}y, \ 68\%\ C.L.$$

REFERENCES

1. Ya.B.Zeldovic and M.Yu.Khlopov, Pisma v ZhETF,34(1981) 148 (JETPh Lett.,34(1981)141)
2. C.W.Kim and K.Kubochera, Phys.Rev.D27(1983)2765
3. W.C.Haxton and G.J.Stephenson, Prog.Part.Nucl.Phys.12 (1984)409
4. R.A.Eramzhayan, G.V.Micelmacher and M.V.Voloshin, Pisma v ZhETF 35(1982)530
5. J.Abad, A.Morales, R.Nunez-Lagos and A.F.Pacheco, J.de Phys.45(1984)C3-147, Anales de Fisica,A80(1984)15
6. M.Doi and T.Kotani, Prog.Theor.Phys.87(1992)1207

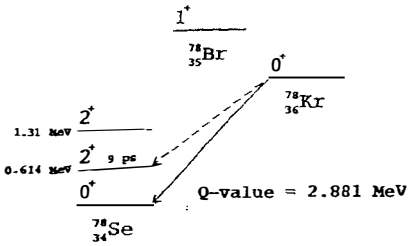

Fig 1: Level scheme of the ^{78}Se -^{78}Br -^{78}Kr triplet.

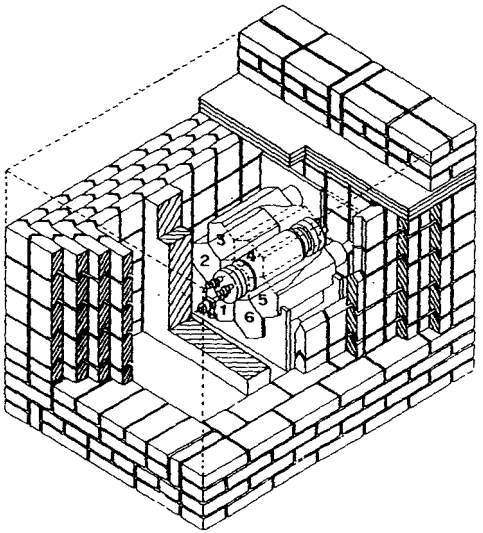

Fig 2: Experimental set-up.

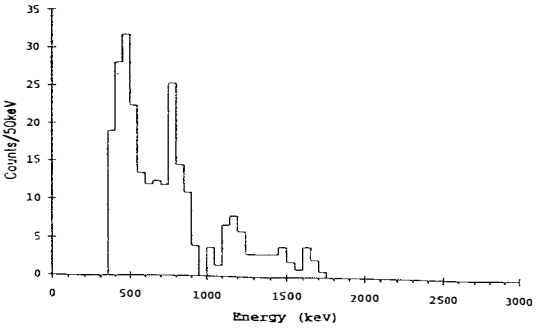

Fig 3: Coincidence spectrum between the IC signal and two 511 keV gammas in the scintillators (within an energy window of 2.35σ) registered in 4434.5 hours.

MEASUREMENT OF THE ββ2ν-DECAY OF ^{76}GE

M. Beck. F. Bensch, J. Bockholt. G. Heusser, H.V. Klapdor-Kleingrothaus*),
B. Maier, F. Petry, A. Piepke, H. Strecker, M. Völlinger

Max-Planck-Institut für Kernphysik, 6900 Heidelberg, Germany

A. Balysh, S.T. Belyaev *), A. Demehin, A. Gurov, I. Kondratenko, D. Kotel'nikov, V.I. Lebedev

Russian Scientific Center-Kurchatov Institute. 123 182 Moscow, Russia

A. Müller

Istituto Nazionale di Fisica Nucleare, I-67010 Assergi, Italia

From the data taken with one of the enriched detectors of the Heidelberg-Moscow ββ-experiment a revised half life of $T^{2\nu}_{1/2} = (1.42 \pm 0.03^{stat} \pm 0.13^{syst}) \cdot 10^{21}$ y for the two neutrino double beta (ββ2ν) decay of ^{76}Ge is derived. With a ^{76}Ge exposure of 19.3 mol·y it represents the first high statistics measurement of this extremely rare effect. The measured decay rate is in good agreement with the theoretical predictions.

The status of the investigation of the zero neutrino ββ-decay modes, indicating a non zero Majorana mass of the neutrino, is briefly reviewed.

From the absence of a signal indicating ββ-decay with Majoron emission in the above data, we conclude that a hypothetical Majoron neutrino coupling has to be smaller than $1.8 \cdot 10^{-4}$ with 90% c.l.. Using the total ^{76}Ge exposure of 56.4 mol·y we extract a half life limit of $T^{0\nu}_{1/2} > 1.5 \cdot 10^{24}$ y with 90% c.l. for the zero neutrino ββ-decay. By this result a Majorana mass of the neutrinos larger than 1.2 eV is excluded.

Presented by: A. Piepke

*) Spokesmen of the Heidelberg-Moscow collaboration

INTRODUCTION

Among the different methods to identify non zero neutrino masses the search for the, B-L symmetry violating, neutrinoless double beta decay plays a unique role, since it distinguishes Dirac from Majorana neutrinos. The physics of the different modes of this very rare second order weak decay, changing the charge of a nucleus by two units, have been discussed in previous publications (see e.g. ref. [1]).

An observation of the neutrinoless decay modes with emission of two electrons ($\beta\beta0\nu$) or with an additional hypothetical Goldstone boson, the so called Majoron, ($\beta\beta0\nu\chi$) would require non standard model physics. Although extremely sensitive this method is sometimes criticized since the neutrino mass deduction has to rely on theoretically calculated nuclear matrix elements.

This article will mainly focus on a measurement of the allowed two neutrino double beta ($\beta\beta2\nu$) decay, which allows us to test whether nuclear physics can reliably parametrize such second order weak processes. The decay rate of the $\beta\beta2\nu$-decay does not depend on any unknown particle physics parameter as the $\beta\beta0\nu$-modes do and can therefore be predicted by nuclear physics. However it has to be mentioned, that the calculations of the $\beta\beta0\nu$- and $\beta\beta2\nu$-matrix elements are substantially different [2].

From the experimental side the detection of the $\beta\beta2\nu$- and $\beta\beta0\nu\chi$-modes are much more difficult than of the $\beta\beta0\nu$-decay. While the latter one has a clear experimental signature in form of a peak at the decay energy of E_0=2038.56 keV, the others, resulting in continuous sum energy spectra of the emitted electrons, are more difficult to distinguish from background. These continua have different shapes and maxima.

EXPERIMENT

In the Heidelberg-Moscow $\beta\beta$-experiment Ge semiconductor detectors, made from isotopically enriched Ge, are used simultaneously as source and high resolution calorimetric detectors for the electrons emitted in the $\beta\beta$-decay of ^{76}Ge. The isotopic abundance of ^{76}Ge is 86% compared to only 7.8% in natural Ge.

At present the Heidelberg-Moscow collaboration is operating three enriched detectors of 6.29 kg total and 6.0 kg active mass in the Gran Sasso underground laboratory in Italy. This corresponds to a source strength of 68.7 mol ^{76}Ge. The shielding thickness of the laboratory is 3500 meters of water equivalent. 4.93 kg·y of measuring time corresponding to a ^{76}Ge exposure of 56.4 mol·y is available. A fourth enriched detector of 2.87 kg, increasing the source strength to 100 mol is under construction and will be installed in 1993. Aim of this experiment is to probe the mass range down to 0.2 eV.

The detectors are operated in a common shield of 10 cm highly radiopure LC2-grade Pb followed by 20 cm of less clean Boliden Pb. The cryostats are made from electrolytic Cu. All construcion materials were carefully selected.

For the analysis of the $\beta\beta2\nu$-decay data taken with the second enriched detector from October 1991 to August 1992 has been used. The measured spectrum (measuring time 1.68 kg·y) is shown in fig. 1. This data taking periode ended with

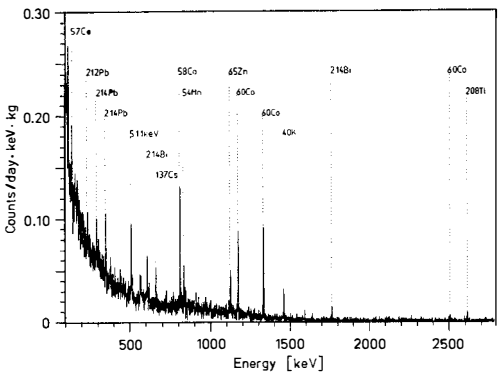

Fig. 1 Measured spectrum of the second enriched detector. The binwidth is 1 keV, the measuring time is 1.68 kg·y. The strongest lines are labled.

the installation of the third enriched detector. In the energy intervals 100-2700 keV, 500-1500 keV and 2000-2100 keV the measured counting rates are 6.36, 5.07 and 0.29 counts/keV·y·kg, respectively.

Since a measurement of the spectral shape is the only criterion to identify a $\beta\beta2\nu$-signal a big number of events is crucial for a reliable analysis. In general the $\beta\beta2\nu$-spectrum is superimposed to continuous background as Compton continua of γ-lines, bremsstrahlung emitted by the construction materials and β-activities of the Ge detectors itsef. These background components have to be identified and then unfolded from the measured spectrum quantitatively. The unfolding can be done reliably only if the measured spectrum is not dominated by background. It should be pointed out, that the subtraction of big numbers, as it was necessary in some previous experiments, is not a reliable method to obtain information about a weak effect.

DATA ANALYSIS AND RESULTS

In a first step 27 identified peaks were removed from the measured data by fitting the continuous background on both sides of each peak and then extending the continuum into the peak region. The resulting 'stripped' spectrum represents the continuous component of the measured spectrum. 15.5% of the counts were thus eliminated in the energy interval of interest from 500 to 1500 keV, containing 72% of the $\beta\beta2\nu$-intensity. The number of simulated background events should be compared to 7219 counts contained in this interval of the stripped spectrum.

To unfold the continuous background a Monte Carlo background model based on the CERN code GEANT 3.14 was developped. For its construction it is most important to know the localization of the different background components, since magnitude and shape of the simulated continuum depends on the geometry and density of the part in which the contamination is placed.

^{54}Mn, ^{57,58}Co and ^{65}Zn decaying totally or partly by EC were identified through their characteristic γ-lines shifted by the energy of the deexitation x-ray to be inside the Ge crystal. The measured peak intensities were used to normalize the activities. Those activities having no EC branch can not be identified in the crystal. ^{54}Mn and ^{57,58,60}Co activities are located in the Cu parts of the cryostat system. This assumption was cross checked through an independent experiment with

Table 1: Localization, absolute activity and contribution to the measured backgound in the evaluation interval.

Isotope	Localization	Activity [μBq/kg]	Fraction [%]
^{54}Mn	Ge	4	0.3
^{57}Co		2	0
^{58}Co		6	0.4
^{65}Zn		20	1.3
^{54}Mn	Cu	27	1.0
^{57}Co		57	0
^{58}Co		152	3.4
^{60}Co		118	13.6
^{232}Th	Cu	70	3.5
^{238}U		36	5.6
^{137}Cs	Cu	20	0.3
^{210}Pb	LC2 Pb	$3.6 \cdot 10^5$	6.7
^{40}K	LC2 Pb	140	3.3

a detector made from natural Ge using a 2.2 to Cu probe of the same production lot with and without inner LC2-grade Pb lining. The measured peak intensities were used to normalize the MC-simulation. The two latter components are cosmogenic activities produced when the materials were above ground (see table 1).

^{210}Pb contained in the LC2-grade Pb of the shield is contributing through the bremsstrahlung of its daughter ^{210}Bi, which β-decays with an endpoint energy of E_0= 1.16 MeV, to the ββ2ν-background. A quantitative analysis of this component is difficult, since no associated γ-quanta are emitted in its decay. The absolute activity was therefore measured by low-level α-spectroscopy of the ^{210}Po decay (a ^{210}Bi daughter). The deviation of the shape of the electron spectrum of the ^{210}Bi decay from an allowed decay was taken into account.

Both natural decay chains are contributing through the Compton continua of numerous γ-lines to the ββ2ν-background. Since several of these lines are identified in the measured spectrum their relative intensities can be used to locate the contamination. A placement in the Cu of the cryostat showed the best agreement with the experimental data. A placement in the LC2-grade Pb could be ruled out in that way, resulting in limits for its ^{232}Th and ^{238}U activities of 286 and 245 μBq/kg, respectively. The absolute activities of the Cu were normalized to the measured peak intensities. A placement in the Ge could be ruled out by the absence of high energetic α-lines in the measured spectrum. Residual uncertainties in the localization were included into the systematic error.

^{40}K localized by neutron activation in the LC2-grade Pb and ^{137}Cs have only a minor influence on the continuous background. The measured peak intensities were used to determine the absolute activities. The simulated Cs background is nearly independent from the placement.

To account for the residual background from 1.6 to 2.8 MeV a phenomenological constant background of 0.15 c/keV·y·kg, extended to lower energies had to be introduced. It contributes 3.5 % of the continuous background. A straight line was chosen to account for unidentified background components and to leave the shape of the background model unchanged.

The sum of the discussed components represents the background model, which thus has been constructed from experimental quantities. It has not been fitted to the measured continuum. From the difference of measured and background counts, according to the discussed model. we deduce a signal to background

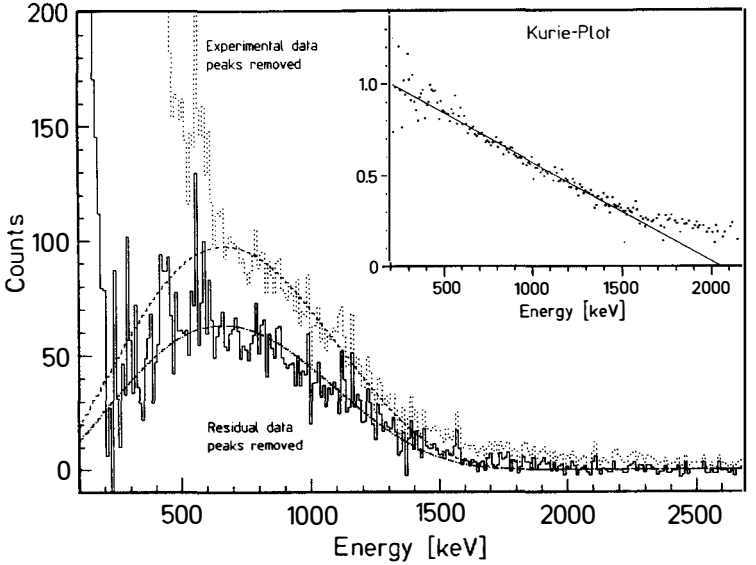

Fig. 2 The dotted spectrum shows the measured continuous background, while the solid spectrum depicts the residual data after background unfolding. The continuous curves are calculated ββ2ν-spectra. In the insert the residual data have been linearized like in a Kurie plot using the shape of the ββ2ν-decay.

ratio of 1.3 : 1 in the evaluation interval, showing that we performed indeed an ultra low background experiment.

To understand whether these non background events are due to ββ2ν-decay we have to investigate their spectral shape. The solid spectrum in fig. 2 shows the residual data after subtracting the background model from the experimental data (peaks removed), while the dotted spectrum shows the measured spectrum. The continuous curves are theoretically calculated ββ2ν-spectra. The lower one is in a wide energy range in good agreement with the residual data. It results from a maximum-likelihood fit of our data, yielding a half life of $T_{1/2} = (1.42 \pm 0.03^{stat}) \cdot 10^{21}$ y. The statistical error was evaluated from the logarithmic likelihood ratio, which shows parabolic behaviour. The upper curve corresponds to a half life of $9.2 \cdot 10^{20}$ y measured in an earlier experiment using also 86% enriched Ge [3], but having a measuring time of only 0.69 mol·y. Their result was evaluated under the assumption, that the detector background is only due to ^{210}Pb. Since our raw data is in good agreement with their published result and the existence of additional background has been shown experimentally their assumption is questionable.

The ββ2ν-spectra of fig. 2 were calculated using the known ββ-decay energy.

Since the statistics of our data is good enough (4135 events are contained in the evaluation interval of the residual spectrum) we can determine the experimental endpoint using a ββ-Kurie plot. Linear regression yields an endpoint energy of (2051 ± 20) keV. The good linearity an the correct endpoint energy shows the excellent agreement of measured and theoretical spectral shape.
Several single β-decay candidates as e.g. ^{68,77}Ge, $^{9\bullet}$Sr and ^{234}Pa were simulated in different materials to test, whether they could produce a similar spectrum. All tested isotopes are either leading to a strongly nonlinear ββ-Kurie plot or to a wrong endpoint energy.

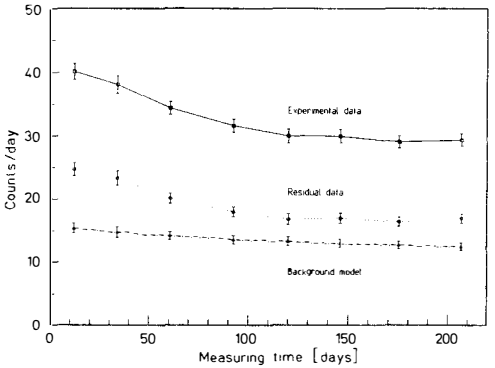

Fig. 3 Time dependence of the integral counting rate from 500 to 1500 keV. Peaks were removed.

Since the evaluated half life is very large the measured counting rate should be constant in time. A further consitency test can be done through the behaviour of the integral counting rate in the evaluation interval as a function of time, displayed in fig. 3. The full measuring time was divided into 30 days intervals. The background model was defined at the end of the measuring periode, then only tabulated half lives were used to calculate its time dependence. Experimental and residual data do not show strong fluctuations, although a decrease of the counting rate in the first 132.5 days of measurement can be seen. It is probably due to the decay of shortlived unidentified background components, which are visible because all data taken after storing the detector underground are included. If a two parameter ML-fit, leaving the half life and the endpoint energy as free parameters, is performed we find for the last 90.5 days (corresponding to a ^{76}Ge exposure of 7.8 mol·y), when the counting rate was constant, $T_{1/2} = (1.58 \pm 0.09) \cdot 10^{21}$ y and $E_0 = (2034 \pm 47)$ keV in comparison to $T_{1/2} = (1.41 \pm 0.05) \cdot 10^{21}$ y and $E_0 = (2053 \pm 29)$ keV if the full measuring time is used. The effect of shortlived unidentified background components should therefore be not larger than 10%.
The systematic error of the measurement includes the uncertainties due to the unsafe localization of ^{137}Cs, ^{232}Th and ^{238}U, statistical errors of the measured peaks used to normalize the model, the error of the ^{210}Pb activity measurement and the error of the simulated detector response. The latter one has been estimated experimentally with a calibrated collimated ^{133}Ba source. The detector was scanned with this source in 19 steps in axial and 14 steps in radial direction.
In summary the discussed data shows strong evidence for the existence of the ββ2ν-decay of ^{76}Ge with a half life of $T^{2\nu}_{1/2} = (1.42 \pm 0.03^{stat} \pm 0.13^{syst}) \cdot 10^{21}$ y.

This result is is in good agreement with the theoretically predicted value of ref. [2] but deviates from an earlier experiment [3].
On the basis of the quantitative understanding of the background the $\beta\beta0\nu\chi$-decay should be visible in the residual data, if the $\beta\beta2\nu$-decay is treated as another background component. In fact $\beta\beta2\nu$-decay is the major and irreducable background of this detector. After subtracting this 'background' we find in the energy interval from 1.1 - 2.05 MeV, containing 72% of the theoretical $\beta\beta0\nu\chi$-spectrum (its maximum is around 1.5 MeV) 208 events, which is on the $2.3\cdot\sigma$ level above zero. Since the spectral shape of these extra events does not match that expected for the $\beta\beta0\nu\chi$-decay they can not be treated as evidence for new physics. Therefore we extract a half life limit of $T^{0\nu\chi}_{1/2} > 1.7\cdot10^{21}$ y with 90% c.l. from that data. Using the theoretically calculated matrix element of ref.[2] and the phase space integral of [4] we conclude that the coupling of the hypothetical Majoron to neutrinos has to be smaller than $1.8\cdot10^{-4}$.
For the analysis of the $\beta\beta0\nu$-decay we use the complete data set of 56.4 mol·y available at present. Nothing has been subtracted from the measured data in this analysis. The average background from 2.0 to 2.1 MeV is 0.31 counts/keV·y·kg. From the absence of a peak at the $\beta\beta$-decay energy we calculate a limit for the $\beta\beta0\nu$-decay rate assuming a Poisson distributed signal superimposed to background. The resulting half life limit is $T^{0\nu}_{1/2} > 1.5\cdot10^{24}$ y with 90% c.l., corresponding to a new neutrino mass limit of 1.2 eV (90% c.l.) using the matrix element of [2].

The exceptional source strength and the extremely low background of the enriched detectors of the Heidelberg-Moscow collaboration has been used to perform the first high statistics measurement of the $\beta\beta2\nu$-decay. Experimental and calculated nuclear matrix element of ref. [2] agree within 40%. It has been shown experimentally, that nuclear physics can parametrize the $\beta\beta2\nu$-decay of ^{76}Ge, giving higher reliability to the constraints placed on non standard model parameters as the Majorana mass of the neutrinos and a Majoron neutrino coupling. Data taking of the experiment continues. With the measured parameters of the experiment a neutrino mass limit of 0.2 eV could be reached within 5 years.

REFERENCES

[1] A. Balysh, M. Beck, S.T. Belyaev, J. Bockholt, A. Demehin, J. Echternach, A. Gurov, G. Heusser, M. Hirsch, H.V. Klapdor-Kleingrothaus, I. Kondratenko, V.I. Lebedev, B. Maier, A. Müller, F. Petry, A. Piepke, U. Schmidt-Rohr, H. Strecker and K. Zuber, Phys. Lett. B283 (1992) 32 and references therein

[2] A. Staudt, K. Muto and H.V. Klapdor-Kleingrothaus, Europhys. Lett. 13 (1990) 31
K. Muto, E. Bender, H.V. Klapdor, Z. Phys. A334 (1989) 177, 187

[3] F.T. Avignone III, R.L. Brodzinski, C.K. Guerard, I.V. Kirpichnikov, H.S. Miley, V.S. Pogosov, J.H. Reeves, A.S. Starostin and A.G. Tamanyan, Phys. Lett. B256 (1991) 559

[4] M. Doi, T. Kotani and E. Takasugi, Phys. Rev. D 37 (1988) 2575

17 KeV Neutrinos

THE ARGONNE 17 keV NEUTRINO SEARCH

S. J. Freedman[1][2][3][4], I. Ahmad[1], K. P. Coulter[1], B. K. Fujikawa[1][2], J. P. Greene[1], J. L. Mortara[1][4], J. P. Schiffer[1][4], W. H. Trzaska[5], and A. R. Zeuli[1]

[1] *Argonne National Laboratory, Argonne, IL 60439*
[2] *Lawrence Berkeley Laboratory, Berkeley, CA 94720*
[3] *University of California, Berkeley, CA 94720*
[4] *University of Chicago, Chicago, IL 60637*
[5] *Texas A&M University, College Station, TX 77843*

ABSTRACT

Perhaps the most puzzling feature of the recent controversy over the 17 keV neutrino is that the positive evidence comes entirely from experiments which measure either the electron energy from beta decay or the bremsstrahlung spectrum following electron capture with solid state detectors. The inconsistency of the positive claims with the negative evidence from magnetic spectrometer experiments suggests the possibility of a universal systematic error in one type of experiment. To help resolve the issue we searched for the effect of a 17 keV/c^2 neutrino in the beta decay of ^{35}S using an apparatus incorporating a high-resolution solid-state detector in conjunction with a super-conducting solenoid. The magnetic field which transports the electrons from the source to the detector enabling us to avoid most of the systematic uncertainties normally found in external source experiments with solid state detectors. In contradiction to previous solid state detector experiments, however, we find no evidence for a massive neutrino between 5 keV/c^2 and 45 keV/c^2 neutrino. The experimental mixing probability is, $\sin^2\theta = -0.0004 \pm 0.0008$ (stat.) $\pm$ 0.0008 (syst.), for a 17 keV/c^2. The sensitivity of our apparatus to neutrino mass was verified in a separate experiment for which a mixed radioactive source containing ^{35}S and ^{14}C, which artificially introduced a distortion in the beta spectrum of ^{35}S similar to that expected from the massive neutrino.

INTRODUCTION

In 1985, J. J. Simpson interpreted an excess of low energy counts in his measurement of a tritium beta energy spectrum as evidence that a "17 keV neutrino" is occasionally emitted in beta decay [1]. His original claim of a 3% mixing probability was later reduced to 1% after including corrections for screening and exchange effects [2,3,4,5] appropriate for tritium bound in the environment of a silicon lattice [6]. Within a year, two new experiments with solid-state calorimeters [7,8], and four others using magnetic spectrometers [9,10,11,12], failed to find the 17-keV-neutino "kink" in measurements with ^{35}S and ^{63}Ni sources. All of these experiments were criticized by Simpson [13], and the controversy ignited when the kink was confirmed in new experiments using sources of ^{3}H [6] ^{35}S [14,15] ^{63}Ni [16], and ^{14}C [17]. Additional jpositive evidence, though less convincing, came from observing distortions in the electron-capture inner bremsstrahlung spectrum of ^{71}Ge [18] and ^{55}Fe [19]. Meanwhile magnetic-spectrometer measurements continued to be negative [20] and the latest versions of these experiments have reached an impressive level of statistical precision [21].

In an effort to resolve the issue measured the beta-energy spectrum from ^{35}S decay ($E_0 - m_e$) ~ 167 keV) using a new approach that eliminates many of the systematic uncertainties inherent in experiments with solid state detectors and external sources [22]. In particular, our geometry is immune to the several electron scattering effects that are inherent in the experiment of Hime and Jelley [15,23].

THEORETICAL FRAMEWORK

In the scenario under present consideration, the neutrino eigenstate that couples in nuclear beta decay is a superposition of a 17 keV/c^2 neutrino- and a massless-neutrino eigenstate,

$$|\nu_e\rangle = \cos\theta\, |\nu_0\rangle + \sin\theta\, |\nu_{17}\rangle . \qquad (1)$$

The usual expression for the electron energy spectrum in allowed beta decay is modified: and we have

$$N(E)\, dE = F(Z,E)\, R(E)\, S(E)\, p\, E\, (E_0\text{-}E)\, \{\cos^2\theta\, (E_0 - E) + \sin^2\theta\, [(E_0 - E)^2 \quad m_{17}^2)]^{1/2}\}\, dE. \qquad (2)$$

Here F(Z,E), R(E), and S(E) are correspondingly, the usual corrections due to Coulomb interaction (the Fermi function), radiative effects, and forbidden matrix elements ; E (E_0) is the electron total (endpoint) energy and p is the momentum. Searches for the 17 keV neutrino in beta decay focus on detecting the spectral distortion introduced by the term proportional to the mixing probability $\sin^2\theta$, in Eq. (2).

DESCRIPTION OF THE EXPERIMENT

The novel feature of the Argonne apparatus illustrated in Fig. 1, is a 60 cm long, 8-coil superconducting solenoid. Six of the solenoid's outer coils operate in series but the two remaining are powered with a second power supply allowing a variety of magnetic field configurations. The axial magnetic field intensity distribution we used is shown at the bottom of Fig. 1. Radioactive sources were inserted on the solenoid axis at the magnetic field maximum. A liquid-nitrogen-cooled, 1.6 cm diameter, 5 mm thick Si(Li) detector was placed in the fringe field, 36 cm from the source. Water-vapor build-up on the detector was avoided with the tubular liquid-nitrogen cold trap indicated in the figure. The typical vacuum pressure during runs was less than 10^{-7} torr.

Electrons from ^{35}S decay moved along helical trajectories which grew in diameter as the field decreased. The magnetic field at the detector was large enough to confine the electrons to the central 9 mm of the detector. The electron incident angle on the detector is reduced because of the decreasing magnetic field, reducing the backscattering probability which is smallest for normal incidence. Backscattering electrons with angles greater than $\theta_C = \sin^{-1}([\, B_D/B_S\,]^{1/2})$,

where B_D and B_S are the field strengths at the detector and the source, were reflected back to the detector by the magnetic mirror effect. The signals from multiple strikes occur within nanoseconds so they were unresolved by the microsecond-time-constant electronics, helping to reduce the usual tail from backscattering.

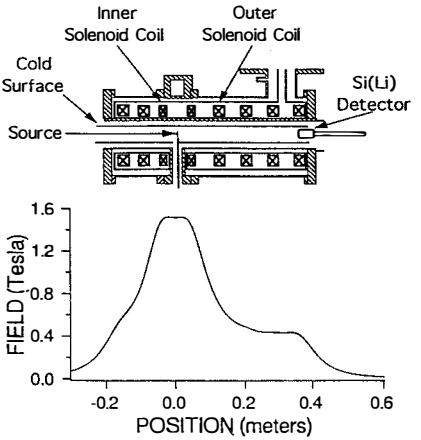

Fig. 1. Schematic view of the central region of the apparatus. The lower curve is the axial magnetic field strength distribution used in the experiment.

The spectrometer has a 2π sr solid angle and very weak sources, less than 0.1 μCurie, with thin support foils, were sufficient. The radioactive sources were all 1.5 mm diameter deposits on 20 $\mu g/cm^2$ carbon foils supported by 1 cm diameter frames. Sources of ^{109}Cd and ^{57}Co for calibrations were made by a standard vacuum evaporation technique. Sources of ^{139}Ce are made with the $^{139}La(p,n)^{139}Ce$ reaction on targets of $^{139}La_2O_3$ on 20 $\mu g/cm^2$ carbon foils with 10.3 MeV protons. Three different thicknesses (≈ 10, 30, and 70 $\mu g/cm^2$) of ^{139}Ce provided measurement points for an extrapolation which allowed us to account for the fact that the ^{139}Ce sources were relatively thick compared to ^{35}S sources. The ^{35}S sources themselves were constructed by allowing the water to evaporate from a drop containing dissolved, carrier free, Na_2SO_4. The average thickness of the Na_2SO_4 residue was less than 0.1 ng/cm^2. All source thicknesses were verified with α particle transmission measurements, although only upper limits were obtained with the thin sources.

The raw data, obtained using electronic pileup rejection, is shown in Fig. 2. The initial count rate was 3000 sec^{-1} of which only 0.5 sec^{-1} was room background. Pileup which escaped the rejection circuit is evident in the figure. The shape of the residual pileup spectrum is reproduced by convoluting the pileup corrected energy spectrum with itself. The resulting form is fit to the data above the endpoint. This procedure converges after a few iterations and it is easily generalized to include third and higher order pileup although higher order effects were negligible. The assumption that there is complete overlap between the unrejected pileup in critical to this procedure, which is valid when electronic pileup rejection is used. To verify that any distortion that might have arisen was not an artifact of the pileup rejection procedure, data was collected in a parallel electronics chamber without a electronic pileup rejection. For this data the pileup rate was ten times higher and complete the disruption of pulse overlap is

no longer valid, For this data, the pileup removal procedure employed the spectrum of observed pileup between ^{35}S electron signals and the signals from an electronic pulser.

The detector response to gamma-rays was studied with ^{182}Ta and ^{57}Co sources. The detector has negligible nonlinearity and the gaussian width for a gamma-ray of energy E_γ is well characterized by a noise width and a statistical term are proportional to energy, $\sigma = (a + b E_\gamma)^{1/2}$. The present experiment requires that we have a detailed understanding of the response to electrons between 120 and 167 keV. The conversion electron lines from ^{139}Ce at 127, 160, and 165 keV (see Fig. 2) conveniently span the analysis region and form the principal constraint on our model of the electron response function. An important feature our geometry, made possible by the superconducting solenoid, was that the detector was far from the source and the solid angle for gamma rays coming from the conversion line sources is negligible. In the previous solid state detector experiments a delicate subtractions of gamma rays were required for the calibrations with conversion lines. The present geometry with the magnetic transport field does imply a high probability for summing Auger and K conversion electrons signals since half of the emitted Auger electrons are detected. A subtraction procedure was required in order to get reliable information on the L and M lines in the presence of an underlying K + Auger electron background. In the important case of ^{139}Ce and ^{109}Cd the shape of the underlying sum spectrum is reliably obtained by convoluting the individual spectra from Auger and K-conversion electrons.

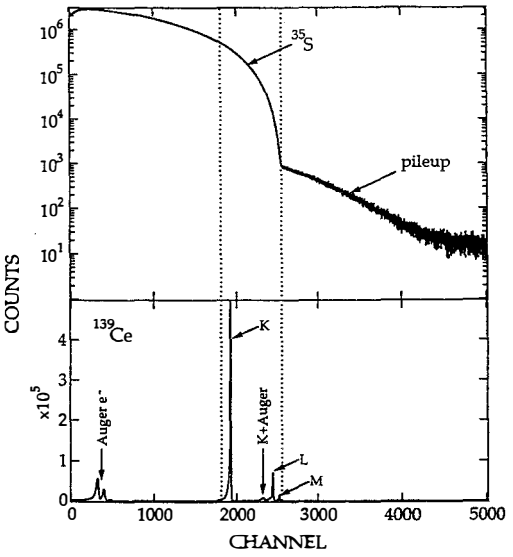

Fig. 2. Raw data from ^{35}S decay. The lower curve is the calibration spectrum from the decay of ^{139}Ce. The region bounded by the dotted lines is used to search for the massive neutrino.

The model of the detector response is similar to those of previous experiments. The full energy peak is characterized as a gaussian with the energy width determined from the gamma ray calibration. The constant term, **a**, in the expression for σ^2 was determined with ^{139}Ce conversion line data, to account for the broadening effects of the detector dead layer on the electron resolution. The shape of the backscattering tail was taken to be of the form, $(E_0 - E)$ E^{α} with $\alpha \approx 1.3$ from a Monte Carlo simulation. The amount in the residual backscattering tail was only about 7% of the incident intensity, being reduced with the aid of the magnetic mirror effect as described above. A Monte Carlo simulation suggested that this fraction is nearly independent of energy.

Another tail, near to the full energy peak (see Fig. 2) is presumably from straggling in the gold ($\approx 40\ \mu g/cm^2$) and SiO_2 detector dead layers. The shape is difficult to model especially because reflected electrons also contribute to this feature. Instead of an analytic expression we used a third order polynomial interpolation of the data near the ^{139}Ce K-electron line to represent the shape of the tail. For the response function at other energies the result is scaled by $C_1/(E+C_2)$, where C_1 and C_2 are determined from a fit to all three ^{139}Ce conversion lines.

The parameters of the resolution function were determined for each of the three ^{139}Ce sources and the final values were obtained by extrapolating to zero thickness. Modeling the resolution function introduces systematic uncertainties but the final conclusions were found to be stable for different characterizations consistent with the ^{139}Ce data. We emphasis that the use of ^{139}Ce conversion lines allowed us to interpolate the modeled response over the critical spectral region. In previous ^{35}S experiments the response functions were extrapolated from lower energy lines, in most cases the ^{109}Cd lines below 90 keV.

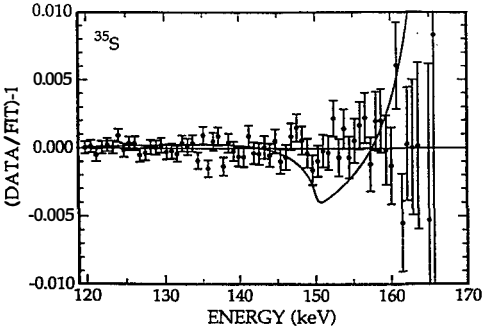

Fig. 3. Residuals from a fit to the pileup-corrected data assuming no massive neutrino ($\sin^2\theta = 0$); the reduced χ^2 for the fit is 0.88. The solid curve represents the residuals expected for decay with a 17 keV neutrino and $\sin^2\theta = 0.85\%$; the reduced χ^2 of the data is 2.82

RESULTS

The Fermi function, which includes the effect of finite nuclear size, was provided by P. Vogel [24] the radiative corrections were from Ref. [25], and the small forbidden corrections from Ref. [26]. In the final fits to the ^{35}S data only two parameters were varied: the overall normalization and the endpoint energy. No arbitrary shape corrections were introduced. The residuals of the fit with $\sin^2\theta = 0$ are displayed in Fig. 3. The distribution is flat, so the assumption of beta decay with a single, massless, neutrino provides a good description of the

data. The solid curve in the figure is the deviations expected for a 17 keV neutrino with $\sin^2\theta = 0.0085$. We obtain $\sin^2\theta = -0.0004 \pm 0.0008$ for 17 keV/c^2. This error is statistical. The largest systematic error appears to be associated with the interpolation of the response function. The total systematic error is no larger than the statistical error. The 95% confidence level limits for mixing probabilities for heavy neutrinos between 5 and 45 keV are shown in Fig. 4. We assigned a systematic equal to the statistical error, and treated the systematic error as if it were statistical in obtaining these limits. A separate analysis of the data taken without pileup rejection gives consistent results and no evidence for the 17 keV neutrino.

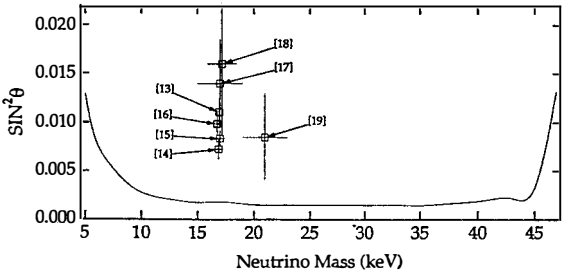

Fig. 4. The 95% cl upper limits on $\sin^2\theta$ from fits to the ^{35}S data for various neutrino masses. The points correspond to the results of previous positive experiments and are labeled by their reference number.

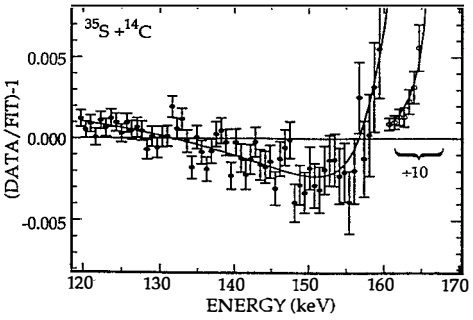

Fig. 5. Residuals from fitting the beta spectrum of a mixed source of ^{14}C and ^{35}S with a pure ^{35}S shape; the reduced χ^2 of the data is 3.59. The solid curve indicates residuals expected from the known ^{14}C contamination. The best fit yields a mixing of 1.4 ± 0 .1% and reduced χ^2 of 1.06.

The value of the fitted endpoint energy is 167.210 ± 0.005 (stat.) ± 0.100 (syst.) keV. The actual endpoint is probably about 60 eV higher because of energy loss in the dead layer. The conservatively estimated systematic error reflects uncertainties in the energy calibration and the effects of possible drifts which have a negligible effect on the conclusions about massive neutrinos.

To assess the reliability of the method, we introduced a known distortion into the ^{35}S beta spectrum and attempted to detect it. A drop of ^{14}C-doped Valine ($(E_0 - m_e) \sim 156$ keV) was deposited on a carbon foil and then a much stronger ^{35}S source was deposited over it. The data from the composite source were fit using the ^{35}S theory, ignoring the ^{14}C contaminant. The fit residuals are displayed in Fig. 5. The distribution is obviously not flat; the solid curve shows the expected deviations from the single component spectrum with the measured amount of ^{14}C. The fraction of decays from ^{14}C determined from the fit to the beta spectrum is 1.4 ± 0.1%. This agrees very well with the value of 1.34% inferred by measuring the total decay rate of the ^{14}C alone while the source was being prepared. This exercise demonstrates that our method is sensitive to a distortion at the expected level. A report of this experiment was recently published in the Physical Review Letters [27].

This work supported, in part, by the US Department of Energy, Nuclear Physics Division, under contract Nos. W-31-109-ENG-38 and DE-AC03-76SF00098.

REFERENCES

1. J. J. Simpson, Phys. Rev. Lett. **54**, 1891 (1985).
2. W. Haxton, Phys. Rev. Lett. **55**, 807 (1985).
3. E. G. Drukarev and M. I. Strikman, Sov. Phys. JETP **64**, 686 (1986).
4. B. Eman and D. Tadic, Phys. Rev. C **33**, 2128 (1986).
5. J. Lindhard and P. G. Hansen, Phys. Rev. Lett. **57**, 965 (1986).
6. A. Hime and J. J. Simpson, Phys. Rev. D **39**, 1837 (1989).
7. T. Ohi *et al.*, Phys. Lett. B **160**, 322 (1985).
8. V. M. Datar *et al.*, Nature (London) **318**, 547 (1985).
9. T. Altzitzoglou *et al.*, Phys. Rev. Lett. **55**, 799 (1985).
10. A. Apalikov *et al.*, JETP Lett. **42**, 289 (1985).
11. J. Markey and F. Boehm, Phys. Rev. C **32**, 2215 (1985).
12. D. W. Hetherington *et al.*, Phys. Rev. C **36**, 1504 (1987).
13. J. J. Simpson, Phys. Lett. B **174**, 113 (1986); see also Ref. (14).
14. J. J. Simpson and A. Hime, Phys. Rev. D **39**, 1825 (1989).
15. A. Hime and N. A. Jelley, Phys. Lett. B **257**, 441 (1991).
16. A. Hime, D. Phil. Thesis, Oxford (1991) unpublished.
17. B. Sur *et al.*, Phys. Rev. Lett. **66**, 2444 (1991).
18. I. Zlimen *et al.*, Phys. Rev. Lett. **67**, 560 (1991).
19. E. B. Norman *et al.*, J. Phys. G: Nucl. Part. Phys. **17**, S291 (1991).
20. M. Chen *et al.*, Phys. Rev. Lett. **69**, 3151 (1992).
21. H. Kawakami *et al.*, Phys. Lett. B **287**, 45 (1992).
22. J. L. Mortara *et al.*, Phys. Rev. Lett. **70**, 394 (1993).
23. A. Hime, Phys. Lett. B **299**, 165 (1993).
24. P. Vogel, private communication.
25. A. Sirlin, Phys. Rev. **164**, 1767 (1967).
26. F. P. Calaprice and D. J. Milner, Phys. Rev. C **27**, 1175 (1983).
27. J. L. Mortara *et al.*, Phys. Rev. Lett. **70**, 394 (1993)

INVESTIGATION OF THE EVIDENCE FOR A 17-KEV NEUTRINO

M.G.Bowler, N.A.Jelley and D.H.Perkins
Department of Physics, Particle and Nuclear Physics, Keble Road,
Oxford OX1 3RH, England.

ABSTRACT

Further measurements have been made of the beta spectrum of ^{35}S using a Si(Li) detector under a variety of source and detector geometries. A long range curvature in the Kurie plots is found which depends on the geometry and is evidence for electrons being scattered from or traversing extra material in the apparatus. Fits to the spectra were made using a fixed backscattering component, an energy loss correction and a flat component, all monitored using ^{109}Cd conversion sources. Good fits to the ^{35}S data assuming no heavy neutrino required the energy loss tail in the electron response function, which contains a few percent of the counts, to be about 1.5 - 2 times larger than indicated by the ^{109}Cd source. None of these five further runs, however, gave a good fit to a 17-keV neutrino admixture at the 0.7% level. A re-analysis of the Hime-Jelley data, including allowance for scattering as well as pile-up effects and the uncertainties in the energy loss tail, no longer shows significant evidence for a 0.7% 17-keV neutrino. Although a complete understanding of instrumental effects on the electron response function has not been achieved, it is concluded in the light of these results that the original data cannot now be regarded as constituting positive evidence for the existence of a 17-keV neutrino.

Talk presented by N.A.Jelley.

Experiments carried out in Oxford in 1990 on the beta-decay of ^{35}S yielded a significant distortion in the beta spectrum 17 keV below the end-point[1]. This distortion was interpreted as further evidence for the existence of a 17-keV neutrino admixture at the 1% level, a hypothesis first put forward by Simpson in 1985 following an experiment on the beta-decay of tritium[2]. In 1990 experimentalists at Berkeley also reported evidence in the beta spectrum[3] of ^{14}C and during 1991 in Oxford studies[4] on ^{63}Ni provided further indications. However, no evidence had been found in experiments using magnetic spectrometers, rather than solid-state detectors. There were some rather inconclusive null experiments until at the "Neutrino 92" conference in Granada the results from two high precision experiments were announced. One on ^{35}S, which was carried out with a solid-state detector, used a magnetic field to collimate the electrons and suppress back-scattering[5]. The other on ^{63}Ni, which had very high statistics, used a magnetic spectrometer[6]. Both reported null results.

At Oxford further measurements were made of the beta spectrum of ^{35}S during 1992 using the same apparatus as in the original work in an attempt to gain further understanding. Spectra were taken under a variety of source and detector geometries. A long range curvature in the Kurie plot was found which depended on the geometry and is evidence for electrons being scattered from or traversing extra material in the apparatus. The electron response in the fits to the ^{35}S spectra was modelled by a fixed backscattering part, which was taken as a constant slope in the region of interest ($0.6E_0$ - E_0), plus a flat component which was allowed to vary and an energy loss correction. The tail of the energy loss had a functional form proportional to the reciprocal of the square of the energy loss. These components were monitored by using ^{109}Cd conversion sources (see figure 1).

In all of these further runs with ^{35}S the collimation was different from that in the original experiment and in four of the five runs a chamfered rather than a square-cut

anti-scatter baffle was used. When fitting to the ^{35}S spectra, using the energy loss extrapolated from the ^{109}Cd source (the amplitude of the energy loss component is proportional to the reciprocal of the square of the velocity of the electron), similar amounts of flat component were found in the ^{35}S as in the ^{109}Cd spectra.

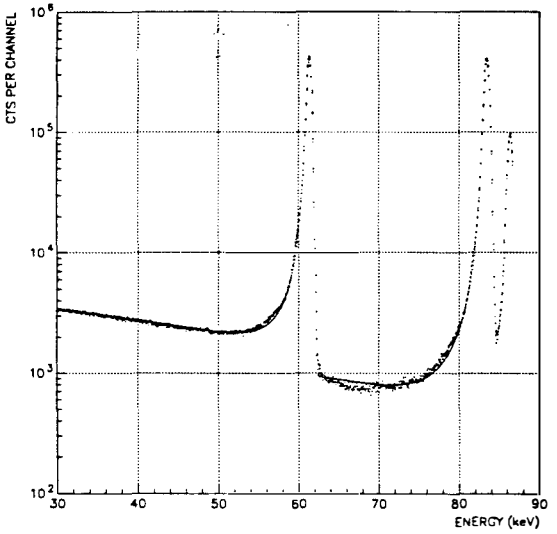

Figure 1 A ^{109}Cd conversion electron spectrum In the fit there was a fixed slope of 0 2 and the fitted curve has 4.5% flat and an energy loss amplitude of 0.39 peaked at 0.2 keV loss

In all but one run no heavy neutrino was preferred to 0.7% of a 17-keV neutrino, and in that one run the χ^2 for the heavy neutrino was rather high. In three of the other runs the χ^2 was acceptable for the no heavy neutrino hypothesis. All runs, however, gave acceptable χ^2 and preferred no heavy neutrino if the energy loss tail was increased by 1.5 - 2 times. This corresponds to a few percent additional electrons in the tail, in the region a few keV below the peak, to the amount extrapolated from ^{109}Cd. A summary of the results is given in figure 2 and fits to one of these runs are shown in figure 3 as the difference (in standard deviations) between theory and experiment.

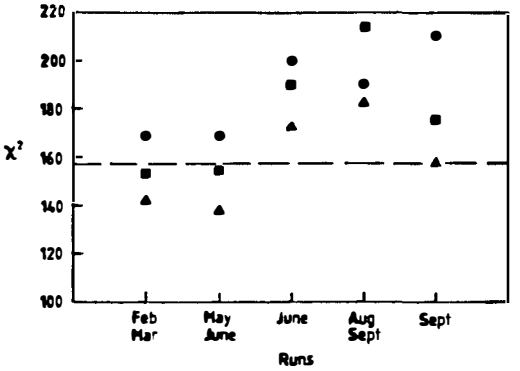

Figure 2 A summary of fits to the five runs (the dashed line indicates the number of degrees of freedom): ■ no heavy neutrino and ● 0.7% of a 17-keV neutrino, energy loss tail as extrapolated from 109Cd; ▲ no heavy neutrino, 1.5 times the energy loss tail extrapolated from 109Cd.

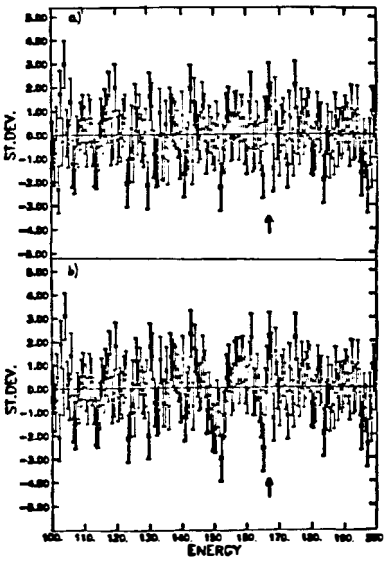

Figure 3 Examples of fits to the ^{35}S run in February-March 1992 (the arrows indicate the end-point of the beta spectrum): a) no heavy neutrino, 1.5 times the energy loss tail extrapolated from ^{109}Cd: $\chi^2 = 142$ for 158 degrees of freedom. b) 0.7% of a 17-keV neutrino, 0.5 times the energy loss tail extrapolated from ^{109}Cd: $\chi^2 = 168$ for 158 degrees of freedom.

A re-analysis of one of the original runs (#2) gave a similar amount of flat in the fit to the ^{35}S as in the fit to the ^{109}Cd. Furthermore, if the energy loss tail was increased by a factor of 2 and a small pile-up correction was made then the no neutrino hypothesis gave a similar χ^2 as the 0.7% 17-keV neutrino hypothesis and both were acceptable (see figure 4, where the fits are plotted as the difference, in standard deviations, between theory and experiment). (A small pile-up correction, previously unsuspected, is necessary to allow for the ~11 keV threshold in the pile-up rejection circuit. The effect of this correction, if the flat component is allowed to vary and the energy loss is as extrapolated from ^{109}Cd, is to lower the χ^2 from 92 to 78 for 75 degrees of freedom for the no heavy neutrino hypothesis. Increasing the energy loss tail by a factor of 2 reduces the χ^2 to 64.)

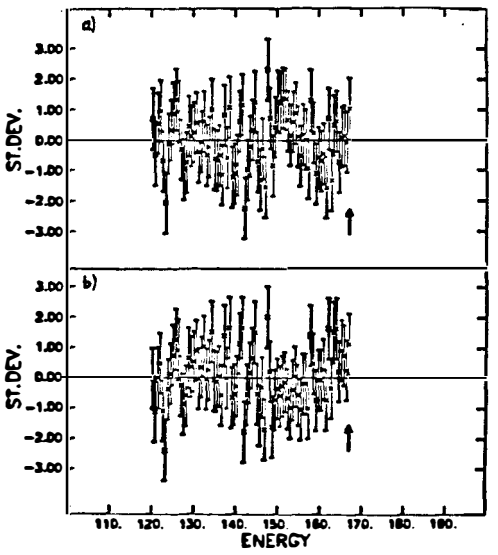

Figure 4 Examples of fits to the ^{35}S run #2 with twice the energy loss tail extrapolated from ^{109}Cd (the arrows indicate the end-point): a) no heavy neutrino $\chi^2 = 64$ for 75 degrees of freedom. b) 0.7% of a 17-keV neutrino $\chi^2 = 64$ for 75 degrees of freedom.

The origin of the increased number of counts (a few percent) in the tail is unclear; in particular in the fits to the ^{35}S spectra there was an increased number whether a square-cut or a chamfered anti-scatter baffle was used. However, while we have not yet achieved a complete understanding of instrumental effects on the electron response function, we are of the opinion, in the light of these results, that the original data cannot now be regarded as positive evidence for a 17-keV neutrino.

REFERENCES

1) Hime, A. and Jelley, N. A., *Phys. Lett.* B**257**, 441 (1991).
2) Simpson, J. J., *Phys. Rev. Lett.* **54**, 1891 (1985).
3) Sur, B. et al., *Phys. Rev. Lett.* **66**, 2444 (1991).
4) Hime, A. and Jelley, N. A., Oxford preprint OUNP-91-21 (1991).
5) Mortara J.L. et al., *Phys. Rev Lett.* **70**, 394 (1993).
6) Oshima, T. et al., KEK preprint 92-184, sub. to *Phys. Rev.* D and Kawakami, H. et al., *Phys. Lett.* B**287**, 45 (1992).

BETA DECAY ANOMALIES AND THE 17-keV CONUNDRUM

A. HIME
Physics Division, Los Alamos National Laboratory, MS D449, Los Alamos, NM 87545, USA

ABSTRACT

Recent developments in pursuance of the 17-keV neutrino are reviewed. Several different experiments found anomalies in β decay spectra which were consistently interpreted as evidence for a heavy neutrino. On the other hand, recent null results definitively rule out the existence of a 17-keV neutrino, as well as escaping criticisms applicable to earlier experiments. While missing links remain, it seems that any strong evidence for a 17-keV neutrino has vanished. Specifically, the anomalies observed in ^{35}S and ^{63}Ni spectra at Oxford can be reinterpreted in terms of electron scattering effects. In addition, the discrepancy amongst internal bremsstrahlung measurements has an instrumental origin, and recent results disfavour a 17-keV neutrino. Anomalies persist in the low energy region of the tritium spectrum which deserve further investigation.

INTRODUCTION

More than seven years have passed since Simpson[1] first reported evidence for a 17-keV neutrino in the β spectrum of tritium implanted into a silicon detector. The result was scrutinized when it was pointed out[2] that an incorrect choice of screening correction and exchange effects in atomic tritium could explain the anomaly. The subject appeared closed following a flurry of negative results[3] from experiments measuring the decay of ^{35}S, all claiming low limits on the mixing probability for a 17-keV neutrino. A detailed report[4] on the β decay of ^{63}Ni at Chalk River also failed to provide any support for Simpson's claim. The 17-keV burial was nevertheless premature. In the first place, further analysis of tritium data[5,6,7] showed that the sudden distortion observed is not easily understood using conventional atomic physics. Secondly, all negative results were criticized[5,8] for incomplete knowledge of systematic effects, specifically for the use of arbitrary shape corrections when analysing magnetic spectrometer data.

The possible existence of a 17-keV neutrino was rekindled after the tritium anomaly persisted in a measurement using a tritiated hyperpure germanium detector[7], an experiment which circumvented many of the uncertainties inherent in the original Simpson experiment. While uncertainties about the state of bound tritium are problematic[7], activity in this field increased when a similar observation was made[8] using a silicon detector with an external ^{35}S source. This work also detailed criticisms of previous experiments claiming to rule out the presence of a 17-keV neutrino. Improvements on the latter technique were investigated at Oxford where consistent observations were made both in the β decay of ^{35}S[9,10] and ^{63}Ni[10,11]. In addition, a group at LBL reported evidence for a 17-keV neutrino based on a measurement employing a ^{14}C doped germanium detector[12].

The evidence in favour of a heavy neutrino derives from measurements on a variety of β emitters, in a host of experimental enviroments, and spanning two orders of magnitude in the threshold energy for a 17-keV neutrino. This, together with a number of null results has formed a most unusual and controversial subject[13]. The purpose of this paper is to bring the subject into perspective and recent developments up to date.

SIGNATURE FOR HEAVY NEUTRINO EMISSION

A description of the signature for heavy neutrino emission in β decay spectra is detailed elsewhere[8,10]. If we consider a two-state model of the electron neutrino, where the weak eigenstate is an admixture of two physical states with masses $M_1 \sim 0$ and M_2, then the β spectrum becomes an incoherent sum of two β spectra with different endpoints. The Fermi-Kurie plot is then defined in the conventional way. The Kurie plot (for an allowed decay) is a linear function of energy in the absence of neutrino masses and is zero at the endpoint energy Q. For non-zero neutrino mass the Kurie spectrum remains linear in regions sufficiently below the endpoint. As the endpoint is approached from below, however, the slope decreases rapidly until it is vertical at the endpoint. In the case of a heavy neutrino admixture the Kurie plot exhibits two components, shown schematically in Fig.1. The spectrum is said to exhibit a "kink" at the threshold energy $(Q - M_2)$ and the size of this kink determines the mixing probability for a heavy neutrino.

Experimental searches for heavy neutrino admixtures in β decay spectra hinge on a comparison of data to the theoretical (*Fermi*) shape. It follows that sensitivity to the physical parameters of interest relies on an experiment's ability to measure this shape accurately. While recognizing a threshold effect in a continuous spectrum is a function of energy resolution, the size of the distortion is governed by the size of mixing. Consequently, constraints on small values of the mixing probability will be dictated by counting statistics and any systematic features of an experiment causing energy dependent shape factors in the measured β spectrum.

The sharpness of the threshold can be seen by considering the interval below $Q - M_2$ over which the Kurie plot remains substantially non-linear. Indeed, this interval is not very wide in units of M_2. In particular, with

$M_2 = 17$ keV, 50% of the distortion occurs in the first 2.6 keV below $Q - 17$ keV. It is often difficult to obtain the statistical accuracy required to observe a kink reliably. A large part of the signal is manifested, however, by the change in slope of the Kurie plot above and below $Q - M_2$. Hence, we see that the signature for heavy neutrino emission in β decay spectra exhibits two features – a local effect, the "kink region", where the spectrum is highly nonlinear and a longer range effect associated with a change in slope of the Kurie plot. It is the latter part of the signal which is most susceptible to (energy dependent) instrumental effects.

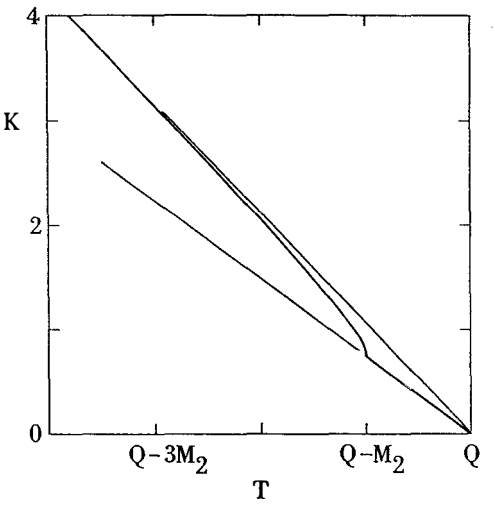

(Fig.1) Schematic diagram showing a two component Kurie plot in the case of maximal mixing of the electron neutrino with one light ($M_1 \sim 0$) and one heavy (M_2) mass eigenstate. The spectrum is characterized by the onset of a "kink" at the threshold energy ($Q - M_2$), and by a change of slope above and below this threshold.

ON ARBITRARY SHAPE CORRECTIONS

It has long been argued[5,8,10] that the null results asserted by magnetic spectrometer searches are largely overstated and that sensitivity to small admixtures of a heavy neutrino is limited by systematic uncertainties associated with instrumental shape corrections. The crux of the argument is that energy dependent shape corrections are not known *a priori* and the need for such corrections becomes apparent only after an attempt at fitting data without such corrections. The problem is usually handled by applying smooth shape corrections in the form of a polynomial in the β energy. Due to the nature of the signal, the addition of unknown instrumental degrees of freedom in a fitting routine create additional correlations with the physical parameters of interest with the result of decreasing the overall sensitivity of a set of data.

The potential hazard in applying "arbitrary" shape corrections is quantified in the Monte Carlo studies by Bonvicini[14], who has demonstrated the ability of a non-linear distortion to bury a heavy neutrino signal

and yet be "well-fitted" by smooth shape corrections. Hence, if instrumental shape corrections cannot be determined *independently* from the β decay measurements, systematic uncertainties can be estimated only by varying the type of correction applied to a set of data and noting any correlation with a heavy neutrino mixing probability. As demonstrated in ref.[14], these correlations are potentially very strong and it is unclear that the earlier magnetic spectrometer searches[3,4] are capable of ruling out a 17-keV neutrino admixed below the 1% level. The only way to overcome such correlations is to determine *a priori* any energy dependent response in an independent experiment. Otherwise, large statistical samples of data must be acquired in order that a "kink" be searched for directly.

RECENT NULL RESULTS

The problem of applying arbitrary shape corrections has been circumvented in a recent magnetic spectrometer measurement[15] of the ^{63}Ni spectrum at the Institute for Nuclear Studies (INS) in Tokyo. Although unkown shape corrections are required, the very high statistics accumulated in the region of interest makes it unlikely that a 17-keV threshold has been missed in this experiment (see Fig.2). At this meeting, Holzschuh discussed the results of a ^{63}Ni measurement using the Zurich toroidal spectrometer where, again, a dedicated search in the "kink region" leaves little room for a 17-keV neutrino.

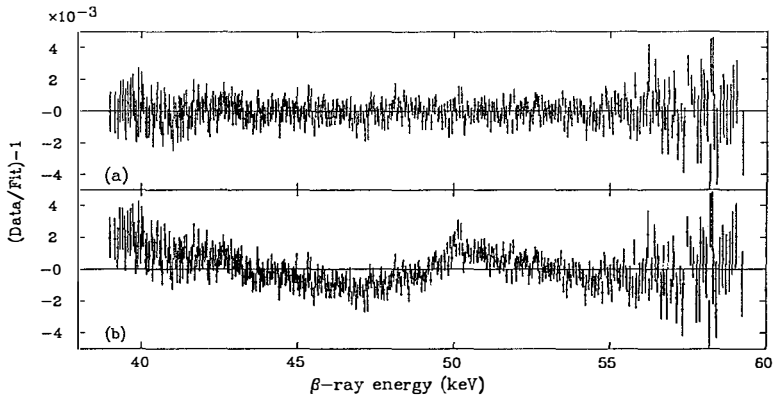

(Fig.2) Data from the INS Tokyo magnetic spectrometer measurement (ref.15) using ^{63}Ni. The 2.4×10^9 events accumulated between 39 and 60 keV allows one to search for a 17-keV "kink" directly. In (a) residuals are shown for the best fit assuming a single component, massless neutrino. Spectrum (b) shows the residuals obtained if one assumes a 1% admixture of a 17-keV neutrino.

While the CalTech group continue to improve their spectrometer as well as performing tests to demonstrate their sensitivity to a heavy neutrino[16], a new ^{35}S measurement has emerged from Princeton. In the latter experiment[17], it has been found that the need for a linear shape correction is greatly reduced when account is made for electrons which back-scatter from the source. The back-scattering contribution has been studied in some detail and the limit on the emission of a 17-keV neutrino appears quite stable against uncertainties in this correction. The accuracy of the Princeton measurement is further demonstrated in that a good fit can be

achieved to the data over a rather wide energy interval, without the need for any further corrections.

Perhaps the most convincing evidence against a 17-keV neutrino comes from the ^{35}S measurement at Argonne Laboratory[18], also discussed by Freedman at this meeting. A silicon detector was used to record electron energy spectra, however, the use of a solenoidal magnetic field provides a natural form of collimation, circumventing potential difficulties associated with electron scattering between the source and detector. The Argonne group have demonstrated the sensitivity of their experiment in an independent measurement with a small component of ^{14}C admixed into a ^{35}S source. A fit to the data reconstructs the spectrum beautifully, a difficult task without an accurate understanding of systematic uncertainties.

SCATTERING IN THE OXFORD GEOMETRY

Experiments at Oxford[9,10,11] employed thin radiation sources in a cylindrical geometry with a cooled silicon detector. The aim was to provide a well defined geometry in which electrons are normally incident on silicon, an improvement on the scheme used at the University of Guelph[8] where no form of collimation was used. Data analysis at Oxford proceeded after removing background and pileup from the raw β spectra, although initial work[9] neglected radiative corrections in the theory. Subsequent analysis[10,11] showed that the conclusions drawn from the data are only weakly sensitive to such corrections. Measurements of the electron response function were performed using internal conversion electron sources prepared in the same fashion, and occupying the same geometry as the β sources. The distortions observed in the Oxford data proved robust against systematic variations in the known instrumental degrees of freedom, such as uncertainties in energy loss and back-scattering effects, or in elements of the background subtraction.

At the previous Moriond workshop, Piilonen[19] presented the results of Monte Carlo calculations of scattering effects in the Oxford geometry and concluded that an incomplete description of the electron response function could be the origin of the anomalies observed. At question is the small amplitude for electrons which scatter into the detector from material between the source and detector. A first glance suggests that such a solution is untenable. Scattering effects are geometry dependent, and the change in geometry from the Guelph to Oxford apparatus was motivated as a systematic check against scattering effects. The null result from Argonne Laboratory strongly suggests, however, that scattering effects are the culprit in the Oxford and Guelph experiments. The focusing field in the Argonne geometry circumvents the need for material between the source and detector with which electrons can interact. We also heard from Abele at this conference who obtained a null result using two silicon detectors in conjunction with a magnetic field to focus electrons into the detectors.

Recently, the present author studied the effects of intermediate scattering[20] described by Piilonen and Abashian[19]. Specifically, account was made for electrons which enter the detector after scattering from an aluminum ("anti-scatter") baffle, those which penetrate the source and detector apertures, as well as electrons which back-diffuse from the source substrate. The sum of these three effects are plotted in Fig.3a along with the more probable effects of energy loss (when electrons traverse the detector contact) and back-scattering (when electrons entering the detector multiple scatter back out of the silicon crystal). The intermediate scattering effects represent second order corrections compared to those of energy loss and back-scattering effects (which were accounted for in the original analysis). Hence, it is non-intuitive that such small effects could play a significant role, particularly when the results proved robust against uncertainties in the dominant components of the electron response function (Fig.3b). Nonetheless, the energy distribution of electrons scattered from the aluminum baffle is concentrated in an energy region as indicated in Fig.3c and its absence in the data analysis plays a much more significant role than first imagined. Indeed, a reanalysis of the Oxford ^{35}S and ^{63}Ni data produces an equally good fit to the data when the heavy neutrino hypothesis is simply replaced by that based on electron scattering effects (see Fig.4).

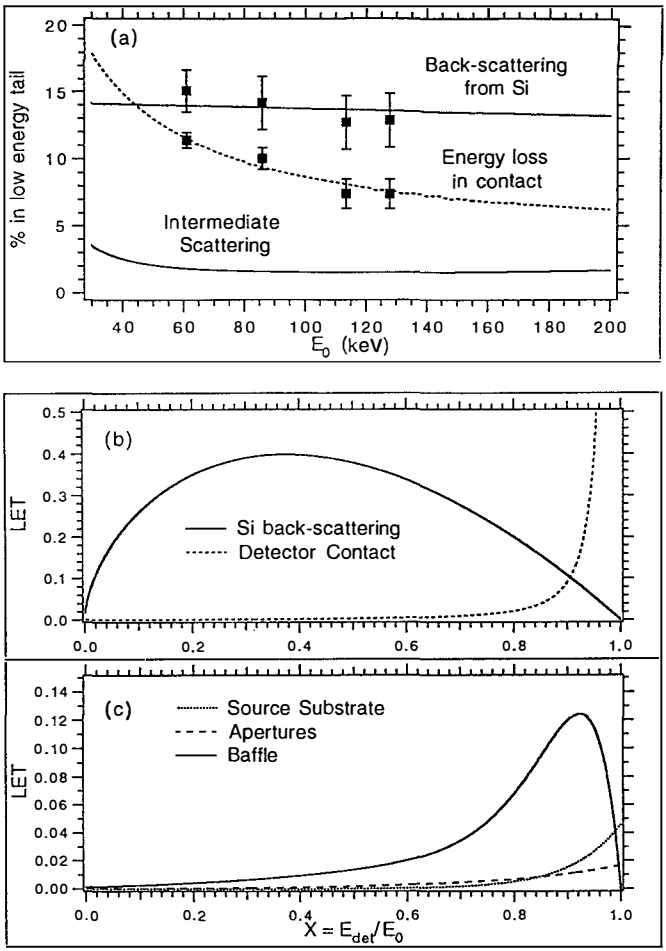

(Fig.3) (a) Energy dependent intensity for the various components of the electron response function appropriate for the Oxford geometry. (b) Low energy tails associated with energy loss and back-scattering effects. (c) Contribution to the low energy tail arising from intermediate scattering effects. The inclusion of intermediate scattering effects is sufficient to suppress the distortions that were previously interpreted as evidence for heavy neutrino emission (see ref.20 for details).

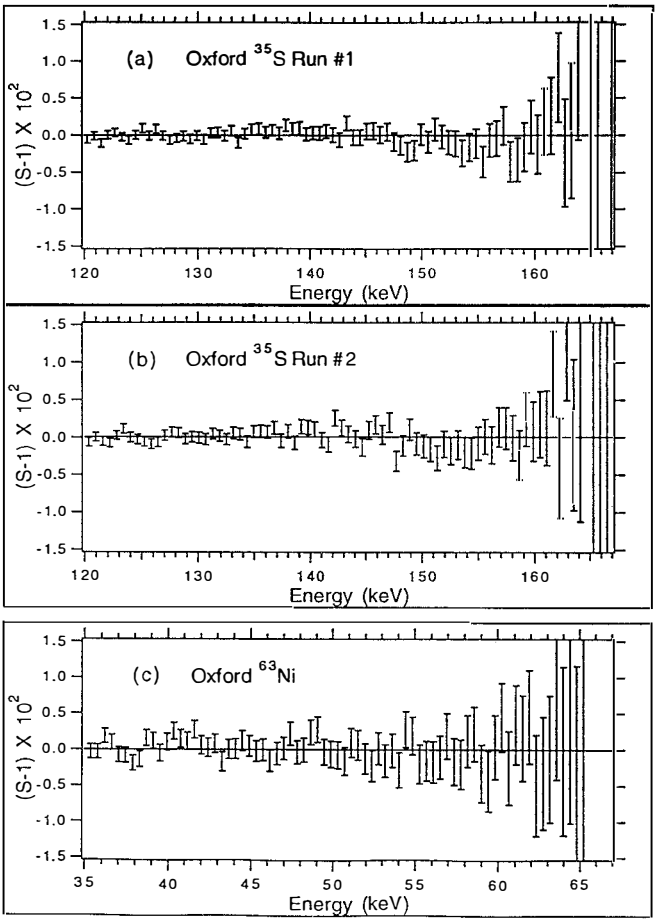

(Fig.4) Residuals obtained from Oxford (a) ^{35}S Run-1, (b) ^{35}S Run-2, and (c) ^{63}Ni data when accounting for intermediate electron scattering effects and assuming a single-component, massless neutrino. Despite the (apparent?) deviation around 150 keV in the ^{35}S shape factors a chi-squared analysis indicates as good a fit as that obtained without intermediate scattering effects but assuming a 17-keV neutrino. Details regarding reanalysis of the Oxford data are presented in (ref.20).

IBEC MEASUREMENTS

The process of inner bremsstrahlung accompanying electron capture (IBEC) offers an alternative means by which one can search for heavy neutrinos. Here, a photon shares phase space with the neutrino in much the same way as does the electron with an (anti)neutrino in β^- decay. While the theoretical (IBEC) spectrum is not as well understood, experimental details make it difficult to achieve sensitivity to heavy neutrino admixtures at the 1% level. Due to the intrinsically low rates, rather large source volumes are required to obtain the desired statistics with the result that the system exhibits a complicated response function for photons.

Searches for a 17-keV neutrino in IBEC spectra have been made, albeit with less definite conclusions. The positive result proclaimed by the Zagreb group[21] using ^{71}Ge lacks the statistics to be convincing. While earlier studies[22] of the ^{55}Fe spectrum failed to find evidence for a 17-keV neutrino, a group at LBL reported[23] an anomaly consistent with the emission of a 22-keV neutrino. Furthermore, a measurement of the ^{71}Ge spectrum at the TANDAR laboratory in Argentina[24] found, not a 17-keV neutrino but an anomaly prescribed by a 14-keV mass eigenstate! While the discrepancy amongst these measurements calls into question their sensitivity, it is a clear indication that fortuitous results can arise when systematics are not completely understood. This point is substantiated in the recent work by the group at Argentina[25], where a more detailed analysis of instrumental response and uncertainties associated with p-wave capture in ^{71}Ge decay leads to an upper limit of 0.5% on the mixing probability for a 17-keV neutrino.

The most convincing IBEC result comes from a recent study[26] of the ^{55}Fe spectrum at LBL. Despite a branching fraction of $\sim 3.3 \times 10^{-5}$, some 1.1×10^7 counts/keV have been accumulated in the region of the expected kink. A qualitative analysis of the second derivative of the spectrum, which shows a clear deviation for a 17-keV neutrino in a Monte Carlo analysis, is flat in the data. A detailed analysis over a narrow region in the data excludes a 0.8% admixture of a 17-keV neutrino at the 7 standard deviation level.

SUMMARY AND CONCLUSIONS

The search for heavy neutrino admixtures at or below the 1% level has proven a most ambitious task, and the problems associated with any of the experiments discussed are dominated by systematic effects. It remains a remarkable coincidence that many different experiments found consistent evidence for the same effect. Is this agreement merely fortuitous? It is clear that recent null experiments can definitively rule out the presence of a 17-keV neutrino, and that criticisms applicable to earlier results have been circumvented. Given the nature and diversity amongst the "positive" experiments a different explanation is required in each case.

The anomalies observed in ^{35}S and ^{63}Ni measurements at Oxford have been reinterpreted in terms of electron scattering effects. On the other hand, the calorimetric measurements employing tritiated solid state detectors and ^{14}C doped germanium do not suffer from such effects. While the LBL group continue to pursue systematics in their ^{14}C experiment, their recent study of the ^{55}Fe IBEC spectrum strongly disfavours the presence of a 17-keV neutrino. Indeed, recent developments show that the previous confusion amongst the various IBEC measurements can be understood in terms of systematic effects.

The low energy region of the tritium spectrum remains intriguing. At this meeting Stoeffl presented results from an "end-to-end" measurement of the spectrum using gaseous T_2 in the Livermore toroidal spectrometer. The low energy region shows a large excess beyond the conventional shape which possibly points to atomic physics not yet realized. It is by no means clear that the Livermore and Guelph tritium experiments measure the same phenomena. It is worthwhile to contemplate whether or not the low energy observations teach us anything about the spectrum near the endpoint. In particular, is there some atomic physics left out in the analysis of the tritium endpoint which might influence our present knowledge of neutrino mass and/or the interpretation of "negative" M_ν^2 values[27]?

REFERENCES

[1] J.J. Simpson, Phys. Rev. Lett. **54**, 1891 (1985).

[2] W. Haxton, Phys. Rev. Lett. **55**, 807 (1985); E.G. Drukarev and M.I. Strikman, Sov. Phys. JETP **64**, 686 (1986); B. Eman and D. Tadic, Phys. Rev. C**33**, 2128 (1986); J. Lindhard and P.G. Hansen, Phys. Rev. Lett. **57**, 965 (1986).

[3] T. Altzitzoglou *et al.*, Phys. Rev. Lett. **55**, 799 (1985); A. Apalikov *et al.*, JETP Lett. **42**, 289 (1985); J. Markey and F. Boehm, Phys. Rev. C **32**, 2215 (1985); T. Ohi *et al.*, Phys. Lett. **B160**, 322 (1985); V.M. Datar *et al.*, Nature (London) **318**, 547 (1985).

[4] D.W. Hetherington *et al.*, Phys. Rev. C **36**, 1504 (1987).

[5] J.J. Simpson, in *Massive Neutrinos in Particle Physics and Astrophysics*, VI'th Moriond Workshop, Tignes, France (1986).

[6] S. Weisnagel and J. Law, Can. J. Phys. **67**, 904 (1989).

[7] A. Hime and J.J. Simpson, Phys. Rev. D **39**, 1837 (1989).

[8] J.J. Simpson and A. Hime, Phys. Rev. D **39**, 1825 (1989).

[9] A. Hime and N. A. Jelley, Phys. Lett. B **257**, 441 (1991).

[10] A. Hime, D.Phil Thesis, Oxford (1991); Oxford preprint OUNP-91-20.

[11] A. Hime and N.A. Jelley, Oxford preprint OUNP-91-21.

[12] B. Sur *et al.*, Phys. Rev. Lett. **66**, 2444 (1991).

[13] A.Hime, in *Results and Perspectives in Particle Physics*, proceedings of the VI'th Rencontres de Physique de la Vallee D'Aoste, La Thuile, Italy, March 3-9 (1991); B.A. Logan and A. Ljubicic, Mod. Phys. Lett. A **6**, 3283 (1991); A. Hime, Mod. Phys. Lett. A **7**, 1301 (1992); J. Jaros, in *Triste Workshop on the Search for New Elementary Particles*, Triste, Italy, May 20-22 (1992); A. Hime, in *Neutrino 92*, XV'th International Conference on Neutrino Physics and Astrophysics, Granada, Spain, June 7-12 (1992).

[14] Giovanni Bonvicini, *Statistical Issues in the 17-keV Neutrino Experiments*, to appear in Z. Phys. C.

[15] H. Kawakami *et al.*, Phys. Lett. B **287**, 45 (1992); T. Ohshima, XXVI'th International Conference on High Energy Physics, Dallas, Texas, USA, August 6-12 (1992).

[16] M. Chen *et al.*, CalTech preprint, CALT-63-638; F. Boehm, in *Neutrino 92*, XV'th International Conference on Neutrino Physics and Astrophysics, Granada, Spain, June 7-12 (1992).

[17] G.E. Berman, M.L. Pitt, F.P. Calaprice, and M.M. Lowry, submitted to Phys. Rev. Lett.

[18] J.L. Mortara *et al.*, Phys. Rev. Lett. **70**, 394 (1992); see also S.J. Freedman in these proceedings.

[19] L. Piilonen and A. Abashian, in *Massive Neutrinos and Tests of Fundamental Symmetries*, XII'th Moriond Workshop, Les Arcs, Savoie-France, Jan. 25 - Feb.1 (1992).

[20] A. Hime, Phys. Lett B **299**, 165 (1993).

[21] I. Zlimen *et al.*, Phys. Rev. Lett. **67**, 560 (1991).

[22] I. Zlimen *et al.*, Physica Scripta **38**, 539 (1988); Fizika **22 (2)**, 423 (1990).

[23] E.B. Norman *et al.*, 14'th Conference on Nuclear Physics, Bratislava, Czechoslovakia, Oct. 20-28 (1990).

[24] D.E. DiGregorio *et al.*, TANDAR preprint, LNY584-L1-SB.

[25] D.E. DiGregorio *et al.*, TANDAR preprint, submitted to Phys. Rev. Lett.

[26] E.B. Norman *et al.*, in XXVI'th International Conference on High Energy Physics, Dallas, Texas, USA, August 6-12 (1992); F.E. Wietfeldt *et al.*, LBL preprint, submitted to Phys. Rev. Lett.

[27] For a recent discussion of measurements at the tritium endpoint see R.G.H. Robertson, in XXVI'th International Conference on High Energy Physics, Dallas, Texas, USA, August 6-12 (1992).

A LOSS-FREE MEASUREMENT OF THE BETA-SPECTRUM OF ^{35}S, AND THE ORIGIN OF THE 17 keV NEUTRINO SIGNALS

H. Abele[1], D. Dubbers[2], G. Helm[1], U. Kania[1], J. Last[3], C. Schmidt[1]
[1] Physikalisches Institut der Universität
Philosophenweg 12
D-6900 Heidelberg, Germany
[2]Fakultät für Physik der Technischen Universität München
[3]Institut Laue-Langevin, Grenoble

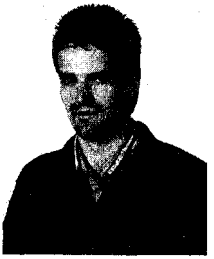

ABSTRACT

We present measurements of the ß-spectrum of ^{35}S, using two energy sensitive silicon detectors in a 4π configuration. A 7 Tesla magnetic field guides the electrons to the detectors. Electrons which are backscattered in one detector are counted in the other detector. No baffles or collimators are needed. In the sum spectra all effects due to electron backscattering are eliminated. No evidence for heavy neutrinos is observed.
When we remove the backscattering suppression, the data show a deviation from the usual electron spectrum that could be misinterpreted as an admixture of a heavy neutrino.

For several years there have been claims that a ≈ 1% admixture of a neutrino of 17 keV mass was seen in the decay spectra of ^{3}H, ^{14}C, ^{35}S, ^{55}Fe, ^{63}Ni and ^{71}Ge, all measured with solid state detectors made of silicon or germanium. No such effects, however, were seen when the beta spectra were measured with magnetic electron spectrometers[1]. The aim of the present experiment was to attack the 17keV neutrino problem with a method of loss-free electron spectroscopy which originally had been developed for the study of free neutron beta decay[4]. This method is very effective for suppressing the loss mechanisms which usually plague electron spectroscopy. A second aim of the experiment was to artificially produce "heavy neutrino signals" by a deliberate deterioration of the experimental conditions, in order to trace possible sources of error in earlier measurements. We did the measurements with the source-detector combination which so far had shown the most pronounced heavy neutrino signals[2),3]. We focussed special attention to the following sources of systematic errors in electron spectroscopy: electrons lose energy due to self absorption both in the source material and in the source substrate; scattering of electrons may occur on their way to the detectors; there backscattering can cause electrons to leave the detector without depositing all of their energy. All these effects can distort the electron spectrum.

Our method avoids all of these difficulties:

- The source substrate is a 5μg/cm^2 (≈200 Å) ^{12}C-foil held by an aluminium ring of 16mm inner diameter. A 2mm diameter droplet of aequeous solution containing the carrier free source was dried onto the centre of the substrate. The energy loss in the source amounts to several electron volts and is negligible. This had been checked earlier with the high resolution magnetic electron spectrometer BILL of the Institute Laue-Langevin[5].
- The source is placed in the 7T magnetic field in the centre of a 0.3m long solenoidal superconducting magnet. The field guides all electrons to two high resolution silicon detectors placed at both ends of the solenoid. This avoids the use of electron baffels or collimators, and allows high resolution electron spectroscopy under a full solid angle of 4π.
- The main feature of our method is the complete suppression of the effects of backscattering on the detectors. An electron which backscatters from one detector is either reflected back onto the same detector by the magnetic mirror effect, or it will follow a magnetic field line and eventually hit the other detector. The total energy of an individual event is obtained by adding the signals from both detectors.

Fig 1. shows the experimental set-up and a graphic description of the backscattering suppression.

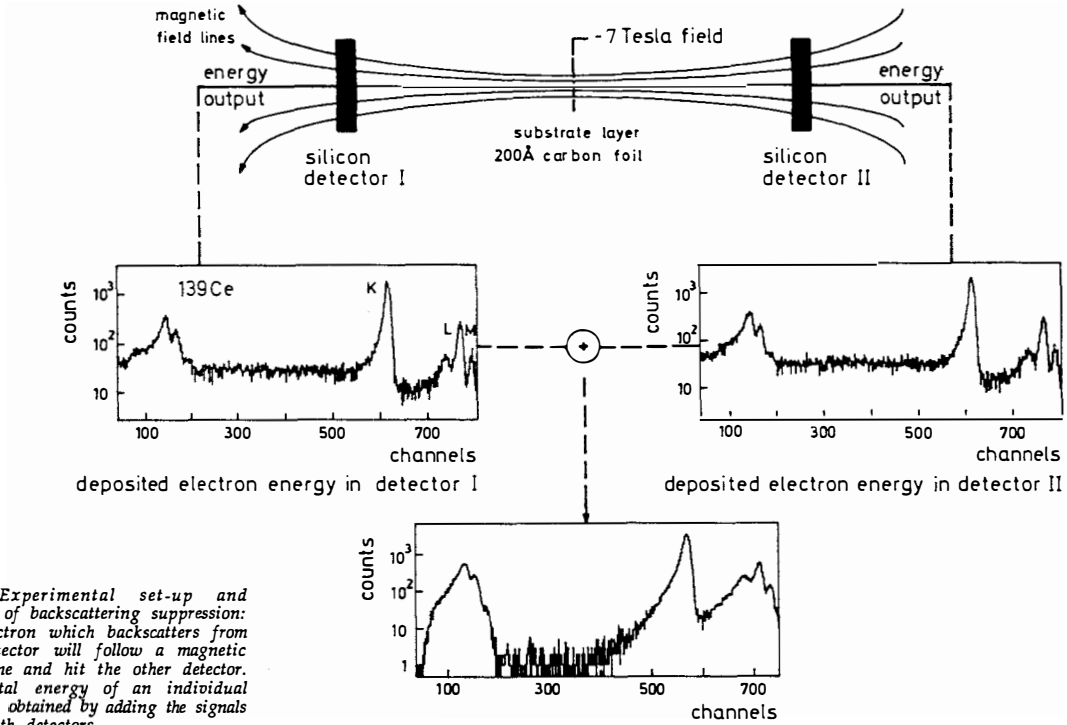

Fig. 1 Experimental set-up and method of backscattering suppression: An electron which backscatters from one detector will follow a magnetic field line and hit the other detector. The total energy of an individual event is obtained by adding the signals from both detectors.

A related method of partial suppression of backscatter events is described by Freedman (these procedings and ref.[6]).

The electronics consist of a NIM system with a CAMAC interface to a personal computer. Each detector has an analogue and a logic channel. Canberra 2001 preamplifiers and Ortec 572 main amplifiers for unipolar shape were used. The analogous detector signals are summed with an Ortec 533 module. A Silena 4418 V-sensing 8 fold ADC stores the sum spectra as well as the spectra from the individual detectors. Measurements were made with and without the use of an electronic pileup reject. In order to keep the pileup rate low, beta activities of 1200/s and 800/s were used and in addition the shaping time was chosen to 1μs.

The spectrometer was calibrated with conversion electron sources ^{109}C d ($E\gamma$=88.03keV), ^{139}Ce ($E\gamma$=165.85), ^{57}Co ($E\gamma$=14.41, 122.06, 136.47) and ^{114}In(m) ($E\gamma$=190.27). The sources are installed near the centre of the spectrometer and are, during beta data collection, hidden behind lead shields, with no direct line of sight from the sources to the detectors. For calibration measurements the sources are moved remotely into the direct line of sight of the detectors. Since the spectrometer has 4π acceptance, Auger electrons often arrive in coincidence with the conversion electrons resulting in additional peaks. The detector response function was derived from the ^{139}Ce and the ^{114}In(m) K conversion lines. It is well described by a gaussian plus a low energy exponential tail due to bremsstrahlung losses in the detector.

For the theoretical description of the ^{35}S ß-spectrum we assume that the electron neutrino is a linear combination of the massless electron antineutrino and a second branch of mass M. As a consequence of an incoherent superposition of two beta spectra the effect of this neutrino mixing results in an observable kink .

The unscreened Fermi function is from Behrens and Bühring[7]. The ratio of the unscreened to screened Fermifunction was provided by Bühring[8], the radiative correction and the shape function are in accordance with Sirlin[9] and Calaprice[10], respectively.

We did measurements of the beta-spectrum of ^{35}S. The data indicate no deviation from the usual spectrum with massless neutrinos. The contour plot of Fig. 2 traces contour lines with respect to the two parameters neutrino mass and neutrino mixing. It was based on a fit in the energy range between 130keV and 157keV. Contour lines are drawn, with the number of standard deviations for each parameter. Our measurements are in full agreement with the theory for massless neutrinos, and the hypothesis of a massive neutrino is excluded with high probability.

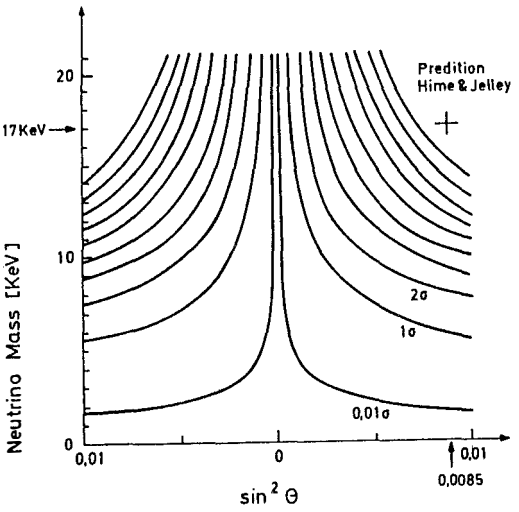

Fig. 2 Contour plot with respect to neutrino mass and neutrino mixing. The contour lines show the deviation in numbers of sigma. The prediction of a heavy neutrino (+) is excluded with high probability.

However, care must be taken when interpreting errors for fits with more than one free parameter: The exclusion region in a four dimensional parameterspace (normalization, end energy, neutrino mass and mixing) becomes less restrictive than suggested by exclusion plots like that of fig. 2; in this case a 17keV neutrino and mixing above 0.35% are excluded with 95%C.L..

Alternatively, our beta spectra can well be described by a polynomial of third order in the energy range of interest. In case of a 17keV neutrino the data should show a sudden change in slope at 150keV. This method was applied to a high statistics measurement on the same system. A polynomial was fitted to a 5keV wide energy band above 150keV. Then the shape with a hypothetical massive neutrino branch was fitted to a 5keV band below 150keV. The only free parameter then is the amount of neutrino mixing and was found to be < 0.13% (95% C.L.). For this second measurement data evaluation is not yet finished. This approach avoids uncertainties associated with the determination of the detector function, the underlaying pile up spectrum and theoretical description. A similar method was already used by Schreckenbach[11].

To study the possible effects of electron scattering in earlier experiments we purposely removed the backscattering suppression in our setup (fig. 1). Fig. 3 shows two spectra: the beta spectrum measured with detector one, and the beta spectrum from the electrons backscattered on detector one and detected in detector two. In a simple source-detector set-up, as used in earlier experiments without a magnetic guide field, both spectra will be superimposed in one detector simultaneously. The spectrum with the higher count rate represents the energy spectrum of electrons which hit the detector directly, the other one corresponds to a spectrum of electrons which scatter on their way to the detector.

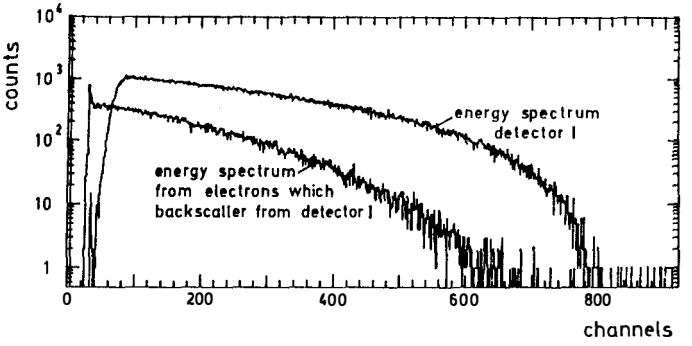

Fig. 3 Production of a heavy neutrino as an artefact

The sum of both spectra causes a signature similar to that of a heavy neutrino branch. In our case the size of the effect depends on the detector material. A fit to the data, taken with a gold window detector (window thickness ≈ 1800Å eq. Si), shows evidence for an artificial heavy neutrino with 60keV mass and a mixing of about 15% (Fig. 4). This large mixing can be explained by the fact that all backscattered electrons contribute. In case of aluminium windows (thickness < 500Å eq. Si), a 30keV neutrino was simulated with a mixing of only 0.9%.

To sum up, we find no evidence for a 17keV neutrino. We have demonstrated, that distortions in the ß-spectrum seen in several experiments could be based on scattering effects. These distortions could be misinterpreted as an admixture of a heavy neutrino.

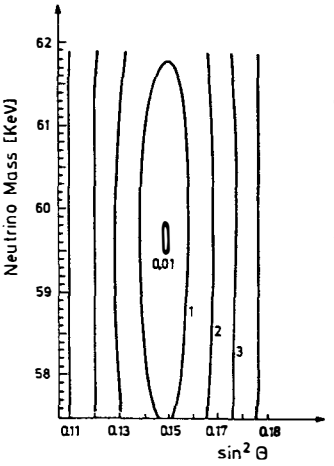

Fig. 4 Contour plot of best fit to an artificial heavy neutrino spectrum (silicon detectors with gold entrance windows)

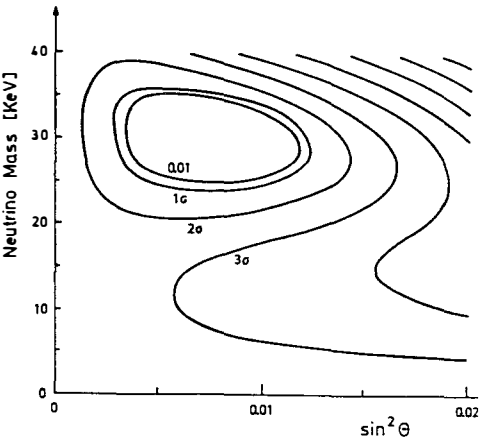

Fig. 5 Contour plot of best fit to an artificial heavy neutrino spectrum (silicon detectors with aluminium entrance windows)

References

1. a review of 17-keV experiments can be found in M. Bahran and G. R. Kalbfleisch, Phys. Rev. D **47** R754 (1993).
2. J.J Simpson and A. Hime, Phys. Rev. D **39**,1825 (1989).
3. A. Hime and N.A. Jelley, Phys. Lett. B **257** 441 (1991).
4. P. Bopp et al., Nucl. Instr. and Meth. A **267** 436 (1988).
5. J. Döhner et al., Nucl. Instr. and Meth. A **284** 123 (1989).
6. J. L. Mortara et al., Phys. Rev. Lett. **70** 394 (1993).
7. H. Behrens and W. Bühring, *Electron Radial Wave Functions and Nuclear Beta-decay* (Clarendon, Oxford, 1982).
8. W. Bühring, Nucl. Phys. A **430** 1 (1984) and private communication.
9. A. Sirlin, Phys. Rev. **164** 1767 (1969).
10. F. P. Calaprice and D. J. Millener, Phys. Rev. C **27** 1175 (1983).
11. K. Schreckenbach et al., Phys. Lett. B **129** 265 (1983).

Search for the 17 keV Neutrino with a High Resolution Magnetic Spectrometer

E. Holzschuh and W. Kündig
Physik-Institut der Universität Zürich, CH-8001 Zürich

A search for the 17 keV neutrino has been performed by measuring the β-spectrum of ^{63}Ni with a high resolution magnetic spectrometer. No indication for a nonzero mixing probability $|U_{ex}|^2$ of a heavy neutrino with a mass m_ν in the range 12 to 22 keV was found. The data show a high degree of internal consistency and, for $m_\nu = 17$ keV, the result, $|U_{ex}|^2 = (0.37 \pm 0.55) \times 10^{-3}$, is compabible with zero within statistics. We conclude that the 17 keV neutrino does not exist with the parameters claimed by several other groups, and thus most likely, does not exist at all.

1. Introduction

One distinctive feature in the long story of the 17 keV neutrino is that all positive results were obtained with solid-state detector spectrometers, whereas measurements with magnetic spectrometers (and several with solid-state detectors) gave only null results (for reviews see [1,2]). So far, nobody has found a consistent, physical explanation for this discrepancy, but we may note one difference between the two types of experiments: a much better energy resolution is possible with magnetic spectrometers than is with solid-state detectors and resolution helps to preserve spectral features.

In fact the admixture of a heavy neutrino with mass m_ν has a quite unique signature in a β-spectrum. Theoretically one expects a singularity of the slope (a 'kink') at an energy $E_0 - m_\nu$ in an otherwise smooth spectrum (E_0 is the endpoint energy). Thus, given enough statistical precision of the data and sufficient energy resolution of the spectrometer, it should be possible to distinguish between a heavy neutrino and other spectrum distortions caused by experimental effects.

In the investigation presented in this paper, we tried to utilize this idea. The magnetic spectrometer, previously used to investigate the tritium endpoint region [3], has a resolution of 17 eV (FWHM), which is quite sufficient to preserve the signature of a 17 keV neutrino. The spectrometer also has high luminosity, which allowed us to take high statistics data. However, with the given setup, it was not possible to avoid backscattering from the solid source. This effect caused a spectrum distortion, which is smooth, but its precise shape could not be determined independently. To cope with this problem, we have taken much more data than would have been necessary otherwise. These extra data allowed us to fit also the shape of the backscattered spectrum and to make a couple of consistency tests.

2. Experimental procedure

The same spectrometer and basically the same procedure as in ref. [3] were used; i.e. the β-spectrum was recorded by stepping a positive high voltage applied to the source while the magnetic field of the spectrometer was kept constant to focus 2.2 keV electrons onto the detector. A new high-voltage supply and a new voltage divider for voltages up to 70 kV were used. The divider was calibrated with an uncertainty of about 10^{-4}.

The ^{63}Ni source was made by vacuum evaporation of metallic nickel. The support was a thick Kapton foil (low Z), with a 100 Å conducting Al layer. The thickness of the nickel layer was 60 Å and had a specific activity of 0.076 mCi/cm^2.

Two runs were performed, a main run A and a second run B. In A, the energy range was divided into four intervals (30 – 45 – 55 – 66.5 – 67.9 keV) and the counting times (2, 5, 3, 10 s/step) were chosen to improve statistics around the energy where the kink of a 17 keV neutrino should show up. The spectrum was scanned in 20 eV steps and a total of 475 interlaced up-down sweeps was accumulated. The raw data of A contain 1894 points and are plotted in figure 1. The energy range of run B was 65.55 – 67.25 keV, scanned in 5 eV steps. It is generally a good test for unaccounted spectrum distortions, to compare the E_0, fitted to data with a large energy range ΔE (as from run A with $\Delta E = 37$ keV), with what one finds from data extending only a small range below E_0 (as run B with $\Delta E = 1.3$ keV). The data of B were only used for such a test.

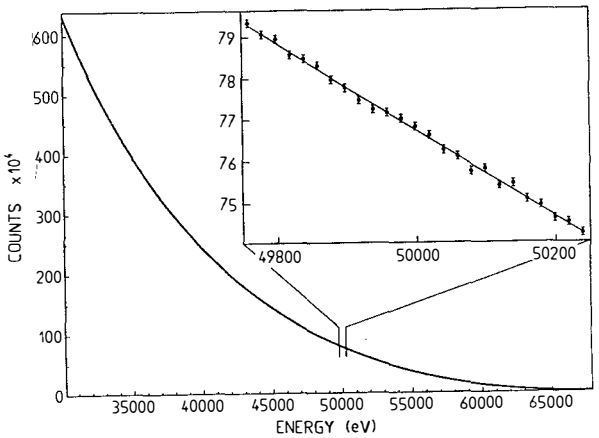

Figure 1: Measured spectrum of ^{63}Ni, scaled for equal counting time along with the best fit. Inset shows part of the data on an expanded scale.

3. Data analysis and results

The model function for the data fit was based on the usual allowed β-spectrum with neutrino mixing and including radiative corrections, etc. This theoretical function was multiplied by the energy dependent solid angle accepted at the source ($S(E)$) and then folded with the spectrometer resolution function and the distributions due to energy loss in the source layer and the excitation of final electronic states. The effect of backscattering from the source and a possible, but much smaller uncertainty of $S(E)$, are smooth functions of energy and were taken into account by a polynomial factor of the form

$$1 + \alpha_1\epsilon + \alpha_2\epsilon^2 + \cdots, \text{ with } \epsilon = E_0 - E.$$

The free parameters of the fit were a spectrum normalization A, endpoint energy E_0, background B, the mixing probability $|U_{ex}|^2$, and the coefficients α_i. The mass of the light neutrino component was set to zero and as no indication for a heavy neutrino was found, its mass m_ν was varied stepwise.

The fitted $|U_{ex}|^2$ is plotted in figure 2 and is compatible with zero. Here, a fourth order

Table 1: Fitted results for assumed orders of the polynomial factor and $m_\nu = 17$ keV.

Order	$\lvert U_{ex}\rvert^2$ (10^{-3})	$E_0 - 66900$ (eV)	χ^2/DOF
2	-1.39 ± 0.39	4.8 ± 3.0	2717 / 1888
3	1.19 ± 0.40	74.8 ± 4.1	1955 / 1887
4	0.37 ± 0.55	65.5 ± 5.9	1951 / 1886
5	0.36 ± 0.55	73.7 ± 7.8	1949 / 1885

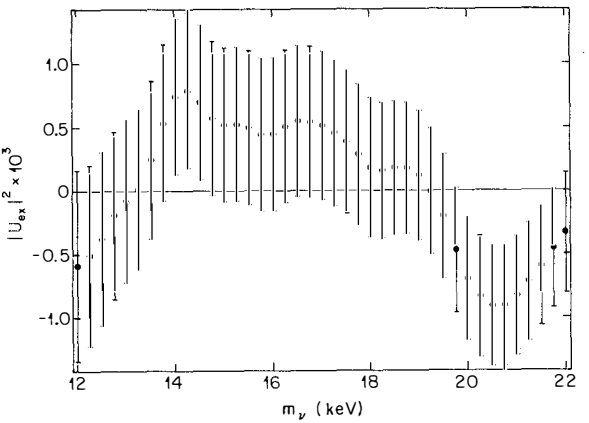

Figure 2: Fitted mixing parameter as a function of an assumed neutrino mass

polynomial was assumed. For $m_\nu = 17\,\mathrm{keV}$, the result is

$$|U_{ex}|^2 = (0.37 \pm 0.55) \times 10^{-3}\,.$$

The residuals of the fit, assuming $|U_{ex}|^2 = 0$ or $|U_{ex}|^2 = 0.0085$ as found by Hime and Jelly [4], are compared in figure 3. The latter hypothesis gave a poor fit and can clearly be ruled out.

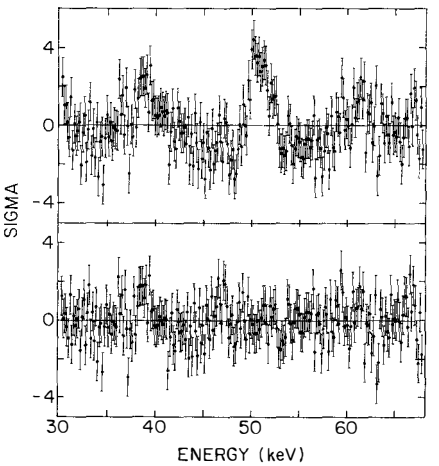

Figure 3: Difference of data and fit divided by the standard deviation, assuming $|U_{ex}|^2 = 0.0085$ (top) or 0 (bottom). For this plot 9 points were added together.

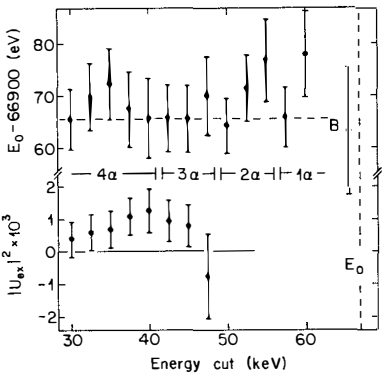

Figure 4: Fitted parameters when the data points below the energy E_{cut} are excluded ($m_\nu = 17\,\text{keV}$). The number of actually fitted α-parameters is indicated. The result of run B is also plotted.

The results as a function of the assumed order of the polynomial factor are given in table 1. With a second order polynomial the fit is bad, however no significant differences result for fourth or fifth order. Hence we take the fourth order as adequate. This conclusion was further tested by excluding the data below an energy E_{cut}. The results are plotted in figure 4 and are, within statistics, independent of E_{cut} (as it should be). For smaller energy ranges, the higher order coefficients (α_i) become indeterminate and have been fixed at their values for the full range. No significant difference results, when they are set to zero instead. The fitted E_0 is stable over the whole energy range and agrees with the value determined from run B. Hence we can conclude that the assumed model is adequate for our data.

The effect of energy loss [5,6] in the source layer and of the excitation of electronic final states [7,8] has also been investigated (see table 2) and were found to cause differences of only about 10^{-4} for $|U_{ex}|^2$. This is smaller than one would naively expect. A likely explanation is that these effects cause smooth spectrum distortions which are taken care of by the polynomial factor. The average energy loss in the source is 11 eV at 50 keV. Comparatively more important is the average excitation energy, computed in ref. [8] to be 85 eV with respect to the electronic groundstate. Our endpoint E_0 agrees with previous results [9,10] if we note that these groups did not take into account the final states.

Table 2: Fitted results when corrections for energy loss (EL), electronic final states (FS), both or none are included in the fit (DOF = 1886).

Correction	$\lvert U_{ex}\rvert^2$ (10^{-3})	$E_0 - 66900$ (eV)	χ^2
None	0.51 ± 0.55	25.8 ± 5.9	1955
EL	0.50 ± 0.55	33.2 ± 5.9	1954
FS	0.37 ± 0.55	57.8 ± 5.9	1951
Both	0.37 ± 0.55	65.5 ± 5.9	1951

To conclude, no indication for the existence of the 17 keV neutrino was found. All consistency tests performed gave null results. A mixing probability of $|U_{ex}|^2 = 0.0085$ would be a 15 σ effect in our data and is completely ruled.

We acknowledge the support by the Paul Scherrer Institut and by the Swiss National Science Foundation.

References

[1] D.R.O. Morrison, Proc. 12th Moriond Workshop (Les Arcs, 1992), ed. G. Chardin *et al.* (Gif sur Yvette, France: Editions Frontieres) p 207.

[2] E. Holzschuh, Rep. Prog. Phys. 55, 1035 (1992).

[3] E. Holzschuh, M. Fritschi and W. Kündig, Phys. Lett. B 287, 381 (1992).

[4] A. Hime and N.A. Jelly, Phys. Lett. B 257, 441 (1991).

[5] M.J. Berger and S.M. Seltzer, ICRU Report 37 (1984).

[6] R.F. Egerton, Electron energy-loss spectroscopy in the electron microscope, Plenum Press (1986).

[7] T.A. Carlson *et al.*, Phys. Rev. 169, 27 (1968).

[8] M.R. Harston and N.C. Pyper, J. Phys. B 17, L839 (1984).

[9] D.W. Hetherington *et al.*, Phys. Rev. C 36, 1504 (1987).

[10] H. Kawakami *et al.*, Phys. Lett. B 287, 45 1992).

ATOMIC/OPTICAL PHYSICS

LARGE, SMALL AND SUPERFICIAL VIOLATIONS OF THE PAULI EXCLUSION PRINCIPLE AND THE SIZE OF THE ELECTRON

Eckehart Nolte
Faculty of Physics, Technical University of Munich,
W-8046 Garching, Germany

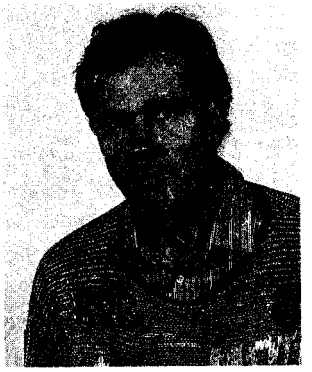

ABSTRACT

With the help of accelerator mass spectrometry, very small upper limits for concentrations of non-Paulian atoms and nuclei have been obtained. These results are discussed in terms of small and superficial violations of the Pauli exclusion principle. Small upper limits for the probabilities of having two electrons, protons or neutrons in the symmetric state with respect to exchange are deduced. For the hypothetical case of a composite electron, the upper limit for the radius of the electron is derived to be smaller than $4 \cdot 10^{-20}$ m.

In nature, only two statistical types of particles are observed : fermions and bosons. Fermions are particles with half-integer spin values, bosons have integer spin. Ensembles of identical fermions are described by a wave function which is completely antisymmetric with respect to exchange of two particles and ensembles of identical bosons are described by a wave function which is completely symmetric with respect to exchange. The resulting statistics are called Fermi-Dirac statistics and Bose-Einstein statistics, relatively. From the completely antisymmetric wave function it is immediately derived that one state cannot be occupied by more than one fermion. This fact is called Pauli exclusion principle (PEP). It was formulated in 1925 by Wolfgang Pauli in order to explain the structure of atoms and the regularities of the periodic table of elements. So far, no violations of PEP are observed.

If we consider hypothetical violations of PEP we have to distinguish the type of violation. One distinguishes three types of violations of PEP : large violations, small violations and superficial violations.

1. LARGE VIOLATIONS OF PEP

Though in nature only two types of statistics, Fermi-Dirac and Bose-Einstein statistics, are observed, quantum mechanics offers equivalently also intermediate statistics called parastatistics, in more detail para-Fermi and para-Bose statistics. The method of field quantization for parastatistics is described e.g. in [1]. For identical para-fermions of order p, up to p para-fermions can occupy one state. Such para-fermions would show large violations of PEP. If we consider for example quarks, these particles can be seen equivalently as para-fermions of order three without colour or as ordinary fermions after introduction of three colours. So, at least in some cases, para-statistics can be reduced to Fermi-Dirac or Bose-Einstein statistics by introduction of a suitable number of degrees of freedom.

2. SMALL VIOLATIONS OF PEP

In quantum mechanics, particle identity makes it impossible to test PEP by looking for forbidden X or γ rays deexciting a state with Fermi-Dirac statistics to a state with a small violation of PEP [2]. A violation of PEP would mean that the wave function of an ensemble of identical particles with half-integer spin is not completely antisymmetric with respect to exchange. Then, ensembles can be found where two such particles occupy the same state.

Our experiments are performed in that way that we look for atoms with three electrons in the K shell and for nuclei with three protons or three neutrons in the nuclear $1s_{1/2}$ shell [3–5]. The detection method is accelerator mass spectrometry (AMS) either with completely stripped ions [6] or with a time-of-flight set-up [7].

Fig. 1 shows the electronic configurations of Paulian Ne (Ar) and F (Cl) and of non-Paulian $\widetilde{Ne}$ ($\widetilde{Ar}$) with three electrons in the K shell.

Since the outer electrons determine the chemical behaviour of elements, non-Paulian $\widetilde{Ne}$ ($\widetilde{Ar}$) with 7 electrons in the L (M) shell and Paulian F (Cl) with the same number of electrons in the L (M) shell are expected to be chemically identical. Our method is to look very sensitively with AMS for non-Paulian $\widetilde{Ne}$ ($\widetilde{Ar}$) atoms in natural F (Cl) samples.

Fig. 2 shows the nuclear configurations for the particle unstable nuclei ^{5}Li and ^{5}He and for non-Paulian nuclei $^{\widetilde{5}}\widetilde{Li}$ and $^{\widetilde{5}}\widetilde{He}$ with

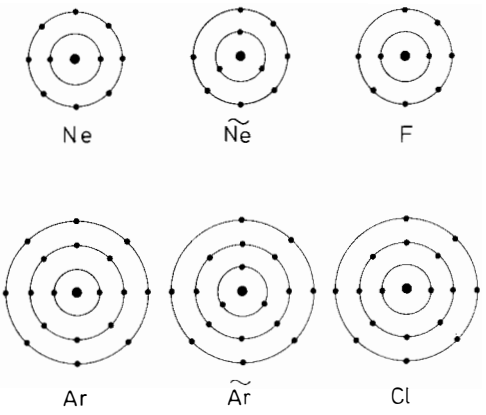

Fig.1: Configurations of atomic electrons for F, Ne and non-Paulian $\widetilde{Ne}$ and for Cl, Ar and non-Paulian $\widetilde{Ar}$

three protons and three neutrons, respectively, in the nuclear $1s_{1/2}$ shell. In samples of natural Li and isotopically enriched ^{6}Li (95.5 %) and of atmospheric He contained in raw neon, non-Paulian nuclei of $^{\widetilde{5}}\widetilde{Li}$ and of $^{\widetilde{5}}\widetilde{He}$ were searched. No events of non-Paulian atoms or nuclei were observed. The spectra were free of background. The obtained experimental limits were [3-5] for non-Paulian atoms:

$$N(^{20}\widetilde{Ne})/N(F) < 6 \cdot 10^{-18} \text{ or } N(^{20}\widetilde{Ne})/N(^{20}Ne) < 2 \cdot 10^{-21} ,$$

$$N(^{36}\widetilde{Ar})/N(Cl) < 8 \cdot 10^{-16} \text{ or } N(^{36}\widetilde{Ar})/N(^{36}Ar) < 4 \cdot 10^{-17}$$

and for non-Paulian nuclei:

$$N(^{\widetilde{5}}\widetilde{Li})/N(^6Li) < 8 \cdot 10^{-18} \text{ and } N(^{\widetilde{5}}\widetilde{He})/N(^4He) < 2 \cdot 10^{-15}$$

for binding energies of $^{\widetilde{5}}\widetilde{Li}$ and $^{\widetilde{5}}\widetilde{He}$ up to 50 and 32 MeV, respectively.

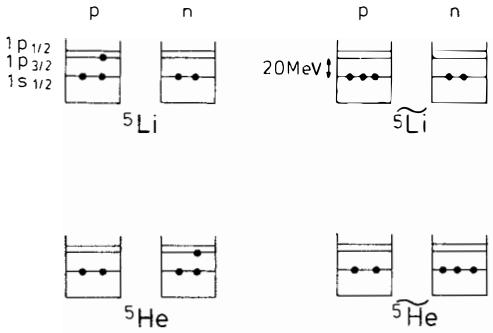

Fig. 2: Configurations of nucleons for ^{5}Li and non-Paulian $\widetilde{^5\text{Li}}$ and for ^{5}He and non-Paulian $\widetilde{^5\text{He}}$

Since transitions from states with Fermi-Dirac statistics to states with a small violation of PEP are strictly forbidden [2], in the interpretation of our data we consider ensembles where PEP is violated from the beginning. The parameter describing the violation is the probability $\beta^2/2$ of having two identical fermions in the symmetric state. A similar consideration was performed by Ramberg and Snow [8] who looked for anomalous X-rays in current carrying copper and who obtained $\beta^2/2 < 2 \cdot 10^{-26}$ for electrons. We deduce limits for $\beta^2/2$ for nucleons by considering β decays to non-Paulian nuclei and primordial nucleosynthesis.

In the β decay of ^{6}Li to $\widetilde{^6\text{Be}}$, the daughter nucleus $\widetilde{^6\text{Be}}$ is proton unstable and disintegrates to $\widetilde{^5\text{Li}}$ and ^{1}H (see Fig. 3). The number of produced $\widetilde{^5\text{Li}}$ nuclei is given by $N(\widetilde{^5\text{Li}}) = N(^6\text{Li}) \cdot \tilde{\lambda} \cdot t$, where $\tilde{\lambda} := \lambda \cdot \beta^2$ is the decay constant for β decay to non-Paulian nuclei, λ is the β decay constant ($\lambda^{-1} \approx 400$ s) and t is the time from the nucleosynthesis till today, $t \approx 10^{10}$ y. From this, we obtain $\beta^2/2 < 5 \cdot 10^{-33}$.

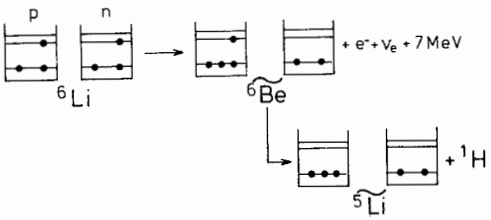

Fig. 3: β-decay of ^{6}Li to non-Paulian $\widetilde{^6\text{Be}}$ and disintegration of $\widetilde{^6\text{Be}}$ in $\widetilde{^5\text{Li}}$ and p

In the primordial nucleosynthesis, $\widetilde{^5Li}$ and $\widetilde{^5He}$ would be produced by the reactions [9]:

$$^2H \;\tilde{+}\; {}^1H \rightarrow \widetilde{^3He}$$

$$^2H \;\tilde{+}\; n \rightarrow \widetilde{^3H}$$

$$\widetilde{^3H} + {}^2H \rightarrow \widetilde{^4He} + n \;,\; {}^3H \;\tilde{+}\; {}^2H \rightarrow \widetilde{^4He} + n$$

$$\widetilde{^3He} + {}^2H \rightarrow \widetilde{^4He} + {}^1H \;,\; {}^3He \;\tilde{+}\; {}^2H \rightarrow \widetilde{^4He} + {}^1H$$

$$\widetilde{^4He} + {}^2H \rightarrow \widetilde{^5Li} + n \;,\; {}^4He \;\tilde{+}\; {}^2H \rightarrow \widetilde{^5Li} + n$$

$$\widetilde{^4He} + {}^2H \rightarrow \widetilde{^5He} + {}^1H \;,\; {}^4He \;\tilde{+}\; {}^2H \rightarrow \widetilde{^5He} + {}^1H$$

The symbol $\tilde{+}$ means that the two reacting protons or neutrons are in the symmetric state. From estimations of the reaction rates [9], the following limits of having two identical nucleons in the symmetric state are deduced: $\beta^2/2 < 2 \cdot 10^{-28}$ for protons and $\beta^2/2 < 3 \cdot 10^{-15}$ for neutrons. These values can be compared with the ones for conducting electrons ($\beta^2 < 2 \cdot 10^{-26}$ [8]) and for protons by considering hydrogen burning in the sun ($\beta^2/2 < 2 \cdot 10^{-15}$ [10]).

3. SUPERFICIAL VIOLATION OF PEP AND THE SIZE OF THE ELECTRON

In a recent publication, Akama et al. [11] pointed out that in case the electron is a composite particle made out of a fermion w and a Boson C (Fig. 4) PEP is violated superficially for electrons though it holds for the constituent fermion w and atomic transitions from states with Fermi-Dirac statistics to states with a small violation of PEP for electrons can occur.

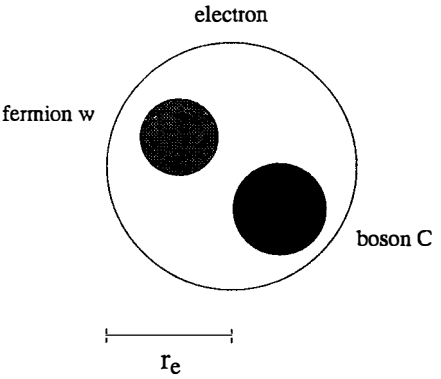

Fig. 4: The electron made hypothetically out of a fermion w and a boson C.

With the atomic number Z and the radius r_e of the electron, the decay constant $\tilde{\lambda}$ for such a transition compared to the normal electromagnetic decay constant λ_{em} is given by [11]:

$$\tilde{\lambda}/\lambda_{em} = 1.7 \cdot 10^{-50}(Z \cdot r_o[10^{-18}m])^6.$$

The non-Paulian atoms $\widetilde{Ne}$ and $\widetilde{Ar}$ would be produced according to

$$N(\widetilde{Ne}) = N(Ne) \cdot \tilde{\lambda} \cdot t \text{ and } N(\widetilde{Ar}) = N(Ar) \cdot \tilde{\lambda} \cdot t$$

where t is the average time from the nucleosynthesis till the formation of galaxies, $t \approx 4.5 \cdot 10^9$ y [3]. From this, we obtain $\tilde{\lambda}^{-1} > 2 \cdot 10^{30}$ y for Ne and $\tilde{\lambda}^{-1} > 4 \cdot 10^{27}$ for Ar [3]. From $\tilde{\lambda}/\lambda_{em} = \beta^2/2$ and with the life times λ_{em}^{-1} of 2.6 fs and 1.0 fs for a K hole in Ne and Ar, respectively, we obtain $\beta^2/2 < 4 \cdot 10^{-53}$ (Ne) and $\beta^2/2 < 8 \cdot 10^{-51}$ (Ar). With the above equation for r_e [11], the following limits for the radius r_e of the electron are deduced: $r_e < 4 \cdot 10^{-20}$ m (Ne) and $r_e < 5 \cdot 10^{-20}$ m (Ar). These results can be compared with limits for r_e in the range of 10^{-18} m obtained from (g - 2) experiments for electrons [12].

4. CONCLUSION

It has been shown that accelerator mass spectrometry is a very powerful tool to set sensitive limits on the validity of the Pauli exclusion principle and on the size of the electron.

REFERENCES

[1] H.S. Green, Phys.Rev.90 (1953) 270

[2] R.D. Amado and H. Primakoff, Phys.Rev.C 22 (1980) 1338

[3] E. Nolte, T. Faestermann, H. Gail, A. Gillitzer, G.Korschinek, D. Müller, R. Scheuer, V.M. Novikov, A.A. Pomansky, D. Miljanic, A. Ljubicic and B.A. Logan, Nucl. Instr. and Meth. B52 (1990) 563

[4] V.M. Novikov, A.A. Pomansky, T. Faestermann, H. Gail, A. Gillitzer, G. Korschinek, D. Müller, R. Scheuer and E. Nolte, Phys.Lett. B240 (1990) 227

[5] E. Nolte, T. Faestermann, A. Gillitzer, G. Korschinek, D. Müller, V.M. Novikov, A.A. Pomansky, A. Ljubicic and D. Miljanic, Z. Physik A340 (1991) 411

[6] P.W. Kubik, G. Korschinek and E. Nolte, Nucl.Instr.and Meth. B1 (1984) 51.

[7] D. Müller, T. Faestermann, A. Gillitzer, G. Korschinek, E. Nolte, R. Scheuer and U. Bittner, Nucl.Instr. and Meth. B52 (1990) 366

[8] E. Ramberg and G.A. Snow, Phys.Lett. B 238 (1990) 438

[9] M.H. Thoma and E. Nolte, Phys. Lett. B291 (1992) 484

[10] R. Plaga, Z.Physik A 333 (1989) 397

[11] K. Akama, H. Terazawa and M. Yasue, Phys.Rev.Lett. 68 (1992) 1826

[12] K. Akama, priv.comm. (1992)

LASER COOLING AND TRAPPING OF NEUTRAL ATOMS

Claude Cohen-Tannoudji
Collège de France et Laboratoire de Spectroscopie
Hertzienne de l'ENS(*), 24 rue Lhomond, 75231 Paris Cedex 05

ABSTRACT

An atom, put in quasiresonant light wave, absorbs and reemits the photons associated with this wave. The exchanges of energy and momentum, which result from these absorptions and emissions of photons by the atom, give rise to radiative forces, which act on the atom, and which allow one to control, with laser beams, its position and its velocity. A new research field, called laser cooling and trapping of atoms, has thus appeared during the last few years and is expanding very rapidly. The first part of the lecture presents a tutorial review of this field, and introduces the basic concepts. The reader is referred to the general references[1)-6)] given at the end of this abstract.

The second part of the lecture deals with two more recent developments dealing with the quantum nature of atomic motion. After a brief description of the so-called "Sisyphus cooling" scheme[1)4)5)], and of its quantum limits[7)8)], recent experiments are described giving evidence for a quantization of atomic motion in a light wave[9)-10)]. Extensions of these experiments to 2 and 3 dimensions have recently been performed, allowing one to bind atoms in regular 2-D or 3-D lattices[11)-13)]. The second development described in the lecture deals with the possibility of achieving a gravitational cavity for neutral atoms[14)]. Recent experimental observations of a multiple reflection of cold cesium atoms on a parabolic electromagnetic mirror formed by an evanescent wave are described[15)].

REFERENCES

(*) Laboratoire associé au C.N.R.S. et à l'Université Paris VI.

1) C. Cohen-Tannoudji, Course given at Les Houches summer school, Session LIII, 1990, in "Fundamental systems in quantum optics", ed. by J. Dalibard, J. M. Raimond and J. Zinn-Justin (Elsevier, 1992).

2) W. D. Phillips, Course given at Les Houches summer school, Session LIII, 1990, in "Fundamental systems in quantum optics", ed. by J. Dalibard, J. M. Raimond and J. Zinn-Justin (Elsevier, 1992).

3) "Laser manipulation of atoms and ions", Proceedings of the Varenna summer school, Course CXVIII, 1991, ed. by E. Arimondo and W. D. Phillips (North-Holland, 1992).

4) Special issue of J.O.S.A. **B** on "Laser Cooling and Trapping of Atoms", J.O.S.A. **B6**, Number 11, November 89, ed. by S. Chu and C. Wieman.

5) C. Cohen-Tannoudji and W. D. Phillips, Physics Today **43**, 33 (1990).

6) S. Chu, Science **253**, 861 (1991).

7) Y. Castin, J. Dalibard and C. Cohen-Tannoudji, in "Light induced kinetic effects on atoms, ions and molecules", p. 5, ed. by L. Moi, S. Gozzini, C. Gabbanini, E. Arimondo and F. Strumia, (ETS Editrice, Pisa, 1991).

8) Y. Castin and J. Dalibard, Europhys. Lett. **14**, 761 (1991).

9) P. Verkerk, B. Lounis, C. Salomon, C. Cohen-Tannoudji, J.-Y. Courtois, G. Grynberg, Phys. Rev. Lett. **68**, 3861 (1992).

10) P. S. Jessen, C. Gerz, P. D. Lett, W. D. Phillips, S. L. Rolston, R. J. C. Spreeuw, C. I. Westbrook, Phys. Rev. Lett. **69**, 49 (1992).

11) A. Hemmerich, T. Hänsch, Phys. Rev. Lett. **70**, 410 (1993).

12) A. Hemmerich, C. Zimmermann, T. Hänsch, Europhys. Lett. **22**, 89 (1993).

13) G. Grynberg, B. Lounis, P. Verkerk, J.-Y. Courtois, C. Salomon, Phys. Rev. Lett. **70**, 2249 (1993).

14) H. Wallis, J. Dalibard and C. Cohen-Tannoudji, Appl. Phys. **B54**, 407 (1992) and references in.

15) C. Aminoff, P. Bouyer and P. Desbiolles, C. R. Acad. Sci. **II 316**, 1535 (1993).

QUANTUM BEHAVIOR OF LASER COOLED ATOMS

William D. Phillips
National Institute of Standards and Technology
PHYS A167, Gaithersburg, MD 20899

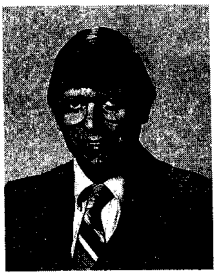

ABSTRACT

We have used atoms, laser cooled to a few microkelvin, in experiments demonstrating quantum behavior. When confined in small potential wells, the motion of the atoms, as deduced from the radiated spectrum, is seen to be quantized. In another experiment, we have transferred eight quanta of photon momentum to laser cooled atoms, in a manner that avoids spontaneous emission and preserves the atomic coherence. This short account of the presentation made at the 1993 Moriond Workshop is not intended as a comprehensive report of that talk, but only as a guide to the literature on the subject, so that the interested reader may more easily find the relevant information.

LASER COOLING AND TRAPPING

Laser cooling and trapping of neutral atoms is reviewed in a number of collections of papers [1-4] (see also the presentation by C. Cohen-Tannoudji at this meeting). Among the key technologies are optical molasses [2,5], a technique whereby atoms are cooled at the intersection of pairs of counterpropagating laser beams, and the magneto-optical trap (MOT) [6], whereby atoms are both cooled and trapped by a similar configuration of laser beams along with a particular magnetic field configuration . We use atoms trapped to densities on the order of 10^{10} cm^{-3} in a MOT and cooled to a few microkelvin in optical molasses for our experiments.

QUANTIZED MOTION OF TRAPPED ATOMS

Interfering light beams induce spatially varying light shifts in atoms. These act as an array of sub-wavelength-size potential wells in which the atoms may be trapped. By observing the fluorescence (emission) spectrum of atoms trapped in such wells, we see the effects of the oscillatory motion of the atoms, as well as the effects of the quantization of the energy of the trapped atoms [7]. We are able to determine the temperature of the atoms, and the fact that they are localized to within 1/15 of the optical wavelength. Similar experiments measuring the absorption spectrum of such atoms have been performed in Paris and Munich [8].

ATOMIC BEAMSPLITTER

Another application of laser cooled atoms to the investigation of quantum behavior is in atom interferometers [9]. In such devices, atoms are made to interfere, exhibiting their wavelike character in much the way that light does in a conventional interferometer. One would like to have the atomic equivalents of beamsplitters and mirrors to make such interferometers work well. A recent suggestion [10] is to have an atomic state adiabatically follow a varying light field in such a way that momentum is given to the atom without any photons being emitted spontaneously. Such an emission would lead to loss of coherence of the atom, and therefore to loss of the interference. The idea relies on the atom remaining in a "dark" state, one that does not absorb the laser light [11]. Recently successful experiments in our laboratory [12] in which eight photon momenta were coherently transferred to laser cooled Cs atoms were inspired by similar experiments elsewhere [13,14] in which population but not momentum was transferred by adiabatic following.

This work was supported in part by the U. S. Office of Naval Research

REFERENCES

[1]. Feature Issue on the Mechanical Effects of Light, P. Meystre and S. Stenholm, eds., J. Opt. Soc. Am. B **2** (1985).
[2]. Feature issue on Laser cooling and trapping of atoms, S. Chu and C. Wieman, eds., J. Opt. Soc. Am., B **6** (1989).
[3]. *Fundamental Systems in Quantum Optics*, J. Dalibard, J. M. Raimond, and J. Zinn-Justin, eds. (Elsevier, 1992). See in particular the lectures by C. Cohen-Tannoudji and W. Phillips.
[4]. *Laser Manipulation of Atoms and Ions*, E. Arimondo and W. Phillips, eds. , proceedings of the Enrico Fermi Summer School, 1991, to be published.
[5]. S. Chu *et al.*, Phys. Rev. Lett., **55**, 48 (1985); P. Lett *et al.*, Phys. Rev. Lett. **61**, 169 (1988).
[6]. E. Raab, *et al.*, Phys. Rev. Lett. **59**, 2631 (1987).
[7]. P. Jessen *et al.*, Phys. Rev. Lett. **69**, 49 (1992).
[8]. P. Verkerk *et al.*, Phys. Rev. Lett. **68**, 3861 (1992); A, Hemmerich and T. Hänsch, Phys. Rev. Lett. **70**, 410 (1993); and works to be published by these groups.
[9]. O. Carnal and J. Mlynek, Phys. Rev. Lett. **66**, 2689 (1991); D. Keith *et al.*, Phys. Rev. Lett. **66**, 2693 (1991); F. Reihle *et. al.*, Phys. Rev. Lett., **67**, 177 (1991); M. Kasevich and S. Chu, Phys. Rev. Lett. **67**, 181 (1991); F. Shimizu *et al.*, Jpn. J. Appl. Phys. **31**, L436 (1992); U. Sterr *et al.*, Appl. Phys. B **54**, 341 (1992); See also the feature issue on Optics and Interferometry with Atoms, J. Mlynek, V. Balykin, and P.Meystre, eds., Appl. Phys. B **54** (1992).
[10]. P. Marte, P. Zoller, and J. Hall, Phys. Rev. A **44**, R4118 (1991).
[11]. A. Aspect, E. Arimondo, R. Kaiser, N. Vansteekiste, C. Cohen-Tannoudji, ref. [2], p. 2112, and references therein. See also the presentation by A. Aspect at this meeting.
[12]. L. Goldner, C. Gerz, R. Spreeuw, S. Rolston, C. Westbrook, W. Phillips, P. Marte, and P. Zoller, to be published.
[13]. U. Gaubatz *et al.*, Chem Phys. Lett. **149**, 463 (1988).
[14]. P. Pillet, C. Valentin, R.-L. Yuan and J. Yu, to be published.

QUANTUM MEASUREMENT IN QUANTUM OPTICS

H.J. Kimble
Norman Bridge Laboratory of Physics 12-33
California Institute of Technology
Pasadena, California 91125

Abstract

Recent progress in the generation and application of manifestly quantum or nonclassical states of the electromagnetic field is reviewed with emphasis on the research of the Quantum Optics Group at Caltech. In particular, the possibilities for spectroscopy with nonclassical light are discussed both in terms of improved quantitative measurement capabilities and for the fundamental alteration of atomic radiative processes. Quantum correlations for spatially extended systems are investigated in a variety of experiments which utilize nondegenerate parametric down conversion. Finally, the prospects for measurement of the position of a free mass with precision beyond the standard quantum limit are briefly considered.

I. Introduction

Over the past fifteen years, a major area of activity in optical physics has been the generation of states of the electromagnetic field with manifestly quantum or nonclassical characteristics.[1–5] One example of a nonclassical field is a squeezed state for which the variance in one of two quadrature amplitudes of the field drops below the level associated with the vacuum state.[1–3] A second example is a field with subPoissonian photon statistics for which the fluctuations in photon number are smaller than those for the Poisson distribution of a coherent state.[4–5] In each case, nonclassical fields are those for which a quantized theory is essential; classical stochastic descriptions are not sufficient. These new states of the field have been applied both to solve questions that date to the origin of the quantum theory and to open new frontiers in optical physics. However, apart from a fundamental significance, these activities in quantum optics are relevant to a number of potential applications since they confront basic issues involved in the measurement and information sciences and attempt to formulate and implement strategies to go beyond the usual quantum limits.

Rather than to attempt an overview of these developments, the purpose of this brief contribution to the Proceedings of the 1993 Moriond Workshop is instead to summarize some recent research in the Quantum Optics Group at Caltech. One source for extended tutorials and a broader view of the diverse activities in the field is the recently published Les Houches 1990, "Fundamental Systems in Quantum Optics".[6]

II. Spectroscopy with Squeezed and Nonclassical Light

Two principal motivations for investigating spectroscopy with nonclassical light are (1) the possibility for enhancements in measurement capabilities beyond the usual quantum limits and (2) the potential for new optical phenomena associated with the fundamental alteration of atomic radiative processes. With regard to the first possibility, we note that squeezed light has been successfully employed to achieve sensitivity beyond the usual vacuum-state (or "shot-noise") limit in Mach-Zehnder[7,8] and polarization[9] interferometers and for the detection of directly encoded amplitude modulation.[10] Likewise, twin photon beams have been utilized for enhanced measurement capabilities where the availability of an independent copy of the quantum noise is exploited for improvement of the

signal-to-noise ratio.[11–14] While these proof-of-principle demonstrations have made clear that the usual, naive limits on quantum measurement associated with the zero-point fluctuations of the electromagnetic field can be surpassed (albeit by initially modest values of $\sqrt{2}$ in minimum detectable signal amplitude), in each case the choice of experimental setup has been driven principally by considerations relating to the convenience of the generation scheme for the particular nonclassical field rather than by the requirements of a specific application. However for spectroscopic investigations,[15] clearly a frequency tunable source of nonclassical light is required. Indeed, although tremendous progress has been made on both theoretical and experimental fronts in the understanding of the generation and application of nonclassical light, there have been until quite recently no frequency tunable sources suitable for spectroscopy. Note that throughout its history, spectroscopy has been carried out with "classical" sources (typically lasers or thermal sources) in that the field is describable in terms of a (possibly stochastic) superposition of the radiation from classical sources.[16]

Within this context, we have developed a frequency tunable source of squeezed light in the Quantum Optics Group at Caltech and have employed it to demonstrate improvement in measurement capability beyond the usual quantum limit for precision spectroscopy.[17,18] More specfically, we have achieved a directly observed quantum noise reduction 6dB below the vacuum-state limit in a balanced homodyne detector, corresponding to a four-fold drop in detection noise below the "shot-noise" limit. Relative to the standard quantum limit in FM saturation spectroscopy, enhanced sensitivity of 3.1dB has been demonstrated for the Doppler-free detection of the $6S_{1/2}, F = 4 \rightarrow 6P_{3/2}, F' = 5$ transition of the D_2 line of atomic Cesium at 852nm. We are continuing this work to explore in both experimental and theoretical detail the ultimate sensitivity limits for quantitative spectroscopic analysis with squeezed light.

While for the above discussion the nonclassical field serves as a passive probe of a frequency dependent atomic response, the second principal motivation for our work is to go beyond this circumstance to investigate fundamental alterations of the atomic radiative processes brought about by coupling to a nonclassical field. If we recall that the Einstein A cooefficient $\Gamma_{||}$ and the Lamb shift can be given an interpretation in terms of a decay rate

and a level shift induced by the fluctuations of the vacuum field, then from the simplest possible viewpoint the theme suggested in 1986 by Gardiner[19] is to replace the "ordinary" vacuum by a squeezed vacuum. This replacement then leads to fundamental changes in the structure of the atom-field equations associated with the nonclassical character of the squeezed "reservoir" to which the atom is coupled. In particular, the Bloch equations for an atom in free-space are modified so that the decay of the atomic polarization now proceeds at two rates $\Gamma_{\perp}^{(\pm)}$, with $\Gamma_{\perp}^{(+)} > \Gamma_{\perp}$ because of enhanced fluctuations and $\Gamma_{\perp}^{(-)} < \Gamma_{\perp}$ due to diminished fluctuations of a squeezed state relative to the vacuum state of the field. Here $\Gamma_{\perp}$ is the usual transverse decay rate for radiative coupling to the vacuum ($\Gamma_{\perp} = \Gamma_{\parallel}/2$). From this beautiful insight offered by Gardiner seven years ago has arisen a small theoretical industry devoted to the analysis of diverse problems in optical physics in the presence of squeezed light. These analyses reveal not only changes in decay rates, but as well concomitant modifications of essentially the whole spectrum of atomic dynamical processes, which derive from the phase sensitivity imprinted by the squeezed reservoir in which the atom is embedded.

Our research in this area is currently directed toward an investigation of two-photon excitation of the $6S_{1/2} \rightarrow 6D_{5/2}$ transition in atomic Cesium. For excitation with squeezed light, correlated pairs of photons should lead to an increase in population of the excited state with a linear dependence on intensity, which is in stark contrast to the usual quadratic dependence for a two-photon process.[20,21]

III. Quantum Correlations via Parametric Down Conversion

The process of parametric down conversion involves the simultaneous creation of a correlated pair of photons. For nondegenerate down conversion, the fields thus generated are distinct modes that can be spatially separated and employed to investigate quantum correlations for extended quantum systems. Our own efforts in this regard have been diverse. In the first place, we have carried out an experiment to demonstrate the Einstein-Podolsky-Rosen paradox for continuous variables[22,23] and have attempted to explore the question of nonlocality for quantum systems with dynamical variables having a continuous spectrum. We have as well studied the quantum fluctuations in optical amplification with a nondegenerate optical parametric amplifier whose internal idler mode is coupled to a

squeezed vacuum.[24] Reductions of the inherent quantum noise of the amplifier have been observed with a mimimum noise level 0.7 dB below the usual noise level of the amplifier with its internal idler mode in a vacuum state. Beyond its relevance to the issue of fundamental fluctuations in quantum amplification, this research is significant in that it represents an attempt to investigate nonlinear optics with nonclassical light. Yet a third experiment has explored possibilities for quantum communication with correlated nonclassical fields and has demonstrated the ability to transmit information with both immunity to interception and signal-to-noise recovery beyond that possible with arbitrary classical sources.[25] Finally, we have exploited the down conversion process in concert with a linear mixing of polarization states to demonstrate back-action evading measurement and a quantum optical tap.

IV. The Standard Quantum Limit (SQL) for the Position of a Free Mass

Perhaps the best known problem in the theory of quantum measurement is that of the Heisenberg microscope, whereby one attempts to ascertain the location of an otherwise free particle. Until recently it had been thought that the resolution for such a measurement of the position of a free mass m is limited by the standard quantum limit $\delta x_{SQL} = \sqrt{\hbar\tau/m}$, with τ as the time between measurements. However, in an interesting series of publications in the 80's, it was determined in quite general terms that the SQL can in fact be breached by way of physically realizable (that is to say, Hamiltonian) interactions.[26–29]

The objective of our current discussion is to specialize this "in principle" situation to the particular case of an optical interferometer by following the work of Unruh,[30] of Jaekel and Reynaud[31] and of Caves[32] who suggested that the SQL could be surpassed by a suitable injection of squeezed light into the interferometer. Of course Caves had first proposed using squeezed light to reduce the phase fluctuations (or sensing noise) in interferometry, albeit with a corresponding increase in the fluctuations in radiation pressure (or the back-reaction noise).[33] In this canonical form, the quadrature-phase amplitudes for the principal axes of the squeezed-vacuum field are chosen to coincide with those of the coherent field that excites the interferometer. A consequence of this choice is that amplitude (back reaction via radiation pressure) and phase (sensing) fluctuations give statistically independent contributions to the uncertainty in the length of the interferometer. However, if one instead makes a "judicious" choice for the orientation of the squeezing ellipse relative

to the complex amplitude of the coherent field, then the "sensing" and "back-reaction" noises become correlated with a nonzero cross correlation that can lead to measurement sensitivity below δx_{SQL}.[30–32]

Of course in practice there are a number of sources of technical noise that can overwhelm the fundamental uncertainty associated with δx_{SQL}. In Figure 1 we summarize the situation with respect to several possible sources of thermal noise. Here the basic model system is a quartz mirror of mass $m = 1$ gm suspended as a pendulum from a thin quartz fiber of length $l = 1$ cm and diameter d = 20 μm. For frequencies above the resonance frequency $f_0 = 5$Hz for the harmonic motion of the pendulum, the response of the mirror "test mass" will approximate that of a "free mass". The displacement noise $\delta q_p(f)$ in the position of the mirror due to the kT of energy excited in the pendulum motion is determined by the exact form of damping for this degree of freedom. For Figure 1a, we follow the work of Saulson[34] and introduce a complex spring constant $k_p(f) = k_o(1 + i\phi_p(f))$, with $k_o = \frac{gm}{l}$ for a "pendulum spring" and with dissipation determined by $\phi_p(f)$ which for simplicity (and due to a lack of detailed emphirical knowledge) is taken to be constant. In particular, we set $\phi_p = Q_p^{-1}$ with Q_p as the quality factor for decay of an initial excitation near f_0. The resulting displacement noise δq_p then follows from equipartition of energy and is given by Eq. (16) of Reference [34], suitably specialized to the pendulum mode of oscillation.

In a similar fashion, one notes that the position of the test mass will be uncertain because of thermal excitation of the eigenmodes of the test mass itself and because of the "violin" modes of the suspension fiber from which the mass is suspended. In Figure 1a the corresponding displacement noises are denoted by $\delta q_m(f)$ and $\delta q_v(f)$, respectively, and are determined from a suitable adaptation of Eq. (38) of Reference [34] with loss coefficients $\phi_m = Q_m^{-1}$ and $\phi_v = Q_v^{-1}$ taken to be independent of frequency. For comparison in Figure 1b we plot the various displacement noises $\delta q_p, \delta q_m$, and δq_v for the more familar case of velocity damping. Note that the quality factors for the various curves in Figure 1 are all exceedingly large; $Q_p = 10^6$, $Q_m = 10^7$, and $Q_v = 10^6$. However, the work of Braginsky and colleagues [35,36] offers the hope that these values are within the realm of the possible. For example, Reference [35] reports a pendulum with $Q_p \geq 10^8$, while Reference [36] describes observations of $Q_m \approx 10^7$ for the internal Q_m of quartz at 1MHz. While these remarkable

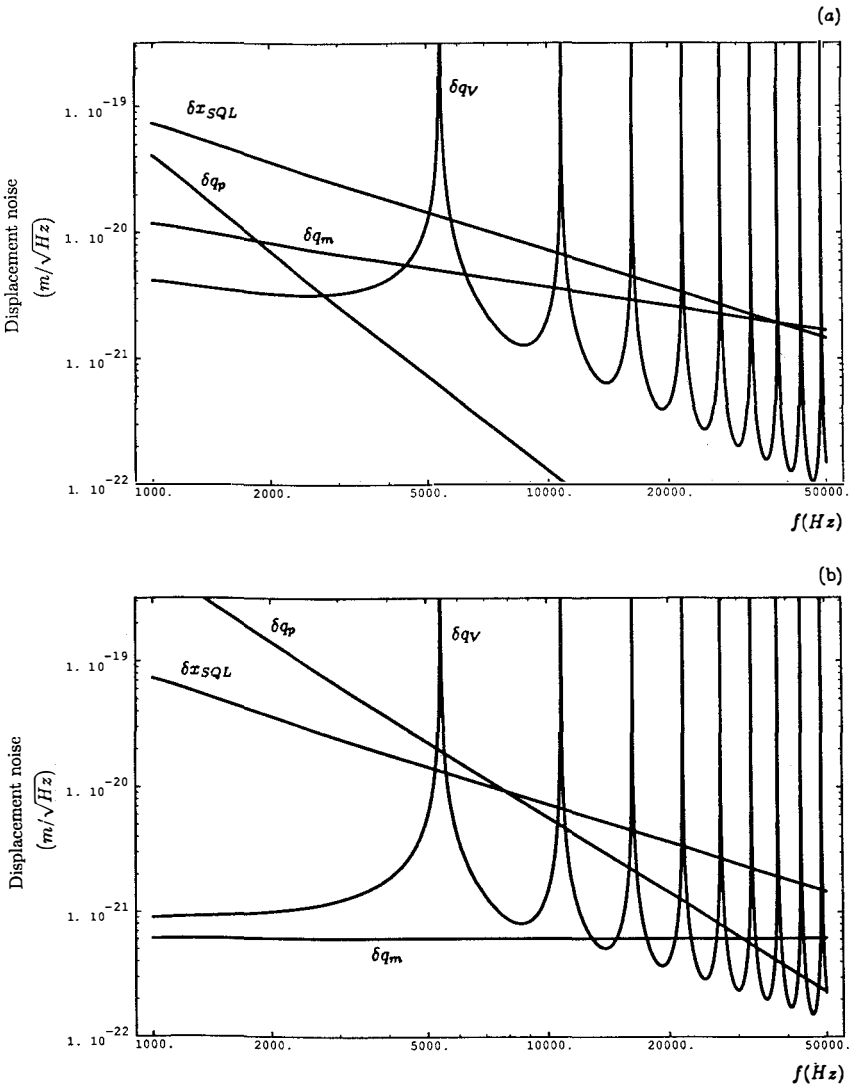

FIGURE 1 - Spectral densities of displacement noise for a suspended mass. δx_{SQL} represents the standard quantum limit for measurement of the position of the mass at frequencies above the pendulum resonance. $[\delta q_p, \delta q_m, \delta q_v]$ are the displacement noises associated with thermal excitation of the pendulum motion, of the internal test mass oscillation, and of the "violin" modes of the suspension fiber, respectively. For (a), damping as described in Reference [34] is assumed, while the more familar velocity damping is employed in (b). In each case, the resonance quality factors are $[Q_p, Q_m, Q_v] = [10^6, 10^7, 10^6]$.

values are thus quite encouraging, we emphasize that there is a paucity of information concerning the form of $\phi(f)$ for high Q materials as would be required for a system as in Figure 1.

To complete this discussion, we must compare these various sources of "extraneous" noise with the fluctuations associated with δx_{SQL}. Such a comparison is made in Figure 1 by noting that the frequency revolved response of a free mass scales as 1/f, with the exact form for δx_{SQL} in terms of a spectral density of amplitude noise given by $\delta x_{SQL}(f) = \sqrt{\hbar/(2m\pi^2 f^2)}$ expressed here as a noise in $m/\sqrt{Hz}$. [37] Although the situation is not one of extreme comfort, there do appear to be windows in frequency space (for either type of damping mechanism in Figure 1a and 1b) where it might be possible to reach the standard quantum limit (that is, to have δx_{SQL} much larger than the other sources of noise). In qualitative terms, a cavity would be formed by two mirrors each with thermal noise as in Figure 1. As the light intensity employed to interrogate the length of this cavity is increased, the phase sensitivity (and hence the inference of length) would improve as $1/\sqrt{N}$ until such time as the back-reaction associated with radiation presence (and scaling as $\sqrt{N}$) begins to dominate. For excitation with a coherent state, the crossover point is the standard quantum limit and represents an optimal comprise between the sensing noise and the measurement-induced back-reaction noise. By contrast, a "judicious" choice of squeezed excitation of the interferometer should lead to sensitivity beyond the standard quantum limit, at least over some frequency intervals. For the situation depicted in Figure 1, the noise floor for the measurement beyond δx_{SQL} would be set by one of the various thermal noises. Note that by making use of very high reflectivity mirrors (R=0.9999984 has been demonstrated in Reference [38]), the laser power required to reach δx_{SQL} could be below 1mW.

Finally, it is a pleasure to acknowledge the essential contributions of many colleagues. The research described in Section II has been carried out by E.S. Polzik, J. Carri, N. Georgiades, and H. Mabuchi, while that discussed in Section III has been accomplished by Z.Y. Ou and S.F. Pereira. J. Kyung and M.P. Winters contributed to the analysis presented in Section IV. This work was supported by the Office of Naval Research and by the National Science Foundation.

References

1. "Squeezed States of the Electromagnetic Field," eds. H.J. Kimble and D.F. Walls, J. Opt. Soc. Am. B4, 1450-1741 (1987).
2. "Squeezed Light," eds. P.L. Knight and R. Louden, J. Mod. Opt. 34, 709-1020 (1987).
3. "Quantum Noise Reduction in Optical Systems," eds. C. Fabre and E. Giacobino, Appl. Phys. B55, 189-298 (1992).
4. R. Loudon, Rep. Prog. Phys. 43, 913 (1980).
5. M.C. Teich and B.E.A. Saleh, in **Progress in Optics Vol. XXVI** ed. E. Wolf (North Holland, Amsterdam, 1988), pp.1-104.
6. Proceedings of Les Houches Session LIII, **Fundamental Systems in Quantum Optics**, eds. J.Dalibard J.M. Raimond, and J. Zinn-Justin (Elsevier Science Publishers B.V., 1992).
7. M.Xiao, L.A. Wu and H.J. Kimble, Phys. Rev. Lett. 59, 278 (1987).
8. K. Bergman, C. Doerr, and H.A. Haus, paper FV1, 1992 Annual Meeting of Optical Society of America, Albuquerque, New Mexico.
9. P. Grangier, R.E. Slusher, B. Yurke and A. LaPorta, Phys. Rev. Lett. 59, 2153 (1987).
10. M.Xiao, L.A. Wu and H.J. Kimble, Opt. Lett. 13, 476 (1988).
11. C.K. Hong, S.R. Friberg, and L. Mandel, Appl. Optics 24, 3877 (1985).
12. J. Mertz, T.Debuisschert, A. Heidmann, C. Fabre, and E. Giacobino, Opt. Lett. 16, 1234 (1991).
13. C.D. Nabors and R.M. Shelby, Phys. Rev. A42, 556 (1990).
14. P.R. Tapster, S.F. Seward, and J.G. Rarity, Phys. Rev. A44, 3266 (1991); P. Kumar, J. Huang, and O. Aytur, SPIE Vol. 1376, "Laser Noise," p. 192 (1990).
15. B. Yurke and E.A. Whittaker, Opt. Lett. 12, 236 (1987).
16. **Nonlinear Laser Spectroscopy**, V.S. Letokhov and V.P. Chebotayev, Springer Series in Optical Sciences, Vol. 4 (Spring-Verlag, Berlin, 1987).
17. E.S. Polzik, J. Carri and H.J. Kimble, Phys. Rev. Lett. 68, 3020 (1992).
18. E.S. Polzik, J. Carri and H.J. Kimble, Appl. Phys. B55, 279 (1992).
19. C.W. Gardiner, Phys. Rev. Lett. 56, 1917 (1986).
20. J. Gea-Banacloche, Phys. Rev. Lett. 62, 1603 (1989); J. Javanainen and P.L. Gould, Phys. Rev. A41, 5088 (1990).
21. Z. Ficek and P.D. Drummond, Phys. Rev. A43, 6247 (1992) and A43, 6258 (1992).
22. Z.Y. Ou, S.F. Pereira, H.J. Kimble, and K.C. Peng, Phys. Rev. Lett. 68, 3663 (1992).
23. Z.Y. Ou, S.F. Pereira, and H.J. Kimble, Appl. Phys. B55, 265 (1992).
24. Z.Y. Ou, S.F. Pereira, and H.J. Kimble, Phys. Rev. Lett. 70, 3239 (1993).
25. S.F. Pereira, Z.Y. Ou, and H.J. Kimble, submitted to Phys. Rev. Lett. (1993).
26. H.P. Yuen, Phys, Rev. Lett. 51, 719 (1983).
27. R. Lynch, Phys. Rev. Lett. 54, 1599 (1985).
28. C.M. Caves, Phys. Rev. Lett. 54, 2465 (1985).
29. M. Ozawa, Phys. Rev. Lett. 60, 385 (1988).

30. W.G. Unruh, in **Quantum Optics Experimental Gravitation and Measurement Theory**, eds. P. Meystre and M.O. Scully (Plenum Press, N.Y., 1983), 647.

31. M.T. Jaekel and S. Reynaud, Europhys. Lett. 13, 301 (1990).

32. C. M. Caves, personal communication (1990).

33. C. M. Caves, Phys Rev. D23, 1693 (1981).

34. P. Saulson, Phys. Rev. D42, 2437 (1990).

35. V.B. Braginsky, V.P. Mitrofanov, and O.A. Okhrimenko, Phys.Lett. A175, 82 (1993).

36. V.B. Braginsky, V.P. Mitrofanov, and V.I. Panov, **Systems with Small Dissipation** (University of Chicago Press, 1985).

37. K.S. Thorne, in **300 Years of Gravitation**. eds. S.W. Hawking and W. Isreal (Cambridge University Press, 1987), p. 430, Eq.(120).

38. G. Rempe, R.J. Thompson, H.J. Kimble, and R. Lalezari, Opt. Lett. 17, 363 (1992).

DISSIPATIVE FORCE ON A SPHERE MOVING IN VACUUM

P.A. Maia Neto, S. Reynaud
Laboratoire de Spectroscopie Hertzienne de l'ENS

and

M.T. Jaekel
Laboratoire de Physique Théorique de l'ENS

ABSTRACT

We derive the spectrum of fluctuations of the vacuum radiation pressure on a spherical perfectly-reflecting mirror, written as a partial-wave series. We study the two opposite limits of large and small spheres. From the fluctuation-dissipation theorem, we obtain the dissipative force exerted upon the mirror when it moves in vacuum. These results are connected to the problem of the ultimate sensitivity limit in a measurement of a length.

Although the zero-point energy of a quantum field diverges, the energy shift when a set of boundaries is introduced may be finite. When two mirrors are set together in vacuum, the zero-point energy shift is negative, giving rise to an attractive pressure between the mirrors [1].

The Casimir pressure may also be obtained as the difference between the mean values of the Maxwell Stress tensor calculated at each side of one of the mirrors. This method, shown to have a widespread class of applications, will be adopted throughout this work. In this local approach, the Casimir radiation pressure clearly appears as a fluctuating quantity.

When there is a single mirror in vacuum, the stresses on each side of the mirror obviously cancel each other, but only in the average. It thus remains a fluctuating radiation pressure [2], to which corresponds the noise spectrum defined as [3]

$$C_{FF}[\omega] = \int dt e^{i\omega t}\Big(\langle F(t)F(0)\rangle - \langle F\rangle^2\Big), \tag{1}$$

where $F(t)$ is the force on the mirror at rest at time t (i.e., the surface integral of the stress tensor over the probing surface). The average is taken over the vacuum state of the field.

The mirror's position cannot be considered as a randomless classical variable, for it will take on the fluctuations of the field to which it is coupled, in the same way that a system coupled to a reservoir at a given temperature is thermalized. At zero temperature, the mirror takes on the quantum fluctuations from its coupling to vacuum fields [4]. We may draw a simple picture of this effect by writing the equation of motion of a mirror of mass m coupled to the vacuum fluctuating force $F_{\rm vac}$:

$$mq''(t) = F_{\rm vac}(t). \tag{2}$$

From Eq. (2), we may guess the quantum fluctuations of position of the mirror. At low frequencies, the noise spectrum $C_{qq}[\omega]$ is then given by:

$$C_{qq}[\omega] = \frac{C_{FF}[\omega]}{m^2\omega^4}. \tag{3}$$

This effect may be relevant in the problem of the ultimate uncertainty limit in the measurement of a length [4, 5].

As well known, the interaction of a system with a reservoir provides as well a damping process: fluctuations and dissipation are closely related via the linear response theory [6]. When a mirror moves in vacuum, it modifies the zero-point electromagnetic field, which then reacts back by exerting a force. This force works against the mirror's motion, in order to compensate the energy radiated.

The force on a moving mirror may be written in the spectral domain as

$$\delta F[\omega] = \chi[\omega]\delta q[\omega], \tag{4}$$

where $\delta q[\omega]$ is the Fourier transform of the mirror's dispalcement, and $\chi[\omega]$ is the susceptibility function to be derived. The linear response relation for the dissipative susceptibility is [6]

$$Im\chi[\omega] = \frac{1}{2\hbar}(C_{FF}[\omega] - C_{FF}[-\omega]). \tag{5}$$

Eq. (5) was explictly shown to hold in the case of a two-dimensional spacetime [3].

Since the field annihilation operators correspond to positive frequencies, one easily derives from Eq. (1) the representation [8]

$$C_{FF}[\omega] = \pi \sum_{\lambda,\lambda'} \delta(\omega - \omega_\lambda - \omega_{\lambda'}) |\langle \lambda, \lambda' | F | 0 \rangle|^2. \tag{6}$$

The sum in Eq. (6) extends over all the field normal modes; $|\lambda, \lambda'\rangle$ is a Fock state containing one photon in the mode λ and one in the mode λ'. The field annihilation operator corresponding to the normal mode λ oscillates at the (positive) eigen-frequency ω_λ. Finally, $|0\rangle$ stands for the vacuum state.

From Eq. (6), we see that the noise spectrum vanishes at negative frequencies and is positive otherwise. It then follows from Eq. (5) that the (odd) function $Im\chi[\omega]$ is positive when $\omega \geq 0$, or in other words that the motional force in vacuum works *against* the mirror, as expected. However, the required property of stability of the mirror's motion does not follow from this property of the noise spectrum. Actually, the motional force derived in the simplest case of a perfect reflecting mirror leads to 'runaway solutions' well-known in classical electron theory.

Those unphysical solutions are probably a consequence of neglecting the recoil effect, which becomes appreciable at very high frequencies. Stability is restored (at least for a two-dimensional spacetime) by taking into account that the mirror becomes transparent at high frequencies, which allows one to consistently neglect the recoil effect [9]. We will assume nevertheless a perfect reflectivity (at all frequencies) throughout this work. Eq. (6) shows that the response at a given frequency ω is related to the pairs of field normal modes whose eigen-frequencies add to give ω. The model of perfect reflection may thus be adopted provided that the mirror bounces slowly enough in order that the much faster mirror's internal degrees of freedom could be adiabatically eliminated. The results we will present for $C_{FF}[\omega]$ correspond to the quasi-static limit and should be regarded as low-frequency approximations.

The simplest non-trivial boundary condition for the electromagnetic field (now in the real 4D spacetime) corresponds to a plane infinite mirror. From Eq. (6), we obtain the spectrum of fluctuations of the force (z-component) on a piston at rest and immersed on the infinite plane of the mirror [7] [8]. Both low and high frequency limits don't depend on the shape of the piston.

For a piston of area A, we have, when $\frac{\omega}{c}\sqrt{A} \ll 1$,

$$C_{FF}[\omega] = \frac{\hbar^2 A^2}{420\pi^3 c^6} \theta(\omega) \omega^7, \tag{7}$$

whereas the result in the opposite (large-size) limit is

$$C_{FF}[\omega] = \frac{\hbar^2 A}{30\pi^2 c^4} \theta(\omega) \omega^5. \tag{8}$$

Then, we may write the dissipative force on the moving piston by using the fluctuation-dissipation connection provided by Eq. (5). When the mirror moves slowly as compared to $\frac{\sqrt{A}}{c}$, we have (small-size limit):

$$\delta F_{\rm damp}(t) = \frac{\hbar A^2}{840\pi^3 c^6} \delta q^{(7)}(t), \tag{9}$$

whereas in the large-size limit the force is

$$\delta F_{\rm damp}(t) = -\frac{\hbar A}{60\pi^2 c^4} \delta q^{(5)}(t), \tag{10}$$

where $\delta q^{(n)}(t)$ stands for the n-derivative of the piston's displacement $\delta q(t)$.

We now consider a spherical perfectly-conducting mirror in vacuum. Here the normal modes correspond to a multipole expansion of the electromagnetic field. Eberlein [10] obtained the correlation functions of a time-averaged force operator on a spherical mirror. We calculated the noise spectrum of the vacuum force on a sphere of radius R from Eq. (6). The result is written as a partial-wave expansion [8]:

$$C_{FF}[\omega] = \frac{2\hbar^2}{3\pi c^2}\theta(\omega)\sum_{l=1}^{\infty}\left\{\frac{l(l+2)}{l+1}\int_0^{\omega}d\omega'\left[\omega'(\omega-\omega')A_{l+1}^{-1}(\frac{\omega' R}{c})A_l^{-1}(\frac{(\omega-\omega')R}{c})+\right.\right.$$
$$+\frac{[\omega'(\omega-\omega')+(\frac{c(l+1)}{R})^2]^2}{\omega'(\omega-\omega')}B_{l+1}^{-1}(\frac{\omega' R}{c})B_l^{-1}(\frac{(\omega-\omega')R}{c})\Big]+$$
$$\left.\frac{2l+1}{l(l+1)}\int_0^{\omega}dx\,\omega'(\omega-\omega')A_l^{-1}(\frac{\omega' R}{c})B_l^{-1}(\frac{(\omega-\omega')R}{c})\right\}, \tag{11}$$

where

$$A_l^{-1}(x) \equiv \frac{1}{(\eta j_l(x))^2+(\eta y_l(x))^2}, \tag{12}$$

and

$$B_l^{-1}(x) \equiv \frac{1}{(\frac{d}{dx}x j_l(x))^2+(\frac{d}{dx}x y_l(x))^2} \tag{13}$$

are the functions describing the penetrability of the centrifugal barrier for the polarizations TE and TM, respectively; $j_l(x)$ and $y_l(x)$ are respectively the Spherical Bessel functions of the first and second kinds.

As in the problem of a flat piston, the small and large-size limits correspond to small and large values of the parameter

$$\beta = \frac{\omega R}{c}. \tag{14}$$

In classical scattering theory, an input l-wave with momentum $\mathbf{k}$ corresponds to a ray of impact parameter

$$b = \frac{l}{|\mathbf{k}|} = \frac{l}{\omega}. \tag{15}$$

When $\beta \ll 1$, the coupling with the l-waves is increasingly weak as l increases (note that there is no s-wave coupling in vector field scattering), and it is sufficient to take the $l = 1$ term in Eq. (11). We then get

$$C_{FF}[\omega] = -\frac{\hbar^2 A^3}{324\pi^4 c^8}\theta(\omega)\omega^9, \tag{16}$$

where

$$A = \pi R^2 \tag{17}$$

is the cross-sectional area of the sphere. Using Eq.s (5) and (16), we obtain the dissipative force on a sphere of small size:

$$\delta F_{\rm damp}(t) = -\frac{\hbar A^3}{648\pi^4 c^8}\delta q^{(9)}(t). \tag{18}$$

In the large-size limit, we may replace the sum over l in Eq. (11) by an integral over a continuous variable, provided we use the analytical continuations of the Bessel functions

in the complex plane of the index. Finally, by using the Debye asymptotic expansion of the Bessel functions, we find

$$C_{FF}[\omega] = \frac{2\hbar^2 A}{45\pi^2 c^4}\theta(\omega)\omega^5. \tag{19}$$

This result is closely related to the geometrical optics limit. When β is very large, the radius is much larger than the wavelength of the relevant normal modes - which are selected by the delta function in Eq. (6). We may thus replace each small region of the sphere by its local tangent plane, and then find a noise spectrum given by the product of a geometrical factor, that takes into account the projection of the normal stress tensor along the direction of motion, and the result for a infinite flat mirror, given by Eq. (8). The comparison between Eqs. (8) and (19) confirms this general result [2]. Finally, we find the dissipative force to be

$$\delta F_{\rm damp}(t) = -\frac{\hbar A}{45\pi^2 c^4}\delta q^{(5)}(t) \tag{20}$$

in this limit.

As a final remark, we stress that the results presented in this paper concern only the *dissipative* part of the force on a moving mirror. Although not relevant for the problem of ultimate sensitivity limits, the analysis of the dispersive part of the force is also an interesting problem. As may be guessed by dimensional analysis, no finite dispersive component may exist in the large-size limit, and indeed a divergent dispersive force was found in the case of a scalar field [11].

One of us (PAMN) thanks the Brasilian Agency CNPq for a grant.

References

[1] H. G. B. Casimir, Proc. K. Ned. Akad. Wet. **51**, 793 (1948).

[2] G. Barton, J. Phys. (London) **A24** , 5533 (1991).

[3] M. T. Jaekel and S. Reynaud, Quantum Optics **4**, 39 (1992).

[4] M. T. Jaekel and S. Reynaud, J. Phys. (Paris) **I3**, 1 (1993).

[5] M. T. Jaekel and S. Reynaud, Europhys. Lett. **13**, 301 (1990).

[6] R. Kubo, Rep. Prog. Phys. **29**, 255 (1966).

[7] G. Barton, "New aspects of the Casimir effect: fluctuations and radiative reaction", preprint 1992; to appear in *Cavity Quantum Electrodynamics* , ed. P. Berman (Supplement: *Advances in Atomic, Molecular and Optical Physics* , Academic Press).

[8] P. A. Maia Neto and S. Reynaud, Phys. Rev. **A47** , 1639 (1993).

[9] M. T. Jaekel and S. Reynaud, Physics Letters **A167**, 227 (1992).

[10] C. Eberlein, J. Phys. (London) **A25** , 3015 (1992).

[11] L. H. Ford and A. Vilenkin, Phys. Rev. **D25** , 2569 (1982).

THE SINGLE-PHOTON TUNNELING TIME

A.M. Steinberg, P.G. Kwiat, and R.Y. Chiao
Department of Physics, University of California, Berkeley, CA 94720, USA

We have measured the time delay for a photon to tunnel across a barrier consisting of a 1.1-μm thick 1D photonic bandgap material (a multilayer dielectric mirror). The peak of the essentially undistorted photon wavepacket appears on the far side of the barrier 1.47 ± 0.21 fs *earlier* than if it had travelled at the vacuum speed of light c. Although the apparent tunneling velocity (1.7 ± 0.2) c is superluminal, this is not a genuine signal velocity, and Einstein causality is not violated. The measured tunneling time is consistent with with the group delay ("phase time"), but disagrees with the "semiclassical time." Interpretational issues are discussed briefly.

Every quantum mechanics text treats the calculation of the tunneling probability. And yet, the issue of how much *time* it takes a particle to tunnel through a barrier, a problem first addressed in the 1930's, remains controversial to the present day. The difficulty arises because the momentum in the barrier region is imaginary. The first answer, the "phase time" (i.e., the group delay as calculated by the method of stationary phase), can in certain limits be paradoxically small, implying barrier traversal at a speed greater than that of light in vacuum [1, 2]. It has generally been assumed that such velocities cannot be physical [3], but in the case of tunneling, no resolution has been universally accepted. This apparent violation of Einstein causality does not arise from the use of the nonrelativistic Schrödinger equation, since it also arises in solutions of Maxwell's equations, which are fully relativistic. Questions have been raised as to the validity of this time, as well as to its interpretation. Alternate definitions of the tunneling time have also been proposed [4]. Some experiments have already been done[5-7], but more are needed in order to clarify the meanings and ranges of validity of the different tunneling times.

We have recently completed an experiment [8, 9] that offers a relatively direct measurement of the time *delay* in tunneling (which may not *necessarily* be identified with an "interaction time"). We employed the process of spontaneous parametric down-conversion, in which pairs of photons are emitted essentially simultaneously (to within tens of femtoseconds). After one particle traverses a tunnel barrier, its time of arrival can be compared with that of its twin (which encounters no barrier), thus offering a clear operational definition of the tunneling time. The magnitude of this time is so small as to be inaccessible to electronic measurement, but a two-photon interference effect [10] can be used to study the overlap of the two photons' wavepackets when they are brought together at a beam splitter, with sub-femtosecond resolution. We have previously used this effect to confirm that single photons in glass travel at the group velocity, and demonstrated that it benefits from a peculiar cancellation of the effects of group-velocity dispersion [11]. Since this technique relies on coincidence detection, the interpretation of the experiment is simple: Each coincidence detection corresponds to a single tunneling event. The particle aspect of tunneling can thus be clearly observed.

In our current apparatus, the tunnel barrier is a multilayer dielectric mirror, which possesses a one-dimensional photonic bandgap [12] that extends approximately from 600 nm to 800 nm; the transmission reaches a minimum of 1% at 692 nm. A particle travelling at c would require 3.6 fs to cross the 1.1 μm-thick barrier. However, over most of the bandgap, the calculated group delay

is less than this, and remains relatively constant near 1.7 fs. It is interesting to note that one of the alternate tunneling times, the semiclassical time of Büttiker and Landauer, also dips below 3.6 fs, but only over a narrower range of frequencies; at the center of the bandgap, this time actually vanishes[13]. This time is obtained by dividing the thickness of the barrier by the velocity ($\hbar|\kappa|/m$ for a massive particle) corresponding to the *magnitude* of the imaginary momentum of the particle in the barrier region, neglecting the effects of coherent reflections between the extremities of the barrier. While in itself, this last approximation is reasonable for barriers much wider than the incident wavepacket, the identification of $\hbar|\kappa|/m$ with an actual velocity is not obvious. Indeed, while the semiclassical time grows linearly with barrier width, for very wide barriers the group delay saturates at a finite limit.

Our apparatus is shown in Fig. 1. A KDP crystal with a $\chi^{(2)}$ nonlinearity is pumped by a cw uv laser at 351 nm. Conjugate pairs of photons are emitted simultaneously in the process of spontaneous parametric down-conversion. We select out nearly degenerate pairs centered at 702 nm, with an rms bandwidth of approximately 6 nm. One photon of each pair travels through air, while the conjugate photon impinges on our sample. This consists of an étalon substrate of fused silica, which is coated over half of one face with the 1.1 μm coating described above, and uncoated on the other half of that face. This sample was periodically placed in each of two positions: In one position, the photon must tunnel through the 1.1 μm coating in order to be transmitted, while in the other position, it travels through 1.1 μm of air. In each position, it traverses the same thickness of substrate. The two conjugate photons are brought back together by means of mirrors, so that they impinge simultaneously on the surface of a 50/50 beam splitter. A coincidence count is recorded when detectors placed at the two output ports of the beam splitter register counts within 500 ps of one another.

If the two photons' wavepackets are made to overlap in time at the beam splitter, a destructive interference effect leads to a theoretical null in the coincidence detection rate. Thus as the path-length difference is changed by translating a "trombone" prism (see Fig. 1), the coincidence rate exhibits a dip with an rms width of approximately 20 fs, which is the correlation time of the two photons. The rate reaches a minimum when the two wavepackets overlap perfectly at the beam splitter. For this reason, if an extra delay is inserted into one arm of this interferometer (e.g., by sliding the 1.1 μm coating into the beam), the prism will need to be translated in order to compensate for this delay and restore the coincidence minimum.

In our experiment, we found that inserting the barrier into the beam caused the center of the

dip to be shifted to a position in which the prism was located *farther* from the barrier. This determines the sign of the effect: The external delay had to be *lengthened*, implying that the mean delay time experienced by the photon inside the barrier was *less than* the delay time for propagating through the same distance in air (see Fig. 1). We performed 12 one-hour runs and one four-hour run, alternating the direction in which we translated the prism in case the direction had a systematic effect on the result (none was observed). In each run, the data with and without the barrier were fitted to separate Gaussians, and the relative shift Δt between their centers was calculated. By averaging the results of all these runs, we found that $\Delta t = -1.47 \pm 0.21$ fs, including estimated systematic errors. The measured delay time is *smaller* by 7 standard deviations than the time it takes to traverse the barrier width at c. (Taking into account the width of the wavepackets, this implies that about 52% of the time, a photon which tunnelled would arrive sooner than one which travelled at c.) It is consistent with the group delay prediction, $\Delta t = -1.9$ fs, but differs greatly from the semiclassical time, $\Delta t = -3.0$ fs.

The normalized data from the 4-hr run are presented in Fig. 2. Each data point with the barrier in the beam has been averaged for 70 seconds, and each point with no barrier for 7 seconds. Since the transmission probability was nearly constant over the bandwidth of our photons, the *form* and *width* of the dip were not appreciably changed by the insertion of the barrier, aside from the overall reduction of the count rate. For this reason, there is physical significance to following the peak of the photon wavepackets. Furthermore, unlike in the electronic case, the shift cannot be understood as arising from the higher speed of the preferentially transmitted energy components before they reach the barrier. The transmission is a weak function of energy near the middle of the bandgap, and photons of all energies travel at the same velocity, except in a few dispersive optical elements. Even the small dispersive effects of those elements, however, have been shown to cancel out in this type of experiment [11, 14].

To study the energy-dependence of the delay time, we "tuned" the barrier by rotating the sample about the vertical axis, thus shifting the center of the bandgap. For the p-polarized photons we employed, this also reduces the bandgap width. A 45° rotation placed our photons close to the band edge, where the semiclassical time diverges, and the transmission probability rises to about 10%. Our results at 23° and at 45° again supported the group delay prediction.

The analogy between quantum mechanical tunneling and evanescent wave phenomena in electromagnetism is well known [6, 8, 15], but there is an important difference between classical

wave propagation and single-particle tunneling. In classical optics, the existence of group velocities greater than c, and even negative ones under certain conditions, is known and has been observed experimentally [16]. This phenomenon is understood as a "pulse reshaping" process, in which a medium preferentially attenuates the later parts of an incident pulse, in such a way that the output peak appears shifted towards earlier times. Einstein causality is not violated in this process; the output peak arises from the forward *tails* of the input pulse in a strictly causal manner, and no abrupt disturbance in the input pulse would propagate any faster than c [3].

In the case of a single-particle wavepacket in standard quantum mechanics, there is no meaning to the question of which "part" of a minimum-uncertainty wavepacket gives rise to a given detection event. If the peak of such a wavepacket is shifted forward in time, this implies that the mean delay between the single-particle emission event and the corresponding detection event may be smaller than d/c, *whenever the particle is transmitted.* The source of this anomaly is that the incident particles are transmitted with low probability. It has been shown by Aharonov and Vaidman [17] that when a "weak measurement" (one with a sufficiently large uncertainty as to leave the state on which the measurement is performed essentially unperturbed) is made on a subensemble defined both by state preparation and by a post-selection of low probability, mean values can be obtained which would be strictly forbidden for any complete ensemble. This has been observed experimentally [18]. We believe that a similar effect is occurring here.

In tunneling, the anomalously large value of the effective velocity of the peak is related to the fact that in the opaque limit, the group delay becomes independent of d. That is, the tunneling process seems to be described not by a characteristic velocity, but rather by a characteristic time. We interpret this to mean that tunneling is a transient effect: For early times, the charging fields inside the bandgap material have not yet built up to their steady-state values, and thus do not suppress transmission as strongly as they do at later times. The relevant time-scale can be estimated from the time-energy uncertainty relation as the reciprocal of the frequency difference between the incident light and the nearest frequency at which transmission is allowed.

Within the conventional interpretation of quantum mechanics, it has so far proven impossible to go beyond a mere calculation and understand *why* the group delay should be so small. It may be that the Bohm-de Broglie pilot-wave interpretation [19] will prove useful in this connection. Insofar as it gives individual particles deterministic trajectories, thus making it possible even before the wave packet encounters the barrier to speak of which subset of the ensemble will be transmitted, this picture is not unrelated to the weak measurement idea. Leavens

has applied this model to the tunneling problem [20] since the durations of these definite trajectories can be easily calculated. Bohm trajectories have the property that they may never intersect one another, and in one dimension, it follows trivially from this that *all* transmitted particles must originate earlier in time than *all* reflected particles. At the present time, this is the closest there is to an explanation of *why* only the early part of an incident wavepacket traverses a tunnel barrier.

In conclusion, our measurements indicate that the peak of the essentially undistorted (but greatly attenuated) single-photon wavepacket appears on the far side of a tunnel barrier *earlier* than it would were it to propagate at the speed of light. There is no genuine violation of Einstein causality, as explained above. This tunneling time does not appear to be a strong function of the angle of incidence, and the data indicate that in our experiment, the group delay (or "phase time") gives a better description of the physically observable *delay* than does the "semiclassical" interaction time. In future experiments, we plan to study the dependence of this delay time on barrier thickness by using the phenomenon of frustrated total internal reflection. We are also looking into the possibility of anomalous delay times off resonance in inverted media, that is, in regimes where the transmission is essentially 100%.

This work was supported by ONR Grant No. N00014-90-J-1259.

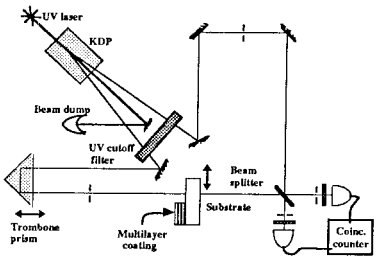

Fig. 1. Experimental setup

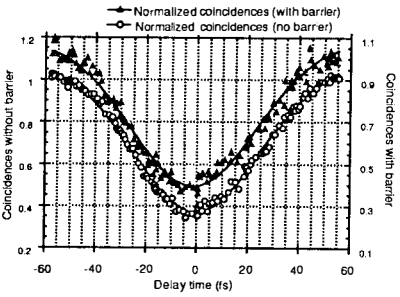

Fig. 2. Coincidence profiles with and without the tunnel barrier essentially map out the single-photon wavepackets.

REFERENCES

[1] L.A. MacColl, Phys. Rev. **40**, 621 (1932).

[2] E.P. Wigner, Phys. Rev. **98**, 145 (1955).

[3] L. Brillouin, *Wave Propagation and Group Velocity* (Academic, New York, 1960).

[4] E.H. Hauge and J.A. Støvneng, Rev. Mod. Phys. **61**, 917 (1989), and references therein.

[5] R. Landauer, Nature **341**, 567 (1989), and references therein.

[6] A. Ranfagni, D. Mugnai, P. Fabeni, G.P. Pazzi, G. Naletto and C. Sozzi, Physica **B175**, 283 (1991), and references therein.

[7] A. Enders and G. Nimtz, J. Phys. I France **2**, 1693 (1992).

[8] R.Y. Chiao, P.G. Kwiat and A.M. Steinberg, Physica **B175**, 257 (1991).

[9] A.M. Steinberg, P.G. Kwiat and R.Y. Chiao, submitted to Phys.Rev.Lett. (1993).

[10] C.K. Hong, Z.Y. Ou and L. Mandel, Phys. Rev. Lett. **59**, 2044 (1987).

[11] A.M. Steinberg, P.G. Kwiat and R.Y. Chiao, Phys. Rev. Lett. **68**, 2421 (1992).

[12] E. Yablonovitch and K.M. Leung, Physica **B175**, 81 (1991), and references therein.

[13] M. Büttiker and R. Landauer, Phys. Scr. **32**, (1985(, and references therein.

[14] A.M. Steinberg, P.G. Kwiat and R.Y. Chiao, Phys. Rev. **A45**, 6659 (1992).

[15] Th. Martin and R. Landauer, Phys. Rev. **A 45**, 2611 (1992).

[16] S. Chu and S. Wong, Phys. Rev. Lett. **48**, 738 (1982).

[17] Y. Aharonov and L. Vaidman, Phys. Rev. **A41**, 11 (1990).

[18] N.W.M. Ritchie, J.G. Story and R.G. Hulet, Phys. Rev. Lett. **66**, 1107 (1991).

[19] D. Bohm, Phys.Rev. **85**, 166 (1952).

[20] C.R. Leavens, Sol.St.Comm. **76**, 253 (1990), and references therein.

CONTROLLING THE QUANTUM FLUCTUATIONS OF LIGHT

C. Fabre
Laboratoire de Spectroscopie Hertzienne de l'ENS, Université P. et M. Curie,
Tour 12, Case 74, 75252 Paris cedex 05, France

ABSTRACT

We describe different possibilities for reducing the quantum fluctuations of a given light beam, using : (i) twin beams and various opto-electronic techniques, (ii) a Kerr medium in an optical cavity made of laser cooled and trapped atoms, (iii) an empty cavity with a moving mirror.

1. INTRODUCTION

In optics, the measurement sensitivity is limited by the noise of the photocurrent. This noise is in most cases mostly due to imperfections in the experimental set-up. When this "technical" part of the noise is reduced, one reaches a noise level which originates from the proper quantum nature of the electromagnetic field. For example, an intensity measurement is limited by the *shot noise*, due to the corpuscular nature of light. Optics is a privileged domain in physics, because the quantum noise level can be reached rather easily using high efficiency photodiodes and low noise electronics. It is then possible to experimentally study the quantum fluctuations of an observable, which enables us firstly to get a deeper insight on the process of quantum measurement, and secondly to tailor them, of course within the limits imposed by the Heisenberg inequality. For example, one can reduce the intensity fluctuations below the shot noise level only by increasing the fluctuations on the conjugate variable, i.e. on the phase of the light field. Squeezing of light quantum fluctuations has been the subject of numerous theoretical studies[1], and more recently of experimental investigations[2]. The purpose of this talk is to describe different ways of controlling the quantum fluctuations of a light beam, and to present some experimental results.

2. ACTIVE CONTROL OF LIGHT FLUCTUATIONS

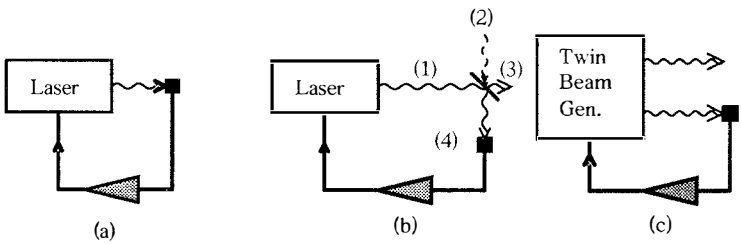

Figure 1

A widely used technique for reducing the fluctuations of a light beam is to actively correct them by some optoelectronics control mechanism. Machida and Yamamoto[3] have in particular shown experimentally that one could reduce these fluctuations well below the shot noise level by monitoring the whole beam intensity and using this information in a feedback loop acting on the semiconductor laser injection current (Fig 1a). However, this configuration does

not produce a usable beam of "quiet" light. If one inserts a beamsplitter in the light beam (Fig 1b), it is easy to show that the fluctuations of the output beam will not be reduced below the quantum level. This is due to the fact that the beamsplitter randomly distributes the photons into its two output ports (3) and (4), and therefore that the resulting photon distributions in beams (3) and (4) are not correlated : the control loop is effective in reducing the quantum noise in beam (4), not in beam (3). As an alternative explanation, one can say that the beamsplitter couples into the system a new noise source, namely the vacuum fluctuations entering through the unused input port (2) (dashed line), that the feedback loop is not able to control.

In order to reduce by active control the intensity quantum noise of a light beam, one can for example use, instead of a beamsplitter, a *Twin Beam Generator*[4] (Fig 1c), which produces two beams having perfectly correlated intensity fluctuations at the quantum level. Measuring one beam provides a perfect information on the quantum fluctuations of the other, which can by used in a control device acting either on the twin beam generator, in a feedback loop configuration (Fig 1c), or on the other beam itself, in a *feedforward* configuration.

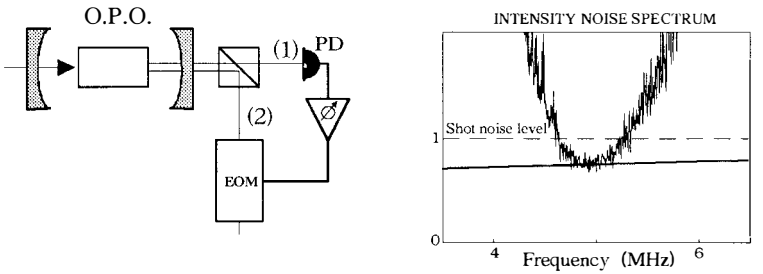

(a) (b)

Figure 2

Parametric splitting of light in a nonlinear crystal provides *twin photons* in the signal and idler modes, i.e. photons which are exactly created at the same time. When such a crystal is inserted in an optical cavity resonant for the signal and idler modes, one gets an Optical Parametric Oscillator (OPO) which produces above some pump threshold intense coherent beams having intensity fluctuations correlated at the quantum level. This was experimentally confirmed[5] and the measured level of quantum correlation between the twin beams turns out to be very large (up to 0.86[6]). Fig 2a shows a sketch of the experiment using twin

beams and active control to produce intensity squeezed light[7]. The OPO contains a KTP crystal as a nonlinear parametric splitting medium and produces c.w. twin infrared beams (1) and (2) of power 1 mW and wavelength close to 1.06 μm when pumped by a frequency doubled YAG laser at 0.53 μm. Twin beam (1) is measured by the photodiode PD, and the resulting photocurrent is used to drive an electro-optic modulator EOM used as a variable attenuator, which corrects the intensity fluctuations of beam (2). Figure 2b shows the intensity noise spectrum of beam (2) with the electronics gain optimized for optimum correction at a frequency equal to 5 MHz : One observes that the noise level is lowered by 24 % below the shot noise level around this frequency. The value of the noise minimum is in agreement with the theoretical calculations taking into account the electro-optic modulator losses, beam 2 excess noise and imperfect quantum correlation between beams 1 and 2 (so lid line in Fig 2b).

Other active correction schemes may be used to control the light fluctuations. A very promising one consists in using the information of the idler beam intensity fluctuations to correct the signal beam fluctuations by *adjustable delays* instead of adjustable attenuation. The photon distribution is thus rearranged without introducing any detrimental losses in the beam. This scheme has been theoretically studied using a Monte-Carlo simulation[8]. One shows that it reduces very efficiently the high frequency part of the intensity fluctuations (above the loop bandwidth, but of course inside the correlation bandwidth). This somewhat surprising result stems from the fact that it is easier by adjusting the delay to modify the photon distribution in short time intervals, which correspond to high noise frequencies.

3.ALL-OPTICAL CONTROL OF LIGHT FLUCTUATIONS

This last technique suggests another possibility for controlling the light fluctuations by a kind of *self-control* mechanism : If one inserts in a light beam a Kerr medium, i.e. a material having an intensity dependent index of refraction, the propagation time in this medium will depend on the instantaneous intensity of the beam. This will modify the photon distribution in the beam, and in some cases, it may reduce its dispersion. Available Kerr media have unfortunately very weak nonlinearities. The effect can be enlarged by inserting the Kerr medium in an optical cavity. One then obtains a bistable device which has been shown theoretically to strongly reduce the quantum fluctuations of the incoming light beam when the system operates close to the turning points of the bistability curve[9].

A fairly good Kerr medium is provided by a set of two-level atoms irradiated close to resonance : the Kerr coefficient varies as δ^{-3}, where δ is the frequency detuning between the field and the atomic resonance, whereas the response time of the system scales as δ^{-2}. Excess noise is coupled to the field of interest through spontaneous emission, when the upper state is populated. Precise theoretical calculations[10] taking into account the atom dynamics and the effect of spontaneous emission show that one gets a significant quantum noise reduction on the cavity output beam when the detuning δ is on the order of 10 γ, where γ is the excited state natural linewidth. This means in particular that it will not be possible to observe this effect with Doppler-broadened atomic lines, i.e. using atoms in gas phase at room temperature. One then needs to work either with atomic beams[11], or with cold atomic samples.

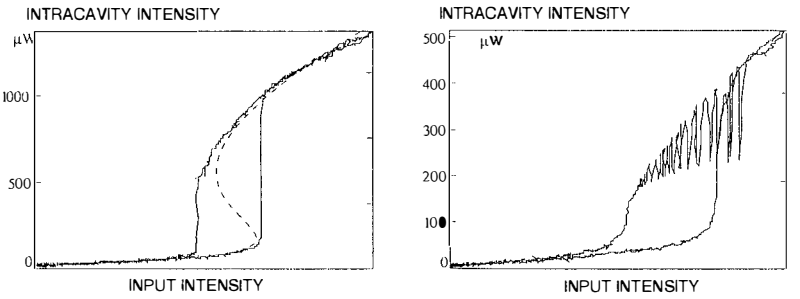

Figure 3

We have chosen to experimentally study this effect using atoms which are trapped and cooled by laser beams. Our nonlinear medium consists in a cloud of 10^8 Cesium atoms trapped and cooled in a magneto-optical laser trap[12]. When inserted in an optical cavity, this medium turns out to have a strong nonlinear behaviour even with very low input powers. Figure 3 gives the intracavity power as a function of input power for different numbers of trapped atoms. One can observe either a bistable behaviour (Fig 3a) or single-mode instabilities (self-pulsing) on the upper branch of the bistability curve (Fig 3b) for very low input powers (the maximum input power in Fig. 3 is 30 μW). We have also observed a spontaneous laser emission out of the cavity without any input beam[13]. We are currently studying the noise properties of a beam having interacting with the cold atoms in the cavity.

4. OPTO-MECHANICAL CONTROL OF FLUCTUATIONS

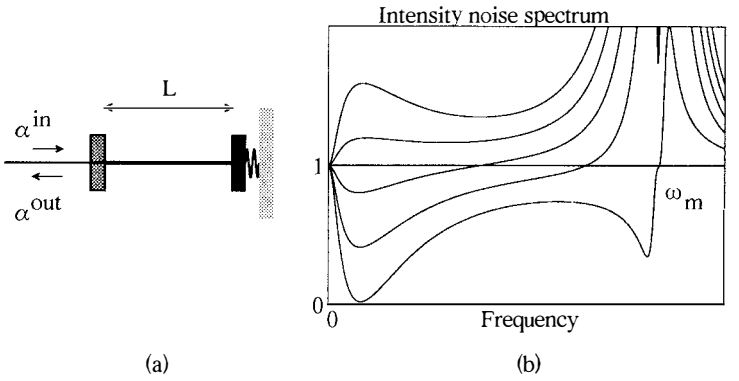

Figure 4

There exist other kinds of effective Kerr media. One of the most promising turns out to be one of the simplest : it consists in an empty cavity with a moving mirror, as sketched in Figure 4a. The mirror is bound by a harmonic force with a mechanical characteristic frequency ω_m, and damped with a decay constant Γ_M. The radiation pressure force due to the intracavity electromagnetic field is responsible for the coupling between the cavity length L and the field variables. In particular, in the c.w. regime, L depends linearly on the mean intracavity intensity, exactly like in a cavity containing a Kerr medium. This gives rise to a bistable regime[14]. One can also show that this system can be unstable and enter a self-pulsing regime. Let us mention that the mirror-field opto-mechanical coupling always leads to a small but non-zero damping force[15], so that such a system is intrinsically lossy. Its noise properties can be theoretically studied using a semi-classical treatment of its quantum fluctuations[16], taking into account the fact that, at finite temperatures, the mirror experiences a Brownian motion which introduces excess thermal fluctuations in the system. Figure 4b gives calculated intensity noise spectra in the vicinity of a turning point of the bistability curve. The lowest curve gives the noise spectrum at zero temperature and shows that one obtains a very large amount of squeezing, not only for small frequencies, like in a Kerr medium, but also around the self-pulsing frequency ω_m. The other curves correspond to increasing values of the temperature (number of thermal phonons in the mirror mode respectively equal to 0, 100, 200, 300, 400, 500 from bottom to top) and for a high mechanical quality factor $\omega_m/\Gamma_m = 10^5$. One observes that the squeezing effect is not completely washed out at low temperatures,

especially in the low frequency region. This means that there is some reasonable hope of experimentally observing such a *mechanical squeezing*.

5. CONCLUSION

We have shown that there are many different possible ways of controlling the quantum fluctuations of light, using either *microscopic devices*, such as the nonlinear properties of cold atoms and molecular crystals, or, perhaps more surprisingly, *macroscopic devices*, such as electronic components or moving mirrors.

Acknowledgements

The results presented here are actually the work of a team including E. Giacobino, S. Reynaud, A. Heidmann, J.M. Courty, J. Mertz, L. Hilico and A. Lambrecht, supported by a EEC contract ESPRIT BRA 3186.

References :

1] see for example C. Fabre, Physics Reports **219**, 215 (1992) and refs in.

2] see special issues of J. Opt. Soc. Am. **B4** (October 1987) and Applied Physics **B55** (September 1992).

3] S. Machida, Y. Yamamoto, Optics Commun. **57**, 290 (1986).

4] H. Haus, Y. Yamamoto, Phys. Rev. **A34**, 270 (1986).
H.P. Yuen, Phys. Rev. Letters **56**, 276 (1986).

5] A. Heidmann, R. Horowicz, S. Reynaud, E. Giacobino, C. Fabre, G. Camy Phys. Rev. Letters **59**, 2555 (1987).
C. Nabors, R. Shelby, Phys. Rev. **A42**, 556 (1990).
O. Aytur, P. Kumàr, Phys. Rev. Letters **65**, 1551 (1990).

6] J. Mertz, T. Debuisschert, A. Heidmann, C. Fabre, E. Giacobino, Optics Letters **16**, 1234 (1991)

7] J. Mertz, A. Heidmann, C. Fabre, E. Giacobino, S. Reynaud, Phys. Rev. Letters **64**, 2897 (1990)

8] A. Heidmann, J. Mertz, "mechanisms for intensity noise reduction by photon control", to be published in J. Opt. Soc. Am. **B**

9] L. Lugiato, G. Strini, Optics Commun. **41**, 67 (1982).
S. Reynaud, C. Fabre, E. Giacobino, A. Heidmann, Phys. Rev. **A40**, 1440 (1989).

10] M.D. Reid, Phys. Rev. **A37**, 4792 (1988).
F. Castelli, L. Lugiato, M. Vadacchino, Nuovo Cimento **B10**, 183 (1988).

L. Hilico, C. Fabre, S. Reynaud, E. Giacobino, Phys. Rev. **A46**, 4397 (1992).

11] M.G. Raizen, L. Orozco, M. Xiao, T. Boyd, H.J. Kimble, Phys. Rev. Letters **59**, 198 (1987).

12] E. Raab, M. Prentiss, A. Cable, S. Chu, D. Pritchard, Phys. Rev. Letters**59**, 2631 (1987).

13] L. Hilico, C. Fabre, E. Giacobino, Europhysics Letters **18**, 685 (1992).

14] A. Dorsel, J. McCullen, P. Meystre, E. Vignes, H. Walther, Phys. Rev. Letters **51**, 1550 (1983).
A. Gozzini, F. Maccarone, F. Mango, I. Longo, S. Barbarino, J. Opt. Soc. Am. **B2**, 1830 (1985).

15] M. Jaekel, S. Reynaud, Europhysics Letters **13**, 301 (1990).

16] C. Fabre, S. Reynaud, A. Heidmann, E. Giacobino "Quantum noise reduction using a cavity with a moving mirror", submitted to Phys. Rev. **A.**

QUANTUM COHERENCE, CLASSICAL LIMIT AND TEMPORAL BELL INEQUALITIES

Juan Pablo Paz
Theoretical Astrophysics, Los Alamos National Laboratory
Los Alamos, NM 87545, USA

ABSTRACT

Using systems of trapped ions one can perform interesting experiments illustrating basic quantum mechanical principles. We describe how a *controlled decoherence* experiment could be conceived using $^9Be^+$ ions in a Penning trap. We also analyze how a similar setup could be used to exhibit violations of temporal Bell inequalities.

1. INTRODUCTION.

Recent developments in ion trapping techniques offer the possibility of performing interesting experiments illustrating basic quantum mechanical principles. An important advantage of these systems is that, being suspended in space by a electromagnetic fields, trapped ions are well isolated from their external environment. Other useful features are the possibilities of manipulating the level structure by applying external static fields and of coherently driving the population by applying resonant laser fields (see [1] for examples of recent experiments).

In this paper we discuss two illustrative experiments that could be performed using trapped ions. In Section 2 we describe a *controlled decoherence* experiment where the interaction between a quantum system (ions in a trap) and its external environment (photons) is induced in such a way that its strength can be controlled. In this way, one could study the *decoherence process*, responsible for the classicalization of the system. In Section 3 we describe a similar setup that could be used to exhibit non–classical effects by demonstrating the existence of violations of "temporal Bell inequalities" (TBI). The above experiments could be naturally combined and used to show how quantum features are gradually suppressed due to the interaction between the quantum system and its environment.

2. CONTROLLED DECOHERENCE

In recent years there has been a renewed interest in the study of the fuzzy interphase between the quantum and the classical regimes. The process of *decoherence* [2] is of fundamental importance in this context since it explains how a quantum system can effectively behave classically. By this process, quantum coherence is dynamically suppressed due to the continuous buildup of nonseparable correlations between the system and its environment. The environment is therefore responsible for the existence of a *superselection rule* preventing the stable existence of the system in the vast majority of the states of its Hilbert space. As shown in many recent papers [2], the *decoherence process* can be very effective in suppressing interference between distinguishable states of measurement apparatus (pointer states) explaining also the classical behavior of objects of "everyday life" (dust grains, cats, etc). However, to our knowledge, there are no laboratory experiments in which *decoherence* is illustrated and studied in a controlled way. A reason for this seems to be the limited control one usually has over the parameters governing the interaction between the quantum system and its environment. In a *controlled decoherence* experiment one should probe the quantum and the classical regimes by varying the strength of the

system–environment interaction. The ideal situation is to have a switch governing the strength of such interaction: when it is strong we observe classical behavior, when it is weak the system behaves quantum mechanically.

Using a system of trapped ions, a ***controlled decoherence*** experiment seems possible. Let us start by describing the quantum system (with no environment): an ensemble of trapped ions. For concreteness, let us think of $^9Be^+$ ions in a Penning trap [1]. Only a few energy levels are available to the ions, for $^9Be^+$ they are the ones forming the hyperfine structure of the $2s^2S_{1/2}$ shell (labeled by the eigenvalue of the z–component of the nuclear and electronic angular momentum $|M_I M_J>$). Let us numerate a few of them (in order of increasing energy) as $|0>=|3/2,1/2>$, $|1>=|1/2,1/2>$, $|2>=|-1/2,1/2>$ and $|3>=|-3/2,1/2>$. This system is well isolated from all external environment, at least for a reasonable timescale. Thus, as the hyperfine sublevels are relatively stable (electric dipole forbidden transitions) there is no spontaneous decay and no irreversible behavior is present in the system. If experiments are performed using this system, characteristic quantum features can be observed (see Section 3).

In order to introduce a controllable interaction with an external environment, we can "open" the system by inducing a coupling with an unstable level $|u>$. For this, we use a laser field, resonant with the transition from the state $|1>$ to $|u>$. For $^9Be^+$, $|u>=(2p^2P_{3/2})$ (a 313 nm transition). This laser is continuously on for the duration of the experiment. Now, the ensemble of ions is interacting with the environment formed by the modes of the quantized electromagnetic field. The strength of this effective interaction, which grows with the intensity of the driving field, can be easily calculated by using simple analytic models based on Bloch equations. A simple estimate is obtained in the limit $\Gamma \gg \gamma \gg \Omega$ where: Γ is the spontaneous decay rate $|u>\rightarrow|1>$ (the only relevant decay), γ is the Rabi frequency between $|1>$ and $|u>$ (proportional to the intensity of the laser field) and Ω is any other frequency present in the system (associated with other driving fields, for example). Thus, the ***decoherence rate*** (at which any initial density matrix approaches diagonality in the basis of the states $|i>$, $i=0,\ldots,3$) is

$$\Gamma_{dec} \propto 2\frac{\gamma^2}{\Gamma} \propto I_{\text{driving}_{|1>\rightleftarrows|u>}}. \tag{1}$$

Therefore, the intensity of the driving laser determines the ***decoherence rate*** and can be used as the switch controlling the ***decoherence process***. To study such process we must now fix the decoherence rate and perform an experiment looking for characteristic quantum features. Repeating the same experiment for different values of the ***decoherence rate***, we

should be able to see the transition from the quantum ($\Gamma_{dec} \to 0$, no driving) to the classical regime ($\Gamma_{dec} \to \Gamma$, strong driving) [3]. What kind of experiment do we perform for each value of the decoherence rate? In the next section we describe one in which one looks for a peculiar non–classical feature (other alternatives are obviously also available).

3. QUANTUM BEHAVIOR AND TEMPORAL BELL INEQUALITIES

The drastic differences between quantum predictions and those derived from other probabilistic theories based on "common sense" assumptions are clearly seen in the usual Bell inequalities [4]. In recent years, another class of inequalities has been proposed to confront quantum mechanics with a class of theories based on two assumptions: (macro) realism and non invasive measurability [5]. The inequalities, involving two–time correlation functions, may also be violated by quantum correlations. Detection of these violations implies the incompatibility of quantum mechanics with the above hypothesis, which are part of our common–sense–based representation of the macroscopic world. Let us present now a short derivation of "temporal Bell inequalities" (TBI) and discuss the measurement strategy that could be used to find their violations with a system of trapped ions.

3.1 The inequalities.

To obtain a TBI let us consider a system with a coordinate Q. We assume that trajectories $Q(t)$ exist (realism), that by repeating an experiment we deal with an ensemble characterized by a probability $P[Q(t)]$ and that measuring the coordinate Q at t_1 and t_2 results in $Q(t_1)$ and $Q(t_2)$ (non–invasiveness). The two time correlation function is

$$K_{12} \equiv K(t_1, t_2) = \int [DQ] P[Q(t)] Q(t_1) Q(t_2), \tag{2}$$

where the integration is over all trajectories $Q(t)$. The inequalities follow from (2) if the coordinate Q is bounded (a condition satisfied by any spin–like variable). The derivation is straightforward: four numbers Q_i ($i = 1, \ldots, 4$) such that $|Q_i| \leq 1$, always satisfy:

$$-2 \leq Q_1 Q_2 + Q_2 Q_3 + Q_3 Q_4 - Q_1 Q_4 \leq 2. \tag{3}$$

Identifying Q_i with the results of four possible measurement of Q (i.e., $Q_i = Q(t_i)$) and integrating (3) over all trajectories (weighting with $P[Q]$), we obtain one of the TBI:

$$|K_{12} + K_{23} + K_{34} - K_{14}| \leq 2. \tag{4}$$

This is analogous to a Bell inequality derived by Clauser et al [4]. The role played here by t_i corresponds to that of the angles of the polarizers in the EPRB case. Quantum

correlations may violate TBI: for an oscillating two-level system with states $|\pm>$ (where $\hat{\sigma}|\pm>=\pm|\pm>$), the correlation function $K(t_1,t_2)=\sum_{s_1,s_2=\pm} s_1 s_2 P(s_1,t_1,s_2,t_2)$, is

$$K(t_1,t_2)=\frac{1}{2}<\hat{\sigma}(t_1)\hat{\sigma}(t_2)+\hat{\sigma}(t_2)\hat{\sigma}(t_1)>=\cos 2\Omega_R(t_1-t_2). \quad (5)$$

This violates the inequalities for some values of the time differences.

3.2 Trapped ions and violations of TBI.

To find violations of TBI, a subtle measurement strategy is required. The correlation functions are obtained from the joint probabilities $P(\sigma,t_1;\sigma',t_2)$, which must be measured by a process that: i) does not introduce noise and dissipation (affecting the coherent evolution between t_1 and t_2) and ii) resembles a classically non-invasive interaction. The basic idea is to create temporal slits allowing the free evolution of the system when it is in a particular state while stopping it otherwise. The possibility of satisfying such requirements has been debated in the context of the SQUID experiments proposed by Leggett [5] to test the existence of macroscopic quantum coherence. The favored strategy, proposed by Tesche, [5] consist of creating records of the state of the system at t_1 and t_2 without making a real measurement. For the SQUID (and in other cases discussed in [6]) these records are created by controlling non-dissipative interactions with auxiliary devices. Here, we use a similar idea with a system of trapped ions. The experiment we propose is thus the simplified version of Leggett–Tesche's SQUID experiment.

Consider the system described in Section 2 (no environment, for the moment). We prepare all ions in level $|1>$ and induce coherent Rabi oscillations between $|1>$ and $|2>$. The ions in these two levels play the role of "the system". The records of the state of the system at time t_1 is created by applying a short π pulse connecting $|1>$ with $|0>$ (the pulse should be short so that the system is effectively "frozen" [6]). Thus, if at t_1 the system is in $|1>$ it will go to $|0>$ and the oscillations will stop. On the other hand, if the ion is in $|2>$, nothing happens and the oscillations continue. In this sense, when the electron is shielded, the scheme is non invasive. The same idea is used at time t_2 when a π pulse connecting $|2>$ and $|3>$ is applied (see Fig.1).

After this pulse sequence is applied, we measure: i) the probability of finding an ion in $|1>$, which is identified with the joint probability $P(|2>,t_1;|1>,t_2)$; ii) the probability of finding an ion in $|3>$, which is identified with the joint probability $P(|2>,t_1;|2>,t_2)$. These joint probabilities can be used to construct the correlation functions that enter in the temporal Bell inequality. The other joint probabilities ($P(|1>,t_1;|i>,t_2)$) should be

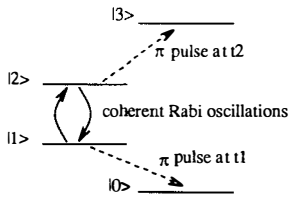

Figure 1: Pulses used for a non invasive measurement of population correlation which test violations of TBI.

determined by applying the same pulses in reversed order. If the correlation K_{ij} is measured in this way (repeating the same measurements for all pairs of times), violations of TBI can be observed. This indicates the existence of non–classical effects: the impossibility of a microscopic description based on an ensemble of non–invasively measurable trajectories.

4. FINAL REMARKS

We discussed two simple illustrative experiments that could be performed using ion traps. When combined, they could allow us to examine some aspects of the quantum to classical transition. Violations of the TBI's should be observed only when the *decoherence rate* is small enough. When the experiment is repeated increasing the rate, the violations will disappear. This is a symptom of classicality although a rather weak one: as happens with the ordinary Bell inequalities, only violations are an unambiguous signal (compatible only with quantum mechanics).

It is a pleasure to thank Günter Mahler for discussions and the organizers of the Rencontre for providing partial support.

REFERENCES

1. W M Itano et al, Phys Rev **A 41**, 2295 (1990); W M Itano et al, Phys Rev **A** (1993) to appear.
2. W H Zurek, Physics Today **44**, 36 (1991), J P Paz, S Habib and W Zurek, Phys Rev **D47**, 488 (1993).
3. See A Peres and A Ron, Phys Rev **A42**, 5720 (1990) for related ideas.
4. J F Clauser and A Shimony, Rep Prog Phys **41**, 1881 (1977) and refs therein.
5. A J Leggett and A Garg, Phys Rev Lett **54**, 857 (1985); C D Tesche, Phys Rev Lett **64**, 2358 (1990)
6. J P Paz and G Mahler, Los Alamos preprint LA–UR–93–0049.

GRAVITATION

Equivalence Principle: Experiments

NEW CONSTRAINTS ON COMPOSITION-DEPENDENT INTERACTIONS WITH RANGES DOWN TO 1 CM

J. H. Gundlach
Physics Department FM-15
Nuclear Physics Laboratory
University of Washington, Seattle, Washington 98195

ABSTRACT

We report the first results from a new torsion-balance that uses a .3 ton Uranium source mass which slowly rotates around the pendulum. The highly symmetric pendulum consists of a Pb-Cu composition dipole suspended from a thin torsion fiber. The counter-balanced source is shaped to minimize gravity gradients. Our instrument has sensitivity for forces with Yukawa ranges down to $\lambda = 1$ cm, and achieves optimal sensitivity for $\lambda > 10$ cm. We set improved limits on interactions coupled to $N - Z$ (isospin) for ranges between $\lambda = 1$ cm and $\lambda = 1000$ km. The results indicate no such new interaction. For interactions coupled to baryon number our result improves limits in the short-range region as well as for $\lambda = 10 - 200$ km.

1. Introduction

The existence of previously undetectable macroscopic-ranged interactions with strengths weaker than gravity has been suggested theoretically as well as investigated in various experiments.[1] Such an interaction would arise from the exchange of ultra-low mass scalar or vector bosons, and is expected to be composition-dependent *i.e.* to violate the universality of free fall. The potential energy of such an interaction between two point masses can be written as

$$V_{12}(r) = \alpha \left(\frac{q}{\mu}\right)_1 \left(\frac{q}{\mu}\right)_2 G\frac{m_1 m_2}{r} e^{-\lambda/r}$$

where α is the coupling constant relative to gravity and q/μ is the test-body charge-to-mass ratio. For an interaction mediated by vector bosons, the charge q could, for instance, be the baryon number, B, the lepton number, L, or any linear combination thereof such as $B - L$. The Yukawa range $\lambda = \hbar c/m_b$ arises from the rest mass of the mediating boson, m_b. Several exotic mechanisms, for instance ones involving gauge symmetry breaking, have been discussed as early 1955 by Lee and Yang [2]. Other exotic scenarios which include a color-singlet two-gluon exchange could also lead to macroscopic range forces which could fall off as a power law as for example $1/r^3$ [3]. Substantial motivation has been brought to the field by Fishbach et al. [4] through the 5th force hypothesis. In addition, there may be spin-dependent forces that arise from the exchange of CP-violating pseudoscalar-scalar axion-like particles. These would lead to an interaction of the form[5] $V_{12}(\vec{\sigma}, \vec{r}) \propto (\vec{\sigma} \cdot \hat{r})(m_b/r + 1/r^2)e^{-m_b r}$ as well as to a spin-spin coupling. Astrophysical considerations limit the mass of the axion to the Turner Window of $10^{-6} < m_a < 10^{-3}$ eV (2 mm$< \lambda <$ 20 cm) [6].

The Eöt-Wash group has previously carried out high-precision searches for new interactions using as source masses local geologic features (λ = 1 m-10 km) [1], the entire Earth (λ = 1000 km-10^8 km) [1], the Sun($\lambda > 10^8$ km), and lately even the Galaxy[7]. However, interactions with ranges below 10 cm, that are of particular interest as argued above, are best probed with laboratory-source experiments. Such experiments offer several advantages:

1. the source geometry can be selected to minimize systematic errors from gravity gradients and yield a well-known strength,
2. the source material can be selected to maximize the charge of interest, and
3. the source field can be easily modulated so that the pendulum orientation does not need to be changed.

The main disadvantage, however, is that source strength is limited by the apparatus size. Naturally, moving-source experiments are very insensitive as equivalence-principle (m_i/m_g) tests.

2. Description of the Experiment

We built a compact, stationary torsion-balance about which a massive source is continuously rotated. A torque on the dipole, related with the proper phase to the position of the source and not explainable by by conventional physics, constitutes our signature of a new interaction. In order to maximize this signal the source was constructed from 3 tonnes of depleted Uranium (^{238}U). Uranium was selected because of its high density and large neutron excess (this makes our source complementary to the geologic source which has essentially no net neutron excess). To enhance our sensitivity to short-range forces, the source is arranged approximately in a semi-cylinder with an inner radius of only 10 cm. It is built from 120 machined trapeziodal pieces of

U placed on a high quality turntable. To eliminate floor tilt, this turntable is counterbalanced by an 800 kg half-ring of Pb with a radius of about 1 m. The turntable is continuously rotated at a rate of about $2\pi/2600s$ (1ω). To check for possible systematic errors due to the magnetic fields or seismic disturbances due to the bearing, the mass and it counterbalance can be rotated with respect to the turntable on a non-magnetic bearing.

The highly symmetric torsion pendulum is suspended from a 0.8 m long, 20 μm dia. W fiber. The pendulum itself consists of an 8 g Be tray with machined positions for four test masses of 10 g each. For the measurements reported here, two of the test bodies were made of solid Cu and the other two from a Pb-Sn alloy with a hollow center. To reduce effects of gravity gradients the test body shapes were selected to have vanishing mass quadrupole and hexadecapole moments. The testbodies can be easily and reproduceably interchanged on the pendulum tray, or replaced with different ones. Any one of the four small right-angle mirrors on the pendulum can be used by an autocollimator to read the angular deflection of the pendulum. The pendulum was operated in a gas atmosphere of 1 torr to damp the swing and compound modes of the pendulum. In addition, the thin torsion fiber is attached to a cylindrically symmetric eddy current damper disk which is hung from a 100 μm thick fiber. This damper is essential for the planned operation at high vacuum (10^{-7} torr) for which our apparatus is equipped with a small 8 l/s ion pump.

The leading systematic errors in our experiment are due to:

1. gravity gradients of the source coupling to pendulum imperfections,
2. thermal variations,
3. apparatus tilt, and
4. electromagnetic effects.

The dominant systematic effect arises from gravitational gradients of the source mass. The gravitational torque can be expressed as a multipole expansion.

$$\tau_{grav} = -4\pi i G \sum_{l=0}^{\infty} \frac{1}{2l+1} \sum_{m=-l}^{+l} m q_{lm} Q_{lm} e^{-im\phi}$$

where q_{lm} and Q_{lm} are the mass spherical multipole moments and fields of the pendulum and the source mass respectively. Any torque with m=1 occurs at the same frequency (1ω) as the signal of a new interaction and must be minimized by careful control of the pendulum and source shapes. We designed the pendulum as well as the source mass with a high degree of symmetry to minimize the low-order multipole moments; the lowest nominal order 1ω coupling occurs at l=7. However machining imperfections in the pendulum and especially in the source, produce lower-order gravitational couplings; in practice the dominant unwanted coupling is through $q_{21}Q_{21}$. We use special gradiometer test bodies to produce a pendulum with a large known q_{21} moment to measure the Q_{21} field of the source and then add Pb trim masses to the source that minimize Q_{21}. A non-magnetic bearing, which bisects the Uranium source allows us to rotate the upper half by 180 deg to generate a very large known Q_{21} gradient and hence to measure the q_{21} moment of the normal pendulum. From the residual $q_{21}Q_{21}$ coupling we expect a 12 nrad deflection (for the data reported here). We use a similar technique to determine higher order m=1 (1ω) couplings.

Due to the 4-fold symmetry of the pendulum, we find torques occurring at 4 times (4ω) the rotation frequency. We minimize this coupling using small trim masses on the turntable to reduce its strav Q_{44} field. If the pendulum is not exactlv centered on the rotation axis of the

turntable a q_{55} moment arises which is proportional to the displacement. The m=5 torque due to the coupling of the q_{55} moment to the Q_{55} field of the source is used to center the pendulum on the source rotation axis to better than 20μm.

We developed a sophisticated computer code to compute all the aspects of gravitational coupling and to design the test bodies and source.

Thermal effects can lead to a coherent pendulum rotation, either through the temperature dependence of fiber properties, effects associated with the residual gas, or dimensional changes of the apparatus. An actively controlled thermal shield isolates the torsion pendulum vacuum vessel from the rotating source mass. A hollow Al mock-up of the Uranium helps symmetrize any convection currents in the air between the source and the heat shield, improving the symmetry of the system. Furthermore the entire experiment is located inside a constant-termperature enclosure. We continuously measure the apparatus temperature at various locations and we found no resolved temperature modulation at 1ω on the vacuum chamber ($\lesssim$ 16 μK at 1ω). We forced strong rotating temperature gradients across the apparatus and modulated the absolute temperature. Linear extrapolation to the measured temperature variation leads us to believe that there are no thermally- induced 1ω torques (real or apparent) above our current noise level.

A tilt of the fiber suspension point causes the pendulum to rotate by 3 percent of the tilt angle. Because a turntable unbalance would deflect the floor we counterbalanced the turntable. We continuously monitor the tilt of the floor and of the torsion balance itself and determine that systematic errors from floor tilt are neglegible. The pendulum is pulled sideways by the gravitational attraction to the source. This bends the fiber at the suspension point by 170 nrad and should produce a 1ω pendulum rotation of 5 nrad.

3. Data Taking

The ability to interchange the test masses on the pendulum (A and B configurations), and to rotate the source on non-magnetic bearings to the opposite side of the turntable, allows us to discriminate most of the above discussed systematic effects from new physics. During one month of data taking we performed the latter flip once and measured with the test masses in the A and B configurations for each source position. Q_{21} and q_{21} were measured whenever the pendulum masses were interchanged or the source position changed. The experiment is highly automated and a datapoint is recorded every 25 seconds using a PC-type computer.

4. Data Analysis

The data were subdivided into segments of 4 source revolutions each and fitted to

$$\Theta(\phi(t)) = \sum_{n=0}^{2} b_n \phi^n + \sum_{n=1}^{6} \left(a_n^{\sin} \sin(n\phi) + a_n^{\cos} \cos(n\phi) \right)$$

where Θ is the angular deflection of the pendulum, and ϕ denotes the angle of the source. The polynomial terms account for a slow drift of the fiber. A new force would manifest itself in the $a_{1\omega}^{\cos}$ amplitude. Our limits for the strength of a new interaction are then derived from the *differences* of $a_{1\omega}^{\cos}$ for the source in 0° and 180° positions on the turntable, and from the *differences* of the A and B testbody configuration:

$$signal = [a_{1\omega}^{\cos}(A\ 0°) - a_{1\omega}^{\cos}(B\ 0°) - a_{1\omega}^{\cos}(A\ 180°) + a_{1\omega}^{\cos}(B\ 180°)]/4$$

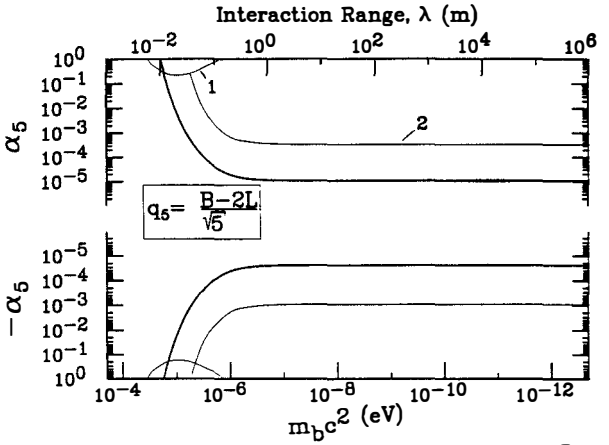

Fig. 1 Our 2σ limits on a new interaction coupled to $q = (B - 2L)/\sqrt{5}$ ($\propto$ isospin) are displayed. Interactions with a coupling stronger than the thick line are excluded. The previous best limits (1) by Hoskins et. al.[8] and (2) Nelson et. al.[9] are also shown.

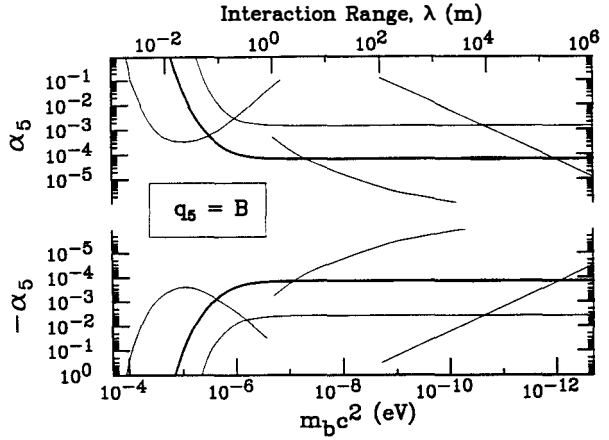

Fig. 2 Our 2σ limits (thick line) for interactions coupled to baryon number. We set new constraints for ranges between 10 cm and 1 m, and also for ranges between 10 km and 200 km where torsion balance experiments using the Earth as a source are insensitive.

The scatter of the individual fits determines the statistical error. The *average* of the coefficients for the A and B configurations shows a systematic 'offset' that is not assoc with the composition dipole itself, but depends on the orientation of the pendulum *body* respect to the source.

5. Results

With 24 days of continuous data using the Pb-Cu test masses we find a deflection of the position dipole due to the Uranium source of $a_{1\omega}^{\cos} = 6 \pm 8$ nrad with the Pb mass being

attracted to the source. The quadrature signal is also unresolved ($a_{1\omega}^{\sin} = -4 \pm 8$ nrad). The 1ω 'offset' which does not change with a test body interchange, but rotates when the pendulum is rotated to a different mirror or when the source is rotated with respect to the turntable, is 76 nrad. Its maximum points at 70 deg away from the center of the source. We are still investigating the origin of this offset, which appears to arise from gravitational coupling of source imperfections to a small misalignment of the pendulum tray (which is not as well controlled as the testbodies themselves).

Assuming a charge $q_5 = (B - 2L)/\sqrt{5}$ (proportional to the third component of isospin), our preliminary result corresponds to a coupling strength $\alpha = -0.7 \pm 0.9$ at $\lambda = 1$ cm and $\alpha = (-7 \pm 9) \times 10^{-6}$ at $\lambda = 1$ m. The corresponding 2σ limits are indicated by the thick line in fig. 1. For this charge our measurement represents a factor > 30 improvement over existing limits for $\lambda > 1$ m. Our limit for $\lambda \leq 1$ m is particularly interesting because it covers the astrophysically-allowed Turner axion 'window'[6]. Our measurement also sets improved constraints on interactions with $q_5 = B$ and ranges between 1 m and 10 m. More importantly, however, our well-characterized source allows us to set new limits for 10 km $< \lambda <$ 200 km where torsion balance experiments using the Earth as source are difficult to interpret.

6. Outlook

We plan to improve the statistical uncertainty of our current data by running with a high vacuum to reduce Brownian noise. Systematic errors are undergoing continued investigation and minimization. A set of Al-Be test bodies will be used for improved sensitivity to baryon number. Furthermore we will test for macroscopic CP-violating forces of the type suggested by Moody and Wilczek[5]. To this end, we are developing a spin-polarized test pendulum. In order to minimize magnetic fields the pendulum is toroidal with the flux-return using magnetism from orbital angular momentum.

I would like acknowledge my coworkers whose work and intellect were important to the success of this experiment: Eric Adelberger, Michael Harris, Blayne Heckel, Greg Smith, and Erik Swanson. This work is supported by NSF grant PHY-9104541.

References

[1] E.G. Adelberger, B.R. Heckel, C.W. Stubbs and W.F. Rogers, Annu. Rev. Nucl. Part. Sci. **41**, 269 (1991), and references therein.

[2] T. D. Lee and C.N. Young, Phys. Rev. **98**, 1501 (1955).

[3] G. Feinberg and J. Sucher, Phys. Rev. D **20**, 1717 (1979).

[4] E. Fishbach, D. Sudarsky, A. Szafer, C. Talamadge and S.H. Aronson, Phys. Rev. Lett **56**, 3 (1986).

[5] J.E. Moody and F. Wilczek, Phys. Rev. D**30**, 130 (1984).

[6] M. S. Turner, Physics Reports, **197**, 67 (1990).

[7] G.L. Smith, E.G. Adelberger, B.R. Heckel and Y. Su, Phys. Rev. Lett. **70**, 123 (1993).

[8] J.K. Hoskins, R.D. Newman, R. Spero, J. Schultz, Phys. Rev. D **32**, 3084 (1985).

[9] P.G. Nelson, D.M. Graham, R.D. Newman, Phys. Rev. D **42**, 963 (1990).

EXPERIMENTAL STUDIES OF GRAVITATION AND FEEBLER FORCES AT GAURIBIDANUR

R. Cowsik, N. Krishnan, S. N. Tandon and C. S. Unnikrishnan
Tata Institute of Fundamental Research
Homi Bhabha Road, Bombay 400 005, India

Abstract

Our interest in torsion balances started in 1981 when we designed the sensitive mass to be a 'gravitational monopole even though it was a compositional dipole' for studies of new composition dependent forces feebler than gravity. Here we report our most recent results obtained with laboratory source masses whose locations can be changed at will to nullify the hypothesized force field while keeping the gravitational field due to them unchanged. Our bounds on the strength of forces coupling to nuclear isospin and B-L respectively are $-5.9 \times 10^{-5} \leq \alpha_I \leq 3.4 \times 10^{-5}$ and $-2.3 \times 10^{-4} \leq \alpha_{B-L} \leq 1.4 \times 10^{-4}$ in units of gravity per atomic mass unit.

Introduction

Seven years ago Fischbach *et al*[1] revived the hypothesis of the existence of a new macroscopic force feebler than gravity which couples to some composition dependent quantity such as the nuclear isospin or baryon number. On the bases of the residual torques in the experiments of Eötvös, Pekar and Fekete[2] and the differences in the value of the Newtonian constant of gravity, G, as measured with the Airy method in mines[3] and that measured in the laboratory, they suggested that there existed a new "fifth-force" which coupled to baryon number with a strength of $\sim 10^{-2}$ of gravity per a.m.u. and had a range of $\sim$ 100m. The potential energy of two macroscopic objects of mass m_1 and m_2 separated by a distance r is then conveniently parametrized in the form :

$$V = -\frac{Gm_1m_2}{r}[1 - \alpha q_1 q_2 \; exp(-\frac{r}{\lambda})] \qquad (1)$$

Here α is the new coupling in units of gravity ($\alpha = f^2/4\pi Gm_H^2$ where m_H = mass of the hydrogen atom) and q the baryon number or any such new charge per unit mass. Keeping in mind the very accurate experiments on the Equivalence Principle by Dicke[4] and by Braginsky[5], gravity itself is assumed to be independent of the composition of the masses m_1 and m_2.

This suggestion of Fischbach *et al* stimulated great interest in the scientific community and helped us direct our new torsion balance to study such composition dependent forces. Our interest in the field started in 1981 when we realized that a torsion balance can be made to respond specifically to composition dependent forces alone by making the mass distribution of its bob spherically symmetric while still keeping its composition bi-modal[6]. In other words, the bob is a gravitational monopole even though it is a compositional dipole. The monopole nature would prevent the balance responding to various gradients of the ambient gravitational field, while the composition dipole **D** couples to any composition dependent force field **E** generating a torque $\mathbf{E} \times \mathbf{D}$. After this initial realization of the basic concept, a torsion balance was built and its sensitivity was increased progressively during a series of experiments; these are described in detail in several of our publications[7,8,9]. Here we will describe the experimental setup briefly and present our latest results.

Experimental Apparatus

The concept of the balance described above is realized by having the pendulum bob in the form of a ring, fabricated by joining together two semi-circular rings, one of copper and the other of lead. Grooves are cut into the lead half so that its mass and first two moments are identical to that of the copper half. Such a ring of total mass $\sim$ 1500g and

radius $\sim$ 9cm is suspended with its plane horizontal by means of a tungsten fibre $\sim$ 110 μm thick and $\sim$ 2.5m long. Because of circular symmetry about the suspension axis, its coupling to gradients in gravity and to the gradients in the environmental parameters such as pressure and temperature is reduced substantially, leaving the errors in the fabrication and tilts of the ring from the horizontal as the dominant contributors to the unwanted torques. This balance is suspended inside an ultrahigh vacuum chamber and is shielded from magnetic disturbances. The whole apparatus is operated at the bottom of a well, about 25m deep, to insulate it from thermal disturbances. The balance executes torsional oscillations with a period of about 795.6s, and the angle of the balance is measured by means of an accurate autocollimator, with a resolution of $\sim 10^{-9}\mathrm{rad}/\sqrt{\mathrm{Hz}}$.

In order to further minimize the coupling of the balance to gradients in gravity (caused by tilts and fabrication errors), the masses constituting the source are configured in a very special way. There are eight mass piles, four of lead and four of brass, each weighing $\sim$ 160 kg. These are suspended with multiple gimbals from a truss so as to occupy the corners of a square parallelopiped with sides nearly 1.4m, and a height of nearly 1.8m. The ratio of the height to the dimension of the sides of the square is chosen to nullify to a high order, the effects of the gravity field on the balance, which is kept at the centre of the mass configuration. When one of the vertical planes of the parallelopiped is occupied by the lead masses and the opposite one by the brass masses, there would be an isospin field normal to these planes. The truss is attached to a bearing and can be rotated at will, for example at the natural period of the balance to drive it in resonance and thereby causing a linear increase in the amplitude of the balance. The lead and the brass masses can be exchanged to nullify the composition asymmetry in the source without altering the gravitational fields appreciably. We have checked that subsequent to any such interchange of the masses, the gimbals keep their centres of gravity unaltered to an accuracy of at least 300μm. This allows us to carry out a "difference experiment" where the signal is defined as the difference between the growth rates in the amplitudes seen in the two aforementioned mass configurations.

We also carried out a series of diagnostic observations applying strong thermal gradients, gravity gradients and magnetic fields in resonance and ensured that their contributions are negligible under the conditions of our experiment.

Results

Before presenting the results from our most recent difference experiments we recapitulate the results we have published[7,9]. The materials Cu and Pb which we have used in the sensitive mass and in the source masses differ substantially in $(N - Z) \equiv I$ (nu-

clear isospin) and consequently we have focussed our attention of forces that couple to this quantum number. Our first publication in 1988 yielded the 2σ upper bound[7] (in standard notation)

$$\alpha_I < 3 \times 10^{-3} \tag{2}$$

This clarified the confusion that then existed, based on experiments which relied on geophysical sources, where claims[10,12] and counterclaims[11] were made about the existence of a finite coupling at the $\sim 5 \times 10^{-3}$ level. The next improvement in our work was published in 1990[9] :

$$-2.3 \times 10^{-4} \leq \alpha_I \leq 2.7 \times 10^{-5} \tag{3}$$

where the negative sign is for attractive couplings and the positive sign is for repulsive couplings. In the most recent set of experiments the rate of growth of amplitude that was expected was

$$\dot{A}_{theo} = \alpha_I \times (5.95 \times 10^{-5})\text{rad/cycle} \tag{4}$$

which is to be compared with the experimental value

$$\dot{A}_{expt} = (-0.73 \pm 1.14_{statistical} \pm 0.5_{systematic}) \times 10^{-9}\text{rad/cycle} \tag{5}$$

The 300μm uncertainty in the relocation of the source masses contributes dominantly to the systematic error. To derive the upper bound on α_I we take $\pm 2 \times \sigma_{statistical}$ and $\pm 1 \times \sigma_{systematic}$, as the latter is the maximum possible offset, and get the result

$$-5.9 \times 10^{-5} \leq \alpha_I \leq 3.4 \times 10^{-5} \tag{6}$$

In terms of the (B-L) quantum number this result translates into

$$-2.3 \times 10^{-4} \leq \alpha_{B-L} \leq 1.4 \times 10^{-4}, \tag{7}$$

while for the phenomenological spin-dependent charge introduced by Hall *etal*[13] our bounds are

$$-1.4 \times 10^{-6} \leq \alpha_S \leq 8.4 \times 10^{-7} \tag{8}$$

These results are valid for all values of $\lambda \gg 1$m. It should be noted that the results of Boynton *etal*[14] improve on these limits for $\lambda > 300$m and those of Adelberger *etal* in this conference yield still better limits over the full range of λ.

We conclude by pointing out that our measurements correspond to an acceleration sensitivity $\delta a \sim 10^{-13}\text{cm s}^{-2}$, and we measure amplitude changes corresponding to a rate of change of energy of the balance of $\sim 10^{-6}\text{eVs}^{-1}$. Our immediate future plans include a torsion balance test of the Principle of Equivalence to an accuracy of 1 part in 10^{13}.

References

1. E. Fischbach *et al*, *Phys. Rev. Lett.*, **56**, 3 (1986)
2. R.v.Eötvös, D. Pekar and E. Fekete, *Ann. Phys. (Leipzig)*, **68**, 11 (1922)
3. F. D. Stacey, S. C. Holding and G. J. Tuck, *Phys. Rev.*, **D33**, 12 (1986)
4. P. G. Roll, R. Krotkov and R. H. Dicke, *Ann. Phys. (NY)*, **26**, 442 (1964)
5. V. B. Braginsky and V. I. Panov, *Sov. Phys. JETP*, **34**, 463 (1972)
6. R. Cowsik, *Ind. Jour. Phys.*, **55B**, 497 (1981)
7. R. Cowsik, N. Krishnan, S. N. Tandon and C. S. Unnikrishnan, *Phys. Rev. Lett.*, **61**, 2179 (1988)
8. R. Cowsik *et al, Ind. Jour. Pure & Appl. Phys.*, **27**, 691 (1989)
9. R. Cowsik, N. Krishnan, S. N. Tandon and C. S. Unnikrishnan, *Phys. Rev. Lett.*, **64**, 336 (1990)
10. P. Thieberger, *Phys. Rev. Lett.*, **58**, 1066 (1987)
11. E. G. Adelberger *et al, ibid*, **59**, 849 (1987)
12. P. E. Boynton *et al, ibid*, **59**, 1385 (1987)
13. A. M. Hall, H. Armbruster, E. Fischbach & C. Talmadge, *Purdue University Preprint* **PURD-TH-90-15**
14. P. E. Boynton and S. H. Aronson, in*Proc. of the X^{th} Moriond Workshop, Les Arcs, France, 1990* eds. O. Fackler and J. Tran Than Van, (Editions Frontieres), p.207

GAUSS'S LAW TEST OF GRAVITY AT SHORT RANGE

M. V. Moody and H. J. Paik
Department of Physics and Center for Superconductivity Research
University of Maryland, College Park, Maryland 20742, USA

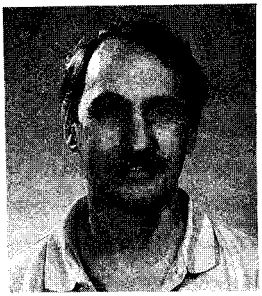

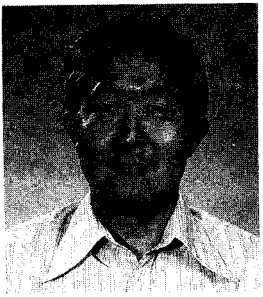

ABSTRACT

A differential equivalent of the inverse-square force law is Gauss's law for the field, $\nabla \cdot \boldsymbol{g} = -4\pi G\rho$, where $\boldsymbol{g} = -\nabla\phi$. Thus, by summing the outputs of an in-line gravity gradiometer rotated into three orthogonal directions, one can perform a near null test of the inverse-square law. The primary advantage of this type of experiment is its reduced sensitivity to the density and metrology errors of the source. We have developed a three-axis superconducting gravity gradiometer and carried out such a test using a 1500 kg lead (Pb) pendulum to produce a time-varying field. This experiment places a new (2σ) limit of $\alpha = (0.9 \pm 4.6) \times 10^{-4}$ at $\lambda = 1.5$ m, where α and λ are parameters of the generalized potential $\phi = -GM/r\,(1 + \alpha e^{-r/\lambda})$. This result represents an improvement of an order of magnitude over the best existing limit at $\lambda = 1.5$ m.

Introduction

Various light-mass bosons have been proposed to explain inconsistencies in particle physics and gravity. The existence of these bosons would give rise to a Yukawa-type potential and appear as a violation of the inverse-square law. Numerous experiments have been performed to search for such a violation.[1] This experiment is unique in that it employs a new instrument, a three-axis superconducting gravity gradiometer (SGG), and is based on a new approach, a test of Gauss's law for gravity.

Gauss's law for the field, $\nabla \cdot \boldsymbol{g} = -4\pi G\rho$, where $\boldsymbol{g} = -\nabla\phi$, is a differential equivalent of the inverse-square force law. Therefore, summing the outputs of an in-line gravity gradiometer rotated into three orthogonal directions produces a null test of the inverse-square law. The primary advantage of this experiment is its relative insensitivity to the source density and metrology errors.[2]

We have performed a laboratory test of the inverse-square law and improved the limit in the resolution of α by a factor of 10 at the range of 1.5 m. The full advantage of the new approach will be realized in a geological-scale experiment, which usually involves a natural source whose density and shape are irregular. The experiment reported here is a stepping stone toward more advanced laboratory and geological-scale experiments with the SGG.

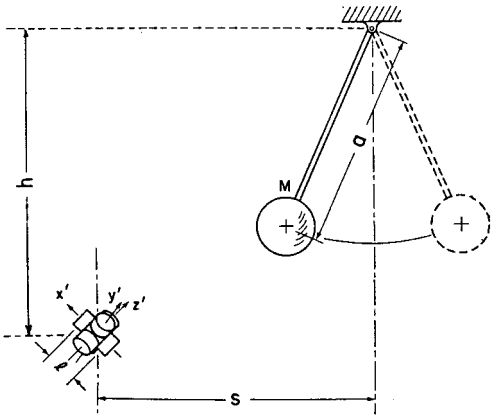

Figure 1. The source-detector configuration in the experiment. Here s is 4.234 m, h is 4.583 m, and the gradiometer baseline, *l*, is 0.1905 m.

Description of the Experiment

The source used in this experiment was a 1498 kg lead (Pb) pendulum confined to a single plane of motion by a shaft and bearings at the pivot. The length of the pendulum is 3.300 ± 0.005 m. Figure 1 shows a schematic of the experiment.

Each axis of the SGG consists of two spring-mass accelerometers in which the proof masses are confined to motion in a single degree of freedom along a common axis, and are coupled together by superconducting circuits. Platform motions appear as common-mode accelerations and are canceled by adjusting the ratio of two persistent currents in the sensing circuit. The sensing circuit is connected to a commercial SQUID amplifier to sense changes in the persistent currents generated by differential accelerations, i.e., gravity gradients. The design and analysis of this gradiometer have been published.[3)]

A three-axis gravity gradiometer is formed by mounting six accelerometers on the faces of a precision cube. The accelerometers on any two opposite faces of the cube form one of three in-line gradiometers. Aligning the diagonal of the cube with the vertical equally biases the three gradiometer axes with respect to the Earth's gravitational acceleration. This orientation also permits the cyclic interchange of the gradiometer axes by a 120° rotation about the vertical.

To increase the resolution of the inverse-square law test in the laboratory, the source should be brought close to the gradiometer. However, as the ratio of the gradiometer baseline to the source-detector separation increases, the finite baseline effect, which results from higher moments of the gradiometer coupling to higher-order field gradients,[4)] becomes significant, and metrological errors become more important. This effect, then, along with the knowledge of the source metrology, establishes a lower limit on the source-detector separation.

Discussion of Errors in the Null Experiment

An ideal gradiometer does not couple to acceleration; however, in reality, misalignment of the sensitive axes of the component accelerometers results in residual coupling to platform motion. A misalignment in the parallelism of the accelerometer sensitive axes couples to translational acceleration, and a misalignment in the concentricity of the sensitive axes couples to angular acceleration.[4)] The errors in

sensitive axes alignment also cause a misorientation of the gradiometer axes. This misorientation gives rise to an error in orthogonality among the three in-line gradiometers and among the cyclic orientations for an individual gradiometer axis. The orthogonality error results in coupling to cross-component gravity gradients.

One can show that, after summing over the three cyclic orientations, only the vertical components of these error terms remain.[5] Then, the orthogonality error couples to the vertical component of the gravity gradient, Γ_{zz}. For the pendulum source, the fundamental component of Γ_{zz} was made to vanish by choosing the source-detector orientation shown in Figure 1.

By confining the data analysis to the fundamental of the pendulum frequency, the error due to direct coupling of the gradiometer to the source-generated linear acceleration of the building was also eliminated. This error removal was possible because the vertical component of this acceleration is limited to the second and other even harmonics. For the fundamental and odd harmonics, the acceleration of the building, which is in the horizontal plane, canceled upon summation over the three cyclic orientations.

To remove the angular acceleration error, the vertical component of angular acceleration and the corresponding error coefficient must be measured. A ring laser gyro (RLG), mounted directly to the turntable with its sensitive axis aligned with the vertical, was used for the acceleration measurement. The error coefficient was measured by shaking the SGG about the vertical axis.

An error in the experiment also arises from a displacement of the center of mass of the SGG upon the 120° rotations, δr. This error can be minimized by choosing an optimum value for the initial SGG azimuthal angle. This error and the error due to an uncertainty in the azimuthal angle of the gradiometer can be reduced to second order effects by independently summing the signals of the three gradiometer axes, i.e., by performing three concurrent measurements of $\nabla \cdot \boldsymbol{g}$.[5]

The final error we need to discuss is centrifugal acceleration. The SGG, like all gravity gradiometers, is inherently sensitive to this error. However, the centrifugal acceleration generates a velocity term, which is in quadrature with the acceleration terms. This error term is rejected by phase-sensitive detection.

Experimental Results and Discussion

For the experiment, the three gradient and three acceleration outputs from the SGG were recorded along with the pendulum position for 33 nights. The turntable was automatically rotated 120° twice each night. After time-averaging the 33 data sets, the data is Fourier-transformed to identify the fundamental component. Because of a faulty superconducting joint in the circuit of one axis, the analysis of the data was limited to the other two axes. Subtracting the term due to torsional motion of the floor and the finite baseline term gives our final result of $(0.58 \pm 3.10) \times 10^{-4}$ E .

The error budget for this result is given in Table I. The random noise comes from the scatter of the $\Sigma\Gamma_i$ data. The gradiometer rotation axis error represents an upper limit corresponding to the worst case in the direction and magnitude of δr. The axis non-orthogonality error is calculated by assuming the maximum error in the polar angle, 0.001 rad. The residual torsional acceleration error comes from the scatter of the RLG data. The source metrology error arises from the uncertainties in the geometric parameters of the experiment.

Figure 2 shows the 2σ limits on positive and negative α versus λ. The strictest limits are $\alpha = (0.9 \pm 4.6) \times 10^{-4}$ at $\lambda = 1.5$ m, which represents an improvement of more than two orders of magnitude over our previous result[6] and an order of magnitude over the best existing limit.[7,8]

Table I shows that the total error could be reduced by a factor of 3 by improving the

Error Source	2σ Level
Random	2.48×10^{-4} E
Gradiometer Rotation Axis	$\leq0.95\times10^{-4}$ E
Gradiometer Axis Non-orthogonality	$\leq0.40\times10^{-4}$ E
Residual Torsional Acceleration	1.12×10^{-4} E
Source Metrology	1.08×10^{-4} E
Magnetic Coupling	$\leq10^{-7}$ E
Total	3.1×10^{-4} E

Table 1. Dominant Errors

random noise of the gradiometer and the gyro. A much more substantial improvement on the result can be achieved with the construction of an improved source.

We are in the process of designing a cylindrical source with proper mass distribution and symmetry to null the first six terms in the multipole expansion of the field at the center and near the end of the cylindrical shell. By modulating between these two points, we expect to achieve a resolution of 10^{-6} in α at $\lambda \approx 0.2$ m. We are also planning a tower experiment for the SGG, which should improve the resolution in α to 10^{-5} at $\lambda \approx 100$ m.

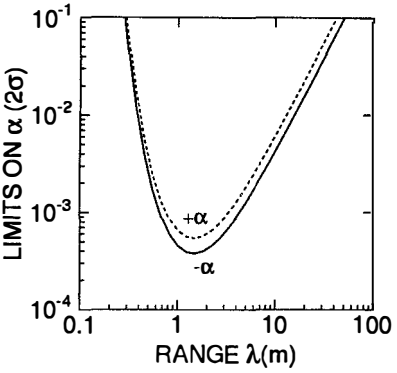

Figure 2. 2σ limits on the Yukawa coupling constant set by this experiment.

Acknowledgements

This work was supported in part by the National Aeronautics and Space Administration under contract NAS 8-38137, and by the U.S. Air Force under contact F19628-87-K-0053. We are indebted to the entire staff of the SGG laboratory for their technical assistance and valuable discussions.

References

1. For a review, see E.G. Adelberger et al, *Ann. Rev. Nucl. Part. Sci.* **41**, 269 (1991), or E. Fischbach and C. Talmadge, *Nature* **356**, 207 (1992).
2. H.J. Paik, *Phys. Rev. D* **19**, 2320 (1979).
3. M.V. Moody, H.A. Chan and H.J. Paik, *J. Appl. Phys.* **60**, 4308 (1986).
4. H.A. Chan and H.J. Paik, *Phys. Rev. D* **35**, 3551 (1987).
5. J.W. Parke, Ph.D. Thesis, University of Maryland, College Park, MD (1990), unpublished.
6. H.A. Chan, M.V. Moody and H.J. Paik, *Phys. Rev. Lett.* **49**, 1745 (1982).
7. J.K. Hoskins et al, *Phys. Rev. D* **32**, 3084 (1985).
8. G. Muller et al, *Phys. Rev. Lett.* **63**, 2621 (1989).

THE SECOND COMING OF TOWER GRAVITY: AN UPDATE

Donald H. Eckhardt, Anestis J. Romaides, Roger W. Sands, and Christopher Jekeli
Phillips Laboratory, Geophysics Directorate (AFMC), Hanscom AFB, MA 01731

Ephraim Fischbach, Carrick L. Talmadge, and Harry Kloor
Physics Department, Purdue University, West Lafayette, IN 47907

ABSTRACT

The Phillips Laboratory and Purdue University are conducting a tower gravity experiment near the town of Inverness, MS. Gravity is measured at six elevations on the 610 m WABG-TV tower as well as on the surface in an 8 km radius about the tower. These data are combined with archived data extending to 300 km. Using previously devised techniques, the surface data are analytically continued and compared with the observations. The current difference at the highest tower elevation surveyed so far, 493 m, is 34 μGal.

INTRODUCTION

In December 1991 the Phillips Laboratory (PL) Geophysics Directorate (formerly AFGL) published the final results of a search for non-Newtonian gravity. The experiment conducted on the WTVD tower in Clayton, NC, led to a null result. Many difficulties were encountered in the North Carolina experiment, not the least of which were systematic effects due to improperly modeled terrain. This led to a bias which resulted from the fact that the gravity survey elevations were not representative of the actual terrain. These problems were compounded by the sparsity of gravity data between 5 and 10 km from the tower, and by the inaccessibility of those areas due to dense regions of trees. Because there were some lingering uncertainties involving the final WTVD results, we embarked on a follow-on tower experiment in an area where all known uncertainties could be minimized.

After a lengthy search, PL selected the 610 m WABG-TV tower located northeast of Inverness, MS. Inverness is about 50 km east of the Mississippi River and about 350 km north of the Gulf of Mexico. The area surrounding the tower is extremely flat out to a distance of 40 km. Also, the area is free of any type of forests, permitting gravity measurements to be made at most desired locations. Furthermore, the existing gravity data in the area are much more extensive than that in Clayton, NC. We believe that, given these advantages, we shall be able to resolve many, if not all, of the previous difficulties.

SURFACE GRAVITY SURVEY AND ANALYTIC CONTINUATION

Based on existing data in the tower area, supplied by the Defense Mapping Agency (DMA), an inner zone survey out to 8 km was deemed sufficient. The survey plan called for a set of concentric rings with up to ten points in each ring. The ring spacing was such that each of the inner ten rings contributed nominally equal weight in the analytic continuation at the top of the tower. This led to ring radii of 150, 300, 450, 600, 800, 1050, 1400, 1900, 2600, and 3600 m from the tower. The remaining rings were placed at distances of 4900, 6400, and 8100 m. PL and Purdue began the near-tower gravity survey in the fall of 1991. The points were positioned using a combination of the Global Positioning System (GPS) and trigonometric leveling using an Electronic Distance Meter (EDM). Positioning all the points using GPS was not possible due to interference from the transmitter near the tower[1]. The EDM points were positioned to an accuracy (relative) of 1 m in the horizontal and 2 cm in the vertical; the GPS points were accurate (relatively) to 3 cm in the horizontal and 4 cm in the vertical. A total of

355 observations contained in 25 survey loops resulted in 123 gravity points surveyed in the region over a period of six months. A least-squares adjustment was performed on the data along with corrections for earth tide, gravimeter drift, and scale factor. The resultant rms error is 13 μGal with no individual errors greater than 30 μGal.

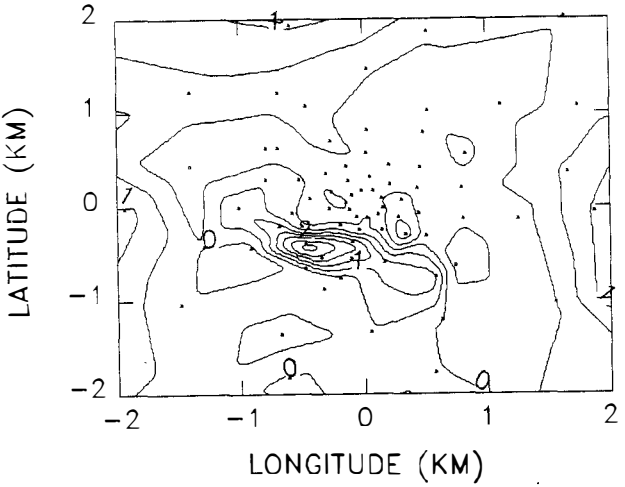

Fig. 1 Survey determined elevations minus digitized elevations contoured at 0.5 m. Dots represent locations of survey points.

The next phase was the removal of the high wave number component of the gravity field from the surface measurements. Using U.S. Geological Survey topographic maps, with a reported accuracy of 76 cm, we digitized the elevations inside a 10 x 10 km region. We interpolated the digital terrain to the points of our survey, determined elevations, and compared the results. The USGS maps are good, but not perfect; the rms difference between our elevations and those of the maps is 85 cm (Figure 1). Especially striking is the effect of the catfish farms (large pools of raised earth where local farmers breed catfish) just south of the tower that do not appear on the USGS maps and thus show up as large elevation differences. Using the comparison results, we corrected the digitized elevations and computed terrain-corrected Bouguer anomalies for all points inside of 10 km. Due to the benign nature of the surrounding terrain the rms terrain correction to the Bouguer anomalies was a mere 0.4 μGal. The resultant gravity field is very smooth with an anomalous horizontal gradient of about 6.7 E in contrast to about 13 E in the North Carolina area (Figure 2).

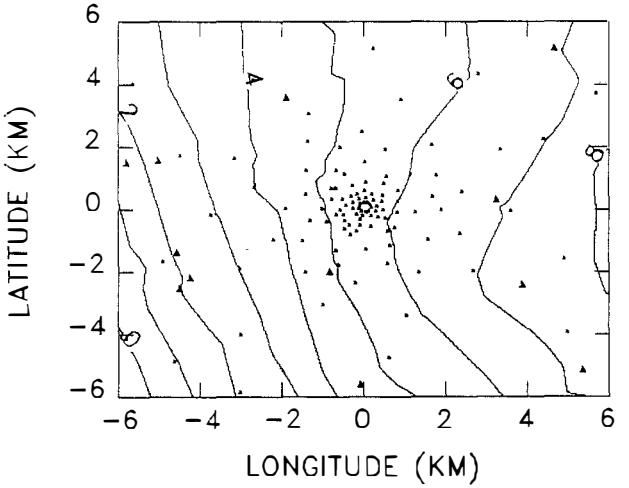

Fig. 2 Terrain-corrected Bouguer anomalies. Dots show the location of PL survey points and triangles show DMA points; contour interval is 1 mGal.

We merged our corrected data with archived data obtained from DMA which were accurate to 1-2 mGal and extended to 300 km from the tower. We selected 7781 points to be used in the analytic continuation from a total of 50292. We obtained digital data from DMA for use in terrain correcting all gravity points, but the voluminous amount of data made for large computational and storage requirements. So, given that the terrain corrections inside 10 km were very small, we computed simple Bouguer anomalies for the DMA points that fell outside of 10 km from the tower. The DMA points within 10 km of the tower were also terrain corrected using the digitized elevation data.

For points outside 10 km, we used a procedure similar to the one in North Carolina. There, we found that the DMA data were biased towards the higher elevations. Given that the bias extended to 20 km from the tower, we assumed a constant bias of 7 m from 20 km out to 200 km. This led to a constantly sloping residual of 42 μGal at the top of the tower and zero at the base[2]. Presumably the DMA data around the WABG tower also contained some outer zone terrain bias despite the flat terrain.

Using the USGS and DMA digitized data together, we computed mean elevations out to 40 km from the tower. We also computed mean elevations of the

gravity data (≤40 km) and compared the results (Figure 3). The figure clearly shows a terrain bias beyond 10 km; the bias continues beyond the boundaries of the figure, growing to as large as 5 m. So, as in the WTVD experiment, the data are biased towards higher elevations even though in the inner survey area (< 10 km) we were very careful to insure unbiased data. We corrected for the bias out to 40 km based on the results of the comparison between digital elevations and gravity elevations shown in Figure 3. We then assumed that the 5 m bias at 40 km is constant out to 300 km (the full extent of the data).

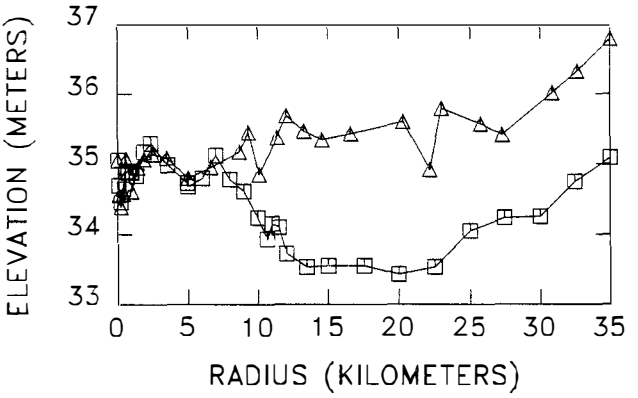

Fig. 3 Azimuthally averaged elevations. Triangles are the elevations of the gravity points. Boxes are the digitized elevations of USGS (<10 km) and DMA (10 - 35 km).

We analytically continued the surface Bouguer anomalies using a combination of a summation of Fourier-Bessel series as a reference field, and a numerical integration technique for the residuals from the reference field[3]. We performed a four-step nested symmetric Bessel function fit. Residuals were computed after each fit which served as input to the succeeding fit at progressively smaller distances; this allowed for the resolution of higher wave numbers. Step 1 is a 35 parameter fit extending to 300 km; step 2 is a 6 parameter fit extending to 7 km; step 3 is a 3 parameter fit extending to 1.3 km; and the final step is a 2 parameter fit extending to 0.3 km. Weights were computed for residuals from this reference field which were then analytically continued. The terrain had been removed prior to analytic continuation, so its effect was then added to the predicted values at the various tower elevations.

TOWER DATA AND PRELIMINARY RESULTS

The tower gravity experiment is currently incomplete. We have measured gravity at five elevations on the WABG tower using the LaCoste-Romberg gravimeter, G-152. The data were collected in four loops with a total of only nine observations. The tower elevations were determined to an accuracy of 2 cm using an EDM. All measurements have been made in less than ideal conditions with wind speeds exceeding 15 km/hr. We estimate the accuracy of the tower data to be in the range 20-25 μGal even though the rms errors are on the order of 10 μGal. An attempt to measure at a sixth elevation, 571 m above ground level, failed. At 571 m, both the galvanometer and the reading line on the gravimeter were disabled, for reasons that are as yet unclear. One possibility is the presence of a very strong magnetic field, although we cannot rule out other effects such as radio frequency interference (RFI). The WABG preliminary results (shown in Table 1) are plotted alongside those of the WTVD tower at commensurate elevations in Figure 4. The agreement is good and, with the exception of the 94 m level, the two results agree to within 16 μGal.

Table 1. Preliminary WABG Analytic Continuation Results

Elevation (m above ground)	Observed (mGal)	Predicted (mGal)	Observed-Predicted (mGal)
0.000	9.445±.009	9.434±.054	0.011±.055
93.845	9.379±.022	9.363±.025	0.016±.033
194.363	9.300±.022	9.305±.019	-0.005±.029
292.564	9.233±.023	9.243±.020	-0.010±.030
388.511	9.148±.023	9.179±.023	-0.031±.033
493.589	9.078±.024	9.112±.026	-0.034±.035

SUMMARY AND FUTURE PLANS

These results leave us with several tasks to perform: 1) obtain more tower data during better weather conditions (wind speeds <15 km/hr); 2) terrain correct the gravity data out to 40 km or beyond; 3) continue error analysis and obtain improved error estimates for analytically continued values; and 4) resolve the problem at the 571 m elevation so that gravity data can be collected. Previous tests have shown that RFI disables the galvanometer but has no effect on the reading line. In addition, mu-metal shielding around the gravimeter should protect it from

stray magnetic fields. So, either the previous tests are somehow incomplete, or there is some other yet unknown cause. Once all the above tasks have been completed to our satisfaction we should be able to present our final results for the WABG tower and for the topic of tower gravity in general.

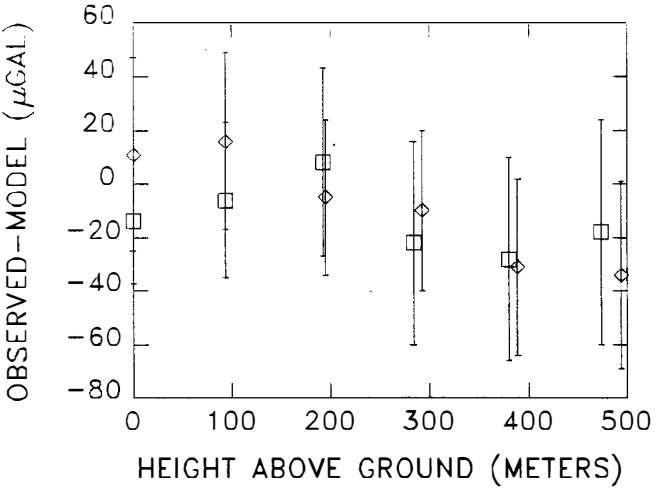

Fig. 4 Observed minus model results for the two tower experiments and their associated errors. The boxes are final WTVD results and the diamonds are preliminary WABG results.

ACKNOWLEDGEMENTS

Our sincerest thanks go to all the people of WABG-TV, especially the station assistant engineer, Mr Glen Naramore, for all his help and cooperation.

REFERENCES

1. A. J. Romaides, R. W. Sands, E. Fischbach, and C. L. Talmadge, submitted to Surveying and Mapping, (1993).

2. C. Jekeli, D. H. Eckhardt, and A. J. Romaides, Phys. Rev. Lett. **64**, 1023 (1990).

3. A. J. Romaides, C. Jekeli, D. H. Eckhardt, and C. L. Taylor, Bulletin Geodesique **65**, 230 (1991).

TORSION BALANCE DEVELOPMENT FOR GRAVITY RESEARCH

M.A. Beilby, R.D. Newman, N. Krishnan and S. Hatamian
Department of Physics, University of California
Irvine, California 92717, USA

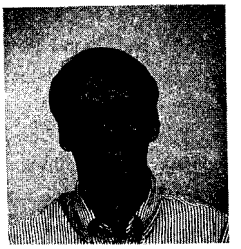

ABSTRACT

The torsion balance, which has proven to be a superb instrument for tests of the equivalence principle and searches for anomalies in Newtonian gravity, is still far from reaching its full potential sensitivity. An improved, rotatable torsion balance is being developed at UC Irvine in an attempt to push the instrument to its full potential. We discuss the performance of this instrument, with emphasis on several critical features: (1) The design of a highly stable suspended torsion balance body, which possesses a compositional dipole moment, yet excludes higher order gravitational moments, and can be trimmed to reduce measured undesired mass multipole moments due to manufacturing imperfections; (2) A feedback system to make the balance co-rotate with its housing, so as to minimize inelastic strain of the torsion fiber; (3) Reduction of thermal noise by maximizing system Q [We currently achieve a Q of 340,000 for a 20 micron bare quartz fiber at 3.6 mHz, corresponding to an amplitude damping time of 1 year. This Q is significantly degraded if a gold and/or silane coating is applied.]; and (4) Isolation from external electromagnetic, thermal, and Newtonian gravitational influences. This instrument is to be used initially for an equivalence principle test, using the sun and earth as a combined acceleration source. The daily and yearly variation in this combined acceleration affords important constraints on the validity of an observed signal.

1. Introduction

1.1 Approaches to an equivalence principle test using a torsion balance

In all tests of the equivalence principle (EP) using a torsion balance, it is necessary to modulate the differential acceleration experienced by the test-mass pairs. There are two different ways in which experiments can modulate this differential acceleration: I) the instrument is fixed to the earth, with the sun used as an accelerating source while the earth rotates the balance as done by Dicke[1] and Braginsky[2] (fixed earth balance); and II) the earth is used as the accelerating source and the balance is rotated in the earth's frame as done originally by Eötvös and more recently by Adelberger[3] (rotated balance). Fixed earth balances have the advantages that: i) the influence of the ambient gravitational and magnetic fields is largely constant and much more easily subtracted from the signals, and ii) the delicate fiber is not stressed by rotating the balance. However, rotating balances have the advantages that: i) they use the acceleration associated with the earth's rotation which is about 2.5 times higher than that towards the sun, and ii) 1/f noise is reduced through a higher frequency of signal modulation. We plan to operate in a mode that uses both the sun and the earth as acceleration sources. Using a rotating balance, the accelerations towards the earth and towards the sun roughly add at night and subtract during the day, so any true signal will have a daily modulation. Furthermore, the resulting modulation of the horizontal components of acceleration is a function of the time of year, due to the tilt of the earth's rotation axis relative to the ecliptic. This modulated signature of a true signal affords a powerful constraint on the validity of any observed signal (further detail is described by Newman[4]).

1.2 Approaches to a rotating balance scheme

There are two ways a balance can be rotated in the earth's frame: i) the balance is continually rotated; or ii) the balance is turned (e.g., 180°) then stopped for data taking (turn/stop mode). Continuous rotation has the advantage that the fiber is only stressed on startup, but a non-uniformity in the rotation rate can simulate a signal. The turn/stop mode has the advantage that data are taken while the balance is at rest, but has the disadvantage that the fiber is stressed as the balance starts and stops. We plan to use the turn/stop mode, and intend to solve the stress problem by co-rotating the balance with the housing using a feedback system with a rotating magnetic field to apply the necessary torque. Another possible method is to make measurements of the torsional period of an oscillating balance at various orientations of the balance housing, the method pioneered by Boynton et al[5]. We use this method to measure the ambient gravitational field gradients.

1.3 Limits to torsion balance performance

For a torsion balance subject to a dissipative damping torque proportional to velocity, the thermal limit on the ability to measure a force difference per unit mass, Δa, on test masses may be written:

$$\frac{\Delta a_{noise}}{\sqrt{Hz}} = \frac{\sqrt{2k_B T \kappa \tau_o / \pi Q}}{p_c} \qquad (1)$$

where the composition dipole moment p_C is the mass dipole moment of one test mass relative to the torsion axis, κ is the torsion constant of the fiber, τ_O is the period of the balance, and $Q=\pi\tau^*/\tau_O$, where τ^* is the amplitude damping time. The parameters of our balance, and our best measured damping times imply a fiber-imposed thermal limit of $\Delta a_{noise}=10^{-13.4}$ cm/s^2 for an observation time of 10^7 seconds. Thermal noise associated with gas damping of the balance will be negligible in comparison with this value for pressures below about 10^{-6} Pa. Achieving the thermal limit for our balance parameters requires an angle readout noise less than about 30 nrad/$\sqrt{\text{Hz}}$ at a frequency of about 0.3 mHz, which is within the capability of our current optical lever.

2. Experimental apparatus

The experiment is housed in the basement of the physics building at UC Irvine, where for added thermal and seismic stability, it is installed in 3 meter deep pit, approximately 2m x 2m wide. The pit is covered by a 0.2m thick styrofoam lid to further attenuate thermal variations. The balance hangs in a vacuum chamber from a 70 cm long, 20 μm diameter quartz fiber which is connected to a 44 cm long, 0.76 mm diameter phosphor bronze fiber, forming a double pendulum. Mounted on the upper fiber is a copper disk encased in a cylindrical C-magnet which provides passive eddy current damping of pendulum modes, while not significantly affecting the torsional mode. The vacuum chamber is pumped by two 30 l/s and two 8 l/s ion pumps. The entire vacuum system is suspended by a dual bifilar suspension to minimize the effect of floor tilts. The entire vacuum housing is rotated by a high precision rotary table, whose angle can be read out by a high precision encoder. A slip ring assembly makes electrical connection between the rotating frame and the lab frame. The balance angle is detected by an optical lever, which reflects light off a mirror on the balance. The light source in the focal plane of the optical lever is the bare 200 μm face of an optical fiber whose other face is illuminated. The vacuum housing near the balance is surrounded by layers of thermal and magnetic shielding as described later.

3. Balance design

A key feature of our experiment is the design of a highly stable, symmetric torsion balance which can be trimmed to reduce measured undesired multipole moments. A prototype has been built and is currently being tested (see figure 1). The balance is made of a cylindrical aluminum

body (1.85 cm x 2.39 cm diameter) which contains 8 through circular holes in which 8 test masses are press fit. Four test masses are copper, and four are lead. A shaft (5.2 cm long x 0.6 cm diameter) with four mirror faces diamond machined on the top and bottom is press fit into a through hole in the center of the body. Sixteen 2 mm holes are drilled into the body to calculated depths, and small masses can be placed in these to reduce measured undesired mass multipole moments. The balance was designed to have all multipole moments equal to zero for all ℓ, m through ℓ=4, except for q_{00} which is proportional to the mass, and design values: $q_{33} = 0.009$ g-cm^3, and $q_{44} = 0.002$ g-cm^4 due to the square mirrors. The mass of the balance is 35 g and its moment of inertia is 25.1 g-cm^2. The measured period using a 70 cm long 20 μm quartz fiber is 312 seconds. Its composition dipole moment, p_c is 5.5 g-cm. The test masses account for 56% of the total mass of the balance. The magnetic moment of the balance has been measured to 2.6 x 10^{-6} erg/gauss, by measuring the angular deflection of the balance in an applied dc magnetic field.

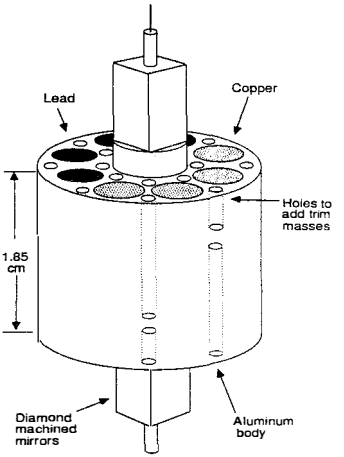

FIG. 1 Torsion Balance

4. Co-rotation of the balance and housing using a rotating magnetic field

Our balance will be operated in a mode where the balance housing is rotated to a position and then stopped for data taking. The process of starting and stopping the balance housing can stress the delicate fiber, if the balance is initially left behind as rotation of the housing begins. We minimize the stress problem by causing the balance to co-rotate with the housing using the torque generated by a rotating magnetic field at the position of the balance. The rotating field is generated by appropriately phased ac currents in two orthogonal pairs of coils flanking the balance housing. The rotation frequency of this field is constant, while its magnitude is servoed to an angular error signal supplied by the optical lever. A typical rotation of the housing involves a period of constant acceleration, followed by an equal period of constant deceleration. During this process a computer monitors the value of the optical lever angular error signal and its derivative, and uses this information along with the known angular acceleration of the balance housing to synthesize the ac currents in the coils required to maintain the balance in a nearly constant angular position relative to the rotating housing. Tests of this system have just begun; in a test rotation of the housing by 25 degrees in 500 seconds and using a 50 Hz ac current in the coils, the balance angular position

remained locked to that of the housing with an rms deviation of approximately 20 μrad, and a peak excursion of less than 100 μrad. A potential problem with this scheme is the few nanowatts of heat generated in the balance, producing a temperature rise of a few microdegrees.

5. Q-tests

We have made extensive tests of the Q demonstrated by a torsion balance suspended by a fused quartz fiber, as a function of chamber pressure and coating type. The fibers were obtained from and are being tested in collaboration with Professor Paul Boynton at the University of Washington. Fibers of 20 μm diameter were tested in three forms: with no coating, with a silane coating (which resists the strength-degrading attack on the fiber by water vapor), and with a gold coating. A simplified 9 g aluminum balance was made with a 5 cm diameter x 0.8 mm thick disk mounted on a 0.6 cm diameter x 2.5 cm long shaft with two small mirrors. We use an interesting method to determine the Q-values of our torsion balances. Consider a balance oscillating with a peak-to-peak amplitude of just over 10 complete revolutions. Towards the peak of an oscillatory swing, the reflected light beam transits on the optical detector, the balance then reaches its peak and swings back, causing another transit on the detector, the transit this time being opposite in direction to the previous one. The short time interval between these two transits is a very sensitive function of the amplitude of the balance, and a record of several successive transit intervals can be used to determine the Q. We are able to determine Q's in excess of 3×10^5 to better than one part in 10^4, in a total measurement span of just four hours (~ 50 oscillations). Figure 2 shows our Q results for various fibers vs. pressure. The best Q was for a bare fiber, with a Q of 3.4×10^5 which corresponds to an amplitude damping time of one year. The effect of gas damping is seen above a pressure of about 5×10^{-7} Torr. There is also substantial reduction seen in the Q-values with coatings of either silane or gold. We are continuing experiments with conductive coatings of other materials with the expectation of finding some which do not cause such a drastic loss in Q.

6. Isolation from external influences

6.1 Newtonian gravitational gradients

When rotating a balance in the earth frame, any gradients in the local gravitational field can couple to gravitational moments of the balance, simulating a signal. Even though the balance is designed to have nearly vanishing multipole moments up to q_{44}, manufacturing imperfections will cause some of them to exist. For this reason, it

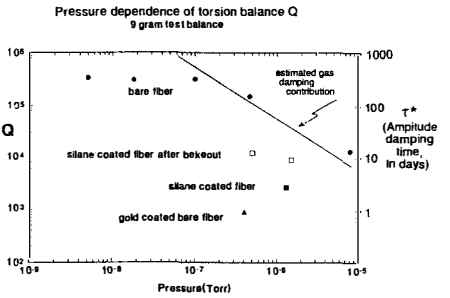

FIG. 2 Q-Test Results

is desirable to reduce gravitational gradients in the vicinity of the balance. This is done by measuring the background gradients using a deliberately asymmetric balance and rotating the housing, and then placing masses that cancel these gradients. The torsional period measurement technique was used to measure the torque on the balance. The lowest order, most troublesome gradient ($\partial g_x/\partial z$, $\partial g_y/\partial z$) was nulled to a level of 1.6×10^{-9} s^{-2}, or 1% of the ambient gradient, by placing two compensating lead masses, each about 100 kg, about 0.5 m from the balance. These were positioned to minimize their coupling to the q_{31} of the balance. The precision with which we were able to measure torque in this procedure suggests a lower limit on the potential sensitivity of $\Delta a = 4 \times 10^{-11}$ cm/s^2 for an observation time of 10^7 seconds. However, this is based on a highly asymmetric balance, limited thermal and magnetic shielding, using a non-conductive fiber, not our best vacuum, and an unstable clock to make the time measurements.

6.2 Thermal and magnetic shielding

A very effective thermal and magnetic shield has been built and tested, which surrounds the vacuum housing near the balance. It is composed of 4 layers of alternating Mu-metal, for magnetic shielding, aluminum and air gap, for thermal shielding. These layers are connected to the housing and are in the rotating frame, and there is one additional layer in the stationary frame. The rotating and stationary shield both contain coils for degaussing. The four layer rotating shield was measured to attenuate temperature differences by a factor of at least 10^4, and to attenuate magnetic fields changes by a factor of 10^6 after degaussing. The stationary shield alone attenuates magnetic fields changes by a factor of 10^3 (no significant improvement was seen when degaussing).

7. Conclusion

We are in the final testing stages of a new rotatable torsion balance, designed in an attempt to realize the full potential of this remarkably capable type of instrument. With our present apparatus, an acceleration sensitivity of 10^{-13} cm/s^2 for integration times of 10^7 seconds appears to be a reasonable target.

1. PG.. Roll, R. Krotkov, and R. H. Dicke, Annal of Physics **26**, 442 (1964)
2. V.B. Braginsky and V.I. Panov, Sov. Phys. JETP **34**, 463 (1972)
3. E.G Adelberger et al, Physical Review D **42**, 3267 (1990)
4. R.D. Newman, in the Proceedings of the 6th Marcel Grossmann Meeting on General Relativity (1991)
5. P.E.Boynton et al, Physical Review Letters **59**, 1385 (1987)

NO NEW FORCES:
SPIN DEPENDENT EFFECTS IN BUDAPEST AND OTHER PLACES

A. M. Hall, H. Armbruster
Department of Physics, Virginia Commonwealth University
Richmond, VA 23284-2000, USA

ABSTRACT

The spin dependent correlation in the Eötvös data has been reproduced elsewhere. While the Eötvös correlation may be due to an experimental error, it can no longer be considered an experimental artifact. If the effect is an experimental error, that same error exists in other experiments and its origin remains unknown. It is possible that the effect is not an error and does in fact represent new physics.

(I) While a "fifth force" does not appear to exist[1] at present experimental sensitivity, the composition dependent Eötvös data remain unexplained.

Consider a charge q equal to the mass of a nucleus multiplied by the intrinsic spin of that nucleus. The total charge Q of a group of nuclei is then:

$$Q = \Sigma N_i M_i s_i \qquad (1)$$

where N is the number of nuclei present, and i is the isotope.

(II) The Eötvös experiment[2] expresses its results for two samples as values of $\triangle K$. A value of $\triangle Q$ may also be calculated using Eq. (1). Figure 1 is a plot of $\triangle K$ vs $\triangle Q$ for the ten samples measured by Eötvös et al.

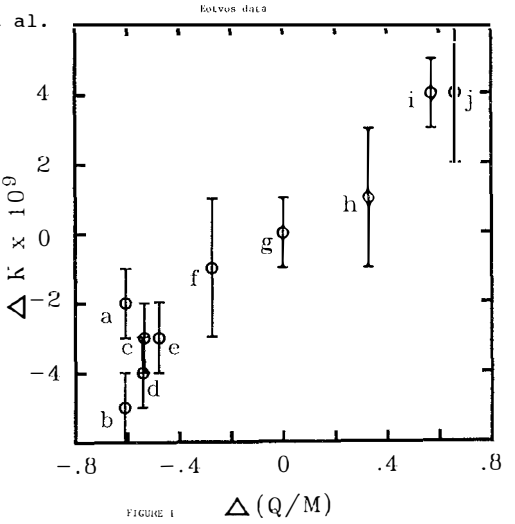

FIGURE 1

(III) Input data on isotope masses[3] are not mutually consistent. Many are mass spectrometer doublet measurements. It is possible to construct loops of these doublets for which the net mass difference should be algebraically zero. The measured departure from zero is called the closure error. The theoretical closure error (including

the potential effects of the charge q) can also be calculated for these loops. Figure 2 is a plot of data taken by Smith[4] (H through Ar^{40}) showing the measured closure error vs the theoretical closure error calculated using the charge q.

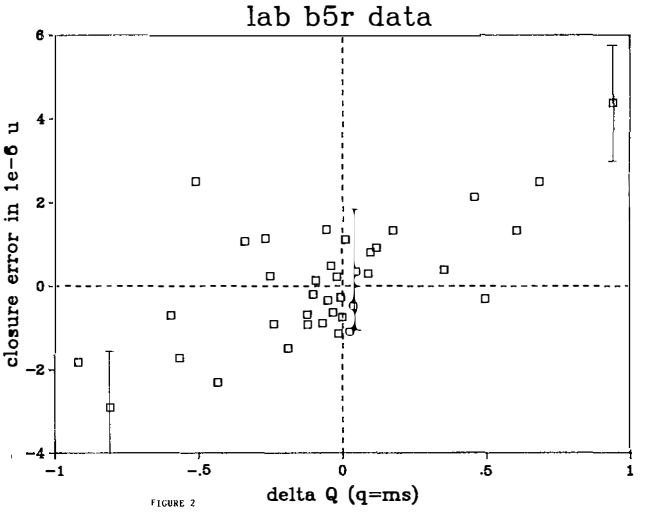

FIGURE 2

(IV) Typical laboratory balances are either of the triple beam (a gravitational force compensates the gravitational weight of the sample), or force restoring type (an electromagnetic force compensates the gravitational weight of the sample). If the balances are properly calibrated, the difference in readings between the balances should be independent of sample composition. A n experiment was conducted in which a series of samples were made whose weights were the same to .1g but whose compositions differed. The composition dependence of the mass measurements could then be tested by looking at the differential balance signal as a function of composition. Figure 3 shows this differential signal as a function of sample composition for Cu (s=1/2) and SiO_2 (s≈0). Other

elements tested include Al, Zn, Sn, In, Bi, and Nb, with results consistent with the spin dependent charge q and Fig. 3. Possible error sources tested for and discounted as causative include: buoyancy effects, electrostatics, magnetic fields, outgassing, temperature fluctuations, density variations, finite size effects, balance linearity, and tidal variations.

(V) If these spin-dependent effects can no longer be dismissed solely as as artifacts of the Eötvös data, they must represent either a previously overlooked error or new physics.

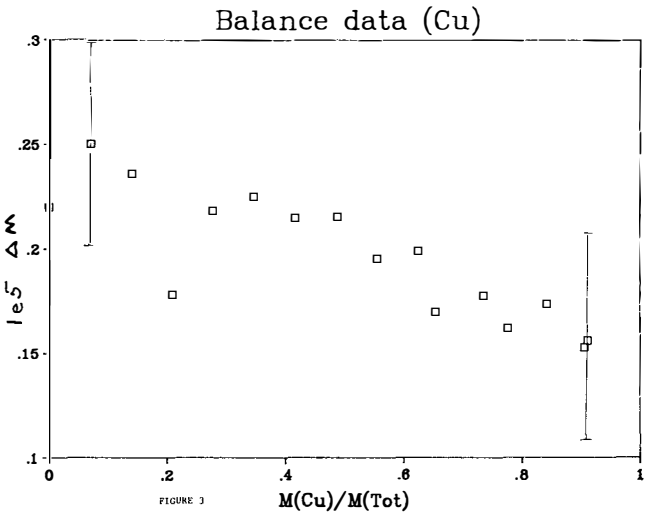

FIGURE 3

References:

1. E. Fischbach et al. , Metrologia **29**, No. 3, 213 (1992).

2. Eötvös R. v., Pekár D., Fekete E., Annalen der Physik (Leipzig), **68**, No. 9, 11 (1922).

3. A. H. Wapstra and K. Bos, Atomic and Nuclear Data Tables, **20**, No. 1, 1 (1977).

4. Smith data is given as Lab B5r in Ref. 3.

SEARCH FOR ANOMALOUS SPIN-DEPENDENT FORCES WITH A POLARIZED-MASS TORSION PENDULUM

Rogers C. Ritter
Department of Physics, University of Virginia
Charlottesville, VA 22901, U.S.

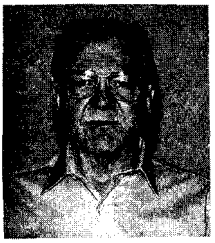

ABSTRACT

With special, intrinsically compensated masses having ~10^{23} polarized electrons, but having no measurable magnetic moment, it has been possible to investigate the existence of weak, hypothetical spin-dependent forces. Postulated spin-spin (pseudoscalar-pseudoscalar) and spin-mass (pseudoscalar-scalar) couplings are tested with two different versions of a torsion pendulum. Both of these two types of experiment yield null results, providing limits on the interactions at ranges greater than about one cm. The spin-spin limit observed is $<9 \times 10^{-12}$ of the strength of the interaction due to the magnetic moments of a like number of polarized, but uncompensated electrons. A limit on the spin-mass dimensionless coupling constant is found to be $g_s g_p/\hbar c < 5 \times 10^{-27}$. This is a new limit on this axionic coupling in the interaction range of 1 to 100 cm.

1. INTRODUCTION

Violation of the principle of equivalence by anomalous spin-dependence is much less tested than violation by composition dependence. There is, nevertheless, a history of its consideration at least from Cartan[1] to the present. Classically, one could motivate such studies by consideration of the Poincare' Group and its invariants[2]. The only invariants are mass and spin (helicity if mass=0). One could consider the mass-mass interaction as the usual gravitation. Hypothetical G(r) and composition-dependent forces could also be in this category. Long range (Yukawa) spin-spin and mass-spin interactions can be postulated as well, and these are the cases we study here.

In 1984 Moody and Wilczek[3] set forth a framework specifically considering anomalous spin-dependence associated with interactions between two fermions. Their motivation was the detection of the invisible axion, which would mediate the interaction. Three types of potentials emerge, somewhat in analogy with the above three classical cases. The virtual axion has vertices which are pseudoscalar at an interacting polarized particle and scalar at an unpolarized particle. The three potentials can be written,

$$V^M = (g_s^1 g_s^2/\hbar c)e^{-r/\lambda}, \tag{1}$$

$$V^D = (g_s g_p/\hbar c)(\hbar^2/8\pi m_p)\,\sigma\cdot r\,(1/\lambda r + 1/r^2)e^{-r/\lambda}, \tag{2}$$

and

$$V^T = (g_p^1 g_p^2/\hbar c)(\hbar^3/m_p^1 m_p^2)[(1/\lambda r^2 + 1/r^3)\,\sigma^1\cdot\sigma^2 - (1/\lambda^2 r + 3/\lambda r^2 + 3/r^3)(\sigma^1\cdot r)(\sigma^2\cdot r). \tag{3}$$

Here, V^M, V^D, and V^T are analogous to the mass-mass, mass-spin, and spin-spin forces. g_s and g_p are the scalar and pseudoscalar coupling constants, λ is the range of the interaction and m_p is the mass of the polarized particle.

A torsion pendulum has been set up in two arrangements to probe (2) and (3). The earlier spin-spin experiment[4] used four cylindrical spin masses with polarization in the vertical direction. The spins of the "attracting masses" external to the vacuum chamber were alternately set to be parallel, and then antiparallel to spins of the "detecting masses" on the torsion beam, as shown schematically in Fig. (1a). To first order in Eq. (3) the terms $\sigma^1\cdot r$ and $\sigma^2\cdot r$ are zero, and the $\sigma^1\cdot\sigma^2$ term changes sign with the change from parallel to antiparallel. The sought-for signal is a change in the pendulum period, or frequency, with this reversal.

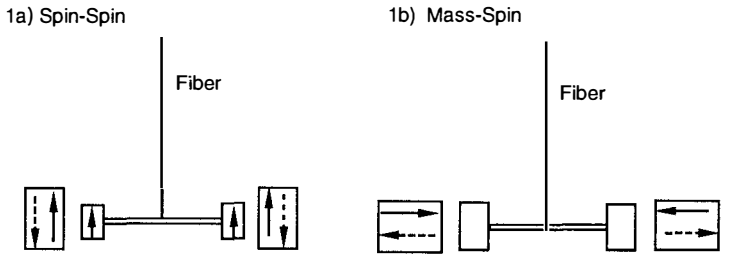

Figure 1. Schematic diagram of spin arrangements for the two experiments. Dashed arrows show the reversed directions of σ.

In the mass-spin experiment[5] the masses on the torsion beam are unpolarized copper, containing ~ 10^{25} interacting nucleons, and the attracting spin masses have their spins horizontal, as shown in Fig. (1b). The expected signal in this case would be the pendulum frequency change which occurs as the spins are reversed in direction relative to the copper masses, which reverses the sign of $\sigma \cdot \mathbf{r}$ in Eq. (2). Here we will consider the earlier spin-spin experiment briefly, and the mass-spin experiment in more detail.

II. THE SPIN-SPIN EXPERIMENT

The primary characteristic of these experiments are the spin masses, of Dy_6Fe_{23}, a "compensating material" in which the intrinsic spin of the electrons is polarized in one direction and the orbital spin opposing at room temperature, so that there is only a small magnetic moment left. The material is well-modelled by two opposing Brillouin functions, having different temperature dependence, so a key feature is the resulting temperature dependence of the magnetic moment of the compound. From temperature dependence of the field on the end surface of the constructed masses, a slope is determined, which can be compared with the model and with measurements made on single crystals of the material. The comparison shows that the material is 75% polarized, and from the g-factor, the number of polarized electrons determined[4].

Major features of both experiments are similar, and details can be found in [4] and [5]. In both cases experimental runs consisted of two halves, each about 3 hours in duration. In each half-run the pendulum period of about 711 s was measured to a few ppm by the centroid of the power spectrum[6], which also contained many diagnostic features. The frequency differences for each run pair form the raw data. In the spin-spin experiment, the geometry was such that a complex series of studies was needed to determine the limits on systematic errors, which were separated into four categories.

After all corrections and error assessment a limit was assigned for the frequency

shift which corresponds to a limit on the dimensionless coupling constants of $(g_p^1 g_p^2/\hbar c) < 1.5 \times 10^{-12}$ for interaction ranges greater than 2 cm. This is to be compared with a recent Ni result[7], about 6 times lower, over the same range. A limit of 1.4×10^{-15} was found by Bobrakov et al[8] using the magnetism induced in a sample by the axionic (or "arionic") coupling. The range and calibration details for this experiment were not given. In 1979 Ramsey[9] analyzed the tensor force between two protons at ranges >> than nuclear distances but still small by macroscopic scales. This yielded a limit for the dimensionless coupling constants of an interaction *between two protons* of about 10^{-4}. The previously discussed limits were for electrons.

3. THE MASS-SPIN EXPERIMENT

The mass-spin experiment consisted of four separate run series, each of about two months duration. Two of the series were as depicted in Fig. (1b), but two others had the spin of one of the masses reversed, so that the signs of $\sigma \cdot \mathbf{r}$ were opposite for the two interacting mass pairs at the two ends of the torsion beam. These special runs should give null results, and therefore served as diagnostic methods for geometric imperfections. In addition, in one of the regular run series, and in one of the null run series the positions of the attracting masses were exchanged, to give further information on the geometric errors. The standard runs should be symmetric under this interchange, while the null runs should be antisymmetric.

Fig. (1b) suggests that the experiment can have systematic error from an offset along the axis of the center of mass of the attracting spin-masses. In a subsidiary experiment we measured this offset with a leveraged balance arrangement shown in Fig. (2). This result accounts to within 0.010 μHz for a measured 5σ frequency difference of -0.160 μHz in the raw data for the main runs.

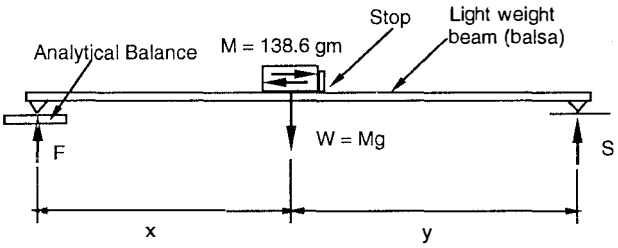

Figure 2. Measurement of center of mass axial offset

The statistical uncertainty of the main runs is determined to be 0.022 μHz, based on approximately 70 run pairs from each of the four series. Including 9 other uncertainties[5], an overall error of 0.047 μHz is assigned, at the 1-σ level. The signal is then $|\Delta f| < (-0.010 \pm 0.047)$ μHz, or a limit $\Delta f < 0.060$ μHz. When this is put into Eq. (2) with the geometry[5], the dimensionless limit is found: $g_s g_p/\hbar c < 5 \times 10^{-27}$ for $\lambda > 3$ cm. Weinland et al[10] used trapped ^{9}Be ions in an NMR experiment with the Earth as a source mass, and found an asymptotic (long range) dimensionless limit of 3×10^{-33}, referring to the neutrons in the ^{9}Be interacting with the Earth. Venema et al[11] used trapped ^{199}Hg and ^{201}Hg ions interacting with the Earth to raise the sensitivity about a factor of six, again referred to the neutrons in the sample. Since the Earth was the source for these NMR experiments, there is a substantial decrease in sensitivity as λ decreases. Adelberger[12] models this case with a spherical source. Under these assumptions the limits on the coupling constants set by the atomic experiments rise above the present torsion pendulum result for ranges greater than about 1 m.

Turner[13] and Raffelt[14] have reviewed the axion existence from astrophysical arguments involving stellar evolution. With an inflationary universe, a window of untested limits exists for axion masses in the range 10^{-6} to 10^{-3} eV, corresponding to a range λ of 0.02 to 20 cm. A search for the heavier axion would require measurements such as that by Ramsey[9] or others, with λ well below one cm.

Colleagues in these experiments are L.I. Winkler, G.T. Gillies, W.-T. Ni, C. Goldblum and C. Speake.

REFERENCES

1. E. Cartan, Ann. Sci. Ec. Norm. Super. **40**, 325 (1923); 41, **1** (1924).
2. Pointed out to me by W. -T. Ni.
3. J.E. Moody and F. Wilczek, Phys. Rev. D **30**, 130 (1984).
4. R.C. Ritter *et al*, Phys. Rev. D **42**, 977 (1990).
5. R.C. Ritter, L.I. Winkler, and G.T. Gillies, Phys. Rev. Lett. **70**, 701 (1993).
6. C.E. Goldblum, R.C. Ritter, and G.T. Gillies, Rev. Sci. Instrum. **59**, 778 (1988).
7. S.-S. Pan, W.-T. Ni, and S.-C. Chen, Mod. Phys. Lett. **7**, 1287 (1992).
8. V.F. Bobrakov *et al*, Pis'ma Zh. Eksp. Teor. Fiz. **53**, 283 (1991) [JETP Lett. **53**, 294 (1991)].
9. N.F. Ramsey, Physica (Amsterdam) **96A**, 285 (1979).
10. D.J. Wineland *et al*, Phys. Rev. Lett. **67**, 1735 (1991).
11. B.J. Venema *et al*, Phys. Rev. Lett. **68**, 135 (1992).
12. E.G. Adelberger *et al*, Ann. Rev. Nucl. Part. Sci. **41**, 269 (1991).
13. M.S. Turner, Phys. Rep. **197**, 67 (1990).
14. G.G. Raffelt, Phys. Rep. **198**, 3 (1990).

CONSTANT OF GRAVITY AND COMPOSITION-DEPENDENT INVERSE SQUARE LAW TEST ON STEP

Ho Jung Paik
Department of Physics and Center for Superconductivity Research
University of Maryland, College Park, MD 20742, USA

ABSTRACT

STEP will carry a dedicated superconducting gravity gradiometer system to determine G to 10^{-6} and to test the $1/r^2$ law at cm ranges to 10^{-6}, both two orders of magnitude improvement over the ground-based experiments. The instrument will consist of two concentric pairs of test masses, which form two independent gradiometers. A pair of source masses, moving along the center axis, will generate gravity signals for both experiments. By making the inner and outer test masses out of different materials and comparing the corresponding test results, composition dependence of the new force will be examined.

Metrology and calibration of the gradiometers are the most important error sources. In order to ensure density homogeneities to better than one part in 10^6, the test masses will be made out of single-crystal dielectric materials. Optical measurement techniques will be employed to determine the shapes to one part in 10^6. The gravity gradient signal from the Earth will be used to calibrate the gradiometers absolutely to the required accuracy.

I. Introduction

The gravitational constant (G) is the oldest known constant in nature, defined in Newton's Universal Law of Gravitation three hundred years ago. The attempt to determine G has become the cornerstone of modern precision experiments. Nevertheless, two hundred years of dedicated efforts on the part of first-rate experimenters, since Cavendish "weighed the Earth" using a torsion balance in 1798,[1] has improved the value of G by only a factor of 100, with the uncertainty still standing at about 1 part in 10^4.

The difficulty in improving the value of G arises fundamentally from the weakness of gravitational coupling. However, modern space technology, coupled with the exquisitely sensitive STEP accelerometers, gives us an opportunity to improve the value of G by two orders of magnitude to 1 part in 10^6, a feat representing two hundred years of progress, if extrapolated linearly from the history of the G experiments!

Closely related with the measurement of G is the Inverse Square Law ($1/r^2$) nature of gravity. If the $1/r^2$ law should be violated, G might not be a *universal constant*, or at least it should be redefined. STEP will also investigate the distance dependence of the gravitational force at short range, improving the limit on α also by two orders of magnitude, to 10^{-6} at $\lambda \approx 1$ cm, where α and λ represent the dimensionless coupling constant and the range of the Yukawa potential superposed with the Newtonian term. Terrestrial torsion-balance experiments have obtained an upper limit of 2×10^{-4} for α at the same range.[2, 3]

In order to perform these experiments, STEP will carry a dedicated gradiometer system composed of two concentric pairs of accelerometers. The two gradiometers will be made of different materials for a *composition-dependent* test of the $1/r^2$ law. This gradiometer system will also allow high-resolution mapping of the Earth's gravity.

The density inhomogeneity of materials and metrology errors limit the ultimate precision of short-range gravity experiments. Single crystals of dielectric materials can be

grown with density homogeneity as high as 1 part in 10^8. For simple shapes with dimensions of centimeters, standard metrology would determine the shapes to 10^{-5}. For transparent materials, this error could be reduced to 10^{-6} or better by using optical measurement techniques. We set 10^{-6} as a common goal for the G and $1/r^2$ experiments.

In addition to the metrology requirements, the G experiment requires an *absolute calibration* of the accelerometers to the accuracy desired for G. In the experiment by Luther and Towler[4], which yielded the presently accepted value of G, gravitational acceleration was calibrated by measuring the resulting increase in the resonance frequency of the torsion fiber. They report, however, that the measurement of this frequency shift was their dominant error source and is one the most difficult to improve.

In space, one finds an elegant solution for acceleration calibration. Modern satellite geodesy has advanced the knowledge of the Earth's gravity to the point of measuring the geocentric gravitational constant, GM_E, to 10^{-9}. The Global Positioning System (GPS) can determine the geocentric position of the spacecraft to 10^{-8}. These can be combined, along with the improved gravity model of the Earth from the STEP geodesy co-experiment, to calibrate the gradiometers to the required accuracy of 10^{-6}.

II. Principles of the Experiments

Figure 1 illustrates the principle of the STEP G and $1/r^2$ experiments. A differential accelerometer is formed by two identical cylindrically symmetric test masses separated by about 0.75 m along their common axis. These act as a gradiometer sensitive to the gradient of the horizontal component of the Earth's gravitational field. The orbit frequency or the second harmonic gradient of the Earth is used to calibrate the gradiometer. In addition to enabling the absolute calibration of the scale factors, the gradiometer configuration improves the resolution by 10^4 by rejecting the spacecraft acceleration by the same factor.

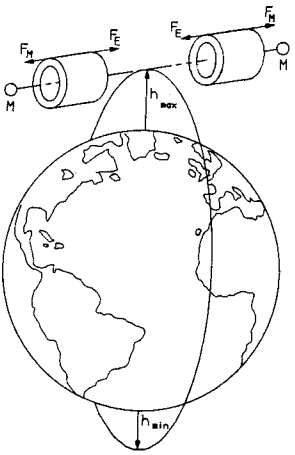

Fig. 1 Principle of the G and $1/r^2$ experiment. The altitude variation of the spacecraft produces a time-varying gravity gradient force from the Earth, F_E, on each test mass. This signal is used to calibrate the gradiometer accurately. The source masses (M) moving along the symmetry axis exert a time-varying gravitational force F_M on each test mass. The absolute value of F_M is used to measure G. Its dependence on the source position is used to test the $1/r^2$ law.

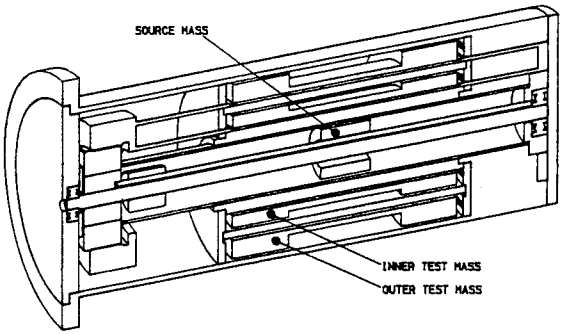

Fig. 2 Cut-away view of one half of the G and $1/r^2$ apparatus. The other half of the apparatus, 75 cm away along the symmetry axis (not shown), contains a mirror image of the instruments shown here. The inner test masses on the two ends form a gradiometer. The outer test masses form a separate gradiometer. The source masses are constrained to move along the symmetry axis by magnetic bearings.

To measure G and to test the $1/r^2$ law, two identical source masses are accurately moved through each test mass along the common axis at a frequency of 3×10^{-3} Hz. The movements are in antiphase to eliminate the net linear and angular momentum of the source motion, and to add the gravity signals at the gradiometer. The maximum differential signal occurs when the source masses are near the ends of the test masses. The source position is modulated between these points and the resulting acceleration signal is used to compute G. The $1/r^2$ test is made by measuring the differential acceleration as a function of the source mass position.

The cylindrical symmetry employed in the experiment reduces several important metrology errors. By constraining each source mass to move along the symmetry axis of the cylindrical test mass and by using the maximum signal, the gravity error arising from the uncertainty in the position of the source mass relative to the test mass becomes second order, both in the axial and radial directions. In order to perform a *near-null test* of the $1/r^2$ law, a particular shape is chosen for the test masses. According to Newton's law, the gravitational field vanishes everywhere inside an infinitely long cylindrical shell. In the test mass, a ring is added on each end of the short cylinder to correct for the missing mass and and create a small region where the Newtonian field almost vanishes (Fig. 2). This near-null geometry greatly reduces the scale factor linearity requirement.

In order to provide redundancy and valuable cross checks for the G, $1/r^2$ and geodesy experiments, a double gradiometer configuration is used. In the design, each test mass in Fig. 1 is replaced by two concentric test masses (Fig. 2). The inner and the outer test mass pairs form two separate gradiometers. *Cross checks* are essential for credibility of such drastically improved, new scientific results as we are seeking in STEP. Further, by constructing the two gradiometers with different materials, the composition dependence of the new force can be examined.

III. Hardware Description

The gradiometer system is composed of two identical instrument packages separated over 75 cm along the axis normal to the orbit plane, as shown in Fig. 1. Figure 2 shows a cut-away view of one of these packages. The source mass is made out of platinum-10% iridium alloy (density of 21.6 g cm^{-3}) and is driven along the symmetry axis to produce time-varying gravity signals. The inner and outer test masses are made out of single-crystal BGO ($Bi_4Ge_3O_{12}$, density 7.1 g cm^{-3}) and single-crystal sapphire (Al_2O_3, density 4.0 g cm^{-3}), respectively. These crystals are transparent and their average atomic numbers are well separated for a composition-dependence test. A single-crystal lead floride (PbF_2, density 8.2 g cm^{-3}) is another candidate for the inner test mass material.

The source mass is a circular cylinder with a hole through the center to accommodate a threaded rod for caging. Each source mass weighs 93.6 g and its dimensions are chosen to make all of its quadrupole moments vanish. It is levitated and driven magnetically. The axial position of the source mass is sensed electrostatically. The required position resolution is 0.01 μm for a small ± 2 mm range from the center and 1 μm for the full range of ± 6 cm.

There are four test masses in the system. Two inner masses are connected together and to two SQUIDs (Superconducting QUantum Interference Device)s by a standard superconducting differencing circuit to form a gradiometer.[5] The two SQUIDs measure the common and differential accelerations, simultaneously. The outer masses form a separate gradiometer. The inner and outer test masses weigh 301 and 334 g, respectively. Since these gradiometers will also be used to obtain geodesy data with a bandwidth from near dc to about 0.02 Hz, we keep the axial differential-mode frequencies above the signal bandwidth, at around 0.1 Hz.

The levitation, sensing, and mode damping schemes for the G gradiometers are

similar to those for the Equivalence Principle (EP) accelerometers. In order to make the test mass a one-dimensional system and thus minimize coupling between the axial and radial degrees of freedom, the radial springs are much stiffer than the axial spring.

Efficient electromagnetic shielding is extremely important to prevent a direct cross talk between the source and detector circuits. The ability of superconductors to perfectly screen electromagnetic fields allows us to achieve the requisite high degree of isolation between the circuits.

IV. Instrument Noise and Experimental Resolutions

The intrinsic noise of a superconducting accelerometer deteriorates at low frequencies due to the 1/f noise of the SQUID. On the other hand, the spacecraft acceleration noise improves as the frequency is lowered toward 10^{-4} Hz since the drag-free controller is optimized for the EP signal frequency. Therefore, there is an optimum signal frequency one can choose for the G and $1/r^2$ experiments, which is about 0.003 Hz. The intrinsic noise of the STEP gradiometers at this frequency is found to be 3.0×10^{-14} m s^{-2} $Hz^{-1/2}$. In order to take full advantage of this low intrinsic noise level, we require that all other disturbances be kept below this level.

The Newtonian accelerations that the near source mass exerts on the inner and outer test masses are plotted in Fig. 3(a) as a function of the source position. The far source mass exerts an acceleration about 10^3 times smaller, which can easily be corrected for. As the two test masses in each gradiometer experience equal and opposite accelerations, the peak signals on the inner and outer gradiometers are 5.8×10^{-9} and 3.0×10^{-9} m s^{-2}, respectively, twice the values given in Fig. 3(a).

Since one is interested only in the peak-to-peak amplitudes, ideally one would like to apply a square-wave modulation to the source position. A practical substitute would be a

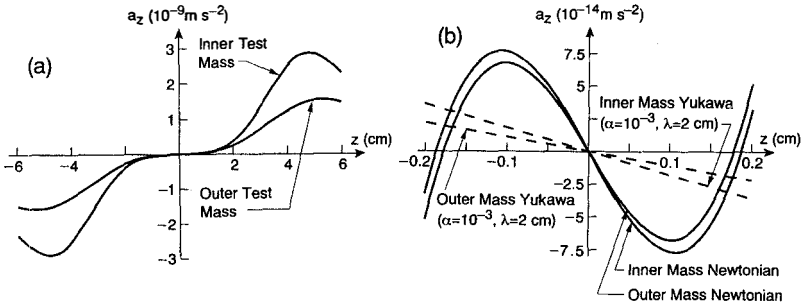

Fig. 3 (a) Newtonian accelerations on the test masses as a function of the source position. The peak values of these signals are measured and compared with the computed values to determine G.
(b) Newtonian and Yukawa accelerations on the test masses near the center as a function of the source position. The Newtonian signals are averaged out by modulating the source position with a proper amplitude. The Yukawa signals are detected at the modulation frequency.

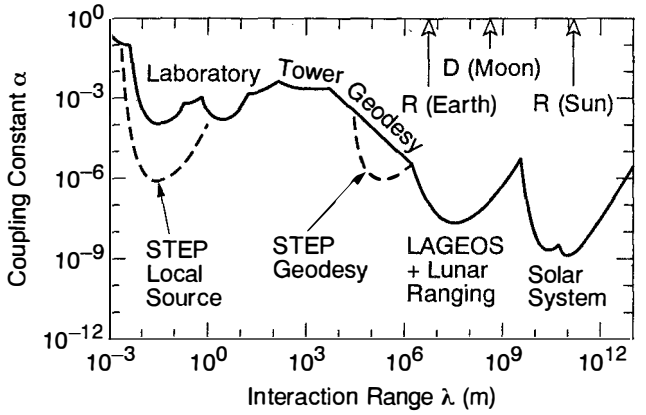

Fig. 4 Existing limits and resolutions expected from STEP for a violation of the $1/r^2$ law. The solid curve represents the existing limits on α as a function of λ, adapted from Ref. 6. The dotted lines represent resolutions expected from STEP.

truncated triangle-wave modulation with the corners smoothed. If the source mass spends roughly half of the time making measurements at the two maximum positions, then the gradiometers can resolve the signals to better than 3×10^{-7} in only 10^4 s.

Figure 3(b) expands the central region of Fig. 3(a), within ± 2 mm of the center, and also shows the Yukawa components corresponding to $\alpha = 10^{-3}$ and $\lambda = 2$ cm. The test mass dimensions have been adjusted to make the Newtonian components oscillate about zero as the source is moved back and forth. Therefore, by modulating the source position between two carefully selected points, the Newtonian signals can be averaged out, while the Yukawa components are detected at the modulation frequency. Figure 3(b) shows that the Newtonian signals must be averaged to 3×10^{-4} in order to resolve α to 10^{-6}.

The strength of $1/r^2$ violation depends on λ. For the source-detector geometry chosen, the Yukawa force becomes a maximum when λ is approximately 2 cm. According to Fig. 3(b), the amplitudes of the differential Yukawa signals for $\lambda = 2$ cm are 7.0×10^{-11} α and 4.0×10^{-11} α m s^{-2}, respectively, for the inner and outer gradiometers. Assuming an integration time of 10^6 s, α can then be resolved to 5×10^{-7} and 7×10^{-7}, respectively. For different values of λ, the resolution of α deteriorates.

The α-λ plot for the STEP $1/r^2$ experiment is shown in Fig. 4, along with the existing limits. Also shown in the figure is the resolution of the $1/r^2$ law at $\lambda \approx 300$ km which would result from the analysis of the orbit fundamental and second harmonic components of the Earth's gravity in the geodesy co-experiment.

The G and $1/r^2$ results obtained with the two gradiometers can be compared to check the composition dependence of the new force. In the absence of any composition dependence, the measurements by the two gradiometers must agree within the experimental error. On the other hand, a disagreement implies existence of a composition-dependent $1/r^2$ law violating force.

V. Absolute Calibration of the Gradiometers

The gradiometers must be calibrated *absolutely* to at least 1 part in 10^6 at the G signal level. Various options have been investigated. The best option appears to be the use of the Earth's gravity gradient as the calibration signal.

The STEP spacecraft will be in a near circular polar orbit at a nominal altitude of 550 km, with residual eccentricity of about 10^{-3}. The sensitive axes of the gradiometers are aligned perpendicular to the orbit plane. The resulting variation in the radial position of the spacecraft, $\Delta R \approx \pm 7$ km, will generate an orbit frequency component of the Earth's gradient, $\Delta\Gamma_E \approx \pm 4$ E, where 1 E = 10^{-9} m s^{-2} m^{-1}. The Earth's quadrupole moment will contribute a second harmonic component of comparable amplitude. These acceleration levels coincide with the levels of the G signals and eliminate calibration errors that could result from nonlinearity of the scale factors.

The calibration signal is contaminated by the errors in the higher harmonic coefficients of the Earth's gravity. Fortunately, the gravity model will be improved by STEP by more than two orders of magnitude. A simulation has confirmed that calibration to 1 part in 10^6 is indeed feasible.

VI. Disturbance Control Requirements

The linear and angular motions of the spacecraft couple to the gradiometers through misalignment of the sensitive axes. With the common-mode rejection to 10^{-4}, the basic drag-free and attitude control of the STEP spacecraft satisfies the linear and angular acceleration requirements.

Angular motion of the spacecraft can also produce errors through modulation of the Earth's gravity gradient and centrifugal acceleration. Fortunately, both of these become

second-order effects due to the orientation chosen for the STEP gradiometers, the inertial orientation with their sensitive axes horizontal. The reduced pointing and pointing stability requirements are satisfied by the attitude control of the spacecraft.

The energetic charged particles, which is one of the most important error sources for the EP experiment, cause significantly less disturbance for the G and $1/r^2$ experiments. However, the helium tide is a potentially critical error source.

A *horizontal* component of the helium tide at the orbit fundamental and second harmonic can contaminate the absolute calibration of the gradiometers. In the worst case, the helium tide could produce an error an order of magnitude greater than allowed for the 10^{-6} calibration. The source masses also pull the helium around, but the effect is negligible due to the smallness of the masses and the symmetry of their motion.

There is a simple solution to the helium problem: Conduct the calibration and the G experiment half way into the mission, at the time when the inner helium tank is full and the outer tank is empty. This will eliminate any chance of a helium tide.

Acknowledgments

I am grateful to Jean-Pierre Blaser for many useful suggestions and performing the helium tide calculation, to Terry Quinn for advising me on various metrology issues, and to Ernst Schrama for carrying out simulations for the gradiometer calibration.

---

1. H. Cavendish, Phil. Trans. Roy. Soc. **88**, 467 (1798).
2. R. Spero, J.K. Hoskins, R. Newman, J. Pellam, and J. Schutz, Phys. Rev. Lett. **44**, 1645 (1980).
3. Y.T. Chen, A.H. Cook, and A.J.F. Metherell, Proc. R. Soc. Lond. A **394**, 47 (1984).
4. G.G. Luther and W.H. Towler, Phys. Rev. Lett. **48**, 121 (1982).
5. H.A. Chan, M.V. Moody, and H.J. Paik, Phys. Rev. D **35**, 3572 (1987).
6. E.G. Adelberger, B.R. Heckel, C.W. Stubbs, and W.F. Rogers, Ann. Rev. Nucl. Part. Sci. **41**, 269 (1991).

STEP SPIN COUPLING EXPERIMENT

C. Speake
School of Physics and Space Research, University of Birmingham, England

T. J. Sumner and D. Shaul
Astrophysics Group, Blackett Laboratory, Imperial College, London, England

Y. R. Jafry
Space Science Department, ESA/ESTEC, Noordwijk, The Netherlands

J. Léon
LAEFF, Madrid, Spain

Abstract

The aim of the STEP Spin-Coupling Experiment (SCE) is to make use of the low-noise, zero -g environment on the STEP spacecraft to search for a new interaction between quantum-mechanical spin and matter. STEP (the Satellite Test of the Equivalence Principle) is a proposed ESA M2 mission to test the Weak Equivalence Principle in a drag-free spacecraft in low-Earth orbit. If approved, the mission would be launched in 2001, and would last a nominal six months. The essence of the STEP mission is to detect any change in the rate of fall of different materials in the Earth gravity field. Superconducting differential accelerometers utilizing SQUID position sensors are at the heart of the instrument.

We present a design of a spin-coupling experiment which shows that a sensitivity of $g_p g_n$ (spin-coupling constants) of 10^{-34} at a range of 1 mm is feasible. This represents a seven order of magnitude improvement over ground-based measurements. The experiment consists of a superconducting differential accelerometer driven by a polarizable source. Superconducting shielding is used to screen the source from the accelerometer to eliminate electromagnetic forces.

We are currently investigating ways of increasing the sensitivity of the experiment by two orders of magnitude. If this can be achieved, the sensitivity will be in the regime required to place new limits on the constants which describe the spin-coupling interaction of the axion.

Introduction

Axions or axion-like particles have scalar and pseudoscalar couplings to matter; they couple both to a "monopole charge" and to a magnetic-like "dipole charge". Only spin-polarized bodies would possess a macroscopic charge of the dipole type. Axion exchange results in monopole-monopole, monopole-dipole and dipole-dipole forces. Moody and Wilczek (1984) have argued that the monopole-dipole forces are the easiest to detect. They postulate a finite range (λ) interaction of the form

$$\mathbf{V_a} = g_s g_p (\frac{\hbar^2}{8\pi m_e}) \hat{\sigma} \cdot \hat{r} \left(\frac{1}{\lambda r} + \frac{1}{r^2} \right) \exp(-r/\lambda) \tag{1}$$

where g_s and g_p are dimensionless coupling constants referring to the scalar and pseudo scalar vertices, m_e is the mass of the fermion within the polarised source (the electron) and $\hat{r}$ is the unit position vector of the nucleon relative to the fermion. The axion interaction is described by two quantities; a spontaneous symmetry-breaking energy scale, F, and the magnitude of CP violation suppression, θ. One property of the axion is that its mass is related to the energy scale F as

$$m_a \simeq 10^{-5} eV (10^{12} GeV/F) \tag{2}$$

Alternatively, the range of the axion-mediated interaction is given as

$$\lambda \simeq 2\ cm (F/10^{12} GeV) \tag{3}$$

Moody and Wilczek's theory leads to

$$g_p g_s = \frac{\theta}{\lambda^2} \times 6 \times 10^{-33} \tag{4}$$

with λ in metres.

There are well accepted limits to the range which suggests that 0.2 mm $\leq \lambda \leq$ 20 cm (these limits are discussed in Kolb and Turner, 1990). Constraints on the value of θ are derived from the electric dipole moment of the neutron which is limited to a maximum value of 5×10^{-25} e cm (Pendlebury et al., 1984). Values of θ are model dependent with a maximum of about 10^{-8} but the majority of models give an upper limit of 10^{-9}. There have been some attempts at deriving a theoretical value for θ, notably Wilczek estimates its value as 10^{-14}. In practice it is difficult to examine ranges as small as 0.2 mm so, if we restrict ourselves to a minimum range of 1 mm, we see that the maximum value that can be expected for the product of the coupling constants is

$$g_p g_s = 6 \times 10^{-36} \tag{5}$$

This is a fairly new area of experimentation and there are, as yet, only a handful of results for the limits on the product of $g_p g_s$. Experimental results up to the end of 1990 are described in the comprehensive review of Adelberger et al. (1991). More recently Venema et al. (1992) employed NMR techniques with mercury atoms to establish an upper limit of 7×10^{-35} for an interaction with a range of 10^6 m. Ritter et al. (1993) performed a torsion balance experiment and have placed an upper limit on $g_p g_s$ of 5×10^{-27} for ranges larger than 10 cm. One would

expect a short range test using NMR techniques to be done in the near future with a sensitivity of about 10^{-28} at 10 cm. It appears then that no experiments have yet approached the sensitivity required to place restrictions on axion theory.

We now present a design of a spin coupling experiment, as part of the STEP payload, which shows that a sensitivity of $g_p g_s$ of 6×10^{-34} at a range of 1 mm is feasible. This represents a seven order of magnitude improvement over the existing ground-based measurements but is two orders of magnitude away from being competitive with the constraints on θ derived from measurements of the electric dipole moment of the neutron.

Experiment design

Moody and Wilczek (1984) proposed an experiment which used a source of high magnetic permeability which could be polarized with a solenoid. A sapphire crystal placed close to the source would then resonantly detect a spin-coupled stress due to the modulation at acoustic frequencies of the spin directions within the source. Moody and Wilczek proposed to use superconducting shielding to eliminate magnetic forces on the crystal due to the leakage of magnetic field from the source. The STEP experiment has adopted this basic experimental arrangement. However, we intend to replace the crystal with a superconducting differential accelerometer. The differential accelerometers will work at a much lower frequency than the sapphire and this will not only improve sensitivity but will also enable us to use commercially available high permeability materials which cannot be polarized at acoustic frequencies. If we have a polarized source with an electron spin density of ρ_s and a test mass of nucleon density ρ_N, then we can use Eq. 1 to calculate the spin-coupled force between them as

$$f_a = \frac{\theta}{\lambda^2} \times 7 \times 10^{-61} \rho_s \rho_N \frac{dI}{dx} \qquad \text{(mks)} \tag{6}$$

where I is the integral from Eq. 1

$$I = \frac{1}{8\pi} \int\int (\hat{\sigma} \cdot \hat{r}) \left(\frac{1}{\lambda r} + \frac{1}{r^2} \right) \exp\left(\frac{-r}{\lambda} \right) dV_1 \, dV_2 \tag{7}$$

In designing the experiment, we must consider the geometry of the monopole-dipole field, and configure the three dimensional sources and test masses to provide the largest signal. We have considered possible designs where the test mass and source were cylindrically symmetric and coaxial and where the spin alignment axis was parallel to the axis of the cylinders. For these coaxial geometries, an expression for dI/dx was derived which reduced the six-order integration to a single numerical integration and this was used to optimise the acceleration signal. As the dimensions of the source and test mass, and the gap between them, are reduced, the acceleration increases because the axion coupling constants vary as $1/\lambda^2$. However, as the size of the test mass becomes smaller, many experimental problems arise. At present, we believe that the smallest range which can be designed for is around 1 mm.

Figure 1 shows the design of the instrument. We employ 16 square-section toroidal polarizable sources which are each coated with superconductor. On the inside of the source assembly, there is a test mass comprising 16 annuli mounted on a former which is supported

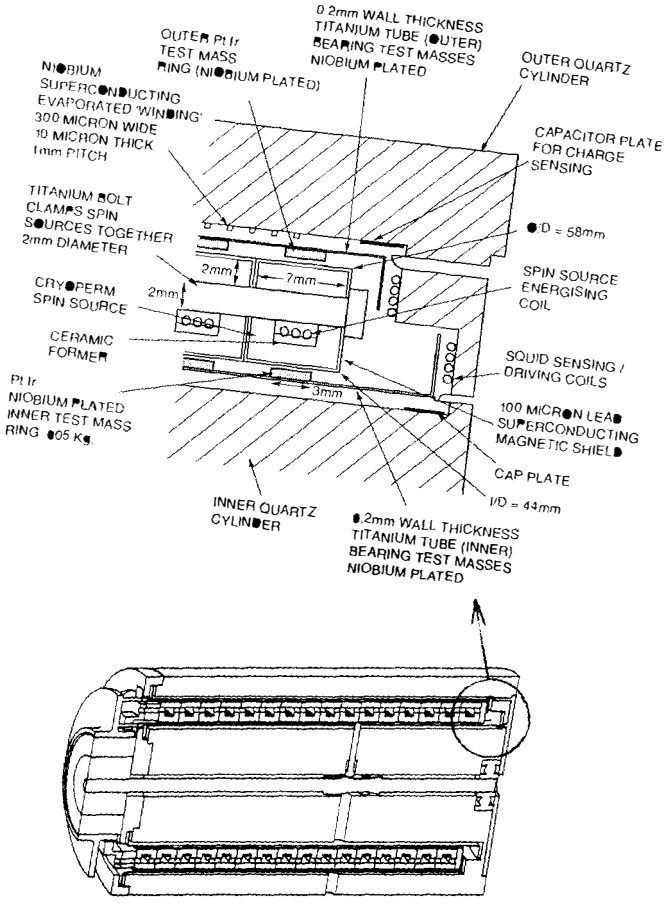

Figure 1. *STEP spin coupling differential accelerometer.*

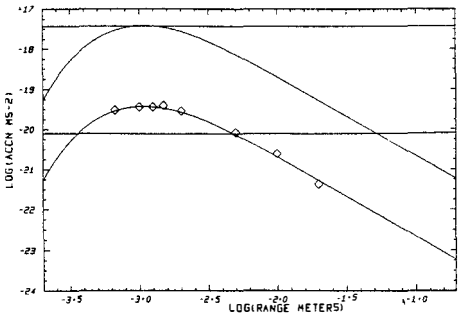

Figure 2: *Putative spin coupling acceleration as a function of range for the exact experimental geometry. The lower and upper curves represent accelerations, calculated analytically, which would be expected from an axion spin coupling with values of* θ *of* 10^{-9} *and* 10^{-7}*, respectively. The diamonds are values calculated using numerical integrations.*

by a superconducting bearing. A similar composite test mass encloses the source, and the test mass pair forms a differential accelerometer. The upper part of the picture shows a close-up of one of the annulus/test mass pairs. The annuli and support tubes are manufactured from platinum-iridium alloy and titanium, respectively. The tubes are completely coated with niobium. Titanium and platinum alloy are chosen because they optimise the ratio of useful test mass (material within the spin coupling field) to the total mass of the test mass assemblies. The titanium and platinum have similar integrated thermal expansion coefficients. Superconducting wires provide current to the sources and a net polarization of spins is created within the sources close to the test mass annuli. The annuli in each of the inner and outer test mass assemblies will then experience a force along the axis of the superconducting bearing; but in opposite directions. The ensuing differential motion is detected by the SQUIDs via two pairs of pancake coils which face the end flanges of the test mass assemblies. The inductance of the coil versus the test mass displacement was calculated numerically (Sumner, 1987), from which we can calculate the acceleration sensitivity of the accelerometer. If the period of the differential mode of the accelerometer is around 500 s, then we obtain an acceleration noise of 10^{-15} m s$^{-2}/\sqrt{\text{Hz}}$. This noise level is limited by the thermal Brownian motion noise.

Active dynamical charge control is achieved by applying appropriate voltages to capacitor plates.

In order to discuss the magnitudes of potential noise sources, we will focus on a nominal noise level goal of 4×10^{-18} m/s^2. This corresponds to a sensitivity to the coupling constant product of 6×10^{-34} or a value of 10^{-7} for θ. Figure 2 shows a plot of the putative spin coupling acceleration signal as a function of range. We see that, if the axion were to have a range of 1 mm, then we might expect to see an acceleration of 4×10^{-20} m s^{-2} (4×10^{-21} g).

The polarizable source

For a high permeability ferromagnetic material, such as iron, the electronic spin density giving rise to the magnetisation is given by

$$\rho_s = B_{\rm int}/(\mu_B \mu_o) \tag{8}$$

where $\mu_B = e\hbar/2m_e$ is the Bohr magneton.

For Cryoperm 10 (a product of Vacuumschmeltze), $B_{\rm int}$ reaches a saturation value of 0.8 T at a magnetic intensity of 8 A/m and the internal field reaches 75% of its saturation value at an intensity of about 2 A/m. The maximum value of the current turns product for each source is about 0.2 Amp-turns.

Disturbances

The spin coupling experiment is subject to the disturbances common to all the STEP experiments (ESA/NASA, 1993), plus a few which are unique to this experiment.

The largest source of random noise will be the residual acceleration of the spacecraft. At a frequency of 2×10^{-3} Hz, the acceleration noise of the spacecraft will be about 4×10^{-11} m s$^{-2}/\sqrt{\rm Hz}$. If the common mode rejection ratio of the differential accelerometer is 10^4, then this residual spacecraft acceleration should limit the experiment to the nominal acceleration sensitivity of 4×10^{-18} m s^{-2} after about 10^6 s. Notice that this residual acceleration is about three orders of magnitude lower than that found in the quietest terrestrial laboratories.

The background spacecraft displacement will produce a background random noise acceleration due to common-mode motion of the test masses relative to trapped flux elements and patch effect fields. At the signal frequency of 2×10^{-3} Hz, the spacecraft displacement noise will be approximately 3×10^{-10} m after averaging for 5×10^5 s. We note, however, that the residual rms SQUID noise after a similar integration time, will be 10^{-14} m. Thus, in principle, we can extract the forces due to spacecraft displacement by cross-correlating the differential acceleration output with the large common mode signal.

A more fundamental noise source comes from fluctuations in any damping forces of thermal origin. Damping due to the residual gas pressure, $p \approx 10^{-11}$ Torr (1.3×10^{-9} Pa) gives, after 5×10^5 s of integration, a sensitivity limit of 8×10^{-19} m/s^2 which is below the target sensitivity. The Q of the differential mode must be at least 2×10^6. We believe this is feasible.

Leakage of magnetic field from the source will exert forces on the test masses. The geometry has been carefully chosen such that the magnetic flux path is closed, thus reducing the leakage to about 10^{-5} T. A (superconducting) lead coating of 0.1 mm isolates each individual source from its neighbour and from the test mass. Aditional shielding will be provided by niobium sheaths, 125 μm thick and separated from the sources by 0.1 mm, which will be mounted independently of the source assembly. It is well established that superconducting shielding can attenuate time dependent magnetic fields by factors of 10^{11} (Vitale et al., 1989).

There will be a fractional change of about 2.5×10^{-5} in the dimensions of each source associated with the magnetisation modulation due to magnetostriction. Any flux which is

trapped on the surfaces of the sources will be displaced by the magnetostriction. The niobium sheaths will prevent this motion from producing spurious forces on the test mass.

The changes in length of the source structure will also create a differential gravitational acceleration of about 10^{-16} m s^{-2}. This is a factor of 25 times larger than our nominal signal but should not present any difficulties because it occurs at the second harmonic.

References

Adelberger, E. G., Heckel, B. R., Stubbs, C. W., and Rogers, W. F. (1991). Searches for new macroscopic forces. *Ann. Rev. Nucl. Part. Sci.*, *41*, 269–320.

ESA/NASA (1993). STEP: Satellite Test of the Equivalence Principle, Report on the Phase A Study. SCI(93)4, ESA/NASA.

Kolb, E. W. and Turner, M. S. (1990). *The Early Universe.* Addison and Wesley.

Moody, J. E. and Wilczek, F. (1984). New macroscopic forces ? *Phys. Rev. D*, *30*, 130–138.

Pendlebury, J. et al. (1984). Search for a neutron electric dipole moment. *Physics Letters*, *136 B*, 327.

Ritter, R., Winkler, L., and Gillies, G. (1993). Search for anomalous spin-dependent forces with a polarized-mass torsion pendulum. *Phys. Rev. Letts.*, *70*, 701–704.

Sumner, T. (1987). A calculation of the effect of a coaxial superconducting shield on the magnetic field distribution of an enclosed coaxial solenoid. *J. Phys. D.*, *20*, 692–696.

Venema, B. J. et al. (1992). Search for a coupling of the Earth's gravitational field to nuclear spins in atomic mercury. *Physics Review Letters*, *68*, 135.

Vitale, S., Bonaldi, M., Falferi, P., Prodi, G. A., and Cerdonio, M. (1989). Magnetization by rotation and gyromagnetic gyroscopes. *Physical Rev. B*, *39*, 11993–12002.

Equivalence Principle: Theory

A NEW MECHANISM FOR CONSTRAINING MACROSCOPIC-RANGED PSEUDOSCALAR FORCES

Dennis E. Krause, Ephraim Fischbach, and Carrick Talmadge
Physics Department, Purdue University, West Lafayette, IN 47907 USA

Daniel Sudarsky
Dept. de Matematicas y Fisica, PUCMM, Santo Domingo, DOMINICAN REPUBLIC

Dubravko Tadić
Zavod za Teorijsku Fizku, University of Zagreb, 41000 Zagreb, CROATIA

Abstract

Present limits on the coupling strength of a long-range pseudoscalar interaction are many orders of magnitude weaker than for scalar or vector interactions, even though all are obtained using similar experimental techniques. Here we explore the reasons for the natural suppression of pseudoscalar forces, and propose a new mechanism which may circumvent this suppression and thereby lead to significantly improved laboratory limits.

1 Introduction

Within the past decade, a significant and successful experimental effort has led to very stringent constraints on new forces mediated by light scalar or vector bosons [1–3]. For such interactions the present constraint on the dimensionless coupling constant $f^2/4\pi$ is approximately 10^{-41} if the range of the force is ≈ 1 m. [1]. However, a similar effort utilizing many of the same experimental techniques has been much less successful in constraining pseudoscalar interactions [4–6]. In this case, the constraint on the analogous coupling constant for such a coupling to electrons is of order 10^{-12} [5, 6], some *29 orders of magnitude smaller than for the corresponding scalar interactions.* The laboratory limits on couplings to nucleons are weaker still. We will begin by showing why these constraints are so much weaker than their scalar counterparts, and then suggest ways to circumvent this problem. Finally we will propose a new mechanism arising from a higher-order 3-body interaction which may overcome these suppression effects, and which may allow the use of Eötvös-type experiments involving *unpolarized* bodies to put new tighter constraints on pseudoscalar forces.

2 Suppression of Pseudoscalar Limits

The simplest interaction of a pseudoscalar field ϕ with a fermion ψ has the form

$$\mathcal{L} = -ig\bar{\psi}\gamma_5\psi\phi, \tag{1}$$

where g is a dimensionless coupling constant ($\hbar = c = 1$) . The lowest order potential obtained from this interaction arises from the exchange of a single massless pseudoscalar boson (Fig. 1), and leads to the following expression for the potential energy between two identical point particles:

$$V_{PS}(r) = \frac{g^2}{4\pi}\left(\frac{1}{2mr}\right)^2\left[\frac{3(\vec{\sigma}_1\cdot\hat{r})(\vec{\sigma}_2\cdot\hat{r}) - \vec{\sigma}_1\cdot\vec{\sigma}_2}{r}\right]. \tag{2}$$

Here m is the mass, $\vec{\sigma}_{1,2}$ the spins, and $\vec{r} = \vec{r}_1 - \vec{r}_2$ is the separation of the fermions. The form of this potential can be contrasted with the more familiar one-boson-exchange potential arising from the exchange of a massless scalar field

$$V_S = -\frac{f^2}{4\pi}\frac{1}{r}, \tag{3}$$

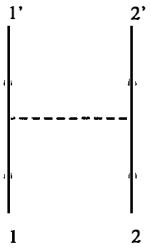

Figure 1: One-boson exchange diagram.

resulting from an interaction of the form

$$\mathcal{L} = -f\bar{\psi}\psi\phi, \tag{4}$$

where f is the dimensionless coupling strength for the scalar field.

We notice two significant differences between the scalar and pseudoscalar potentials. First, the pseudoscalar interaction is spin-dependent, and hence experiments searching for its effects must use polarized matter. This introduces severe technical difficulties, since the pseudoscalar interaction then must compete with the relatively strong magnetic dipole interaction whose potential has the same functional form as Eq. (2). However, these problems may be minimized by using materials such as Dy_6Fe_{23} in which the magnetic moments arising from the spin and orbital angular momenta cancel.

The second important difference between the pseudoscalar and scalar interactions is that the pseudoscalar potential is suppressed by a factor of $(1/2mr)^2$ relative to the scalar potential. For example, if the fermions exchanging bosons are electrons, and their separation is 1 meter (the scale of the spin-dependent experiments), then

$$\frac{V_{PS}}{V_S} \sim \left(\frac{g}{f}\right)^2 \left(\frac{1}{2mr}\right)^2 \sim \left(\frac{g}{f}\right)^2 \times 10^{-26}. \tag{5}$$

Thus, *if the coupling strengths of the two interactions are equal ($f = g$), the pseudoscalar force will still be 26 orders of magnitude weaker than the scalar force!* In other words, the limit on the pseudoscalar coupling g will be 26 orders of magnitude poorer than for the scalar coupling constant f using experiments with similar intrinsic sensitivity. This suppression has its origin in parity conservation: While a scalar boson is emitted by a fermion in an s-state, the pseudoscalar boson must be emitted in a p-state to conserve parity, and this

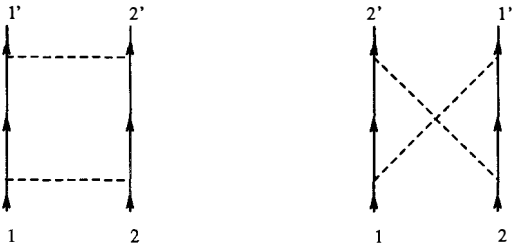

Figure 2: Two-boson exchange diagrams.

introduces an angular momentum suppression factor. Therefore, if one is to obtain limits on f comparable to g, the sensitivity of the spin experiments must be increased by at least 26 orders of magnitude, a challenge that will not likely be met in the near future.

3 Overcoming Suppression Effects

3.1 2-Boson Exchange Mechanism

Any hope of setting better limits involves finding a mechanism which will overcome these suppression effects. One alternative would be to look at higher order potentials. For example, the pseudoscalar potential arising from the exchange of two pseudoscalar bosons (Fig. 2) leads to the potential [7, 8]:

$$V_{PS}^{(4)}(r) = \frac{g^4}{64\pi^3 m^2 r^3} = \left(\frac{g^2}{4\pi}\right)^2 \left(\frac{1}{2mr}\right)^2 \frac{1}{\pi r}. \tag{6}$$

While this removes the necessity of using spin polarized matter, the $(1/2mr)^2$ suppression remains. Furthermore, this interaction is suppressed by an additional factor $g^2/4\pi$ compared with the single boson exchange potential. Evidently, all higher-order potentials involving a single pseudoscalar field will be similarly suppressed.

3.2 3-Body Mechanism

The preceding discussion suggests that we could improve the limits on pseudoscalar couplings if we could write an effective Lagrangian in a form which simulates a scalar interaction,

$$\mathcal{L}_{eff} = -Q(g)\bar{\psi}\psi\phi \tag{7}$$

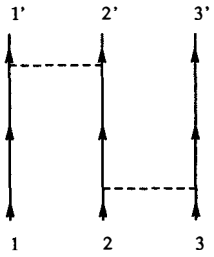

Figure 3: A 3-body potential diagram.

where $Q(g)$ is an effective charge depending upon the more fundamental coupling constant g. If this interaction is to conserve parity and time reversal when ϕ is a pseudoscalar field, $Q(g)$ must itself be a pseudoscalar quantity. Assuming that such an interaction exists, then the potential between two bound systems A and B arising from massless pseudoscalar exchange will have the form

$$V_{eff} = -\frac{1}{4\pi}\frac{\langle Q_A\rangle\langle Q_B\rangle}{r} \tag{8}$$

where $\langle Q_A\rangle$ is the expectation value of $Q(g)$ for system A, etc. The form of V_{eff} is identical to that for the usual scalar interaction, *except* that the charges are pseudoscalar quantities. If one could identify and calculate the effective charges for a pair of bodies (with the only unknown being the fundamental coupling constant g), then one could use the limits on scalar interactions from Eötvös-type experiments to constrain g.

We next show how an effective interaction of the form given by Eq. (7) might arise. Such an interaction involves the exchange of a pseudoscalar boson in an s-state which is impossible for a fermion when parity is conserved. However it is possible if the boson is emitted from a ***bound*** system, say a nucleus, which has internal degrees of freedom. To see this, consider three particles, #1, #2, and #3, interacting via the exchange of pseudoscalar bosons. In addition to the usual 2-body interactions, one can show that there exist 3-body (and, in fact, n-body) interactions among these particles (Fig. 3) [9]. If two of the particles, say #1 and #2, are located close to one another, and both are distant from #3, then the 3-body interaction reduces to an effective 2-body interaction between the pair of particles (representing a bound system) and the distant third particle (Fig 4). Then Q_{12} plays the role of the pseudoscalar charge Q of our effective Lagrangian $\mathcal{L}_{eff}$ given by Eq. (7) and leads

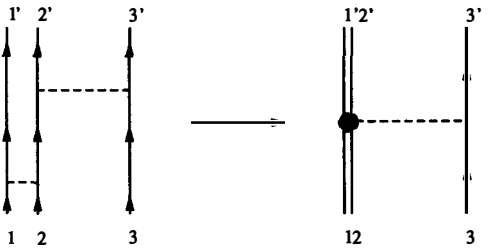

Figure 4: A 3-body interaction becomes an effective 2-body interaction if one particle is moved far away from the other two particles.

to the 2-body potential

$$V(r) = \langle Q_{12} \rangle \left(\frac{-g_3}{8\pi m_3} \frac{\vec{\sigma}_3 \cdot \vec{r}}{r^3} \right). \tag{9}$$

where $\vec{r}$ is now the displacement vector between the center of mass of particles #1 and #2, and the distant mass #3. One first calculates the general 3-body pseudoscalar potential for a pseudoscalar field and then moves one of the particles far way from the other two, creating an effective 2-body interaction. Then, by comparing this result with Eq. (9), the charge Q_{12} can be identified. For a single, massless pseudoscalar field, Q_{12} for two fermions was found to take the form

$$Q_{12} = \frac{g^3}{2\pi} \left(\frac{1}{2mr_{12}} \right)^2 \left[\frac{(\vec{\sigma}_1 - \vec{\sigma}_2) \cdot \vec{r}_{12}}{r_{12}} \right] \tag{10}$$

where $\vec{r}_{12} = \vec{r}_1 - \vec{r}_2$. This effective 2-body interaction significantly changes the complexion of the suppression effects plaguing the usual one-boson exchange potential. While the factor $(1/2mr)^2$ is still present, r is no longer the separation of the two bodies, but rather the distance between the two bound particles. Thus, for two nucleons in a nucleus,

$$\left(\frac{1}{2mr} \right)^2 = \left(\frac{1}{2mr_{12}} \right)^2 \sim 1, \tag{11}$$

effectively removing the suppression. However, this result was obtained at a cost: The effective interaction between two nuclei would be of order $(g^2/4\pi)^3$, making the effect actually smaller than the usual one-boson potential.

To yield a significant effect, two distinct pseudoscalar fields are used: One is the massless pseudoscalar field discussed above, and the other a massive pseudoscalar (say, the pion) with mass m_π. In this way, it can be shown that the pseudoscalar charge Q_{12} for two bound

nucleons now takes the form

$$Q_{12} = \frac{g_\pi^2}{2\pi}\left(\frac{\mu_\pi}{2m}\right)^2 \left\{\left[\frac{1}{\mu_\pi r_{12}} + \frac{1}{(\mu_\pi r_{12})^2}\right] e^{-\mu_\pi r_{12}}\right\} \left[\frac{(g_2\vec{\sigma}_1 - g_1\vec{\sigma}_2)\cdot\vec{r}_{12}}{r_{12}}\right], \tag{12}$$

and the suppression factor becomes

$$\left(\frac{1}{2mr}\right)^2 \sim \left(\frac{m_\pi}{2m_N}\right)^2 \sim 10^{-2}, \tag{13}$$

where m_N is the nucleon mass, and this is an improvement of ~ 24 orders of magnitude over the usual one-boson-exchange potential. Furthermore, this interaction is now of order $g^2/4\pi$ in the pseudoscalar coupling constant, and of order $(g_\pi^2/4\pi)^2$ in the pion coupling constant.

It is instructive to understand in intuitive terms how the large suppression factor arising from Eq. (2) has been avoided. From Eq. (5) we see that for the exchange of a light pseudoscalar by *free* nucleons the suppression factor is of order

$$\left(\frac{\hbar/m_N c}{r}\right)^2 \sim \left(\frac{10^{-18}}{r/1\,\mathrm{m}}\right)^2 \tag{14}$$

where r is their separation, and where we have reinstated the factors $\hbar$ and c. However, for the emission of a pseudoscalar by a *bound* system, there is another dimensionless parameter that can be formed utilizing the factor $1/m_N$ that arises from γ_5, namely,

$$\frac{\hbar/m_N c}{size\ of\ bound\ system}. \tag{15}$$

This factor is much closer to unity for typical bound systems as we see from Eq. (13). Since the same intuitive argument would apply to bound electrons, we can take over the preceding discussion to bound atomic systems as well, which may be experimentally more interesting as we discuss below. We note that even for pion-exchange between electrons, the Q_{12} mechanism gives a larger amplitude for emission of a light pseudoscalar than does the emission by a free electron.

To calculate the force arising from this mechanism between two macroscopic bodies, one still needs to calculate their total charges. Since Q_{12} is a pseudoscalar quantity, the expectation value $\langle Q_{12}\rangle$ for a test mass will vanish in general unless both parity (P) and time reversal (T) symmetries are broken. While the weak interaction is available to break P, T violation has only been observed indirectly in the neutral kaon system, and its connection to ordinary, non-strange matter is not evident. A solution to the problem of obtaining a non-zero expectation value for a pseudoscalar operator in ordinary matter may lie with the so-called Zeldovich moment.

The electric dipole moment $\vec{d}$ of a particle is odd under P and even under T as can be seen from its definition:

$$\vec{d} = e\vec{r}. \tag{16}$$

However, in quantum mechanics, we know that $\vec{d}$ must be proportional to the spin angular momentum $\vec{s}$ which is even under P and odd under T. It follows that $\vec{d} = 0$ unless *both* P and T are violated, i. e., parity-violating weak interactions alone are insufficient to produce an electric dipole moment. Zeldovich has shown that while these conditions apply to stable particles, the situation is more complicated for unstable particles [10, 11]. Bernreuther and Nachtmann [12] have explicitly demonstrated that the interference of phases arising from the weak interaction and the coupling of the atom to the electromagnetic vacuum leads to a non-zero expectation value of the electric dipole moment for an excited deuterium atom.

The same mechanism that produces the Zeldovich moment should yield a non-zero expectation value for the pseudoscalar charge Q_{12} for unstable systems. Since some fraction of ordinary matter is thermally excited, these effects may be detected in a sensitive Eötvös-type experiment. This would lead to new constraints on pseudoscalar interactions from laboratory experiments.

4 Conclusions

We have seen that the one boson exchange potential for a pseudoscalar interaction is highly suppressed compared to its scalar counterpart. This suppression may be circumvented by considering an effective 2-body force emerging from a higher order 3-body interaction. Calculations presently underway suggest that this mechanism may allow the use of conventional Eötvös-type experiments to set more stringent constraints on pseudoscalar couplings. Complete details of these results will be published elsewhere.

References

[1] E. G. Adelberger, B. R. Heckel, C. W. Stubbs, and W. F. Rogers, Annu. Rev. Nucl. Part. Sci **41**, 269 (1991).

[2] E. Fischbach and C. Talmadge, Nature **356**, 207 (1992).

[3] E. Fischbach, G. T. Gillies, D. E. Krause, J. G. Schwan, and C. Talmadge, Metrologia **29**, 213 (1992).

[4] R. D. Newman, D. M. Graham, and P. G. Nelson, in *New and Exotic Phenomena*, Proceedings of the XXIInd Rencontre de Moriond (VIIth Moriond Workshop), edited by O. Fackler and J. Trân Thanh Vân (Editions Frontières, Gif-sur-Yvette, 1987), p. 599.

[5] S. -S. Pan, W. -T. Ni, and S. -C. Chen, Mod. Phys. Lett. A **7**, 1287 (1992).

[6] R. C. Ritter, C. E. Goldblum, W. -T. Ni, G. T. Gillies, and C. C. Speake, Phys. Rev. D **42**, 977 (1990).

[7] V. M. Mostepanenko and Yu. I. Sokolov, Sov. J. Nucl. Phys. **46**, 685 (1987).

[8] D. Sudarsky, C. Talmadge, and E. Fischbach (unpublished).

[9] H. Primakoff and T. Holstein, Phys. Rev. **33**, 1218 (1939).

[10] Ya. B. Zeldovich, Sov. Phys. JETP **12**, 1030 (1961).

[11] J. S. Bell, Nuovo Cimento **25**, 452 (1962); J. S. Bell and G. Karl, Nuovo Cimento **41A**, 487 (1977).

[12] W. Bernreuther and O. Nachtmann, Z. Phys. A **309**, 197 (1983).

STRING THEORY AND THE EQUIVALENCE PRINCIPLE

Thibault DAMOUR
Institut des Hautes Etudes Scientifiques, 91440 Bures-sur-Yvette, France
and
DARC, CNRS-Observatoire de Paris, 92195 Meudon Cedex, France

ABSTRACT

By means of two examples (concerning the antisymmetric tensor field $B_{\mu\nu}$, and the dilaton field Φ or its four-dimensional avatars) the types and levels of violation of the Equivalence Principle that could follow from String Theory are discussed.

Thanks to the work of Feynman, Weinberg, Deser and others[1], it is known that General Relativity (and in particular its historical basic postulate termed the "Equivalence Principle") follows uniquely from the assumption that the gravitational interaction is mediated *only* by a massless, spin-2 field, plus the usual requirements of consistent field theories (causality, absence of ghosts, ...). On the other hand, most attempts at unifying gravity with the other interactions predict the existence of "partner" fields to the usual gravitational spin-2 field. In String Theory the original (ten-dimensional) tensorial gravitational field $G_{\mu\nu}$ has two partners: a scalar field Φ (called the dilaton) and an antisymmetric tensor field $B_{\mu\nu}$. One does not know at present how to connect in detail the field content of string theory to the four-dimensional "low-energy" world described by the Standard Model and General Relativity. In particular, one of the least understood issues is that of the generation of mass for initially massless fields (such as $G_{\mu\nu}$, Φ and $B_{\mu\nu}$). The purpose of the present contribution is to discuss, by means of two examples, what types of observable violations of the Equivalence Principle could arise if Φ and $B_{\mu\nu}$ survive down to the low-energy world as massless or nearly massless fields.

Consider first $B_{\mu\nu}$[2]. Because of its original gauge invariance, $\delta B_{\mu\nu} = \partial_\mu A_\nu - \partial_\nu A_\mu$, the only macroscopic couplings that the B field could be expected to have are of the Pauli type: field-strength coupling $H.\tilde{J}$, where $H_{\lambda\mu\nu} = \partial_\lambda B_{\mu\nu} + \partial_\mu B_{\nu\lambda} + \partial_\nu B_{\lambda\mu}$. Introducing the dual of the 3-form $\tilde{J}^{\lambda\mu\nu}$ (a 1-form J_α), and integrating by parts, this coupling can be rewritten as

$$\frac{1}{2} f \varepsilon^{\mu\nu\alpha\beta} B_{\mu\nu} \partial_\alpha J_\beta, \tag{1}$$

where f is a dimensionless coupling constant. It is well known that if $B_{\mu\nu}$ remains exactly massless, it describes only one scalar degree of freedom (the coupling (1) then translates into a coupling to the divergence of J_μ). It has been recently pointed out[2] that a more interesting situation arises if $B_{\mu\nu}$ somehow acquires a (very) small mass μ (corresponding to a macroscopic range). In that case one can show that $B_{\mu\nu}$ describes a massive vector degree of freedom (a "fifth force") coupled to the "current" J_μ with the strength

$$g_5 = \kappa \mu f, \tag{2}$$

where κ is the gravitational coupling constant ($\kappa^2 = 4\pi G$). Besides the usual composition-dependent interactions mediated by the coupling (2), such a "string-inspired" massive B field could also exhibit many novel matter couplings and thereby provide a useful phenomenological foil to the standard theories of gravity.

If we turn our attention to the dilaton field Φ (or, in fact, any massless scalar field

surviving in 4 dimensions) the situation can be even more interesting. Indeed, it has been recently noticed[3] that massless scalar fields exhibiting generic field-dependent couplings to matter have a natural tendency to relax, during the cosmological expansion, towards a state where they decouple from matter. The work of Ref. 3) considered the case where the scalar field is coupled to the trace of the energy-momentum tensor, i.e. where scalar interactions do not violate the Equivalence Principle. More recently, it has been realized[4] that this mechanism can be extended to the physically interesting case of the dilaton or its four-dimensional avatars. A long-standing problem of String Theory is to "get rid" of all the massless scalar fields coupled to matter with gravitational strength which seem to lead to unacceptably large violations of the Equivalence Principle and variations of the gauge coupling constants. The mechanism of Refs 3), 4) might succeed in solving this problem *without* requiring all the potentially dangerous fields to acquire a mass. As discussed in Ref. 4), one (or several) massless scalar fields, with Equivalence-Principle-violating couplings could exist now, and have been driven by the cosmological expansion to a very weakly coupled state. In fact, some natural numerical estimates lead us to expect that these fields would cause a non universality of the acceleration of free fall at the level

$$\delta a/a \lesssim 10^{-4} Z^{-3/2} \simeq 6 \times 10^{-11}, \tag{3}$$

where $Z \simeq 1.34 \times 10^4$ is the redshift separating us from the end of the radiation era. The estimate (3) is tantalizingly close to the present experimental limits, and provides a new, strong motivation for experiments (notably STEP[5]) pushing beyond the precision of Equivalence Principle tests.

REFERENCES

1. See e.g. R.M. Wald, Phys. Rev. D **33**, 3613 (1986) and references therein.
2. T. Damour, S. Deser and J. McCarthy, Phys. Rev. D **45**, R3289 (1992); and Phys. Rev. D **47**, 1541 (1993).
3. T. Damour and K. Nordtvedt, submitted to Phys. Rev. Lett. (1993).
4. T. Damour and A. M. Polyakov, in preparation.
5. See the contributions of M. Sandford, H. J. Paik and Y. Jafry to these proceedings.

Gravitational Waves and Other Gravitational Topics

SPACE EXPERIMENTS WITH HIGH STABILITY CLOCKS

ROBERT F. C. VESSOT
Smithsonian Astrophysical Observatory, Cambridge, Massachusetts, 02138, USA

ABSTRACT

Modern metrology depends increasingly on the accuracy and frequency stability of atomic clocks. While *accuracy* of measurement with respect to the defined second of time is important for many aspects of metrology, the precision of experimental measurements depends very much upon the *stability* of the clock during the data-taking process. Today's atomic hydrogen masers produce signals with fractional frequency stability better than 1×10^{-15} over intervals of 10^3 to 10^5 seconds Applications of such high-stability oscillators (or clocks) to experiments performed in space are described and estimates of the precision of these experiments are made in terms of clock performance. Use of multi-link microwave systems to cope with the Doppler effect of spacecraft motion and of signal propagation through the earth's troposphere and ionosphere are described, including methods using time-correlation to cancel localized disturbances in very long signal paths. Analyses of proposed tests of relativistic gravitation, of operation of a very long baseline interferometry (VLBI) system operated in space, and of a possible measurement of the quadrupole moment of the sun's mass distribution are discussed. A proposed space borne four-stationVLBI system is described that could compare, with a precision of 3×10^{-15} rad/sec, the rotation of a local inertial frame based on the velocity of light with the inertial frame defined by distant radio stars.

1 Introduction

Just as the invention of the telescope was a major factor in the revolution in science during Renaissance times, advances in clock technology will continue to revolutionize science. One of the most powerful devices in support of science in our era is the uparalleled precision of measurement made possible by atomic clocks. Modern metrology increasingly depends on precise measurement of time and frequency.

This discussion is meant to provide a picture of where we stand in the present state of clock development, a review of the techniques for clock-related space experiments, and of some space experiments that are now technically feasible

2 Present State of Clock Technology and Systems for Space Experiments

An estimate of the progress of clock development is shown in Figure 1, which shows that the frequency stability of highly stable oscillators has improved by a factor of about 10 every decade since the 1960 era, when atomic clocks were first introduced.

The most commonly used definition of frequency stability is the Allan deviation, $\sigma_y(\tau)$. This is the one-sigma expectation of the fractional frequency difference $\Delta f/f$ (designated by the subscript y), between time-adjacent frequency measurements, each made over time intervals of duration, τ. The functional relationship of $\sigma_y(\tau)$ versus (τ) depends on the Fourier spectrum of of the phase variations.[1)]

An estimate of the time dispersion of a clock or oscillator for a future time interval, τ, can be obtained from the relation

$$\sigma_{\Delta t}(\tau) \sim \tau\, \sigma_y(\tau) \qquad (1)$$

Oscillator performance given by $\sigma_y(\tau)$ can provide statistical estimates of the limits imposed by clock performance on the precision of measurements.

Figure 2 shows $\sigma(\tau)$ versus τ plots for recently developed stored ion devices[2)] atomic hydrogen masers[3)], and for the binary pulsar[4)] This figure also includes the Allan deviation of disturbances caused by the earth's troposphere and ionosphere on signals traversing vertically. In the following discussions of experimental techniques, the H maser performance data in Figure 2 will be used as a basis for numerical examples.

2.1 Measurements using Electromagnetic Signals

2.1.1 The effects of oscillator instability on measurements of distance and of range-rate using Doppler data.

In the case of distance measurements made from the one-way propagation of light we can obtain an estimate of range dispersion from time dispersion given in Equation 1, by writing

$$\sigma_{\Delta r}(\tau) = c\, \tau\, \sigma_y(\tau) \qquad (2)$$

where c is the velocity of light.

The one-way Doppler frequency shift of signals from an oscillator transmitting at a frequency, f, moving with velocity v_r toward the receiver is

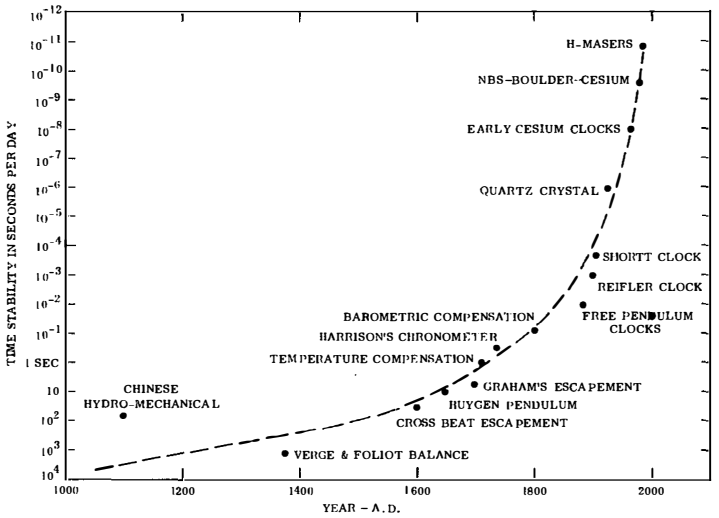

Figure 1 Progress in clockmaking since AD-1000

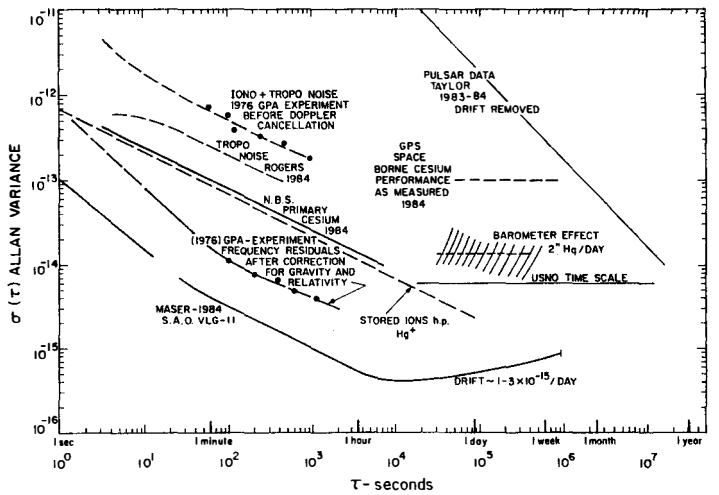

Figure 2. Sigma versus tau plots of frequency stability of oscillators and of stability degradation owing to signal propagation through the earth's ionosphere and troposphere.

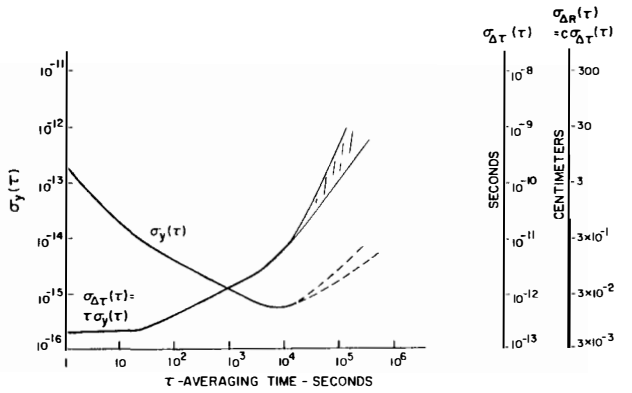

Figure 3. A nomograph showing estimates of time dispersion and range distance error contributed by an oscillator when frequency stability is described in terms of $\sigma_y(\tau)$.

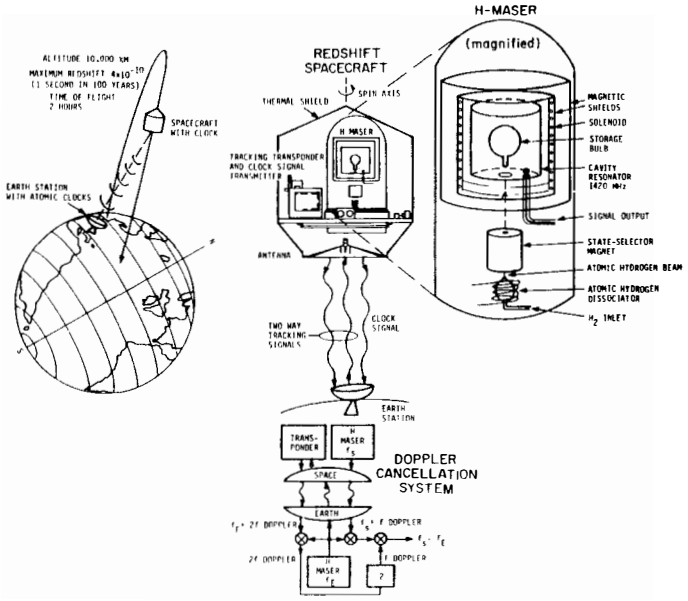

Figure 4. The 1976 SAO/NASA gravitational redshift experiment.

$$\frac{\Delta f}{f} = \frac{v_r}{c}$$

The contribution of the oscillator to the imprecision of determining range rate, v_r, during measurement intervals, τ , is given by

$$\sigma_{vr}(\tau) = c\,\sigma_y(\tau) \qquad (3)$$

Figure 3 is a nomograph of range-rate error and range distance error based on the H-maser data in Figure 2. On the left hand axes are scales for $\sigma_y(\tau)$ and the corresponding one-way Doppler frequency range-rate measurement error, $\sigma_{vr}(\tau)$. On the right hand axes are the scales for time dispersion, $\sigma_{\Delta\tau}(\tau)$, and the corresponding one-way range measurement error.

2.1.2 A Systems or Cancelling First-Order Doppler and Signal Propagation

The concept of one-way and two-way Doppler measurements leads naturally to the three-link Doppler-cancelling system used in the 1976 SAO/NASA test of the gravitational redshift, now referred to as Gravity Probe A (GP-A).[5] This "Doppler cancellation" scheme was pivotal to the success of the experiment. By measuring the Doppler effects in a *separate* two-way system and subtracting one-half the number of two-way cycles from the phase of the received signal in the one-way microwave link connecting the space vehicle clock to the earth station, the propagation effects were *systematically* removed.

Figure 4 schematically describes the phase-coherent analog system that was used in the 1976 SAO-NASA test of the gravitational redshift. (Today's technology permits digitally recording the one - and two-way signals and processing the data in a computer.) With this system, the fractional output frequency variations obtained by subtracting one-half of the two-way Doppler cycles from the one-way cycles received by the earth station is given in the expression:

$$\frac{f_s - f_e}{f_0} = \frac{(\phi_s - \phi_e)}{c^2} - \frac{|\vec{v}_e - \vec{v}_s|^2}{2c^2} - \frac{\vec{r}_{se} \cdot \vec{a}_e}{c^2} \qquad (4)$$

Here the total frequency shift is f_s-f_e, and f_0 is the clock downlink frequency. The term $(\phi_s - \phi_e)$ is the Newtonian potential difference between the spacecraft and earth station, $\vec{v}_e$ and $\vec{v}_s$ are the velocities of the earth station and the spacecraft, r_{se} is the vector distance between the spacecraft and earth station, and a_e is the acceleration of the earth station in an inertial frame. For the 1976 test, an earth-centered frame with axes aimed at the fixed stars was sufficiently "inertial" to satisfy the requirements of the the two-hour experiment.

The first term is the gravitational redshift resulting from the difference in the Newtonian gravitational potential between the two clocks, the second term is the second-order Doppler effect of special relativity, and the third term is the result of the acceleration of the earth station during the light time, r/c, owing to the earth's rotation. During the two-hour near-vertical flight, the first-order Doppler shifts were as large as $\pm 2 \times 10^{-5}$ and the noise from ionospheric and tropospheric propagation effects was at a level of about 1×10^{-12} at $\tau \sim 100$ sec, as shown in the top left curve of Figure 2. After the frequency variations predicted in Equation 4 were fitted to the data, we concluded that the error in the fit of the data was within $(+2.5 \pm 70) \times 10^{-6}$ of Einstein's prediction.[6] The residuals were analyzed after subtracting the predicted frequency variation over the time

of the mission. The resulting Allan standard deviation of the frequency residuals is shown in Figure 5. Here we see that the stability of the frequency comparison made through the three-link system over signal paths of 10,000 km, in the presence of Doppler shifts of magnitude ± 44kHz plus the ionospheric and tropospheric noise shown in Figure 2, is comparable to the frequency comparison made between the two reference masers in the same room, reaching 6×10^{-15} stability at about 10^3 sec.

A closer look at the system in Figure 4 is provided in Figure 6 to show how phase coherence throughout the system was provided by ratio frequency synthesizers. We see that there was a considerable difference in the S-band (2 GHz) frequencies, owing to the transponder's turn-around frequency ratio, 240/221. Because of variations in the ionospheric electron content in the signal path, there would have been serious problems from variations in phase delay owing to the frequency differences in the three microwave links[7]. This error was removed by choosing the frequency ratios so that the dominant ionospheric effects in the three signal paths were cancelled at the output of mixer M3 in Figure 6. [8],[9]

2.1.3 A Symmetrical Four-Link System to Provide Time-Correlated Doppler Data

The three-link system can be made symmetrical by providing a transponded signal back to the spacecraft as shown in Figure 7. Here one-way, two-way, and Doppler-cancelled data are recorded at both stations of the system. Each record is made in terms of the proper time scale kept by the station's clock. In cases where the stations are widely separated so that the light time between stations is long compared to the intervals required for measurements, a dominant, spatially localized noise process can be cancelled *systematically* by time-correlating the data from the two stations. To illustrate this process, Figure 8 shows the continuum of space-time paths of the four signals in Figure 7. Here the dots signify the clocks, and the arrows, $E_1(t)$ and $E_2(t)$, signify signal outputs representing earth-based one-and two-way data at a particular epoch in the continuum. $S_1(t)$ and $S_2(t)$ represent one- and two-way data recorded in space. By time-correlating the Doppler responses we can systematically cancel a strong localized noise source such as the earth's troposphere and ionosphere.[10],[11]

For example, let us consider the frequency variations in Doppler outputs $E_1(t)$, $E_2(t)$, $S_1(t)$, and $S_2(t)$ shown in Figure 6. We see that the iono-tropo noise pattern received from the the spacecraft transmitted at time t_i and received at earth at time t_i+R/c is the same as the noise received at the spacecraft at time (t_i+2R/c). By advancing $E_1(t)$ by time R/c with respect to $S_1(t)$ and subtracting the two data sets we can systematically remove the noise in the $S_1(t_i+2R/c) - E_1(t_i+R/c)$ combined data set at the small expense of increasing the random noise in the data by $\sqrt{2}$. In situations where the localized dominant noise is substantially larger than the nonlocalized random noise, this process can be highly effective.

2.1.3.1 Relativistic Doppler Shifts and Redshifts with the 4Four-Link System

The Doppler-cancelled signal outputs $S_o(t)$ and $E_o(t)$ in Figure 7 contain relativistic and gravitational information that can be time correlated. Equation 4 is repeated below as $E_o(t)$, along with its counterpart expression at the spacecraft, $S_o(t)$:

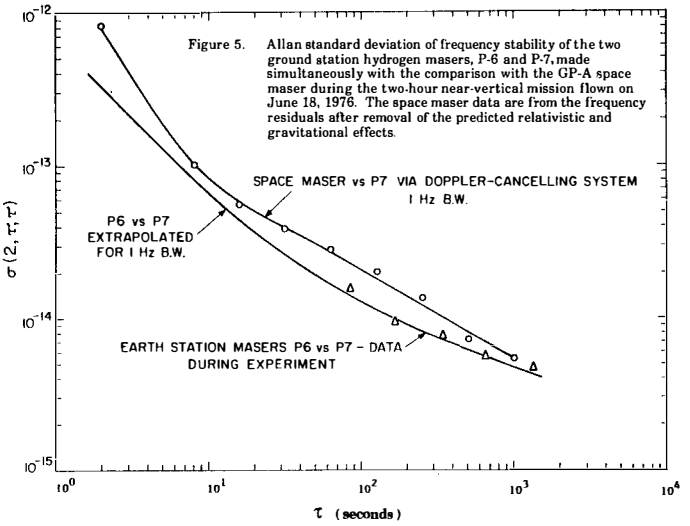

Figure 5. Allan standard deviation of frequency stability of the two ground station hydrogen masers, P-6 and P-7, made simultaneously with the comparison with the GP-A space maser during the two-hour near-vertical mission flown on June 18, 1976. The space maser data are from the frequency residuals after removal of the predicted relativistic and gravitational effects.

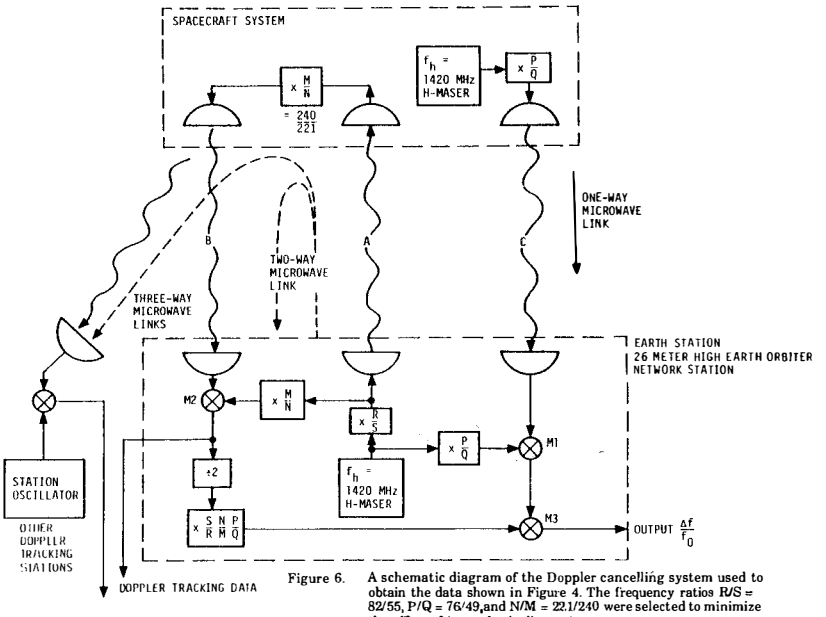

Figure 6. A schematic diagram of the Doppler cancelling system used to obtain the data shown in Figure 4. The frequency ratios R/S = 82/55, P/Q = 76/49, and N/M = 221/240 were selected to minimize the effect of ionospheric dispersion.

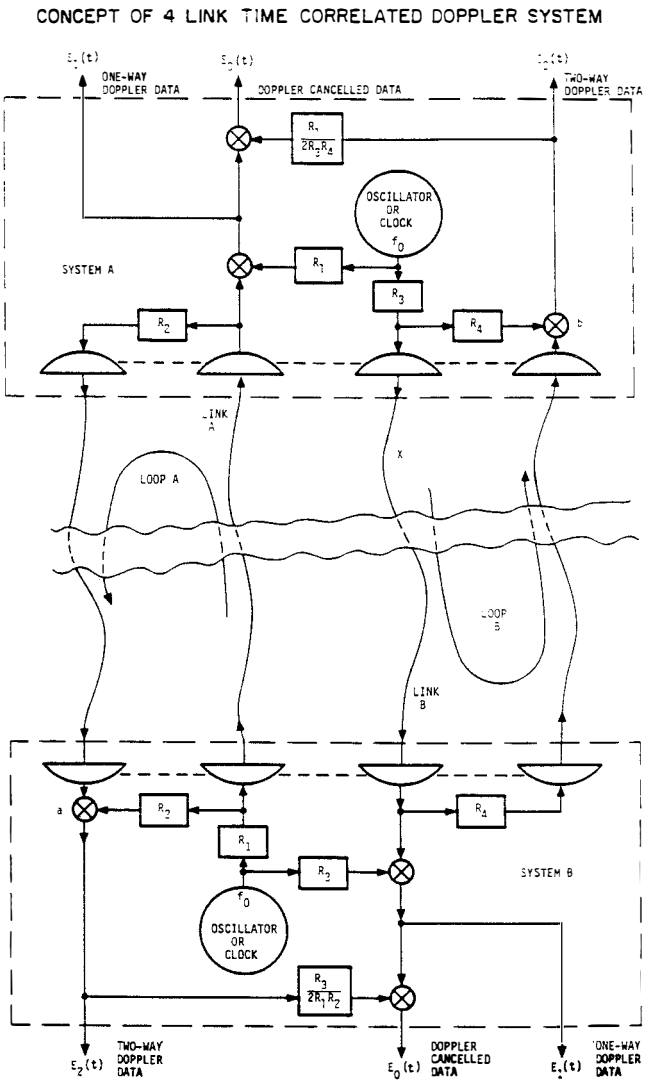

Figure 7. A four-link Doppler cancelling system that allows time correlated data to be obtained both at the earth and space terminal.

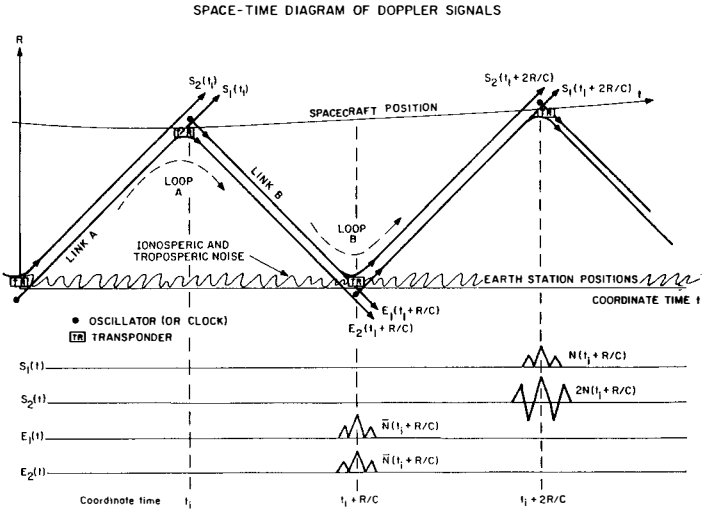

Figure 8. A space-time diagram of the signals as shown in Figure 7, showing how time correlation of the data can systematically remove a dominant and localized noise source.

ERROR ANALYSIS OF A PROPOSED ORBITING REDSHIFT TEST AND COMPARISON WITH THE 1976 NASA-SAO GP-A ROCKET PROBE EXPERIMENT

	GP-A TEST 2 HOURS	PROPOSED ORBITING TEST 1 ORBIT	30 ORBITS
RANDOM NOISE -- $\Delta f/f$			
H-MASER AND MICROWAVE SYSTEM NOISE	13×10^{-15}	$<1\times10^{-16}$	$<1\times10^{-16}$
UNCANCELLED ATMOSPHERIC NOISE	2.5×10^{-15}	2.5×10^{-15}	0.50×10^{-15}
UNCANCELLED IONOSPHERIC NOISE	5.0×10^{-15}	2.0×10^{-15}	0.37×10^{-15}
RSS	14.2×10^{-15}	3.2×10^{-15}	0.58×10^{-15}
POSSIBLE SYSTEMATIC BIAS ERRORS -- $\Delta f/f$			
GROUND STATION CLOCKS	3.0×10^{-15}	1.0×10^{-15}	1.0×10^{-15}
SPACE CLOCK	4.5×10^{-15}	1.0×10^{-15}	1.0×10^{-15}
SPACECRAFT TRACKING ERROR	3.3×10^{-15}	1.0×10^{-15}	1.0×10^{-15}
RSS	6.3×10^{-15}	1.7×10^{-15}	1.7×10^{-15}
RSS COMBINED RANDOM AND SYSTEMATICS -- $\Delta f/f$	15.5×10^{-15}	3.6×10^{-15}	1.8×10^{-15}
VARIATION OF $\Delta f/f = \Delta\Phi/c^2 + 1/2\ V^2_{rel}/c^2$	2.2×10^{-10}	9.6×10^{-10}	9.6×10^{-10}
FRACTIONAL ACCURACY OF TEST			
$\frac{\text{RSS COMBINED RANDOM AND SYSTEMATICS}}{\Delta\Phi/c^2 + 1/2\ V^2_{rel}/c^2} =$	70×10^{-6}	3.8×10^{-6}	1.9×10^{-6}

TABLE I

$$E_O(t) = \frac{\phi_S - \phi_e}{c^2} - \frac{|\vec{v}_S - \vec{v}_e|^2}{2c^2} - \frac{\vec{r}_{se} \cdot \vec{a}_e}{c^2} \quad (5)$$

$$S_o(t) = \frac{\phi_e - \phi_S}{c^2} - \frac{|\vec{v}_e - \vec{v}_S|^2}{2c^2} - \frac{\vec{r}_{es} \cdot \vec{a}_S}{c^2} \quad (6)$$

By adding these two time-ordered data sets we cancel the first term and double the magnitude of the second term representing the second-order shift. Conversely, if we subtract the data sets, we double the first-term representing the gravitational red (blue) shift and cancel the second term. In both instances we must account for the acceleration of the earth and space stations along the line of sight in a suitable inertial frame.

3 Future Tests of Relativistic Gravitation with Clocks

3.1 A Test of Relativistic Gravitation with a Clock in a 24-Hour Eccentric Earth Orbit

The original concept for testing the Gravitational Redshift called for operating a spaceborne clock in a spacecraft placed in a highly eccentric 24-hour earthorbit.[12] Low inclination orbits with eccentricities as high as 0.6 can produce apogee-to-perigee redshifts of about 4.8×10^{-10}, and still keep the spacecraft in view of an earth station with a minimum elevation angle greater than 15 degrees. Accompanying the redshift there is a second-order Doppler shift of comparable magnitude, which produces a combined frequency variation of 9.6×10^{-10} in the Doppler cancelled data described in Equation 9.

Table 1 shows an error analysis of the combined gravitational redshift and second-order Doppler test made in 1976 using a near-vertical trajectory.[13] The improvement from 70 parts per million to 2 parts per million in the proposed test results partly from improved clocks, but mostly from the longer averaging intervals and estimates of the smaller systematic bias errors made possible by having time for adjusting and tuning the space maser before taking data.

3.2 A Proposed Extension of the GP-A Experiment to Test General Relativity with a Solar Probe

A series of studies is in progress of relativistic gravitation tests with a clock in a space probe in a polar orbit approaching within 4 solar radii of the sun's center.[14] The 14 hour time of travel from pole-to-pole is in the region of best performance of the hydrogen maser. This test is intended to reveal the behavior of the second order in the redshift, $[\Delta\phi/c^2]^2$.

During the 10 hours before and after perihelion, the value of Φ/c^2 varies from 5.3×10^{-7} at perihelion to 2.0×10^{-7} at times ± 10 hours from perihelion. During the same time interval, the second-order redshift $[\Phi/c^2]^2$, varies from 2.81×10^{-13} to 4×10^{-14}, as shown in Figures 9 and 10. Taking the Allan standard deviation of today's H-masers over 10 hours averaging time as 6×10^{-16}, the inaccuracy of measurement imposed by the maser instability for the first-order measurement is 1.8×10^{-9}, the corresponding inaccuracy for the second-order measurement is 2.5×10^{-3}.

The sun's gravitational potential is complicated by having a number of multipole components. The largest of these is the solar quadrupole moment, J_2, which must be accounted for in the measurement of the second order term in the redshift.

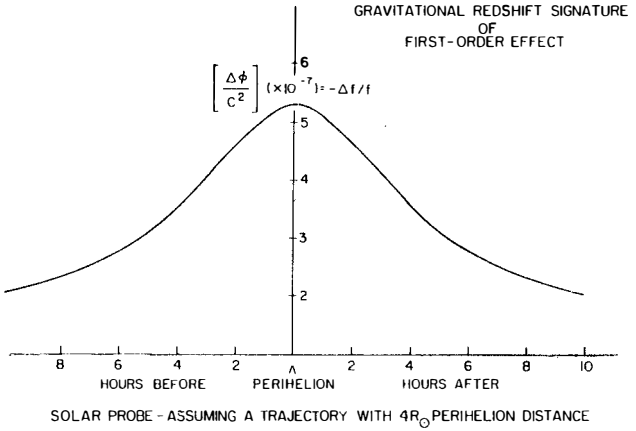

Figure 9. The gravitational redshift signature at first order in $\Delta\phi/c^2$ for a clock passing over the poles of the sun with 4-solar radius distance from the sun's center when over the equator.

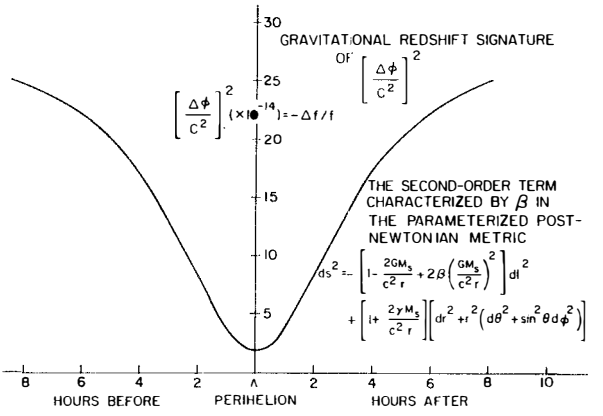

Figure 10. Second-order redshift signature for a clock passing over the poles of the sun with 4-solar radius distance from the sun's center when over the equator.

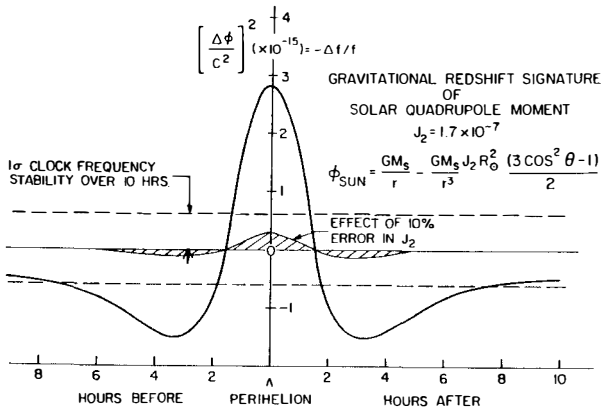

Figure 11. Gravitational redshift signature at first order in $\Delta\phi/c^2$ of the solar quadrupole moment, J_2, assumed to be 1.7×10^{-7}

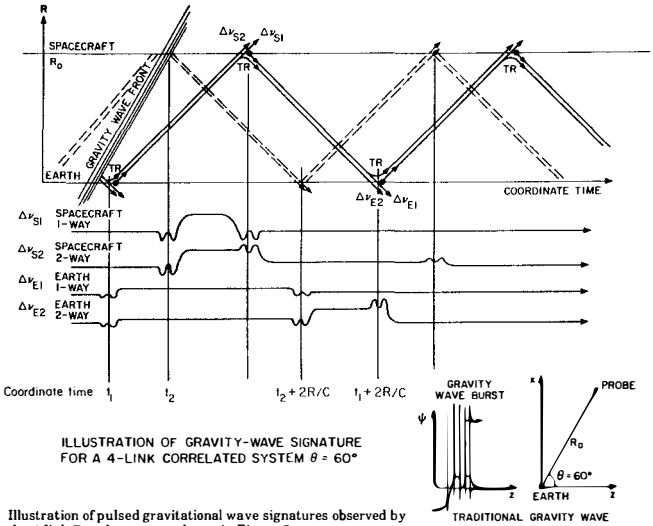

Figure 12. Illustration of pulsed gravitational wave signatures observed by the 4-link Doppler system, shown in Figure 7.

Measurements of J_2 have been made from solar oscillations,[15] and we can estimate the effect of the uncertainty in these measurements from the behavior of the J_2 signature in the data during the 14-hour pole-to-pole passage.

At order c^{-2} the first-order redshift has the following behavior:

$$\frac{\phi}{c^2} = \frac{\mu}{r} + \frac{\mu}{r^3} J_2 R^2_{sun} \frac{3\cos^2\vartheta - 1}{2} = \frac{\Phi_1}{c^2} + \frac{\Phi_2}{c^2} \qquad (11)$$

where $\mu = GM_{sun}/c^2$. Assuming $J_2 = 1.7 \times 10^{-7} \pm 0.17 \times 10^{-7}$, then at perihelion, $r = 4R_{sun}$, $\vartheta = \pi/2$, and $\Phi_2/c^2 = -2.8 \times 10^{-15}$.

At about ±7 hours from perihelion, $\vartheta = 0$, $r = 8R_{sun}$, and $\Phi_2/c^2 = +7.0 \times 10^{-16}$.

The frequency variation caused by the J_2 contribution to the sun's redshift is shown in Figure 11 before and after perihelion. Its peak-to-peak magnitude is 3.5×10^{-15}. If we have an error of 10% in the estimate of J_2, the uncertainty in its contribution to the redshift over this interval is about 3.5×10^{-16}, comparable to the instability of the clock. The error contribution will have a distinctive $(3\cos^2\vartheta - 1)/r^3$ signature in contrast to the very smooth $1/r$ dependence of the first-order redshift and the $1/r^2$ dependence of the second-order redshift, as shown in Figures 9 and 10. To achieve the precision of measurement of β and J_2, the position of the probe must determined to 1 m rms. and its velocity to within .005 cm sec^{-1}. This is within the tropospheric constraints shown in Figures 2 and 3.

An important feature that makes this experiment possible is the ability to take Doppler-cancelled data at the probe. In Figure 8, we have shown how the localized noise near earth can be cancelled by correlation. While the spacecraft Doppler cancellation system can systematically remove the effect of the tropo-iono noise when it produces the $S_0(t_i+2R/c)$ data, this is not the case for the earth station Doppler-cancelled output E_0. In the earth station cancelled Doppler there would be about 1000 sec of time delay between the uplink transmission and reception from the transponder. During this interval the combined atmospheric and ionospheric delay could have varied considerably.

A joint study by NASA's Jet Propulsion Lab and the Smithsonian Astrophysical Observatory is in progress to evaluate the feasibility of this experiment.[16]

3.3 Detection of Pulsed Gravitational Radiation using Doppler Techniques

During the long travel time to the sun there will be an opportunity to search for gravitational radiation using Doppler techniques.[17],[18] While evidence for such radiation has not been observed directly, the orbital decay of a binary pulsar has been observed since 1975 and its rate continues to follow closely the predicted behavior for loss of energy by gravitational radiation.[19]

When a gravitational wave intercepts an electromagnetic wave, it distorts the frequency of the wave by an amount $h=\Delta f/f$. It should be possible to detect gravitational waves by observing Doppler shifts of a signal that is transmitted by a highly stable microwave (or laser) transmitter and detected by a receiver located at a distance that is greater than about one-half the wavelength of the gravitational wave.

An example of possible Doppler detection[20] of a pulsed gravitational wave using the four-link Doppler measurement system is shown in Figure 12. Here the wavefront

of the gravitational pulse is assumed to intercept the earth-probe line at an angle, $\theta = 60$ degrees. The effect of the pulse would be observed three times in the Earth 2-way Doppler trace as follows:

$$\frac{df}{f} = \frac{(1-\mu)\psi(t_R)}{2} - \mu\psi\left[t_R - L\frac{(1+\mu)}{c}\right] + (1+\mu)\psi\left(t_R - 2\frac{L}{c}\right) \qquad (13)$$

- by a Doppler shift of the gravitational wave disturbing the earth station at $t=t_1$, while it is receiving a signal transmitted earlier by the spacecraft.
- by its "echo" when the earth station receives a transponded signal at $t = t_1 + 2R/c$.
- by the disturbance when the gravitational wave arrives at the spacecraft at time t_2 and reported at earth at $t = t_2+R/c$.

The spacing of the pulses, their time signature designated by the parameter $\psi(t)$, and the relative magnitude and sign of the signature are described by a single parameter, $\mu = \cos\theta$ [21),22)]. Here t_R signifies arrival time at the first station. The one-way transmission from the spacecraft would show the pulses at t_1 and at $t_2 + R/c$.

A similar set of five observations of the same gravitational pulse is available at the spacecraft. In this case $\mu = \cos(\pi+\theta)$ and another set of five manifestations of the pulse appears in the spacecraft data. While only four of the ten pulses, i.e.,those from the two one-way Doppler signals, are unique, the other six are obtained from other paths through the electronics system and provide redundancy to help prevent interpreting noise as gravitational wave signals.

If one of the stations is on earth, noise from the earth's troposphere and ionosphere would be the main limitation to the sensitivity of detection. Reduction of ionospheric noise is possible by operating at higher frequencies than the currently used S-band (2 GHz) and X-band (10 GHz) systems. Future tracking systems are planned to operate at 33 GHz and even higher.

However, tropospheric noise cannot be reduced by such techniques and will substantially degrade the stability of a signal. Studies show that the Allan deviation of the tropospheric noise for signals passing vertically has a $\tau^{-2.5}$ behavior for intervals between 20 and 200 sec, with $\sigma_y(100\ \text{sec}) = 8 \times 10^{-14}$, as shown in Figure 2[23)]. While it is possible to model the tropospheric frequency shifts using other data, such as the columnar water vapor content and the local barometric pressure, tropospheric propagation variations will nevertheless severely limit the detection of gravitational radiation with transponded two-way Doppler signals.

By implementing the process shown in Figure 8, nearly complete rejection of such spatially localized sources as near-earth tropospheric and ionospheric variations and earth station antenna motion noises could be obtained. With both clock systems operating in space and at frequencies where the noise from the solar corona ionization is not significant, the principal nongravitational noise sources will likely be from the buffeting of the space vehicles by nongravitational forces such as light pressure, particle collisions, and sporadic outgassing of the spacecraft. Here, again, since these disturbances are localized at the ends of the system, the time signatures of the noises are separated by R/c, and can be distinguished from the patterns expected from pulsed gravitational waves, which have signatures that depend only on the parameter μ of equation 13.

4 High Resolution Very Long Baseline Interferometry (VLBI) Astronomy in Space

4.1 The Effect of Oscillator Instability on the Measurement of Angles

High precision measurement of the angle between the propagation vector of a signal and the direction of a baseline, defined as the line between the phase centers of two widely separated radio telescope antennas, can be made with VLBI techniques shown in Figure 13.[24] Here, two radio telescopes, separated by a distance, L, each detect the arrival of radio noise signals from a distant radio star. After heterodyning to a lower frequency the noise signals are recorded as a function of time and the two sets of noise data are subsequently time-correlated. The observable quantities from the correlation process are the correlated amplitude and the relative phase of the signals detected at the widely separated points on the wavefront. VLBI measurements have been used in light deflection tests of relativistic gravitation.[25]

The stability limit on the successive measurements of angle imposed by the oscillator instability on successive measurements of angle taken τ seconds apart is

$$\sigma_{\Delta\theta}(\tau) \sim \frac{c\,\tau\,\sigma_y(\tau)}{L \sin\theta}, \tag{14}$$

where θ is the angle between the propagation vector and the baseline. The result of correlating the noise data obtained from a common source by the two stations is the production of fringes. The spacing between the fringes is $\lambda/L\ \mathrm{Sin}\theta$, where λ is the average wavelength of the signals arriving at the antennas. The visibility of the fringes depends on the extent to which the signals arriving at the antennas are correlated.

The angular resolution of the interferometer is given by the change of fringe phase, ϕ, with θ

$$\frac{d\phi}{d\theta} = \frac{2\pi L}{\lambda} \tag{15}$$

The error in successive angular measurements owing to the instability of the clocks in a terrestrial system with L = 6000 km, assuming $\sigma_y\,(10^3\ \mathrm{sec}) = 1 \times 10^{-15}$, and $\theta = \pi/2$, is given by

$$\sigma_{\Delta\theta}\,(10^3\ \mathrm{sec}) = 5 \times 10^{-11}\ \mathrm{rad\ or}\ 2\ \mu\ \mathrm{arcsec}.$$

However this is far smaller than the present actual limit of 100 μ arcsec level from terrestrial stations with an 8000-km baseline operating at 7 mm wavelength.[26] The effects of tropospheric and ionospheric fluctuations impose limits that are far more serious than clock instability.

By operating VLBI stations in space, limits in angular resolution owing to tropospheric and ionospheric propagation and baseline distance, imposed by the size of the earth, can be overcome . A successful demonstration of a spaceborne radio telescope operating as a VLBI terminal was made in 1986[27] using NASA's orbital Tracking and Data Relay Satellite System (TDRSS) system as a spaceborne radio telescope in conjunction with a number of radio telescopes on earth.

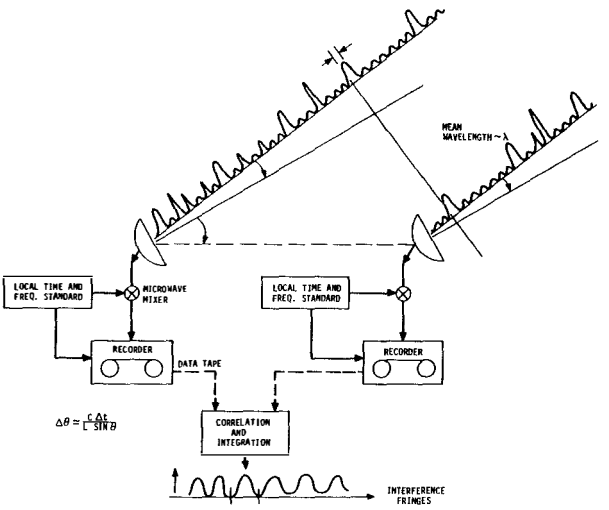

Figure 13. Schematic of the Very Long Baseline Interferometry (VLBI) technique used in radioastronomy.

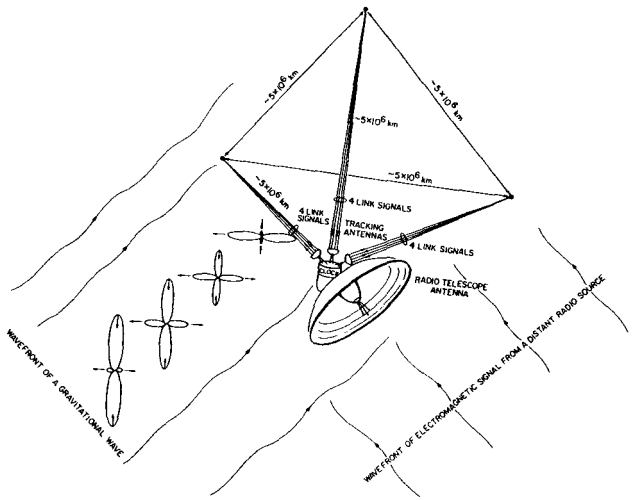

Figure 14. An array of four spaceborne radio telescopes, each connected to the other by the system shown in Figure 7.

As an example of the limits that a spaceborne two station system could achieve, let us consider a spaceborne system where $L = 5 \times 10^6$ km, $\sigma_y(10^4 \text{ sec}) = 4 \times 10^{-16}$, and $\theta = \pi/2$. In this case,

$$\sigma_{\Delta\theta}(10^4) = 2 \times 10^{-13} \text{ rad or } 0.05 \ \mu\text{arcsec} .$$

For $\lambda = 1$ mm we have $\lambda/L = 2 \times 10^{-13}$ rad and we see that the limit imposed by clock stability with 10^4 sec integration time is capable of resolving fringes at 1-mm wavelengths in a spaceborne system with baseline distances of 5×10^6 km. The numbers in this example are chosen to be close to present estimates of the limits for having reasonably well correlated flux at the two stations at the distances chosen.[28)]

Terrestrial VLBI systems are now used to record polar motion and rotation of the earth and to monitor the movements of the earth's tectonic plates. While *relative* positions of radio stars, and features of their brightness distribution, can be made with a precision of a few tenths of a milliarcsecond, the *absolute* directions in space of the baselines between VLBI stations depend on the choice of a frame of reference. This reference is usually taken from the positions of very distant radio sources.

4.2 *A Spaceborne Four Terminal (VLBI) Array that Establishes an Inertial Reference Frame, a "Gedanken" System to Exercise our Imaginations.*

Having already stretched the VLBI technique to baseline distances of 5 million kilometers, let us go several steps further and postulate the existence of an array of four such stations in the form of a tetrahedron that defines a three-dimensional figure in space that is in an orbit about the sun. (The station separations need not be equal.) Figure 14 shows such an array. Each station contains a clock that is synchronized to a coordinate time scale and is connected to its three neighbors by the four link system shown in Figure 7.[29)] The six baseline distances can be precisely measured, using one-way and two-way Doppler techniques discussed earlier, and thus precisely define the *configuration* of the array as a function of time.

Defining the *orientation* of the array of six baselines poses an interesting problem. Distant radio stars define the conventionally used inertial frame. By invoking the Sagnac effect,[30)] we can define *another inertial frame* based on the velocity of light, and it should be possible to compare the orientation of the array determined in terms the two reference frames.

To describe the application of the Sagnac process, we visualize the arrival times of light signals sent in opposite senses about a closed path on a surface rotating at Ω rad/second. If the projected area of the closed path, perpendicular to the rotation axis, on that surface is A, then the difference in the arrival times of light signals going around the path in opposite senses is $\Delta\tau = 4\Omega A/c^2$. By measuring the difference in arrival times of signals going in opposite senses about a triangle defining one face of the tetrahedron, we can obtain the component of rotation normal to that face. From the four triangles that define the tetrahedron we have an overdetermination of the rotation and can make an estimate of the accuracy of its measurement.

For the array shown in Figure 14, the limitation due to the accuracy of the detection of changes in rotation rate, $\Delta\Omega$, is 1.2×10^{-15} rad/sec. If the array is located at 1 AU from the sun, such a rotation measurement would include the Einstein–deSitter precession of 2×10^{-2} arcsec/yr (3×10^{-15} rad/sec) owing to the bending of space-time by the sun's gravity.

This array could compare with very high precision the frame of reference defined by the most distant radio sources with an inertial frame defined by the local isotropy and constancy of the velocity of light. The measurements could be accomplished in a short period of time. (This period would probably mostly be taken up in steering the array's antennas to a series of selected radio sources.)

WHAT COULD THIS SYSTEM TELL US ABOUT OUR UNIVERSE ? Could it provide a way to observe some aspects of the behavior of the missing matter? Perhaps theorists could be tempted to speculate about scenarios that could be revealed with this system.

5 Conclusion

Since the mid 1960s the frequency stability of atomic clocks (or oscillators) has been improving by a factor of about ten every decade, so far with no end in sight. The units of time and frequency, and the now redefined unit of distance through the velocity of light, are solidly based on atomic frequency standards. This metrology, in a local sense, has been made consistent with present concepts of gravitation and relativity. We now make measurements of astronomical and astrophysical objects near the edge of our universe with clocks that operate using quantum processes whose dimensions encompass staggeringly smaller distance scales. As the performance of atomic clocks improves and their uses are extended in astrophysical measurements, perhaps there will be some surprises about the nature of our universe.

References

[1] J. Ruttman and F.L. Walls, "Characterization of frequency stability in precision frequency sources," Proc. IEEE, vol. 79, 1991.

[2] D. J. Wineland, J.C. Bergquist, J.J. Bollinger, W.M. Itano, D.J. Heinzen, S. L. Gilbert, C.H. Manney, and M.G. Raizen, "Progress at NIST toward absolute frequency standards using stored ions," *IEEE Trans. on Ultrasonics, Ferroelectrics and Frequency Control*, vol. 37, no. 6, Nov. 1990.

[3] R.F.C.Vessot, E.M. Mattison, W.J. Klepczynski, G.M.R. Winkler, I.F. Silvera, H.P. Godfried, and R.L. Walsworth, "Present clock stability and realistic prospects for the future," in *Proc. Fourth Marcel Grossman Meeting on General Relativity* (R. Ruffini, Ed.) Rome, Italy, June 17-21, 1985

[4] L.A. Rawley, J.H. Taylor, M.M. Davis, and D.W. Allan, "Millisecond pulsar PSR 1937 + 21: A highly stable clock," *Science*, vol. 238.

[5] R.S. Badessa, R.S. Kent, R.L. Nowell, and C. L. Searle, "A Doppler-cancellation technique for determining the altitude dependence of gravitational redshift in an earth satellite," *Proc. IRE*, vol. 48, p. 758, 1960.

[6] R.F.C. Vessot, M.W. Levine, E.M. Mattison, E.L. Blomberg, T. E. Hoffmann, G.U. Nystrom, B.F. Farrell, R. Decher, P.B. Eby, C.R. Baugher, J.W. Watts, D.L. Teuber, and F.D. Wills, "Tests of relativistic gravitation with a space-borne hydrogen maser," *Phys. Rev. Lett.*, vol. 45, pp. 2081-2084, Dec. 1980.

[7] A.J. Tucker and B.M. Fannin, "Analysis of ionospheric contributions to the Doppler shift of C.W. signals from artificial earth satellites,"
J. Geophys. Res., Space Physics, vol. 73, no. 13, pp. 4325-4334, 1968.

[8] R.F.C. Vessot and M.W. Levine, "Performance data of space and ground hydrogen masers and ionospheric studies for high-accuracy frequency comparison between space and ground clocks," in *Proc. Twenty-eighth Annual Symp. Frequency Control*, U.S. Army Electronics Command, Ft. Monmouth, NJ, 1974, pp. 408-414.

[9] R.F.C. Vessot and M.W. Levine, NASA Experimental Final Redshift Report, GPA Project Report, Contract NAS8-27969.

[10] R.F.C.Vessot and M.W. Levine, "A time-correlated four-link Doppler tracking system," in A Closeup of the Sun (M. Neugebauer, and R.W.Davies, Eds.) JPL Publication 78-70, NASA, 1978.

[11] T. Piran, E. Reiter, W.G. Unruh, and R.F.C. Vessot, "Filtering of spacecraft Doppler tracking data and detection of gravitational radiation," *Phys. Rev. Lett., D*, 34, no. 4, p. 984, 1986.
[12] D. Kleppner, R.F.C. Vessot, and N.F. Ramsey, "An orbiting clock experiment to determine the gravitational redshift," *Astrophys. Space Sci.* , vol. 6, pp. 13-32, 1970.
[13] L.L. Smarr. R.F.C. Vessot, C.A. Lundquist, R. Decher, and T. Piran, "Gravitational waves and redshifts: A space experiment for testing relativistic gravity using multiple time-correlated radio signals," *Gen. Rel. and Grav.* vol. 15, no. 2, pp. 129-163, 1983.
[14] M. Neugebauer and R.W. Davies, *A Closeup of the Sun*, JPL Publications 78-70, NASA, 1978.
[15] T. M. Brown, J. Christensen-Dalsgaar, W.A. Dziembowski, R. Goode, D.O. Gough, and C.A. Morrow, "Inferring the sun's internal angular velocity from observed P-mode frequency splitting," *Astrophys. J.*, vol. 343, p. 526, 1989.
[16] This work is being studied under NASA contract numberNAS-918 by J.D. Anderson, T.P. Krisher and E Lau of JPL and E.M. Mattison and R.F.C. Vessot of SAO.
[17] F. B. Estabrook, "Gravitational wave searches with ground tracking networks," *ACTA Astronautica*, vol. 17, no. 5, pp. 585-587, 1988.
[18] J. W. Armstrong, J.D. Anderson, and E.L. Lau, "Application of hydrogen maser technology to the search for gravitational radiation,"in *Proc. of Twenty-first Annual Precise Time and Time Interval (PTTI) Applications and Planning Meeting*, Redondo Beach, CA. Nov. 28-30, 1989, pp. 259-263.
[19] J. H. Taylor and J.M. Weisberg, "Further experimental tests of relativistic gravity using the binary pulsar PSR 1913 + 16," *Astrophys. J.*, vol. 345, pp. 434-450, Oct, 1989.
[20] A. J. Anderson, "Probability of long period (VLF) gravitational radiation," *Nature*, vol. 229, pp. 547-548, 1971.
[21] F. B. Estabrook and H.D. Wahlquist, "Response of Doppler spacecraft tracking to gravity waves," *Gen. Rel. Grav.*, vol. 6, pp. 439-447, 1975.
[22] K. S. Thorne and V.B. Braginsky, "Gravitational-wave bursts from the nuclei of distant galaxies and quasars: proposal for detection using Doppler tracking of interplanetary spacecraft," *Astrophys. J. Lett.*, vol. 204, L1, 1976.
[23] A.E.E. Rogers, A.T. Moffet, D.C. Backer, and J.M. Moran, "Coherence limits in VLBI observations at 3-millimeter wavelength," *Radio Sci.*, vol. 19, no. 6, pp, 1552-1560, 1984.
[24] A.E.E. Rogers and J.M. Moran, Chapter 5, "Interferometers and Arrays," Chapter 5 in *Methods of Experimental Physics*, Astrophysics, M.L. Meeks, Ed., vol. 12. New York: Academic Press, 1976.
[25] E. B. Formalont and R.A. Sramek, "Measurement of the solar gravitational deflection of radiowaves in agreement with general relativity," *Phys. Rev. Lett.*, vol. 36, p. 1475, 1976.
[26] N. Bartel, V. Dhawan, T. Krichbaum, D.A. Graham, I.I.K. Pauliny-Toth, A.E.E. Rogers, B.O. Rönnäng, J.H. Spencer, H. Hirabayashi, M. Inoue, C.R. Lawrence, I.I. Shapiro, B.F. Burke, J.M. Marcaide, K.J. Johnston, R.S. Booth, A. Witzel, M. Morimoto, and A.C.S. Readhead, "VLBI imaging with an angular resolution of 100 microarcseconds,"*Nature*, vol. 334, no. 6178, pp. 131-135, 1988.
[27] G.S. Levy, C.S. Christensen, J. F. Jordan, R.A. Preston, C.D. Edwards, R.P. Linfield, S.J. DiNardo, L. Skjerve, J.S. Ulvestad, T. Hayashi, T. Nishimura. T. Taskano, T. Yamada, T. Shiomi, H. Kunimori, N. Kawaguchi, M. Inoue, M. Morimoto, H. Hirabayashi, B.F. Burke, A. Whitney, D.L. Jauncey, C.H. Ottenhoff, K. Blaney, and W. Peters, "Results and communications considerations of the very long baseline interferometry demonstration using the tracking and data relay satellite system," *Acta Astron.*, vol. 15, no. 6/7, pp. 481-487, 1986.
[28] V.V. Andrejanov *et al.* "Quasat, A VLBI Observatory in Space," in *Proc. Workshop* , Gross Enzersdorf, Austria, June 18-22, 1984, ESA Publication SP-213.
[29] R.F.C. Vessot, "Clocks and spaceborne tests of relativistic gravitation," in*Advances in Space Research*, Eds. (R.D. Reasenberg and R.F.C. Vessot Eds.) Pergammon Press, vol.9, No. 9, 1989.
[30] E.J. Post, "Sagnac Effect," *Rev. Mod. Phys.* , vol. 39, p. 475, 1967.

A SHORT REVIEW OF THE VIRGO PROJECT

Jean-Yves VINET
Groupe VIRGO
Laboratoire de l'Accélérateur Linéaire
Orsay
and
Laboratoire d'Optique Appliquée
Ecole Polytechnique
Palaiseau (France)

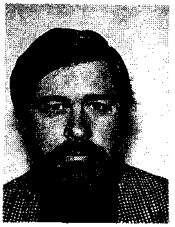

ABSTRACT

VIRGO is a French-Italian project of optical gravitational radiation detector. We outline the goals, the technological aspects and the scientific context of the project.

INTRODUCTION

Exotic astrophysical objects like pulsars, close and compact binary stars or supernovae have been theoretically shown to radiate gravitational waves. A first direct detection of such waves predicted by the General Relativity theory is a crucial experiment, and beyond, will provide a new observational window opening on strong gravitational field events. The

extreme weakness of radiative gravitational effects on earth-based devices (relative light distances distortions as small as 10^{-22}) implies special technological efforts and improvements in several domains.

1 SOURCES OF GRAVITATIONAL EVENTS

To emit significant gravitational radiation power, a matter distribution must have a large dynamical quadrupole moment either transient or steady. Only astrophysical objects like stars, or binary stars contain a mass in relation with the requirements of Einsteins's equations. Three classes of sources are currently discussed in relativistic astrophysics :

- ***stable rotators*** like white dwarfs binaries are numerous monochromatic very low frequency sources (< 50 mHz) . More interesting, in terms of frequency are the asymmetrical pulsars. The gravitational frequency can reach the kHz region but the amplitude depend on the asymmetry. They allow however an arbitrary signal integration time, reducing the effective noise of the detector.

- ***end of unstable rotators*** : Very close compacts objects have unstable orbits as they radiate gravitational energy. Finally they are expected to coalesce, emitting a final chirp of gravitational radiation of characteristic signature. The gravitational amplitude has been estimated as 3.10^{-21} for 1.5 solar masses elements in the Virgo cluster (about 15 Mpc) [1]. Accurate knowledge about the wave form allows a huge enhancement in the signal to noise ratio for such events.

- ***transient quadrupoles*** : In supernovae explosions, during the resulting collapse, asymmetry in the matter flow may induce rapidly varying quadrupole moments. The corresponding gravitational wave is a short isolated pulse. Typically, the expected peak amplitude for a supernova at 15 Mpc is 10^{-23} for a collapse of an iron stellar core to a neutron star, and $3\ 10^{-21}$ for a collapse to a black hole [1].

Discussion of the occurence rate of each type of events can be found in more detailed works . But our conclusion is that the VIRGO system must have a noise spectral density equivalent to $3\ 10^{-23}\ Hz^{-1/2}$ in order to detect at least several events per year.

2 THE VIRGO SYSTEM

2-1 The interferometer

The main subsystem of VIRGO is a Michelson inteferometer with arms containing 3km long optical resonators.

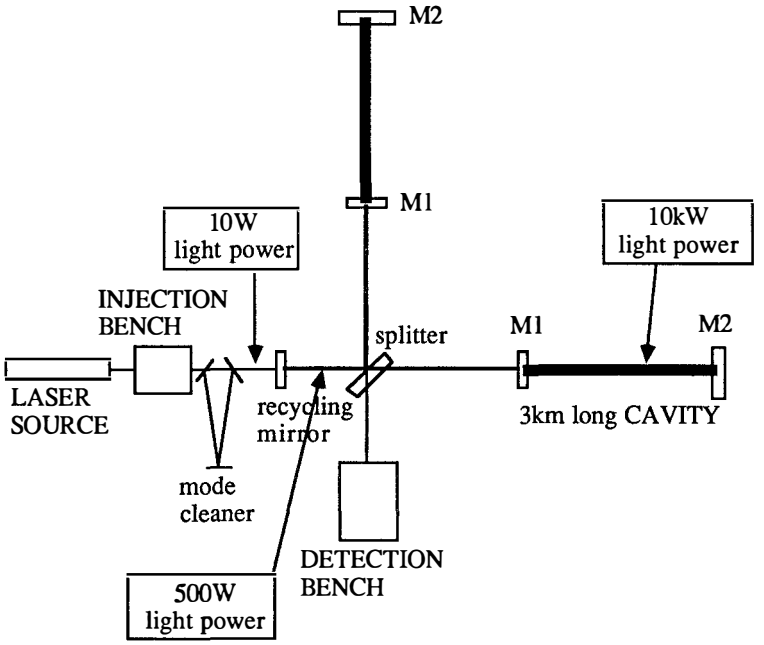

Gravitational waves produce a differential phase change in the optical amplitudes reflected by the two orthogonal cavities, phase change which is converted in a detected power variation after interference [2]. A recycling mirror is used in order to achieve a resonance which increases the light power reaching the beamsplitter. A mode cleaner filters residual direction fluctuations of the laser beam.

2-2 Supermirrors

Stringent requirements have been found for the mirror quality. In order to achieve recycling, the wavefront must remain clean after reflexion on each cavity at resonance. It has been found that the mirror surface *aberrations* must be less than $\lambda/100$ (peak to peak).

Moreover, the global efficiency of the mirror is essential. If a fraction of the incoming light power is converted into heat, temperature gradients appear, resulting in index gradient, and thermoelastic distortions. The *dissipative losses* must be smaller than a few ppm. If now a fraction of the incoming ligth power is scattered, the light scattered under angles larger than a mRd will interact with the walls of the vacuum vessel (see below), then recombine with the main beam, introducing noise. The *scattering losses*, must therefore be smalleer than a few ppm.

The beam geometry requires a 10cm diameter mirror as M1, and a 30 cm diameter mirror as M2. These dimensions are unusual for the preceding figures. But in fact, the dimensions of the substrate will be much larger because a large mass is needed. It is well known that the eigenmodes of an isolated solid resonator are excited by thermal (brownian) forces, so that each has an energy kT. The corresponding motion of the mirror faces is proportional to $M^{-1/2}$ this is why we must have a large *mass* (> 50 kg).

The brownian motion of the faces is also proportional to $Q^{-1/2}$ where Q is the *quality coefficient* of the mode. Q is directly related to the dissipation of sound waves. We shall use a kind of silica with acoustic losses giving a Q of 10^6.

2-3 the laser

The light source must be a highly stable and still powerfull laser. The challenge is to reach a power > 10W with a frequency noise spectral density $< 10^{-4}$ Hz $Hz^{-1/2}$ at 10 Hz. We develop a diode pumped Nd:YAG laser (slave) injected by a smaller, ultrastable similar laser (master). Injection technique allow to associate the stability of the master and the power of the slave [3]. The wavelength is 1.06 μm , corresponding to the near infrared.

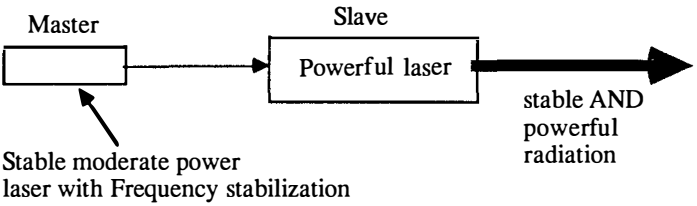

The master laser is locked on a prestabilization reference cavity of high finesse, isolated from thermal and mecahnical noises. The beam cleaner is one more filtering process.

2-4 The seismic isolation

In order to isolate the mirrors (test masses) from the ground vibrations, we have developped [4] a multistage gas spring attenuator which provides a (tested) attenuation of 10^{-10} at 10 Hz. This is an essential feature of VIRGO, which decreases the lower bound of the detection band, giving access to a wider class of sources.

2-5 The vacuum system

The whole optical system and its suspension must be operated in a vacuum to reduce pressure and corresponding refractive index fluctuations. A pressure of 10^{-7} torr would be sufficient, but in order to have a reasonable life time for the pumps, a mean operation pressure of 10^{-9} has been fixed (see at the end of the paper the configuration of the vacuum vessel). The large dimensions of the cavities (3km long and 1.2 m diameter) the size of the seismic attenuators (7 m high) result in a very large (more than 20,000 m^2) internal area for the vacuum vessel. The outgassing rate of the walls must remain very low, and we test stainless steel processing which guarantee a tolerable residual outgassing.

3 THE VIRGO TEAMS

The total manpower amounts to about 50 engineers and 50 physicists (Italians and French). Four Italian I.N.F.N. teams are involved, at

Frascati, Napoli , Perugia and Pisa . France provides five C.N.R.S teams at Annecy (LAPP), Lyon (IPN) , Paris (E.S.P.C.I.) and Orsay (LAL and LOA-polytechnique). But the tasks are numerous : infrastructure, seismic isolation, vacuum system, automatic alignment, data acquisition, thermal noise studies, interferometry, laser systems, general control and command, vacuum system, supermirror realization and supermirrors metrology, data acquisition, management and analysis...

4 THE VIRGO CLUSTER

A number of laboratories neither directly nor mainly involved in VIRGO have nevertheless wanted to mark their common interest for the project by creating a working group. The represented teams come from astrophysics, cosmology, and quantum optics (Groupe d'Astrophysique Relativiste at Meudon Observatory, Laboratoire de Gravitation et Cosmologie Relativistes and Laboratoire de Spectroscopie Hertzienne at University of Paris),. A number of cooperations are initiated with Australian groups (the AIGO teams) and with Indian groups (the IUCAA at Puna). Cooperation with LIGO has begun in the domains of supermirrors, development of software for optical studies, and scattered light reduction.

REFERENCES

1) Gravity-Wave Astrophysics Astrophysics
G. Schäfer
Relativistic Gravity Research : Proceedings of the 81 WE-Heraeus Seminar
Springer-Verlag 1992

2) Optimization of long-baseline optical interferometers for gravitational wave detection
J.-Y. Vinet et al.
Phys. Rev. D 38, 2, p. 433-447 (1988)

3) 18 W Single-Frequency Operation of an Injection-Locked, CW, Nd:Yag Laser
O.Crégut, C.N.Man, D.Shoemaker, A.Brillet, A.Menhert, P.Peuser, N.P.Schmitt, P.Zeller, K.Wallmeroth
Physics Letters, 140 , 294 (1989)

4) A. Giazotto
Phys. Rep. (1989) p.182-365

OPTICAL CONFIGURATIONS FOR THE VIRGO INTERFEROMETER

Patrice Hello *
Laboratoire de l'Accélérateur Linéaire - Groupe Virgo, Bâtiment 208
Université Paris-Sud, F-91405 Orsay, France

ABSTRACT

We present, in this paper, the potential optical configurations for the VIRGO interferometer, as well as for other similar antennas (LIGO...), and the implications for its sensitivity for the detection of gravitational waves (GW's). The dual recycling arrangement may particularly relax the severe optical specifications required in a power recycling interferometer. Finally, we present a new idea to improve the symmetry of the interferometer.

* : E-mail : HELLO@FRLAL51.BITNET

1. DETECTION OF GW'S BY THE VIRGO INTERFEROMETER

First of all, VIRGO is basically a Michelson interferometer; the principle of GW detection is based on the fact that an incident GW differentially changes the lengths of the arms (due to its quadrupolar nature), and so changes the interference field. It can be easily shown that maximal sensitivity is achieved when the interferometer is tuned at a dark fringe. Practically, a high power laser is needed in order to decrease the shot noise and kilometric arms (3 km for VIRGO) are required to decrease the influence of other noises (mainly seismic and thermal noises) on the signal to noise ratio. Use of Fabry-Perot cavities as arms is for optimising the storage time of the light in the arms with respect to the GW period.

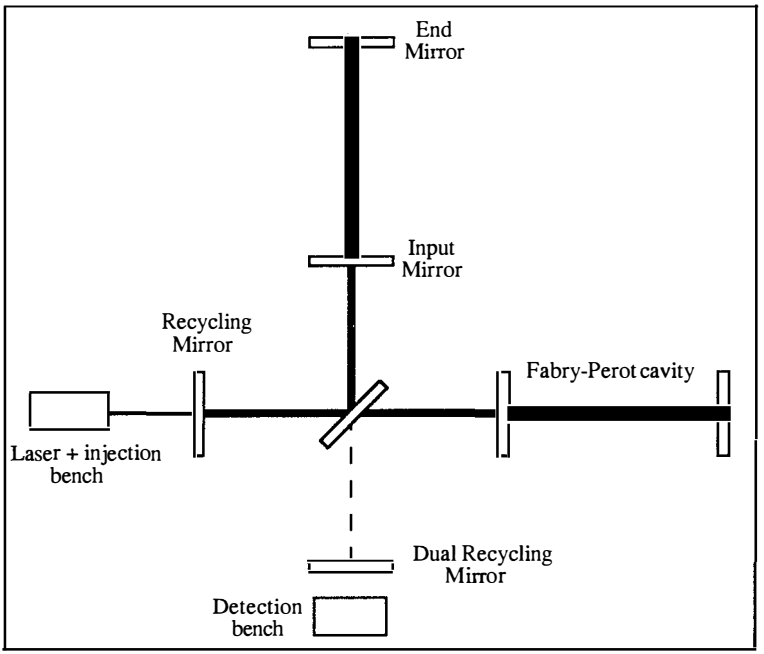

Fig.1 : recycling configurations for the Virgo GW detector

2. POWER RECYCLING AND THE QUALITY OF OPTICS

The idea of the power recycling (PR) is due to R. Drever [1]; this technique (see Fig.1) consists in increasing the circulating power in the interferometer, by adding a new mirror before it, in order to make a resonant Fabry-Perot cavity (the "recycling cavity").
A shot-noise limited recycling interferometer could in principle reach the strain sensibility level of $h \approx 3\ 10^{-23}\ Hz^{-1/2}$, which is the goal of VIRGO. However, the power in the recycling cavity, thus the sensitivity, can be directly reduced by defects of optics or asymmetry of the interferometer. We have then built simulation tools in order to determine the effect of a large class of optical imperfections and fix the tolerances [2, 3]. Non linear effects of high powers stored in the arm cavities have been also studied : effect of the radiation pressure [4] or thermal effects due to optical power absorption in the mirrors [5]. The found tolerances are rather stringent [6] (e.g. a surface quality requirement about $\lambda/100$ peak-valley in the beam zone) and imply a wide technological effort.

3. DUAL RECYCLING AND LOST LIGHT RECOVERY

While the effect of the PR is to reduce the shot-noise level, the signal recycling, due to Meers [7, 8], tends to increase the signal level. Indeed, from the point of view of the light, the effect of a GW is to add two sidebands at frequencies $\nu_0 \pm \nu_g$, to the carrier laser frequency ν_0; if we add a mirror at the output port of the interferometer (see Fig.1), we form an other cavity which may enhance the detected signal, one sideband being resonant. The combination of the PR (recycling of the carrier) and of the signal recycling (recycling of one of the sidebands) has been called dual recycling (DR) by Meers.
One very important consequence of the DR is that we can relax the optical tolerances, because of the recycling of the lost light ("bad" light) leading to a reduction of the total losses. This effect has been experimentally proved [9], and numerically checked [10]. An illustration is given on Fig.2, where we can see the recovery of the power in the PR cavity, use of the DR technique (simulation made at Orsay in collaboration with David McClelland, using fast numerical methods [11]).

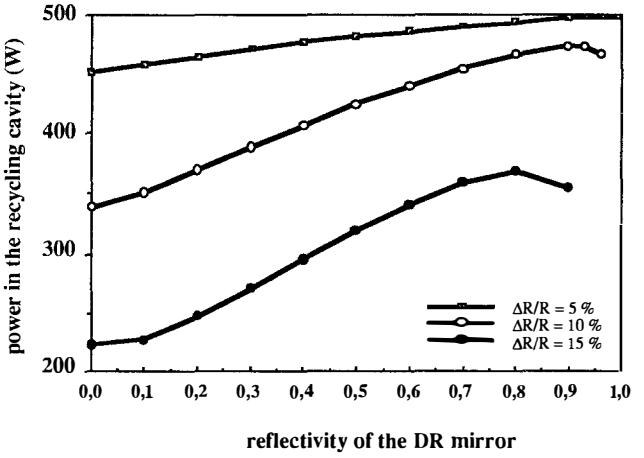

Fig.2 : the power in the PR cavity as a function of the reflectivity of the DR mirror for various curvature mismatches.

4. IMPROVEMENT OF THE SYMMETRY OF THE INTERFEROMETER

One important figure is the symmetry of the interferometer. Non perfect symmetry particularly makes the detection highly sensitive to the laser frequency noise. State of the art (asymmetry $\approx 10^{-3}$ between the two arms) prescribes a laser frequency stabilization at the level $\Delta\nu \approx 10^{-6}$ Hz. $Hz^{-1/2}$, in order to reach $h \approx 3\ 10^{-23}\ Hz^{-1/2}$. A mean of symmetrization is going to be tested at Orsay; the idea is simple : since the optical index depends on temperature, we can change the optical path in a mirror by heating it, and thus control its apparent reflectivity, taking advantage of the Fabry-Perot effect between the coated face ($R \approx 90$ %) and the uncoated face ($R \approx 4$% for Silica); if the mirror is, say, the input mirror of a Fabry-Perot cavity, we may change the reflectivity of the cavity itself. We may finally compensate for a lack of symmetry between the two arm cavities.

5. CONCLUSION

In spite of the severe optical specifications for the VIRGO detector [6], as

well as for LIGO, we can be optimistic : even with not as good optics as required, VIRGO/LIGO GW detectors should achieve the planned strain sensitivity about 3 10^{-23} $Hz^{-1/2}$ by use of "advanced" techniques, such as the dual recycling, or other to be tested.

REFERENCES

1) R. Drever, in *Gravitational Radiation*, N. Deruelle and T. Piran eds (North Holland, 1983)
2) P. Hello, Thesis (Université Paris-Sud, Orsay, 1990)
3) J.Y. Vinet, P. Hello, N. Man and A. Brillet, J. Phys. France **I2**, 1287-1303 (1992)
4) L. Bel, J.L. Boulanger and N. Deruelle, Phys.Rev.A**37**, 1537-1570 (1988), and references therein.
5) P. Hello and J.Y. Vinet J. Phys. France I, to appear (March 1993)
6) A. Brillet et al, VIRGO : Final Concept Design (unpublished)
7) B.J. Meers, Phys.Rev.D**38**, 2317-2326 (1988)
8) B.J. Meers, Phys.Lett.A**142**, 465-470 (1989)
9) B.J. Meers and K.A. Strain, Phys.Rev.D**43**, 3117-3130 (1991)
10) D.McClelland, C.M.Savage, A.J.Tridgell, R. Mavaddat, preprint (1993), submitted to Phys.Rev.D
11) J.Y. Vinet and P. Hello, preprint (1993), submitted to Journal of Modern Optics

SINGULARITIES IN GENERAL RELATIVITY

Pankaj S. Joshi
Tata Institute of Fundamental Research
Homi Bhabha Road, Bombay 400 005
India

ABSTRACT

We consider here the singularity problem in general relativity with a special reference to those forming in gravitational collapse. The relevance of recent results on collapse models involving perfect fluid, dust and imploding radiation shells is examined in connection with the fundamental problem of cosmic censorship. It is pointed out that the occurrence of naked singularities in gravitational collapse need not depend on geometric symmetries of the space-time assumed such as self-similarity, or the specific equation of state used. Such an analysis of gravitational collapse would be useful for any possible rigorous formulation and proof of the censorship hypothesis. It is argued that to begin with, a physical formulation for censorship should be developed which captures the basic spirit of the hypothesis, and some possibilities are indicated.

The singularity theorems in general relativity[1] establish the occurrence of space-time singularities in gravitational collapse and cosmology under a wide range of general conditions which have considerable physical plausibility. Such conditions include, amongst others, a suitable causality condition, the positivity of mass-energy density, the generic condition which implies that every non-spacelike trajectory must come across atleast once a non-zero stres-energy density, and a suitable convergence condition in the form of formation of trapped surfaces in the case of gravitational collapse. Such singularities then occur in the form of geodesic incompleteness in the space-time. Two basic areas used in order to infer the existence of such singularities are the topic of general global properties of a space-time obeying Einstein equations (which are used very weakly in the proofs of the singularity theorems) and the gravitational focusing of congruences of non-spacelike trajectories in a space-time.

Such results on the existence of space-time singularities however, do not make any further statement on the nature and structure of the singularities they establish. For example, they do not imply that physical quantities such as densities and curvatures must necessarily diverge along such incomplete non-spacelike geodesics in the limit of approach to the singularity as it happens in the case of the big bang singularity in the past at $t = 0$, or in the case of the Schwarzschild singularity at $r = 0$. Neither do they imply that the singularities forming in gravitational collapse must be necessarily hidden inside an event horizon, and hence invisible to an out side observer who is far away from the collapsing star. Such a situation requires a detailed analysis of the nature and structure of the space-time singularity which might occur under a specific situation and a determination is needed which would ensure whether the given singularity is physically meaningful or not in terms of the classification available for the physical significance of the singularity[2].

A particularly interesting question regarding the singularities occurring in gravitational collapse is whether these are necessarily covered by an event horizon and hence invisible to an out side observer at infinity. In the idealized case of the collapse of a homogeneous spherically symmetric dust ball[3], the space-time metric interior to the dust ball is given by the closed Friedmann metric, which is matched at the boundary by the exterior schwarzschild metric. All the matter collapses to a space-time singularity at $r = 0$ which is completely covered by the event horizon at $r = 2m$. Such a singularity cannot emit any messages to an out side observer.

The statement that such a situation would persist in a generic gravitational collapse as well, when departures from the assumptions such as homogeneity of the matter distribution, the dust form of matter etc. are allowed for is called the *cosmic censorship hypothesis*[4]. A rigorous formulation and proof of the cosmic censorship hypothesis, ruling out the occurrence of naked singularities of gravitational collapse has been one

of the most outstanding open problem in gravitation theory. Such a hypothesis lies at the very foundation of the theory and applications of the black holes. As it turns out, the attempts for different formulations and proofs for the same have run into one or the other difficulty after the conjecture was proposed. As far as a general proof for any suitably formulated version of the censorship is concerned, the main difficulty appears to be that we seem to require much more knowledge on general global properties of Einstein's equations and solutions than it is known presently[5].

Under the situation, we would argue that what is needed first is to develop a physical formulation of the censorship principle which captures the basic spirit of the conjecture. This should be based necessarily on a detailed examination of collapse scenarios other than the exact homogeneous dust collapse case to examine the possibilities arising in order to have insights into the issue of the final fate of gravitational collapse.

Several results have been obtained recently in this direction, analyzing the gravitational collapse of dust, perfect fluid as well as collapsing shells of radiation which provide certain insights into the final fate of collapse and show that shell-focusing naked singularities form at the center of spherically symmetric collapsing configurations.

In the following we discuss some of these results briefly and then consider the implications. For the sake of simplicity, through out we confine to self-similar gravitational collapse. To begin with, consider a shell of radiation collapsing at the center in an otherwise empty space-time[6]. The gravitational potentials in (u, r, θ, ϕ) coordinates are described by the Vaidya metric given by,

$$g_{uu} = -\left(1 - \frac{2m(u)}{r}\right), \quad g_{ur} = 1, \quad g_{\theta\theta} = r^2, \quad g_{\phi\phi} = r^2 \sin^2\theta \tag{1}$$

The stress-energy tensor describes the imploding radiation and is given by,

$$T_{ij} = \sigma k_i k_j \tag{2}$$

where k_i is a null vector. The collapse is characterized by the mass function $m(u)$ and the requirement of self-similarity implies that it must have a linear form,

$$m(u) = \lambda(u) \tag{3}$$

where $\lambda \geq 0$. A naked singularity forms in this case at the center $u = 0, r = 0$ provided $\lambda \geq 1/8$ and as shown in Ref.6, not just isolated trajectories but families of non-spacelike trajectories with a non-zero measure are emitted from this naked singularity. Further, a powerful curvature growth is observed along all these trajectories in the limit of approach to the naked singularity where we have,

$$R_{ij}V^iV^j \propto \frac{1}{k^2} \tag{4}$$

k being the affine parameter along the geodesic. It follows that this is an essential singularity in terms of the classification of singularities.

The analysis such as above provides certain insights into what is possible in gravitational collapse in general relativity. For example, it follows that the cosmic censorship conjecture cannot be valid in the form that all naked singularities must be in some sense gravitationally weak[7]; and that the curvatures could diverge very powerfully along the non-spacelike trajectories in the limit of approach to the naked singularity.

Similar analysis can be carried out for the cases of collapse of dust and perfect fluids as well[8], in which cases similar conclusions on the structure and formation of the naked singularity are obtained, namely, the formation of a naked singularity, emergence of a non-zero measure of non-spacelike trajectories from the same provided the positivity of the energy density holds, and a powerful curvature growth in the above sense along the non-spacelike trajectories in the limit of approach to the naked singularity in the past[9]. In the case of a perfect fluid, the condition for the formation of the naked singularity can be written in the form of a forth order algebraic equation which must have real positive roots.

One could however, argue in order to generate a physical formulation for the cosmic censorship that the forms of matter such as dust, perfect fluid or collapsing radiation are not really 'fundamental' forms of matter which must cease to be good approximations as the collapse progresses to an advanced stage. Alternatively, one could suggest[10] that these may be regarded only as approximations to more basic entities such as a massive scalar field and a massless scalar field (in the eikonal approximation). Thus, one would like to know whether naked singularities occur for a scalar field coupled to gravity, or for similar matter fields other than forms of matter such as dust, perfect fluid or collapsing radiation.

To examine this question in some detail, we consider a collapse scenario involving matter only subject to the restriction of positivity of energy but with a general equation of state[11]. The non-zero metric components for a spherically symmetric space-time are $(t,r,\theta,\phi = 0,1,2,3)$,

$$g_{00} = -e^{2\nu}, \quad g_{11} = e^{2\psi} \equiv V + X^2 e^{2\nu}, \quad g_{33} = g_{22}\sin^2\theta = r^2 S^2 \sin^2\theta, \tag{5}$$

where V is defined as above and due to self-similarity ν, ψ, V and S are functions of the similarity parameter $X = t/r$ only. The remaining freedom in the choice of coordinates r and t can be used to set the only off-diagonal term T_{01} of the energy momentum tensor T_{ij} to zero (using comoving coordinates). We assume the matter to satisfy the weak energy condition, i.e.

$$T_{ij}V^iV^j \geq 0, \tag{6}$$

for all non-spacelike vectors V^i. The relevant field equations for a spherically symmetric self-similar collapse of the fluid under consideration can be written as[12],

$$G^0{}_0 = \frac{-1}{S^2} + \frac{2e^{-2\psi}}{S}(X^2\ddot{S} - X^2\dot{S}\dot{\psi} + XS\dot{\psi} + \frac{(S - X\dot{S})^2}{2S}) - \frac{2e^{-2\nu}}{S}(\dot{S}\dot{\psi} + \frac{\dot{S}^2}{2S}) \quad (7)$$
$$= 8\pi r^2 T^0{}_0,$$

$$G^1{}_1 = \frac{-1}{S^2} - \frac{2e^{-2\nu}}{S}(\ddot{S} - \dot{S}\dot{\nu} + \frac{\dot{S}^2}{2S}) + \frac{2e^{-2\psi}}{S}[-SX\dot{\nu} + X^2\dot{S}\dot{\nu} + \frac{(S - X\dot{S})^2}{2S}] \quad (8)$$
$$= 8\pi r^2 T^1{}_1,$$

$$G^2{}_2 = 8\pi T^2_2, \quad G^0{}_1 = \ddot{S} - \dot{S}\dot{\nu} - \dot{S}\dot{\psi} + \frac{S\dot{\psi}}{X} = T^0{}_1 = 0. \quad (9)$$

Using the last equation above, the first two equations can be combined to get

$$\dot{V}(X) = Xe^{2\nu}[H - 2], \quad (10)$$

where $(\cdot)$ is the derivative with respect to the similarity parameter $X = t/r$ and $H = H(X)$ is defined by

$$H = r^2 e^{2\psi}(T^1{}_1 - T_0{}^0) \quad (11)$$

For matter satisfying weak energy condition, it follows that $H(X) \geq 0$ for all X. Using the field equations above and methods similar to those used in a perfect fluid collapse[9], one can see that the singularity at $t = 0, r = 0$ is naked when the equation $V(X) = 0$ has a real simple positive root, i.e.

$$V(X_0) = 0, \quad (12)$$

for some $X = X_0$.

It is also seen that a non-zero measure of future directed non-spacelike trajectories will escape from the singularity provided

$$0 < H_0 = H(X_0) < \infty. \quad (13)$$

Using the equations of non-spacelike geodesics in a self-similar space-time (see e.g. Joshi and Dwivedi in Ref.9), it is seen that these escaping trajectories near the naked singularity are given by,

$$r = D(X - X_0)^{\frac{2}{H_0 - 2}}. \quad (14)$$

Here D is a constant labeling different integral curves, which are the solutions of the geodesic equations, coming out of the naked singularity. It is seen that $H_0 > 0$ will hold if the weak energy condition above is satisfied and when the energy density as measured by any timelike observer is positive in the collapsing region near the singularity. In this

case, when $H_0 < \infty$, families of future directed non-spacelike geodesics will come out, terminating at the naked singularity in the past. On the other hand, for $H_0 = \infty$, a single non-spacelike trajectory will come out of the naked singularity. This characterizes the formation of naked singularity in self-similar gravitational collapse. Such a singularity will be at least locally naked and considerations such as those in Ref.9 can be used to show that it could be globally naked as well provided $V(X_0) = 0$ has more than one real simple positive roots.

We note that the existence of several classes of self-similar solutions to Einstein equations in the cases such as dust, radiation collapse etc. indicated above, where the gravitational collapse from a regular initial data results into a naked singularity, points out that such a condition will be realized for a wide variety of self-similar collapse scenarios. For example, for the case of radiation collapse with a linear mass function discussed above, the above initial condition corresponds to a restriction on the parameter λ (which is the rate of collapse) given by $0 < \lambda \leq 1/8$. In general, one could treat this condition for the existence of a naked singularity as an initial value problem for the first order differential equation given above governing $V(X)$.

One could examine the curvature strength of the naked singularity here as well, which provides an important test of its physical significance. As in the case of radiation and perfect fluid, this turns out to be a strong curvature naked singularity as specified in terms of the classification of singularities[2]. Consider the radial null geodesics coming out which are given by,

$$\frac{dt}{dr} = e^{\psi - \nu}. \tag{15}$$

Then,

$$\lim_{k \to 0} k^2 R_{ij} V^i V^j = \frac{4H_0}{(2 + H_0)^2} > 0. \tag{16}$$

It follows that this is a strong curvature naked singularity in the sense that the volume forms defined by all possible Jacobi vector fields vanish in the limit of approach to the naked singularity, in which case the space-time may not admit any continuous extension.

Are the results such as above confined to the case of self-similar gravitational collapse only ? Several results[13] worked out for the non-self-similar collapse of dust and radiation indicate that this is not the case.

The considerations such as above suggest that it may be useful to develop first a physical formulation of the cosmic censorship conjecture which captures its basic spirit before a rigorous and provable formulation for the same can be arrived at. A possibility is suggested in this direction by the results on self-similar collapse, namely that if the weak energy requirements indicated above are violated in the final stages of collapse, then even though a naked singularity may exist (in the sense that a single null geodesic might escape from the singularity), no families of non-spacelike trajectories may terminate at

the naked singularity in the past. Further, this will no longer be a strong curvature singularity as described above. For all practical purposes such a naked singularity may not be taken seriously and the physical spirit of cosmic censorship hypothesis would be in tact. It is not clear what mechanism may be invoked to achieve such a violation of energy condition in the advanced stages of gravitational collapse. Of course, the quantum effects may become important in the very final stages of collapse, and the quantum gravity corrections would be relevant at extremely small lengths of the order of the Planck scales. In fact, such a possibility of violation of energy conditions has been discussed recently in the context of worm hole space-times[14].

It would appear that the final fate of gravitational collapse remains an issue involving exiting possibilities. Even if a successful quantum theory of gravity was some how to dispense with all the space-time singularities, one would nonetheless have to take account of essentially singular, high density regions of matter and radiation predicted by the classical theory. One would like to conclude that the phenomena of gravitational collapse, and in particular the issue of its final out come requires much more investigation than it has received so far. In the absence of a mathematically rigorous formulation and proof for the censorship conjecture, it would seem that the first task is to develop a suitable physical formulation which captures the essence of censorship. Such a formulation should be based on a detailed analysis of the gravitational collapse scenarios.

References

1. S.W. Hawking and G.F.R.Ellis (1973), 'The Large Scale Structure of Space-time', Cambridge University Press, Cambridge.
2. F. J. Tipler, C. J. S. Clarke and G. F. R. Ellis (1980), 'General Relativity and Gravitation' Vol 2, ed A Held (New York : Plenum)
3. J. Oppenheimer and R. Snyder (1939), Phys.Rev. 56, p.455.
4. R.Penrose (1969), Riv. Nuovo Cimento 1, p.252 ; for recent reviews, see also W.Israel (1986), Can.J.Phys. 64, p.121 and D.M.Eardley (1987), in 'Gravitation and Astrophysics' (Cargese, 1986), Proc. of the NATO Advanced Study Institute, Cargese, France (ed. B.Carter and J.Hartle).
5. W.Israel (1984), Found.Phys. 14, p.1049.
6. For an analysis on the structure, formation and curvature growth near naked singularity in this case, see for example, I.H.Dwivedi and P.S.Joshi, Class.Quantum Grav. 6, p.1599 (1989); Class.Quantum Grav. 8, p.1339 (1991); and references therein.
7. See for example, Ref.2 above and also R.P.A.C.Newman (1986), Class.Quantum Grav. 3, p.527. and W.Israel in Ref.4 above.

8. For some references, see e.g. D.Eardley and L.Smarr (1979), Phys.Rev. D19, p.2239; D.Christodoulou (1984), Commun.Math.Phys. 93, p.171; R.P.A.C.Newman (1986), Class.Quantum Grav. 3, p.527; A.Ori and T.Piran (1990), Phys.Rev. D42, p.1068; B. Waugh and K.Lake (1991), Phys.Rev. D40, p.2137; K. Lake (1992), Phys.Rev.Lett. 68, p.3129.
9. P.S.Joshi and I.H.Dwivedi (1992), Commun.Math.Phys. 146, p.333; Class.Quantum Grav. 9, L69 (1992); To appear in Phys.Rev.D (1993).
10. See for example D. M. Eardley in Ref.4.
11. P.S.Joshi and I.H.Dwivedi (1993), To appear in Lett.Math.Phys.
12. M.E.Cahill and A.H. Taub (1971), Commun.Math.Phys. 21, p.1; G.Bicknell and R.N.Henriksen (1978), Astrophys.J. 225, p.237.
13. K.Lake (1991), Phys.Rev. D43, p.1416; P.S.Joshi and I.H.Dwivedi, J.Math.Phys. 32, p.2167 (1991); Gen.Relat.Grav. 24, p.129 (1992); Phys.Rev. D45, p.2147 (1992) and see also Ref.9 above.
14. Morris M. S. , Thorne K. S. and Yurtsever U. (1988), Phys. Rev. Lett. 61, p.1446.

COALESCING BINARIES AND PLUNGE ORBITS

Gerhard Schäfer and Norbert Wex
Max-Planck-Gesellschaft, Arbeitsgruppe Gravitationstheorie
an der Friedrich-Schiller-Universität Jena
O-6900 Jena, Federal Rep. of Germany

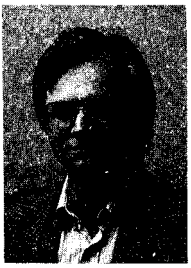

ABSTRACT

Innermost stable circular orbits may play an important role in the final stage of the time evolution of coalescing binaries with compact components. The paper gives a critical overview of our knowledge of the location of those orbits.

1. INTRODUCTION

It is a quite remarkable property of the motion of a test body in the exterior static relativistic gravitational field of a compact spherically symmetric heavy object (black hole, neutron star) that there exists an Innermost Stable Circular Orbit (ISCO). Inside this orbit test bodies, slightly perturbed, spiral into the center through conservative forces. This is what Einstein's theory of gravitation predicts in the domain of exact solutions.

In the case of objects with comparable masses, i.e. binary systems, things are more complicated and exact solutions are not known. The main reason for this is the emission of gravitational waves. Whereas the motion of a small body in the gravitational field of a heavy object is stationary with excellent accuracy (in the test-body limit the stationary motion is even exact), the stationary motion of a binary system is only a rough approximation to its exact motion because of stronger gravitational wave emission. (The gravitational wave emission is proportional to the mass-factor $\nu := m_1 m_2/(m_1 + m_2)^2$ which is maximal for equal masses.) Counted in powers of GM/ac^2, where G and c denote the Newtonian gravitational constant and the velocity of light, respectively, and where $M(= m_1 + m_2)$ is the total mass of the system and a a typical radial extension, the stationarity of the binary motion terminates already at the second post-Newtonian approximation (2PNA), i.e. at the order c^{-4}, because of the entering of gravitational radiation damping at the order c^{-5}, whereas in the test-body case the stationary part does not terminate. In the small-body case gravitational radiation damping will cause a modest inspiral. After crossing the ISCO the inspiralling motion will accelerate rapidly and the final plunge will be driven mainly by conservative forces. This coalescing picture is expected to be valid also in case of the motion of binaries although the gravitational radiation emission will surely play a more important role in the final plunge. (In the binary case with gravitational radiation damping the ISCO radius is determined by the time-symmetric (stationary) part of the dynamics.)

In Sec. 2 the post-Newtonian approximation (PNA) is confronted with the exact value of the Schwarzschild-test-body-ISCO radius. In Sec. 3 we critically review our knowledge of the location of the ISCO in binary systems.

2. APPROXIMATE TEST-BODY DYNAMICS IN SCHWARZSCHILD SPACETIME

The most compact objects in Einstein's theory of gravitation are black holes. (We shall discuss only non-rotating objects.) Their radial extension is naturally defined by the radius (Schwarzschild radius) of their sphere of "no return" (event horizon) which encloses the singular ("point-like") matter. Three different coordinate systems, covering the spacetime outside the event horizon, will be important in our discussion: Schwarzschild, R, harmonic, ρ, and ADM, r, coordinates, in the following abbreviated by SCs, HCs, and ACs, respectively. They are related by the equations

$$R = \rho + \frac{GM}{c^2} = r\left(1 + \frac{GM}{2c^2 r}\right)^2 . \tag{1}$$

The Schwarzschild radius takes respectively the following values in the three coordinate systems: 2 GM/c^2, GM/c^2, and $GM/2c^2$. The ISCO radius, in our three coordinate systems, is located at 6 GM/c^2, 5 GM/c^2, and 4.95 GM/c^2, respectively. Neutron stars are the most compact stars known. Their masses are about 1.4 solar masses and their radii, in HCs, are expected to lie in the range from 5 to 14 km, depending on the equation of state. These radii have to be compared with an ISCO radius of about 10 km. Therefore, besides black holes there might also exist neutron stars for which the ISCO radius has physical meaning.

The energy H_0 (divided by the reduced mass) of a test body in the Schwarzschild spacetime moving on circular orbits, as function of a reduced radius, r, and a reduced angular momentum, J, reads in ACs (M, here the mass of the heavy body, and G are put equal to 1),

$$\frac{H_0}{c^2}(r,J) = \frac{1-1/2c^2r}{1+1/2c^2r}\sqrt{1+\left(1+\frac{1}{2c^2r}\right)^{-4}\frac{J^2}{c^2r^2}} - 1. \qquad (2)$$

The corresponding expressions in HCs and SCs follow by the application of the transformations (1), holding J fixed. We have given the energy expression explicitly only in ACs because SCs do not exist for binary systems and also, for these systems, an ordinary Hamiltonian structure is not attainable in HCs beyond the 1PNA. For the Schwarzschild spacetime our ACs are isotropic in space. From the Hamiltonian (2) the radius of the ISCO is obtained by the aid of the equations

$$\frac{\partial H_0(r,J)}{\partial r} \;=\; 0 \;=\; \frac{\partial^2 H_0(r,J)}{\partial r^2}. \qquad (3)$$

The nPNA of the energy H_0 is defined as its Taylor expansion in powers of c^{-2} up to the order c^{-2n}. Table 1 shows ISCO–radii for different nPNAs in ACs, HCs and SCs, which, for later comparison, were transformed to HCs, using eq. (1). Only odd–PNAs show ISCOs. Their radii monotonically approach the exact value. Using an Euler–Lagrange–equations–of–motion approach in HCs, the values for the PNA–ISCO radii given in Table 2 were obtained by Kidder et al.[1]. There the odd–PNA radii converge from below and the even–PNA radii from above. It can be seen that the Hamiltonian–PNA approach in SCs converges faster than the Euler–Lagrangian–PNA approach in HCs.

Table 1. Schwarzschild–ISCO radii (unit GM/c^2) for nPNAs of the test–body Hamiltonians H_0^{ADM}, H_0^{harm}, and H_0^{Sch} given respectively in ADM, harmonic, and Schwarzschild coordinates

Approx.	H_0^{ADM}	H_0^{harm}	H_0^{Sch}
1PNA	11.1	11.1	5.35
3PNA	7.58	7.70	5.07
5PNA	6.56	6.63	5.01
7PNA	6.08	6.14	5.001
9PNA	5.81	5.85	5.000

Table 2. Schwarzschild–ISCO radii (unit GM/c^2) for nPNAs of the test–body Euler–Lagrange equations of motion in harmonic coordinates, according to Kidder et al. (KWW)

Approx.	KWW
1PNA	—
3PNA	—
5PNA	4.784
7PNA	4.985
9PNA	4.999

Approx.	KWW
2PNA	6.505
4PNA	5.364
6PNA	5.048
8PNA	5.004
10PNA	5.000

The different values for a specific PNA (see Tables 1 and 2) indicate that the PNA–ISCOs are located outside the domain of validity of the individual PNAs. Notice that the Hamiltonian and the Euler–Lagrangian forms of the PNAs, independently of the coordinate systems used, always give identical results, if restricted to their domain of validity.

3. ISCOs AND COMPACT BINARIES

The motion of compact binaries is known only up to the 2.5PNA. Extrapolating Table 2 to the binary case the 2PNA might be expected to give the exact ISCO with an accuracy of about 30%. In the binary case the 2PNA–ISCO radius, in the HCs, was found to be 6.8 GM/c^2 [1]. Numerical integration of the 2.5PNA dynamics in the same coordinate systems showed a plunge behavior near 7 GM/c^2, for equal masses[2].

In modifying a procedure, suggested and applied by Clark and Eardley[3] for the binary dynamics at 1PNA (quadratic Schwarzschild–test–body–Hamiltonian approach in SCs augmented by two times the 1PNA–binary part in HCs), Kidder et al.[4],[1] "improved" the 2PNA dynamics in HCs by the addition of all higher test–body–PNA terms to their equations of motion. From this "hybrid" dynamics they obtained an ISCO radius of 6.03 GM/c^2, for equal masses. The difference of only about 10% between the 2PNA and the hybrid ISCO–equal–mass radius compared to the difference of 30% between the 2PNA and the exact ISCO–test–body radius indicates that in the hybrid dynamics the 2PNA–binary part plays a dominate role, which suggests that the higher order PNA–binary parts might contribute essentially to the final result.

The modification of Kidder et al.[4] applied to our Hamiltonian approach, in ACs, results in the expression[5]

$$H(r,J) \equiv H_0(r,J) + H_\nu(r,J), \tag{4}$$

$$H_\nu := \nu\left[\frac{1}{8c^2}\left(3\frac{J^4}{r^4} - 4\frac{J^2}{r^3}\right) + \frac{1}{16c^4}\left(5(\nu-1)\frac{J^6}{r^6} - 2(3\nu+20)\frac{J^4}{r^5} + 64\frac{J^2}{r^4} - 12\frac{1}{r^3}\right)\right],$$

where $H_0(r,J)$ is given in equation (2). The application of the conditions (3) to the expression (4) gives an ISCO radius of 7.50 GM/c^2, in the HCs and for equal masses. The result differs by about 20% from the corresponding result by Kidder et al. In view of the fast convergence of the Hamiltonian–PNA approach in the case of the Schwarzschild–test–body–ISCO radius in SCs, we transformed the expression (4) to some pseudo–SCs, using eq.(1), and applied our critical point analysis, eq.(3), to that expression (in the binary part of the Hamiltonian, H_ν, only the 2PNA terms were kept). The result is 5.32 GM/c^2, where the radial coordinate is transformed back to its original ADM expression and then changed into its harmonic one, using the transformation which is valid also in the case of binary systems[5]. This result differs quite remarkably from our previous result and the result of Kidder et al., see Table 3. The diversity of the presented results clearly shows the strong influence of higher order PNA–binary terms on the ISCO radius.

Within an Hamiltonian variational approach with standing gravitational waves at spatial infinity, time independent as viewed from a rotating frame of reference, Blackburn

and Detweiler[6] found an equal-mass-binary-ISOC radius in an ADM-like coordinate system of 0.6 GM/c^2, far outside the domain of applicability of their approach. To render possible a comparison of their result with the other results the numerical values of the energy, H, and the angular momentum, J, both coordinate independent quantities, are added in Table 3. (For the small value of 0.6 GM/c^2 the transformation to binary HCs is not known.) This Table also shows the result obtained by Clark and Eardley[3]. Their hybrid dynamics, based on 1PNA-binary terms, yields an equal-mass-ISCO radius far away from the hybrid 2PNA-binary-ISCO radii of Kidder et al. and us. 1PNA results, however, should not be given too much weight as can be seen from the Tables 1 and 2; their values there for the ISCO radii, if well defined at all and not spurious like in Table 2, deviate from the exact value in a disproportionate manner.

Table 3. Approxiomate ISCO radii in harmonic coordinates (unit GM/c^2) and related energy (unit νMc^2) and angular momentum (unit $\nu GM^2/c$), obtained by Clark and Eardley (CE), Blackburn and Detweiler (BD), Kidder et al. (KWW), and us in ACs (SW1) and pseudo-SCs (SW2) for equal-mass binaries

	CE	BD	KWW	SW1	SW2
ρ	2.4	—	6.03	7.50	5.32
H	−0.07	−0.7	−0.037	−0.047	−0.059
J	3.2	0.9	3.83	3.71	3.42

We conclude that presently the best estimate for the equal-mass-binary-ISCO radius, in HCs, seems to be 6 GM/c^2 ±20%. Deeper investigations are obviously needed.

REFERENCES

[1]L.E. Kidder, C.M. Will and A.G. Wiseman, Coalescing binary systems of compact objects to (post)$^{5/2}$-Newtonian order. III. The transition from inspiral to plunge, preprint Washington University, WUGRAV-92-15 (1992).

[2]C.W. Lincoln and C.M. Will, Phys. Rev. D **42** (1990) 1123.

[3]J.P.A. Clark and D.M. Eardley, Astrophys. J. **215** (1977) 311.

[4]L.E. Kidder, C.M. Will and A.G. Wiseman, Class. Quantum Grav. **9** (1992) L125.

[5]N. Wex and G. Schäfer, Innermost stable orbits for coalescing binary systems of compact objects—a remark, preprint Jena University, December 1992.

[6]J.K. Blackburn and S. Detweiler, Phys. Rev. D **46** (1992) 2318.

GRAVITATIONAL RADIATION REACTION

Luc BLANCHET
Département d'Astrophysique Relativiste et de Cosmologie,
Centre National de la Recherche Scientifique (UPR176),
Observatoire de Paris, 92195 Meudon Cedex, France

ABSTRACT

Gravitational radiation reaction effects, in the dynamics of an isolated system, are computed by means of a post-Minkowskian approximation method (or nonlinearity expansion method). These effects arise from a specific "antisymmetric" component of the gravitational field (in the exterior region of the system), a solution of the wave equation of the type half-retarded minus half-advanced, which is investigated to all orders of nonlinearity. The antisymmetric component of the linear field (in a suitable coordinate system) defines a four-tensor potential for the radiation reaction forces in the linear theory, which generalizes the usual Burke and Thorne scalar potential. The complete nonlinear potential, up to the 1.5PN relative level, involves, besides the leading-order Burke-Thorne potential, reaction terms which parametrize the recoil force acting on the centre of mass of the system, and purely nonlinear reaction terms, depending on the full past dynamics of the system, which are associated with the "tail" effect.

1. INTRODUCTION

Gravitational radiation reaction effects, which are due to the reaction to the emission of gravitational radiation, play an important role in highly dynamical systems, such as coalescing compact binary star systems, whose radiation will be observed by future gravity-wave detectors (notably, laser interferometer detectors like VIRGO and LIGO). The dominant reaction effects have already been accurately measured, by Taylor and collaborators, in the dynamics of the binary pulsar PSR 1913+16. In view of these present and future astrophysical observations, it is important to have at hand powerful *theoretical* methods for the computation of gravitational radiation reaction in isolated systems. This contribution reports some recent work[1] in which we have defined such a method, able, in particular, to deal with radiation reaction effects of *nonlinear* origin.

The *leading-order* radiation reaction force in general relativity has been obtained by Burke[2] and Thorne[3], using a method of matched asymptotic expansions. This force arises at the so-called 2.5 post-Newtonian (2.5PN) approximation in the equations of motion, that is basically at the approximation of order c^{-5} when $c \to \infty$, where c is the velocity of light. Later, Chandrasekhar and Esposito[4], and many subsequent authors[5-8], obtained similar results (although in different coordinate systems), using systematic post-Newtonian methods. *Higher-order* radiation reaction forces necessitate the control of higher-order post-Newtonian approximations. For instance, the 3.5PN approximation is required for the computation of the total reaction force acting on the centre of mass of the system (or "recoil" force). The post-Newtonian method, however, is faced with severe inconsistencies in the higher-order approximations.

We have based our investigation of gravitational radiation reaction on a particular *post-Minkowskian* method (i.e., a method of nonlinear expansion of the field around Minkowski space-time) which has been developed in recent years[9,10] on foundations laid by Bonnor[11] and by Thorne[12]. Essentially, this method deals first with the nonlinear gravitational field in the *exterior* region of the system, and then uses an asymptotic matching, *à la* Burke and Thorne, to the inner field computed, for instance, by means of a post-Newtonian algorithm. Post-Minkowskian methods do not present any sign of inconsistency, and it has been shown that the nonlinearity expansion, in the exterior region, can be iterated *ad infinitum*. Furthermore, one can say that the post-Minkowskian method contains the post-Newtonian one, because the expansion when $c \to \infty$ can be performed afterwards in each terms of the nonlinearity expansion. The difficulties encountered by the post-Newtonian method in the higher-order approximations can be more clearly understood within the framework of the post-Minkowskian method. They lie in the appearance of non-local (in time) terms in the inner metric of the system, or "hereditary" terms (depending on the full past dynamics of the system), which are associated with radiation reaction effects of nonlinear origin[10]. This occurs at the 4PN approximation in the metric (or in the equations of motion).

Let us consider an isolated system S, described by some stress-energy tensor $T^{\mu\nu}$. We assume that the velocities of the constituents of S are small with respect to the velocity of light, and that the gravitational field generated by S is everywhere weak. To compute the radiation reaction forces acting within S, we proceed as follows. First, we consider the

gravitational field, satisfying the condition of retarded potentials, in the exterior (vacuum) region of S, and we determine there a specific *antisymmetric* component of the field, i.e. a solution of the wave equation which is the difference between retarded waves and the corresponding advanced waves (and which is parametrized by some retarded functionals of the stress-energy tensor of S). These waves change sign if we change the condition of retarded potentials to a condition of advanced potentials. Then, we use an argument of continuation inside S (which has in fact to be justified by an explicit matching to the field of S) to conclude that these antisymmetric waves form a radiation reaction potential for the radiation reaction forces acting *inside* S.

2. LINEAR RADIATION REACTION

At the linear level, the gravitational field $h_1^{\mu\nu}$ (say the harmonic coordinates trace-reversed perturbation of the Minkowski metric) in the exterior region of S can be expressed as a retarded multipole moment series of the form

$$h_1^{\mu\nu} = \sum_{l=0}^{+\infty} \frac{(-)^l}{l!} \partial_L \left\{ \frac{1}{r} \mathcal{F}_L^{\mu\nu} \left(t - \frac{r}{c} \right) \right\} . \tag{1}$$

We denote by ∂_L a product of l space derivatives $\partial_L = \partial_{i_1} \dots \partial_{i_l}$ (with $L = i_1 \dots i_l$). The multi-indexed functions $\mathcal{F}_L^{\mu\nu}$, which are functions of the retarded time $t - r/c$, can be viewed as some (reducible) "multipole moments". They are related to the stress-energy tensor of S by

$$\mathcal{F}_L^{\mu\nu}(t) = -\frac{4G}{c^4} \int d^3\mathbf{x}\, \hat{x}_L \int_{-1}^{1} dz \delta_l(z) T^{\mu\nu}(\mathbf{x}, t - z|\mathbf{x}|/c) . \tag{2}$$

Here, $\hat{x}_L$ denotes the trace-free part of a product of l space coordinates $x_L = x^{i_1} \dots x^{i_l}$. The expression (2) involves a weighted time average which is physically due to the time delays of the propagation of the waves inside S (with finite velocity c). The weighting function $\delta_l(z)$ is given by

$$\delta_l(z) = \frac{(2l+1)!!}{2^{l+1} l!} (1 - z^2)^l \quad ; \quad \int_{-1}^{1} dz \delta_l(z) = 1 . \tag{3}$$

A complete analysis[12] shows that the most general solution (modulo an arbitrary gauge transformation) of the linearized equations in the exterior of S is parametrized by only two sets of independent components of the functions $\mathcal{F}_L^{\mu\nu}$, namely two sets of irreducible multipole moments M_L and S_L which in the limit $c \to \infty$ reduce to the usual Newtonian expressions of mass type and spin type multipole moments, respectively. Now, the *antisymmetric* component of the exterior linearized field (1) is obtained by replacing in (1) each retarded wave by the corresponding antisymmetric (half-retarded minus half-advanced) wave. Antisymmetric waves are given by the formula

$$\partial_L \left\{ \frac{\mathcal{F}_L^{\mu\nu}(t - r/c) - \mathcal{F}_L^{\mu\nu}(t + r/c)}{2r} \right\} = -\frac{\hat{x}_L}{(2l+1)!! c^{2l+1}} \int_{-1}^{1} dz \delta_l(z)\, {}^{(2l+1)}\mathcal{F}_L^{\mu\nu}(t - zr/c) . \tag{4}$$

Note that (4) involves the same weighting function $\delta_l(z)$ as in the expression (2) of the multipole moments themselves. [We denote by ${}^{(2l+1)}\mathcal{F}_L^{\mu\nu}$ the $(2l+1)$-th time-derivative of

$\mathcal{F}_L^{\mu\nu}$.] The right-hand-side of (4) clearly shows the interesting characteristics of antisymmetric waves. When $c \to \infty$, these waves have the small order of magnitude c^{-2l-1}, contrasting with the order of magnitude 1 of the corresponding retarded or symmetric waves (we assume that the functions $\mathcal{F}_L^{\mu\nu}$ do not depend on c). Furthermore, viewing the expansion $c \to \infty$ as a near-zone expansion $r \to 0$, we find that the waves (4) are *regular* (C^∞) in a neighbourhood of the spatial origin $r = 0$, where S is located. Thus these waves, which are solutions of the vacuum (homogeneous) linearized equations, will as well appear by continuation in (or will have to be added by matching to) the field constructed in the interior of S, where they will imply a small correction in the equations of motion of S which can be interpreted in the usual way as a radiation reaction force. Using the decomposition of the moments $\mathcal{F}_L^{\mu\nu}$ into irreducible mass moments M_L and spin moments S_L, and using a suitable coordinate system, we can define[1] a *four-tensor* potential for the radiation reaction forces in the linear theory, which generalizes, in a precise sense, the usual Burke-Thorne scalar potential.

3. NONLINEAR RADIATION REACTION

The previous considerations neglected the important role of the nonlinearities of Einstein's equations in the radiation reaction problem. At the n-th post-Minkowskian order of approximation, we have to satisfy a wave equation of the type

$$\Box h_n^{\mu\nu} = N_n^{\mu\nu}(h_m; m \leq n-1) \tag{5}$$

(together with a condition of harmonic coordinates), where $h_n^{\mu\nu}$ denotes the n-th nonlinear iteration of the gravitational field (so that $Gh_1^{\mu\nu} + \cdots + G^n h_n^{\mu\nu} + \cdots$ is equal to the metric density perturbation), and where $N_n^{\mu\nu}$ denotes a nonlinear source, which is a nonlinear functional of the previous iterations $h_m^{\mu\nu}$ (with $m \leq n-1$) and their derivatives. We refer to[9] for a precise implementation of an algorithm solving (5) (and the condition of harmonic coordinates) for any n, and for the proof that the nonlinear series so obtained constitutes the most general solution of Einstein's equations in the exterior of S (modulo an arbitrary coordinate transformation). Now, the antisymmetric component of the nonlinear field, solution of (5), that is associated with nonlinear radiation reaction effects, is given by the unique decomposition of the usual (regularized) integral of the retarded potentials of the source, say $\mathrm{FP}\Box_{\mathrm{Ret}}^{-1} N_n^{\mu\nu}$, in terms of what we call the integral of the *instantaneous* potentials, say $\mathrm{FP}I^{-1} N_n^{\mu\nu}$. The symbol FP stands for "Finite Part" and reminds that one must apply the regularization procedure of [9] to deal with the integral of nonlinear sources (which are valid only in the exterior of S). This regularization procedure is in fact needed for a correct definition of $\mathrm{FP}I^{-1} N_n^{\mu\nu}$. The instantaneous integral defines, like the retarded integral, a solution of the wave equation with source $N_n^{\mu\nu}$ (i.e., we have $\Box(\mathrm{FP}\Box_{\mathrm{Ret}}^{-1} N_n^{\mu\nu}) = \Box(\mathrm{FP}I^{-1} N_n^{\mu\nu}) = N_n^{\mu\nu}$), but it has the particularity of depending on the values of the source $N_n^{\mu\nu}$ at only one single instant, namely the current instant t at which the field is evaluated. The solution $\mathrm{FP}I^{-1} N_n^{\mu\nu}$ is useful in practical computations of post-Newtonian expansions of the nonlinear field; however, its theoretical interest is that it delineates the terms which are *not* associated with radiation reaction. More precisely, we can

write the decomposition[1)]

$$\mathrm{FP}\Box_{\mathrm{Ret}}^{-1} N_n^{\mu\nu} = \mathrm{FP} I^{-1} N_n^{\mu\nu} + \sum_{l=0}^{+\infty} \frac{(-)^l}{l!} \partial_L \left\{ \frac{\mathcal{G}_{nL}^{\mu\nu}(t-r/c) - \mathcal{G}_{nL}^{\mu\nu}(t+r/c)}{2r} \right\} , \tag{6}$$

where the second term is a multipolar series of antisymmetric waves which is associated with radiation reaction effects of n-th nonlinear origin. The "multipole moments" $\mathcal{G}_{nL}^{\mu\nu}$, parametrizing the antisymmetric waves in (6), are given by the following *retarded* functionals of the source

$$\mathcal{G}_{nL}^{\mu\nu}(t) = \mathrm{FP} \left\{ \frac{-1}{4\pi} \int d^3\mathbf{x}\ \hat{x}_L \int_1^{+\infty} dz \gamma_l(z) N_n^{\mu\nu}(\mathbf{x}, t - z|\mathbf{x}|/c) \right\} , \tag{7}$$

where the weighting function $\gamma_l(z)$ is simply related to the weighting function $\delta_l(z)$ appearing in (2) and (4). Namely, we have

$$\gamma_l(z) = -2\delta_l(z) \quad ; \quad \int_1^{+\infty} dz \gamma_l(z) = 1 . \tag{8}$$

Note that the integral from one to infinity of the function $\gamma_l(z)$ is divergent, and that its value has to be computed by complex analytic continuation in l.

Finally, with the radiation reaction tensor potential of the linear theory, and with the equations (6)-(8) above (together with an appropriate algorithm for the construction of the nonlinear metric), we obtain[1)] the complete nonlinear radiation reaction potential up to the 1.5PN relative level (or 4PN level in the equations of motion). At the Newtonian level, the potential agrees with the scalar potential of Burke and Thorne. At the 1PN level, the potential involves both scalar and *vector* components which parametrize the radiation recoil force. And at the 1.5PN level, the potential contains a non-local in time contribution, of purely nonlinear origin, which is associated with the "tail effect", i.e. the effect of the scattering of the outgoing radiation off the (approximate) Schwarzschild space-time generated by S.

REFERENCES

[1] L. Blanchet, Phys. Rev. D, in press (15 May 1993).
[2] W.L. Burke, unpublished Ph. D. Thesis, California Institute of Technology (1969).
[3] K.S. Thorne, Astrophys. J. **158**, 997 (1969).
[4] S. Chandrasekhar and F.P. Esposito, Astrophys. J. **160**, 153 (1970).
[5] J.L. Anderson and T.C. DeCanio, Gen. Relat. Grav. **6**, 197 (1975).
[6] A. Papapetrou and B. Linet, Gen. Relat. Grav. **13**, 335 (1981).
[7] G.D. Kerlick, Gen. Rel. Grav. **12**, 467 (1980); **12**, 521 (1980).
[8] R. Breuer and E. Rudolph, Gen. Rel. Grav. **13**, 777 (1981).
[9] L. Blanchet and T. Damour, Philos. Trans. R. Soc. London A**320**, 379 (1986).
[10] L. Blanchet and T. Damour, Phys. Rev. D**37**, 1410 (1988).
[11] W.B. Bonnor, Philos. Trans. R. Soc. London A**251**, 233 (1959).
[12] K.S. Thorne, Rev. Mod. Phys. **52**, 299 (1980).

NON-PERTURBATIVE STRONG-FIELD EFFECTS IN TENSOR–SCALAR GRAVITY

Gilles Esposito-Farèse
Centre de Physique Théorique – CNRS Luminy, Case 907
F 13288 Marseille Cedex 09 (France)

Abstract : This talk presents the results of a recent work in collaboration with Thibault Damour. We show that a wide class of tensor–scalar theories of gravity can pass all present solar-system tests and still exhibit non-perturbative strong-field deviations away from general relativity in systems involving neutron stars. This is achieved without requiring either large dimensionless parameters, fine tuning or the presence of negative-energy modes. This study provides new motivations for experiments probing the strong-field regime of gravity, notably binary-pulsar experiments.

1. Introduction

Most of the experimental tests of general relativity have been performed in the solar system, *i.e.* in conditions where the gravitational field is extremely weak. For instance, the surface potential GM/Rc^2 of the Sun is about 10^{-6}, and it is smaller than 10^{-9} for the Earth. A few tests have also been possible in the strong-field regime thanks to the observation of binary pulsars, which involve neutron stars whose surface potentials are about 0.2. However, it is difficult to determine what features of Einstein's theory have really been tested by such observations if one does not compare its predictions with those of alternative theories of gravity. This is the motivation for studying the strong-field behaviour of contrasting theories, and thereby to suggest new tests of relativistic gravity.

The most natural alternatives to general relativity are the so-called tensor–scalar theories, in which gravity is mediated by one tensor ($g_{\mu\nu}$) together with one or several scalar fields (φ^a). Indeed, it seems very difficult to introduce consistently vector fields or extra tensor fields (besides $g_{\mu\nu}$) in the gravitational interaction, as discussed in section V of reference 1. On the contrary, massless scalars participating in the gravitational interaction arise naturally in theoretical attempts at unifying gravity with other interactions or at quantizing gravity (Kaluza–Klein theories, supergravity, strings, non-minimal generalizations of Einstein's theory), and recent extended inflationary models furnish new motivations for considering tensor–scalar theories.

Before studying the behaviour of such contrasting theories in the strong-field regime, it is necessary to check whether they are consistent with all weak-field tests. In the case of tensor–scalar theories, only two parameters are sufficient to describe all possible post-Newtonian deviations from general relativity. Their standard notation is β, γ, but in order to distinguish them from the underlying theory parameters introduced below, we shall decorate them with a tilde : $\tilde{\beta}, \tilde{\gamma}$. The bounds imposed at the one sigma level by solar-sytem experiments read

$$|\tilde{\beta} - 1| < 2 \times 10^{-3} \quad , \quad |\tilde{\gamma} - 1| < 2 \times 10^{-3} \; . \tag{1}$$

The question that we want to address is therefore the following : do theories exist which satisfy these tight constraints (*i.e.* which are very close to general relativity in the weak-field regime) but nevertheless exhibit large deviations from Einstein's theory in the strong-field regime ?

We gave a first answer to this question last year at the Moriond meeting[2,3] by considering tensor–multi-scalar theories involving at least two scalar fields. We showed that it was then possible to have strictly the same post-Newtonian limit as general relativity (*i.e.* $\tilde{\beta} = \tilde{\gamma} = 1$ strictly) without constraining the strong-field deviations. However, the bad feature of this class of theories is that one of the scalars must carry negative energy. In fact, it is possible to show[3] that a wide sub-class of them does not lead to any classical unstability, but it is clear that they would be ill-defined at the quantum level (although we do not know how to quantize gravity).

The aim of this talk is to present a new and much better answer to the preceding question : tensor–scalar theories which do not involve any negative-energy mode can satistfy the constraints (1) and still exhibit non-perturbative strong-field deviations away from general relativity[4].

2. Action and weak-field constraints

The non-perturbative strong-field effects we wish to point out are already present in the simplest case of a theory involving only one scalar field. For clarity, we shall therefore restrict our attention to tensor–mono-scalar theories although the multi-scalar case is not much more difficult to write[3]. In order to satisfy the weak equivalence principle, we consider only 'metric theories', in which the action of matter depends only on *one* metric tensor, say $\tilde{g}_{\mu\nu}$, without any explicit dependence on the scalar field φ. However, as was first pointed out by Pauli and Fierz, this tensor $\tilde{g}_{\mu\nu}$ is not necessarily the one, say $g_{\mu\nu}$, which appears in the Einstein–Hilbert action describing a spin-2 field. Indeed, they can be related by a conformal transformation

$$\tilde{g}_{\mu\nu} \equiv A^2(\varphi) g_{\mu\nu} \ , \tag{2}$$

where $A(\varphi)$ is a function of the scalar field. The action describing the class of tensor–mono-scalar theories can therefore be written as[5]

$$S = \frac{c^3}{16\pi G} \int \sqrt{-g} \mathrm{d}^4x (R - 2g^{\mu\nu}\partial_\mu\varphi\partial_\nu\varphi) + S_{\mathrm{matter}}[\psi, \tilde{g}_{\mu\nu}] \ , \tag{3}$$

where g denotes the determinant of $g_{\mu\nu}$, $g^{\mu\nu}$ its inverse, and R its curvature scalar (with the sign conventions of reference 6). The action of matter is supposed to describe all non-gravitational physics, *i.e.* for instance the Standard Model of electroweak and strong interactions. The square brackets mean that S_{matter} depends functionally on the material fields, globally denoted as ψ (including gauge fields), and on the tensor $\tilde{g}_{\mu\nu}$ which is a mixing of spin 2 ($g_{\mu\nu}$) and spin 0 (φ) degrees of freedom. The field equations which derive from this action read

$$R_{\mu\nu} - \frac{1}{2} R g_{\mu\nu} = 2\partial_\mu\varphi\partial_\nu\varphi - \partial_\rho\varphi\partial^\rho\varphi g_{\mu\nu} + \frac{8\pi G}{c^4} T_{\mu\nu} \ , \tag{4a}$$

$$\Box\varphi = -\frac{4\pi G}{c^4}\alpha(\varphi) T^\rho_\rho \ , \tag{4b}$$

where the contractions of indices, the Dalembertian $\Box$, and the Ricci curvature tensor $R_{\mu\nu}$ correspond to the metric $g_{\mu\nu}$ (and not $\tilde{g}_{\mu\nu}$), and where $T^{\mu\nu} \equiv (2c/\sqrt{-g})(\delta S_{\mathrm{matter}}/\delta g_{\mu\nu})$.

The function $\alpha(\varphi)$ involved in (4*b*) is the logarithmic derivative of the conformal factor $A(\varphi)$ defined in (2). It describes the coupling of φ to matter, and is therefore directly linked with the magnitude of this scalar field generated by a massive body. From now on, our discussion will be focussed on this function. Let us denote as φ_0 the (cosmologically imposed) background value of the scalar field, and expand $\alpha(\varphi)$ in powers of $(\varphi - \varphi_0)$ as

$$\frac{\partial \ln A(\varphi)}{\partial\varphi} \equiv \alpha(\varphi) = \alpha_0 + \beta_0(\varphi - \varphi_0) + \cdots \ , \tag{5}$$

where α_0, β_0, ...are constants. Only α_0 and β_0 are probed by the weak-field experiments performed in the solar system. Indeed, the post-Newtonian parameters $\tilde{\beta}$ and $\tilde{\gamma}$ read[3]

$$\tilde{\gamma} - 1 = -2\frac{\alpha_0^2}{1+\alpha_0^2} \quad , \quad \tilde{\beta} - 1 = \frac{1}{2}\frac{\alpha_0^2\beta_0}{(1+\alpha_0^2)^2} \ , \tag{6}$$

and therefore the constraints (1) can be rewritten as

$$\alpha_0^2 < 10^{-3} \quad , \quad \alpha_0^2|\beta_0| < 4 \times 10^{-3} \ . \tag{7}$$

In conclusion, solar-system experiments impose a small value for α_0, but do not constrain directly $\beta_0 = 8(\bar{\beta} - 1)/(1 - \bar{\gamma}^2)$.

On the contrary, strong-field effects depend on all the expansion (5) of the coupling function $\alpha(\varphi)$. However, the post-Newtonian formulae can be generalized in the strong-field regime[3] by simply replacing α_0 and β_0 by body-dependent parameters α_A, β_A, where A labels a compact body with radius R_A and mass M_A. Their expansion in powers of the surface potential GM_A/R_Ac^2 read

$$\alpha_A = \alpha_0 \times \left[1 + a_1 \frac{GM_A}{R_Ac^2} + a_2 \left(\frac{GM_A}{R_Ac^2}\right)^2 + \cdots\right] , \tag{8a}$$

$$\beta_A = \beta_0 + b_1 \frac{GM_A}{R_Ac^2} + b_2 \left(\frac{GM_A}{R_Ac^2}\right)^2 + \cdots , \tag{8b}$$

where $a_1, a_2, \ldots, b_1, b_2, \ldots$ are constants which depend only on the theory [*i.e.* on the series (5)] but not on body A. A quick way to estimate the order of magnitude of α_A is to compute $\alpha(\varphi_c)$, where φ_c is the value of the scalar field at the center of body A. These formulae show clearly why only α_0 and β_0 are probed by experiments in the solar system, where the surface potentials GM/Rc^2 are extremely small.

It can be shown[3] that any deviation from general relativity in an observable quantity involves at least two α_A factors. For instance, in a binary pulsar where A denotes the pulsar and B its companion, the orbital motion depends on products like $\alpha_A\alpha_B$, $\alpha_A^2\beta_B$, ..., and combinations like $\alpha_A\alpha_B\beta_A\beta_B$, ...also appear in the gravitational radiation. Therefore, any observable deviation from general relativity can be written formally as

$$\alpha_0^2 \times \left[c_0 + c_1 \frac{GM}{Rc^2} + c_2 \left(\frac{GM}{Rc^2}\right)^2 + \cdots\right] , \tag{9}$$

where $c_0, c_1, \ldots$ are theory-dependent constants, and GM/Rc^2 denotes globally the surface potentials of all the bodies. Hence our problem is to determine if this series in GM/Rc^2 can be large enough to compensate the small value of α_0^2 imposed by solar-system experiments (7). A possible answer would be to choose some very large parameters in the expansion (5) of $\alpha(\varphi)$, so that some of the constants $c_1, c_2, \ldots$ in (9) would compensate both α_0^2 and the powers of GM/Rc^2. However, such a choice would be *ad hoc*, and we shall restrict our attention to theories which do not involve large dimensionless parameters.

3. Non-perturbative effects

The simplest tensor–scalar theory is the Jordan–Fierz–Brans–Dicke theory[7-9]. It is determined by a constant coupling function $\alpha(\varphi) = \alpha_0 = 1/\sqrt{2\omega + 3}$, and the body-dependent parameters (8) read then simply : $\alpha_A = \alpha_0$, $\beta_A = 0$. Therefore, this theory and general relativity do not differ more in the strong-field regime than in the solar-system, and the constraints (7) show that one cannot expect deviations larger than $\sim 0.1\%$ even near neutron stars.

Let us now consider the next simplest theory, which is determined by a linear coupling function

$$\alpha(\varphi) = \beta_0\varphi = \alpha_0 + \beta_0(\varphi - \varphi_0) , \tag{10}$$

where β_0 is a constant, and $\alpha_0 \equiv \beta_0\varphi_0$. The background value φ_0 is supposed to be small enough in order to satisfy the weak-field constraints (7), *i.e.* $\beta_0^2\varphi_0^2 < 10^{-3}$ and $|\beta_0^3|\varphi_0^2 < 4 \times 10^{-3}$.

One can see heuristically in a toy model how the quantity (9) can be of order unity even for a vanishingly small α_0. Let us neglect the curvature of space-time, and suppose that the matter density ε and the pressure p take constant values inside a neutron star. In the interior of the star, the field equation (4*b*) reads $(1/r)\mathrm{d}^2(r\varphi)/\mathrm{d}r^2 = \kappa^2\beta_0\varphi$, where r is the radial coordinate and $\kappa^2 \equiv (4\pi G/c^4)(\varepsilon c^2 - 3p)$. There are therefore two different solutions depending upon the sign of β_0 :

$$\varphi \propto \sinh(\kappa\sqrt{\beta_0}r)/r \quad \text{if } \beta_0 > 0, \qquad \varphi \propto \sin(\kappa\sqrt{|\beta_0|}r)/r \quad \text{if } \beta_0 < 0. \tag{11}$$

By matching these interior solutions with the exterior one $\varphi = \varphi_0 + \text{constant}/r$, one can thus compute the value of the scalar field at the center of the star :

$$\varphi_c = \varphi_0/\cosh(\kappa\sqrt{\beta_0}R) \quad \text{if } \beta_0 > 0, \qquad \varphi_c = \varphi_0/\cos(\kappa\sqrt{|\beta_0|}R) \quad \text{if } \beta_0 > 0, \tag{12}$$

where R denotes the radius of the star. Hence the scalar field inside the star is even smaller than the background value φ_0 if $\beta_0 > 0$. In other words, the theory is even closer to general relativity in the strong-field regime than it is in the solar system ! On the contrary, φ_c is given by a function which has a pole at $\kappa\sqrt{|\beta_0|}R = \pi/2$ if $\beta_0 < 0$. Therefore, if β_0 is close enough to $-(\pi/2\kappa R)^2$, φ_c [and $\alpha_A \approx \alpha(\varphi_c)$] can be of order unity even if φ_0 is vanishingly small. As $GM/Rc^2 \approx \kappa^2R^2/3$ is typically of order 0.2 for a neutron star, we expect that this non-perturbative amplification of φ will take place for $\beta_0 \lesssim -4$, *i.e.* for $(\tilde{\beta}-1)/(\tilde{\gamma}-1) \gtrsim +1$ in terms of the post-Newtonian parameters (6). Therefore, this toy model shows that non-perturbative effects can occur in a theory which does not involve any large dimensionless parameter : here, the compensation of the small value of α_0 is due to a *pole*.

The numerical integration of the exact field equations (4) has been performed in reference 4. Numerical methods were necessary not only because the curvature of space-time obviously cannot be neglected in the vicinity of a neutron star (and therefore one has to solve coupled differential equations for $g_{\mu\nu}$ and φ), but also because one must choose a realistic equation of state to describe nuclear matter inside a neutron star. We plot in Figure 1 the body-dependent parameters (8) as functions of the baryonic mass of a neutron star (*i.e.* its number of baryons multiplied by the mass of a baryon), for the equation of state EOS II of reference 10, and for a coupling function $A(\varphi) = \exp(-3\varphi^2)$ (*i.e.* $\beta_0 = -6$). We chose for φ_0 the maximum value consistent with the solar-system constraints (7). This figure shows that the curvature of space-time has the effect of "damping the resonance" we found in the previous toy model : $-\alpha_A$ never diverges, but it takes large values over a wide interval of masses (from 1 to 3 solar masses), whereas in our previous heuristic argument it was non-negligible only over a tiny interval concentrated near the pole. In other words, the curvature not only suppresses the dangerous divergence we found, but also allows the non-perturbative effects to appear for almost any neutron star without requiring fine-tuning. Note that the divergence of β_A at the maximum mass is physically not relevant because the star becomes anyway dynamically unstable there. To give an order of magnitude of observable deviations from general relativity, let us compute the strong field analogues of the post-Newtonian parameters $\tilde{\beta}$, $\tilde{\gamma}$ which govern the motion of a binary system of two identical neutron stars [They are given by equation (6)

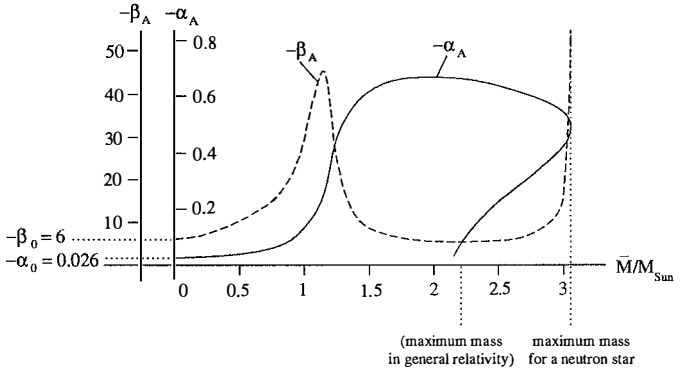

Figure 1 : The body-dependent parameters α_A and β_A for the model $A(\varphi) = \exp(-3\varphi^2)$.

in which we replace α_0 and β_0 by α_A and β_A.]. For $1.5M_{\rm Sun}$ neutron stars, we find that the strong-field analogue of $\tilde{\gamma}$ is about 0.4, whereas it is equal to 1 in general relativity. Similarly, the maximum value of $-\beta_A$ in Figure 1 corresponds to a strong-field analogue of $\tilde{\beta}$ which is close to -1, instead of $+1$ in general relativity.

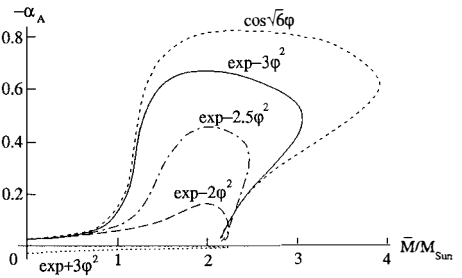

Figure 2 : The body-dependent parameter α_A for several coupling functions $A(\varphi)$.

Figure 2 shows how these strong-field effects depend on the coupling function $A(\varphi)$ defined in equation (2). In each case, we chose the maximum value of φ_0 consistent with the solar-system constraints (7). For the models $A(\varphi) = \exp(\beta_0\varphi^2/2)$, these numerical results confirm the conclusions of our previous heuristic argument : there exist appreciable deviations from general relativity as soon as $\beta_0 \lesssim -4$, *i.e.* $(\tilde{\beta}-1)/(\tilde{\gamma}-1) \gtrsim +1$. Note that when $\beta_0 > 0$, the theory is closer to general relativity in the strong-field regime than in the solar system. Finally, we see by comparing two functions which have the same curvature at the origin, $A(\varphi) = \exp(-3\varphi^2)$ [*i.e.* $\alpha(\varphi) = -6\varphi$] and $A(\varphi) = \cos\sqrt{6}\varphi$ [*i.e.* $\alpha(\varphi) = -6\varphi - 12\varphi^3 - \cdots$], that strong-field effects probe a large segment of the coupling function.

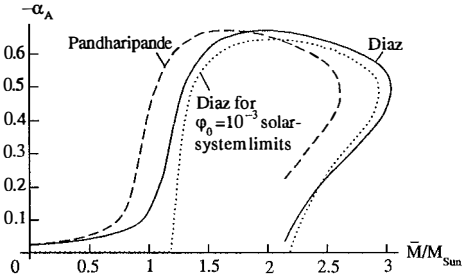

Figure 3 : The body-dependent parameter α_A for two different equations of state, and for a very small value of φ_0.

Figure 3 illustrates the robustness of the strong-field effects over a change of nuclear equation of state (Diaz : equation EOS II of reference 10; Pandharipande : equation A of reference 11), for the model $A(\varphi) = \exp(-3\varphi^2)$. Indeed, the magnitude of the effects is almost constant, although the masses for which the effects occur have been shifted. The comparison between the cases $\varphi_0 = 4.3 \times 10^{-3}$ (maximum allowed by solar-system constraints) and $\varphi_0 = 4.3 \times 10^{-6}$ in Figure 3 also underlines how strong-field effects free themselves from weak-field constraints when they develop. Hence a great enhancement of the precision of solar-system tests would not change our conclusions.

Conclusion

We have presented the first examples of relativistic theories of gravity which (i) are consistent with all solar-system experiments, (ii) are very different from general relativity in the vicinity of neutron stars, (iii) do not involve any negative-energy mode, and (iv) do not need any large dimensionless parameter nor fine tuning. This class of theories can be very useful as contrasting alternatives to general relativity, and can suggest new tests of the strong-gravitational-field regime. Their confrontation with the experimental data of binary pulsars will be done this year in collaboration with T. Damour and J. Taylor.

References

1. Damour T 1992 in Les Houches Summer School LVII *Gravitation and Quantizations*
2. Contributions of T Damour and G Esposito-Farèse to the *Proceedings of the XXVIIth Rencontres de Moriond* (1992) Editions Frontières
3. Damour T and Esposito-Farèse G 1992 *Class. Quant. Grav.* **9** 2093
4. Damour T and Esposito-Farèse G 1993, submitted to *Phys. Rev. Letters*
5. Bergmann P G 1968 *Int. J. Theor. Phys.* **1** 25; Nordtvedt K 1970 *Astrophys. J.* **161** 1059; Wagoner R V 1970 *Pys. Rev. D* **1** 3209
6. Misner C W, Thorne K S and Wheeler J A 1973 *Gravitation* (Freeman)
7. Jordan P 1949 *Nature* **164** 637; 1955 *Schwerkraft und Weltall* (Vieweg, Braunschweig); 1959 *Z. Phys.* **157** 112
8. Fierz M 1956 *Helv. Phys. Acta* **29** 128
9. Brans C and Dicke R H 1961 *Phys. Rev.* **124** 925
10. Diaz-Alonso J and Ibañez-Cabanell J M 1985 *Astrophys. J.* **291** 308
11. Arnett W D and Bowers R L 1977 *Astrophys. J. Suppl.* **33** 415

A POSSIBLE RESOLUTION OF THE BLACK HOLE INFORMATION LOSS PARADOX

J. W. Moffat
Department of Physics
University of Toronto
Toronto, Ontario M5S 1A7, Canada

ABSTRACT

The problem of information loss in black hole formation and the associated violations of basic laws of physics, such as conservation of energy, causality and unitarity is reviewed. The problem can be avoided in the nonsymmetric gravitational theory, if the NGT charge of a black hole and its mass satisfy an inequality that does not violate any known experimental data and allows the existence of white dwarfs and neutron stars. The observational evidence for black holes is reviewed and recent equations of state that allow compact stars with large critical mass to exist are discussed.

Hawking's discovery of black hole radiance,[1] led him to state that the accepted principles of relativity and quantum mechanics cannot be reconciled with this phenomenon[2]. All suggested resolutions of the paradox result in violations of cherished physical laws, such as the conservation of energy, causality and unitarity[3]. Consider a pure quantum state describing the infalling matter of a star. Such a state can be described by a density matrix, $\rho = |\psi><\psi|$ with vanishing entropy, $S = -\mathrm{Tr}\rho\ln\rho$. If, for sufficiently large M, the falling matter collapses to form a black hole, it will begin emitting Hawking radiation. If the back-reaction of the emitted radiation on the geometry is neglected, an approximation expected to hold until the mass M becomes comparable to the Planck mass M_{Pl}, then the radiation is thermal and is described by a mixed quantum state. The radiation is approximately described by a thermal density matrix with a nonzero entropy, $S \sim M^2/M_{Pl}^2$. The entropy is interpreted as an absence of information, and because it is nonvanishing, the information contained in the initial quantum state that fell into the black hole does not subsequently escape in the form of Hawking radiation. Information has been lost and unitarity has been violated. If the black hole evaporates completely, then an initially pure quantum state that was precisely known becomes a mixed state, and we can only assign probabilities to what the final state will be. Thus, information is destroyed in principle.

The problem begins with the formation of an arbitrarily large, classical black hole, which emits Hawking radiation. We cannot expect to invoke arguments based on some, as yet, unknown quantum gravity theory to cure the problem, since such a theory is only operative at the Planck length, $L_{Pl} \sim 10^{-33}$ cm. This would suggest

that we must seek an alternative to Einstein's gravitational theory i.e. we must modify the short distance behavior of gravity and prevent the formation of black holes. If black holes cannot form, then there is no Hawking radiation or information loss and the paradox has been removed. In order to prevent singularities and black holes from existing, we must make gravity repulsive in certain situations. The simplest modification of Einstein's theory is the Brans-Dicke scalar-tensor theory[4]. However, in this theory gravity is always attractive, so that the theory predicts singularities and black holes as in GR.

The nonsymmetric gravitational theory (NGT) is a mathematically and physically consistent theory of gravitation, which contains GR in a well-defined limit [5]. In this theory, the $g_{\mu\nu}$ decomposes according to the rule:

$$g_{\mu\nu} = g_{(\mu\nu)} + g_{[\mu\nu]}, \tag{1}$$

where $g_{(\mu\nu)} = \frac{1}{2}(g_{\mu\nu} + g_{\nu\mu})$ and $g_{[\mu\nu]} = \frac{1}{2}(g_{\mu\nu} - g_{\nu\mu})$. The affine connection $W^{\lambda}_{\mu\nu}$ decomposes according to

$$W^{\lambda}_{\mu\nu} = W^{\lambda}_{(\mu\nu)} + W^{\lambda}_{[\mu\nu]}. \tag{2}$$

The NGT contracted curvature tensor in terms of the W-connection is given by

$$R_{\mu\nu}(W) = W^{\beta}_{\mu\nu,\beta} - \frac{1}{2}(W^{\beta}_{\mu\beta,\nu} + W^{\beta}_{\nu\beta,\mu}) - W^{\beta}_{\alpha\nu}W^{\alpha}_{\mu\beta} + W^{\beta}_{\alpha\beta}W^{\alpha}_{\mu\nu}. \tag{3}$$

The field equations are

$$G_{\mu\nu}(W) = 8\pi G T_{\mu\nu}, \tag{4}$$

$$\mathbf{g}^{[\mu\nu]}{}_{,\nu} = 4\pi \mathbf{S}^{\mu}, \tag{5}$$

where $G_{\mu\nu} = R_{\mu\nu} - \frac{1}{2}g_{\mu\nu}R$ and $\mathbf{g}^{\mu\nu} = \sqrt{-g}g^{\mu\nu}$. The energy-momentum tensor for a perfect fluid in NGT is of the form[6]:

$$T^{\mu\nu} = (\rho + p)u^{\mu}u^{\nu} - pg^{\mu\nu}, \tag{6}$$

where ρ and p are the density and pressure and $u^{\mu} = dx^{\mu}/ds$. We interpret S^{μ} as the conserved particle number of the fluid:

$$S^{\mu} = \sum_{i} f_i^2 n_i u^{\mu}, \tag{7}$$

where f_i^2 are the coupling constants associated with stable fermion particles i, and n_i denotes the particle density. The net NGT charge associated with a body is defined by

$$\ell^2 = \int \mathbf{S}^0 d^3x \tag{8}$$

and because of the identity:

$$\mathbf{S}^{\nu}{}_{,\nu} = 0, \tag{9}$$

the ℓ^2 of a body is a conserved quantity. The matter response equations are

$$\frac{1}{2}\left(g_{\sigma\rho}\mathbf{T}^{\sigma\alpha} + g_{\rho\sigma}\mathbf{T}^{\alpha\sigma}\right)_{,\alpha} - \frac{1}{2}g_{\alpha\beta,\rho}\mathbf{T}^{\alpha\beta} + \frac{1}{3}W_{[\rho,\nu]}\mathbf{S}^{\nu} = 0, \tag{10}$$

where $W_{\mu} = W^{\alpha}_{[\mu\alpha]}$.

A cooling star of mass greater than a few solar masses cannot reach equilibrium as either a white dwarf or a neutron star in GR, and a similar situation prevails in NGT for standard phenomenological equations of state[7]. Savaria has found solutions to the time dependent, spherically symmetric collapse equations in NGT[8]. He proved that, if the final state of the collapsing matter is described by an equation

of state for which the repulsive NGT force dominates, then it is possible to produce a bounce mechanism which can prevent the formation of a black hole, without violating the Hawking-Penrose[9] positivity condition: $T_{\mu\nu}u^{\mu}u^{\nu} > 0$.

In NGT, there are no negative energy contributions, even in the presence of repulsive forces. This is an important aspect of the theory, which makes it a viable modification of GR. The flux of gravitational waves at infinity is the same as in GR, i.e. it is finite and positive definite[10].

For the case of a time dependent, spherically symmetric spacetime, the line element in polar coordinates is given by

$$ds^2 = \gamma(r,t)dt^2 - \alpha(r,t)dr^2 - R^2(r,t)d\Omega^2, \tag{11}$$

where $d\Omega^2 = d\theta^2 + \sin^2\theta d\phi^2$. We choose $w(r,t) = g_{[10]} \neq 0$ and $f(r,t) = g_{[23]} = 0$ in order to satisfy the physical boundary condition of asymptotic flatness at infinity.

From (10), we get for a perfect fluid the conservation law:

$$\dot{\rho} = -(\rho + p)\frac{\partial}{\partial t}\ln(\gamma^{-1/2}\sqrt{-g}), \tag{12}$$

and

$$p' = \frac{1}{2}(\rho + p)\frac{\gamma'}{\gamma} - \frac{1}{6\pi}\frac{s}{wR}W_{[0,1]}, \tag{13}$$

where $\dot{\rho} = \partial\rho/\partial t$ and $p' = \partial p/\partial r$. Moreover,

$$s(r,t) = \frac{2\pi R w S^0}{R'} = \frac{d\ell^4}{dR^4}. \tag{14}$$

For the spherically symmetric collapse of a pressureless fluid, the solutions for $\alpha(r,t)$ and $w(r,t)$ are given by

$$\alpha(r,t) = \frac{[R'(1+\ell^4/R^4)]^2}{(1-\frac{2GM}{r})(1+\frac{\ell^4}{r^4})}, \tag{15}$$

$$w(r,t) = \frac{\ell^2}{R^2}R'\left[(1-\frac{2GM}{r})(1+\frac{\ell^4}{r^4})\right]^{-1/2}. \tag{16}$$

The collapse cannot be isotropic unless $\ell^2 = 0$ (the GR limit). It can be shown that for a pressureless fluid, $dM/ds = 0$, so that $M = M(r)$ is a constant of the motion as in GR. We identify $M(r)$ as the mass contained within a sphere of radius r. Moreover, due to (9), $\ell^2 = \ell^2(r)$ is also a constant of the motion and will be identified as the NGT charge contained within the sphere. Another constant of the motion is given by

$$E(r) = \left[\left(1+U^2-\frac{2GM}{R}\right)\left(1+\frac{\ell^4}{R^4}\right)\right]^{1/2} - \frac{1}{2}\frac{M\ell^2\ell_t^2}{m_t R^4}, \tag{17}$$

where $U = dR/ds$ and ℓ_t^2 and m_t are the ℓ^2 charge and mass of a test particle.

We are interested in the case when the repulsive NGT forces are at a maximum, which corresponds to neglecting the tensor force contribution in (10) and (17). We assume that the fluid is at rest at $t = 0$:

$$R(r,0) = r, \quad \dot{R}(r,0) = 0. \tag{18}$$

Then, (17) yields

$$E(r) = [(1-\frac{2GM}{r})(1+\frac{\ell^4}{r^4})]^{1/2}. \tag{19}$$

Let us further assume that the gravitational field is weak, so that

$$\frac{2GM}{r} << 1, \quad \frac{\ell^4}{r^4} << 1. \tag{20}$$

Solving the equation:

$$\dot{R}(r,t) = 0, \tag{21}$$

we find that the collapsing star with initial density $\rho(r,0)$ and zero pressure will not form an event horizon and a black hole when:

$$\ell \geq \left(\frac{8}{3^{3/4}}\right) GM. \tag{22}$$

When $M = M_{\odot}$, the collapse is halted before the event horizon is reached for $\ell \geq 5.2$ km.

It is not expected that the basic mechanism preventing black hole formation in stellar collapse will be significantly modified when the approximations made above are relaxed, but further work must be carried out to investigate this issue.

For a Wheeler GEON (gravitational electromagnetic entity)[11], it was shown by Wheeler[12], and Brill and Hartle[13], that such objects are unstable i.e. they will either disperse or collapse. Although it is unlikely that such objects exist, we must consider their behaviour in NGT. Because the photon number density n_γ is not conserved, we have $\ell_\gamma^2 = 0$ and $g_{[\mu\nu]} = 0$, and NGT reduces to GR for photon GEONS (i.e. pure photon stars). Therefore, if photon GEONS exist, we cannot prevent their collapse to a black hole with the resultant loss of information due to Hawking radiation. On the other hand, for neutrino GEONS[14], NGT will prevent their collapse to a black hole, because the NGT charge for neutrinos, $\ell_\nu^2 \neq 0$,

thereby guaranteeing that these objects can be prevented from collapsing to black holes. However, as with photon GEONS, we consider that such systems are highly unlikely to exist as astrophysical objects.

We shall postulate as a general principle in Nature, that since the initial big bang at t=0, matter always dominated over anti-matter. Thus, matter genesis was initiated at t=0 by means of a violation of particle number conservation and an associated CP violation. In NGT, this breaks the principle of equivalence, since the excess of matter coupled to the NGT field $g_{[\mu\nu]}$, violates the equivalence principle. We also postulate that at the end-point of gravitational collapse, the repulsive NGT force dominates, so as to prevent the formation of black holes of arbitrarily large or small mass. A consequence of this is that no naked, local singularities of the type generated by gravitational collapse can ever be observed in Nature, nor can event horizons be produced together with Hawking radiation. In NGT there will be no absolute loss of information, as occurs in GR, and the laws of quantum mechanics and thermodynamics will not be violated.

The values of the NGT charge necessary to prevent the formation of black holes are not expected to contradict any experiments in the solar system[5] (this is certainly true for pressureless collapse), nor will they prevent the formation of white dwarfs or neutron stars[7]. It will be interesting to investigate the astrophysical consequences of the objects that form when stellar collapse is halted in NGT, and to ascertain whether stable systems can be formed with possibly unique observational signatures that could distinguish them from black holes.

The best evidence for black holes is based on observations of binary systems such as Cyg X-1, LMC X-3, and 0620-00[15]. None of these sources has shown X-ray bursts or pulses, which are considered evidence of a neutron star. Consider the best known case of Cyg X-1, which was identified with the optical source HDE 226868 in a binary system with an orbital period of 5.6 days. Analysis of the B star's radial velocity curve showed that if the primary star's mass is normal for its spectral type and luminosity, then the estimated mass of the unseen companion, $M_x \sim 10 - 16\, M_\odot$[16], is too large to be a neutron star.

However, this criterion is based on GR and the choice of an equation of state for matter at or greater than nuclear densities. Recently, studies have shown that an equation of state obtained from alternative exotic types of matter, such as soliton stars[17], or an equation of state based on effective field theories of bulk nuclear matter producing Q-stars[18], can lead to stable compact objects with masses as large as $\sim 400\, M_\odot$. In the case of Q-stars, the equation of state is built on an effective Lagrangian for nuclear matter, which is in agreement with known experimental properties of the nuclear physics of bulk nuclear matter. This equation of state does not violate causality or any known physical law. Adapting such equations of state in NGT will lead to stable compact objects with $M \geq 20\, M_\odot$, which are not black holes but could have the characteristic signatures of compact objects such as Cyg X-1 and 0620-00.

Acknowledgements

This work was supported by the Natural Sciences and Engineering Research Council of Canada. I thank M. Clayton, N. Cornish, P. Savaria and D. Tatarski for helpful and stimulating discussions.

References

1. S. Hawking, Commun. Math. Phys. **43**, 199 (1975); Phys. Rev. D**13**, 191 (1976); J. D. Bekenstein, Phys. Rev. D**7**, 2333 (1973); Phys. Rev. D**9**, 3292 (1974).
2. S. Hawking, Phys. Rev. D**14**, 2460 (1976).
3. For reviews, see: T. Banks, M. E. Peskin, and L. Susskind, Nucl. Phys. B**244** 125 (1984); J. Preskill, "Do Black Holes Destroy Information?" California Institute of Technology preprint CALT-68-1819 (1992); S. B. Giddings, Phys. Rev. D**46**, 1347 (1992); "Toy Models for Black Hole Evaporation" UCSBTH-92-36 hep-th/9209113 (1992); J. A. Harvey and A. Strominger, "Quantum Aspects of Black Holes", preprint EFI-92-41 hep-th/9209055 (1992).
4. C. Brans and R. H. Dicke, Phys. Rev. **124**, 925 (1961).
5. J. W. Moffat, Phys. Rev. D**35**, 3733 (1987); For a review, see: *Gravitation 1990: A Banff Summer Institute, ed. R. B. Mann and P. Wesson (Singapore: World Scientific) p. 523 1991.*
6. D. Vincent, Class. Quantum Grav. **2**, 409 (1985).
7. P. Savaria, Class. Quantum Grav. **6**, 1003 (1985); L. Campbell, J. W. Moffat, and P. Savaria, Astrophys. J. **372**, 241 (1991).
8. P. Savaria, Class. Quantum Grav. **9**, 1349 (1992).

9. R. Penrose, Phys. Rev. Lett. **14**, 57 (1965); S. Hawking, Proc. R. Soc. London **A300**, 187 (1967).

10. It has recently been claimed that NGT suffers from radiation flux instability and bad asymptotic behaviour: T. Damour, S. Deser, and J. McCarthy, Phys Rev. D**45**, R3289, (1992); *ibid* D**47** 1541 (1993). These results have been shown to be incorrect: N. Cornish, J. W. Moffat, and D. Tatarski, Phys. Lett A **173**, 109 (1993); "Gravitational Waves from an Axi-Symmetric Source in the Nonsymmetric Gravitational Theory", preprint 1993 (submitted to Phys. Rev. D); N. Cornish and J. W. Moffat, Phys. Rev. D (to be published).

11. J. A. Wheeler, Phys. Rev. **97**, 511 (1955); *Geometrodynamics*, Academic Press Inc. New York, 1962.

12. J. A. Wheeler, *Relativity, Groups and Topology*, ed. C. and B. DeWitt (New York: Gordon and Breach 1964); B. K. Harrison, K. S. Thorne, M. Wakano, and J. A. Wheeler, *Gravitation Theory and Gravitational Collapse*, University of Chicago Press, Chicago and London, 1965.

13. D. R. Brill and J. B. Hartle, Phys. Rev. **135**, B271 (1964).

14. D. R. Brill and J. A. Wheeler, Rev. Mod. Phys. **29**, 465 (1957).

15. A. P. Cowley, Annu. Rev. Astron. Astrophys. **30**, 287 (1992).

16. B. L. Webster and P. Murdin, Nature **235**, 37 (1972); C. T. Bolton, Astrophys. J. **200**, 269 (1975).

17. T. D. Lee, Phys. Rev. D**35**, 3637 (1987); T. D. Lee and Y. Pang, *ibid* D**35**, 3678 (1987).

18. S. Bahcall, B. W. Lynn, and S. B. Selipsky, Astrophys. J. **362**, 251 (1990).

CONFERENCE SUMMARIES

NEUTRINO MASS AND MIXING: SUMMARY OF THE NEUTRINO SESSIONS

Thomas J. Bowles
Physics Division, MS D449
Los Alamos National Laboratory
Los Alamos, New Mexico 87545

ABSTRACT

A great deal of experimental and theoretical effort is underway to use neutrinos as a probe for Physics Beyond the Standard Model. Most of these efforts center on the questions of the possible existence of non zero neutrino mass and mixing. Sessions at the Moriond conferences have dealt with these questions at most of the meetings during the last several years and this year was no exception. Presentations covering most of the current and planned research in this field were presented and discussed. Although there is, at present, no definitive evidence for a non zero neutrino mass and mixing, several unresolved problems (in particular solar neutrinos) do seem to be indicating the likely existence of new neutrino properties. It is likely that before the end of this decade, efforts now being initiated will be able to determine whether or not the hints we are now seeing are really due to new physics.

INTRODUCTION

Neutrinos play a dominant role in both particle physics, astrophysics, and cosmology. In the our present understanding of the strong, weak, and electromagnetic forces, the group structure of the Standard Model is $SU(3)_C \otimes SU(2)_L \otimes U(1)_{EM}$. In the Weinberg-Salam-Glashow Standard Electroweak Model, left-handed neutrinos are in a doublet, while right-handed neutrinos are in a singlet, and therefore do not interact with the other known particles. In this model, the neutrinos are intrinsically massless and conserve lepton number. However, while the W-S-G provides an amazingly accurate picture of our present cold Universe, it has a number of deficits. The Standard Model does not explain the origin of the group structure, it does not reduce the number of coupling constants required, nor does it offer any prediction for the physical masses of the particles. Thus, it is generally assumed that the Standard Model is but a subset of some larger gauge theory. A wide variety of Grand Unified field Theories (GUTs), Super Symmetric Models (SUSY) and Superstring models have been proposed as the model for this larger structure. In general, these models predict non zero neutrino masses and contain mechanisms that provide for lepton-number violation. Thus, a variety of new phenomena are predicted, including finite neutrino masses and the possibility that neutrinos can oscillate from one type to another.

In astrophysics, neutrinos play direct roles in the energy-producing reactions in stars, as well as being the primary driving force in supernova explosions. As the cross sections for neutrinos are so small (typically 10^{-40} cm^2), they generally do not interact as they exit a star and thus they can provide a direct means of probing the stellar interior. In contrast, the energy we observe radiated from stars takes of order 10^6 years to reach the surface of the star and suffers so many interactions that any direct information is lost.

Finally, in Standard Big Bang cosmology, the number density of relic neutrinos is comparable to that of photons, and is therefore of order 10^9 times higher than that of baryons. Thus, if neutrinos have even a very small mass (of order a few tens of eV), they will be the dominant form of matter in the Universe and may be an explanation for dark matter. Even with masses of only a few eV, they will strongly influence the large scale structure of the Universe.

STATISTICAL AND SYSTEMATIC CONCERNS IN SEARCHES FOR NEW PHYSICS

In searching for new physics beyond the Standard Model, one is usually looking for rare phenomena or slight deviations from an expected shape. It is extremely important in carrying out such experiments that the statistical and systematic analyses do not bias the results in any way which might either hide a real effect or introduce a spurious effect. Knapp* pointed out the difficulties and problems that one can encounter in doing fairly straightforward statistical analyses of the data. The case in point was analysis of the tritium beta decay experiments, but the point applies equally well to many experiments. In analyzing the tritium data, one has very few events in the region of interest and therefore must use Poisson statistics. However, one can use either the Neyman's or Pearson's fitters, and one finds different results fitting the same data set with the two different fitters. In general Neyman's X^2 underestimates the area fitted while Pearson's X^2 overestimates the area. These effects can lead to an apparent (but spurious) ν_e mass of more than -100 eV^2 to + 40 eV^2. Thus, in general, one must carry out Monte Carlo checks of the fitters and derive an unbiased fitter in order to ensure that the result is correct. Knapp* went on to discuss possible systematic errors which could also affect the results of the tritium beta decay experiments. Many of these ideas apply generally to all experiments, such as the idea that one must take a penalties error of 1-σ every time one tries to fit the same data set under different assumptions or with different cuts when trying to maximize the experimental sensitivity for a particular result when that result is already known from an earlier round of fitting. The moral of the story is that there is a real danger of bias in analyzing data when you already "know" the answer.

BETA DECAY

There are three known flavors of neutrinos: electron, muon, and tau (together with their corresponding antineutrinos). Neutrinos may also be classified as Dirac, in which case the right- and left-handed neutrinos ν_R and ν_L and their antiparticles $\bar{\nu}_R$ and $\bar{\nu}_L$ are distinct states, or Majorana, in which case $\nu \equiv \bar{\nu}$, so that there are only two states ν_R and ν_L. Electron and muon neutrinos have been directly observed in many experiments. The tau neutrino has not yet been directly observed, but is assumed to exist as it is required in the Standard Model and from LEP results. By observing the beta decay spectra of nuclei,

muons, and tau particles, one can kinematically reconstruct the events, and the existence of a finite neutrino mass will produce a well-defined distortion in the spectra.

Tau Neutrino

The best limit on the ν_τ mass comes from the ARGUS collaboration at DESY. By observing the decay of a tau to 5-pion final states, one can constrain the tau neutrino mass by looking for events very close to the endpoint. A total of 20 events has been observed, and coupled with recent new measurements of the tau mass, provides an upper limit of 31 MeV (95% CL).[1] With higher statistics and improved resolution, one might hope to achieve limits of 10 MeV in the future.

Muon Neutrino

The most stringent limit on the ν_μ mass comes from measurements of the μ momentum following the decay of stopped pions. The most recent determination of m_{π^+}, coupled with the muon data of Abela et al[2], gives $m_{\nu_\mu} < -0.097(72)$ MeV, which, using the Bayesian prescription[3], yields an upper limit of 270 keV (90% CL).

However, new measurements at the Paul Scherrer Institute (PSI) of m_{π^+} have resulted in a reevaluation[4] of the Abela et al. data. This results in a new value of $m_{\nu_\mu} < -0.127(25)$ MeV, resulting in a 5-σ negative central value. The difficulty is that m_{π^+} is determined using pionic X-rays and the precision is limited principally by theoretical uncertainties such as electron screening and strong interactions (eg., absorption from the 3d state). Thus, the measurement using stopped pions has a severe systematic problem and cannot be used.

The next best method of determining m_{ν_μ} mass is using π decay in flight in which both the π and μ momenta are directly measured. This method is relatively insensitive to m_π and m_μ. The measurement of Anderhub et al.[5] at PSI thus provides the most reliable limit on m_{ν_μ} of $m_{\nu_\mu}^2 = -0.14(20)$ MeV^2, resulting in an upper limit of $m_{\nu_\mu} < 500$ keV (90% CL).

Electron Neutrino

Tritium beta decay offers an almost ideal means of searching for a neutrino mass. It is a superallowed decay, the endpoint energy is quite low (18.6 keV), and the atomic final-state effects can be well understood. In these experiments, the beta decay spectrum is

measured over a wide region far below the endpoint and then the expected spectral shape in the endpoint region is extrapolated assuming a zero neutrino mass and including all effects (energy loss, spectrometer resolution, decay to different atomic final states, backscattering, background, variation of spectrometer acceptance efficiency with energy) that can distort the spectrum. One then measures the spectrum in the endpoint region and compares it with the extrapolated spectrum. A deviation between the extrapolated and measured spectra can be indicative of a finite neutrino mass.

Originally, a Russian group initially claimed to see evidence for a ν_e mass of 35 eV, which was later reduced to 26 eV.[6] Of particular concern in these measurements was the use of a tritiated amino acid (valine) as the source material that required extensive (and somewhat uncertain) theoretical calculations to take into account the atomic and molecular final-state effects. At present, five other experiments have reported results using much simpler source materials, ranging from pure molecular tritium to tritiated molecular compounds.

The measurement of the Livermore group was reported by Stoeffel*. This experiment uses a gaseous T_2 coupled to a magnetic spectrometer. In comparison to the Los Alamos experiment (which used a similar system), the resolution is improved, the backgrounds are lower, and the system can scan over the entire tritium spectrum. Stoeffel reports a limit of 8 eV (95% CL), but also obtains a best fit value with a negative m_ν^2. It is also interesting that there is a strong surplus of counts at very low energies, below about 1.4 keV. This occurs at about the energy where Simpson saw evidence for a distortion in the T decay spectrum in a solid state detector implanted with T that was interpreted as evidence for a 17-keV neutrino. The Livermore observation may (or may not) be coupled to this. At any rate, this increase was not expected and may be important in trying to resolve the source of the apparent excess of counts near the endpoint.

Bonn* reported on the measurement at Mainz, which uses a frozen T_2 source and an electrostatic spectrometer. This is the first measurement of the tritium beta decay spectrum in which the backgrounds have been sufficiently suppressed in the spectrometer that electrostatic analysis could be used. The spectrometer acceptance is quite high while at the same time the resolution is quite good. The data clearly shows counts due to tritium beta decay to within 20 eV of the endpoint. The quoted limit is $m_{\bar{\nu}_e} < 7.2$ eV (95% CL). There is one systematic effect which is not yet understood, and which appears to be

common to all of the experiments. That is the apparent excess of counts in the region of the endpoint, which results in a best fit value which gives a negative $m\bar{\nu}^2$. In the case of the Mainz experiment, Bonn* reported that this shows up as an apparent 5% branch of some other state at about 75 eV below the endpoint. Further studies of possible sources of this effect are now underway.

Lobashev* reported on the efforts of the group at the Institute for Nuclear Research in Moscow, which will use a gaseous T_2 source coupled to an electrostatic spectrometer. The resolution should be quite good (about 2 eV) with high acceptance from the source. The T_2 source is now being brought into operation, which will then allow one to see if the backgrounds are still acceptably low with T_2 in the source. A goal of this experiment is to be able to measure the beta spectrum below the first excited state in T_2 (at 41 eV) with enough statistics and signal to background that one can search for a non zero neutrino mass without the complications of any excited final states.

As shown in Table 1, all five experiments rule out the ITEP result. However, it must also be noted that all five experiments find a best fit for $m\bar{\nu}_e^2$ which is negative. In fact, the weighted average of the five experiments is $m\bar{\nu}_e^2 = -59 \pm 26\ eV^2$. Physically, this corresponds to an observed excess of events in the endpoint region, rather than a deficit, which would be indicative of a finite neutrino mass. Using the Bayesian method, these combined data results in a limit on $m\bar{\nu}_e$ of 5 eV (95% CL). However, as the result is 2.3-σ negative, this limit must be viewed with some suspicion.

Table 1. Limits on the mass of ν_e.

Group	$m\bar{\nu}_e^2$ (eV^2)	95% CL Limit (eV)
Los Alamos[7]	-147 + 68 + 41	9.3
Zurich[8]	-24 + 48 + 61	11.5
INS Tokyo[9]	-65 + 85 + 65	13
Livermore[10]	75 + 41 + 30	8.0
Mainz[11]	-39 + 34 + 15	7.2

The origin of the negative central value could be due to either 1) a statistical fluke, 2) an undetermined systematic error in the experiments, or 3) difficulties with the theoretical description of the spectrum. The chance that it is a statistical fluctuation is only 1.2%, assuming that $m_{\bar{\nu}_e}$ is actually zero. An independent check for possible systematic problems has been made by comparing the endpoint measurements from the experiments with the known T-^{3}He mass difference. One finds very good agreement at the few eV level, making it less likely (but not ruling out) that the explanation is a systematic error. However, additional studies of possible effects are clearly warranted and are under way.

Finally, there are two possible uncertainties in the theoretical description of the spectrum. The first is that the effect of decays populating different atomic and molecular final states comes entirely from theory. But in the case of tritium, it is believed that these final-state distributions can be calculated with high accuracy, and in fact several different calculations agree quite well. The other possibility is that some new physics is involved; for example, tachyonic neutrinos, capture of relic neutrinos from the Big Bang, the existence of new particles, etc.. Stephenson* presented the idea that new scalar particles may exist which couple only to neutrinos. The existence of these new particles, if the neutrinos and scalar particles have masses less than about 10 eV, would cause the neutrinos to cluster around matter. This clustering would lead to density enhancements sufficiently large to produce appreciable effects on the neutrino spectrum in tritium beta decay and produce the sort of effect of negative $m_{\bar{\nu}}^2$ observed. Remarkably, the existence of such new scalar particles does not seem to be precluded by any other measurements to date. While it may be that this and other ideas may prove to be ruled out by other data, one should not preclude the possibility that the tritium beta decay experiments are sensitive to new physics, and further theoretical work is merited.

Nonetheless, the use of the Bayesian method provides a relatively stable limit for $m_{\bar{\nu}_e}$, and it is unlikely that $m_{\bar{\nu}_e}$ can exceed 10 eV. Such a limit not only rules out the ITEP claim, but also eliminates $\bar{\nu}_e$ (or ν_e) as the dominant component of dark matter.

17-keV NEUTRINOS

The initial claims of evidence for the existence of a 17 keV neutrino with a few per cent branch in tritium beta decay have been followed by a wide range of subsequent experiments. In these experiments, one observes the admixture of a heavy (17-keV)

neutrino with a much lighter (< few eV) neutrino, which results in a kink in the beta spectrum where the beta spectrum with the heavier neutrino kicks in on top of the light neutrino beta spectrum. Physically, in order for this process to occur, not only must the neutrino have a non zero mass, but lepton number must also be violated.

A total of eight experiments claimed to observe evidence for a 17-keV neutrino with a branch of about 0.85%.[12] All of these were remarkably consistent with the best fit to the mass and the branching ratio observed. All were also carried out using solid state detectors. In contrast, more than fourteen experiments (mostly carried out using magnetic spectrometers) claimed not to observe evidence for a 17-keV neutrino with limits on the branching set as low as 0.1% (95% CL).[12]

The most convincing of the experiments observing a 17-keV neutrino are those of Hime and Jelley[13] at Oxford using ^{35}S and ^{63}Ni sources with a solid state detector. An important experiment checking the Oxford results was carried out at Argonne National Laboratory[14] by Freedman* et al using a ^{35}S source placed in the bore of a superconducting magnet. The field profile could be tuned so that as betas spiral along the field lines, their phase space is compressed by the decreasing field so that they strike a solid state detector at the end of the magnet bore at close to normal incidence. Most betas that backscatter from the detector are reflected back by the magnetic pinch effect and are recollected in the detector. This scheme has the advantages of magnetically collimating the betas and of reducing backscattering effects. The results of this measurement observed no evidence for a 17-keV neutrino. This, together with work by Piilonen and Abashian, prompted Hime to reevaluate their data. He carried out careful Monte Carlo calculations of possible scattering effects from intermediate surfaces (such as a thin baffle placed between the source and detector so as to preclude the detector observing betas that might strike the walls of the vacuum chamber). Hime* found that including these intermediate scattering effects could account for the observed distortions in the spectra.[15] This is somewhat surprising, as these effects occur at the one percent level, whereas backscattering and energy-loss effects come in at more than the ten percent level. The backscattering and energy loss effects had been varied in the analysis by a few percent, but they could not account for the observed distortions by any reasonable variation. The problem was that the spectral form of the backscattering and intermediate scattering effects are different, and produce different effects. The new analysis is also in better

agreement with the total response function as determined by conversion line measurements. New data from Oxford, as reported by Jelley*, taken with steps implemented to reduce intermediate scattering effects, show no distortions consistent with a 17-keV neutrino.

Additional experiments have also been recently carried out which also do not see any evidence for a 17-keV neutrino. Holzschuh* reported a limit of < 0.1% (95% CL) for a 17-keV branch using a ^{63}Ni source in the Zurich magnetic spectrometer used to study tritium beta decay. An experiment which uses a setup similar to that used at Argonne was reported by Abele*. In this detector, a thin ^{35}S source is placed at the center of the solenoid with detectors at both ends so that all events into 4π are collected. This makes it possible to further suppress the effects of backscattering by adding the energy deposited in both detectors from a backscattered event. The limit determined was a branching ratio for a 17-keV neutrino < 0.5% (95% CL). Thus, while the ^{14}C measurements of the Berkeley group and the tritium data of Simpson still remain unexplained, it is clear that a 17-keV neutrino does not exist with a branching ratio in the fraction of a percent range.

NEUTRINO CROSS SECTIONS

A stringent test of the Standard Model can be carried out by precision measurements of neutrino-electron elastic scattering which provides allows a precise determination of the Weinberg angle. While a number of measurements have been made at accelerators, only one measurement with limited precision has been carried out at a reactor. Thus, Broggini* discussed plans for a new measurement of ν_e elastic scattering at a reactor using a high pressure gas time projection chamber (TPC). In addition, this experiment is designed to search for a magnetic moment of ne with a sensitivity of 2-3 x 10^{-11} Bohr magnetons, which would represent more than an order of magnitude improvement over the current limits.

Other measurements of interest in testing the Standard Model and the structure of the weak interactions have recently been carried out at the ISIS spallation neutron source at the Rutherford Laboratories. Kleinfeller* reported on results from the KARMEN detector of searches for neutrino oscillations and measurements of charged and neutral current interactions in carbon. The data indicate that flavor universality is conserved within 1-σ with an uncertainty of σ = 20% and in general the charged and neutral current cross

sections on carbon are as expected, except that there appears to be some discrepancy between measurements at ISIS and Los Alamos of the inclusive charged current cross section on carbon.

DOUBLE BETA DECAY

The pairing force in nuclei results in a number of cases in which beta decay from a nucleus with (Z, A) is not energetically allowed to a daughter with (Z-1, A), but double beta ($\beta\beta$) decay from the (Z, A) parent is energetically allowed to a daughter with (Z-2, A). This can proceed by three possible mechanisms: two ν $\beta\beta$ decay, no ν $\beta\beta$ decay, and no ν $\beta\beta$ decay with the emission of a Majoron. The two ν $\beta\beta$ decay is an allowed second-order process requiring no new physics. No ν $\beta\beta$ decay requires that the neutrino have a mass, that lepton number be violated, and that the neutrino is a Majorana neutrino. No ν $\beta\beta$ decay with Majoron emission has, in addition, the requirement that a new particle, the Majoron (a massless Goldstone boson) also exists.

The most stringent limits on the neutrino mass in no ν $\beta\beta$ decay come from the experiments using Ge solid state detectors, which are highly enriched in ^{76}Ge. In this case, the detector is also the sample. The best limit to date comes from a Moscow-Heidelberg collaboration. Piepke* has reported a limit on no ν $\beta\beta$ decay of $< 1.6 \times 10^{24}$ yrs (90% CL). Using calculated nuclear matrix elements, one can then use this result to set a limit on the mass of a Majorana electron neutrino of < 1.2-1.4 eV (90% CL). Larger isotopic ^{76}Ge detectors with lower backgrounds are under construction and one might hope to reach sensitivities of 0.1 eV ultimately.

Similar levels of sensitivity may be reached using other detectors. Busto* reported work on a liquid ^{136}Xe time projection chamber which has provided a limit for no ν $\beta\beta$ of 4.2×10^{23} yrs (90% CL), corresponding to a limit on the Majorana neutrino mass of < 3 eV (68% CL). With anticipated reductions in backgrounds, it seems feasible to reach lifetimes of about 10^{25} yrs.

Some efforts have been made in studies of double positron decay, positron-electron capture decay, and electron capture-electron capture decay as reported by Pomansky*. However, as measurements in ^{85}Kr have only reached lifetimes of $< 2.0 \times 10^{21}$ yrs (68% CL) for double positron decay and lifetimes of 5.8×10^{21} yrs (68% CL) for positron-

electron capture decay, substantial work remains to be done to make these competitive with $\beta\beta$ decay.

Finally, it may be possible to push sensitivities down through the use of other cryogenic detectors. Garan* reported that considerable progress has been made during the last year in understanding the physics of metastable superconducting granulated detectors. These detectors seem to offer the possibility of low background measurements in double beta decay, solar neutrinos, and searches for monopoles and dark matter. It now seems possible to make energy measurements with these devices, rather than acting as integrating detectors above some threshold.

Perhaps the most interesting possibility is that of no ν $\beta\beta$ decay with Majoron emission. Measurements using a Time Projection Chamber with enriched ^{82}Se, ^{100}Mo, and ^{150}Nd samples[16] have observed an excess of events below the endpoint that might be consistent with Majoron emission with a branching ratio of a few x 10^{-4}. This is intriguing, as recent experiments using Ge detectors[17] have also seen an excess at about this level. The Moscow-Heidelberg group also sees an excess in their enriched ^{76}Ge detector. However, Piepke* has reported that after making a (large) background subtraction, the shape of the spectrum is not consistent with Majoron emission with an upper limit of 1.8 x 10^{-4} (90% CL) on the branching ratio. Further work is under way to study the origin of this excess.

NEUTRINO OSCILLATIONS

Theory

If the neutrino has a non zero mass and lepton number is also violated, then the physical neutrinos that we observe (e, μ, and τ) are not mass eigenstates. Instead there exist three mass eigenstates (ν_1, ν_2, and ν_3) with masses m_{ν_1}, m_{ν_2}, and m_{ν_3}. The three physical neutrinos are linear combinations of these mass eigenstates. For simplicity, one can consider the case of only two neutrinos, ν_e and ν_μ. Then, ν_e is predominantly composed of ν_1 with a small admixture (determined by a mixing angle θ between ν_1 and ν_2) of ν_2. It is then possible for ν_e to oscillate into ν_μ as it propagates. The probability for oscillation to occur is:

$$P(\nu_e - \nu_\mu) = \sin^2 2\theta \ \sin^2\{1.27 \times \Delta m^2(eV^2) \times L(m)/E_\nu(MeV)\}$$

where $\Delta m^2 = |m_{\nu_2}{}^2 - m_{\nu_1}{}^2|$.

A variety of searches, both terrestrial and nonterrestrial, has been carried out and no definitive evidence for neutrino oscillations has been found in terrestrial experiments.[18]

Atmospheric Neutrinos

Cosmic rays (primarily protons and gammas) striking the upper atmosphere produce showers of pions and muons that decay, yielding ν_e and ν_μ with typical energies of around 1 GeV. The flux of these neutrinos can be calculated to about 30% accuracy and is sufficiently large that they can be observed in large underground detectors. By measuring the ratio of electron- to muon-neutrinos, one can search for neutrino oscillations in a manner that is relatively free of the individual flux uncertainties, as the ratio can be calculated to about 5% accuracy, as reported by Gaisser*. As the distance traveled by the neutrinos ranges from 10 to 10,000 km, one has sensitivity to small values of Δm^2 that are otherwise inaccessible.

Barloutaud* provided a review of measurements of atmospheric neutrinos have been carried out by a number of large underground detectors: Kamiokande and IMB (which are both large water Cherenkov detectors), Frejus, NUSEX, Baksan, and Soudan II (which are either scintillator based detectors or tracking calorimeters). In their analyses, they compare the observed ratio of ν_μ/ν_e divided by the Monte Carlo (MC) calculated ratio of ν_μ/ν_e. The results, as reported by Kielczewska* for IMB and Kaneyuki* for Kamiokande, are given in Table 2.

Table 2. Atmospheric neutrino data.

Group	ν_μ/ν_e(Data)/ν_μ/ν_e(MC)
Kamiokande[19]	$0.60\ +0.07/-0.06 \pm 0.05$
IMB-3[20]	$0.54 \pm 0.05 \pm 0.12$
	$1.01 \pm 0.03 \pm 0.11$[a]
Frejus[21]	$1.06 \pm 0.18 \pm 0.15$
	$0.87 \pm 0.16 \pm 0.08$[b]
NUSEX[22]	$0.99\ +0.35/-0.25 \pm ?$

[a] Stopping/through muons
[b] Fully contained events

The most sensitive of the detectors, Kamiokande and IMB, observe a significant deficit of the relative number of ν_μ compared to ν_e. The systematic uncertainties are 8% for Kamiokande and 22% for IMB (attributed mostly to uncertainties in the MC simulations). A possible explanation of this deficit may be attributed to neutrino oscillations. If so interpreted, the allowed range for the Kamiokande result is shown in Figure 1. IMB does not make any claim to observe neutrino oscillations, due to their much larger systematic uncertainties.

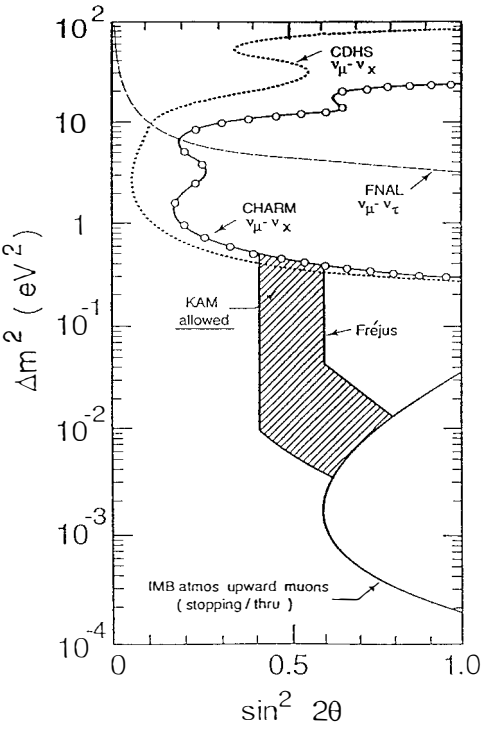

Figure 1. Range of neutrino oscillation parameters for atmospheric neutrinos allowed by the Kamiokande data. Also shown are limits set by atmospheric neutrino data from IMB and Frejus, as well as limits from accelerator searches for neutrino oscillations.

It may well be that the deficit is due to a systematic effect rather than new physics. Two major concerns have been raised. First, it is quite difficult to separate electrons from muons at low energies (a few hundred MeV) based on the differences in the observed rings. IMB and Kamiokande jointly plan to check this by building a 1 kiloton water Cherenkov detector at KEK by using beams of charged particles (π, μ, and e) to check the accuracy of the identification. It is also interesting that recently Soudan II, which is a tracking calorimeter, observed the same deficit, albeit with large statistical uncertainties at present. Second, there is possible concern that the cross sections used in the Monte Carlo calculations may be incorrect. These cross sections are calculated using the Fermi Gas Model (FGM), as the momentum transfer is low at these energies, and nuclear effects are important. But data recently published of measurements made at LAMPF of ν_μ cross sections on ^{12}C are at some variance with the FGM predictions.[23] Preliminary theoretical work apparently does not find any large differences with improved nuclear models.[24] It may be possible to check the cross sections by exposing the KEK test detector to a beam of low-energy neutrinos. This possibility is being investigated, but it will require upgrades of the accelerator and construction of a neutrino beam line, and so is unlikely to happen very soon.

Experiments at Reactors and Accelerators

In order to test the possibility that neutrino oscillations are being observed in measurements of atmospheric neutrinos (and solar neutrinos, as discussed below), a number of experiments have been proposed. Parke* reviewed the numerous possibilities for long baseline experiments that would be sensitive to Δm^2 range of 10^{-3} to 10^{-4} eV^2. All of these experiments would require either an upgrade to an existing accelerator and construction of new neutrino beam lines and/or construction of new large underground detectors. Perhaps the most plausible candidates for a long baseline experiment would involve an upgrade of the KEK accelerator and installation of a new neutrino beamline with the Super Kamiokande detector located 250 km away. Other plausible possibilities would involve Fermilab with an upgraded Soudan detector or CERN with the ICARUS detector. All of these experiments are designed to try to cover the region of allowed parameter space from the results of the atmospheric neutrino experiments. Bilenky* has pointed out the importance of searching for $\nu_\mu \rightarrow \nu_\tau$ oscillations. If one takes indications

from the solar neutrino, atmospheric neutrino, and COBE results, together with the see-saw mechanism (in which neutrino masses are expected to scale as the square of the quark or lepton masses), then one might expect to observe $\nu_\mu \rightarrow \nu_\tau$ oscillations with small, but observable, mixing angles and values of Δm^2 in the few eV^2 range. Thus, the long baseline experiments are well justified by theoretical expectations.

Another class of experiments potentially able to shed some light on the atmospheric neutrino problem involves searching for neutrino oscillations using nuclear reactors as an intense source of antineutrinos. Mascaarenhas* reported on work underway at Cal Tech which would use the San Onofre reactor in California as the source with a 12-ton detector located 1 km away under about 20 meters water equivalent (mwe) of shielding. This experiment would use the $\nu_e + p \rightarrow e^+ + n$ reaction with a four-fold coincidence requirement of the prompt e^+ signal, the two annihilation gammas of the e^+, and the neutron capture gamma ray. Another possible experiment using the CHOOZ reactor in France was described by Kerret*. This experiment could take advantage of a large underground chamber with 300 mwe of shielding which exists at a distance of 1 km from the CHOOZ reactor, which is under construction and scheduled to come on line in 1996. This experiment would employ an 8-ton Gd-loaded scintillator and be sensitive to neutrino oscillations down to a Δm^2 of about 10^{-3} eV^2. Finally discussions are underway to carry out an experiment with a new large scintillation detector to be located in the old IMB proton decay chamber at the Morton Salt Mine in Ohio.[25] This experiment would use the Perry reactor, which is at a distance of 13 km from the IMB site, as the source of antineutrinos. The detector would be a 1-kiloton scintillator detector and would be sensitive to neutrino oscillations down to a Δm^2 of about 10^{-4} eV^2.

Finally, the importance of $\nu_\mu \rightarrow \nu_\tau$ oscillations is being addressed by the NOMAD experiment at CERN, as presented by Levy*. This type of oscillation is favored with a ν_τ mass in the range of 1 eV if the solar neutrino experiments are indicating oscillations of $\nu_e \rightarrow \nu_\mu$ and the seesaw model is correct. The detector, which is a large tracking detector consisting of drift chambers followed by a total radiation detector and muon chambers, coupled with a decay-in-flight neutrino beam will be capable of reaching limiting values of Δm^2 of about 0.4 eV^2 and mixing angles with $\sin^2 2\theta$ of about 4×10^{-4} (90% CL). This more or less encompasses the region of parameter space expected for $\nu_\mu \rightarrow \nu_\tau$ oscillations if the solar neutrino and atmospheric neutrino results are in fact indicative of neutrino

oscillations and if the see saw mechanism is the correct model for determining how the masses of the neutrino generations scale.

SOLAR NEUTRINOS

Perhaps the most outstanding discrepancy between prediction and measurements in current particle physics comes from the solar neutrino problem, in which the radiochemical chlorine experiment of Davis et al. observes a deficit of high-energy neutrinos of a factor of four.[26] This experiment is sensitive primarily to the ^{7}Be and ^{8}B neutrinos produced by fusion reactions in the Sun. A deficit of a factor of two of the ^{8}B neutrinos has been confirmed by the Kamiokande (K III) experiment, as reported by Kaneyuki*. Kamiokande II (III) is an upgraded version of a large real-time water Cherenkov detector that was originally built to search for proton decay. The observed deficits appear to be statistically quite significant with small systematic errors, so that the ratio of the measured rate compared to the Bahcall-Pinsonneault Standard Solar Model (SSM)[27] predictions are: ϕ(Cl)/SSM = 0.23 ± 0.02 ± 0.03 and ϕ(KII)/SSM = 0.49 ± 0.04 ± 0.06. Different SSM give somewhat different predictions. For example, using the Turck-Chieze et al[28] SSM, ϕ(Cl)/SSM = 0.23 ± 0.02 ± 0.03 and ϕ(KII)/SSM = 0.63 ± 0.05 ± 0.08. While the differences are appreciable, they are still insufficient to resolve the problem. However, the predicted fluxes are extremely temperature dependent, as the ^{8}B (^{7}Be) flux scales with the core temperature of the Sun (T_c) as $\phi(^8B) \propto T_c^{18}$ ($\phi(^7Be) \propto T_c^8$). Thus, a 5% decrease in T_c can lower the fluxes to be in agreement with the observations.

Pinsonneault* presented the results of the most recent SSM calculations. These now include the effects of helium diffusion, opacities which are in better agreement with helioseismology data, updated Fe abundances, and better atomic physics calculations. The Bahcall-Pinsonneault results have not changed appreciably from earlier models, while the updated results of the Turck-Chieze et al model is now in closer agreement to the Bahcall-Pinnsoneault. Still, all is not perfect with the models. Pinnsoneault noted that the measured abundances of ^{7}Li and CNO isotopes in the convective zone are in strong disagreement with the SSM predictions. Pinsonneault felt that the likely source of this difference was due to effects of rotation and mixing which are not included in the SSM. Preliminary work to incorporate these effects indicate that it is likely that the prediction of

the abundances will come closer in line with observations while the maximal effect on the ^8B neutrino flux is a decrease of 7%.

Morrison* and Kocharov* discussed many of the possibilities which have been proffered to show that the solar neutrino problem does not exist. Many Nonstandard Solar Models have been invoked to try to lower the core temperature of the Sun, incorporating effects such as turbulent diffusion, massive mass loss, strong magnetic fields, a burnt-out core, etc. However, all of these models have run into problems in trying to reproduce other measured parameters (e.g., the luminosity) of the Sun. Other explanations offered by Morrison included incorrect nuclear cross sections, the need to use selected subsets of data from the solar neutrino experiments which are in better agreement with the SSM predictions, and other possibilities too numerous to list. However, subsequent speakers addressed essentially all of the concerns raised and the general consensus was that the solar neutrino problem is real.

Other explanations to resolve the solar neutrino problem involving new physics (such as Weakly Interacting Massive Particles (WIMPs), neutrino magnetic moments, neutrino decay, neutrinos oscillations, etc. have also been proffered. Petcov* reviewed the status of theoretical work on MSW oscillations[29], vacuum oscillations[30], and solutions involving magnetic moments of the neutrino[31]. Akhmedov* demonstrated the possibility of $\nu \rightarrow \bar{\nu}$ oscillations via natural mechanisms which exist within the Sun involving a handedness to the magnetic fields due to the rotation of the Sun. Nunokawa* discussed neutrino spin precession with flavor mixing as a possible solution to the solar neutrino problem and concluded that this mechanism cannot yet be ruled out. Pal* discussed neutrino interactions in matter which might ultimately be of interest in solar neutrino studies, although the effects are quite small compared to current sensitivities. Finally, Halprin* discussed the possibility that neutrino oscillations could occur even in the case of massless neutrinos through a flavor changing gravitational interaction and used the current results of the solar neutrino experiments to rule out part of the parameter space for this type of interaction.

Most of the explanations involving new physics have been ruled out or disfavored by either laboratory or astrophysical measurements. While vacuum oscillation and magnetic moment solutions are still possible, it appears that perhaps the most likely particle physics solution is that of matter enhanced neutrino oscillations, the Mikheyev-Smirnov-

Wolfenstein (MSW) oscillations. In order to try to resolve the source of the deficit, two radiochemical gallium experiments, SAGE (Soviet-American Gallium Experiment) and GALLEX (GALLium EXperiment) were mounted. The threshold of the gallium experiments is sufficiently low that it is sensitive to the dominant flux of low-energy p-p neutrinos, which are produced in the primary energy producing reaction of the Sun, the fusion of two protons. The flux of the p-p neutrinos is determined to about 2% accuracy in a relatively model independent manner and is directly coupled to the measured solar luminosity. The gallium experiments have now announced their first results, and also find a significant deficit. Bowles* reported that SAGE finds the deficit (compared to the Bahcall-Pinsonneault SSM) to be ϕ(SAGE)/SSM = 0.44 +0.13/-0.18 ± 0.11 while Stolarczyk* reported that GALLEX observes ϕ(GALLEX)/SSM = 0.62 ± 0.13 ± 0.06. Spiro* showed analyses demonstrating that the runs in the three radiochemical experiments are all distributed statistically, as expected. Thus, as the results of these two experiments appear to be Poisson distributed and are dominated by statistical uncertainties, Spiro* felt it seems reasonable to take a weighted average to obtain ϕ(Ga)/SSM = 0.55 ± 0.11 as the result of the combined gallium experiments. If one assumes only that fusion reactions power the Sun and that the Sun is in thermal equilibrium, one expects a minimal rate in the Ga experiments of 0.60 SSM. A rate significantly lower than this would require one to invoke new physics, rather than a change in the astrophysical models of the Sun, as the solution to the solar neutrino problem. Thus, while the Ga experiments seem to favor a particle physics solution, they are not yet precise enough to definitely rule out an astrophysics solution. In addition, it will be important to check the quoted efficiencies of the gallium experiments using an artificial neutrino source. Both SAGE and GALLEX are planning to do this with intense ^{51}Cr sources. However, using the results of the four experiments, a recent analysis[32] indicates that any model invoking a cooler Sun is ruled out at the 99.99% CL. All four experiments are consistent with the hypothesis of MSW oscillations, and the regions in the parameter space of Δm^2 versus $\sin^2 2\theta$ are shown[32] in Figure 2. There are two allowed solutions, the one with $\sin^2 2\theta \approx 10^{-2}$ is called the nonadiabatic solution, while the one with $\sin^2 2\theta \approx 0.6$ is called the large mixing angle solution. These solutions differ in their prediction of the energy dependence of the effect of oscillations on the solar neutrino spectrum.[32] The nonadiabatic solution gives strong suppression of the ^{7}Be and

^{8}B neutrinos but leaves the p-p neutrinos essentially unaffected. The large mixing angle solution provides for a roughly equal suppression of neutrinos at all energies.

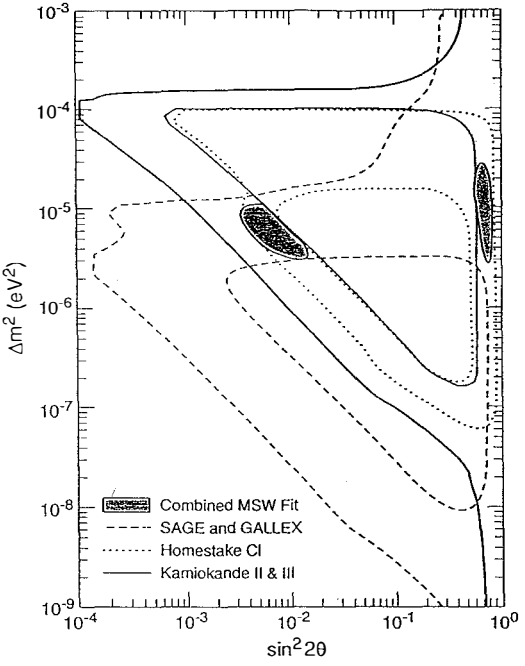

Figure 2. Allowed region of neutrino oscillation parameters for solar neutrinos. The limits set by the chlorine, Kamiokande, and combined gallium experiments are as indicated by the inset legend.

In order to determine the origin of the solar neutrino problem, it now appears that model-independent tests must be made. This could done by either directly measuring the solar neutrino spectrum and looking for the distortions predicted by the MSW oscillations, or to measure the flux of ν_e and compare it to measurements of the total flux of $\nu_e + \nu_\mu + \nu_\tau$. Four experiments to do this are either under way or working on prototype development. The Sudbury Neutrino Observatory (SNO) experiment, as reported by B. Robertson*, is a large water Cherenkov detector using 1 kiloton of heavy water (D_2O). In this experiment, one will be able to directly measure the ^{8}B neutrino spectrum by observing the energetic electron emitted in the charged current (CC) reaction $\nu_e + d \rightarrow p +$

$p + e^-$. In addition, one can measure the total flux of all neutrinos above a 2.2-MeV threshold by observing the neutron created in the neutral current (NC) reaction $\nu_e + d \rightarrow p + n$. While the canonical plan to detect neutrons in SNO is by adding 2.5 tons of NaCl and observing the gamma from neutron capture on the Cl, work is underway to develop ultra low background ^3He proportional counters to provide neutron detection, as reported by H. Robertson*. Finally, in SNO one can also observe the elastic scattering (ES) reaction $\nu_e + e^- \rightarrow \nu_e' + e^{-\prime}$. In the Super-Kamiokande project, as reported by Kaneyuki*, a 50-kiloton water Cherenkov detector will be built to study the elastic scattering (ES) reaction. This experiment will give rates almost 100 times higher than Kamiokande and will be able to measure the ^8B neutrino energy spectrum from the recoil electron spectrum. The SNO and Super-Kamiokande projects expect to come on the air in the fall of 1995 and spring of 1996, respectively. In another detector under development, the Borexino project[33] would use 300 tons of scintillator viewed by an array of photomultipliers to directly observe the ^7Be neutrinos via the ES reaction. This experiment is under development and hopes to come on line about 1996. Finally, a 3-ton prototype of a liquid argon time projection chamber has demonstrated the feasibility of full track reconstruction over drift distances of a few meters, as reported by Montanari*. Thus, this detector looks quite a lot like an electronic bubble chamber in its ability to reconstruct tracks and identify particles. Plans are now under way to use this technique in a 5-kiloton ICARUS detector, which would detect ^8B solar neutrinos primarily by the ES reaction. These experiments will provide real-time information with better resolutions, lower backgrounds, and count rates almost 100 times higher than previous solar neutrino experiments. One thus expects that they should be able to determine the origin of the solar neutrino problem in a model-independent manner before the end of this decade.

One detection scheme for solar neutrinos, proposed by Weber, that involves use of coherent scattering from sapphire crystals to detect solar neutrinos, seems not to be feasible. Measurements by McHugh* of the scattering of solar neutrinos from sapphire crystals mounted on a water balance indicate an absence of coherent effects, with a limit of about 2% (68% CL) of that expected. It appears the cross sections are incoherent for scattering from crystals, which results in cross sections reduced by many orders of magnitude from that for coherent scattering, thus rendering a solar neutrino experiment impossible.

SUPERNOVA NEUTRINOS AND DARK MATTER

The dark matter problem, in which more than 90% of the Universe is comprised of some unknown (nonbaryonic) form of matter was reviewed by Caldwell* with some additional discussion by Krauss*. The need for dark matter now seems to be well established and ir.tensive experimental efforts are underway to determine the origin of the dark matter. Searches for MAssive Compact Halo Objects (MACHOs) are underway by three groups using the gravitational microlensing technique. Initial tests indicate they have sufficient sensitivity to observe objects with masses greater than 10^{-7} solar masses in the halo of our galaxy. One year of observations are now being analyzed and within the next year or so we should know if MACHOs are a dominant form of dark matter. The recent observations of COBE (COsmic Background Explorer) and IRAS (InfraRed Astronomical Satellite) seem to indicate the need for about 20-40% of hot dark matter mixed in with cold dark matter in order to reproduce the observed large scale structure of the Universe. A prime candidate for the hot dark matter is a tau neutrino with a mass of about 7 eV. Axions are also still a dark matter candidate and efforts are under way to build a large cryogenic cavity inside a superconducting magnet which would allow detection of axions by their coupling to the magnetic field. Weakly Interacting Massive Particles (WIMPs) have been largely ruled out as dark matter candidates by experiments using ultra low background solid state detectors in which a WIMP would be detected by observation of the recoil nucleus when the WIMPs scatter in the detector. Finally a number of efforts are under way using cryogenic detectors which have the potential of being able to observe the nuclear recoils from neutralinos (the lightest stable SUperSYmmetric particle) scattering in the detectors. Thus, it is hoped that the origin of dark matter may be determined within the next decade.

If the tau neutrino has a mass in the few eV range, as possibly indicated by COBE and IRAS, it is of crucial importance to find a means to measure such a mass. Neutrino oscillations, such as the NOMAD experiment, provide one means to probe this mass range. However, a more direct means is by studies of the neutrinos emitted in supernova explosions, as discussed by Krauss*. A great deal of detailed modeling of supernovas has now been carried out and the question of the effect of a non zero neutrino mass has been looked into. If a supernova goes off in our galaxy during the operating lifetime of SNO and Super Kamiokande (and any other large detectors which are operational), the count

rates that one expects to see are of order 10^3 events in SNO and 10^4 events in Super Kamiokande. With such high statistics, the detailed evolution of the neutrino pulse can be studied. It appears that both model-dependent and model-independent effects of a non zero neutrino mass should be observable for masses of tens of eV. Studies also indicate, although with less reliability, that it may be possible to determine neutrino masses as low as a few eV. Thus, there is some hope that a nearby supernova may provide the best information on a possible tau neutrino mass in the few eV to few tens of eV range.

CONCLUSIONS

At present, laboratory measurements are all consistent with the hypothesis that neutrinos are massless. In particular, there is not a 17 keV neutrino. Nonetheless, extensions beyond the Standard Model generically predict non zero neutrino masses. There are possible indications of new physics in no n bb decay with emission of a Majoron with a branching ratio of around 10^{-4}. However, while an unexplained excess of events below the endpoint is observed in all of the experiments, the data are probably inconsistent with Majoron emission. There appear to be systematic effects in the tritium beta decay experiments which are not completely understood. The consistent observation of a best fit of negative m_ν^2 could possibly indicate the presence of new physics, but a great deal of work remains to be done before one can seriously consider new physics as the solution to this problem. Possible evidence for neutrino oscillations is observed in atmospheric neutrinos and solar neutrinos. In the case of atmospheric neutrinos, only one experiment has the sensitivity to claim consistency with neutrino oscillations. A number of possible systematic effects may also account for the observations, and further studies are under way. In the case of solar neutrinos, four experiments all see significant deficits below the rates predicted. Various analyses indicate it is unlikely that changes to the Standard Solar Models can accommodate the results. The most likely consistent explanation is that we are observing matter-enhanced MSW neutrino oscillations. Yet, given the extreme dependence of the neutrino fluxes on the core temperature of the Sun, it is difficult to definitively rule out astrophysical solutions. But a new round of experiments will provide model-independent tests, which should provide the solution to the solar neutrino problem in the next five to seven years. Finally, measurements of the 3 K microwave background radiation seem to favor that some fraction of the dark matter may

be comprised of a (tau) neutrino with a mass of several eV. If the large solar neutrino detectors now under construction should be lucky enough to observe a supernova within our galaxy during their lifetimes, it may be possible to address the question of a tau neutrino mass of several eV.

It is clear that the new round of experiments under construction and being discussed will greatly impact our understanding of neutrino mass and mixing. If we are fortunate, the early indications we are seeing with the present round of experiments will be borne out with new data by the end of this decade. It may well be that these experiments are providing us with the first window to the long-sought new physics beyond the Standard Model.

REFERENCES

Numerous references giving the name of a researcher in this text refer to presentations made at this Moriond conference by the person listed. Further information about each of the named references may be found in articles by the presenter listed in these proceedings.

1. Albrecht A., to be published in Proc. 26th Intl. Conf. on High Energy Physics, Dallas, TX (1992).
2. Abela, R. et al. 1984. Phys. Lett. **B146**: 431 (1984).
3. Particle Data Group, Phys. Lett. **B170**: 1 (1986).
4. Frosch, R. (private communication.) (1992).
5. Anderhub, H.B. et al, Phys. Lett. **B114**: 76. (1982).
6. Boris, S. et al, JETP Lett. **45**: 333 (1987).
7. Robertson, R.G.H. et al, Phys. Rev. Lett. **67**: 957 (1991).
8. Holzschuh, E. Proc. XV Intl. Conf. on Neutrino Physics and Astrophysics, Granada, Spain, June 6-12, Nucl. Phys. B (Proc. Suppl.) **31**: 42 (1993).
9. Kawakami H. et al, Phys. Lett. **B256**: 105 (1991).
10. Stoeffel, W. and Decman, D., Many Aspects of Neutrino Physics, Fermilab Workshop, Batavia, IL, Nov. 14-17 (unpublished) (1991).
11. Backe, H. et al, Proc. XV Intl. Conf. on Neutrino Physics and Astrophysics, Granada, Spain, June 6-12, Nucl. Phys. B (Proc. Suppl.) **31**: 46 (1993).
12. Hime A., Mod. Phys. Lett. A7: 1301 (1992).
13. Hime, A. et al, Phys. Lett. **B260**: 441 (1991); Hime, A. and Jelley, N., Oxford Univ. Preprint OUNP-91-21 (to be published) (1991).
14. Mortara, J.L. et al, Phys. Rev. Lett. **70**: 394 (1993).
15. Hime, A., Phys. Lett **B299**: 165 (1993).
16. Elliott, S.R. et al, Proc. XV Intl. Conf. on Neutrino Physics and Astrophysics, Granada, Spain, Nucl. Phys. B (Proc. Suppl.) **31**: 68 (1993).
17. Avignone, F.T. III, et al, Phys. Lett. **B256**: 559 (1991).
18. Schneps, J., Proc. XV Intl. Conf. on Neutrino Physics and Astrophysics, Granada, Spain, Nucl. Phys. B (Proc. Suppl.) **31**: 307 (1993).
19. Hirata, K.S., et al, to be published in Proc. 26th Intl. Conf. on High Energy Physics, Dallas, TX (1992).
20. IMB Collaboration, Phys. Rev. Lett. **66**: 2561 (1991); Phys. Rev. Lett. **69**: 1010 (1992).

21. **Frejus** Collaboration, Phys. Lett. B**245**: 305 (1991).
22. NUSEX Collaboration, Europhys. Lett. 8: 611 (1989).
23. Koetke, D.D. et al, Phys. Rev. C**46**: 2554 (1992).
24. Vogel, P., to be published in the Proceedings of the 5th International Workshop on Neutrino Telescopes, ed. Baldo-Ceolin, M., Venice (1993).
25. Steinberg, R.I., (private communication)
26. Cleveland, B.T. et al, to be published in Proceedings of the Franklin Symposium in Celebration of the Discovery of the Neutrino, ed. Steinberg, R.I., Franklin Institute Press, Philadelphia (1993).
27. Bahcall, J.N., Pinsonneault, M.H., Rev. Mod. Phys. **64**: 885 (1992).
28. Turck-Chieze, S., Lopes I., to appear in May, 1993 Astroph. J. (1993).
29. Krastev, P.I., Petcov, S.T., Phys. Lett. B**299**: 99 (1993); Krauss, L.M., Gates, E., White, M., Phys. Lett. **B299**: 94 (1993); White, M., Krauss, L., Gates, E., Phys. Rev. Lett. **70**: 375 (1993).
30. Krastev, P.I., Petcov, S.T., Phys. Lett. **B285**: 85 (1992).
31. Okun, L.B., Voloshin, M.B., Vysotskii, M.I., Yad Fiz. **44**: 677 (1986); Lim, C.-S., Marciano, W., Phys. Rev. D**37**: 1368 (1988); Akhmedov, E.Kh., Phys. Lett. **B213**: 64 (1988).
32. Bludman, S.A., Hata, N., Kennedy, D.C., Langacker, P.G., Phys. Rev. D**47**: 2220 (1993).
33. Raghavan, R.S., Proc. 25th Intl. Conf. High Energy Phys., ed Phua, K.K., Yamaguchi, Y., World Scientific, Singapore: 482 (1991).

GRAVITY WITH LEVITY

E.G. Adelberger
Physics Department, FM-15
University of Washington, Seattle, WA 98195

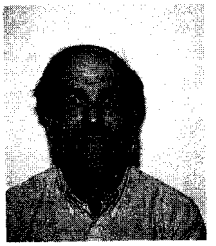

ABSTRACT

The gravitation sessions of this workshop are briefly summarized and a personal overview of the field is presented.

I was asked to give this summary talk only after I got to the workshop, and then discovered that the last of the sessions I was supposed to cover ended only a few hours before I had to give my talk. So perhaps you will forgive me for not being able to prepare a beautiful and comprehensive summary talk such as the one we just heard from Tom Bowles, and for delivering instead a light-hearted overview.

For many years gravitational physics was essentially uncoupled from the rest of physics. The theory, general relativity, seemed completely unrelated to the quantum field theories that formed the basis of particle physics; the experimental techniques, which involved the study of macroscopic classical objects, had little in common with those used in most other areas of physics; and gravitational effects are so weak that they could be ignored in the microscopic arena that occupied the attention of the 'mainstream' physicists. Much of this has changed in recent years, particularly in theory, where attempts to unite particle physics and gravity (for example via super-strings) are now well known. But one of the most interesting things about this workshop was learning other ways in which gravitation has worked its way into the rest of physics. But let us start with the main dish and then go on to the dessert.

The classic torsion-balance technique continues to produce new and interesting tests of the universality of free fall (UFF). The new aspects come largely from a different way of looking at the UFF. Instead of the traditional check of the gravitational weak equivalence principle which was cast in terms of the parameter

$$\eta(A,B) = 0.5[(m_i/m_g)_A - (m_i/m_g)_B]/[(m_i/m_g)_A + (m_i/m_g)_B],$$

we now think in terms of searching for new non-gravitational Yukawa interactions that may lie hidden 'under' gravity. The relevant parameters are the coupling constants, ranges, charges, and possible spin-dependence of the hypothesised interactions. This naturally opens up new areas for investigation: instead of assuming that any violation of the UFF has an infinite range as does gravity, we now must consider all ranges, from the Planck length (1.6×10^{-35} m) up to infinity! From this point of view, there are two enormous gaps in our experimental results: one between the ranges that have been probed with mechanical experiments ($\sim$1 mm$\geq \lambda \geq \infty$) and the very small distances probed by particle experiments, and a second between the length scales probed by existing accelerators and the Planck length. I find it interesting that there may be a special interest in a length scale intermediate between infinity and the Planck length that is quite accessible to torsion-balance techniques. This scale ($\lambda \approx 0.3$ m) is associated with a mass $m = M_Z^2/M_P$, where M_Z and M_P are the Z^0 and Planck masses respectively, and m is a 'see-saw' mass acquired by some hypothetical, originally massless, scalar boson[1].

This new way of looking at UFF tests has stimulated the development of a generation of instruments designed to be sensitive over a wide range of length scales[2]. At this conference we heard new results from the Eöt-Wash group testing the UFF on the galactic length scale to probe the dark matter at the center of our galaxy, and for ranges down to 1 cm to probe length scales characterized by exchange-boson masses up to 10^{-5} eV. The Virginia group reported sensitive new tests for spin-dependent forces using electron-polarized test bodies and sources. Previous results, notably from the Irvine group, probed spin-independent interactions with ranges down to a fraction of a mm. But we have essentially no sensitive results for length scales much shorter than 1 mm. This seems to be an area where the techniques of atomic physics (laser-cooled atoms and atomic fountains) and materials science (atomic force microscopy and various nanotechnologies) could be fruitfully applied.

We heard interesting talks and a round-table discussion about STEP, a proposed high-quality drag-free satellite for testing the equivalence principle with a designed sensitivity of 1 part in 10^{17}. This represents a remarkable factor of 10^5 improvement over the most precise result quoted for a laboratory experiment[3]! It is clear that a satellite offers substantial advantages (a

≈600 times larger signal and probably a more benign environment compared to ground-based experiments) and some significant disadvantages (you have one shot at the experiment and cannot change things on the basis of experience). To attain this fantastic level of precision one will have to anticipate all the subtle systematic errors that one normally discovers by incremental development of an apparatus. It is good to see that these problems are being tackled by a large and diverse group, and I wish them the best of luck. I should point out that a successful result from STEP will not eliminate the role of laboratory UFF experiments. This has to do with the question of the range of the UFF-violating interaction. Although the satellite sees a factor of ≈600 larger signal for an interaction with $\lambda >> r_{earth}$, the situation is reversed for shorter ranges where a laboratory experiment can have a signal that is enormously larger than that from a satellite orbiting ~500 km above the earth.

We heard relatively little at this workshop about gravity-wave observatories. These new interferometric instruments, now being actively developed in the US and in Europe, are designed not to study gravity itself (the existence of gravity waves has been very convincingly demonstrated in precise studies of the binary pulsar by Taylor's group at Princeton) but to study astrophysics (the properties of neutron stars revealed by the gravitational radiation emitted in the final stages of an in-spiraling binary system, *etc.*) This is a very high-tech area where much work is still needed before we can expect to detect events. The Italian VIRGO project reported impressive developments in vibration isolation, one of the key factors that limit the detector performance. Hopefully, we will hear more on technical progress in gravity-wave detectors in next year's Moriond Workshop.

Finally, it was nice to see McHugh's results that convincingly disproved Weber's claim of enormously enhanced coherent ν scattering cross-sections from crystals such as sapphire. While very few people accepted Weber's theoretical arguments or his data, it is nevertheless good to have a careful experimental test of his claim. The 17 keV neutrino was not the only anomaly whose funeral was announced at this workshop.

So far I have discussed only experiments, and not done justice to theory. That is because I am not really competent to do so. But, speaking as an experimentalist, I was very interested to hear Damour's talk on general relativity as a cosmological attractor of scalar-tensor theories. After hearing so many theorists explaining why we shouldn't see any violations of the UFF, it was refreshing to hear a scenario in which an effect could be lurking within the reach of future experiments. I have long enjoyed DeRujula's wonderful analogy between physicists and farmers. The theorist is like a farmer who takes his pig, the experimentalist (you can already tell that this joke was invented by a theorist), to a field to dig for truffles. The grateful pig of course loves truffles and digs industriously through the dirt. But if he finds a truffle, the farmer immediately takes it away. However, there is one problem with this analogy; the farmer only leads his pig to fields that are known to contain truffles. Now it may be asking too much of our 'farmer' colleagues to lead us 'pigs' to fields that are known to contain truffles, but it is good for our morale when the farmer can at least conceive of a way in which the field *may* contain truffles!

As I said at the beginning, gravity is creeping into all fields of physics. This workshop covered particle physics (ν's), atomic physics and gravitational physics. It was exciting to hear about the lovely laser cooling and interrogation techniques that have advanced to the point where gravity can be studied using atoms in free fall. The rapid developments in the techniques of atom-interferometry may also have spin-offs for experimental gravity–could one use an atomic Sagnac interferometer to test the Lense-Thirring precession? In fact, even particle physics experiments are now able to detect gravity! I assume many of you have seen the plot of the diurnal variations in the energy of the LEP ring shown in Figure 1. The energy variation is caused by the solid-earth tides (primarily from the moon) distorting the ring's shape. But

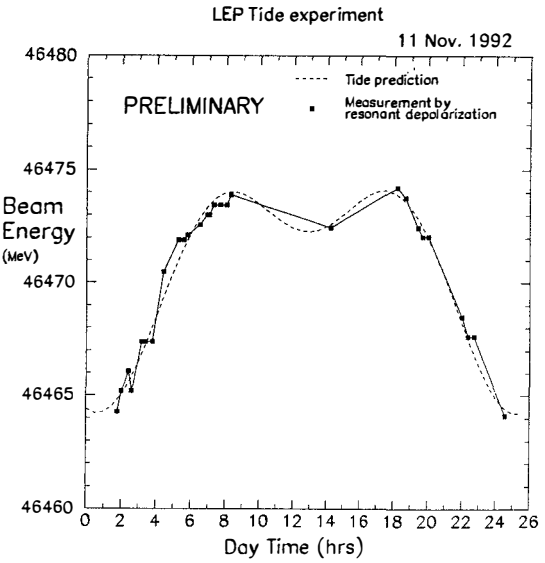

Figure 1: Variation of the energy of the LEP ring at CERN due to tidal effects. Because the RF frequency is constant, the energy reflects the circumference of the ring. Note the predominant 24 h period of the tidal effect.

how many of you stopped to ask why the effect appears to have a dominant 24 h period, when everyone knows that the tides have a 12 h period? This puzzled me when first saw the data, but I think I now understand it. If the moon were directly above or below the ring, tidal effects would symmetrically shrink the ring radius so that the circumference (which dictates the beam energy because because the RF frequency is constant) is *decreased* by a factor proportional to a/r where a is the ring radius and r the distance to the moon. On the other hand when the moon in in the plane of the ring it distorts the circular ring into an ellipse so that its circumference is *increased* by a factor proportional to $a/2r$. Now if the earth's rotation axis were perpendicular to plane of the moon's orbit this would lead to a tidal circumference variation with a 12 h period. But because the earth's rotation axis is inclined and LEP is neither on the equator nor on the pole, one gets a 24 h period as well. This is an amusing problem for you to work out and then assign to your students.

I would like to close by thanking Thibault Damour for organizing such a balanced, wide-ranging, and interesting session, and the speakers for giving such lively and stimulating presentations. This Moriond Workshop amply demonstrated that, in spite of the title of this little talk, gravity should not be taken lightly.

References

[1] I am endebted to Christoff Wetterich for this observation.

[2] E.G. Adelberger, C.W. Stubbs, B.R. Heckel and W.F. Rogers, Ann. Rev. Nucl. Part. Sci. **41**, 269 (1991).

[3] V.B. Braginsky and V.I. Panov, Zh. Eksp. Teor. Fiz. **61**, 873 (1971) [Sov. Phys. JETP **34**, 463 (1972)].

ERRATUM

Erratum

DARK MATTER AND THE POSSIBLE EXPANSION OF SPIRAL GALAXIES

D. F. Bartlett and Tyler Pike*, Department of Physics,
University of Colorado, Boulder, CO 80309-0390

We would like to correct a significant error in our earlier report to the Moriond conference of January, 1990.[1] At that time we showed that Warmel's study of the Doppler shifts of the 21-cm line in hydrogen[2] could be interpreted as indicating substantial expanding (or contracting) motions in several galaxies within the Virgo cluster. If true, these motions might help provide an alternative for dark matter as the cause for the flat rotation curves of spiral galaxies.

We now believe that the evidence was faulty, caused by our lack of appreciation for "beam smearing". The Westerbork Synthesis Radio Telescope used for these observations is aligned along an E-W axis. The resulting poor resolution in the N-S direction causes highly elliptical resolution ellipses in Warmel's contour plots for the velocity of a galaxy's hydrogen towards the earth. The effect is to pull contours of equal velocity in the N-S direction leading us to to confuse galactic rotation with expansion. In particular, the very significant radial motion we originally reported in the contour plots for NGC 4222 and NGC 4294 can be ascribed to beam smearing.

The former galaxy has now been observed by Cayatte et al[3] as part of a study using the tri-axial Very Large Array which leads naturally to analyses with little beam smearing. It is interesting that Cayatte's equivelocity contours for this galaxy show no evidence for radial motions.

1. D. F. Bartlett and Tyler Pike in **Proc. of 25th Rencontre de Moriond** pp. 433-438, O. Fackler and J. Tran Thanh Van, eds. (Editions Frontièrs, 1990).

2. R.H. Warmels, "The HI Properties of Spiral Galaxies in the Virgo Cluster, 1. Westerbork Observations of 15 Virgo Cluster Galaxies," Astron. Astrophys. Suppl. **72**, 19-56 (1988).

3. V. Cayatte, J. H. van Gorkom, C. Balkowski, and C. Kotanyi, "VLA Observations of Neutral Hydrogen in Virgo Cluster Galaxies, I. The Atlas", Astronomical Jrnl. **100**, 604-634 (1990).

*Now at University of California, Berkeley.

List of Participants

ADELBERGER Eric
C E R N
PPE Div.
1211 Geneve 23
Switzerland

AKHMEDOV Eugeni
Kurchatov Inst.
of Atomic Institute
Moscow 123182
Russia

AMSLER Claude
Physik Institut der Univ. Zurich
Schberggasse 9
CH-8001 Zurich
Suisse

ASPECT Alain
Inst. d'Optique
Centre Universitaire d'Orsay,B.P. 147
91403 Orsay Cedex
France

BANNER Marcel
C E N Saclay
DAPNIA
91191 Gif sur Yvette Cedex
France

BARDON Marcel
National Science Foundation
Room V-501
Washington D.C. 20550
USA

BARLOUTAUD Roland
C E N Saclay
DAPNIA
91191 Gif sur Yvette Cedex
France

BEILBY Mark
Univ. of California at Irvine
Department of Physics
Irvine CA 92717
USA

BEL Nicole
Observatoire de Meudon
5, Place Janssen
92195 Meudon
France

BILENKY Samoil
Univ. di Torino, Dept di Fisica Teorica
Via Pietro Giuria
10125 Torino
Italy

BLANCHET Luc
Observatoire de Meudon
5, Place Janssen
92195 Meudon Cedex
France

BLASER Jean-Pierre
Paul Scherrer Institut
Dept di Fisica Teorica
CH-5232 Villigen PSI
Switzerland

BOSHIER Malcolm
Yale University, Physics Dept.
P.O.Box 6666
New Haven CT 06511
USA

BOWLES Thomas
Los Alamos Nat. Lab.
MS D449
Los Alamos NM 87545
USA

BROGGINI Carlo
INFN
Laboratorio Nazionale Del Gran Sasso
67010 Assergi AQ
Italy

BUSTO José
Université de Neuchatel
rue Breguet
CH2000 Neuchatel
Switzerland

CALDWELL David
Universita of California
Department of Physics
Santa Barbara CA 93106
USA

CASTIN Yvan
Depart. de Physique de l'E.N.S.
24, rue Lhomond
75231 Paris
France

CELNIKIER Ludwig
Observatoire de Meudon
5, Place Janssen
92195 Meudon
France

CHARDIN Gabriel
C E N Saclay
DAPNIA
91191 Gif sur Yvette Cedex
France

CHU Steven
Stanford Univ.
Physis Dept
Stanford CA 94305
USA

COHEN-TANNOUDJI Claude
Collège de France
24, rue Lhomond
75231 Paris
France

CONTI Enrico
INFN, Universita di Padova,
Via Marsolo 8
35131 Padova
Italy

COWSIK Ramanath
Indian Inst. of Astrophysics
Sarjapur Rd, Koramangla
Bangalore 560034
India

DAMOUR Thibault
I. H. E. S
35, route de Chartres
91440 Bures sur Yvette
France

de KERRET Hervé
Collège de France
11, Pl. M. Berthelot
75231 Gif sur Yvette
France

DE RUJULA Alvaro
C E R N
Theory Div.
1211 Geneve 23
Switzerland

DEWEY Scott
N I S T
Building 235, Room E19
Gaithersburg 20899
USA

ECKHARDT Donald
PL/GPE
Hanscom AFB Ma 01731
USA

ESPOSITO FARESE Gilles
CNRS Marseille
Case 907
13288 Marseille Cedex 09
France

EVERITT C.W. Francis
WW-Hansen Experimental Physics
Laboratory
Stanford CA
USA

FABRE Claude
Univ. P. et M. Curie
Case 74, 4 Pl. Jussieu
75252 Paris Cedex 05
France

FACKLER Orrin
Lawrence Livermore Laboratory
P.O.Box 808, L-403
Livermore CA 94550
USA

FALLER Jim
University of Colorado
J I L A, Box 440
Boulder CO 80309
USA

FISCHBACH Ephraim
Purdue University
Physics Dept
W. Lafayette IN 47907
USA

FONTAINE Gérard
I N2 P3
20, rue Berbier du Mets
75013 Paris
France

FREDKIN Edward
Boston University
Department of Physics
Boston MA 02215
USA

FREEDMAN Stuart
Univ. of California at Berkely
Department of Physics
Berkeley CA 94720
USA

GAISSER Thomas
Bartol Research Institute
University of Delaware
Newark DE 19716
USA

GARRETA Denis
CEN Saclay
CERN
1211 Geneve 23
Switzerland

GIACOBINO Elisabeth
Univ. P. et M. Curie
Case 74, 4 Pl. Jussieu
75252 Paris
France

GIRARD Ta
Centro de Fisica Nuclear
av. Gama Pinto 2
1699 Lisboa
Portugal

GOUANERE Michel
L A P P
B.P. 110
Annecy Le Vieux 74941 Cedex
France

GREENE Geoffrey
N I S T
Bld 235 RmE126
Gaithersburg MD 20899
USA

GRIMUS Walter
Univ. of Vienna, Theoretical Physics,
Boltzmanngasse 5
1090 Vienna
Austria

GRUWE Magali
U L B - V U B
CO 230, Boulevard du Triomphe
B-1050 Bruxelles
Belgium

GUNDLACH Jens
University of Washington
NPL GL-10
Seattle Wa. 98195
USA

HALL Andrew
Physics Department,
Virginia Commonwealth University,
Box 2000, Richmond Va 23284
USA

HALPRIN Arthur
University of Delaware
Dept of Physics & Astronomy
Newark DE 19716
USA

HEINZEN Daniel J.
University of Texas
Dept; of Physics
Austin TX 78731
USA

HELLO Patrice
Université de Paris Sud
L A L, Groupe Virgo - Bât 208
91405 Orsay Cedex
France

HIME Andrew
Los Alamos Nat. Lab.
MS D449
Los Alamos NM 87545
USA

HOLZSCHUH Eugen
Inst. der Universität Zürich
Schönberggasse 9
8001 Zürich
Switzerland

JAFRY Yusuf
ESA/ESTEC
Space Science Department, Postbus 299
2000 AG Noordwijk zh
Netherl.

JELLEY Nick
Nuclear Physics Laboratory
Kebble Roadd
Oxford OX1 6RX
United Kingdom

JOSHI Pankaj
Tata Institute of Fundamental Research
Homi Bhabha Rd, Colaba
Bombay 5
India

KANEYUKI Kenji
Tokyo Institute of Technology
2-12-1 Oh-Okayama Meguro-ku
Tokyo 152
Japan

KIELCZEWSKA Danuta
Institute of Experimental Physics
Hoza 69
00-681 Warsaw
Poland

KIMBLE H. Jeff
Bridge Laboratory of Physics,
California Inst. of Technology,
MC-12-33, Pasadena CA 91125
USA

KLAGES Hans
Kemforschungszentrum
Karlsruhe, Postfach 3640
D-7500 Karlsruhe 1
Germany

KLEINFELLER Jonny
Rutherford Appleton Laboratory
Particle Physics Department, Chilton
Didcot OX11 0QX
United Kingdom

KLOOR Harry
Purdue University
Physics Department
West Lafayette IN 47907
USA

KNAPP David
Lawrence Livermore Nat. Lab.
L-421
Livermore CA 94550
USA

KOCH-MIRAMOND Lydie
C E N Saclay
Optics Section
91191 Gif sur Yvette Cedex
France

KOCHAROV Grant
A.F. IOFFE Physical Institute
26, Polytekhnicheskaya
St Petersburg 194021
Russia

KRAUSS Lawrence
Yale University
Center f. Theor. Physics, Sloane Lab.
New Haven CT 06511
USA

KRISHNAN N.
Universita of California
Physics Dept
Irvine Ca 92717
USA

KROLAK Andrzej
Polish Academy of Sciences
Siadeckich 8
00-950 Warsaw
Poland

KUNDIG Walter
Inst. der Universität Zürich
Schönberggasse 9
8001 Zürich
Switzerland

LABERRIGUE-FROLOW Jeanne
Université P et M Curie, LPNHE,
4 Pl. Jussieu, Tour 33 R de Ch.
75252 Paris Cedex 05
France

LEVY Jean-Michel
Univ. Paris VI/VII
4, Pl. Jussieu, Tour 33
75252 Paris
France

LOBASHEV Vladimir
Inst. for Nuclear Research
60th Anniv. Oct. Rev prosp. 7a
Moscow 117312
Russia

LORENZ Eckart
Max Planck Inst. Physics
Föhringer Ring 6
Munchen 40
Germany

MAIA NETO Paulo-Américo
Univ. P. et M. Curie
Case 74, 4 Pl. Jussieu
75252 Paris
France

MASCARENHAS Nicholas
California Inst. of Technology
161-33
Pasadena CA 91125
USA

MAUROGORDATO Sophie
Observatoire de Meudon
5, Place Janssen
92195 Meudon
France

Mc HUGH Martin
Philipps Laboratory
GPEG
Hanscom AFB MA 01731
USA

MLYNEK Jürgen
Univ. Konstanz, Fak. f. Physik,
Postfach 5560
D-7750 Konstanz
Germany

MOFFAT John
Univ. of Toronto
Dept of Physics
M5S 1A7 Toronto Ontario
Canada

MONTANARI Claudio
I N F N, , Dip. Fisica Nucl.
Sez. di Pavia
27100 Pavia
Italy

MONTANET François
CPP Université de Marseille II
Case 907
13288 Marseille
France

MONTANET Lucien
C E R N
CERN
1211 Geneve 23
Switzerland

MOODY Martin
University of Maryland
Dept. of Physics
20742 CollegePark MD
USA

MORAND R.
L A P P
B.P. 110, Chemin de Bellevue
74941 Annecy le Vieux
France

MORETTI Mauro
S I S S A
2 Via Beirut
34013 Trieste
Italy

MORRISON Douglas
CERN
Division PPE
Geneva 23
Switzerland

MOURS Benoit
L A P P
B.P. 110, Chemin de Bellevue
74941 Annecy le Vieux
France

NELSON Peter
Max Planck Inst. für Quantenoptic
Ludwig Prandtl Str. 10
D-8046 Garching
Germany

NEUMAIER Stefan
C E R N
Div. PPE
Ch-1211 Geneva 23
Switzerland

NOLTE Eckehart
Fakultät für Physik E17
T U M
8046 Garching
Germany

NORDTVEDT Ken
I H E S
35, Route de Chartres
91440 Bures sur Yvette
France

NUNOKAWA Hiroshi
National Lab. for H.E. Physics
K E K, 1-1 Oho Tsukuba-shi
Ibaraki-Ken 305
Japan

OROZCO Luis
State Univ. of N.Y. at Stony Brook
Department of Physics
Stony Brook N.Y. 11794-3800
USA

PAIK Ho Jung
Univ. of Maryland
Dept of Physics
College Park MD 20742
USA

PAIN Reynald
Université Paris VI et VII
4, Pl. Jussieu ,Tour 33, RdC
75252 Paris Cedex 05
France

PAL Palash
Center for Particle Physics
Dept of Physics
Austin Tx 78712-1081
USA

PAPAGEORGIOU Elena
Université de Paris Sud
LPTHE, Bât. 211
91405 Orsay Cedex
France

PARKE Stephen
Fermilab, Theoretical Physics ,
P.O.Box 500
Batavia IL.
USA

PAZ Juan Pablo
Los Alamos National Lab.
Theoretical astrophysics
Los Alamos NM 87545
USA

PELTONIEMI Juha
Universitat de Valéncia
Dr. Moliner 50
46100 Burjassot
Spain

PEREZ Patrice
C E N Saclay
DAPNIA
91191 Gif sur Yvette Cedex
France

PESSARD Henri
L A P P
B.P. 110, Chemin de Bellevue
74941 Annecy le Vieux
France

PETCOV Sergey
S I S S A
Via Beirut No 2-4
34013 Trieste
Italy

PHILLIPS William
N I S T
Phys A 167
Gaithersburg MD 20899
USA

PIEPKE Andreas
Max Planck Institut
P.O.Box 10 39 80
6900 Heidelberg
Germany

PINSONNEAULT Marc
Yale University, Dep. of Astronomy ,
Mail Box 6666
New Haven CT 06511
USA

POMANSKY Alexander
Baksan Observatory I N R
Kabardino-Balkarskaya, Respublika
361609 Baksan
Russia

PREDA Anna
INFN
Sezione di Milano, Via Celoria, 16
20133 Milano
Italy

RAIMOND Jean-Michel
E N S , Spectroscopie Hertzienne,
24 rue Lhomond
75231 Paris Cedex 05
France

RAMSEY Norman
Harvard Univ.
Lyman Physics Lab.
Cambridge MA 02138
USA

RITTERS Rogers
University of Virginia
Dept of Physics
Charlottesville Va 22901
USA

ROBERTSON Barry
Queen's University
Physics Department
Kingston Ontario
Canada

ROBERTSON Hamish
Los Alamos National Lab.
MS D449
Los Alamos NM 87545
USA

ROSOWSKY André
C E N Saclay
DAPNIA
91191 Gif sur Yvette Cedex
France

ROUSSEAU David
Université d'Aix - Marseille II
C. P. P. M., Case 907
13288 Marseille Cedex 09
France

RUFFINI Remo
I C R A
Univ. "La Sapienza", P.le Aldo Moro
00185 Roma
Italy

SALOMON Christophe
E N S, Spectroscopie Hertzienne,
24, rue Lhomond
75231 Paris
France

SANDFORD Michael
Rutherford Appleton Lab.
Chilton
Didcot, Oxon OX11 0QX
U.K.

SCHAFER Gerhard
Max Planck Gesellschaft
Universität Jena, Max-Wien-Platz 1
6900 Jena
Germany

SCULLY Marlon
Univ. of New Mexico
800 Yaje Blvd. NE
Albuquerque, NM 87131
USA

SONA Pietro
I N F N, Dipartimento di Fisica,
Largo E. Fermi 2
50125 Firenze
Italy

SPIRO Michel
C E N Saclay
DAPNIA
91191 Gif sur Yvette Cedex
France

STEINBERG Aephraim
U.C. Berkeley, Physics Dept;
366 Leconte Hall
Berkeley CA 94720
USA

STEPHENSON Gerard J. Jr
Los Alamos Nat. Lab.
P-Do MS D434 LANL
Los Alamos NM 87545
USA

STOEFFL Wolfgang
Lawrence Livermore Nat. Lab.
P.O.Box 808
Livermore CA 94550
USA

STOLARCZYK Thierry
C E N Saclay
DAPNIA
91191 Gif sur Yvette Cedex
France

TALMADGE Carry
Purdue University
Physics Department
West Lafayette IN 47907-1396
USA

TRAN THANH VAN Jean
Univ. de Paris Sud
Bât. 211
91405 Orsay Cedex
France

UROS CORRALES Victor
Université V et VII
4, Pl. Jussieu - Tour 33-B.P. 200
75252 Paris Cedex 05
France

VESSOT Robert
Smithsonian Astro. Observatory
Garden Street
Cambridge MA 02138
USA

VINET Jean-Yves
Université de Paris Sud
L A L, Bât. 200
91405 Orsay Cedex
France

WARK Dave
Nuclear Physics Laboratory
Kebble Roadd
Oxford OX1 6RX
United Kingdom

WAYSAND Georges
Université Paris VI et VII
Tour 23, 2, Pl. Jussieu
75251 Paris Cedex 05
France

WEI Yi
FB. Physik, Universität Wuppertal
5600 Wuppertal 1
Germany

WILKERSON John
Los Alamos National Lab.
MS D449
Los Alamos NM 87545
USA

WILL Clifford
Washington University,Dpt of Physics
Campus Box 1105
St Louis MO 63130
USA

YODH Gaurang
University of California at Irvine
Department of Physics
Irvine CA 92717
USA